AN INVESTIGATION INTO PIPELINES SUBJECTED TO LATERAL SOIL LOADING

MICHAEL J. PAULIN


CENTRE FOR NFLD. STUDIES
MEMORIAL UNIVERSITY
OF NEWFOUNDLAND

An Investigation into Pipelines Subjected to Lateral Soil Loading

by

Michael J. Paulin, M.Eng., P.Eng.

A Thesis Submitted to the School of Graduate Studies in Partial Fulfilment of the Requirements for the Degree of Doctor of Philosophy

Faculty of Engineering & Applied Science

Memorial University of Newfoundland

October, 1998

St. John's Newfoundland Canada

Abstract

With the increased use of pipelines for carrying gas, oil, water, and electrical cables, the response of the pipeline to soil movements in the vicinity of the pipeline needs to be understood. These movements may be due to adjacent earth works, landslides, thaw settlement of permafrost, frost heave or a variety of other causes. These soil movements set up stresses within the pipeline and, depending upon the magnitude of these stresses and the nature of the pipeline, may cause damage to or failure of the line. Several consequences may be associated with pipeline failure and include loss of life, damage to the environment, and economic costs. The stresses which are generated by the soil movements are dependant upon a number of parameters, which include the nature of the soil, the properties of the pipeline, and the geometry of the pipeline/soil/backfill system.

The state-of-practice (SOP) for pipeline design for areas where soil may move relative to the pipeline involves discretizing the pipeline into elastic-plastic segments which are connected to sets of springs/sliders which simulate the soil. As the springs replace the soil, their force-displacement characteristics should correspond to the actual soil response if a meaningful analysis is to be conducted. Much of the theory behind the interaction parameters used in the SOP are derived from theories developed for other geotechnical applications such as pile/soil or anchor plate/soil interaction; there is little or no verification of the mechanisms or the magnitude of forces which arise during pipeline displacement. This thesis presents a research program conducted to examine one aspect of pipeline/soil interaction; that of lateral

pipeline/soil interaction.

The objectives of the research program outlined in this thesis were to: (1) conduct physical model testing of lateral pipeline/soil interaction in cohesive soil to ascertain the effects of trench width, burial depth, interaction rate, backfill properties, and stress history of the soil on the interaction using the centrifuge technique to maintain similitude between model and full-scale; (2) determine the characteristics of normalized force-displacement curves or interaction factors so that they can be used generically; (3) assess the displacement patterns and failure mechanisms of the soil around a pipeline; and (4) generate conclusions and recommendations regarding current and proposed methods of analysing lateral pipeline/soil interaction through comparison with experimental results.

This thesis demonstrates that: (1) the trench width had little or no effect on an undrained interaction; (2) the undrained load on a pipeline increased with increasing burial depth; and (3) the pipeline displacement rate (and thus drainage conditions) had a significant effect on the loads transferred to the pipeline by the soil (for this particular soil/backfill system). The pipeline displacement rate effect is significant because the current state-of-practice for cohesive media is based on an undrained interaction between the pipeline and the soil which can significantly underestimate the ultimate load transferred to the pipeline. Also, the displacements required to reach these ultimate loads are significantly underestimated in existing guidelines for the soil/backfill system considered. Results from existing and proposed analysis methods to predict pipeline/soil interaction curves are encouraging.

The undrained force-displacement response could be reasonably predicted and ultimate loads can be predicted within $\pm 20\%$ using existing methods of analysis. Experimentally derived methods of undrained analysis provided reasonable fit to the experimental data; an average of within 10% of the ultimate lateral load might be expected. Other potential methods based on undrained anchor/soil and pile/soil interaction resulted in predictions of ultimate loads within 20% of those measured experimentally. Pile/soil interaction p-y curves were found to provide reasonable predictions to the experimental data. Bearing capacity solutions showed potential to bound the actual ultimate load. Passive earth pressure solutions were found to yield reasonable undrained prediction for cases where the pipeline was shallow ($H/D < 2$).

Predicted drained (c-ϕ) ultimate loads on the pipelines were consistently underestimated using existing methods. Drained analysis methods from the experimental data could be expected to predict the force-displacement response of the experimental data to within $\pm 20\%$. Drained anchor/soil interaction analysis methods underestimated the experimental data. Drained pile/soil interaction methods provided reasonable fits to the data in cases. Cohesionless soil p-y curves were found to overestimate the actual experimental force-displacement response. Cohesionless soil bearing capacity solutions were found to overestimate while passive earth pressure solutions tended to underestimate the ultimate lateral loads.

Acknowledgements

This research program was completed at Memorial University of Newfoundland through funding provided by NOVA Gas Transmission Limited of Calgary, Alberta. Financial support to assist in the completion of the thesis was provided by the Natural Sciences and Engineering Research Council of Canada (NSERC).

I am greatly thankful to my supervisors, Dr. Jack Clark, Principal Consultant of C-CORE, and Dr. Ryan Phillips, Director of Centrifuge & Experimental Modelling at C-CORE, under whose guidance and supervision the project was carried out. Thanks to Dr. Farrokh Poorooshasb for introducing me to the use of centrifuge modelling in geotechnical engineering. Thanks to Dr. Arisi Swamidas of the Faculty of Engineering and Applied Science for his review of my thesis. Appreciation goes out to Mr. Raymond Boivin of NOVA for his insight into this research program.

The significant contribution of Faculty of Engineering and Applied Science graduate student, Ling Lin, who conducted a significant portion of the proof activities for this project is acknowledged. The contributions of the C-CORE Centrifuge Centre team to this project are also acknowledged and greatly appreciated especially the efforts of Don Cameron, Shawn Hurley, Dan King, Rick Meaney, Dave Millan, Steve Smyth, Karl Tuff, Xiaojun Xiao, and Fanyu Zhu.

Finally, but not least, thanks to Janet for her patience, encouragement, and assistance over the past three years and during the preparation and defence of this thesis.

Table of Contents

List of Figures

List of Tables

Notations

Lowercase

a	Acceleration
c	Soil Cohesion
cm	Centimetre
c'	Drained Soil Cohesion
c_a	Pile Adhesion
c_u	Undrained Shear Strength
$c_{u\text{-}avg}$	Average Undrained Shear Strength above the Pipe Invert
d_{50}	Mean Grain Size
e	Void Ratio
e	Exposed Pile Head Length
f_x, f_y, f_z	Force or Load per Unit Length
g	Gravity
h	Linear Distance
h	Depth to the Pipe Springline
k	Coefficient of Permeability
km	Kilometre
kN	KiloNewton
kPa	Kilopascal
kW	Kilowatt
k_h	Coefficient of Horizontal Subgrade Reaction
k_x, k_y, k_z	Linear Soil Springs
m	Metre
min.	Minute
mm	Millimetre
p	Lateral Force or Load per Unit Length
p, p'	Mean Effective Stress, Effective Mean Effective Stress

q	Overburden Pressure
q, q'	Deviator Stress, Effective Deviator Stress
q_c	Cone Tip Resistance
q_{ult}	Predicted Ultimate Lateral Pressure
s	Anchor Plate Shape Factor
s	Coefficient for the Effect of Overburden Pressure
sec.	Second
t	Time
u	Pore Pressure
u_x, u_y, u_z	Displacements
v	Velocity
w	Water Content
w_l	Liquid Limit
w_p	Plastic Limit
x, y, z	Principal Directions
y	Lateral or Horizontal Displacement
y_c	Deflection at 50% of P_{ult}

Uppercase

A	Projected Cross-Sectional Area
A	Load Reduction Factor
A	Cone Factor
B	Breadth or Thickness of Pile
BC	Bearing Capacity
C	Depth of Soil Cover to Top of Pipe
C_D	Drag Coefficient
C_k	Empirical Factor to Estimate K_{h70}
CPT	Cone Penetration Test
D	Pipeline or Pile Diameter

D	Height of Anchor Plate, Foundation Width, Width of Anchor Plate
D_{BO}	Distance into the Trench Wall to Breakover
E	Energy
F	Force
F	Central Point Load
F"	Normalized Force
F_{ch}	Correction Factor for Backfilled Trench
F'_c	Factor for the Effect of Cohesion on Anchor Behaviour
F_D	Drag Force
F_x, F_y, F_z	Maximum Force per Unit Length
F'_γ	Factor for the Effect of Unit Weight on Anchor Behaviour
G_s	Specific Gravity of Soil Solids
H	Depth to Bottom of Trench/Pipeline or Anchor Plate
H/D	Embedment Ratio
I_p	Plasticity Index
J	Empirical Pile Coefficient from Matlock (1970)
K_c	Net Lateral Soil Pressure Coefficient
K_{cr}	Resultant Net Lateral Soil Pressure Coefficient
K_{h70}	Secant Slope at 70% of Maximum Force
K_o	Coefficient of Earth Pressure at Rest
K_p	Passive Earth Pressure Coefficient
L	Length of Pipeline, Pile, Foundation or Anchor Plate
L	Embedded Length of Pile
LDT	Linear Displacement Transducer
M	Mass
N	Acceleration or Scaling Factor
NPS	National Pipe Schedule

N_c	Lateral Interaction Factor or Resistance Coefficient or Horizontal Bearing Capacity Factor or Breakout Factor for Cohesive Soils
N_c^*	Limiting or Critical Breakout Factor for Anchor Plates in Cohesive Soils
N_c	Cone Factor
N_k	Cone Factor
N_{BO}	Normalized Resistance at Breakover
N_{TW}	Normalized Resistance at Trench Wall
$N_{0.5D}$	Normalized Resistance at 0.5D Penetration
N_{1D}	Normalized Resistance at 1D Penetration
N_γ	Lateral Interaction Factor or Horizontal Bearing Capacity Factor or Anchor Capacity Factor for Frictional Soils
OCR	Overconsolidation Ratio
PP	Passive Pressure
PPT	Pore Pressure Transducer
P_{ult}	Ultimate Lateral Load Per Unit Length
P_{ult-x}, P_{ult-y}, P_{ult-z}	Ultimate Load or Force per Unit Length
Q_u	Ultimate Load Capacity for a Laterally Loaded Pile
RPM	Revolutions Per Minute
R_c	Ratio of Native Soil to Backfill Undrained Strength
R_ψ, R_R, R_K	Correction Factors for the Effects of Soil Dilatancy, Anchor Roughness, and Initial Stress State for Anchor Plates in Cohesionless Soil
SM	Secant Modulus
S_{AB}	Slope of Interaction After Breakover
S_{BB}	Slope of Interaction Before Breakover
TW	Trench Wall
U_x, U_y, U_z	Limiting Displacement to Maximum Force per Unit Length
W	Trench Width

Y"	Normalized Displacement
Y_{ult}	Lateral or Horizontal Displacement to Ultimate Load
Z	Depth Below Soil Surface
Z_{cr}	Critical Depth After Which Pile Load Does Not Increase
0.5D	0.5 Diameter Penetration
1D	1 Diameter Penetration

Greek

ϵ	Strain
ϵ_c	One-Half the Strain at Maximum Stress
γ	Saturated Unit Weight of Soil
γ'	Effective Unit Weight of Soil
γ_w	Unit Weight of Water
ϕ	Angle of Friction
ρ	Bulk Density
σ	Total Stress
σ'	Effective Stress

Chapter 1

Introduction

1.1 Background

> "Underground pipelines are the arteries of our nation, the lifeblood of our society. They work silently and continuously, 24 hour a day, 365 days a year, to deliver the energy to enable our country to thrive."

The above is a quotation from the Opening Address (Itzkovitch, 1994) to *Managing Pipeline Integrity - An Issues Workshop on Pipeline Lifecycle*. The statement indicates the importance in today's society of the national pipeline infrastructure which continues to age. It also implies the significant role pipelines will continue to play in the future as the move is made into new frontiers to exploit and transport natural resources. To put in perspective the importance of Canada's pipeline infrastructure, the amount of oil currently transported daily from Calgary to Toronto by the nations pipeline system is equivalent to over 39,000 trailer truck loads. Similarly for gas, 15,000 truck loads per day would be required from Calgary to Toronto to ship an equivalent amount of light natural gas (Yungblut, 1994).

There are over 1,000 companies which own and operate 90,000 kilometres of oil and gas pipelines in Canada (Itzkovitch, 1994; Yungblut, 1994). The age of the major pipelines in Canada's pipelines infrastructure in 1994 ranged from 32-52 years (McCarthy, 1994) and it

has been suggested that, based on current reserve levels, the system (with additions where necessary) will be required for another 40-50 years (Yungblut, 1994). It has also been suggested that if a new system was to be installed, the cost would place a substantial strain on the Canadian economy and that Canadian gas could not be fiscally competitive in the eastern Canadian market (Yungblut, 1994). In 1992, the initial cost (in US dollars) of one kilometre of pipeline in the US was reported to be over $650,000 (C-FER, 1994). In 1978, there was very nearly 1 million miles of pipelines for crude oil alone in the US (Williams, 1979). Worldwide, pipelines account for 80% of all natural gas transmission (Itzkovitch, 1993). Onshore, pipelines are subjected to loading hazards as a result of landslides or slope instability, seismic activity, adjacent earth works, frost heave, thaw settlement of permafrost, and vehicle loading (see, for example, Rizkalla and McIntyre, 1991; ASCE, 1984; O'Rourke and Ahmed, 1985; Selvadurai, 1992; Vinson and Palmer, 1989).

The search for oil, gas, and other natural resources has led countries, such as Canada, to look to the oceans to supplement their land based reserves. Economical exploitation and transportation of these natural resources will depend on overcoming seabed geotechnical and oceanographical problems. Of the offshore resources being explored, oil and gas accounts for approximately 90% of the total value and it has been estimated that 30% of the worlds total hydrocarbon resources lie offshore (Poulos, 1988). To transport the oil and gas, a pipeline is usually required to transport the hydrocarbons to shore or at least to a riser system where it can be picked up by a tanker. Pipelines are operated in a physically and technically demanding environment which can be subject to severe weather, shifting sediments, and the

threat of corrosion. Near-term plans by the offshore pipeline industry will have pipelines operating in water depths as deep as 3,000 feet (National Research Council, 1994). In the United States, over 20,000 miles of pipelines are operated offshore and more than one-third is beyond its 20 year design life (Omnes, 1995) as it was installed in the 1950's and 1960's (Baalist, 1995). One-quarter of all natural gas and one-ninth of all crude oil in the United States is carried in offshore pipelines (Baalist, 1995). The first U.K. offshore pipeline was put into operation in 1967. In 1991, there were in excess of 100 major offshore pipelines in the U.K. sector of the North Sea with a combined length of over 4,000 miles; in addition, there were over 400 smaller pipeline systems with a total length of more than 1,000 miles (Adams, 1991). In all of the North Sea, there are more than 600 pipelines having a total length of around 7,000 miles (Adams, 1991).

These pipelines must be designed in consideration of environmental forces and loadings. Such environmental forces may include waves, earthquakes, currents, ice, ice scour, and seafloor stability problems such as flowslides, slumping, and creeping soils (see, for example, Poulos, 1988; Clark *et al.*, 1994; Sangrey, 1977; Audibert *et al.*, 1979). All of these phenomena can move, damage, or expose once buried pipelines.

It is clearly of concern that as pipelines both onshore and offshore grow older, the techniques and methodologies to assess their serviceability reflect their actual state. Also, new pipelines must be confidently designed to account for potential hazards listed above. The failure frequency for onshore pipelines in Canada is currently at 0.00004 events per kilometre-year

(Ashworth, 1994). Between 1991 and 1994, there were six major pipeline ruptures reported in Canada, three of which resulted in fires (Ashworth, 1994). Onshore, the potential exists, especially in remote regions, for damage to facilities, danger to facility personnel, pollution, forest fires, and hazards to the general public including loss of life. Offshore, pipeline structural failures could also result in loss of life, damage to facilities, pollution of fishing grounds and pollution of coastal areas. New technologies and methodologies are needed to accurately reflect the state of the pipeline and the behaviour of the pipeline under operating conditions in order to predict when and where pipeline failure may occur.

1.2 Nature of the Problem

With the increased use of pipelines for carrying gas, oil, water, communications, and electrical cables both onshore and offshore, the response of the pipeline to soil movements in the vicinity of the pipeline needs to be understood. These movements may be due to landslides, seismic activity, adjacent earth works, thaw settlement of permafrost, frost heave or a variety of other causes. As the soil moves relative to the pipeline as exemplified in Figure 1.1, loads are imposed on the pipeline which will tend to distress the pipeline. Portions of the pipeline are anchored in or loaded by the moving soil mass, while adjacent portions of the pipeline are anchored in the intact soil and tend to restrain the pipeline. These soil movements and restraints set up stresses within the pipeline and, depending upon the magnitude of these stresses and the nature of the pipeline, may cause damage to or failure of the line. The stresses which are generated by the soil movements and restraints are dependent upon a number of parameters, which include the type of soil, the properties of the

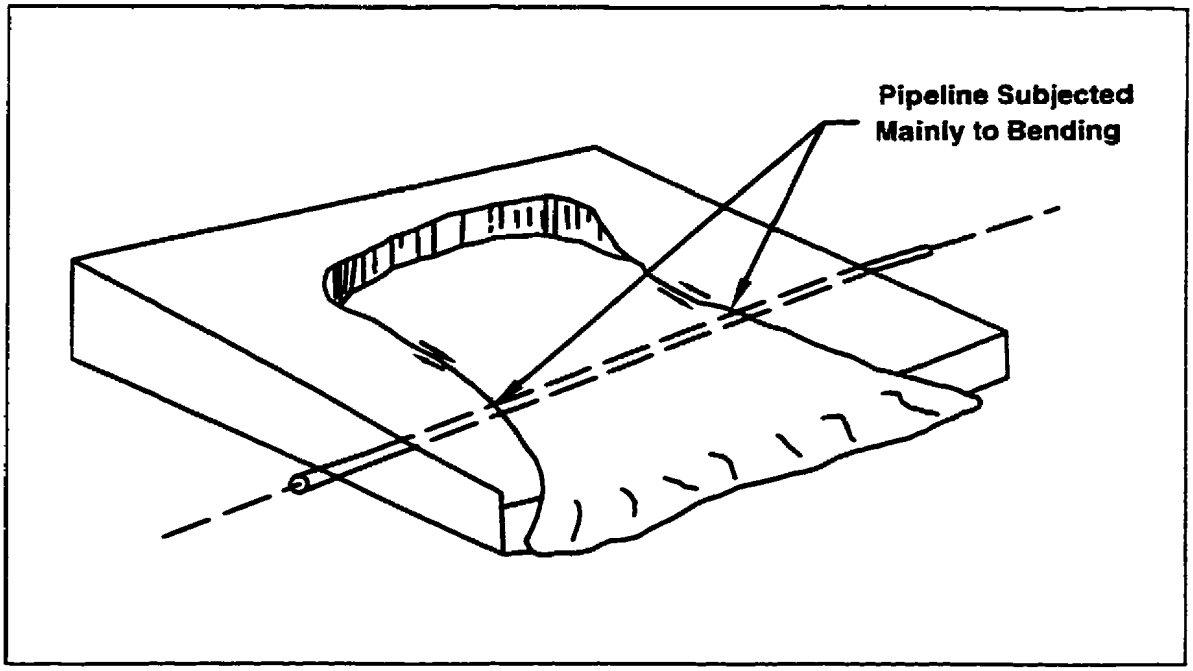

Figure 1.1 - Example of a pipeline subjected to lateral loading (after O'Rourke and Lane, 1989).

pipeline, the geometry of the pipeline/soil/backfill system, the differences in the properties between the backfill and the native soil, the variability of the soil properties along the pipeline route, the conditions of the pipeline/soil interface, the orientation of the pipe to the differential soil movement, and the rate of loading between the pipeline and the soil (Selvadurai, 1985).

Relative movements between buried pipelines and the surrounding soil can be caused by landslides or creeping soils in regions where pipelines move along slopes which do not correspond with hill crests or valleys. Studies carried out by NOVA Gas Transmission Limited (Paulin *et al.*, 1994) have shown that typical rates of ground movements for creeping type landslides experienced by the industry range from less than 1 cm/year to 6 cm/year.

Studies by SNAM in Italy have indicated slope movements on the order of 18 cm/year (Venzi *et al.*, 1993). Primarily lateral movements occur when pipelines move across slopes while primarily longitudinal movements occur when a pipeline passes perpendicularly over the crest of a hill. A combination of these movements occurs in a variety of other configurations. The load transfer behaviour between a pipeline and the surrounding earth is not considered to be well understood.

Pipelines generally traverse large areas and may cross areas of seismic hazard. Seismic hazards which could affect pipelines both onshore and offshore are generally characterized as: (1) ground failures, which include faulting, landslides, liquefaction, densification and ground cracks; (2) ground motion; (3) tsunamis and seiches; and (4) tectonic uplift and subsidence (Yeh, 1988; ASCE, 1984). Of the types of ground failures discussed by the Committee on Gas and Liquid Fuel Lifelines (ASCE, 1984) and reviewed in the next chapter, only massive landslides with deep translation and rotational movement are considered virtually impossible to design against (ASCE, 1984). However, the authors of the "guidelines" state that many areas that have potential for deep-seated movement can be identified and avoided.

Offshore, pipelines could be subjected to seafloor movements such as mudslides (Poulos, 1988), slumping (Audibert *et al.*, 1979), soil loading due to creeping soils (Sangrey, 1977), mud lumps which occur in developing river deltas (Milz and Broussard, 1972), or loading from ice scour through subscour deformation (Clark *et al.*, 1994). Poulos (1988) presents

three major mechanisms of instability in marine soils. These are gravity forces, hydraulic forces and earthquake or tectonic activity. Poulos (1988) subclassifies gravity forces into basic instability and creep phenomena. Basic instability may be the result of shear stresses in the soils which exceed the shear strength simply by excessive deposition of weak soils on steep slopes (Bea, 1985). Soil movement due to instability is usually rapid, with large displacements occurring within a period of time ranging from a few minutes to a few days (Poulos, 1988). Poulos (1988) also acknowledges that creep under constant stress may occur in marine clays. Soil movement is dependent upon a number of factors including stress level and environmental conditions; movement may take place over time periods ranging from a few hours to thousands of years (Poulos, 1988). Hydraulic forces such as waves may cyclically load the seabed and generate excess pore pressures within the seabed. Such excess pore pressures may affect the stability of the seafloor (Poulos, 1988). Earthquakes and tectonic activity can also pose hazards to structures due to ground shaking and such seafloor failures as slumping (slope stability) or flow slides due to liquefaction (Poulos, 1988). Slope failures may be natural but they may also be caused by construction activities such as dredging and anchor dragging (Sylwester and Holmes, 1989).

Relative movements and the resulting interaction between the pipeline and the soil can also be important in pipeline design where thermal buckling may be a hazard (Luscher *et al.*, 1979). The combination of pipeline design and restraint offered by the soil must be such that it will offer sufficient resistance to pipeline movement if it tends to buckle.

When a buried pipeline is subjected to ground movements as described above, the pipeline's integrity and operating safety are both matters of concern both from a lifeline and an environmental point of view. The state-of-practice for pipeline design in areas where the soil may move relative to the pipeline involves performing finite element or related numerical analyses. The industry standard for pipeline/soil interaction analysis is considered to be that in which the pipeline is modelled as a series of straight beam finite elements connected to the soil by a series of individual springs/sliders (Zhou and Murray, 1993). The springs/sliders represent the elastic-plastic behaviour of the soil. The beam elements are assigned cross-sectional stiffness coefficients characteristic of the pipeline (Zhou and Murray, 1993). Parameters describing the interaction curves or soil springs are commonly input to the computer based programs to determine the stress or strain states of the pipe with regards to soil displacement and to determine the point where remedial action need be taken (Rizkalla *et al.*, 1992). Pipeline response to large horizontal soil movements can be determined from such computer based analyses and provide a basis for design (O'Rourke and Lane, 1989).

In these models, the total interaction is represented as three distinct interactions; axial, transverse horizontal, and transverse vertical as shown in the schematic of Figure 1.2. Figure 1.3 presents schematic force-displacement curves for pipeline/soil interaction in the three directions x, y, and z. The notations f_x, f_y, and f_z represent the force per unit length transmitted to the pipe by the soil and the notations u_x, u_y, and u_z represent the displacements. Generally, there is considered to be a maximum force per unit length that can be transmitted by the soil to the pipe which is represented by F_x or $P_{ult\text{-}x}$, F_y or $P_{ult\text{-}y}$, and F_z or $P_{ult\text{-}z}$ (O'Rourke

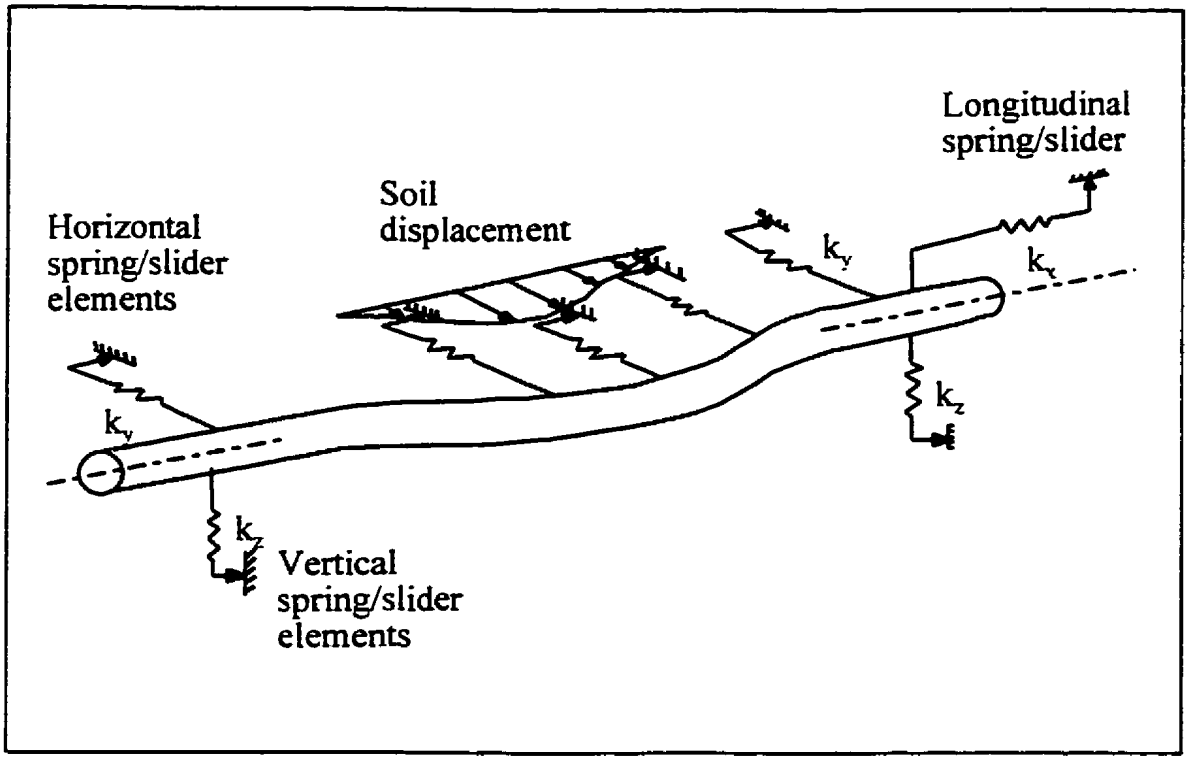

Figure 1.2 - Schematic representation of soil reactions (after O'Rourke and Lane, 1989).

and Lane, 1989). These maximum forces occur after some limiting displacements designated as U_x, U_y, and U_z for the longitudinal, lateral, and vertical directions, respectively (O'Rourke and Lane, 1989). The parameters describing these spring elements have generally been assumed from other soil/structure interaction studies (e.g. anchor plates and piles) (Rizkalla *et al.*, 1992). The actual response between a pipeline and the soil is nonlinear (normally approximately hyperbolic) but is often simplified by means of a bilinear relationship as shown in Figure 1.4 (Bea, 1985). The springs describing the soil are independent of one another and so there is no connection between adjacent soil zones. This assumption of independent slices of soil (the behaviour of each which is governed by a soil spring) will not truly replicate the observed behaviour and will produce conservative designs (Kettle, 1984).

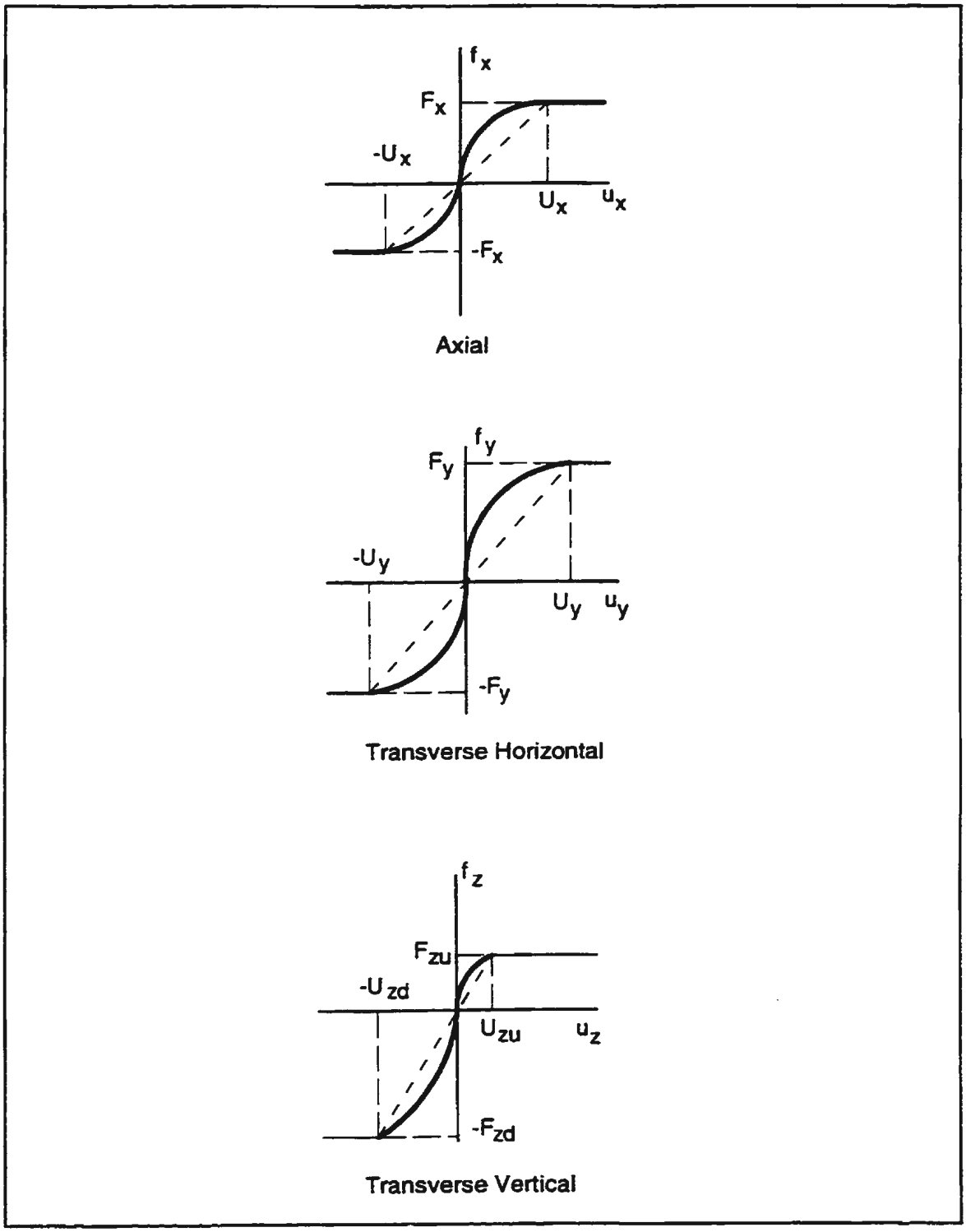

Figure 1.3 - Force-displacement curves for pipeline/soil interaction (after O'Rourke and Lane, 1989).

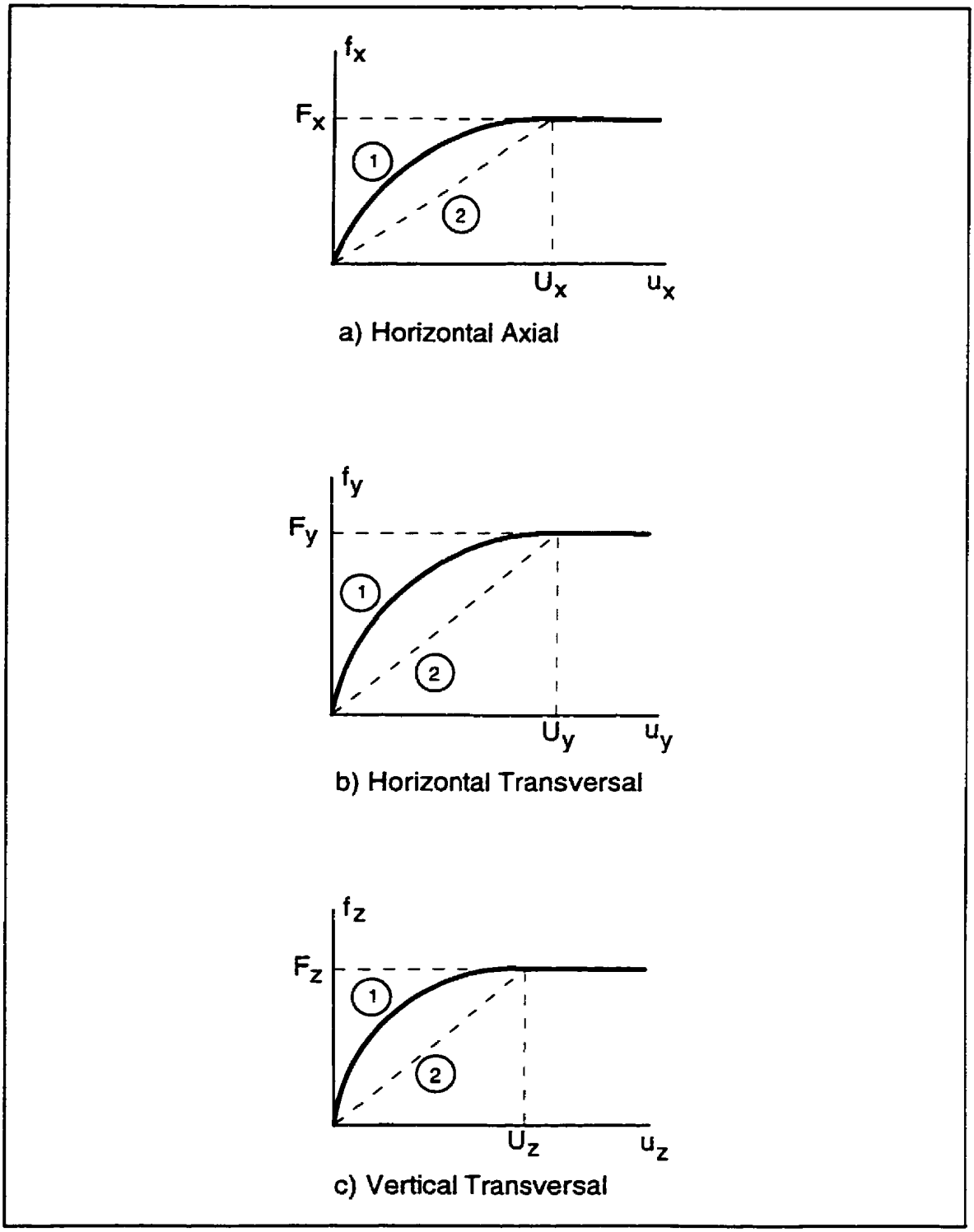

Figure 1.4 - Load-deformation relationships for soil restraints or loadings: 1 = actual nonlinear relationship or hyperbolic approximation; 2 = simplified bilinear representation (after Bea, 1985).

More recently, two-dimensional soil spring models have included shear elements to link together adjacent soil springs which noticeably improved pipe strain predictions of a full-scale buried pipeline subjected to frost heave (C-FER, 1995).

Selig and Nash (1988) commented on buried pipeline research needs at an ASCE conference on pipeline infrastructure (Bennett, 1989). These needs were identified at a workshop prior to the conference which was convened with representatives from universities, consulting engineering and research organizations, pipe and/or equipment manufacturers, constructors, users, and government agencies. A partial list of research needs identified by the workshop included: (1) experimental verification to advance the understanding of pipeline/soil interaction principles, to evaluate and improve designs, or design techniques, and to provide a basis for the development of new products and installation methods; (2) study of pipeline/soil interaction resulting from time-dependent soil and material properties and develop improved design methods incorporating this behaviour; (3) development of standard soil stress-strain and volume change data to use in analytical models for predicting pipeline/soil interaction. From this information, establish reliable values of the soil parameters for design applications so that designers can select appropriate values based on rapid field and laboratory techniques without having to conduct difficult or extensive testing; and (4) obtain more information on the nature and magnitude of loads on pipelines, such as those associated with installation, vehicles, dynamic events, ground movements, and temperature variations.

1.3 Purpose of the Study

The purpose of the study described in this thesis is to consider one aspect of pipeline/soil interaction in cohesive soils; that of lateral pipeline/soil interaction. Given the expense and technical difficulty associated with full-scale testing and the uncertainty in the results which would be gained by small-scale modelling at 1 gravity, research has been undertaken using the technique of centrifuge modelling to maintain similitude between model and full-scale. A review of centrifuge modelling and its applications are presented as Chapter 4 of this thesis.

The objectives of the experimental program were to examine the phenomenon of lateral pipeline/soil interaction in cohesive soil and, specifically, to:

(1) determine the shape of the load-displacement curves,

(2) determine the characteristics of normalized force-displacement curves or interaction factors,

(3) assess the effect of pipeline trench depth, trench width, interaction rate, backfill properties, and stress history of the soil upon the interaction,

(4) determine the displacement pattern and mechanism of failure of the soil around a pipeline,

(5) develop analytical methods to predict pipeline loads, and

(6) generate conclusions and recommendations regarding current and proposed methods of analysing lateral pipeline/soil interaction through comparison with experimental results.

1.4 Thesis Outline

This thesis is organized into nine chapters in an attempt to logically proceed through the reasoning behind the research, the work itself, the results and their analysis, comparison of the results, and conclusions arising from the results. Chapter 2 reviews the literature relevant to this study and includes a review of literature dealing with lateral pipeline/soil interaction, current methods of analysis and design, previous research, and other potentially relevant literature. Chapter 3 states the research objectives and outlines the scope of the program. Chapter 4 presents an overview of centrifuge modelling. Chapter 5 describes the experimental tests as well as the facilities and equipment used. Chapter 6 outlines the experimental procedure and testing while Chapter 7 contains the experimental results. The data are analysed in Chapter 8 and results are compared with accepted methods of pipeline/soil interaction analysis and proposed analytical analyses. The thesis closes with a summary, conclusions and recommendations which are contained in Chapter 9. Selected details, observations, and data from the experimental program are contained in the appendices. Any reference to a figure or table with a designation beginning with a letter (i.e Figure A.1) refers to a table or figure in that particular appendix (i.e. Appendix A). Further details and results on the experimental program described herein can be found in: Lin (1995); Paulin *et al.* (1993); Paulin and Phillips (1994); Paulin and Phillips (1995); Paulin and Phillips (1996).

Chapter 2

Literature Review

2.1 Lateral Pipeline/Soil Interaction

2.1.1 Onshore Pipelines

In 1993, a working group on Design and Construction/Geotechnical Science and Engineering of the *Issues Workshop on Pipeline Lifetime* identified the effects of natural hazards, such as earthquakes and landslides, as a key issue (CANMET, 1993). Typical landslide types are depicted in Figure 2.1. During selection of a pipeline route, care is taken to define the best possible route around unstable slopes. However, it is generally accepted that occasionally pipelines must be operated on or in adverse ground conditions (Rizkalla *et al.*, 1993) as pipelines are often constrained to right-of-ways or must be constructed on existing properties and potential hazards cannot be avoided. Ground movements in such areas may induce an accumulation of strain in the pipeline which may in turn pose a hazard to its integrity. Yeh and Lai (1992) suggest that it is unlikely that pipelines could survive the large deformations associated with deep seated translational soil movements. However, the authors state that if the potential soil instability involves slumps or other shallow landslides, a properly designed pipeline system may be a means of reducing risks and promoting long-term performance of the pipeline.

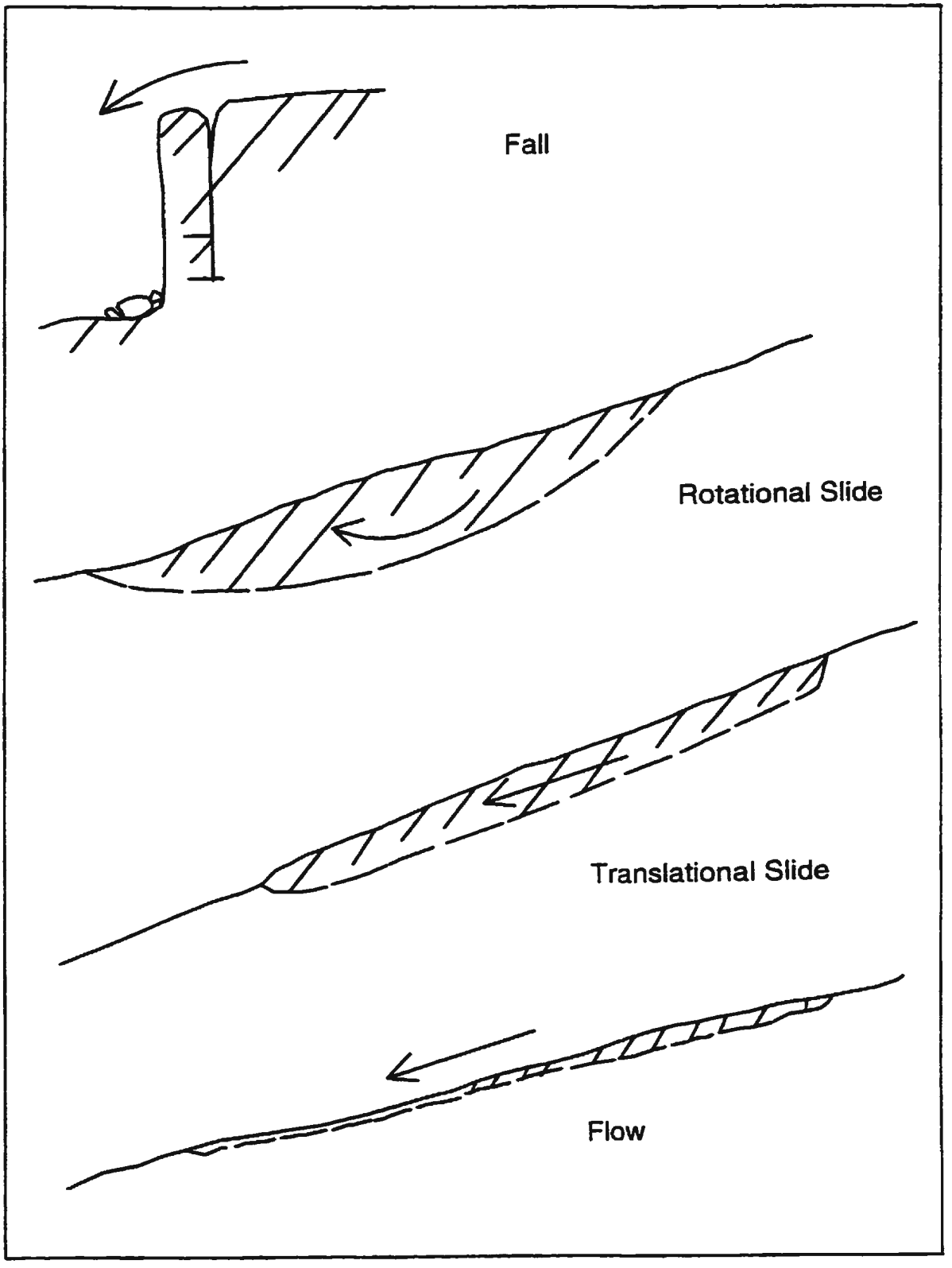

Figure 2.1 - Typical landslide types (after Winterkorn and Fang, 1975).

In 1955, a 25 inch natural gas pipeline was installed by Northwest Pipeline Corporation across Douglas Pass in western Colorado (Bukovansky *et al.*, 1985). The area was known for its landslides and although the pipeline designers were aware of the potential hazard, they accepted the risk due to highway and access considerations.

The first landslide to disrupt the pipeline occurred in 1962 when a long section of the line was damaged and 4,400 feet of new pipeline was required to reroute the pipeline outside the slide zone. In 1963 and 1979, the same thing happened in other areas requiring 3,200 and 1,200 feet respectively of new pipeline. Pipeline monitoring began in 1984 to detect slope deformations and increases in pipeline strain. The authors suggest that through monitoring, potential problems can be detected and mitigating measures can be implemented to prevent pipeline failure.

Mitigating measures in the Douglas Pass area consisted of stress-relieving the pipeline through the excavation of a trench around and parallel to the pipeline. The authors state that through such a procedure, strains in the pipeline decreased immediately and the pipeline moved up slope in the trench, sometimes to the opposite wall of the trench. During one excavation reported by the authors, the pipeline moved across the bottom of the excavated trench before finally "climbing" out the up slope wall of the trench. Another case is reported where an unstable slope moved approximately 10 feet perpendicular to the pipeline without damage to the line due to mitigation techniques. The authors conclude that hazard mitigation through excavation is quick, relatively inexpensive, and reliable.

Rizkalla and McIntyre (1991) describe mechanisms in northern Alberta which contribute to slope instability and could induce excessive stress or strain in a pipeline. Erosion of river banks and down cutting of its channel bed are considered to be the basic causes of instability. Contributing to the instability are the presence of weak zones such as low strength soil or rock layers which determine the lateral extent and depth below the ground surface of the instability. Secondary contributors include mechanism such as valley floor rebound which contributes to deep-seated creep-like ground movements.

Cavanagh and Rizkalla (1992) reported on a gas pipeline crossing the Simonette River in western Alberta which ruptured in 1978 and resulted in an explosion and fire. The damage to the pipeline occurred after only two years of operation and involved less than a two metre length of the pipeline. Subsequent investigation at the site indicated that slope instability and movement (both laterally and longitudinally to the pipeline) was at least partially responsible for the rupture. Following the incident, in 1979, slope monitoring instrumentation was installed at the site to assess loading caused by the slope movement. Monitoring of the unstable pipeline right-of-way continued and by September of 1980, the slope movement totalled approximately 40mm (Couperwaite and Marshall, 1989). In December of 1980, it was suspected that strains in the pipeline were reaching critical values, so a section of the pipeline was excavated and permitted to rebound to an unstrained condition. Similar excavations had to be undertaken in 1982, 1983, and 1988 to strain relieve the pipeline and it is expected that periodic excavations will need to be undertaken every 5 to 10 years.

Boivin and Cavanagh (1992) describe the case of two high pressure gas pipelines in northwestern Alberta which were located in unstable slopes. The pipelines were 273 and 406mm in diameter. Instrumentation (slope indicators) installed at the site indicated slope movements ranging from 1 to 17 mm/month moving in directions varying from primarily perpendicular to primarily parallel to the pipeline. When the pipeline was finally excavated for stress-relief purposes, over 300mm of rebound in each pipeline was noted. Based on the risk to the pipeline and the remoteness of the site, the authors recommended that the pipeline be rerouted at high cost using directional drilling to locate the pipeline beneath the unstable zones of the slope.

In 1986, a pipeline in western Alberta ruptured and fire occurred in an area of known instability which was only 10km from a small town (Wong, 1992). The NPS 30 pipeline, which had a wall thickness of 15.9mm, was located within a massive and deep seated landslide. Soil conditions at the pipeline were essentially silty-clays with a liquid limit, plastic limit and water content of approximately 43%, 16%, and 21% respectively and an undrained shear strength ranging from 50-100kPa (Wong, 1992). The rupture was caused by bending and buckling of the pipeline due to excessive soil movement, primarily parallel to the pipeline axis (Novacorp, 1992). The rupture put the pipeline out of commission for the 78 hours required to complete temporary repairs. Another 2.5 months were required to complete permanent repairs. Subsequent measurements of the rate of slope movement averaged 25 to 50 mm/year but Wong (1992) cautions that slope movements could be accelerated due to unfavourable climatic conditions. The author estimated through stress

Boivin and Cavanagh (1992) describe the case of two high pressure gas pipelines in northwestern Alberta which were located in unstable slopes. The pipelines were 273 and 406mm in diameter. Instrumentation (slope indicators) installed at the site indicated slope movements ranging from 1 to 17 mm/month moving in directions varying from primarily perpendicular to primarily parallel to the pipeline. When the pipeline was finally excavated for stress-relief purposes, over 300mm of rebound in each pipeline was noted. Based on the risk to the pipeline and the remoteness of the site, the authors recommended that the pipeline be rerouted at high cost using directional drilling to locate the pipeline beneath the unstable zones of the slope.

In 1986, a pipeline in western Alberta ruptured and fire occurred in an area of known instability which was only 10km from a small town (Wong, 1992). The NPS 30 pipeline, which had a wall thickness of 15.9mm, was located within a massive and deep seated landslide. Soil conditions at the pipeline were essentially silty-clays with a liquid limit, plastic limit and water content of approximately 43%, 16%, and 21% respectively and an undrained shear strength ranging from 50-100kPa (Wong, 1992). The rupture was caused by bending and buckling of the pipeline due to excessive soil movement, primarily parallel to the pipeline axis (Novacorp, 1992). The rupture put the pipeline out of commission for the 78 hours required to complete temporary repairs. Another 2.5 months were required to complete permanent repairs. Subsequent measurements of the rate of slope movement averaged 25 to 50 mm/year but Wong (1992) cautions that slope movements could be accelerated due to unfavourable climatic conditions. The author estimated through stress

lengths less than 400m. Lateral displacement of some pipelines were noted during the survey.

2.1.2 Pipelines Subjected to Seismic Events

Serious damage to a pipeline due to excessive strains can occur as the result of large seismic ground movements such as faulting, liquefaction, lateral spreading, landslides, and slope failure (Yeh and Lai, 1992; Yeh, 1988). Faulting is defined by ASCE's Committee on Gas and Liquid Fuel Lifelines (ASCE, 1984) as the relative displacement of adjacent parts of the earth's crust as shown in Figure 2.2. The fault can move horizontally, vertically, or a combination of the two. During an earthquake, this displacement occurs suddenly but it can also occur gradually over a period of time due to tectonic activity. Landslides are mass movements of the earths crust which can be triggered by seismic vibrations. Landslides include rockfalls, slumps and shallow slides, and deep translation and rotational movement some of which were depicted previously in Figure 2.1. Slumps and shallow slides are caused primarily by inertial forces but densification of loose soil or liquefaction of an underlying layer may assist in the creation of such a failure. Sudden deep-seated translation and rotational movement usually affects large areas and may involve significant displacement of the soil mass. These deep slides are often caused in part due to liquefaction of underlying sediments or sand lenses (ASCE, 1984). Ground failures associated with liquefaction can be classified as lateral spreading, flow failure, and loss of bearing capacity. Lateral spreading occurs as the result of the liquefaction of an underlying layer of soil as shown in Figure 2.3. Movements are typically on the order of several feet although displacements up to several tens of feet could occur. Lateral spreading generally occurs on slopes with inclinations

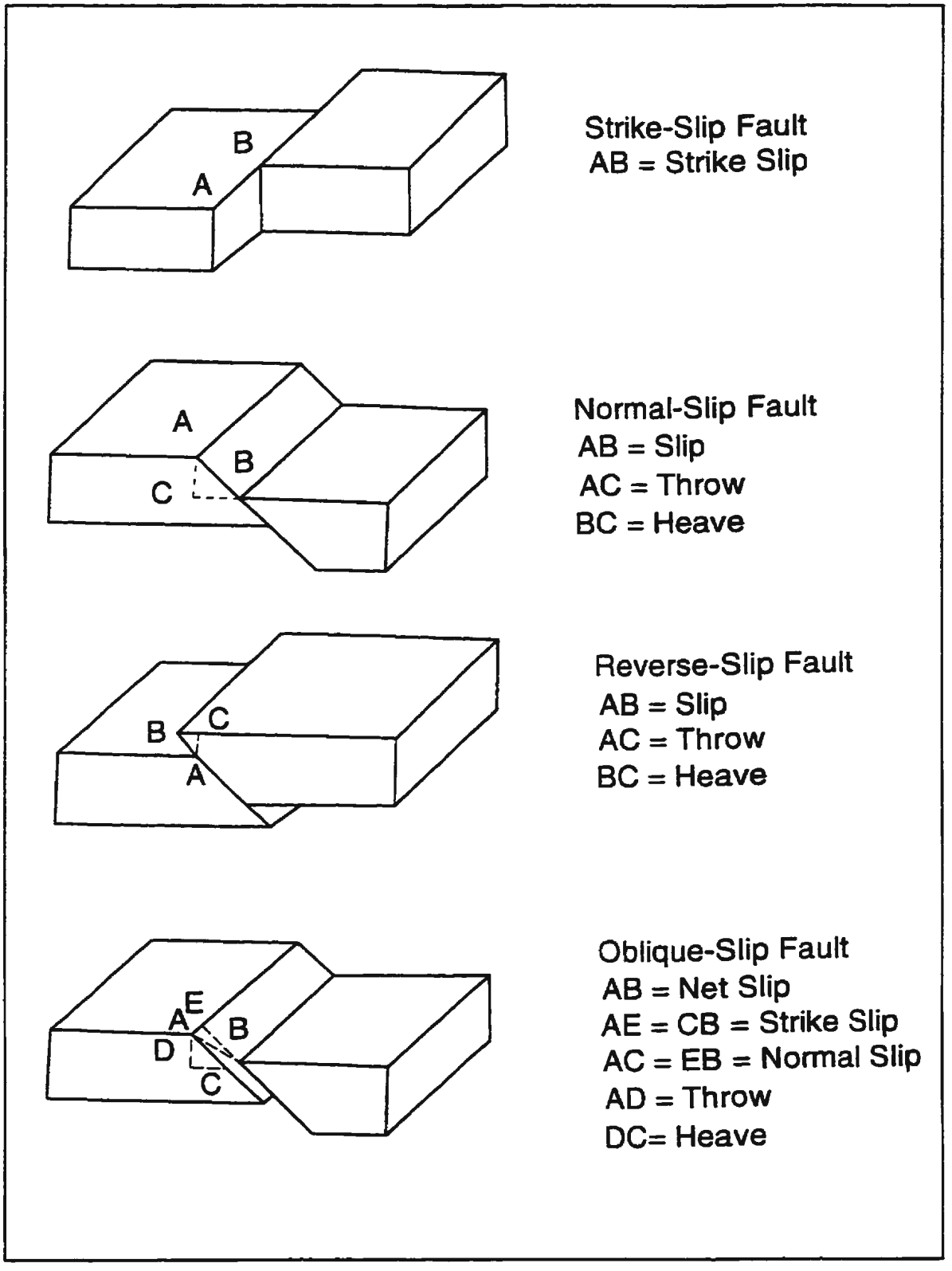

Figure 2.2 - Types of fault movements (after ASCE, 1984).

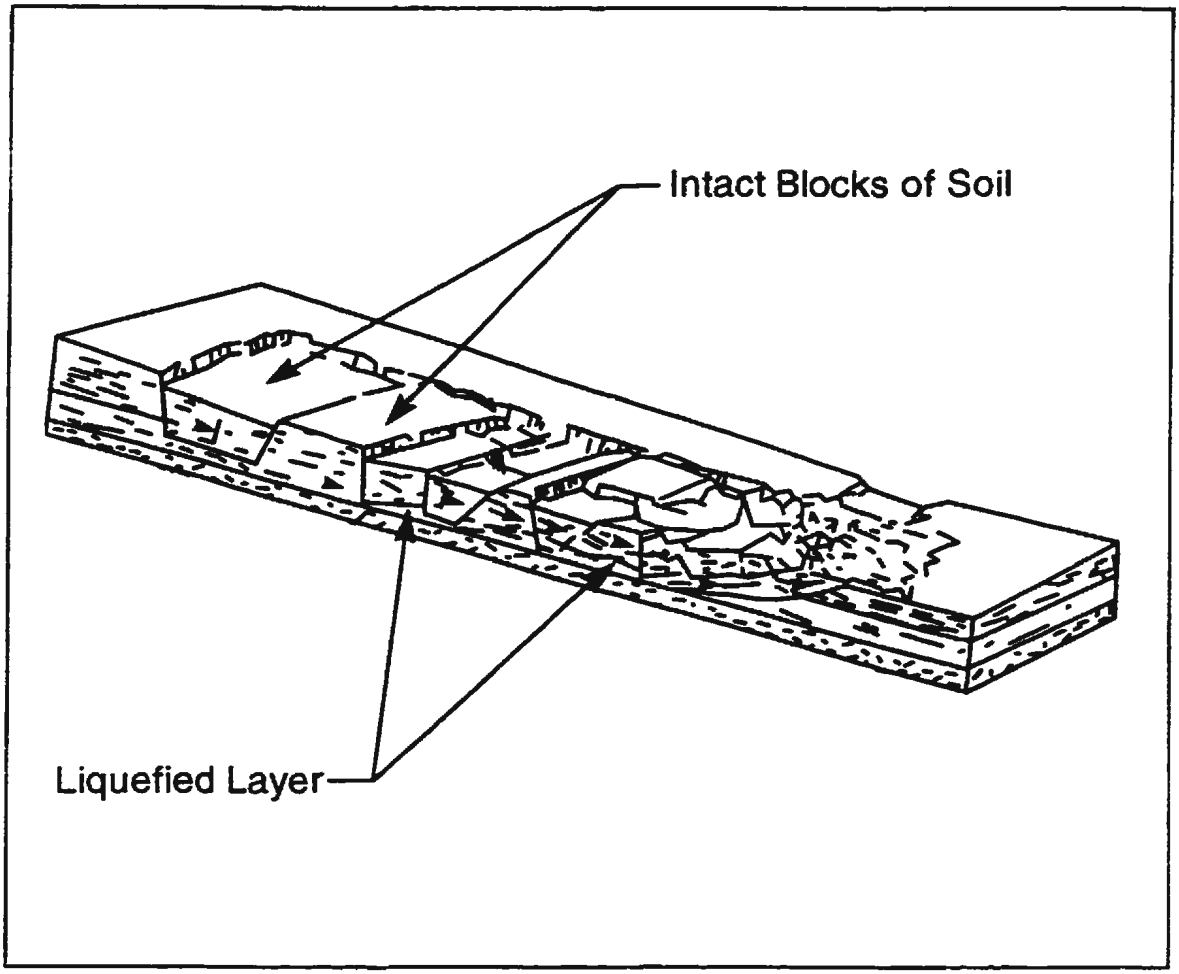

Figure 2.3 - Lateral spread ground failure (after O'Rourke and Lane, 1989).

ranging from 0.3 to 3 ° (O'Rourke and Lane, 1989). Lateral spreading is considered to be one of the most common mechanisms of ground deformation caused by liquefaction during an earthquake (O'Rourke and Lane, 1989). Flow failures or flow slides usually consist of completely liquefied soil which may contain intact blocks of earth transported within the liquefied mass. Flow slides usually occur in loose saturated sand deposits with slopes greater than 5 ° and many develop under water. Other liquefaction type failures include loss of bearing capacity and buoyancy effects.

Numerous pipeline failures have been attributed to seismic activity (ASCE, 1984). As mentioned previously, pipelines usually traverse large areas and it is likely in seismic areas that a pipeline will cross areas of potential faulting and liquefaction. Therefore, in the design of these pipelines, the potential for large ground displacements must be evaluated and designed for (O'Rourke and Lane, 1989). Faulting can load a pipeline if the fault is close to the buried pipeline. A strike-slip fault or oblique-slip fault could load the pipeline laterally or with lateral component (ASCE, 1984). Landslides could load a pipeline laterally or with a lateral component as competent material has the potential to move relatively large distances. Lateral spreading can be especially destructive to buried pipelines (ASCE, 1984) as they tend to involve the movement of surficial soils in a competent state carried along with the liquefied underlying soil. Horizontal displacements in a lateral spread are maximum at the centre of the slide and are generally distributed over its width (O'Rourke and Lane, 1989). Lateral spreads may be the most detrimental hazard for pipelines (O'Rourke and Lane, 1989). They occur relatively often and the locations of lateral spreads may be difficult to identify in advance as they can occur on relatively gentle slopes and involve the movement of competent blocks of soil; the full passive pressure soil resistance can be mobilised against a buried pipeline (O'Rourke and Lane, 1989). Flow failures may cause large amounts of soil to flow tens of metres at speeds up to tens of kilometres per hour (O'Rourke and Lane, 1989). These flow failures may subject the pipeline to viscous drag forces which may be as great or greater than forces associated with lateral spreading depending on the velocity of the flow. They are considered one of the worst geotechnical hazards for buried structures due to the catastrophic nature of the deformation and the fact that they often carry intact soil and

other objects in the debris (O'Rourke and Lane, 1989).

Lateral spreading was the most common and most disruptive liquefaction induced ground failure during the 1906 San Francisco earthquake. Extensive damage to bridges, roads, structures, and pipelines was reported (O'Rourke and Lane, 1989). Horizontal displacements of up to 7.6m were reported for pipelines; these were caused by lateral spreading. Due to damage to the water distribution network, fire fighting capabilities of the city were seriously reduced and over 500 city blocks were damaged or destroyed by fire (O'Rourke and Lane, 1989).

During the 1964 Anchorage earthquake, all utilities and communications were knocked out in the south-central portion of Alaska. Lateral spreading was considered to be responsible for some 200 breaks in the gas distribution system and severe damage to the water distribution (over 100 breaks) and sewer systems (O'Rourke and Lane, 1989).

Most damage during the 1971 San Fernando, California earthquake was caused by seismic induced landslides and lateral spreading. Lateral spreading was considered to be the main cause of the failure of gas transmission lines during the earthquake (ASCE, 1984) which resulted in several explosions (O'Rourke and Lane, 1989). Explosion craters 3-4 metres in diameter were formed by the sudden release of high pressure gas. O'Rourke and Tawfik (1983) reported that, in total, 11 transmission pipelines crossed areas of lateral spreading and liquefaction induced landslides. In general, the pipelines were buried in medium dense sand

and silty sand above the water table (O'Rourke and Tawfik, 1983). Other accounts suggested that there were over 2,400 breaks in water, natural gas, and sewer pipelines reported in the areas of fault displacement (McCaffrey and O'Rourke, 1983). The maximum horizontal displacement and width of lateral spreads were reported to be 1.75 and 340m respectively (O'Rourke and Lane, 1989). Pipeline displacements up to 0.7m were noted after the earthquake (O'Rourke and Lane, 1989). Some pipelines were repaired but other were extensively damaged and had to be abandoned. Gas pipelines which were 660 and 324mm in diameter and which were perpendicular to the flow were found to have failed while 1,370mm diameter water pipelines were only slightly damaged (O'Rourke and Lane, 1989). Damaged pipelines ranged in diameter from 170mm to 1,524mm buried with a depth of cover ranging from 1-2m (O'Rourke and Tawfik, 1983). As the result of critical pipeline failures in the natural gas distribution and transmission systems in the Los Angeles area, the distribution of natural gas to the San Fernando Valley was prevented (Eguchi and Taylor, 1988).

Extensive damage to gas, water and sewage pipelines was attributed to liquefaction caused by the 1983 Nihonkai-Chuba Earthquake in Japan. Horizontal displacements of soil greater than 5.0m were reported and most of the damage was done to the gas distribution network. 8,757m of the 60,000m of precast reinforced concrete sewage network were damaged. It was found after the earthquake that there was a high correlation between pipeline break locations and areas of lateral spreading (O'Rourke and Lane, 1989).

The Hyogoken-Nanbu or Kobe earthquake struck south-central Japan on Tuesday, January 17th, 1995. One account (Earthquake Engineering Research Center (EERC), 1995) suggests the earthquake caused 5,415 deaths and 34,500 injuries. Over 150,000 houses collapsed or were severely damaged, and over 7,000 houses were burned down in subsequent fires. Estimates of direct dollar losses are about US $150 billion. Extensive liquefaction of natural and artificial fill deposits caused extensive damage to port facilities and underground utilities.

It has been estimated that 1,800 water distribution pipeline failures occurred during the above-mentioned earthquake (Chung, 1996). It is speculated that much of this damage was associated with joint separation from liquefaction induced lateral spread. In general, geotechnical failures governed the poor performance of the water systems. Landslides, consolidation, and liquefaction or lateral spread stopped the flow of water from the source, damaged two major and one small water treatment plant, and tore the distribution system apart. With regards to the gas system, major trunk lines, pipelines, and distribution mains totalled 49,430km in Kobe at the time of the earthquake. There were 490km of transmission or major trunk lines in the system with a typical diameter of 600mm and a typical wall thickness of 12mm; no damage was reported to these lines. There were over 5,000km of medium pressure gas distribution lines at the time of the earthquake to which there were between 90 and 100 reported repairs but no observed leakage. However, no major damage was reported in these lines which had been subjected to large permanent ground deformation at several locations. The low pressure distribution system (43,895km) sustained the greatest

damage, the predominant type of which was failure at threaded or screw joints of steel piping and leakage and cracking at the joints of cast and ductile iron pipelines. There were no repairs in polyethylene piping which accounts for approximately 5% of the services. There were 5,190 repairs to distribution mains and branches within city streets, compared with 10,161 damaged service lines and 11,108 locations of damage where piping was attached to buildings.

2.1.3 Offshore Pipelines

Poulos (1988) defines environmental considerations on pipeline design as waves, currents, mudslides, fault movements, geotechnical properties and bathometry. The author points out that it is often difficult to avoid seabed instability problems and it is therefore necessary to determine potential extent and characteristics of hazards to which a pipeline may be subjected. Rawat (1978) suggests that additional investigations of subbottom deposits may be required to determine the possibilities of slides or liquefaction as the result of dynamic loading. The author also suggests that topographic features such as potentially unstable slopes and faults should be considered during pipeline route selection and recognised in design.

The potential instability of marine sediments is considered to be a major design concern for a variety of offshore structures in a variety of geographic locations. The integrity of offshore structures such as oil platforms, subbottom storage tanks, and pipelines is highly dependant on the stability of the seabed on which they are founded (Pamukcu *et al.*, 1983). Poulos

(1988) appreciates the potential for lateral loading of offshore structures due to the movement of submarine soil by the mechanisms described previously and the author suggests these loadings could be significant and may even produce forces which exceed those produced from a design storm. Liquefaction of the seabed may pose hazards to offshore structures such as pipelines, anchors, and platforms. Poulos (1988) also poses the question as to the magnitude of the forces developed against a structure, such as a pipeline, if the slide reaches the structure. If the slide contains debris, the results could be even more devastating.

Silva *et al.* (1989) state that one of the dominant processes causing offshore mass wasting is rotational slumping or translational slides. If the sliding surface or shear plane is concave, and the slipping sediment mass undergoes a backward rotation, the failure is generally termed a slump (Garrison and Bea, 1977). However, if the sliding surface, and therefore the movement of the sediment mass are roughly parallel to the bottom, the feature is generally called a slide (Garrison and Bea, 1977). Slumps are also considered to be blocks of soil which have undergone translation and or rotation along a fault but have experienced only minor internal deformations (Laine *et al.*, 1986). Mudslides are forms of seabed deformation which have undergone sufficient liquefaction to promote internal shear flow and deformation; the material in the slide behaves like a viscous fluid but may carry intact blocks of seabed.

Submarine slides can be initiated on very flat slopes. Most of the cases cited by Edgers and Karlsrud (1982) occurred on slopes less than 6 ° inclined to the horizontal and some have

even occurred on slopes as gentle as 1 °. Many submarine slides can runout 10's to 100's of kilometres and volumes of material up to 30km^3 can be involved. Velocities cited by the authors ranged from 0.8 m/sec. up to 20-30 m/sec. It is obvious that a pipeline could not be designed to withstand these high volume, high velocity slides, but if an existing or planned pipeline is in an area where a smaller amount of material might move or creep, then it might be designed to withstand the forces generated.

Silva *et al.* (1989) state that there is a significant amount of geological and geophysical evidence that deformations of submarine slopes occur due to creep. The authors state "By creep we mean very slow deformations of a surficial or buried sedimentary layer, that occur over many years under the driving forces of gravity". Silva *et al.* (1991) suggest that, based on geological evidence, creep deformations have occurred and may still be occurring on submarine slopes. Pratson and Laine (1989) also state that creep is considered as a down slope process (mass transport process) in this context.

Sangrey (1977) explains that an aspect of dynamic loading which is important in marine geotechnical engineering is rate of loading effects. The author states that slow rate of loading effects are caused by the creep of clay slopes which can lead to failure or large deformation of the soil mass. Sangrey (1977) also warns that marine geotechnical engineering problems offshore could involve stressing of structures such as pipelines as soil interacts with them during creep caused by self-weight (gravity) stresses. Experimental data collected by Templeton *et al.* (1985) in the Mississippi Canyon indicated seafloor movement rates ranging

from approximately 40 to 240mm per year.

API (1993) recommends that offshore pipeline designs should take into account forces caused by and resulting stresses from soil movement but they do not offer guidelines for the determination of the forces. Natural phenomena which the recommendations name are effects of earthquakes, hurricanes, cyclones, typhoons, and gross seafloor movements which may subject a pipeline to large lateral forces. API (1993) suggests that it may not be possible to quantify the effect of these phenomena but rather to reroute the pipeline around a potential seafloor movement zone. The recommendations also state that the seabed route should avoid potential mudslide areas.

Instabilities such as submarine landslides are a real hazard in coastal areas of the British Columbia offshore. Some have already occurred and such events will continue to occur (Pelletier, 1979). The west coast has a seismic regime which is unparalleled in any other Canadian waters. Seismic shocks could trigger submarine landslides and seismic activity is also associated with faulting. On the east coast of Canada tectonic factors include faults and earthquakes; the latter could initiate slumping, submarine landslides, or turbidity currents (Pelletier, 1979).

In the U.K. sector of the North Sea, Adams (1991) defines a pipeline "incident" as "an occurrence which directly results or threatens to result in loss of containment of a pipeline". Adams (1991) also reports that there has been 145 pipeline incidents over the years. Of these,

94 have involved steel pipelines, 12 have involved flexible pipelines, and 39 have involved pipeline fittings such as flanges, connectors, and valves. Of the 94 steel pipeline incidents, 8 incidents were the result of natural hazards such as mudslides.

In the Mississippi Delta offshore, large volumes of soils are transported over large distances by storm-wave induced submarine slope failures. Over 27 years, increases and decreases in seabottom elevation have been observed to have occurred (Bea and Bernard, 1973). Unconsolidated mud accumulations, rapidly deposited during high river flows, move down slope in mass movements when disturbed by storm waves. Pipelines and structures in the path of such movements can be moved or otherwise exposed to severe stresses which may cause failure (National Research Council, 1994).

Reifel (1979) conducted a review of literature up until 1978 to obtain information relating to storm related damage of pipelines in the Gulf of Mexico. The author concluded that there are several instances where slides or slumps initiated by severe storms have caused significant pipeline damage. The review findings of Reifel (1979) on pipeline damage are summarized in Table 2.1.

Mandke (1995) presented pipeline failure data from Hurricane Andrew at an international workshop on damage to underwater pipelines. Hurricane Andrew passed through the Gulf of Mexico on August 25, 1992. Severe storm winds gusting to 160 miles per hour and significant wave heights estimated to be at 35-40 feet interacted with close to 2,000 oil and

Table 2.1 - Selected review findings of Reifel (1979)

Event	Comments
Hurricane Carla, 1961	Mudslides and slumping damaged 30 flowlines in water depths greater than 30 feet.
Hurricane Camille, 1969	An 8 inch pipeline was severed by a mudslide in 300 feet of water.
Hurricane Carmen, 1974	A mudslide severed 3.5-12.75 inch pipelines, risers, and flowlines in water depths ranging from 40-138 feet. The pipelines were buried with 10 inches of soil cover.
Storm, 1/5/75	A mudslide damaged a 12.75 inch unburied pipeline in 55 feet of water.
Storm, 3/20/75	A 12.75 inch unburied pipeline was damaged as a result of a mudslide in 55 feet of water.
Hurricane Eloise, 1975	A mudslide damaged a 8.5 inch buried pipeline with 3 feet of soil cover. The water depth was 217 feet. 400 feet of pipeline and riser had to be replaced.
Storm, 3/28/77	A 12.75 inch pipeline was damaged due to a mudslide which resulted in a spill of 250 barrels of oil. The pipeline had been buried with 3 feet of cover. As a result, 3,000 feet of damaged pipeline were replaced.

gas production facilities. Over 480 pipeline and flowline segments were damaged. Mandke (1995) reports that the principal causes of pipeline failure were: material failures, equipment failures, operational errors, corrosion or erosion, natural hazards such as storms and mudslides, and third party damage due to anchors, jack-up rigs, supply boats, trawling, etc. A total of 485 pipeline incidents were reported, of which 10 failures were the result of due to mudslides. Of the pipe damaged in the mudslides, sizes ranged from 6 to 18 inches in diameter and two of the more serious incidents required replacement of 1,000 and 2,630 feet of pipeline segment.

2.2 Analysis and Design of Laterally Loaded Pipelines

2.2.1 Onshore Pipelines

A review of the development of lateral pipeline/soil interaction formulations leading to the current state-of practice was prepared by Rizkalla *et al.* (1992). They present early efforts to estimate the ultimate load transferred to a laterally loaded pipeline using the classic geotechnical passive earth pressure solution (i.e. Terzaghi and Peck, 1967) or the Meyerhof solution (Meyerhof, 1953) for a horizontally loaded strip footing. The authors go on to state that the former approach was dismissed because of the methods insensitivity to burial depth; this tended to lead to overestimates in design. The latter approach was not developed further. Later solutions were based on the research of Mackenzie (1955) which was based on anchor plate/soil interaction and the works of Hansen (1948 and 1961) which were based on piles subjected to lateral earth movements. Rizkalla *et al.* (1992) suggest that it is reasonable to define the current state-of-practice formulations most often used in routine design to include both the works of Rowe and Davis (1982a) based on the elasto-plastic finite element analyses of vertically oriented smooth anchors and the Committee on Gas and Liquid Fuel Lifelines' (ASCE, 1984) recommendations based on Hansen's (1961) work on laterally loaded piles.

In the 1970's, the Trans-Alaska Pipeline was constructed to transport crude oil from Prudhoe Bay to Valdez. The pipeline is 1,285 kilometres long and has a diameter of 48 inches with wall thicknesses of 0.462 and 0.562 inches. The buried portion (less than half) of the pipeline has 3 feet or more of soil cover (Luscher *et al.*, 1979). The authors state that large axial compressive forces could develop in a pipeline which is constructed during cold weather and

later operated at higher temperatures. To prevent compression buckling in straight-line portions of the pipeline and to prevent excessive displacements (which could lead to excessive stress and strain) in bends, the designer must ensure the soil offers adequate resistance to pipeline movement.

The finite element program PIPLIN was used in the design of the Trans-Alaska Pipeline to assess the pipeline/soil interaction (Luscher *et al.*, 1979). A limit of 15cm was assigned to lateral horizontal pipeline movement and the soil resistance was modelled using elastic-perfectly-plastic soil springs. Luscher *et al.* (1979) suggest the lateral pipeline force is resisted by the passive resistance of the soil as shown in Figure 2.4 and is analogous to a buried deadman anchor undergoing horizontal displacement. The authors also suggest the controlling variables to the lateral resistance are the shear strength parameters for the soil and the depth of cover.

For granular soils, the authors calculated the lateral resistance based on the Rankine passive earth pressure reduced by a factor, A (Figure 2.5), as suggested by Ovesen and Stromann (1972) to account for the pipe height being less than the total height of the trench. The ultimate lateral resistance is therefore calculated from

$$P_{ult} = \frac{1}{2} \gamma' H^2 K_p A \qquad [2\text{-}1]$$

where the coefficient of passive earth pressure, K_p, is calculated from

$$K_p = \tan^2 (45 + \phi/2). \qquad [2\text{-}2]$$

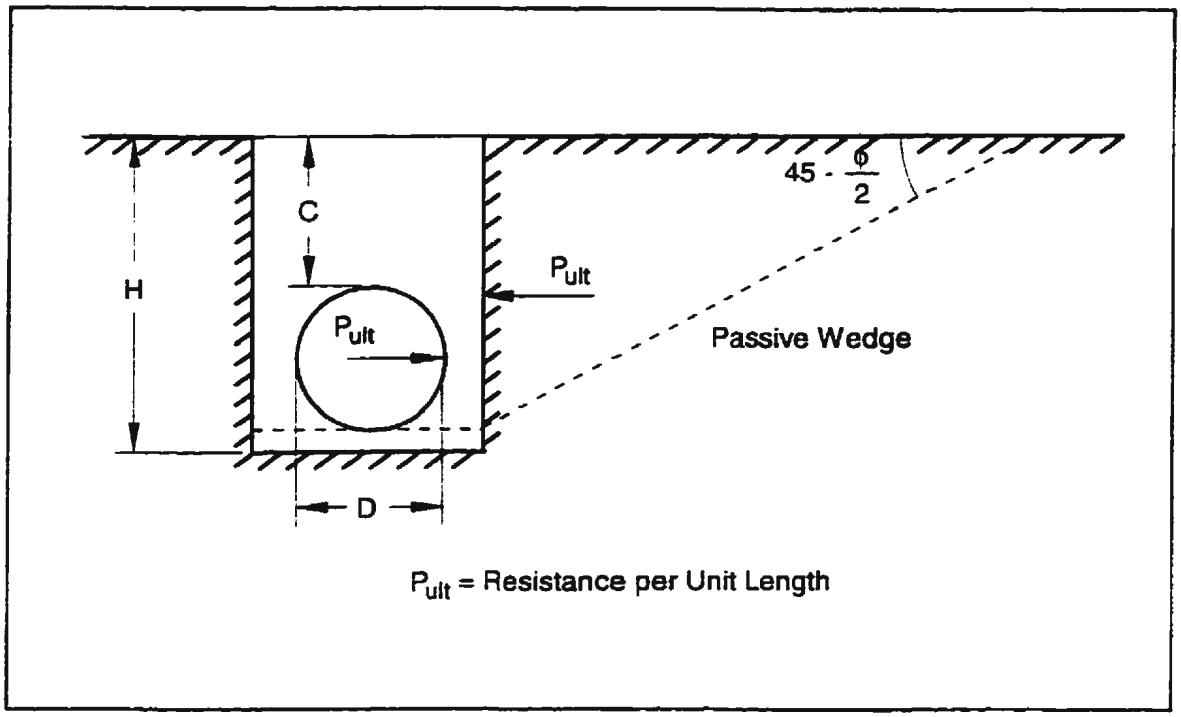

Figure 2.4 - Sidebend resistance model (after Luscher et al., 1979).

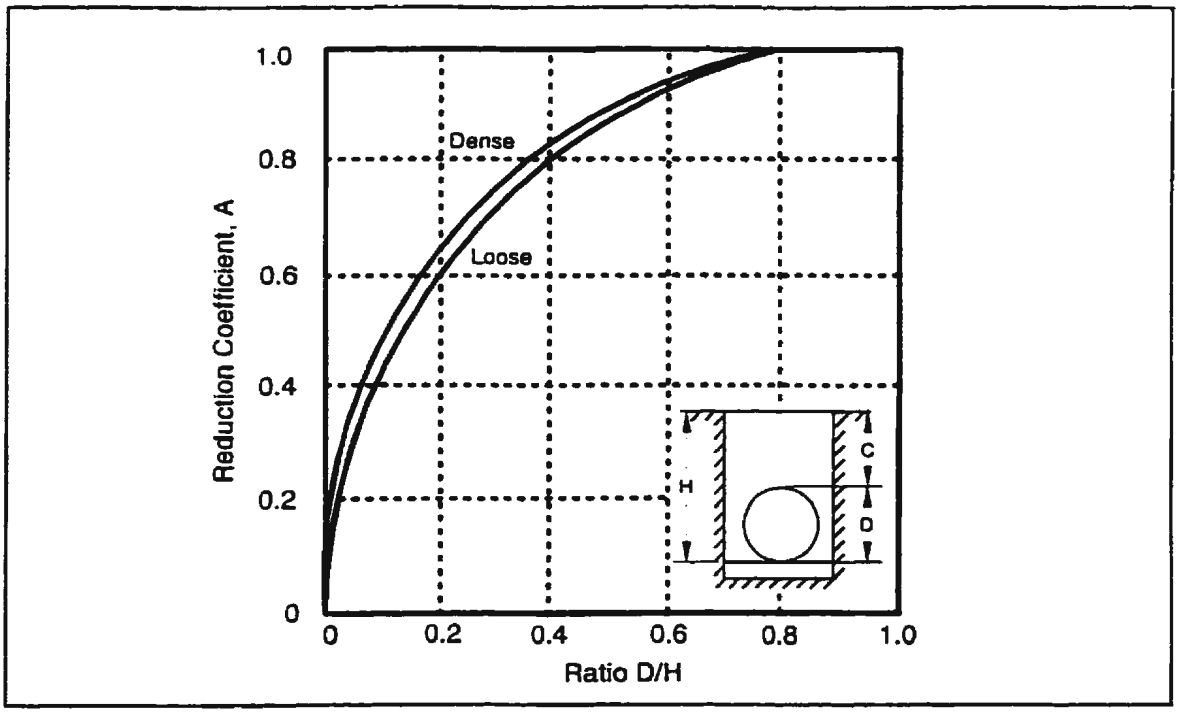

Figure 2.5 - Lateral resistance coefficient (after Luscher et al., 1979).

In these equations, P_{ult} is the ultimate lateral soil resistance per unit length, γ' is the effective unit weight of the soil, H is the depth of the trench, and ϕ is the internal angle of friction of the soil. For cohesive fine-grained soils, the authors suggest the ultimate resistance to pipeline movement can be expressed by

$$P_{ult} = N_c \, c_u \, D \qquad [2\text{-}3]$$

where c_u is the undrained shear strength, D is the pipeline diameter, and N_c is the lateral resistance coefficient based on the works of Mackenzie (1955) on deadman anchorages. The variation of N_c with embedment ratio is presented later in Figure 2.14.

In the 1980's, the ASCE Technical Council on Lifeline Earthquake Engineering formed the Committee on Gas and Liquid Fuel Lifelines to study the effect of seismic activity on lifelines. The resulting document (ASCE, 1984) was intended to provide guidance for the seismic design of most major components of pipeline systems. The transverse horizontal (lateral) soil loading theory presented in the document is inferred from footing and vertical anchor plate pull out capacity theory and laboratory tests on model pipelines simulating horizontal pipeline movements by particularly Audibert and Nyman (1977) and Trautmann and O'Rourke (1983).

The guideline presents, for sand, a hyperbolic p-y curve of the form

$$p = \frac{y}{A' + B'y} \qquad [2\text{-}4]$$

where

$$A' = 0.15 Y_{ult} / P_{ult} \qquad [2\text{-}5]$$

and

$$B' = 0.85 / P_{ult}. \qquad [2\text{-}6]$$

It is suggested the ultimate lateral soil load on the pipeline, P_{ult}, and the displacement to ultimate load, Y_{ult}, be calculated from

$$P_{ult} = \gamma' \, h \, N_{\gamma} \, D \qquad [2\text{-}7]$$

and

$$Y_{ult} = 0.07 \text{ to } 0.10 \, H \qquad [2\text{-}8]$$

for loose sand;

$$Y_{ult} = 0.03 \text{ to } 0.05 \, H \qquad [2\text{-}9]$$

for medium sand; and

$$Y_{ult} = 0.02 \text{ to } 0.03 \, H \qquad [2\text{-}10]$$

for dense sand where h is the depth to the pipe springline and H is the depth to the base of the pipeline. The guidelines suggest two models can be used to obtain the horizontal bearing capacity factor, N_{γ}. The first is based on the work of Audibert and Nyman (1977), which is discussed in Section 2.3, who adapted Hansens (1961) model for vertical piles subjected to lateral loading and found good agreement with experimental results. The adapted curves to determine N_{γ} are presented in Figure 2.6. The second model is based on the work of Trautmann and O'Rourke (1983), which is discussed in Section 2.3, who found good agreement between theory for vertical plate anchors subjected to horizontal loading (Ovesen and Stromann, 1972) and experimental results. Design curves were developed for the horizontal bearing capacity factor as presented in Figure 2.11 of the next section. The guideline (ASCE, 1984) cautions that horizontal bearing capacity factors based on the model

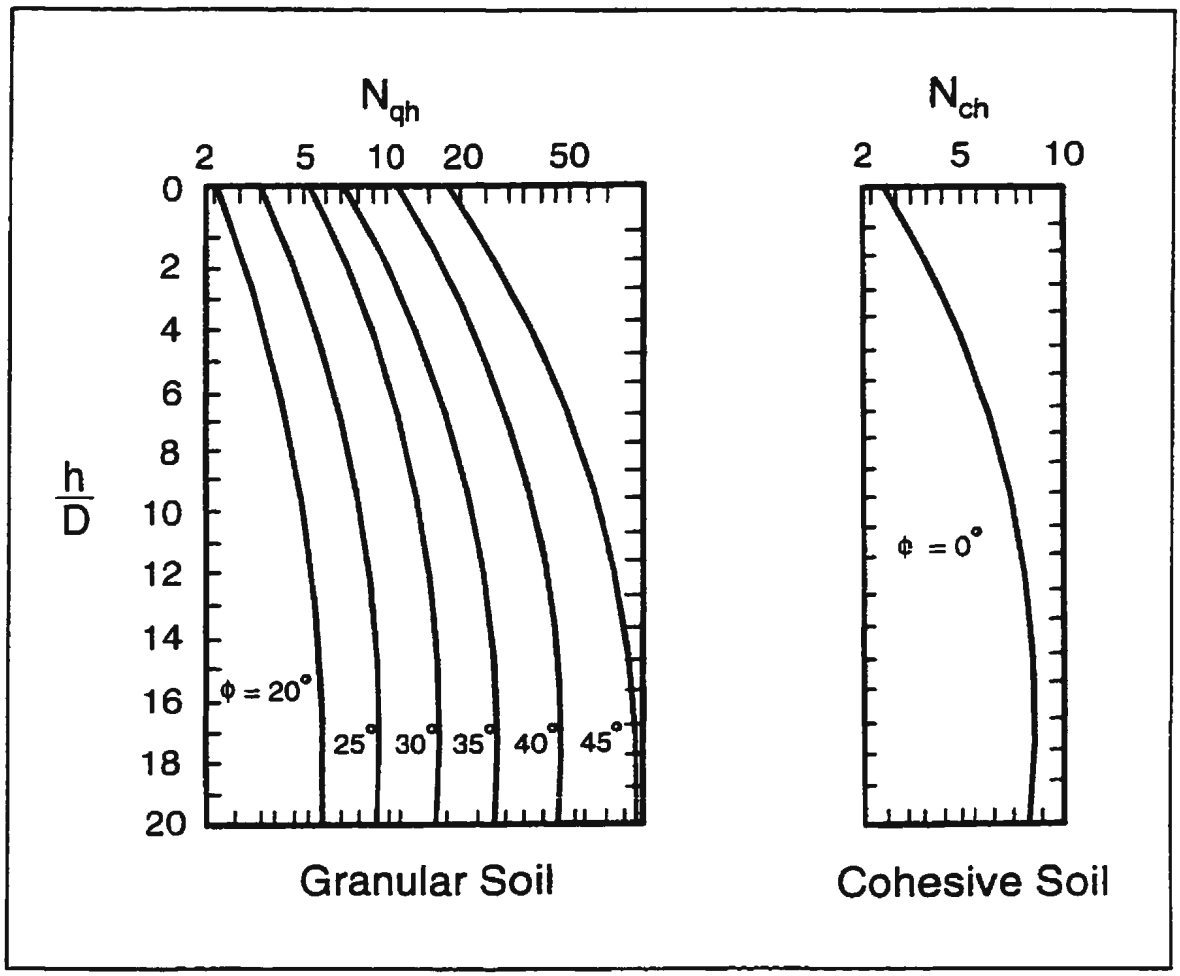

Figure 2.6 - Horizontal bearing capacity factors as a function of depth to diameter ratio for pipelines (after ASCE, 1984).

of Hansen (1961) are 50 to 100% larger than those of the Ovesen and Stromann (1972) based model for similar burial geometry and soil properties.

For clays, the guidelines (ASCE, 1984) suggest a modified Hansen (1961) model for cohesive soils can be used. The expression for the maximum horizontal pipeline force, P_{ult}, is given by

$$P_{ult} = c_u N_c D \qquad [2\text{-}11]$$

where N_c is the horizontal bearing capacity factor for vertical strip footings which are horizontally loaded. This factor is also presented in Figure 2.6 as a function of h/D. The guidelines also suggest the p-y relationship for cohesive soils is similar to Equation [2.4], with Y_{ult} occurring at approximately 3 to 5% of H.

Selvadurai (1985) suggests that due to complexities and uncertainties associated with modelling soil response, often the soil mass surrounding the pipeline can be idealized as an elastic region. The author states that such a model can be used for a first approximation of the analysis of complex soil interaction problems. However, it is apparent that, as the soil does not behave as an elastic material at moderate displacements, such an analysis will be of limited application.

Rizkalla and McIntyre (1991) acknowledge that in the design of buried pipelines, consideration must be given to landslide ground movements in the immediate vicinity of a buried pipeline. To determine local slope failure mechanisms and extent may require several years of geotechnical monitoring and thus a design incorporating slope stabilization or avoidance may not be feasible. It may be therefore required to design accepting the fact that slope movement would induce loads on a pipeline and to operate on a "monitor and excavate" philosophy. However, the authors admit that it is unlikely that a pipeline could withstand a sudden, catastrophic ground movement greater than 2m. In design, the authors suggest that ground movement induced loads can be estimated using the recommendations of the ASCE Committee on Gas and Liquid Fuel Lifelines (ASCE, 1984) using interaction

rates of 10mm per year for creep-like ground displacements or 25mm per year for more pronounced slope movement (in the absence of measured rates of ground movement). The authors also suggest that subsurface ground movement and periodic pipeline deformation surveys be coupled with finite element analysis to monitor the subsequent integrity of the pipeline system.

Novacorp (1992) conducted a stress analysis of the pipeline system described by Wong (1992). The analysis was conducted with the nonlinear finite element program PIPLIN-PC which models the pipeline as a series of beam elements coupled to the soil via a series of interaction parameters or soil springs. The interaction parameters were chosen based on the recommendations of the Committee on Gas and Liquid Fuel Lifelines (ASCE, 1984). Results of the analysis indicated that strain relief operations would need to be conducted approximately every two years based on maximum slope movements of 20 mm/year. Recommended remedial measures included excavating within 100m of the excessive slope movement along the axis of the pipeline and attempting to uncouple the pipeline from the native soil through the use of a light weight aggregate as backfill.

Rizkalla *et al.* (1992) state that a simple engineering analysis of the lateral pipeline/soil interaction problem can be reduced to the following expression:

$$P_{ult} = D\ c_u\ N_c \qquad [2\text{-}12]$$

where P_{ult} is the ultimate (per unit length) load transferred to the pipe. The authors imply that the interaction factor used in Equation [2-12] can be based either on the work of Rowe and

Davis (1982a) or the recommendations of the Committee on Gas and Liquid Fuel Lifelines (ASCE. 1984).

The authors (Rizkalla *et al.*, 1992) conclude that much of the work related to the formulation of spring-slider pipeline/soil interaction models has been adapted from other branches of geotechnical engineering. Most attention has been focused on predicting the ultimate resistance to pipeline movements. The experimental work that does exist to verify the predictive capability of spring-slider models is largely laboratory based, uses idealized soils, and does not adequately address the influence of construction-related factors on pipeline/soil interaction.

Onshore regulatory codes published by the CSA (CSA, 1994) do not offer any guidance on how to design for slope movements. Under "Other Loading and Dynamic Effects", the Standard explains that additional loadings other than the specified operating loads are not specifically addressed in the document. However, the standard dictates that the designer must determine whether supplemental design criteria are necessary for additional loadings including slope movements, fault movements, and seismic-related earth movements.

Rajani *et al.* (1993) proposed an approximate 3-D analytical design solution for pipelines subject to transverse soil movements and which accounted for embedment and breakaway conditions behind the pipeline. The authors developed non-dimensional load-displacement and moment-displacement relationships and presented these in the form of charts. The

authors claim that these charts permit hand calculations for rapid verification of structural design of pipelines subjected to transverse landslide soil movements. The soil is assumed to be an elastic, perfectly-plastic, isotropic, homogeneous medium whereas the pipe is assumed to be a linear elastic beam. The ultimate soil resistance developed due to the lateral movement of the pipeline is evaluated based on the numerical solutions developed by Rowe and Davis (1982a) for anchor plates in cohesive soil.

Although the curves presented by the authors have been developed in terms of undrained shear strength (c_u), Ranjani *et al.* (1993) suggest that it is possible to apply the method using drained strength parameters. The ultimate soil resistance (P_{ult}) for a frictional soil can be converted to an equivalent undrained strength. The ultimate soil resistance for a frictional soil under drained conditions and for a cohesive soil under undrained conditions respectively are determined from the following two equations:

$$P_{ult} = 0.5\ \gamma\ K_p\ (H^2 - C^2) \qquad [2\text{-}13]$$

and

$$P_{ult} = N_c\ D\ c_u \qquad [2\text{-}14]$$

where C is the depth of soil cover to the top of the pipe and N_c is the Rowe and Davis (1982a) lateral interaction factor.

Rajani *et al.* (1993) state that an equivalent undrained shear strength can be evaluated for any drained soil parameters by equating the above two expressions. However, the authors suggest that for many soil conditions, the undrained rapid response will generally produce the highest

resistance and will therefore be the most conservative. The authors also suggest that, in general, the backfill material will have a lower strength than the surrounding ground and therefore for preliminary design it would be appropriate to apply the shear strength of the natural ground to the analysis as this will result in higher calculated stresses in the pipeline which would be the case if the pipeline began to interact with the trench wall.

2.2.2 Offshore Pipelines

Audibert *et al.* (1978) state that it is the responsibility of the pipeline engineer to design pipelines to remain stable and to provide ten to forty years of safe operation while exposed to such possible loading conditions as mudslides, seismic action, and hydrodynamic forces. The authors suggest that pipeline/soil interaction has been characterized by coefficients of subgrade reaction and, for the sake of mathematical convenience, these coefficients were considered to be constant. However, the use of simple linear elastic relationships (constant coefficient of subgrade reaction) does not allow for a limit restraint or ultimate load to be reached and generally leads to overly conservative results (too high stresses predicted in the pipelines). The authors stress that the load-deformation relationships (p-y curves) for the springs thus cannot be linear elastic but must represent the nonlinear, stress-dependent behaviour of soils.

Audibert *et al.* (1980) acknowledge that subsea pipelines must be designed to resist potential seabed instabilities. The authors suggest p-y curves can be developed based on the hyperbolic relationship presented by Audibert and Nyman (1977) which is outlined in Section 2.3.

Ultimate resistances are calculated using recommendations of the Committee on Gas and Liquid Fuel Lifelines (ASCE, 1984) adapted from Hansen's (1961) theory. The displacement to ultimate load, Y_{ult}, can be calculated from

$$Y_{ult} = 0.02H \qquad [2\text{-}15]$$

for loose sand and

$$Y_{ult} = 0.015H \qquad [2\text{-}16]$$

for dense sand. The authors (Audibert *et al.*, 1980) recommend a Y_{ult} value of about 3 to 5% of H for clays. Alternatively, Bea and Audibert (1980) suggest, for clays, the displacement to ultimate load can be calculated from

$$Y_{ult} = 0.04 \text{ to } 0.06 \ H. \qquad [2\text{-}17]$$

The forces on an object in the path of an oncoming slide are dependant on the thickness and velocity of the slide (Edgers and Karlsrud, 1982). Two methods are suggested by the authors and are based upon the ultimate capacity of laterally loaded piles (if the flow is considered to be a deformable continuum) and on drag forces during flow around submerged structures (if the flow is considered to be a fluid).

For the analogy to laterally loaded piles, the authors present the general equation for soft soil as

$$P_{ult} = N_c \ c_u \ D \qquad [2\text{-}18]$$

where D is the projected width of the foundation and N_c is a bearing capacity coefficient, generally empirically determined.

Based on the work of Stevens and Audibert (1979) and Bea *et al.* (1980), the authors present estimated values of N_c ranging from 4 at the mudline to a value of 12 at a depth equivalent to 4 pile diameters. The authors conclude that the data base for N_c is limited and there is "virtually no information available on the effects of structure shape, size, and neighbouring member interactions". Bea and Arnold (1973) suggest for isolated cylindrical members located at a depth sufficient to be free of soil surface effects, N_c falls in the range of 8 to 12 while at the soil surface, N_c falls in the range of 2 to 5. A study of N_c factor data by Bea *et al.* (1975) led the authors to recommend an N_c value of 10 at depth below the soil surface and 3 at the soil surface.

Edgers and Karlsrud (1982) also suggest that the forces exerted on a structure may be estimated by the examination of the hydrodynamic drag on a submerged object. The general equation is

$$F_D = \frac{1}{2} C_D \rho A v^2 \qquad [2\text{-}19]$$

where F_D is the drag force, C_D is the drag coefficient, ρ is the density of the flow, A is the projected cross-sectional area of the structure, and v is the velocity of the flow. Similar analyses have been considered in the analysis of mudslide forces on pipelines (i.e. Bea and Aurora, 1982; Norem, 1993).

Poulos (1988) suggests that the principles used in the analysis of offshore pipeline/soil interaction are identical to the principles used for analysing pile/soil interaction. The pipeline is modelled as a simple structural member which is connected to the soil mass via a series

of springs. The author also suggests that the lateral soil spring characteristics can be based on the works of Audibert and Nyman (1977), Bea and Aurora (1982), and Wantland *et al.* (1979).

As with the onshore codes, offshore regulatory codes and standards, such as that published by the CSA (CSA, 1994), appear to offer little guidance to assist in the quantification of pipeline loading resulting from soil movement. API Recommended Practice 1111 (API, 1993) states that specific geographic locations are subject to natural phenomena that can expose an offshore pipeline to unusual forces; gross sea bottom movement may subject a pipeline to large lateral forces. The Practice states that the design of offshore pipelines should consider these dynamic forces particularly with regard to the stability of the pipeline and the resulting stresses; however, the Practice does not offer guidance on how to quantify these forces. ASME (1995) in their Code for gas transmission and distribution piping systems state that there are a number of physical parameters or design conditions which govern design of an offshore pipeline system so that it meets installation, operation, and other post-installation requirements. These factors include marine soils and seismic activity. The Code states the design environmental loads which should be considered include those arising due to dynamic soil related loadings such as those resulting from mudslides and soil liquefaction. But again, this practice makes no recommendation on how to quantify such loadings.

2.3 Previous Research Into Lateral Pipeline/Soil Interaction

2.3.1 Conventional Research

A number of analytical and experimental studies have focused on pipeline/soil interaction in the longitudinal (e.g. Hmadi and O'Rourke, 1988), lateral (e.g. Audibert and Nyman, 1977), and vertical directions (e.g. Trautmann *et al.*, 1985). Studies have also focused on the loading of pipelines due to static or surcharge loading from embankments or vehicles (e.g. O'Rourke and Ahmed, 1985) and the effect of trenching on adjacent pipelines (e.g. Kyrou and Kalteziotis, 1985). This section will focus only on studies where research was conducted into lateral pipeline/soil interaction.

The soil resistance against horizontal movement of a buried pipeline or conduit is generally called the coefficient of horizontal subgrade reaction, k_h (Audibert and Nyman, 1977). This coefficient is not a unique soil parameter but rather varies with contact pressure, the geometry of the interface, the type of soil, and the density of the soil. Audibert and Nyman (1977) conducted a literature review and found that there was limited information available on analytical methods to determine values of k_h for buried conduit or culverts and that methods for obtaining the coefficient are poorly understood and inaccurate. The authors point out that k_h will vary continuously along any nonlinear force-displacement curve and thus recommend that appropriate p-y or force-displacement curves be developed for the pipeline under consideration. The authors also state that numerical formulations proposed in the literature are inadequate for the safe design of conduits subjected to lateral soil movement.

An experimental program was conducted by the authors to determine p-y curves for a buried pipeline in sand, to reveal failure mechanisms, and to investigate the influence of such parameters as pipeline diameter, embedment ratio and soil density. The tests were conducted in a testing box which was filled with air-dried medium Carver sand. This sand has a uniformity coefficient of 2.7 and the grain size varies primarily between 3 and 0.2mm. The sand was spread in 25mm layers using a slumping technique to achieve a loose condition and dynamic compaction to achieve a dense sample. Three model pipeline test sections were used which had diameters of 25mm, 60mm, and 111mm. Cover ratios (depth of cover / pipe diameter) investigated were: 1, 3, 6, 12, and 24; 1, 3, and 6; 1 and 2 respectively for each of the model pipeline diameters. The ends of the pipelines were connected to a hydraulic ram outside the test box via cables which passed through the walls of the test box. Pipeline force and displacement readings were continuously monitored.

Failure mechanisms were observed through a plexiglass wall on one of the sides of the testing box. Typical failure mechanisms for shallow to intermediate and deep burial are presented in Figure 2.7. The authors note for shallow to intermediate burial that a front passive wedge bounded by a logarithmic spiral failure surface formed in front of the model pipeline. For deep burial conditions, a confined zone of soil flow was observed to extend 1 diameter in front of the pipeline for dense sand and 2 to 3 pipeline diameters for loose sand. The authors normalized their data with respect to the maximum soil pressure, P_{ult}, and a displacement to maximum soil pressure, Y_{ult}, as

$$\bar{p} = \frac{p}{P_{ult}} \qquad [2\text{-}20]$$

for $p \leq P_{ult}$ and

$$\bar{y} = \frac{y}{Y_{ult}} \qquad [2\text{-}21]$$

for $y \leq Y_{ult}$ and found that the trend of the normalized curves could be described by

$$\bar{p} = \frac{\bar{y}}{0.145 + 0.855\bar{y}} \cdot \qquad [2\text{-}22]$$

A rearrangement of the above equations by the authors led to their recommended formulae for the analytical prediction of p-y curves

$$p = \frac{y}{A' + B'y} \qquad [2\text{-}23]$$

with

$$A' = \frac{0.145\ Y_{ult}}{q_{ult}} \qquad [2\text{-}24]$$

and

$$B' = \frac{0.855}{q_{ult}} \qquad [2\text{-}25]$$

and where q_{ult} is the predicted ultimate lateral pressure acting on the pipeline.

The authors compared the experimental ultimate lateral pressure (P_{ult}) results with those predicted by Hansen's (1961) method (q_{ult}), found good agreement, and recommended that this method be used to estimate the ultimate lateral pressure in the above equation. A value for Y_{ult} equivalent to 1.5 to 2% of the depth of embedment was also recommended. The authors also present suggestions for the bilinear representation of the hyperbolic p-y curve. Nyman (1984) incorporated the work of Audibert and Nyman (1977) with the work of Vesic (1971) and Meyerhof (1973) to evaluate soil response against the oblique motion of pipes.

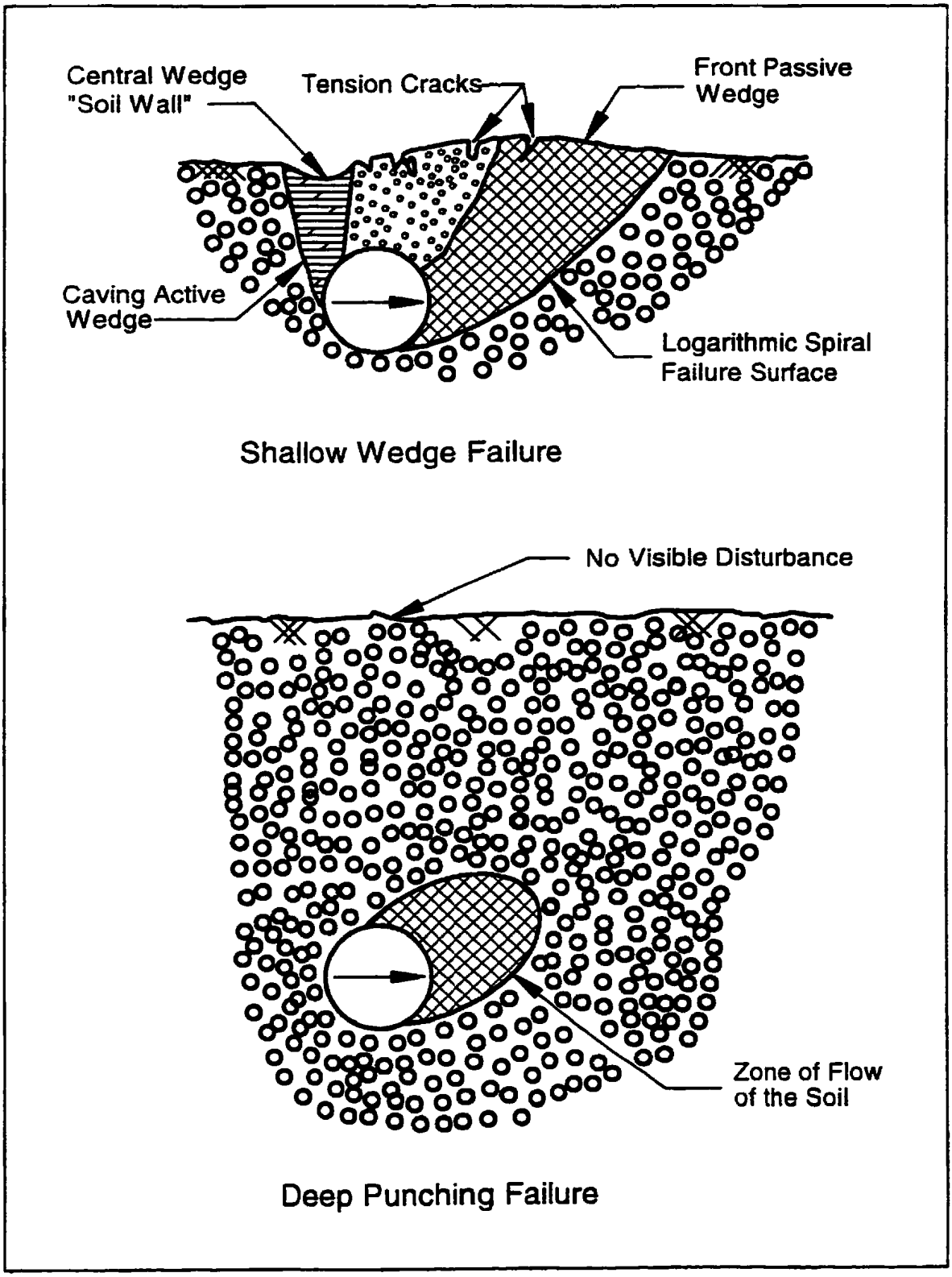

Figure 2.7 - Pipeline/soil interaction (after Bea, 1985).

Audibert and Nyman (1977) also conducted a field test to assess their proposed method of developing p-y curves. The test was conducted in a natural deposit of Carver sand with a unit weight of 16.8kN/m^3 and an estimated angle of friction of 35 °. The pipeline test section was 2.36m in length, had a diameter of 229mm, and the springline was located 80cm below the soil surface. The calculated ultimate load was found to be only 6% less than that measured while the calculated displacement to ultimate load approximately 10% lower than the experimental value. The authors found the p-y curve developed using the proposed method gave a reasonable approximation to the curve obtained from the field data.

Wantland *et al.* (1982) suggest that soil resistance to lateral pipeline movement is similar to the bearing capacity of a foundation although consideration must be given to the complexity of the geometry of the pipeline/soil interface and the proximity of the soil surface. The authors suggest that an upper bound plasticity mechanism for bearing capacity should be able to be applied to a laterally loaded pipeline as shown in Figure 2.8. Using the foundation analogy, the maximum lateral resistance to displacement would be $5.14c_uD$ at H=2D where c_u is the undrained cohesion, D is the pipeline diameter, and H is the depth of burial measured to the base of the pipeline. The author recognized that the actual maximum lateral resistance for a pipeline may be different from the value suggested by plasticity theory and a greater depth of embedment might be necessary to achieve this maximum value. The lateral resistance of the soil is expressed by the authors as

$$P_{ult} = N_c \, c_{u\text{-}avg} \, D \qquad [2\text{-}26]$$

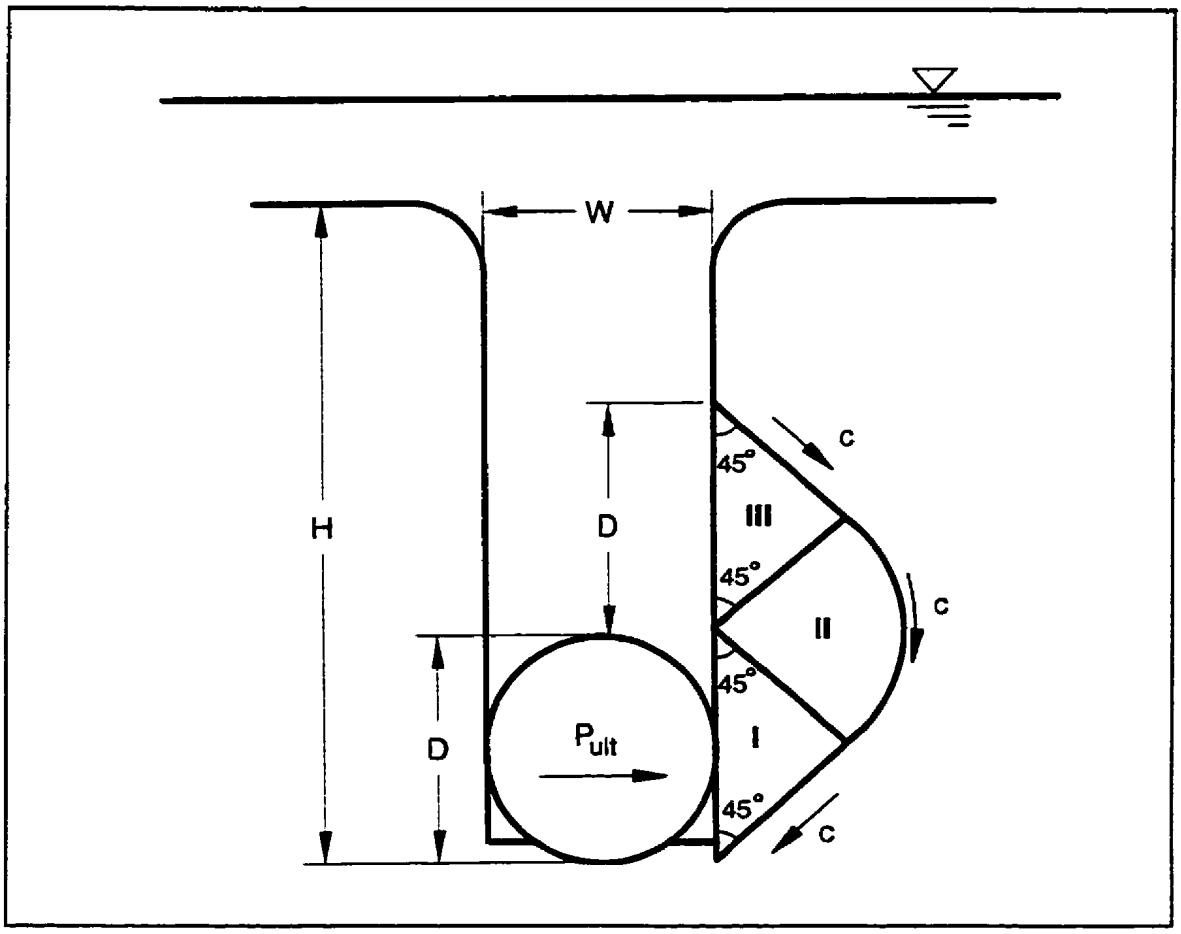

Figure 2.8 - Assumed flow pattern for pipe embedded in open trench (after Wantland et al., 1979).

where N_c is a lateral bearing capacity factor dependant primarily on H/D, pipe shape, and unit weight of the soil, and $c_{u\text{-}avg}$ is the average cohesion for a distance 2D above the pipeline invert. If H is less than D, Equation [2-26] is modified to

$$P_{ult} = N_c \, c_{u\text{-}avg} \, H. \qquad [2\text{-}27]$$

Wantland *et al.* (1982) also conducted experimental studies to determine the effects of pipe weight, pipe diameter, embedment depth, loading rate, and type of soil on the resistance

developed during lateral displacement of a pipeline.

The first test series was conducted in an estuary in an underconsolidated highly plastic montmorillonitic clay with an undrained shear strength ranging from 1-2kPa with depth. The pipeline test sections were 2.875 and 4.50 inches in diameter and 20.5 feet in length. The pipelines were tested with different amounts of ballast to change the buoyant weight. During testing, the pipelines were placed on the bottom without trenching, allowed to settle under their own weight, and then winched laterally at 1 foot/min. for several feet. A continuous load displacement record was made during the pull.

The second test series was conducted in the laboratory using kaolin clay at the liquid limit to model an underconsolidated clay. Shear strengths were measured and found to be approximately 1.4-1.7kPa within the range of depths of interest. The pipeline test segments were 22.75 inches long with diameters of 1.5 and 3.0 inches. The pipelines were ballasted so that the pipeline specific gravities were constant from test to test and the ends of the pipeline were sealed to prevent any clay from entering. Depths of embedment ranging from less than 1D to 6D were investigated under displacement rates of 0.14 and 0.70 inches/minute. The resistance to movement as a function of time was recorded during pipeline displacement.

The results from both test series are presented in Figure 2.9 where the dimensionless factor N_c was calculated for each test and plotted as a function of the ratio H/D. The authors have

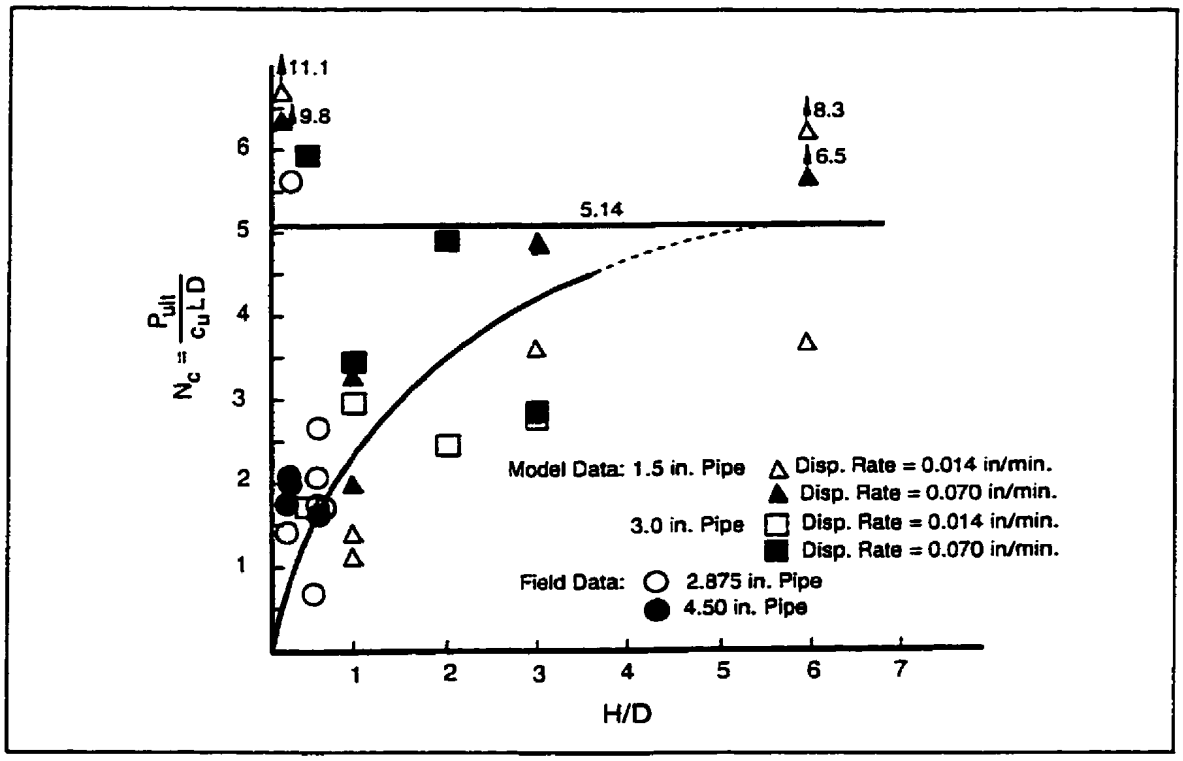

Figure 2.9 - Relationship between N_c and embedment ratio (after Wantland et al., 1979).

drawn a curve on the figure thought to be representative of the observed trend for the lateral bearing capacity factor. The authors conclude that Equation [2-26] and Equation [2-27] used in conjunction with Figure 2.9 can be used to determine the ultimate lateral resistance of a pipeline in a very soft clay near the liquid limit. It is also suggested that an upper limit to N_c appears to be on the order of 5 to 6 and that N_c is not significantly influenced by pipeline diameter. Finally it was observed the rate of displacement did not significantly affect the lateral resistance within the rate of displacements studied and for the particular soils used in the investigation.

Trautmann and O'Rourke (1985) conducted an experimental program to investigate the

lateral force-displacement response of buried pipe. A review of the literature by the authors indicated that formulations utilizing the coefficient of horizontal subgrade reaction were inadequate for the design of buried pipelines. The authors also found that various analytical models used to estimate the maximum lateral resistance of buried pipelines led to predictions differing by as much as 240%.

The goals of the experimental program were to characterize force-displacement behaviour in terms of a simple model suitable for design practice and to compare the results with other published results. The tests were varied to ascertain the effects of burial depth, soil density, pipeline diameter, and pipeline surface roughness. The tests were conducted in a test compartment measuring 1.2m by 2.3m in plan by 1.2m deep. Two 1.2m long pipeline test sections were used which had diameters of 102mm and 324mm and wall thicknesses of 6.4 and 9.5mm. The pipelines were connected to a hydraulic ram outside the test box via stiff rods which passed through the walls of the test box and which were strain gauged to measure loads. The sand was placed in 25mm layers using a spreader to achieve a constant density of either 14.8, 16.4 or 17.7kN/m^3. Corresponding peak direct shear friction angles were 31 °, 36 ° and 44 ° respectively. Thirty tests were conducted in the different sands at h/D ratios of 1.5, 3.5, 5.5, 8 and 11. To determine the effects of pipeline roughness, a pipeline was covered with sandpaper for two of the tests and covered with plastic film coated with oil for two other tests.

The test results are presented in Figure 2.10 as non-dimensional force, N_γ, which is defined

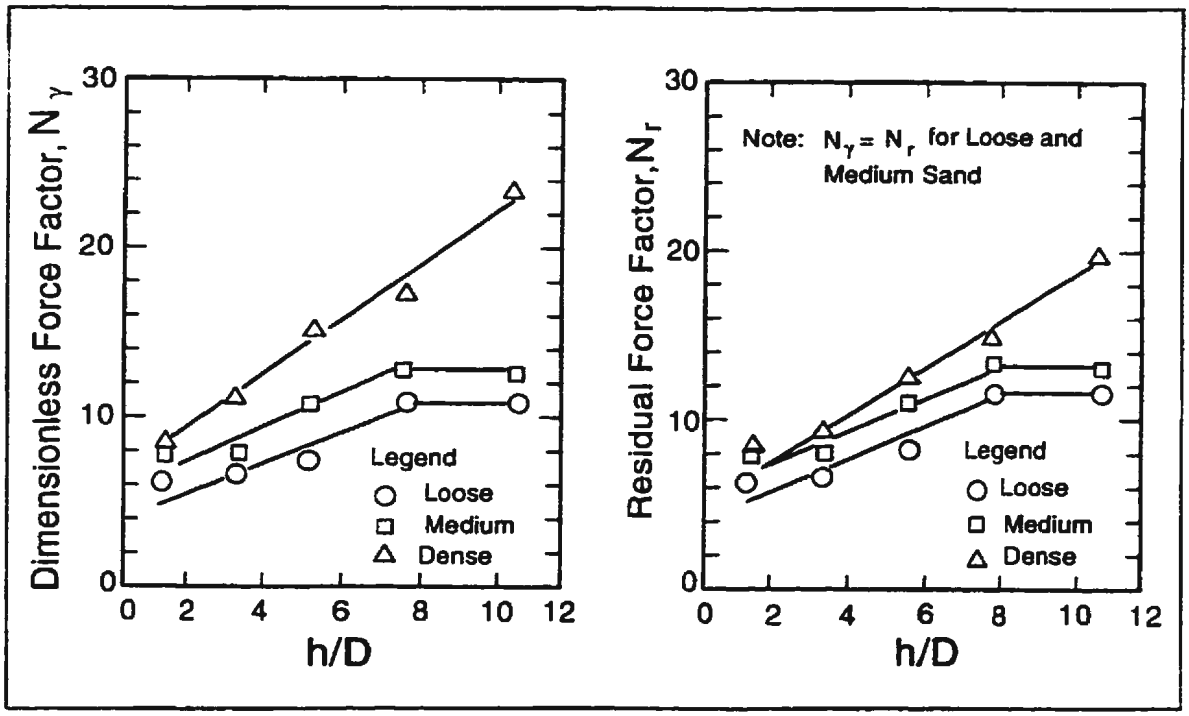

Figure 2.10 - Plot of N_γ versus h/D for pipe loading tests (after Trautmann and O'Rourke. 1985).

as

$$N_\gamma = \frac{P_{ult}}{\gamma\ h\ D\ L} \qquad \text{[2-28]}$$

versus embedment ratio. In the above equation, P_{ult} is the maximum measured force, γ is the soil unit weight, h is the depth to the pipe springline, D is the pipe diameter, and L is the length of the pipeline segment. The displacement at P_{ult} is termed the dimensionless displacement, Y_{ult}. For dense sand the peak force could be easily identified but for loose sand Y_{ult} was taken as the point where the force-displacement curve became linear. The displacements to maximum force were found to vary with density and were 0.13h, 0.08h, and 0.03h respectively for the loose, medium, and dense sand. The pipeline surface roughness

was found to have little effect on soil response; N_γ for the rough pipeline was only 10% greater than from the smooth pipeline. Soil density was found to have significant impact as shown in Figure 2.10. The N_γ values for the larger diameter pipe were found on average to be only 8% greater than the smaller diameter pipe in loose sand and only 1% higher in the dense sand. The authors conclude from this that the data can be extrapolated to pipeline diameters greater than 324mm.

A comparison of the test results was made with the analytical models of Hansen (1961), Ovesen (1964), Neely *et al.* (1973), and Rowe and Davis (1982b). The comparison indicated the best agreement was with the models of Ovesen (1964) and Rowe and Davis (1982b) while the models of Hansen (1961) and Neely *et al.* (1973) overpredicted the measured forces by 150 to 200%. Because of the close correspondence of results with Ovesen's (1964) analytical method, the authors developed the plot of Figure 2.11 based on the work of Ovesen (1964) and proposed that this chart could be used in pipeline design. The authors further analysed their experimental data and found that there was a hyperbolic relationship between normalized force (F") and normalized displacement (Y") which could be expressed as

$$F'' = \frac{Y''}{0.17 + 0.83\ Y''} \qquad [2\text{-}29]$$

in which

$$F'' = \frac{(p/(\gamma\ h\ D\ L))}{N_\gamma} \qquad [2\text{-}30]$$

and

$$Y'' = \frac{(y/D)}{(Y_{ult}/D)} \qquad [2\text{-}31]$$

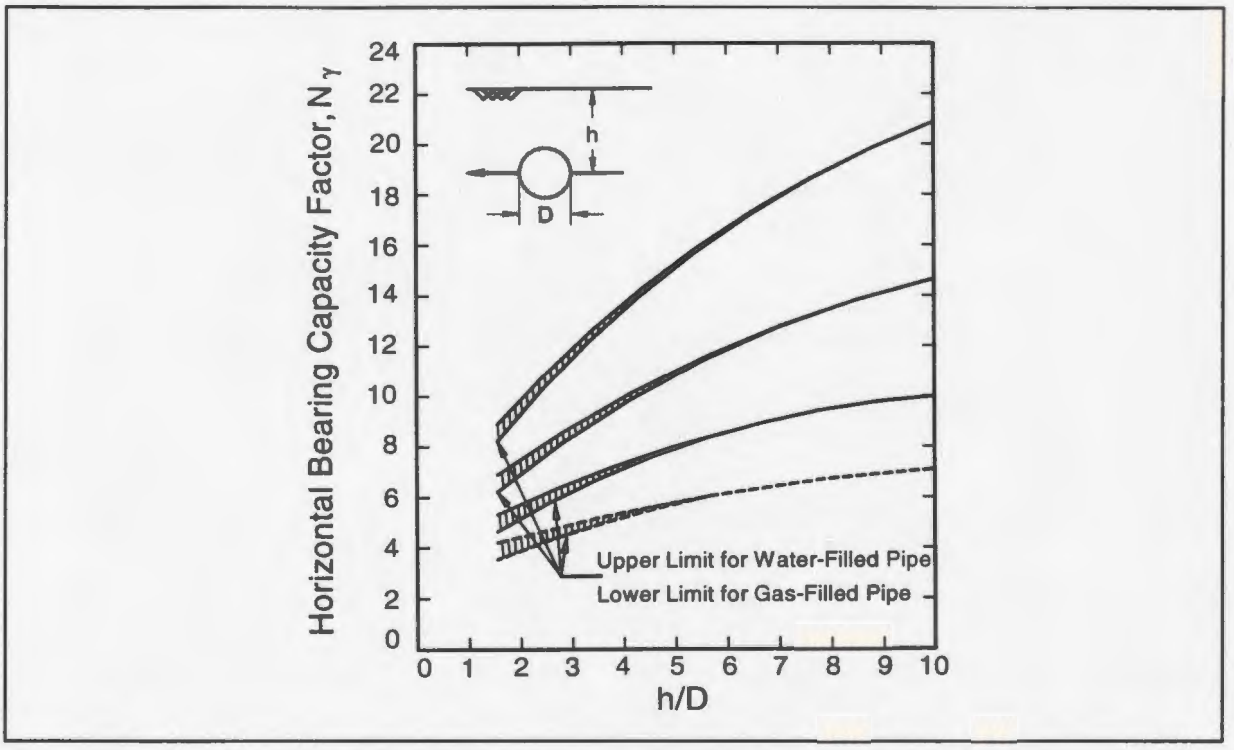

Figure 2.11 - Horizontal bearing capacity factors, N_γ, for sand as a function of h/D (after ASCE, 1984).

and where p is the force measured at each increment of displacement, y. If a bilinear relationship is needed for the force-displacement curve, the authors suggest that Figure 2.11 can be used to determine the maximum lateral force and the elastic horizontal soil stiffness should be taken as a secant slope defined at 70% of the maximum force. This is given by the following expression:

$$K_{h70} = C_k \, N_\gamma \, \gamma \, D \, L \qquad \text{[2-32]}$$

where K_{h70} is the secant slope of the bilinear relationship defined at 70% of the maximum force. C_k has been determined to be 20, 30, and 80 respectively for loose, medium, and dense sand and the displacements at maximum horizontal force have already been presented.

O'Rourke and Lane (1989) conducted research to characterize liquefaction induced lateral spreading and conducted a parametric study to evaluate the response of a buried steel pipeline as a function of the magnitude of horizontal displacements associated with lateral spreading, the width of the slide and the properties (unit weight and strength) of the displaced soil mass. Displacement patterns were modelled after those observed during the 1906 San Francisco earthquake and the pipeline/soil interaction was analysed using a computer program, UNIPIPE. The authors argue that analytical models must account for the nonlinear behaviour of both the pipeline and the soil as large ground displacements can load pipelines well into the plastic range. The model allowed for the analysis of stress and deformation resulting from a combination of bending, axial compression, and internal pressure.

For the parametric study, the soil movement was assumed to cross perpendicular to the axis of the pipeline and the study focused on the horizontal displacements induced by the lateral spreading. The soil displacements were assumed to be symmetric across the width of the slide, the maximum occurring at the centre. The ends of the pipeline were anchored away from the margin of the slide. The pipeline analysed was a 610mm steel pipeline with a wall thickness of 9.5mm and no internal pressure. The depth of burial was set at 1.2m to the top of the pipeline. The interaction of the pipeline and the soil was modelled using a bi-linear relationship based on the works of Audibert and Nyman (1977), Trautmann and O'Rourke (1985), and Tawfik and O'Rourke (1986).

As part of the investigation, five analyses were conducted. During the analyses, the

maximum soil displacement was held at 1.5m. For three of the analyses, the width of the lateral spread was modelled as 10, 30, and 50m with a soil unit weight of 18.8kN/m^3, an internal friction angle of 35 °, and a pipeline/soil interface friction angle of 28 °. For the remaining two analyses, the width of the lateral spread was maintained at 30m and the input parameters (soil unit weight, internal friction angle, and pipeline/soil interface friction angle) were taken as 20.4kN/m^3, 40 ° and 32 ° to 20.4kN/m^3, 45 ° and 36 ° respectively.

The results indicated that the smallest width of lateral spread led to the largest relative movements between the pipeline and the soil. This is significant as the resistance of the soil against the pipeline is fully mobilized at relatively small lateral spread displacements. The soil unit weight and shear strength were shown to only have a small influence on the interaction. The authors conclude that pipelines should be sited to avoid potential narrow zones of lateral spreading and that failure zones with widths less than approximately 20m may induce relatively high plastic deformations in pipelines similar to that studied.

Yeh and Lai (1992) conducted an analytical analysis of laterally loaded pipelines to determine the effect of magnitude of the soil displacement, the effect of width of the sliding zone, the effect of internal angle of friction of the soil, and the effect of pipeline burial depth. The model developed by the authors utilized the concept of a beam on an elastic foundation. The soil resistance to horizontal pipeline movement in the model was based upon the work of Hansen (1961) for piles subjected to lateral loading. The baseline analysis was for a 1,067mm diameter pipeline with a wall thickness of 14.3mm placed in a sand with a density

of 1,760kg/m^3. The baseline parameters used in the analysis were 200cm, 8,000cm, 20° and 90cm for the lateral movement of the soil, width of the sliding zone, internal angle of friction of the sand, and pipeline cover depth, respectively.

To investigate the effect of soil movement, slide magnitudes of 50-450cm were also investigated. The results indicated that a critical condition in the pipeline was reached for a lateral soil movement of approximately 205cm. The width of the sliding zone was varied to determine the critical value which was found to be less than or equal to 67.7m which indicates that narrow zones of instability are more hazardous to a pipeline. Friction (ϕ) angle values of 20°, 25° and 30° were investigated but no significant effect on the stress condition of the pipeline was found by varying this parameter. Variation of cover depth from 60 to 120cm in the analysis indicated that the load transferred to the pipeline increased with increasing burial depth.

SNAM (Boizoni *et al.*, 1993) have developed a numerical analysis tool to assess the stress state of a pipe buried in an unstable slope. A complete nonlinear finite element analysis was implemented and reduced-scale models were used to refine the finite element simulation. Besides providing a benchmark for numerical simulations, the reduced-scale physical models were intended to provide a better understanding of the soil/structure interaction and especially the effects of the pipeline configuration with respect to the ground movement.

Venzi *et al.* (1993) describe these reduced-scale (1:10) physical model experiments

conducted to study the behaviour of a pipeline undergoing lateral interaction with the soil. The model pipeline used in the investigation had a diameter of 50mm and a wall thickness of 1mm and was said to represent a full-scale NPS 20 pipeline with a 10mm wall thickness. The pipeline was buried in three clayey soil blocks adjacent to one another. Details on the soil used during testing are provided by Boizoni *et al.* (1993). To simulate prototype soil conditions, a surcharge was placed on the model soil surface. The experimental setup permitted the horizontal displacement of the central clay block which rested on a sliding support plate to create a relative displacement between the blocks of soil.

The experiments modelled a 100m long section of pipeline subjected to a lateral ground movement of 1.84m acting on the central 53m section of pipe. No details on the results of the experimental program are presented by the authors. However, the authors claim good agreement between the experimental results and the results of a complete finite element analysis of the prototype-scale pipeline.

Ng (1994) conducted research to examine the behaviour of buried trenched pipelines subjected to external loading. The author carried out numerical analyses to simulate *in situ* pipe loading tests with the claim that such analyses can improve the understanding of the behaviour of buried pipelines subjected to differential ground displacements.

The results of lateral push tests were used for the validation of a two stage analysis technique, developed by British Gas, for the modelling of laterally loaded pipelines. Stage

I used a 2-D plane strain finite element analysis to predict the restraining effect of the soil as a function of pipe displacement. These predictions were then used in Stage 2 which models the lateral behaviour of the pipe using an elastic beam on elastic foundation program. This elastic beam on elastic foundation program had been modified to include the effects of plastic behaviour of the pipe material, change in shape of the cross-section, and shear deformation in the pipe. The author used different soil models to represent the backfill in the FE analysis and assumed different interface conditions between the soil and pipe and between the backfill and natural ground.

Results of the research indicated that the tensile stress developed at the rear of the pipe significantly affected the predicted pressure-displacement relationship. Satisfactory agreement to the field data was obtained from analyses using a non-linear elastic model and an elasto-plastic model together with interface elements around the pipe and along the trench or using a no tension procedure. A 2-D finite element model was used to carry out a parametric study to investigate the influence of the relative strength between natural ground and backfill, trench width, and angle of trench sides.

Ng (1994) compared the results of his field lateral loading tests to empirical relationships suggested by other researchers to assess the validity of the relationships. Table 2.2 shows values of interaction factor, N_c, for six formulations from the literature together with N_c values back-calculated from the field tests where

Table 2.2 - Predicted values of N_c for the lateral pipe loading test by the proposed formulations and modified formulation to include the effects of existence of a backfilled trench (From Ng, 1994)

Original Results From	Proposed Formulation	$N_c = \frac{P_{ult}}{c_u D}$	N_c from Eq. [2.34]
Reese (1958)	$N_c = 2 + \frac{\gamma Z}{c_u} + 2\sqrt{2}\frac{Z}{D}$	7.2	8.5
Matlock (1970)	$N_c = 3 + \frac{\sigma'}{c_u} + 0.4\frac{Z}{D}$	4.7	5.5
Poulos and Davis (1980)	$N_c = 3 + \frac{\gamma Z}{c_u} + 0.5\frac{Z}{D}$	4.8	5.7
Rowe and Davis (1982a)	N_c = 2 *to* 11.5 (for actual values see ref.)	No breakaway - 9.4 Immed. breakaway - 4.2	No breakaway - 11.1 Immed. breakaway - 5.0
Randolph and Houlsby (1984)	$N_c = 2 + \frac{\gamma Z}{c_u} + 1.5\frac{Z}{D}$	5.2	6.1
ASCE (1984)	N_c = 2.8 *to* 7.8 (for actual values see ref.)	5.5	6.5
Field Experiment	----	7.3	7.3

$$N_c = \frac{P_{ult}}{c_u D} \qquad [2\text{-}33]$$

and where P_{ult} is the ultimate load on the pipe, c_u is the undrained shear strength of the soil around the pipe, and D is the pipe diameter. As stated earlier, the current state-of-practice formulations most often used in routine design are those of Rowe and Davis (1982a) and the ASCE recommendations (ASCE, 1984) based on Hansen's (1961) model. The author concluded that most formulations underpredict the value of N_c.

Ng (1994) points out that the empirical formulations are all based on the assumption that the soil condition is homogeneous; however, most pipes are laid in an excavated trench and then backfilled with a material usually weaker than the natural or native ground. Based on his parametric finite element analysis, Ng (1994) demonstrated that the existence of two distinct materials could influence the overall behaviour of the pipeline under external loading. Again based on his parametric analysis, Ng (1994) introduced a factor F_{ch} which could be included in a general equation to determine P_{ult} and which corrects N_c for the influence of a backfilled trench. The proposed general equation was

$$P_{ult} = c_u \, D \, N_c \, F_{ch} \qquad \text{[2-34]}$$

where F_{ch} is presented in Figure 2.12 and c_u is the undrained shear strength of the backfill. In the figure, W is the trench width and R_c is the ratio of native soil to backfill undrained shear strengths. The values of F_{ch} shown in Figure 2.12 are only applicable for a trench with vertical sides but the author developed corrections for different angles of trench sides. The last column of Table 2.2 shows recalculated N_c using developed correction factors and Ng (1994) suggests the value of N_c proposed by the Committee on Gas and Liquid Fuel Lifelines (ASCE, 1984) agrees quite well with the field test result.

Ng (1994) states that the pipe displacement to ultimate load suggested by the Committee on Gas and Liquid Fuel Lifelines (ASCE, 1984) underpredicts the actual value measured from field tests which was 0.111h where h was the depth to the pipe springline. From the results of the author's parametric study, relationships for the non-dimensional ultimate displacement, Y_{ult}/h, as a function of R_c for different W/D ratios for trenches for vertical

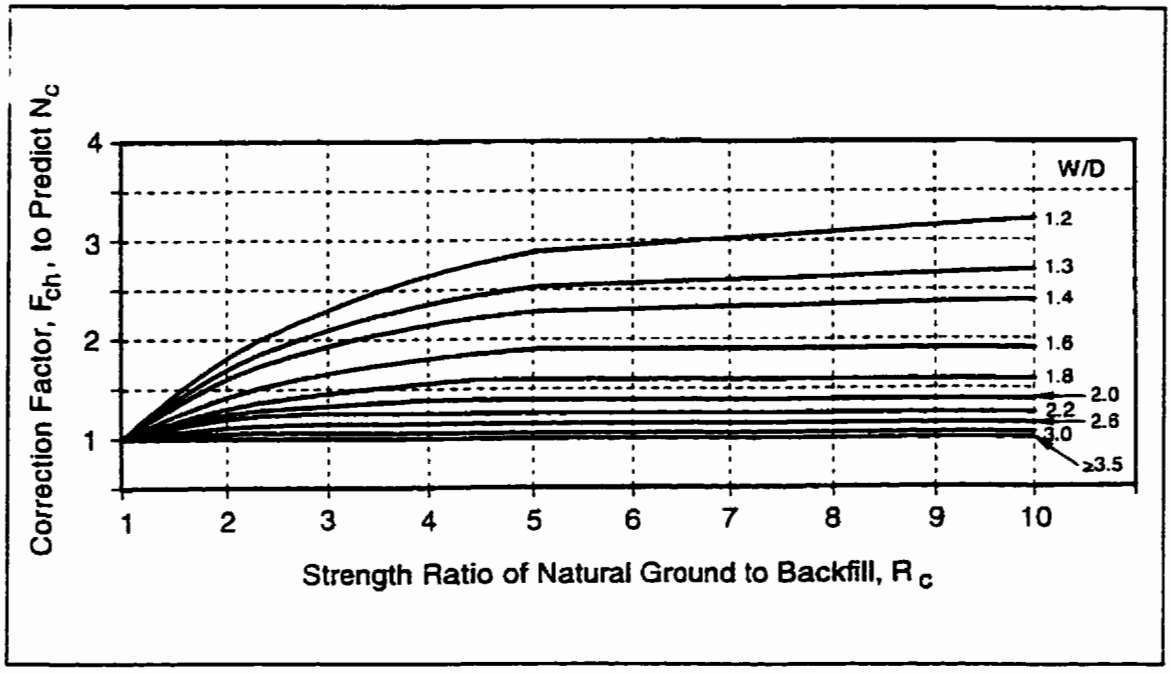

Figure 2.12 - Relationship of correction factor F_{ch} versus R_c at different W/D ratios for a trench with vertical sides (after Ng, 1994).

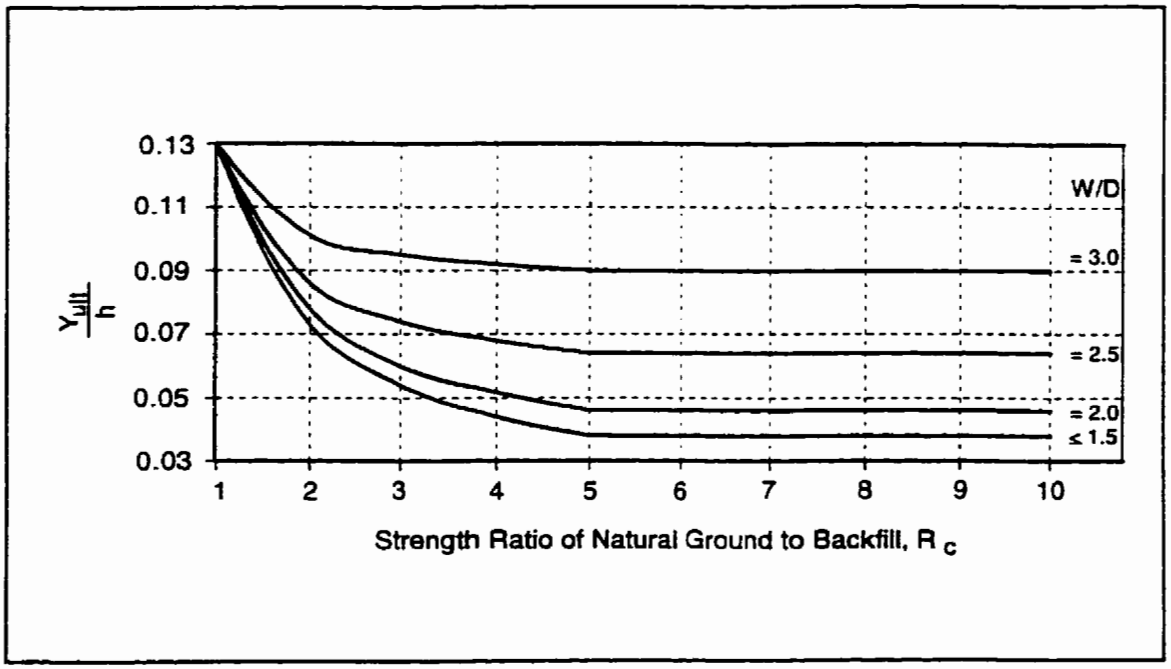

Figure 2.13 - Relationship between non-dimensional ultimate displacement versus R_c at different W/D ratios for a trench with vertical sides (after Ng, 1994).

sides were developed as shown in Figure 2.13. A correction factor was also developed for trenches with non-vertical sides.

With regards to a mathematical formulation which can be used to estimate the non-linear p-y curve, Ng (1994) used the hyperbolic p-y curve formulations provided by Audibert and Nyman (1977), Trautmann and O'Rourke (1985), and Georgiadis *et al.* (1992) to fit the p-y curve derived from the field test. It was found that the formulation by Trautmann and O'Rourke (1985) provided the best agreement. However, the best agreement with the normalized data from the 2-D finite element analyses and parametric study was provided by Audibert and Nyman (1977). Ng (1994) comments that both formulations gave good predictions for the shape of the p-y curve and the differences between them is small. The author suggests that either can be used in practice or the mean value of the two formulations can be used:

$$p = \frac{y}{\frac{0.16\,Y_{ult}}{P_{ult}} + \frac{0.84y}{P_{ult}}}. \qquad [2\text{-}35]$$

In summary, Ng (1994) concluded that a non-linear p-y curve can be estimated using the above equation. The ultimate pressure on the pipeline can be estimated using Equation [2-34] where N_c can be taken to be the Hansen (1961) bearing capacity factor suggested by ASCE (ASCE, 1984) and where F_{ch} values are taken from Figure 2.12 to correct for the presence of a backfilled trench. Figure 2.13 can be used to determine the displacement to ultimate load, Y_{ult}.

2.3.2 Centrifuge Modelling

A number of tests have been carried out in the centrifuge to investigate pipeline/soil interaction. These include investigations on: the effect of rising groundwater levels on buried pipes (English and Schofield, 1973); flexible circular pipes subjected to surface loading (Valsangkar and Britto, 1979); the long term behaviour of large-span culverts in cohesive soils (McVay *et al.*, 1994); thaw induced settlement of pipelines (Smith, 1991); the influence of excavations on buried pipes (Kusakabe, 1984; Phillips, 1986); and the effect of earth pressures on buried flexible pipes (Tohda *et al.*, 1985; Takada *et al.*, 1985).

Dickin (1988) conducted centrifuge model tests to investigate the lateral displacement of vertical anchor plates and pipelines in sand. The author states that predictions of soil restraint against the lateral movement of buried pipelines have been made using design methods developed originally for vertical anchor plates but that there is no experimental evidence to suggest anchor plates behave in a similar fashion. Dickin (1988), therefore, conducted a centrifuge study to investigate the force-displacement response of 1m high vertical anchor plates and 1m diameter pipelines with an embedment ranging from 1 to 11m.

The tests were conducted on 25mm pipelines and plates which were subjected to a centrifugal acceleration of 40g enabling the prototype behaviour to be investigated. The tests were conducted in dry Eirth sand which was poured from a hopper to both loose (γ = 14.5kN/m^3) and dense (γ = 16kN/m^3) conditions. The sand had a uniformity coefficient of 1.5 and 80% of the grains were between 0.125mm and 0.250mm.

No major differences in the force-displacement response between the plates and pipes were noted by the author especially at deeper embedment. Dickin (1988) therefore proposed that the assumption that a laterally displaced pipeline can be regarded as a laterally displaced anchor plate in theoretical calculations of lateral resistance is broadly validated. The author also compared dimensionless breakout factors with those predicted by Ovesen and Stromann (1972) and Rowe and Davis (1982b). The dimensionless breakout factor, N_γ, is defined as

$$N_\gamma = \frac{P_{ult}}{\gamma D h L} \qquad [2\text{-}36]$$

where P_{ult} is the ultimate displacement resistance, γ is the unit weight of the soil, D is the pipeline diameter, h is the depth to the pipe springline, and L is the length of the pipeline. Comparison between theoretical and experimental breakout factors in dense sand indicated the method of Ovesen and Stromann (1972) yielded reasonable results while the theory of Rowe and Davis (1982b) overpredicted the experimental breakout factors especially at higher embedment ratios. For loose sand, both analytical methods overpredicted the experimental breakout factors by approximately 100% for all embedment ratios.

Rizkalla *et al.* (1992) conducted a series of 1:50 scale centrifuge tests to investigate lateral pipeline/soil interaction in a cohesive soil (overconsolidated kaolin clay). The aims of that study were to prove that the centrifuge technique was appropriate for this application, to determine the interaction factors (and the overall interaction curves) for a particular soil, and to determine the effects of ditch geometry on these interactions.

The tests were conducted in a centrifuge strongbox which was 360mm deep and with internal dimensions of 800mm by 1200mm. Four pipelines were tested during each centrifuge flight and were displaced at a nominal speed of 1mm/sec. The clay sample was prepared by mixing clay powder with water, placing the slurry in the strongbox, and consolidating the sample one-dimensionally in a press to a vertical effective stress of 160kPa. The sample was then carved to accommodate the pipelines and the actuator and the pipelines placed into the trenches. The pipelines were backfilled with a kaolin clay slurry. The trench geometry was varied so that cover depths of 0.92 and 1.52m (prototype-scale) and ditch widths of 2 and 2.75m (prototype-scale) were investigated.

Most of the author's goals were achieved. The major concern was an inability to model a distinct backfill material to provide conclusions about the effect of ditch width and depth. They concluded that centrifuge modelling is a suitable technique for investigating lateral pipeline/soil interaction The main consideration presented by the authors was that current state-of-practice formulations based on the works of Rowe and Davis (1982a) and Hansen (1961) appeared to be unconservative, predicting loads acting on the pipeline about 50% lower than those measured experimentally. A reanalysis of the data from the experimental program in light of desiccated soil condition data yielded interaction factors consistent with the above formulations (Paulin *et al.*, 1998).

Krstelj (1996) conducted centrifuge testing to examine the behaviour of laterally loaded pipelines in dry and saturated sand. The goal of the research was to study the forces caused

by: (1) the case of undeformed sand moving relative to a pipeline which is the case when there is liquefaction in a sublayer (lateral spreading); and (2) the case of deformed or liquefied sand moving relative to a pipeline (flow failure).

Tests were conducted both at 1g and using the Princeton geotechnical centrifuge with pipes representing prototype diameters from 0.02 to 1.3m. Static dry, static saturated and dynamic saturated tests were conducted, the latter achieved by means of an electro-hydraulic shaker. As a result of the testing program, Krstelj (1996) confirmed that the normalized ultimate loads dropped by about 20% for any ten-fold increase in pipe diameter (for the depths and diameters tested). The author also found that the initial slope of the force-displacement curve decreased by a factor of three for the same ten-fold increase in the pipe diameter.

The author compared experimental results with recommendations provided by the Committee on Gas and Liquid Fuel Lifelines (ASCE, 1984). It was observed that the theoretical results proposed by Ovesen (1964) compared well with the data recorded during the dry soil loading tests while the formulation proposed by Hansen (1961) overpredicted the experimental measurements by as much as 100%.

Krstelj (1996) found that the series of experiments with the monotonic loading in the saturated sand indicated that the normalized ultimate force under undrained conditions could be expected to increase, depending on the velocity of the applied loading, by 80% or more over its "drained value". The author suggests that this finding is significant in that tests in dry

sand can seriously underestimate the magnitude of ground restraint during the large ground deformations. Tests in which the effective stress in the soil was permitted to drop to zero, yielded little to no resistance between the pipe and liquefied soil.

2.4 Literature Applicable to the Analysis of Lateral Interaction

2.4.1 Anchor Plate/Soil Interaction

The lateral or transverse horizontal component of force is the restraint provided by the soil in response to the horizontal displacement of the pipeline. Such an interaction is considered to be similar to that of a vertical anchor plate (O'Rourke and Lane, 1989).

Mackenzie (1955) conducted small-scale model tests on rectangular and strip deadman anchors in purely cohesive soils to evaluate the application of passive earth pressure theories and the theory of Hansen (1948) on the dowel-like action of piles. The author also wanted to determine if the anchor strength would reach a limiting value with cover depth.

The tests were conducted in a steel tank filled with clay into which the anchor was placed and displaced horizontally to failure. To simulate deep tests, a water surcharge was placed on the soil surface. The model anchor was square in cross-section with a height, D, of 25.4mm, a width, also D, of 25.4mm and a length, L, of 254mm. To simulate plane-strain conditions, lubricated steel plates were placed adjacent to the end of the anchor to eliminate end effects. The plates were lubricated in an attempt to minimize end friction. The anchor

was displaced by two steel cables attached to the end of the anchor which passed through the soil and out the end of the test box.

The soil used in the experiments was a silty-clay with a liquid limit of 92% and a plastic limit of 30%. Tests were conducted with soil at water contents of approximately 63% (c_u=2.5kPa, γ=15.7kN/m^3) and 45% (c_u=21kPa, γ=16.5kN/m^3). The testbed was prepared by hand compacting the clay (after mixing) below, around, and above the anchor to the desired soil cover. Soil cover ranged from 0 to 432mm. A total of twenty tests were performed; ten at the first water content and ten at the second. Loading was achieved through a dead load system.

Mackenzie (1955) found that when the cover was shallow, the anchor acted like a continuous wall; the ruptured and disturbed soil surface indicated a conventional passive wedge type failure. Strain to failure increased with burial depth. For deep anchors, failure surfaces were found to be similar to those of the deep failure mechanism assumed for laterally loaded piles (soil flow around the anchors). In cases of shallow anchor cover (0-50mm), passive wedge theory was found to yield close agreement beyond which it deviated significantly. The data also suggested a very definite trend towards a limiting resistance for deeper anchors but did not reach limiting values (11.43c_uD) suggested by Hansen's (1948) pile-dowel theory. Use of bearing capacity as an approximate method of estimating the anchor strength by considering the anchor as a deep buried footing with a vertical load, yielded values which were too low by approximately 50% and this theory was discarded as a viable means of calculating anchor strength.

The author suggested a correction be applied to passive wedge theory so that it fit the experimental data. A correction which appeared to work well was $(D/H)^{0.5}$ which resulted in the equation:

$$P_{ult} = \sqrt{\frac{D}{H}} \left[\frac{\gamma H^2}{2} + 2 H c_u \right] \qquad [2\text{-}37]$$

for depths up to approximately 203mm (shallow to medium depths) where H is the depth of soil to the bottom of the anchor. The limiting condition was found to be

$$P_{ult} = 8 D c_u \qquad [2\text{-}38]$$

for depths greater than 250mm (deep anchors). Between anchor depths of 200 and 250mm, both equations tend to overpredict the capacity of the anchor.

The author concludes that the passive wedge theory of failure can be used for horizontally loaded surface anchors (H=D) in clay but does not apply to deadman anchors with substantial cover and will yield strengths in these cases which are on the unsafe side. Also, the theory of Hansen (1948) can not be applied to anchors in clay and will overpredict the ultimate capacity of deep anchors. The author also states that the rate of loading may increase the ultimate load carrying capacity of the anchor but offers no insight in the correlation between the two. Finally, the author suggests that the resistance of deadman anchors can be calculated based on the derived relations presented above in Equation [2-37] and Equation [2-38].

Rowe and Davis (1982a) suggest that because Mackenzie's (1955) small-scale model tests were conducted over a prolonged period of time (approximately two hours), that the tests may not have been completely undrained. The authors suggest that the parameters from such tests may lie between drained and undrained values.

Tschebotarioff (1973) reanalysed the continuous (plane-strain) anchor data of Mackenzie (1955) and plotted it in non-dimensional form as shown in Figure 2.14. N_c is known as the breakout factor and is expressed in non-dimensional form as

$$N_c = \frac{P_{ult}}{D\ c_u} \qquad [2\text{-}39]$$

where P_{ult} is the ultimate resistance per unit length of the anchor, D is the height of the anchor, and c_u is the undrained shear strength of the clay. As shown in Figure 2.15, H is the depth of embedment measured from the surface of the soil to the bottom of the anchor plate. Tschebotarioff (1973) suggested the data presented in the figure could be used in design if proper factors of safety were used.

It is obvious from the plot, that the breakout factor, N_c, increases with embedment ratio (H/D) up until a limiting breakout factor, N_c^*, at which point it remains relatively constant (Das, 1990). The embedment ratio at which this occurs is known as the critical embedment ratio, $(H/D)_{CR}$ (Das, 1990). From Figure 2.14, it is observed that the values of N_c^* and $(H/D)_{CR}$ were approximately 9 and 12 respectively. Anchors with an embedment ratio less

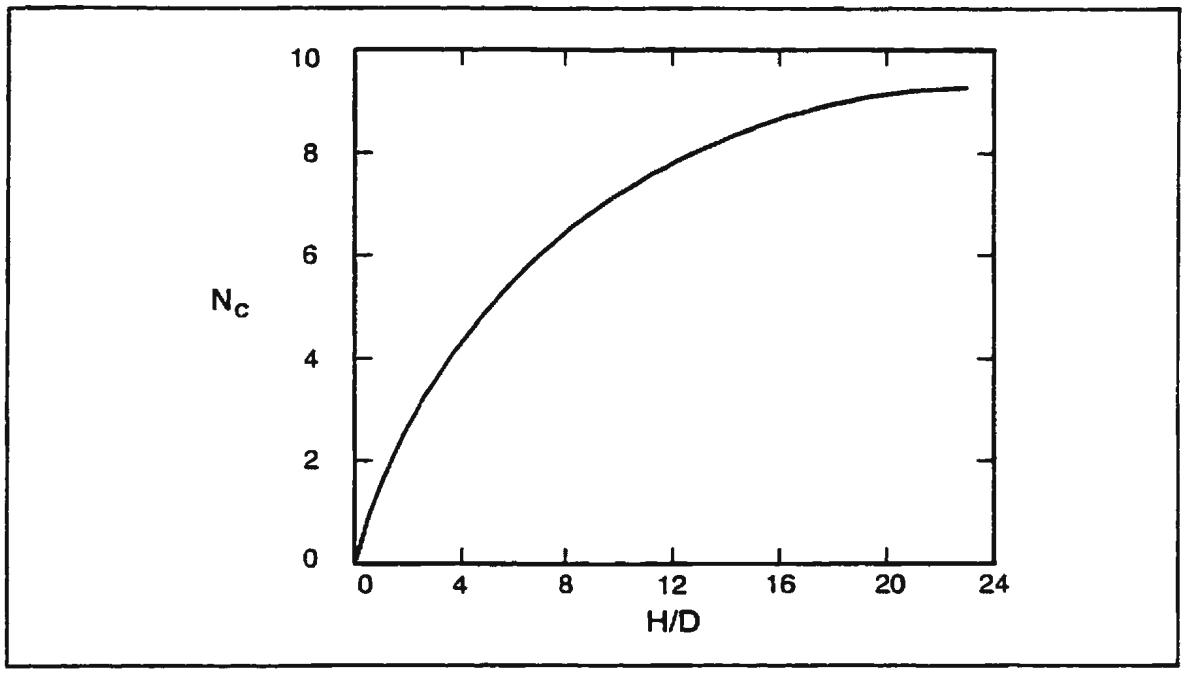

Figure 2.14 - Average plot of N_c versus H/D for strip anchors in clay based on the works of Mackenzie, 1955 (after Das, 1990).

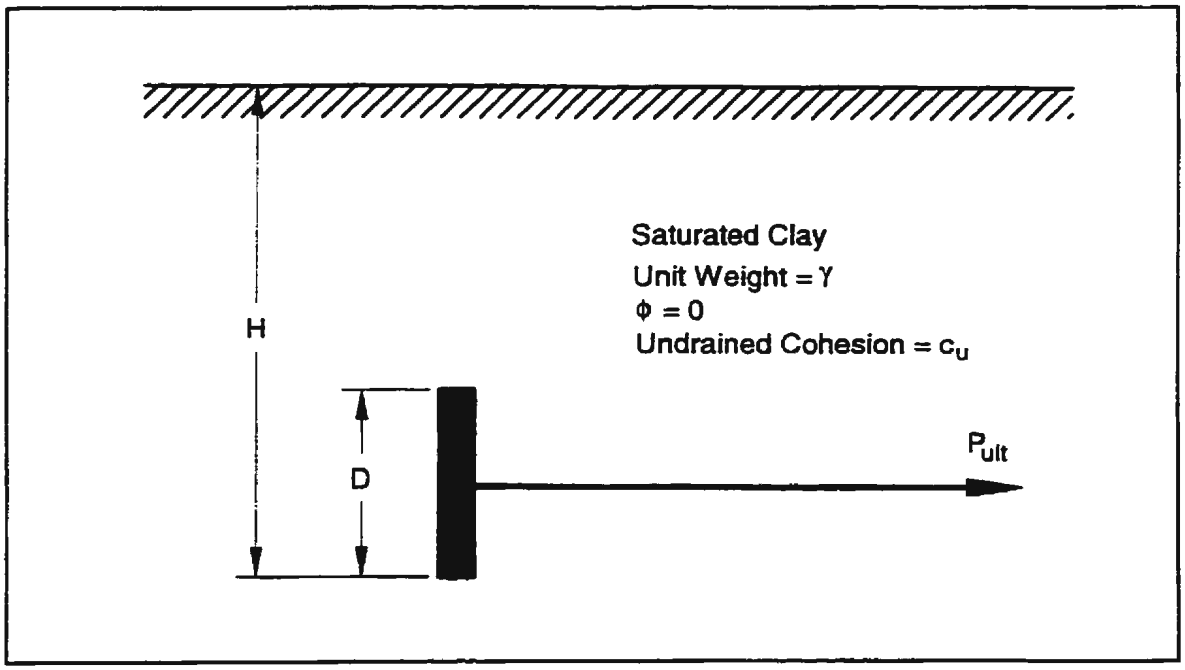

Figure 2.15 - Geometric parameters of vertical anchor plate embedded in saturated clay (after Das, 1990).

than $(H/D)_{CR}$ are considered to be shallow anchors and those with an embedment ratio greater than the critical value are considered to be deep anchors (Das. 1990).

Kovacs *et al.* (1975) present the theories of Hansen (1948) and Mackenzie (1955) for the design of block ground anchors but offer no insight on which would be the preferred method of design.

Rowe and Davis (1982a) conducted a theoretical investigation into the behaviour of horizontally and vertically orientated anchor plates in cohesive soil. Poulos (1988) suggests the use of these results in the analysis of anchor plates for offshore applications. The study was conducted using an elasto-plastic finite element analysis assuming the soil was a homogeneous, isotropic saturated clay. The anchor was considered to be of height D. buried to a depth H (Figure 2.16). and was thin and perfectly rigid. The anchor was also considered to be an infinite strip to simulate plane-strain conditions. As part of the analysis, the effects of anchor embedment, layer depth, overburden pressure, breakaway condition, anchor roughness, thickness and shape were analysed. The breakaway conditions are defined as "immediate breakaway", where the back of the anchor separates from the surrounding soil or "no breakaway" where the back of the anchor always remains in contact with the soil.

Rowe and Davis (1982a) noted that shallow anchor failure was characterized by plastic flow to the soil surface but that deep anchor failure was characterized by more local failure as shown in Figure 2.17. The depth at which the response of the anchor is no longer

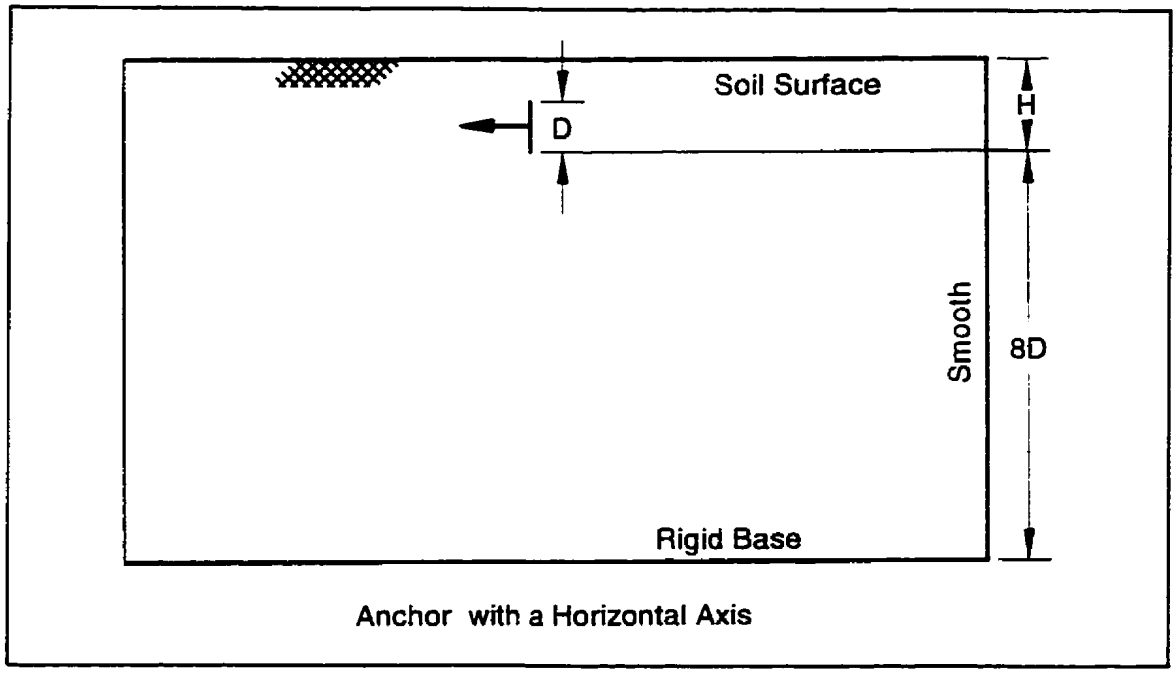

Figure 2.16 - Anchor plate finite element model (after Rowe and Davis, 1982a).

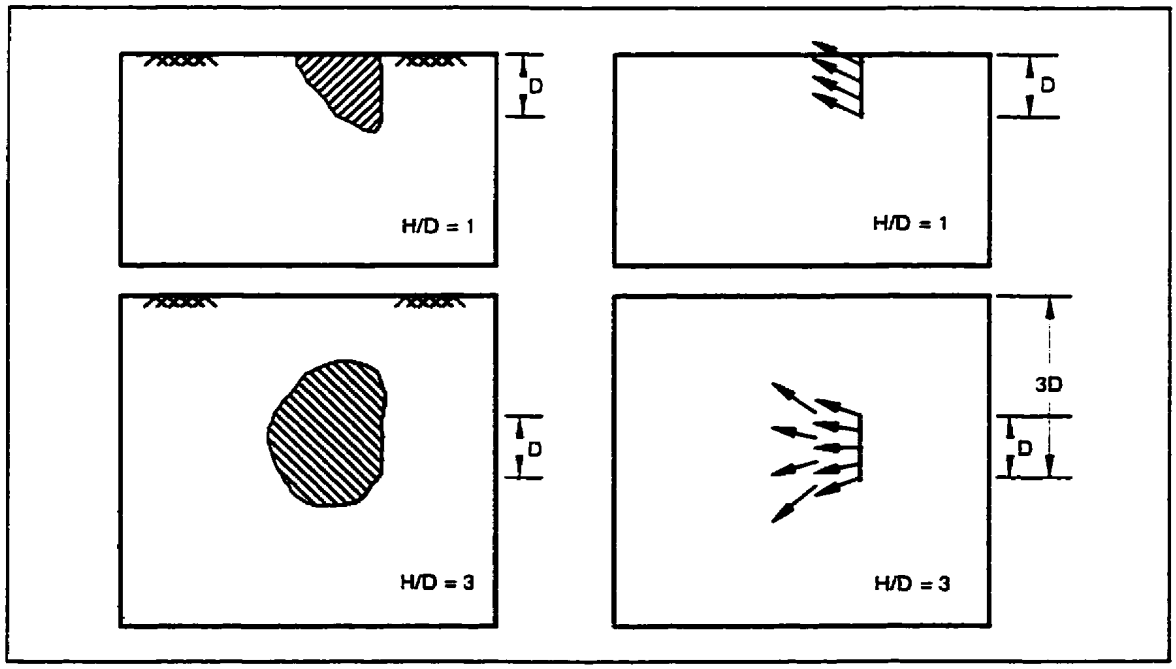

Figure 2.17 - Plastic regions and velocity fields at failure for shallow and deep anchor plates; immediate breakaway (after Rowe and Davis, 1982a).

appreciably affected by the location of the soil surface is termed the critical embedment ratio and deeper embedment will not have a significant effect on the anchor capacity. Horizontally loaded anchors were found to have a critical embedment ratio of approximately 3 for both the "immediate breakaway" and the "no breakaway" condition.

The authors suggest the ultimate undrained capacity of horizontally loaded anchor plates can be expressed by

$$P_{ult} = c_u F_c' D \qquad [2\text{-}40]$$

where F_c' is the lower value obtained by

$$F_c' = N_c + \frac{s\,q}{c_u} \qquad [2\text{-}41]$$

or

$$F_c' = N_c^*. \qquad [2\text{-}42]$$

N_c is the dimensionless anchor capacity factor for an unbonded anchor with the immediate breakaway condition. N_c^* is the dimensionless anchor capacity factor for a fully bonded anchor with the "no breakaway" condition, q is the initial overburden pressure at the level of the anchor plate and s is a coefficient for the effect of overburden pressure on the anchor capacity. The results of the authors' analysis are presented in Figure 2.18 where N_c and N_c^* are plotted as a function of the embedment ratio. For a vertical anchor, the authors suggest

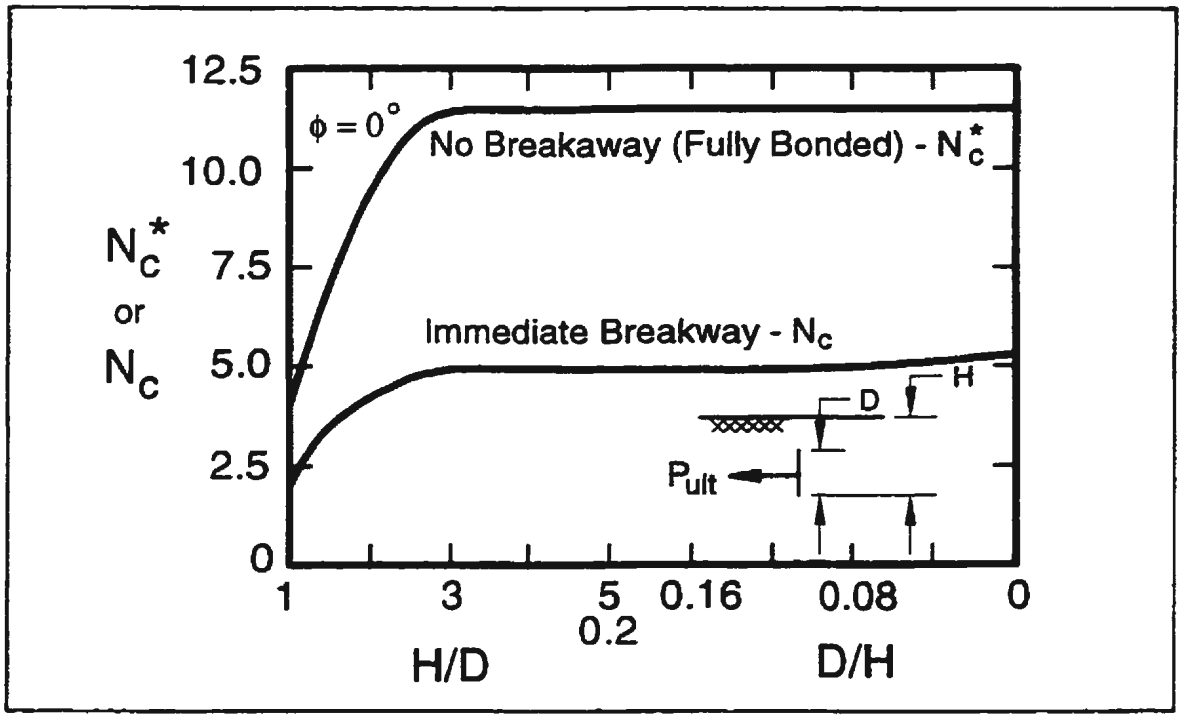

Figure 2.18 - Rowe and Davis (1982a) anchor capacity factors for a vertical plate anchor in clay (after Poulos, 1988).

that s varies from $0.5K_0$ for H/D=1 to $s=0.96K_0$ for H/D=3 and for embedment ratios in between, linear interpolation can be used. For deep anchors (H/D > 3), the authors suggest that s can be taken to be unity.

Rowe and Davis (1982a) compared their theoretical results to the horizontally-loaded small-scale anchor model tests conducted by Mackenzie (1955) and Ranjan and Aurora (1980). The authors state that the comparison suggests the theoretical predictions provide reasonable limits for the model anchor behaviour even though Mackenzie (1955) and Ranjan and Aurora (1980) made no attempt to measure adhesion or suction behind the anchor.

The authors conclude that the theoretical solutions obtained from their study provide reasonable bounds to the observed behaviour of model anchors. They also suggest that the results presented may be used in hand calculations to estimate the undrained (rapid loading) failure load of anchor plates. The authors state that if the rate of loading is slow, drained analysis using the drained shear strength and angle of friction may be more appropriate as presented in Rowe and Davis (1982b).

Rowe and Davis (1982b) extended their theoretical analysis of anchor plates in sand to the case of a cohesive-frictional soil. The anchor capacity is given as

$$P_{ult} = c' F_c' + \gamma' H F_\gamma' \qquad [2\text{-}43]$$

where c' is the drained cohesion, F_c' is the factor for the effect of cohesion on anchor behaviour, H is the depth of embedment, γ' is the effective unit weight of the soil above the anchor, and F_γ' is the factor for the effect of unit weight. F_c' is determined from

$$F_c' = N_c + \frac{q}{c'} \qquad [2\text{-}44]$$

where N_c is the anchor capacity factor for immediate breakaway and q is the surcharge pressure.

F_γ' is expressed approximately as

$$F_\gamma' = N_\gamma \; R_\psi \; R_R \; R_K \qquad [2\text{-}45]$$

where F_γ' is the basic anchor capacity factor for the effect of soil weight; R_ψ, R_R, and R_K are correction factors for the effect of soil dilatancy, anchor roughness and initial stress state respectively. The variation in N_c and N_γ with angle of internal friction, ϕ, is presented in Figures 2.19 and 2.20. Details on the calculation of the correction factors presented in Equation [2-45] are given by Rowe and Davis (1982b). Poulos (1988) also suggests that these theoretical results can be used for the design of offshore anchors in clay under drained conditions.

Das *et al.* (1985) conducted small-scale laboratory model tests to determine the ultimate pullout resistance of vertical anchor plates embedded in saturated clay. The tests were conducted in a test box approximately 1m square with aluminum anchors which were 9.5mm thick, 50.8mm high and which ranged in length from 50.8 to 254mm. The model anchor plates thus represented length-to-height ratios (L/H) of 1, 2, 3, and 5.

The clay used in the experiments had a liquid limit of 39% and a plastic limit of 14%. The clay was hand compacted in 25.4-50.8mm layers and during testing the average moisture content was measured to be 27%. The average moist unit weight of the clay after compaction was measured to be 19.2kN/m^3 with an average undrained shear strength, c_u, of 16kPa.

Twenty model tests were conducted as part of the experimental program: five with each model tested at embedment ratios of 1, 2, 3, 4, and 5. The load was applied through a deadweight system with a time of 5-8 minutes between each load step. The failure load (P_{ult})

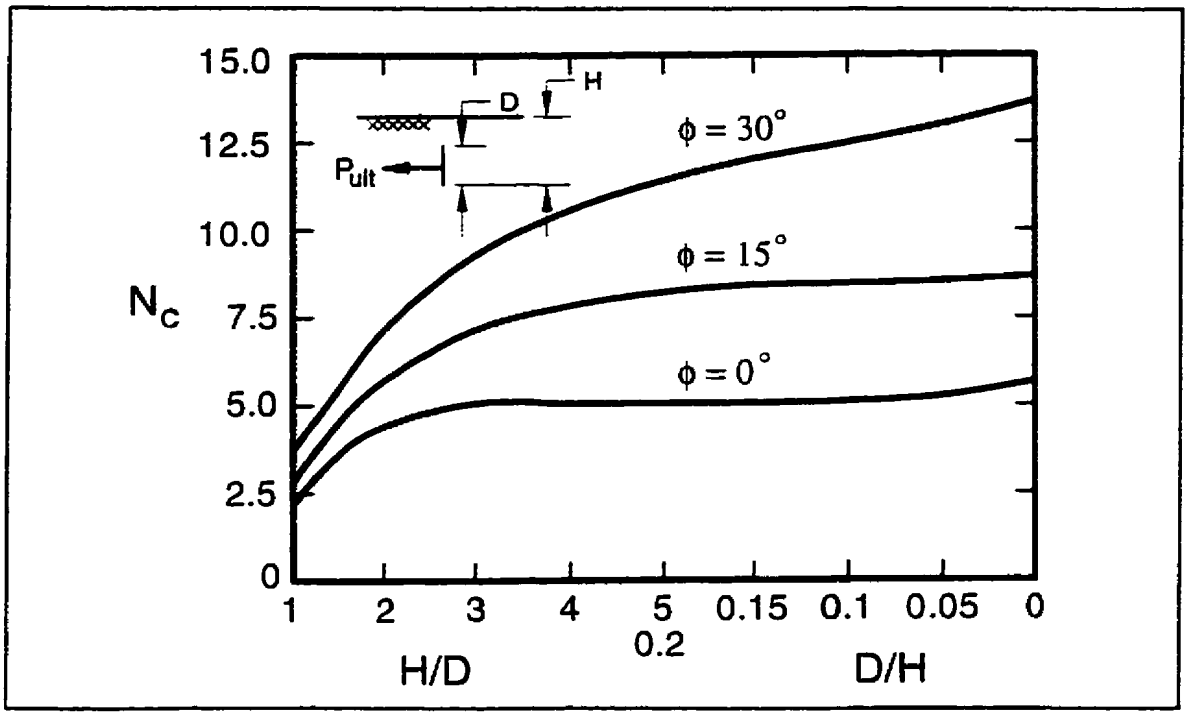

Figure 2.19 - Rowe and Davis (1982b) N_c for a vertical anchor plate with immediate breakaway (after Poulos, 1988).

during testing was defined as the load at which the anchor was completely pulled out of the soil or the point at which the load-displacement curve became linear.

The authors noted during the tests that for anchors with embedment ratios up to approximately 4, surface cracks appeared immediately above the anchors and at ultimate load, a rupture surface in front of the anchors was visible. For deeper anchors (H/D=5), surface cracks only appeared as the load approached the ultimate load.

The test results are presented in Figure 2.21 in the non-dimensional form

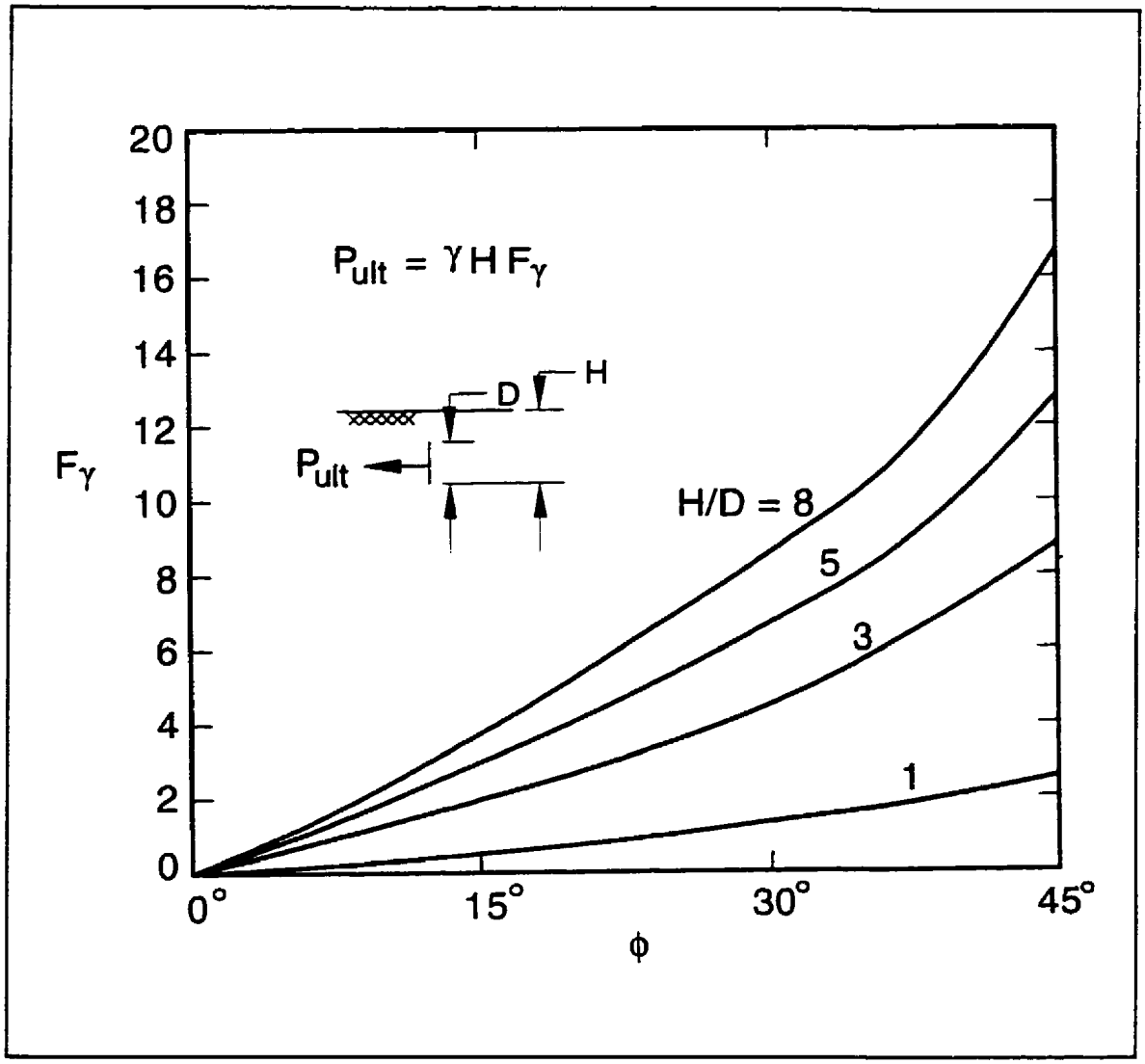

Figure 2.20 - Rowe and Davis (1982b) variation of N_γ anchor capacity factor with angle of friction for a vertical anchor plate (after Poulos, 1988).

$$N_c = \frac{P_{ult}}{D\ c_u} \qquad \text{[2-46]}$$

where N_c is termed the breakout factor. The authors suggest the data represents shallow anchor conditions as the breakout factor for all plates continues to increase with embedment

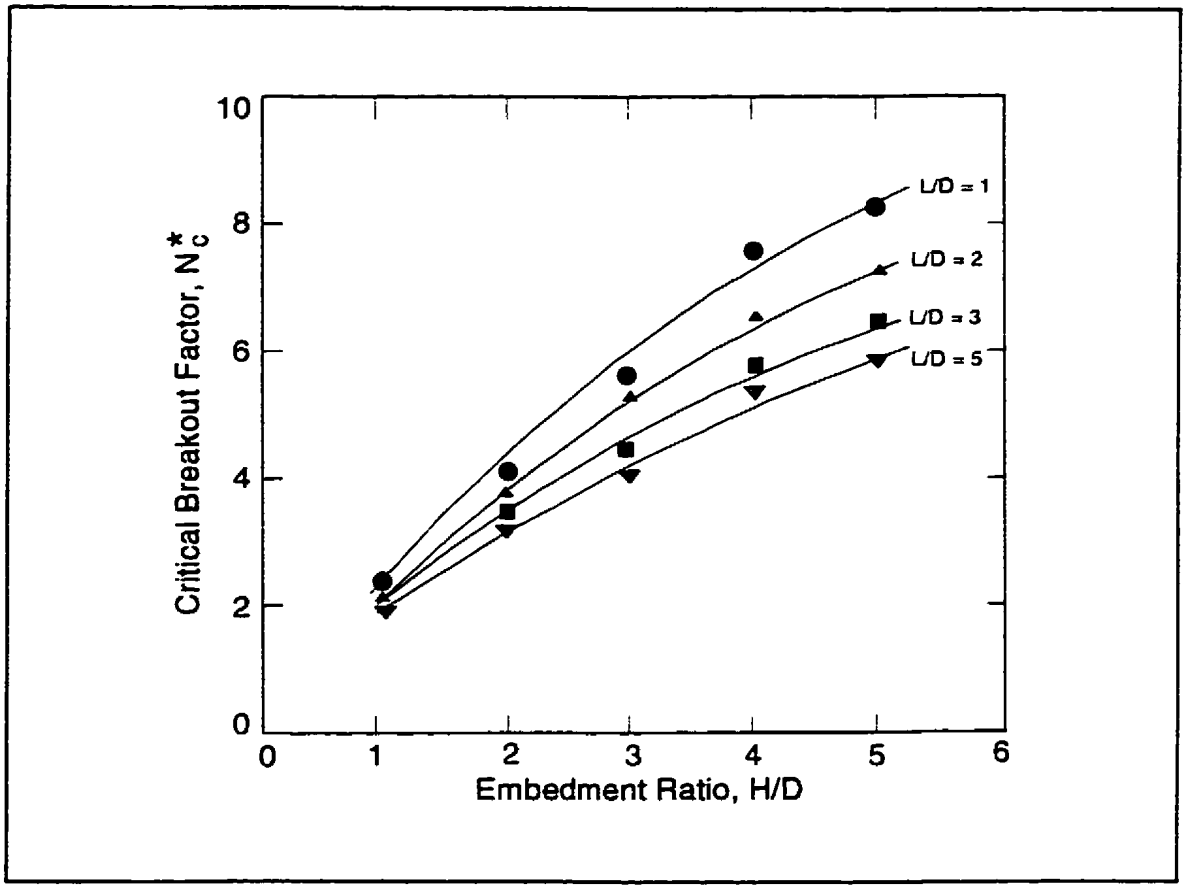

Figure 2.21 - Plot of experimental breakout factor with embedment ratio (after Das et al., 1985).

ratio and does not reach a limiting value which would be expected for deep anchors.

The authors also suggest that for $L/H \geq 5$, the interaction can be assumed to be a plane-strain condition. Based on this assumption, the authors presented the following equation

$$P_{ult} = s\ D\ c_u\ N_{c_{(L/D=5)}} \qquad [2\text{-}47]$$

for $H/D \leq 5$ which is the limit of the experimental data and where s is a shape factor dependant on L/D and embedment ratio; for $L/D \geq 5$ (plane-strain conditions), s would be

equal to 1 and for $L/D \leq 5$ (non plane-strain conditions), s would be greater than 1. The variation of the shape factor with L/D and embedment ratio based on experimental data is presented in detail by Das *et al.* (1985). The authors also found that

$$N_{c_{(L/D=5)}} = 2\ (H/D)^{0.74} \qquad [2\text{–}48]$$

and combining equations arrived at

$$P_{ult} = 2\ D\ c_u\ (H/D)^{0.74} \qquad [2\text{–}49]$$

for shallow continuous anchors ($H/D \leq 5$).

The authors conclude that the ultimate pullout resistance for shallow vertical anchors subjected to horizontal pull can be conveniently expressed in the form of the non-dimensional breakout factor N_c. They also conclude that, for shallow anchors, the breakout factor increases with embedment ratio and also increases with a decrease in width to height (L/D) ratio, Finally, the authors acknowledge that larger scale tests are needed to validate the results.

A series of laboratory model tests were conducted by Das (1987a) to investigate the ultimate pullout resistance of vertical strip anchor plates in saturated or near saturated clay. The anchors used in the study had dimensions of 50.8mm (height) by 228.6mm (length) and a thickness of 4.76mm. The test box was only 0.4mm wider than the length of the anchor plate so the sides of the box were polished to reduce friction effects.

Two types of clayey soil were used in the experiments. The first had a liquid limit of 32%, a plasticity index of 13% and was tested under two conditions: with an average moisture content (w) of 24.5 and 17.6%, a moist unit weight (γ) of 19.7 and 20.8kN/m^3 and an undrained shear strength (c_u) of 20.3 and 42.5kPa. The second soil had a liquid limit of 39% and a plasticity index of 25%. The tests were conducted under four soil conditions: with moisture contents ranging from 16.5 to 27%; with moist unit weight ranging from 19.1 to 20.6kN/m^3; and with undrained shear strengths ranging from 16 to 52kPa. The degree of saturation of both soils during testing varied from 92 to 97.5%.

The testing procedure and definition of ultimate load were the same as those described for Das *et al.* (1985). The ultimate pullout resistance was expressed by the author using a non-dimensional breakout factor, N_c, defined as

$$N_c = \frac{P_{ult}}{D\ c_u} \qquad [2\text{-}50]$$

where P_{ult} is the ultimate resistance per unit length of the anchor, D is the height of the anchor, and c_u is the undrained shear strength of the clay. The results for the breakout factor as a function of embedment ratio obtained are presented in Figures 2.22 and 2.23. From the figures, the authors discovered that the magnitude of the breakout factor increased with embedment ratio up to a limiting value (N_c^*) at which point the embedment ratio is termed the "critical embedment ratio", $(H/D)_{cr}$. The critical embedment ratio was found to be approximately 6.5 for medium to stiff clays, (c_u > 40kPa). The average value of N_c^* was

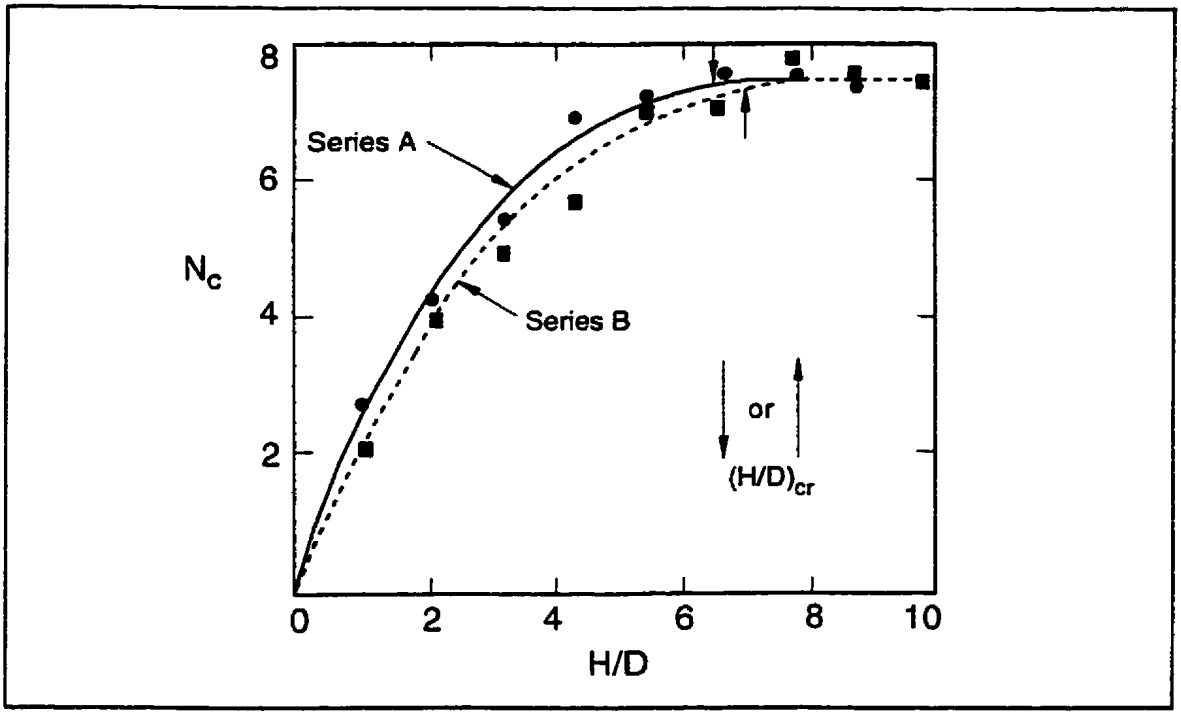

Figure 2.22 - Variation of N_c with H/D; soil type I (after Das, 1987a).

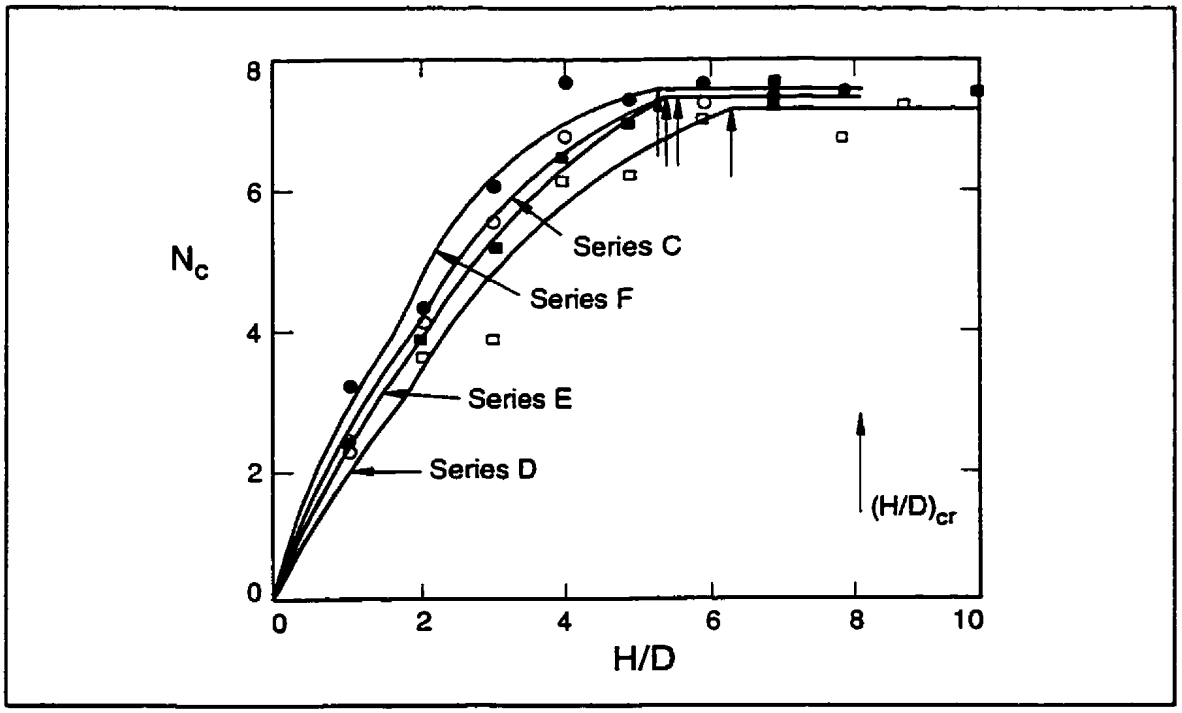

Figure 2.23 - Variation of N_c with H/D; soil type II (after Das, 1987a).

found to be approximately 7.5. Based on the results, the author presents the following formulae to describe the ultimate resistance:

$$(H/D)_{cr} = 4.31 + 55.5x10^{-3}c_u \leq 6.5; \qquad [2\text{-}51]$$

for deep anchors where $(H/D) > (H/D)_{cr}$,

$$P_{ult} = N_c^* D c_u \approx 7.45 c_u ; \qquad [2\text{-}52]$$

and for shallow anchors where $(H/D) \leq (H/D)_{cr}$,

$$P_{ult} = 7.45 c_u D \frac{(H/D)/(H/D)_{cr}}{0.42 + 0.58 [(H/D)/(H/D)_{cr}]}. \qquad [2\text{-}53]$$

The author concludes that the ultimate capacity of a vertical strip anchor can be expressed as the non-dimensional breakout factor presented above. Also, the critical embedment ratio is a function of the undrained shear strength of the clay and can be determined from the experimentally derived expression of Equation [2-51]. Finally, for deep anchors, the breakout factor reaches an ultimate value of approximately 7.5.

Comments on Centrifuge Testing

Boon and Craig (1978) state that much of the data which has been used to validate design methods for anchor plates in sand has primarily been the result of small-scale laboratory tests. The authors' concern is that scale effects might give rise to uncertainty in the extrapolation of the design methods to the full-scale field situation. The authors conducted

vertically loaded anchor plate tests in sand (plane-strain configuration) at various gravity levels ranging from 1 to 54 using a centrifuge to assess the effects of changes in stress level on the failure of an anchor. Comparison of the results with accepted methods of analysis (Meyerhof, 1973) indicated that the design of full-scale field anchors in cohesionless soil based on the results of 1g small-scale experiments may be in error due to the difference in stress levels between the two conditions. The authors conclude that the centrifuge offers a means of providing correct stress levels in the soil in order to obtain design data from the model tests.

Ovesen (1981) demonstrated that small-scale conventional (1g) model test results are subjected to scale error. The author accomplished this through small-scale uplift capacity tests and centrifuge tests on circular slabs with a diameter of 29.1mm. The author concludes that scale effects could cause errors when extrapolating model test results for the design or assessment of full-scale anchor slabs; this may result in an overestimation of anchor uplift capacities.

Dickin and Leung (1983) state that much of the work reported in the literature on the horizontal pullout resistance of vertical anchors in sand tends to be from small-scale (D = 25-100mm) laboratory tests. The authors suggest that, because of the complex behaviour of the soil, the accuracy of predicted full-scale behaviour of anchor plates based on model test data should be questioned. The authors conducted what they consider to be the first centrifuge model tests of vertical anchors subjected to horizontal pull. For comparison purposes, a

series of 1g tests were also conducted on the small-scale (D = 25mm) anchors. Comparison of results indicated overprediction of full-scale anchor resistances by direct extrapolation of small-scale results. Overpredictions as large as 80% were noted from extrapolation of results from a 1g, 25mm plate to a 1m prototype modelled in the centrifuge. The results from the centrifuge model tests were also compared with selected existing theories and most of the theories yielded somewhat reasonable agreement including the results of Rowe and Davis (1982b). The authors conclude that a more reliable design methodology for full-scale anchor plates would result from centrifuge model tests. Rowe (1984) suggests that, based on the data provided by Dickin and Leung (1983), the design charts published by Rowe and Davis (1982b) can be used to obtain a convenient and reasonably accurate method to assess anchor capacity. Rowe (1984) also suggests that for situations where the capacity of anchor plates is critical, centrifuge model tests may play an integral part in the design process.

Dickin and Leung (1985) compared the results from existing design methods and centrifuge model tests (Dickin and Leung, 1983) on vertical anchor plates in dense sand. The authors concluded that a number of design theories yielded acceptable agreement with observations for shallow continuous anchor plates ($H/D < 6$). However, theoretical analyses for deep anchor plates yielded a wide range in predictions (especially in dense sand) and tended to overpredict measured horizontal anchor capacity.

2.4.2 Pile/Soil Interaction

Vertical piles resist lateral loads by deflecting and transferring the load to the adjacent soil. It appears reasonable to consider a pipeline as a short, stiff, fixed-head (no rotation) pile in analysing pipeline/soil interaction to determine both the p-y curve and the ultimate load on the pipeline. Poulos and Davis (1980) state that two criteria must be satisfied in the design of piles subjected to lateral load. The first is that the factor of safety against ultimate failure must be adequate and the second is that the deflection at working loads must be acceptable. Prakash and Sharma (1990) suggest that methods of calculating the lateral resistance of vertical piles can be broadly divided into two categories: (1) methods of calculating the ultimate lateral resistance; and (2) methods of calculating deflection at working load.

Several methods of determining the ultimate lateral resistance of a vertical pile are found in the literature, the most common being those of Hansen (1961) which can be applied to c, ϕ, and c-ϕ soils and Broms Method (Broms, 1964a; Broms, 1964b) which can only be applied to c or ϕ soils. Both of these methods are suggested as means to determine the ultimate resistance by the Canadian Foundation Engineering Manual (1992).

Methods of calculating the pile deflection at working load suggested in the literature include the subgrade reaction approach, the elastic continuum approach, and the p-y approach. The first two approaches treat the interaction of the pile and soil as a linear analysis and are discussed further in Chapter 8. The final approach considers the nonlinear interaction between the pile and the soil; methods of analysis are discussed in this section. The nonlinear

soil response as a pile is subjected to a lateral load is usually referred to as a p-y curve and can be evaluated based on laboratory results or backcalculated from field performance data (Canadian Foundation Engineering Manual, 1992). Prakash and Sharma (1990) suggest the method of Matlock (1970) to determine the entire p-y curve for laterally loaded piles in soft to firm clay, the method suggested by Reese and Welch (1975) to establish curves in stiff clay, and the method of Bhushan *et al.* (1979) for stiff overconsolidated clays. Reese (1990) states that the development of p-y curves for the design of offshore piles are principally based on the work of Matlock (1970) and Reese *et al.* (1975).

Ultimate Resistance

Hansen (1948) investigated the stabilizing effect of piles in clay for the case where a structure is founded on a pile foundation and the sliding surface of a slope failure intersects a number of piles similar to the condition shown in Figure 2.24. The piles will resist the movement of the soil mass along the sliding surface to an ultimate resistance. The author shows that the ultimate soil reaction for a square pile varies between $8.3c_uD$ and $11.4c_uD$ where c_u is the undrained shear strength of the clay. The author suggests the ultimate resistance for a round pile should be taken as

$$P_{ult} = 10\ c_u\ D \qquad [2\text{-}54]$$

where D is the pile diameter.

Poulos and Davis (1980) considered the ultimate lateral resistance of relatively slender

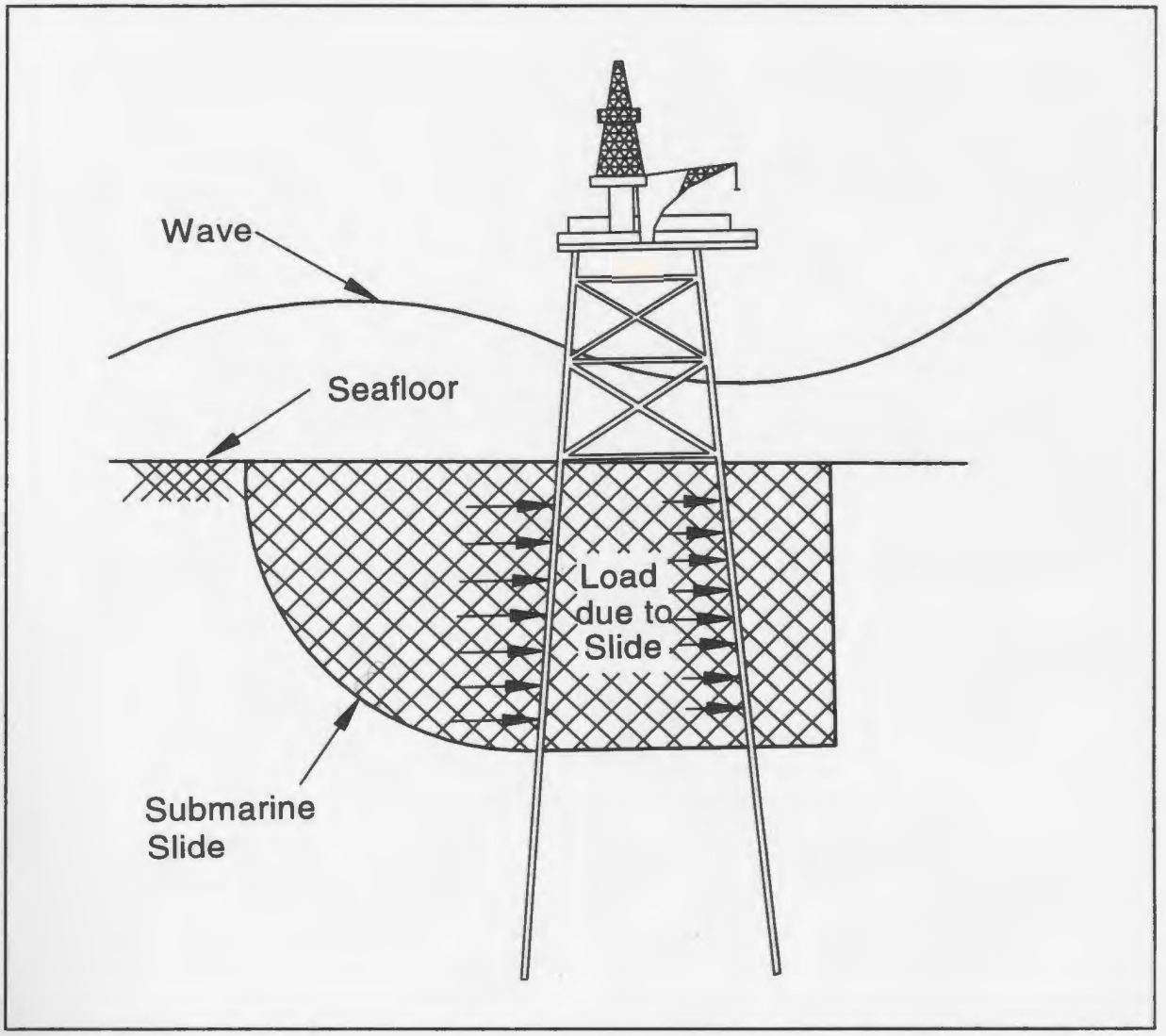

Figure 2.24 - The problem of forces on piles due to lateral soil movements (after Poulos, 1988).

vertical piles having negligible base resistance where either the soil fails or the pile fails. In a purely cohesive soil, the authors suggest that the ultimate lateral resistance, P_{ult}, increases from the soil surface to a finite value at a depth of approximately 3D where D is the pile diameter. The authors suggest that, at this depth, plasticity theory can be used to determine P_{ult} as the failure involves plastic flow of soil around the pile in the horizontal plane only. The ultimate resistance of the soil can be expressed as

$$P_{ult} = N_c \, c_u \, D \qquad [2\text{-}55]$$

where c_u is the cohesion of the soil, N_c is the lateral resistance factor which depends on the shape of the pile section, and the ratio of pile adhesion to soil cohesion, c_a/c. Figure 2.25 presents the distribution of lateral resistance suggested by Poulos and Davis (1980) for an unrestrained (free-headed) pile while Figure 2.26 presents values of N_c obtained from plasticity theory as a function of pile shape and c_a/c. The authors also suggest that the lateral resistance at depth in purely cohesive soil can usually be taken as $9c_uD$ regardless of the shape of the pile and value of c_a/c. Others have also suggested the same value (i.e. Broms, 1964a; Wolters, 1973; Poulos, 1988).

Hansen (1961) derived the ultimate lateral soil resistance of rigid piles, with width D, against transversal soil forces. The method proposed by the author is based on active and passive earth pressure theory and applies to the general case of a $c - \phi$ soil. The author assumes that the pile will not fail and will rotate as a rigid body about a point at a certain depth. The differences in failure mechanisms at various depths was taken into consideration during derivation of ultimate resistance. The ultimate pressure per unit area at depth, Z, was expressed as

$$P_{ult} = q \, N_\gamma \, D + c_u \, N_c \, D \qquad [2\text{-}56]$$

where q is the vertical effective overburden pressure and N_γ and N_c are constants that are a function of ϕ and Z/D. These constants are presented in Figure 2.27. The author claims that

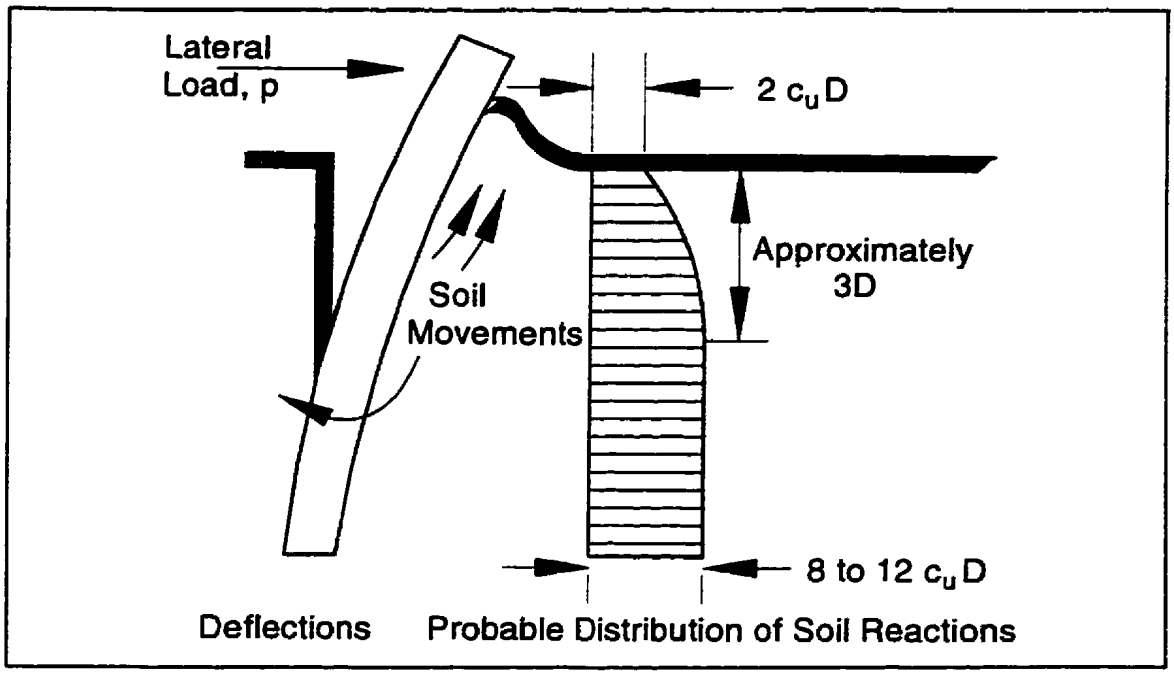

Figure 2.25 - Distribution of lateral resistance (after Poulos and Davis, 1980).

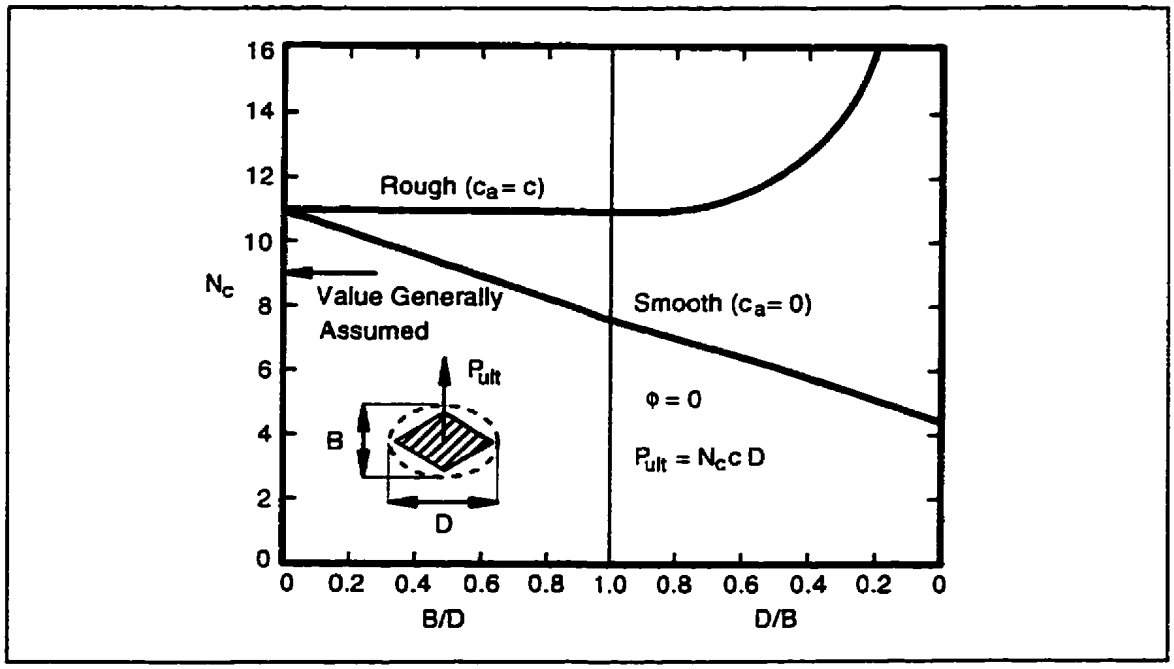

Figure 2.26 - Effect of aspect ratio and adhesion ratio on lateral resistance for a purely cohesive soil (after Poulos and Davis, 1980).

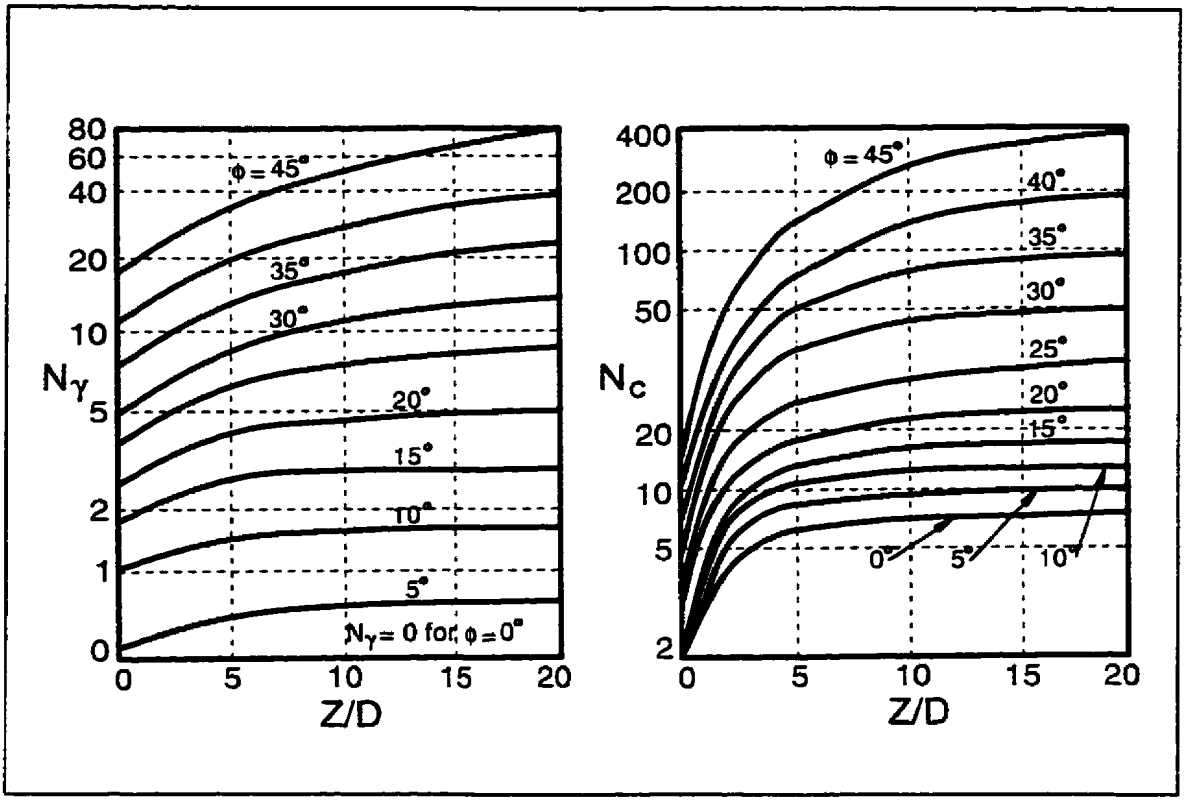

Figure 2.27 - Coefficients N_γ and N_c for laterally loaded piles (after Prakash and Sharma, 1990).

this method will enable a quick and direct determination of the lateral load on a pile.

Christian (1961) carried out a series of tests on wooden piles in sand to investigate the validity of the theory presented by Hansen (1961). Twenty-six tests were conducted on square piles (5cm by 5cm) buried to depths of 25 and 50cm and with horizontal loads placed 5 and 22.5cm above the sand surface. The tests were conducted in both loose and dense sand and the piles were either driven into the sand or were placed in position before pouring the sand. The author concludes that Hansen's (1961) theory gives a reasonable (although a little conservative) approximation to the test results provided that ϕ is taken as corresponding to

a plane-strain condition.

Broms (1964a) considers the ultimate lateral resistance of both free- and fixed-head piles driven in cohesive soils. During lateral movement of the pile, soil close to the ground surface (to a depth of approximately 3 pile diameters) is considered to move in an upward direction away from the pile while deeper soil moves laterally from the front to the rear of the pile. The ultimate lateral resistance was defined as "the failure which takes place when the lateral resistance of the supporting soil is exceeded along the total length of the laterally loaded pile". The author presents data on the lateral resistance of free-headed piles, based on plasticity theory, which varied from 8.28 to $12.56c_uD$, the actual value of which depends on roughness and shape of the pile. The value $9.14c_uD$ is presented for smooth, circular piles. The case for a short restrained pile is depicted in Figure 2.28a and the corresponding soil reaction is shown in Figure 2.28b. The author assumes that the lateral soil reaction is equal to zero to a depth of 1.5 pile diameters and equal to $9c_uD$ below this depth where D is the pile diameter. The ultimate lateral resistance can then be calculated from

$$P_{ult} = 9\ c_u\ D\ (L - 1.5D) \qquad [2\text{-}57]$$

where P_{ult} is the ultimate lateral resistance and L is the pile length. The distribution of ultimate soil reaction (both free-head and restrained) is shown in Figure 2.29.

p-y Approach

Matlock (1970) suggests that soil resistance to laterally loaded piles may be a highly

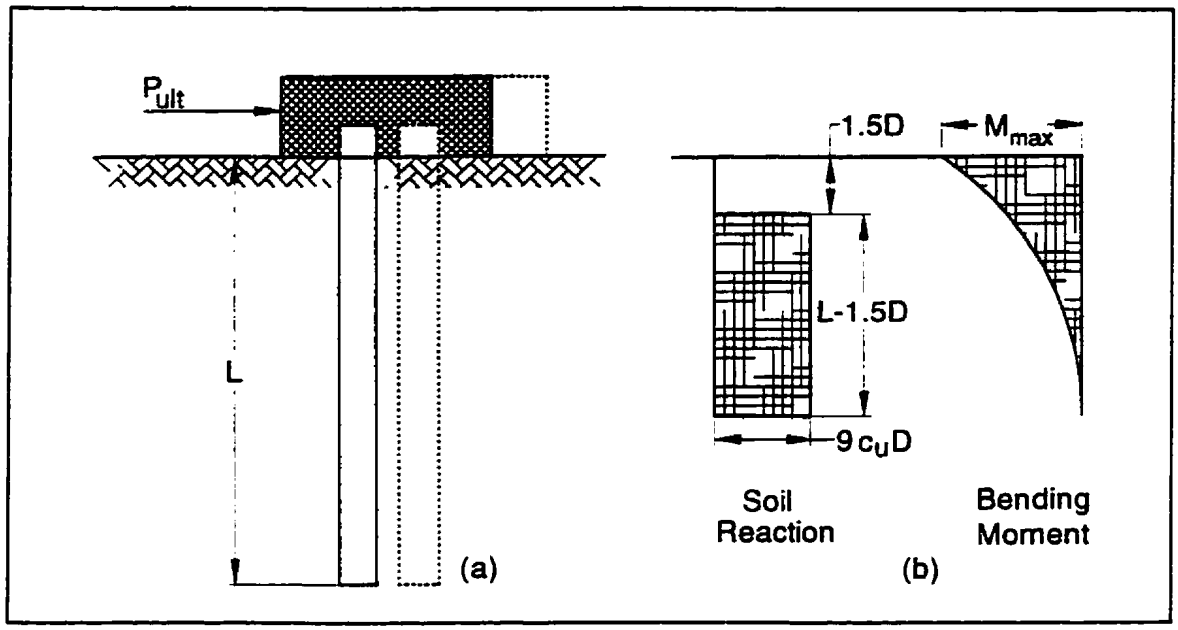

Figure 2.28 - Short pile under lateral loads in cohesive soil: (a) translational movement for a fixed head pile; (b) soil reaction and pile bending moment (after Prakash and Sharma, 1990).

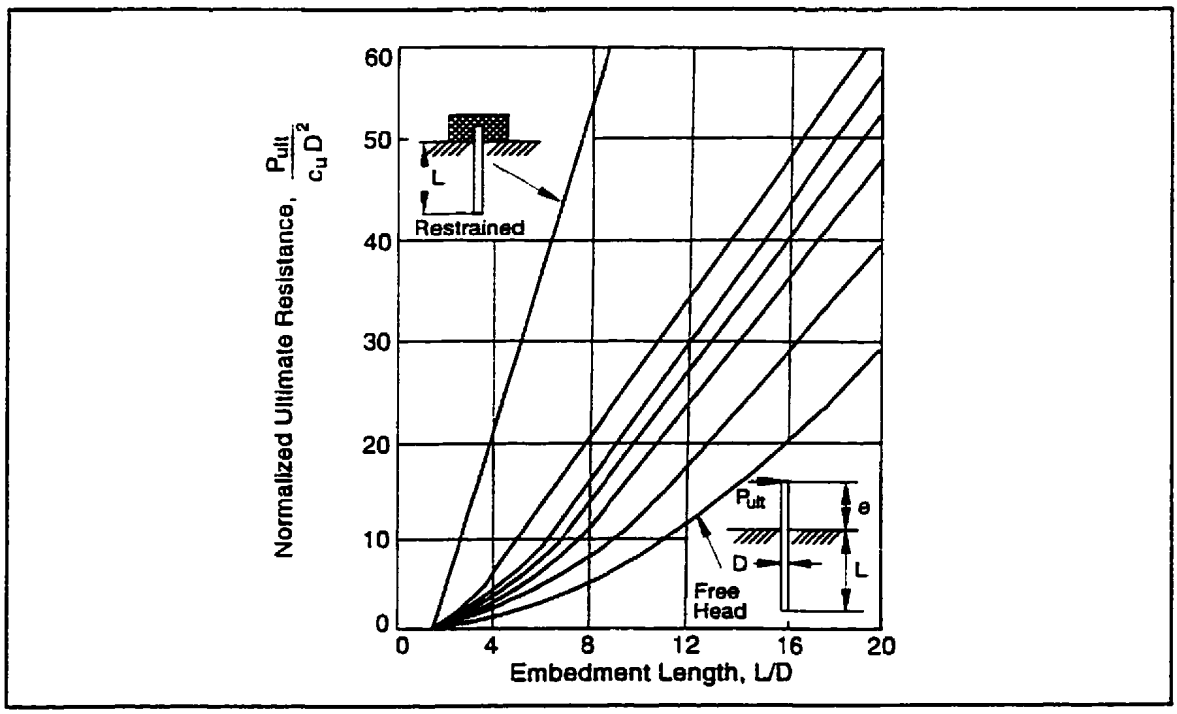

Figure 2.29 - Ultimate load capacity of short piles in cohesive soils (after Prakash and Sharma, 1990).

nonlinear function of the deflection and that a difficult part of the design of such piles is the determination of the soil resistance characteristics (p-y curves). The author states that the p-y curve is influenced by, among other things, the general form of the pile deflection, the variation of soil properties with depth, and the state of stress and strain throughout the affected soil zone.

A research program was conducted to investigate the short term static behaviour of laterally loaded piles. The program involved model tests in the laboratory, field testing with an instrumented pile, and development of analytical methods and correlations. The field load tests were conducted with a steel pile, 12.75 inches in diameter, with an embedded length of 42 feet. The pile was instrumented with strain gauges and loading (both free and restrained head) was achieved through a hydraulic ram. Testing was conducted at two sites, both in clay, the first with an undrained shear strength of 38kPa and the second with an undrained shear strength of 14kPa. The experimental field p-y curves were used as the principal basis for a methodology for development of p-y curves presented by the author.

Matlock (1970) proposes that the ultimate resistance per unit length of pile may be expressed as

$$P_{ult} = N_c \, c_u \, D \qquad [2\text{-}58]$$

where D is the pile diameter, c_u is the soil strength, and N_c is a non-dimensional ultimate resistance coefficient. The author suggests that N_c varies from a value of 3 at the soil surface

to the ultimate value of 9 at a critical depth below the ground level, Z_{cr}, for a cylindrical pile. For the case where the soil strength and effective unit weight, γ, are constant with depth, Z_{cr} can be calculated from

$$Z_{cr} = \frac{6\ D}{\frac{\gamma\ D}{c_u} + J} \qquad [2\text{-}59]$$

where J is a factor which is determined empirically. Matlock (1970) suggests a J value of 0.5 for soft clay and a value of 0.25 for stiffer clays. The variation of N_c with depth can be described by the following equations:

$$N_c = 3 + \frac{q}{c_u} + J\frac{Z}{D} \qquad [2\text{-}60]$$

for $Z < Z_{cr}$, and

$$N_c = 9 \qquad [2\text{-}61]$$

for $Z \geq Z_{cr}$ where q is the overburden pressure and Z is the depth below the ground surface.

To construct the p-y curve as shown in Figure 2.30 at a particular depth, the ultimate resistance must first be calculated using the method described above. The point y_c is the deflection where the lateral resistance is 50% of P_{ult} and is determined from

$$y_c = 2.5\ \varepsilon_c\ D \qquad [2\text{-}62]$$

where ε_c is one-half the strain at maximum stress from a laboratory stress-strain curve

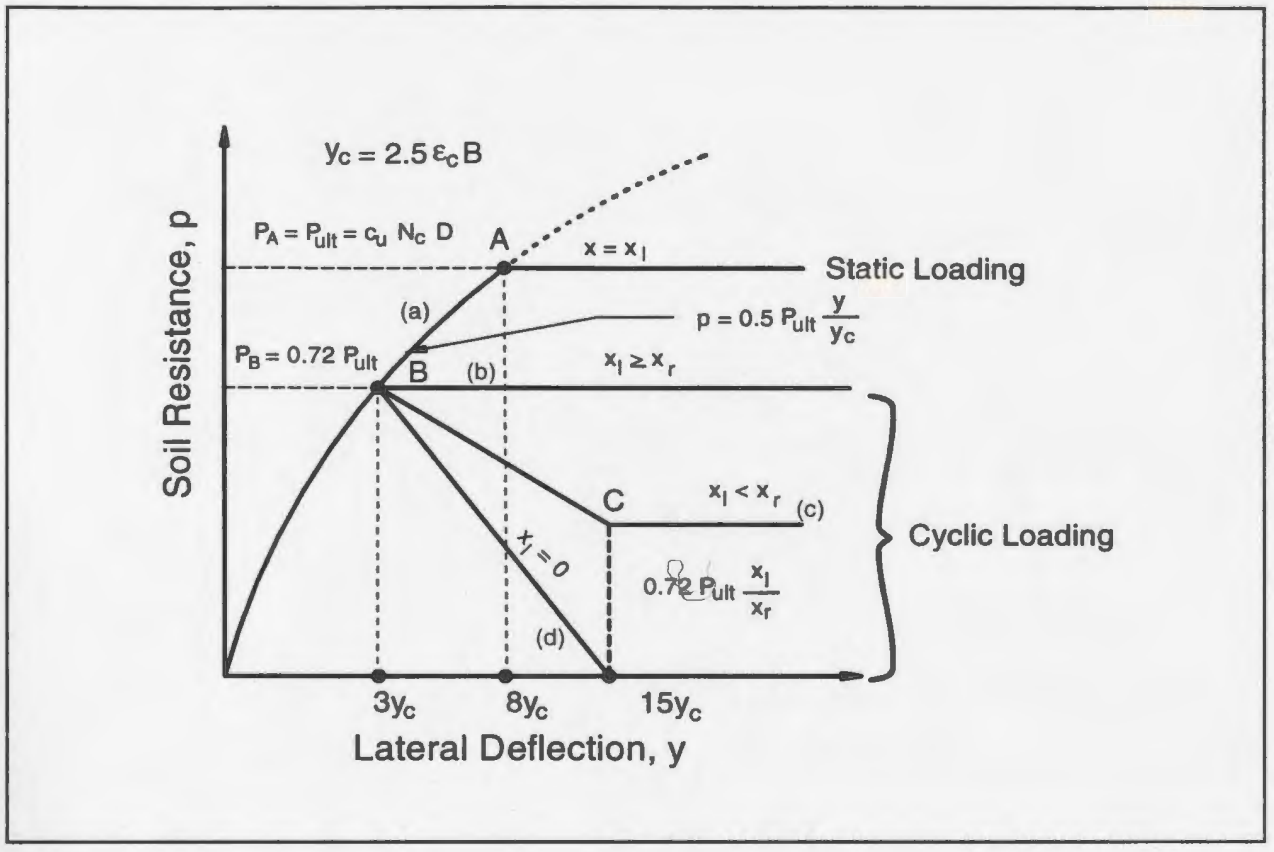

Figure 2.30 - Establishing the p-y curve for soft to firm clay (after Prakash and Sharma, 1990).

determined from undrained triaxial compression tests. The lateral deflection at the ultimate soil resistance is equal to $8y_c$. Matlock (1970) suggests that, in the absence of laboratory tests, a value of ε_c may be assumed to be 0.005 for brittle and sensitive clays and 0.020 for remoulded soils or unconsolidated sediments. The author also suggests a value of 0.010 is probably satisfactory for most purposes. The shape of the p-y curve is expressed by the equation

$$p = 0.5\ P_{ult}\ [\frac{y}{y_c}]^{\frac{1}{3}}. \qquad \text{[2-63]}$$

Matlock (1970) compared the bending moment distributions from the field tests with predicted distributions using p-y curves estimated from the methods presented above and found good comparison. The author concludes that a satisfactory correlation was established for short-term static loadings and the procedure can be applied to pile design in submerged clay soils which are naturally consolidated or slightly overconsolidated.

To develop p-y curves for laterally loaded piles in stiff clay, it is suggested in the literature (i.e. Prakash and Sharma, 1990; Poulos and Davis, 1980) that the method proposed by Reese and Welch (1975) be used. Reese and Welch (1975) suggested that the ultimate soil resistance to a laterally loaded pile shaft would be the smaller of the values obtained from

$$P_{ult} = (3 + \frac{q}{c_u} + 0.5\frac{Z}{D})\, c_u\, D \qquad [2\text{-}64]$$

and

$$P_{ult} = 9\, c_u\, D \qquad [2\text{-}65]$$

where q is the overburden pressure from the soil surface to depth Z, c_u is the average undrained shear strength from the soil surface to depth Z, and D is the width of the pile. The points describing the p-y curve for y less than $16y_c$ are determined from

$$p = 0.5\, P_{ult}\, (y/y_c)^{\frac{1}{4}} \qquad [2\text{-}66]$$

and for y greater than $16y_c$

$$p = P_{ult}. \qquad [2\text{-}67]$$

The constant, y_c, is determined from

$$y_c = 2.5\ D\ \varepsilon_c \qquad [2\text{-}68]$$

where, as before, y_c is the deflection at $0.5P_{ult}$ and ε_c is the strain at one-half the maximum principal stress resulting from a laboratory undrained triaxial compression test.

To develop p-y curves for laterally loaded piles in stiff, overconsolidated clay, Prakash and Sharma (1990) suggest the method proposed by Bhushan *et al.* (1979) be used. The method is similar to that described above for stiff clays but Equations [2-64], [2-66], and [2-68], respectively are replaced by

$$P_{ult} = \left(3 + \frac{q}{c_u} + 2\frac{Z}{D}\right) c_u\ D \qquad [2\text{-}69]$$

and

$$p = 0.5\ P_{ult}\ (y/y_c)^{\frac{1}{2}} \qquad [2\text{-}70]$$

and

$$y_c = 2\ D\ \varepsilon_c. \qquad [2\text{-}71]$$

Comments on Centrifuge Testing

Numerous lateral pile/soil interaction investigations have been successfully carried out in the centrifuge (i.e. Nunez *et al.*, 1988; Hamilton *et al.*, 1991). Researchers have concluded that the geotechnical centrifuge offers a useful alternative to field tests for studying the lateral resistance behaviour of piles as results from laterally loaded pile investigations were shown to agree well with predictions using established analyses. Results of centrifuge tests have also been validated by verifying the model scaling laws through modelling of models tests at different "g" levels which have been shown to provide close agreement when prototypes were compared (Nunez *et al.*, 1988; Hamilton *et al.*, 1991).

One test program where good agreement was obtained between centrifuge and large-scale field testing for laterally loaded piles was reported by Wesselink *et al.* (1988). The authors reported on laterally loaded pile tests performed in calcareous sand in support of offshore platform strengthening efforts. These tests were conducted as there were no relevant performance data available for this type of soil and the behaviour of the strengthening system was sensitive to the lateral stiffness of the foundation piles. Onshore pit tests on 0.356m diameter piles were conducted with the same reconstituted sand to provide a tie to the full-scale piles and to verify the centrifuge modelling. Using the p-y curves developed in the centrifuge study, a prior prediction of the field testing provided results to within 15% of the pit test results.

2.5 Summary of Literature Review

A review of the literature has indicated that both offshore and onshore pipelines are potentially subject to rapid and slow rates of lateral loading due to the movement of soil relative to the pipeline. These movements may be due to gravity effects or they may be the result of seismic activity and rates of ground movements can vary from several millimetres per year to several metres per second. These soil movements in the vicinity of the pipeline can cause excess stress and strain in the pipeline which can lead to failure. To prevent failure, remediation techniques can be employed (where possible) at significant expense.

In most analytical models used to evaluate pipeline/soil interaction, the pipeline is represented as a beam or a cable. The beam is assigned appropriate material and section properties to model the behaviour of the pipeline. This beam is generally connected to a series of discrete nonlinear springs to simulate the soil reactions. The characteristics of the soil springs which are input to the program defines the amount of loading or restraint subjected to the pipeline for a given displacement. Parameters describing the interaction curves or soil springs are commonly input to the computer based programs to determine the stress or strain states of the pipe with regards to soil displacement and to determine the point where remedial action need be taken. Pipeline response to large horizontal soil movements can be determined from such computer based analyses and provide a basis for design.

There are a number of suggested and potential methods to determine the ultimate load or force-displacement (p-y) curves for pipelines in the literature. Formulations discovered

during the current literature review are presented in Table 2.3. Many of those methods have been based on other soil/structure interaction studies (e.g. anchors plates and piles). There is little pipeline-specific theoretical or experimental results available to compare with and validate accepted methods. The experimental results which are available tend to be small in scale and may not be confidently extrapolated to the full-scale for design or analysis purposes. Investigations in the literature also give no consideration for the geometry of the problem in the case where a pipeline must be trenched and backfilled. Most of the experimental pipeline studies in the literature were conducted in sand and very little consideration has been given to the problem in cohesive soils. Those methods which do consider cohesive soils generally use undrained shear strength in the analysis which may not be appropriate for slow rates of loading. In summary, there is a lack of information regarding the true lateral force-displacement or p-y curves for pipelines in cohesive soils.

Table 2.3 - Summary of existing and potential lateral pipeline/soil interaction methods

Reported By	Proposed Formulation	Basis	Comments
Luscher *et al.* (1979)	$P_{ult} = \frac{1}{2} \gamma' H^2 K_p A$	Rankine passive earth pressure.	For granular soils where H is the depth of the trench and A is a "load reduction" factor.
Luscher *et al.* (1979)	$P_{ult} = N_c c_u D$	Lateral resistance of deadman anchorages.	For cohesive soils. N_c is a lateral resistance coefficient based on the works of Mackenzie (1955).
ASCE (1984)	$P_{ult} = \gamma' h N_\gamma D$	Laterally loaded piles and vertical plate anchors subjected to horizontal load.	For granular soils. N_γ is a horizontal bearing capacity factor based on the works of Hansen (1961) or Ovesen and Stromann (1972).
ASCE (1984)	$P_{ult} = c_u N_c D$	Laterally loaded piles.	For cohesive soils. N_c is a horizontal bearing capacity factor based on the works of Hansen (1961).
Rizkalla *et al.* (1992)	$P_{ult} = D c_u N_c$	Laterally loaded anchor plates.	For cohesive soils. N_c is an interaction factor based on the works of Rowe and Davis (1982a).
Ranjani *et al.* (1993)	$P_{ult} = 0.5 \gamma K_p (H^2 - C^2)$	Passive earth pressure.	For frictional soil where H is the depth to the base of the trench and C is the soil cover above the pipe.
Ranjani *et al.* (1993)	$P_{ult} = N_c c_u D$	Laterally loaded anchor plates.	For cohesive soils. N_c is an interaction factor based on the works of Rowe and Davis (1982a).
Edgers and Karlsrud (1982)	$P_{ult} = N_c c_u D$	Laterally loaded piles.	For cohesive soils. N_c is a bearing capacity coefficient generally empirically determined.
Edgers and Karlsrud (1982)	$F_D = \frac{1}{2} C_D \rho A v^2$	Hydrodynamic drag on a submerged object.	C_D is the drag coefficient, ρ is the density of flow, A is the projected area, and v is the velocity of the flow.

Table 2.3 cont... - Summary of existing and potential lateral pipeline/soil interaction methods

Reported By	Proposed Formulation	Basis	Comments
Audibert and Nyman (1977)	$P_{ult} = \gamma\ h\ N_\gamma\ D$	Small-scale laboratory tests.	For granular soils. N_γ is a horizontal bearing capacity factor based on the works of Hansen (1961).
Wantland *et al.* (1982)	$P_{ult} = N_c\ c_{u\text{-}avg}\ D$	Small-scale field and laboratory tests.	For cohesive soils. $c_{u\text{-}avg}$ is the average cohesion for a distance 2D above the pipeline invert.
Trautman and O'Rourke (1985)	$P_{ult} = \gamma\ h\ N_\gamma\ D$	Small-scale laboratory tests.	For granular soils. N_γ is a horizontal bearing capacity factor based on the works of Ovesen and Stromann (1972).
Ng (1994)	$P_{ult} = N_c\ c_u\ D$	Field tests and finite element analyses.	For cohesive soils. N_c is a horizontal bearing capacity factor based on the works of Hansen (1961).
Dickin (1988)	$P_{ult} = \gamma\ h\ N_\gamma\ D$	Centrifuge model testing of vertical anchor plates and pipelines.	For granular soils. N_γ is a horizontal bearing capacity factor based on the works of Ovesen and Stromann (1972).
Mackenzie (1955)	$P_{ult} = \sqrt{\frac{D}{H}}\ \left[\ \frac{\gamma\ H^2}{2} + 2\ H\ c_u\ \right]$	Small-scale deadman anchor tests.	For cohesive soil. H is the depth to the base of the anchor.
Mackenzie (1955)	$P_{ult} = 8\ D\ c_u$	Small-scale deadman anchor tests.	For cohesive soils. This is a limiting condition on the above equation.
Tschebotarioff (1973)	$P_{ult} = N_c\ c_u\ D$	Reanalysis of the Mackenzie (1955) data.	For cohesive soils. N_c comes from the Mackenzie (1955) data.

Table 2.3 cont... - Summary of existing and potential lateral pipeline/soil interaction methods

Reported By	Proposed Formulation	Basis	Comments
Rowe and Davis (1982a)	$P_{ult} = c_u F_c' D$	Finite element analyses of horizontally loaded vertical anchor plates.	For cohesive soils. F_c' is a function of embedment ratio.
Rowe and Davis (1982b)	$P_{ult} = c' F_c' + \gamma' H F_\gamma'$	Finite element analyses of horizontally loaded vertical anchor plates.	For c-ϕ soils. F_γ' is a function of internal angle of friction and embedment ratio.
Das *et al.* (1985); Das (1987)	$P_{ult} = N_c D c_u$	Small-scale laboratory tests on horizontally loaded vertical anchor plates.	For cohesive soils. N_c is based on experimental results.
Dickin and Leung (1983)	$P_{ult} = \gamma' H F_\gamma'$	Centrifuge model tests.	For cohesionless soils. Formulation is based on the works of Rowe and Davis (1982b).
Hansen (1948)	$P_{ult} = 10 c_u D$	Stabilizing effect of piles in clay.	For cohesive soils.
Poulos and Davis (1955)	$P_{ult} = N_c c_u D$	Laterally loaded piles.	For cohesive soil. N_c is a function of pile shape and ratio of pile adhesion to soil cohesion.
Hansen (1961)	$P_{ult} = q N_\gamma D + c_u N_c D$	Laterally loaded piles.	For c-ϕ soils. N_γ and N_c are a function of embedment ratio and soil angle of internal friction.
Matlock (1970); Reese and Welch (1975); Bhushan *et al.* (1979)	$P_{ult} = N_c c_u D$	Laboratory and field tests on laterally loaded piles.	For cohesive soils. N_c varies from 3 at the soil surface to a maximum value of 9 at a critical depth. Different formulations for soft, stiff, and stiff overconsolidated clays.

Chapter 3

Research Objectives and Scope

3.1 Problem Definition

A review of the literature has indicated that there are a number of suggested methods for pipeline/soil interaction design and analysis. Most of the methods utilize parameters borrowed from other geotechnical analyses such as anchors plates and piles. There is little pipeline-specific theoretical or experimental results available to compare to and validate accepted methods. The experimental results which are available tend to be small in scale and may not be confidently extrapolated to the full-scale for design or analysis purposes. Investigations in the literature also give no consideration for the geometry of the problem in the case where a pipeline must be trenched and backfilled. Most of the experimental pipeline studies in the literature were conducted in sand and very little consideration has been given to the problem in cohesive soils.

Several difficulties arise in undertaking either physical or numerical modelling studies of lateral pipeline/soil interaction as presented by Rizkalla *et al.* (1992). Figure 3.1 shows a laterally displaced pipeline and indicates the various aspects of the problem that presents modelling complexities. As the pipeline moves, the soil behind the pipeline may separate from the back of the pipe or move with it which presents a modelling consideration. The soil

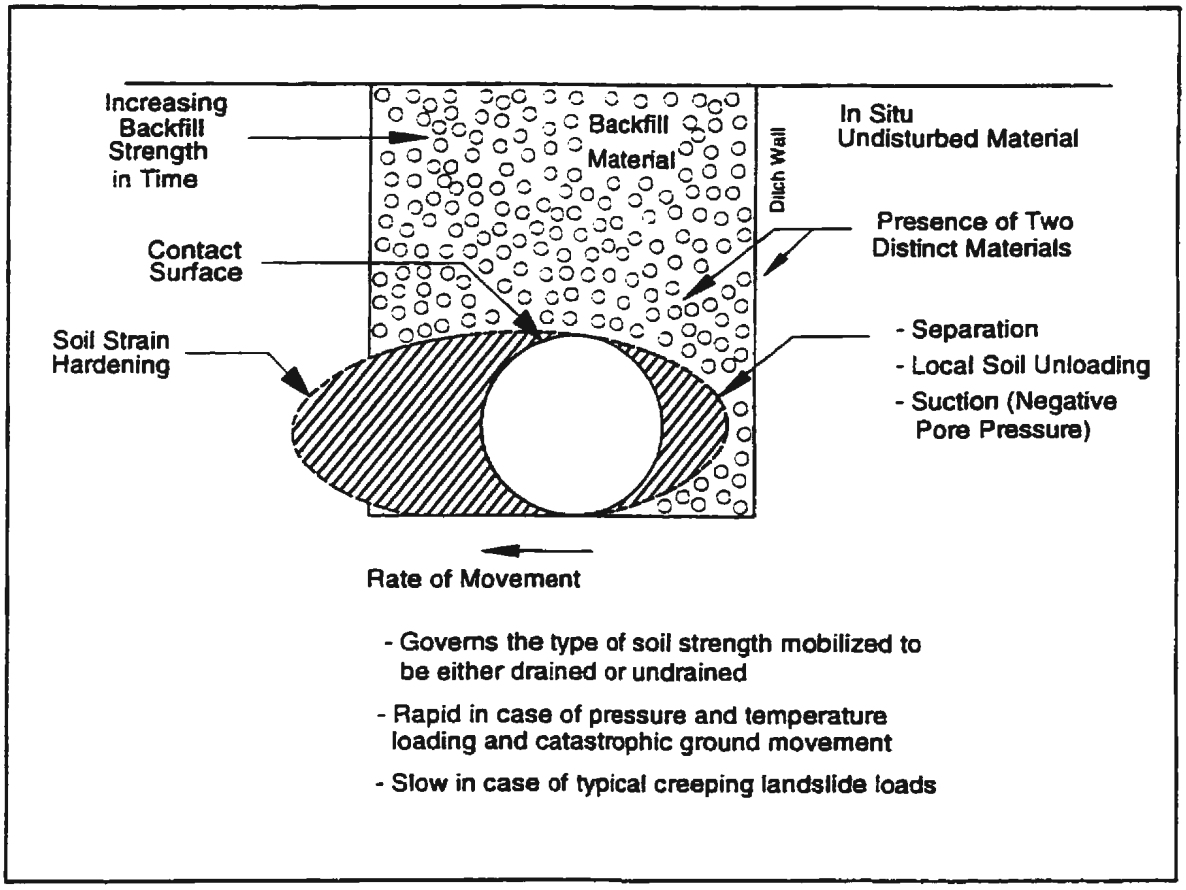

Figure 3.1 - Aspects of lateral pipeline/soil interaction that present modelling difficulties (after Rizkalla et al., 1992).

strain hardening or softening in front of the pipe poses varying degrees of modelling difficulties. These aspects may also be a function of the rate of pipeline displacement against the soil which must also be considered. To model the behaviour of the soil as closely as possible under prototype-scale stress levels, the physical modelling technique of centrifuge modelling can be utilized.

3.2 Research Objectives

Within the general confines of lateral pipeline/soil interaction, the objectives of the research

outlined in this document are to:

(1) Conduct physical model analyses of lateral pipeline/soil interaction to ascertain the effects of trench width, burial depth, interaction rate, backfill properties, and stress history of the soil on the interaction.

(2) Within the physical model analysis, conduct a modelling of models study to ensure the results correspond and therefore can be confidently extrapolated to full-scale.

(3) Generate solutions to the physical model lateral pipeline/soil interaction problem studied above using accepted methods of pipeline/soil interaction analysis found in the literature.

(4) Generate solutions to the physical model lateral pipeline/soil interaction problem studied above using conventional soil mechanics methods.

(5) Compare and contrast the solutions generated using the above methods.

(6) Generate conclusions and recommendations regarding the methods of analysing lateral pipeline/soil interaction presented in the thesis.

3.3 Scope of the Research

The work will quantify the normalized force-displacement response of pipelines through the use of physical modelling. The proposed research considers only the case of a pipeline which is subjected to lateral loading in cohesive soils with cohesive and cohesionless backfills. The interaction is considered to be two-dimensional. The mechanical response of the pipeline will not be considered but rather the pipeline used in the research will be rigid to satisfy the requirements of plane-strain interaction. No attempt is made to model actual field soil

conditions but rather accepted modelling soils will be used to generate generic solutions to the problem. The parameters to be investigated during the physical model analysis will be a limited variation in trench width, burial depth, interaction rate, backfill properties, and stress history of the soil.

The focus of the research is on the physical modelling aspect. However, for the results to have meaning, they must be compared to some benchmark. Therefore, the results will be compared to those obtained through accepted methods of pipeline/soil interaction analysis in the literature and methods developed during the analysis of model data.

Chapter 4

Overview of Centrifuge Modelling

4.1 Introduction

Centrifuge modelling has been shown (e.g. Schofield, 1980; Murff, 1996) to be a useful technique for modelling gravity dependent phenomena. Centrifugal acceleration is used to simulate gravity and allows for correspondence of stress fields between model and full-scale, permitting accurate modelling of geotechnical and tectonic phenomena. Such accurate modelling increases general understanding and permits calibration and verification of numerical and theoretical models of full-scale situations. The use of centrifuge modelling in countries where it is more established has had considerable impact on the state-of-practice of engineering and physical science. A number of centrifuge modelling facilities are available for use in North America and more are planned so that engineers and scientists can have access to centrifuge modelling facilities.

4.2 Basis for the Use of Centrifuge Modelling

Many mechanical processes which occur in the lithosphere are significantly affected by the Earth's gravitational acceleration. These processes include soil mechanics, plate tectonics, ice mechanics, ocean dynamics and many others. The study of these phenomena can be

undertaken in a variety of ways, including analytical, numerical and experimental. Each of these methods has its limitations.

An analytical study is perhaps the most attractive method of analysis, in that it provides a mathematical description of a problem. This method is limited by the necessity of assembling a set of equations that faithfully describe the process in question and the applied loading and boundary conditions. In general, only solutions to highly idealized problems may be obtained (with simple constitutive models and boundary conditions).

Numerical modelling permits the solution of more complicated boundary condition problems in that a large problem with a complex boundary is approximated by several smaller problems with simple boundaries. This has resulted in the popularity of numerical modelling, and in particular, finite element modelling for the solution of real engineering problems. However, the limitations with material description equations remain, and some new limitations arise because of the computational technique itself (such as numerical instability). The casual use of numerical modelling for engineering design can be misleading, because a solution can be obtained which predicts allowable stresses and deformations and yet is incorrect (because of an error or oversimplicity in describing the material or the boundary conditions, or because of limitations imposed upon the calculation by the author of the code). Thus numerical modelling solutions for phenomena about which there is little knowledge require corroboration by other means.

Experimental investigations involve full-scale observations or small-scale modelling of phenomena. Full-scale observation should be the best way of gaining an understanding of a problem; however, difficulties with control, making measurements and time considerations (i.e. phenomena of long duration or phenomena whose occurrences are unpredictable) not to mention cost, restrict repeated full-scale observations for many types of events.

Small-scale modelling of a full-scale prototype offers advantages in that the model may be constructed more easily, thus saving time and money, and the model test may be conducted in a controlled environment. However, for a model test to have practical significance, similarity of significant parameters must be maintained between the model and the full-scale prototype; small-scale modelling at 1 gravity has limitations. If the material to be modelled has a linear stress-strain response (such as steel in its elastic range) then correspondence between model and prototype occurs; however, for these conditions, numerical or analytical solutions often suffice and are less expensive than physical modelling. If a nonlinear material response is being investigated (such as soil), the results of small-scale modelling are often only qualitatively applicable to the full-scale. This is because the ratio of stresses (due to self-weight) to strength is different for the model and full-scale prototype. Attempts to maintain a similarity in this ratio generally require the use of an analogue material in the model. This does not usually scale all of the relevant strength and stiffness properties concurrently. Hence, a decision must be made at the time of the experimental design as to which strength property will be scaled; if this decision is erroneous, or if more than one strength property is significant, the effectiveness of the small-scale 1 gravity physical modelling will be

reduced. Also, the scaled down strengths of model materials make them difficult to handle. This limits the factor by which the full-scale prototype can be reduced. The centrifuge modelling technique avoids some of these problems and can therefore be used to complement analytical studies, numerical modelling, full-scale observations and small-scale 1 gravity modelling.

4.3 Description of Centrifuge Modelling

The centrifuge modelling technique replicates gravitational effects by the centrifugal acceleration experienced by an object in circular flight (Schofield, 1980). The rationale behind this modelling approach is as follows. Consider the earth embankment shown in Figure 4.1. If a full-scale (prototype) earth structure is represented by a model manufactured of the same material to a scale of N (every linear dimension in the prototype being N times greater than in the model), then the vertical stress levels due to self-weight will be N times greater at any position in the prototype than at the corresponding point in the model. The behaviour of this model will not replicate the prototype because of the dissimilarity of stress level. However, if the model weight is increased to be N times greater than that in Earth's gravitational acceleration (g), the stress distribution between prototype and model will be identical as shown in Figure 4.2. The model weight is increased by placing the model under a centrifugal acceleration equivalent to N times g. If the same soil is used in model and prototype, the strain fields should also be identical, since the constitutive laws governing the soils are the same and correspondence between the stress fields is maintained. Furthermore, if any external loadings are to be added to the self-weight loading, these must be scaled so

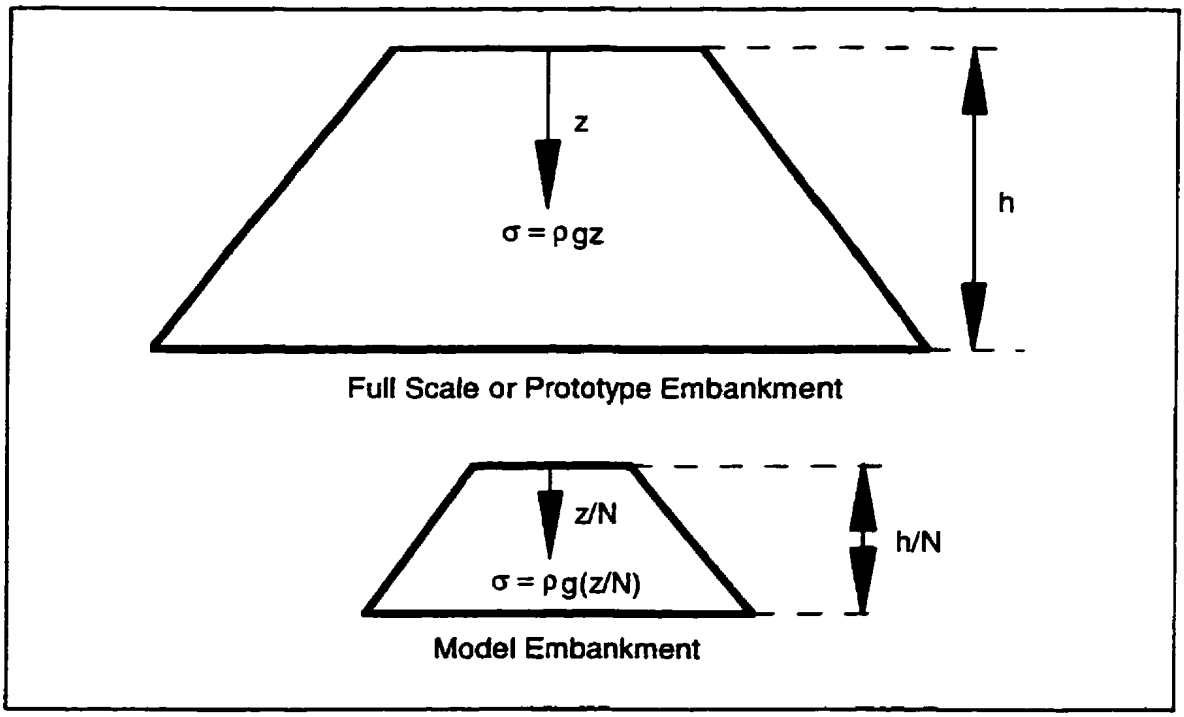

Figure 4.1 - Full-scale and 1g model embankment.

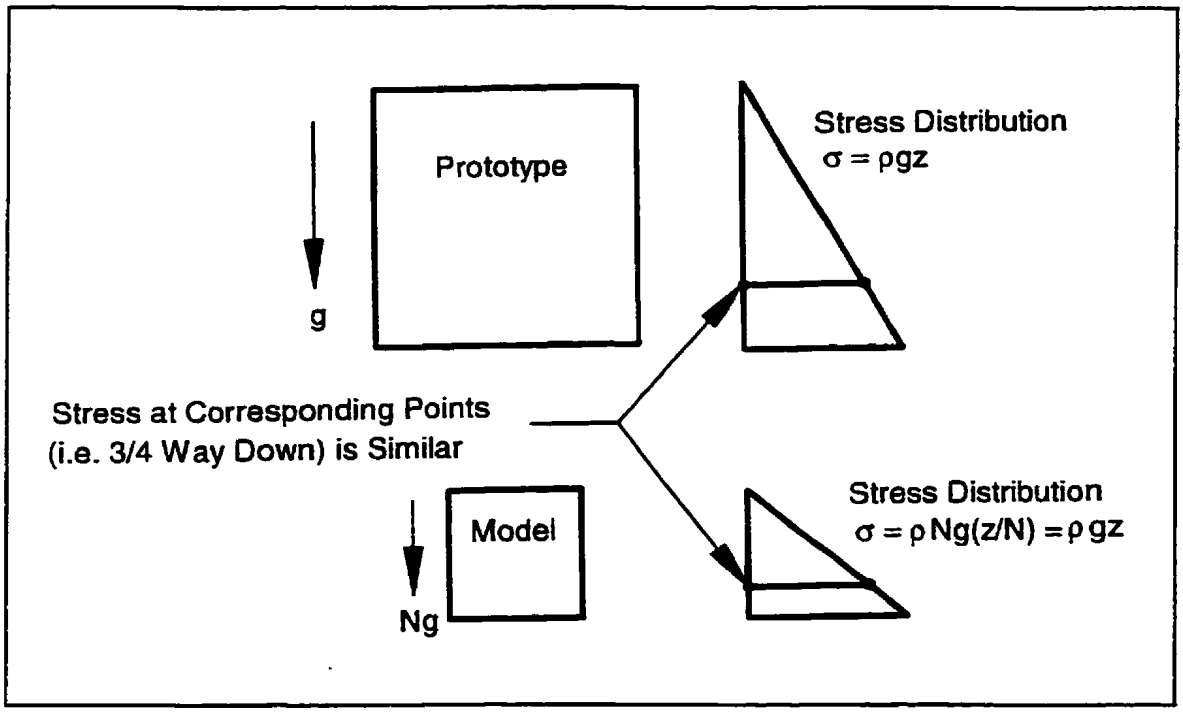

Figure 4.2 - Stress distributions in full-scale and model.

that the correspondence of stress fields is maintained. If these conditions are met, the reaction of the model to the external loading should be similar to the prototype or full-scale behaviour, and will provide a valuable understanding of the deformations and failures involved in the full-scale events.

Modelling of models is a technique whereby the applicability and accuracy of centrifuge modelling can be tested. In this technique, a full-scale phenomenon is tested at a variety of scale factors (e.g. 1/50, 1/100 and 1/200) and the scaled results are compared. If these results correspond, it indicates that the scaling has been correctly undertaken (at least within the range of gravitational accelerations chosen) and that the results should be applicable to the full-scale. If the results do not correspond, then processes which do not scale with acceleration are significant and can be identified.

4.4 Scaling Laws

All modelling requires that certain conditions be established between the model and full-scale event. Similarity rules not only establish conditions which must be satisfied during construction of the model, but also provide the relations needed to transfer the results from the model back to full-scale (Corté, 1989). These scaling laws can be derived using the techniques of dimensional analysis or by considering the explicit governing equations. Dimensional analysis can also simplify problems by reducing the number of variables to a smaller number of dimensionless parameters which can be used as guides to experimentation and can help in the presentation of results.

It is possible to derive a series of scaling factors for use in centrifuge modelling. Since the stress-strain behaviour of soil is dependent on the effective confining stress, it is desirable to make the confining stress in the model identical to that in the prototype. This can be denoted by

$$\sigma_m = \sigma_p \qquad [4\text{-}1]$$

where the subscripts "m" and "p" refer to quantities in the model and prototype respectively. If the model is built to a scale of 1/N, then, with regards to linear distances,

$$h_m = \frac{1}{N} h_p \qquad [4\text{-}2]$$

where "h" refers to any linear distance. The same type of prototype soil (of mass density ρ) is normally used in the model (when modelling a particular prototype) as the behaviour depends on the soil type. Therefore,

$$\rho_m = \rho_p \qquad [4\text{-}3]$$

Vertical stress due to self-weight in the full-scale is given by the equation

$$\sigma_p = \rho_p a_p h_p \qquad [4\text{-}4]$$

where "h" is the depth of the soil (a linear dimension) and "a" is the acceleration that the soil is subjected to (equal to 1 gravity in the prototype). Similarly,

$$\sigma_m = \rho_m a_m h_m. \qquad [4\text{-}5]$$

Substituting Equation [4-4] and [4-5] into Equation [4-1] yields

$$\rho_m a_m h_m = \rho_p a_p h_p \qquad [4\text{-}6]$$

and substituting Equation [4-2] and [4-3] into the left-hand side of Equation [4-6] results in

$$\rho_p a_m \frac{1}{N} h_p = \rho_p a_p h_p. \qquad [4\text{-}7]$$

Reducing yields

$$a_m = N a_p. \qquad [4\text{-}8]$$

Therefore, one way to ensure stress similarity between model and prototype is to increase the acceleration level to be N times greater in the model than in the prototype. This condition can be approximated by use of the centrifuge. Other scaling relationships which apply to centrifuge modelling are presented in Table 4.1.

4.5 Applications of Centrifuge Modelling; An Overview

Centrifuge modelling has led to a much better understanding of mechanical processes in which gravity is significant (e.g. Craig, 1985; Corté, 1988; Ko and McLean, 1991; Taylor, 1995). The main discipline in which centrifuge modelling has been used is in geotechnical engineering and includes soil statics, soil dynamics, cold regions studies, and environmental engineering. Examples of applications in each of these areas are load carrying capacity of

Table 4.1 - Some common centrifuge scale factors

Parameter	Scale Factor
Length	$h_m = 1/N\ h_p$
Stress	$\sigma_m = \sigma_p$
Density	$\rho_m = \rho_p$
Acceleration	$a_m = N\ a_p$
Angle of Friction*	$\phi_m = \phi_p$
Shear Strength	$(c_u)_m = (c_u)_p$
Strain	$\varepsilon_m = \varepsilon_p$
Force	$F_m = 1/N^2\ F_p$
Mass	$M_m = 1/N^3\ M_p$
Energy	$E_m = 1/N^3\ E_p$
Inertial Time	$t_m = 1/N\ t_p$
Diffusion	$t_m = 1/N^2\ t_p$

Note: Subscript **m** denotes model, **p** denotes prototype.
* - when using prototype soil.

laterally loaded piles, behaviour of dynamically loaded gravity-base structures, subsea deformation due to ice scour, and hazardous waste disposal in the seabed, respectively. Another area of application for the centrifuge is in earth sciences, for example structure formation and reservoir engineering. The results of such studies have often had an immediate and significant effect upon the state of the practice in engineering and have allowed an innovative concept to proceed with confidence.

A promising beginning has been made in the area of ice mechanics. Lovell and Schofield (1986) showed that sea ice grown in a centrifuge displayed the characteristics of real sea ice. Smith (1991) investigated the thawing of permafrost in a centrifuge and demonstrated the

suitability of the technique for many other cold regions applications. In view of the increasing amount of hydrocarbon exploitation being undertaken in cold regions such as northern Canada, the US, Europe and Russia, this is a promising new area for the application of centrifuge technology.

Theoretical studies by Zelikson (1985) and Poorooshasb (1990) showed that a certain class of hydrodynamic problems may be investigated using the centrifuge technique. If experimental results corroborate theory, the centrifuge technique will complement existing seakeeping tanks, wave tanks and hydrodynamic basins as a major tool in experimental fluid dynamics.

In structural geology, a number of experiments have been conducted in which the development of folds and faults has been investigated (Dixon 1988). The theories behind the formation of the Himalayas have also been tested (Peltzer and Garnier, 1988). These studies show that the centrifuge technique is applicable to both deep and shallow structural geology.

The above paragraphs describe the attributes of centrifuge modelling and recommend its use for a variety of applications. This does not imply, however, that centrifuge modelling should be used to the exclusion of all other methods of analysis. Any engineering or scientific analysis should consider the use of numerical/analytical work or full-scale work as well as centrifuge work. In fact, for many large-scale projects, a preferred method of analysis would be to conduct a small number of full-scale observations (very expensive), coupled with a

medium number (5-10) of centrifuge tests (moderately expensive) and use these to calibrate and validate analytical or numerical calculations. Of course, full-scale observations or numerical/analytical calculations may be very difficult for a particular problem.

In summary, it may be said that centrifuge modelling represents a significant increase in the usefulness of physical modelling as a provider of solutions to real engineering and scientific problems. Some problems with the technique do exist, but these can usually be circumvented, and the degree of accuracy of the modelling can be tested by modelling of models. The technique can be used to greatly increase the quality of confidence in civil engineering design, and can be used to further the understanding of processes in natural sciences.

Chapter 5

Experimental Overview, Facilities, and Equipment

5.1 Introduction

In this chapter, the experimental methods, facilities and test apparatus used to investigate the problem of pipeline/soil interaction are described. The design of the experimental program including the basis for the selection of variables is first presented. Detail is then provided on: the physical model tests; the soil used in testing; the research facilities, equipment and instrumentation used in the simulation and monitoring of an idealized pipeline/soil interaction; and, the data acquisition and data processing systems.

5.2 Experimental Program Design

The findings from the literature review and the concepts of centrifuge modelling as well as input from industry were applied to the problem to develop a reduced-scale model program to investigate pipeline/soil interaction. The objective of the model tests was to use centrifuge modelling to collect accurate data for well-defined physical events. These data would then be used to examine the effects of variation in burial depth, trench width, pipeline/soil interaction rate, stress history of the soil, and backfill properties and to conduct a modelling of models study to ensure the results correspond and could be

confidently extrapolated to full-scale.

The centrifuge testing environment places practical limitations on the methods used to achieve this objective. The size of the model was limited by the payload capacity of the centrifuge and the physical dimensions of the model it could carry. For the most part, the equipment used in the present study had been developed for use in a previous study and therefore flexibility in the experimental program was somewhat limited. The enhanced acceleration environment of the centrifuge limited options regarding test control, instrumentation, and data acquisition; proven techniques, apparatus, and procedures developed for centrifuge modelling were used whenever possible.

The experimental program was developed in consultation with industry. It was decided to investigate the interaction of a large diameter (0.95m) gas transmission pipeline as opposed to a smaller pipeline associated with distribution systems. It was also decided to investigate embedment ratios ranging from 1 to 4.42. It was felt this range would include a transition from shallow to deep burial because, with anchor plates, this transition has been suggested to occur at an embedment ratio of approximately 3 (see, for example, Rowe and Davis (1982a)). Trench widths investigated were to range from 1.5 to 3m to see if variation of this parameter had any influence on the process. The effect of variation in backfill type was also to be investigated to see how the utilization of different backfill types affected the interaction.

It was also thought important to investigate the effect of interaction rate as most of the accepted methods of analysing this problem are based on rapid undrained interaction but, in the field, the interaction rate could be on the order of millimetres per year. The pipeline loading system used in the study would permit approximate equivalent prototype interaction rates as low as 0.29m/year and as high as 657m/year; it was felt that the difference between the two rates was adequate.

Native material soil strength as high as was possible was desired so that the undrained shear strength might approach that commonly found in the field (50-100kPa) plus it was desired to have a significant difference between native material and the backfill; a fairly soft backfill was developed to achieve this difference. A practical limitation on achieving higher strength in the native material was the restriction that the soil could only be consolidated to a maximum effective stress of 400kPa. It was also desired to see what effect a lower soil strength would have on the interaction so a lower preconsolidation stress (160kPa) was also investigated.

Finally, it was considered important that a modelling of models study be conducted as part of the program to ensure that the results corresponded and could be confidently extrapolated to the full-scale.

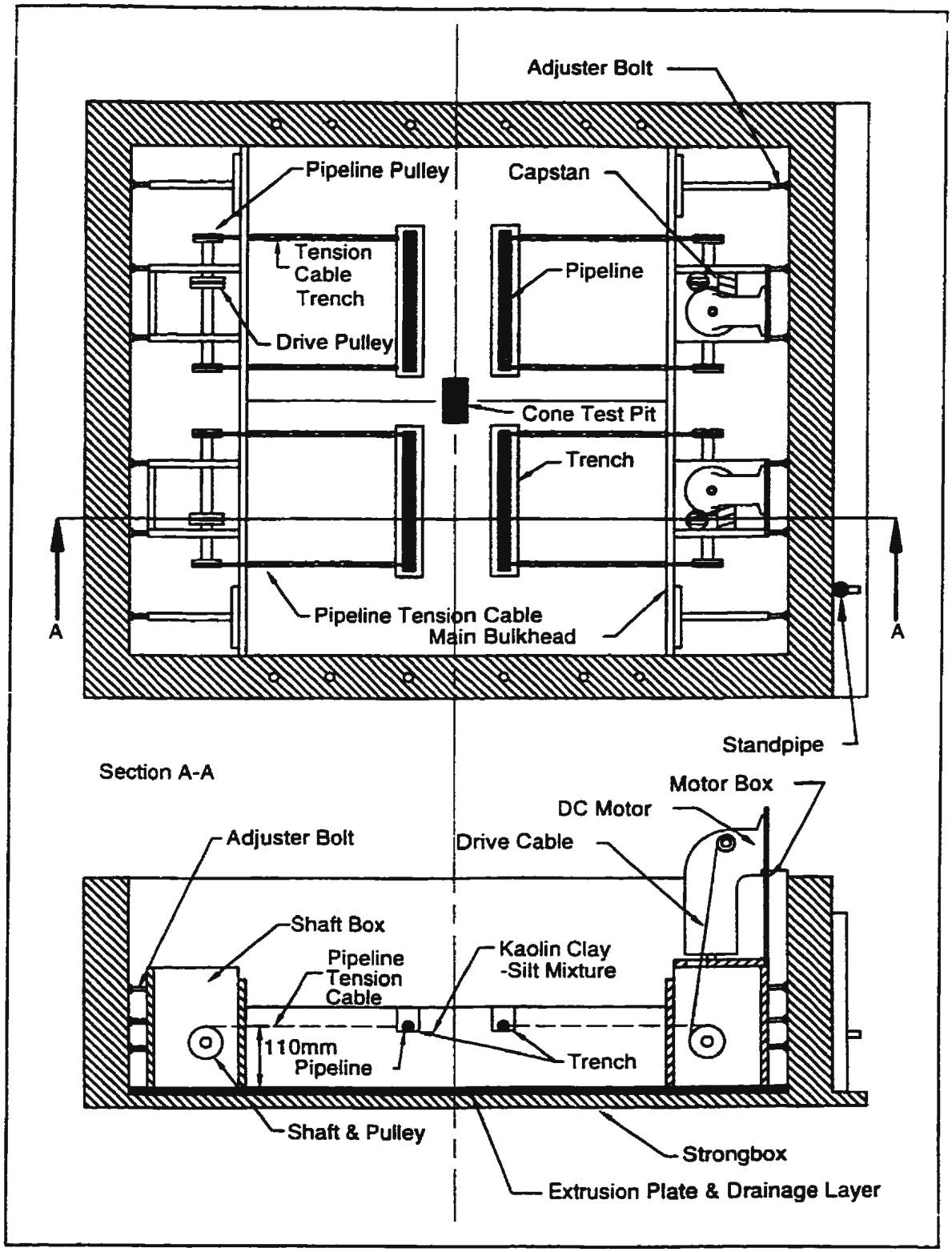

Figure 5.1 - Typical experimental setup.

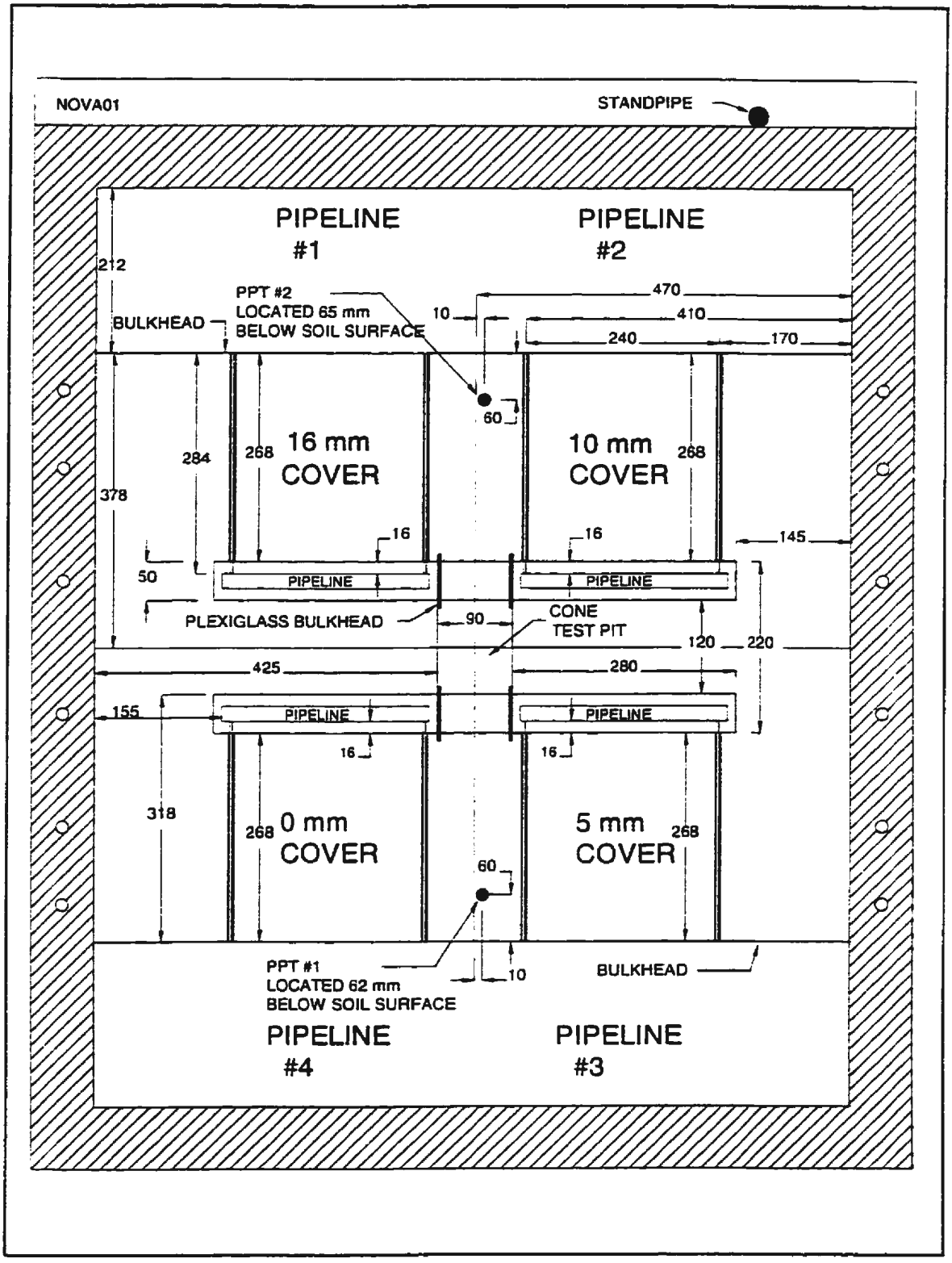

Figure 5.2 - Typical model configuration.

5.3 Description of Physical Model Tests

A typical model configuration is shown in Figure 5.1 and Figure 5.2. The samples were prepared in an aluminum C-CORE strongbox which was 940 by 1,180mm in internal plan and 400mm deep. The central section of the strongbox contains clay (native soil) which is retained by means of two bulkheads which are positioned by means of adjuster bolts at the rear of the shaft boxes.

Four pipelines were tested during each centrifuge test as shown in the figures. The pipelines were placed into trenches and backfilled during model assembly. Each pipeline was located at a predetermined depth below the soil, in a trench of predetermined width and during centrifuge testing was pulled through the soil at a predetermined rate by a pair of tension cables. These tension cables were connected to variable speed DC motors by means of pipeline pulleys mounted on a shaft. Data were collected prior to, during and after the displacement of each pipeline.

A total of nine tests was planned for the test series. These tests are presented in Table 5.1 where quantities are presented at prototype-scale. The baseline test was a 1:50 model tested at an acceleration level equivalent to 50 gravities representing the case where a 0.95m diameter pipeline was buried in a 2.5m wide ditch which had been backfilled with 0.8m of slurry backfill; the native material had been preconsolidated to 400kPa and the pipeline displaced at a rate of 315 m/year. The purpose of each test was to investigate the

Table 5.1 - Planned test series

Test	Pipeline Diameter (m)	Cover Depth (m)	Ditch Width (m)	Displacement Rate (m/year)	Preconsolidation Stress (kPa)	Backfill Type
Test 01	0.95	0, 0.25, 0.5, 0.8	2.5	315	400	Slurry
Test 02	0.95	1.35, 1.9, 2.5, 3.25	2.5	315	400	Slurry
Test 03	0.95	0.8	1.5, 2.0, 2.5, 3.0	315	400	Slurry
Test 04	0.95	0.8	2.5	0.4, 3, 32, 630	400	Slurry
Test 05	0.95	0, 0.25, 0.5, 0.8	2.5	315	400	Slurry
Test 06	0.95	0, 0.25, 0.5, 0.8	2.5	315	400	Slurry
Test 07	0.95	0.8	2.5	0.3, 3.2, 31.5, 315	400	Slurry
Test 08	0.95	0.8	2.5	0.3, 3.2, 31.5, 315	160	Slurry
Test 09	0.95	0.8	2.5	0.3	400	Slurry,Compacted Native Material, Chunks of Native Material, Fine Sand

following: Test 01 - the effect of variation in shallow cover depth; Test 02 - the effect of variation in deep cover depth; Test 03 - the effect of variation in trench width; Test 04 - the effect of variation in interaction rate; Test 05 - the effect in variation of model scale (1:25 scale); Test 06 - the effect in variation in model scale (1:100 scale); Test 07 - the effect of variation in interaction rate; Test 08 - the effect of variation in native soil preconsolidation pressure; and Test 09 - the effect in variation of backfill type.

There was one other major difference between some of the tests. Test 01 through Test 06 were designed so that a number of surface displacement measurements were taken during the interaction of the pipeline with the soil. These measurements were not incorporated into Test 07 through Test 09 but rather a different model pipeline was used which utilized a pressure transducer to measure the suction conditions at the rear of the pipe during pipeline displacement.

5.4 Description of Soil

5.4.1 Choice of Modelling Soil

Kaolin clay is a standard modelling soil which has been extensively used in centrifuge modelling (and geotechnical engineering research in general) to investigate the fundamental behaviour of soils. The limitation with kaolin clay, however, is that it is a highly plastic clay that does not model the behaviour of most field soils realistically. Recently, emphasis has been placed on research into developing model soils which can replicate *in situ* behaviour.

A study by Rossato *et al.* (1992) on the properties of pure kaolin and a kaolin-silt-sand (KSS) mixture showed that the kaolin has a lower undrained shear strength than most clays and that a KSS mixture consolidated from slurry might be used as an alternative, more realistic model soil. Springman (1993) studied another mix (kaolin and silica rock flour - KRF) using direct shearbox tests and concluded that the behaviour of both the KSS and KRF mixtures were closer to those of "real" soils.

Activities conducted to support this research program (Paulin *et al.*, 1993; Lin, 1995) focused mainly on producing a high strength modelling soil that better simulates field conditions for use in the physical model tests. The modelling soil which was developed (50% speswhite kaolin clay + 50% Sil-Co-Sil silt; by weight) yielded undrained shear strengths greater than 50kPa at a depth where the effective stress was 95kPa and the OCR was 4.2 while at 50g on the centrifuge. The grain size distributions of the kaolin, the silt, and the kaolin/silt mixture are presented in Figure 5.3. This material was reconstituted in a mixer at a 70% water content and consolidated to a 400kPa effective stress level. The use of Vaseline on the soil surface prevented desiccation and therefore prevented a highly nonlinear undrained shear strength profile. Thus test conditions were repeatable from test to test and controllable. A baseline trench backfill of the same mixture with a 65% water content was selected (termed "slurry backfill") as it was easy to work with and yielded undrained shear strengths approximately 6-10 times lower than the native material after consolidation in the centrifuge. Vaseline on the trench walls also reduced the migration of pore fluid from the backfill into the preconsolidated material preventing subsequent softening. The reduction of porewater

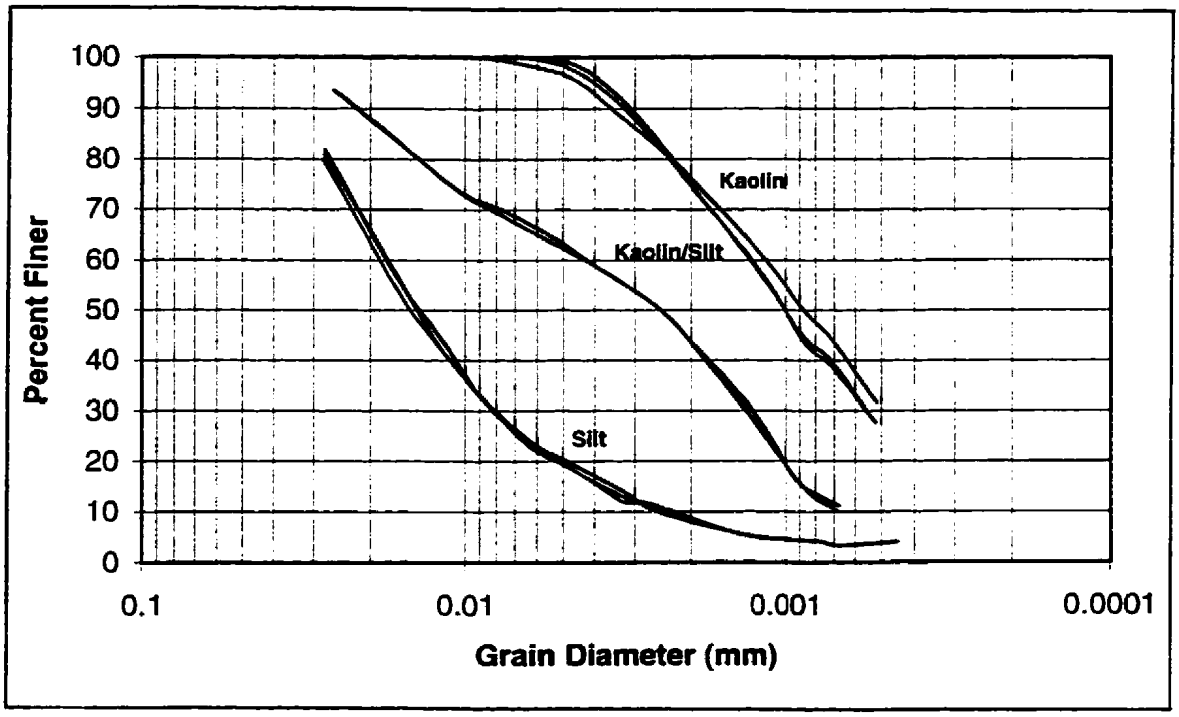

Figure 5.3 - Grain size distribution of kaolin, silt, and kaolin/silt mixture.

migration and the selection of the backfill resulted in a distinct difference between backfill and native material which was another objective of that study.

The research on the developed modelling soil included standard laboratory geotechnical classification tests, direct shearbox tests and shear vane tests. The shearbox and shear vane tests were conducted at 1g in the laboratory to determine the variation of undrained shear strength with overconsolidation ratio and mixture (i.e. 50% kaolin - 50% silt). The test data was then used to formulate empirical relationships between undrained shear strength, effective stress level, and overconsolidation ratio. From these empirical relationships, correlations between cone penetrometer tip resistance and undrained shear strength have been developed (Lin, 1995).

5.4.2 Laboratory Testing

As described above, the silty clay used during this test series was a mixture by weight of speswhite kaolin clay (50%) and Sil-Co-Sil silt (50%). This material has been described in detail by Paulin *et al.* (1993) and Lin (1995). Selected laboratory test results on the soil mixture are summarized in Table 5.2.

5.4.3 Triaxial Testing

The 50-50 mixture of kaolin clay and silt has been subjected to both drained and undrained triaxial testing. During triaxial sample preparation, the attempt was made to subject the clay to the same stress history as the soil used for the centrifuge model. The mixture had initially been one-dimensionally consolidated to a vertical effective stress of 400kPa. Following removal of the vertical loading, the soil was cored and a sample placed in the triaxial cell. Back-pressure was incrementally increased until B-values of 94 to 95% were achieved. The samples were then isotropically consolidated under a 25kPa effective stress during which time drainage was permitted. An isotropic effective consolidation stress of 25kPa was chosen as it was similar to the vertical effective stress found at the springline of a pipe with a prototype equivalent of 0.8m cover during centrifuge testing at 50 gravities when a soil which had been preconsolidated to 400kPa was used.

Consolidated Undrained (CU) Test

Head (1986) presents a method for calculating the shearing rate for undrained triaxial compression testing of clay using isotropic triaxial consolidation data. Using this method,

Table 5.2 - Laboratory test results on the 50% kaolin - 50% silt mixture

Test	Results
Liquid Limit - Fall Cone (w_l)	35.0%
Plastic Limit (w_p)	22.0%
Plasticity Index (I_p)	13.0%
Specific Gravity (G_s)	2.624
Coefficient of Permeability, k (cm/s)	1.5×10^{-8}
Mean Grain Size, d_{50} (mm)	0.0005
Grain Size Analysis	Clay < 2μ approximately 35%

the calculated suggested rate was 0.0424 mm/min. However, the actual shearing rate used was a slightly faster; 0.0625 mm/min.

Figure A.1a of Appendix A presents the isotropic consolidation data used to calculate the shearing rate. The stress-strain and pore pressure change-strain data are presented in Figure A.1b and A.1c. The total and effective stress paths are presented in the p-q and p'-q space of Figure A.1d.

Consolidated Drained (CD) Test

Head (1986) presents a method for calculating the shearing rate for drained triaxial compression testing of clay using isotropic triaxial consolidation data. Based on this method, the calculated suggested rate was 1.69×10^{-3} mm/min. or about 6 days to reach 15% strain.

Figure A.2a presents the isotropic consolidation data used to calculate the shearing rate. The stress-strain, pore pressure change-strain, and volumetric-axial strain data are presented in Figures A.2b, A.2c, and A.2d respectively. The total and effective stress paths are presented in the p-q and p'-q space of Figure A.2e. Apparent from Figure A.2e is the fact that the sample was not fully drained but rather was only partially-drained.

Comparison of Triaxial Results

Drained and undrained stress paths from the two triaxial tests are presented in Figure A.3. These data will be used in Chapter 8 to derive parameters used for pipeline/soil interaction analyses. From the plot, it can be observed that, for the same material, the ultimate undrained shear strength is approximately 1.25 times the "drained" shear strength for these conditions. It is also obvious from the data that while Sample #2 was subjected to a very slow rate of loading, it was not completely drained.

5.5 Research Facilities

5.5.1 The C-CORE Centrifuge Centre

The C-CORE Centrifuge Centre is a research facility located between the Captain Robert A. Bartlett building and the S. J. Carew building on the campus of Memorial University of Newfoundland. The centrifuge centre was constructed and equipped through funding from the Canada/Newfoundland Offshore Development Fund, the Technology Outreach Program of Industry, Science and Technology Canada and the Natural Sciences and

Engineering Research Council Canada.

The centre comprises a two storey building, containing laboratories and workshops with offices upstairs and a containment structure housing an Acutronic 680-2 centrifuge. The containment structure has three levels. The upper level provides a stiff ceiling for the main centrifuge chamber to resist the aerodynamic excitation imposed by the centrifuge in rotation. The upper level also houses the electrical slipring capsule and associated interfaces. The intermediate level is the main centrifuge chamber which is accessible by forklift from the main building. The main chamber is 13.5m in diameter and 4.2m high. The 300mm thick reinforced concrete chamber wall is aerodynamically clean inside and retains a rockfill safety berm outside. The lower level is underground and contains the centrifuge drive unit with associated controllers and the refrigeration unit. The two storey building includes sample preparation and investigation areas, an x-ray bay, mechanical and electrical workshops, coldroom, data processing areas and offices including areas for visiting researchers or clients. The building also has access to Memorial University's computer capabilities. The plan of the C-CORE Centrifuge Centre is shown in Figure 5.4.

5.5.2 The Acutronic 680-2 Centrifuge

This Acutronic 680-2 centrifuge, shown in Figure 5.5, is capable of testing models to 200g and has a radius of 5.5m to the surface of the swinging platform. The test package centroid is typically at a nominal working radius of approximately 5m. At the maximum centrifuge rotational speed of 189 rpm, the acceleration of the package is approximately 200g. The

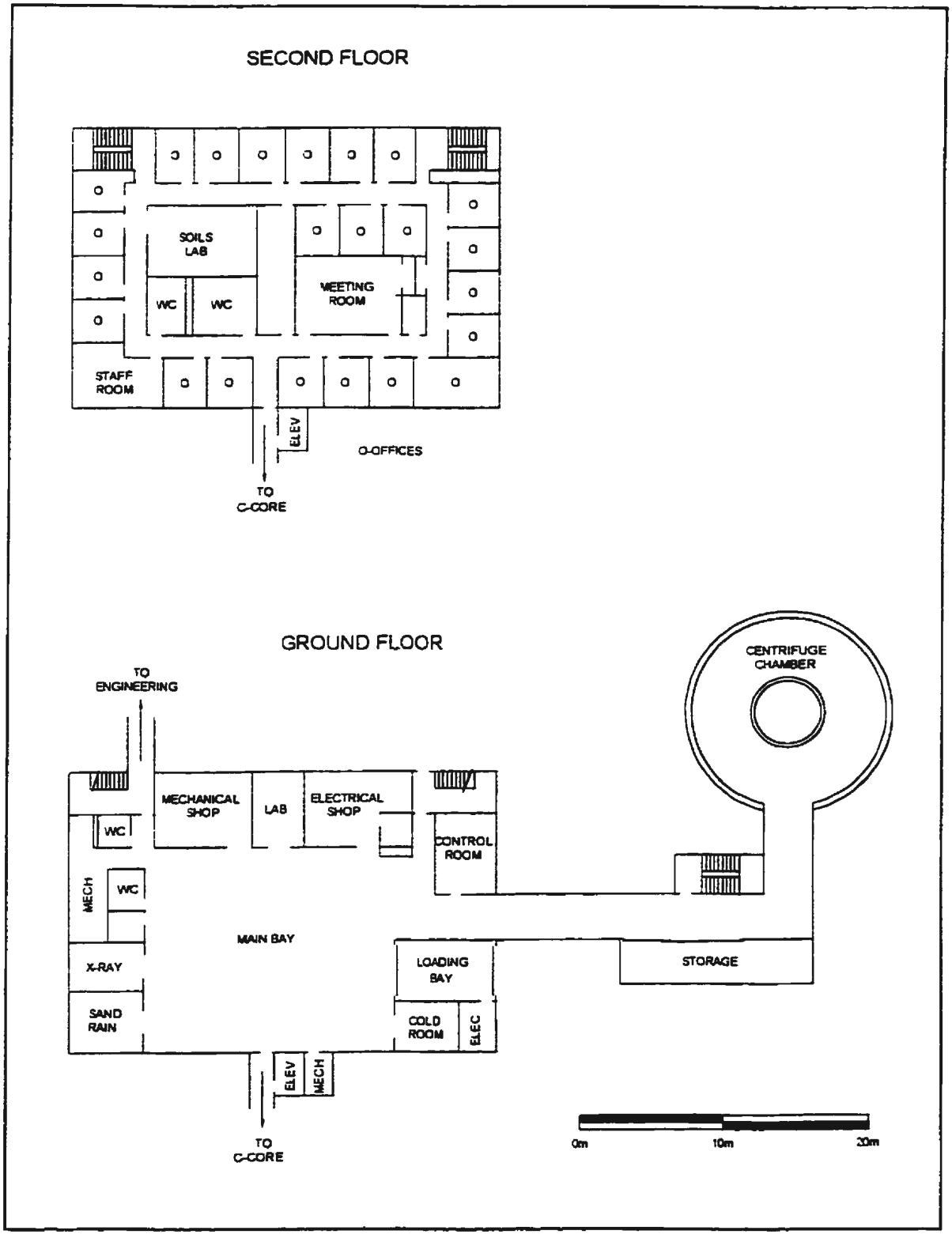

Figure 5.4 - Plan of the C-CORE Centrifuge Centre.

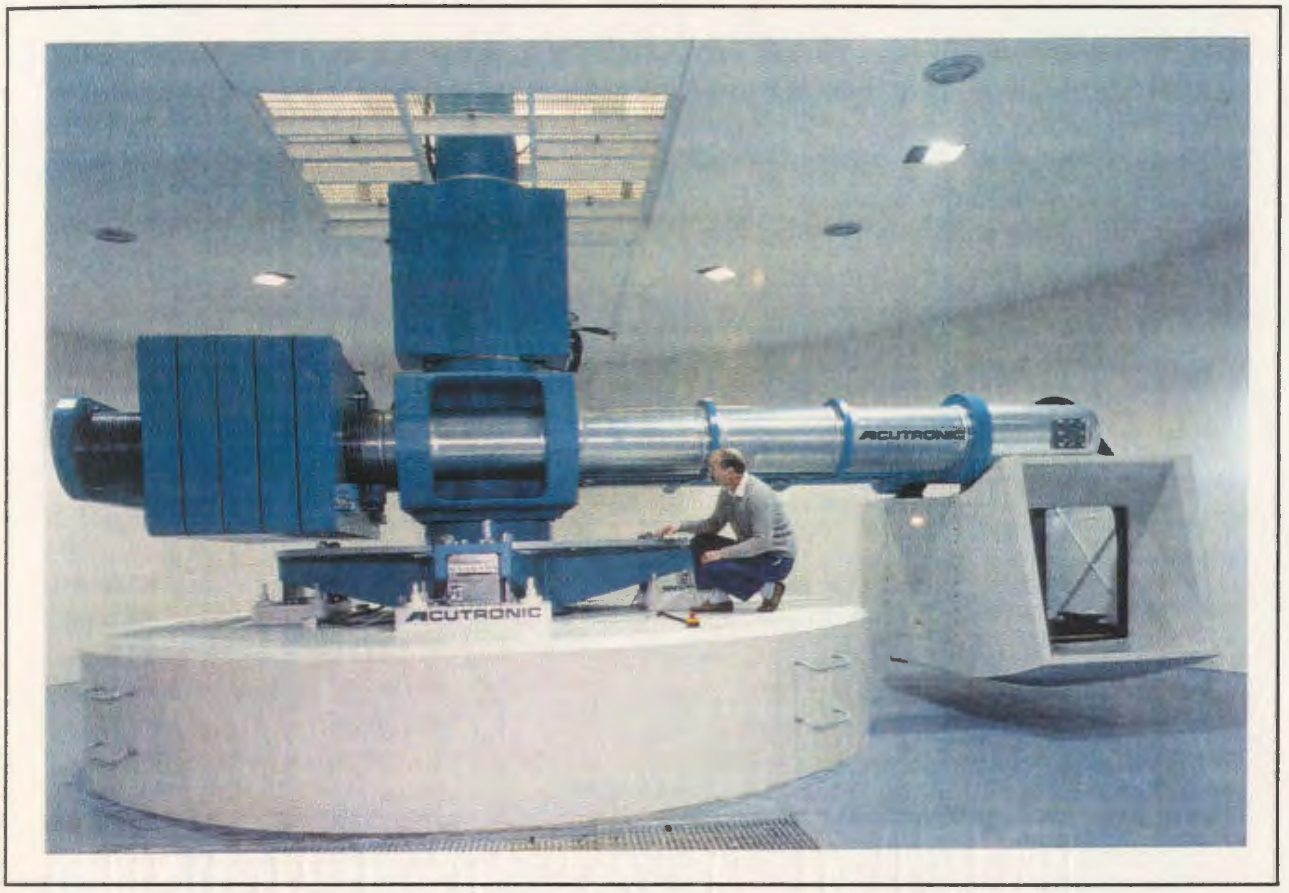

Figure 5.5 - C-CORE Acutronic 680-2 centrifuge.

C-CORE centrifuge has a maximum payload capacity of 100g x 2.2 tonnes = 220g-tonnes at the 5m working radius. This capacity reduces to 130g-tonnes at 200g due to the increased self-weight of the platform. The capacity and specifications of the Acutronic 680-2 are presented in Figure 5.6. The maximum payload size is 1.1m high by 1.4m long and 1.1m wide.

The centrifuge arm consists of two parallel steel tubes held apart by a central drive box and spacers as shown in Figure 5.7. The swinging platform is suspended on pivots from the

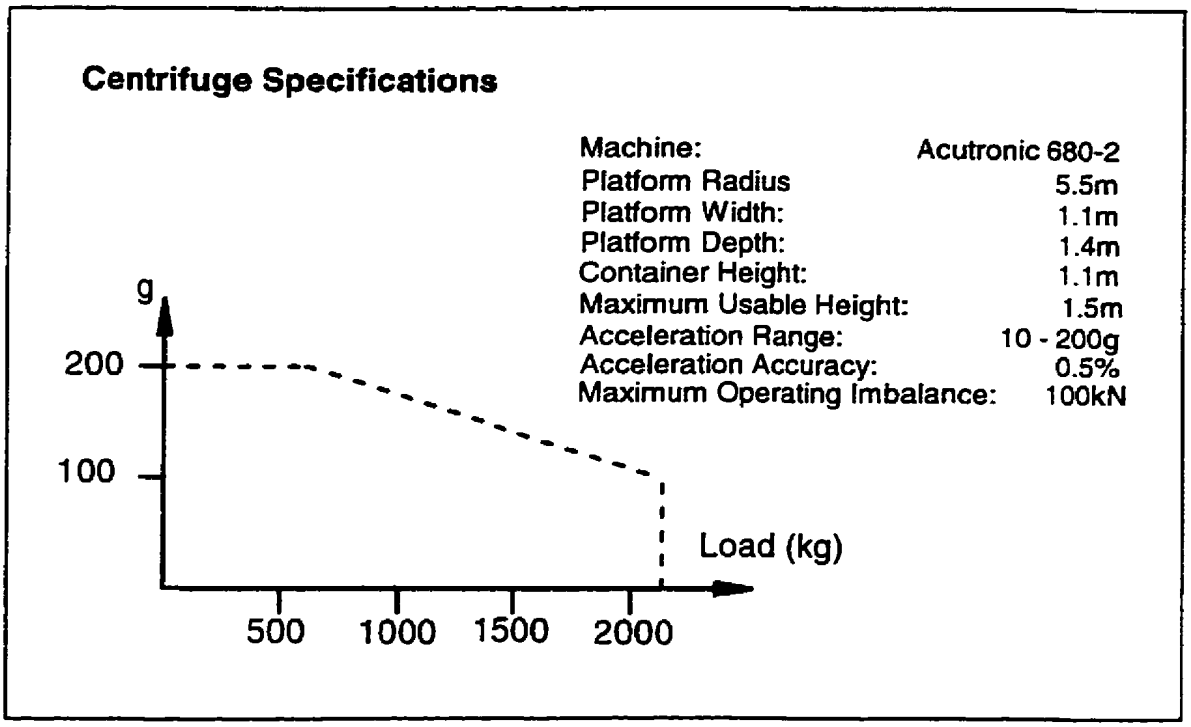

Figure 5.6 - Capacity and specifications of the Acutronic 680-2.

ends of the load carrying beams and is covered by an aerodynamic shroud to reduce drag. The platform and the payload are balanced by a 20.2 tonne mass counterweight. The position of this counterweight is adjusted by driving a series of gearwheels along screwthreads on the outside of the parallel steel tubes using an electric motor.

The centrifuge arm rotates on a set of tapered roller bearings inside the central drive box and is mounted on a stationary shaft. This shaft is attached to the concrete base through a four branch star support suspended on four springs. Each of the four springs is strain-gauged to sense imbalance within the centrifuge arm to within 10kN.

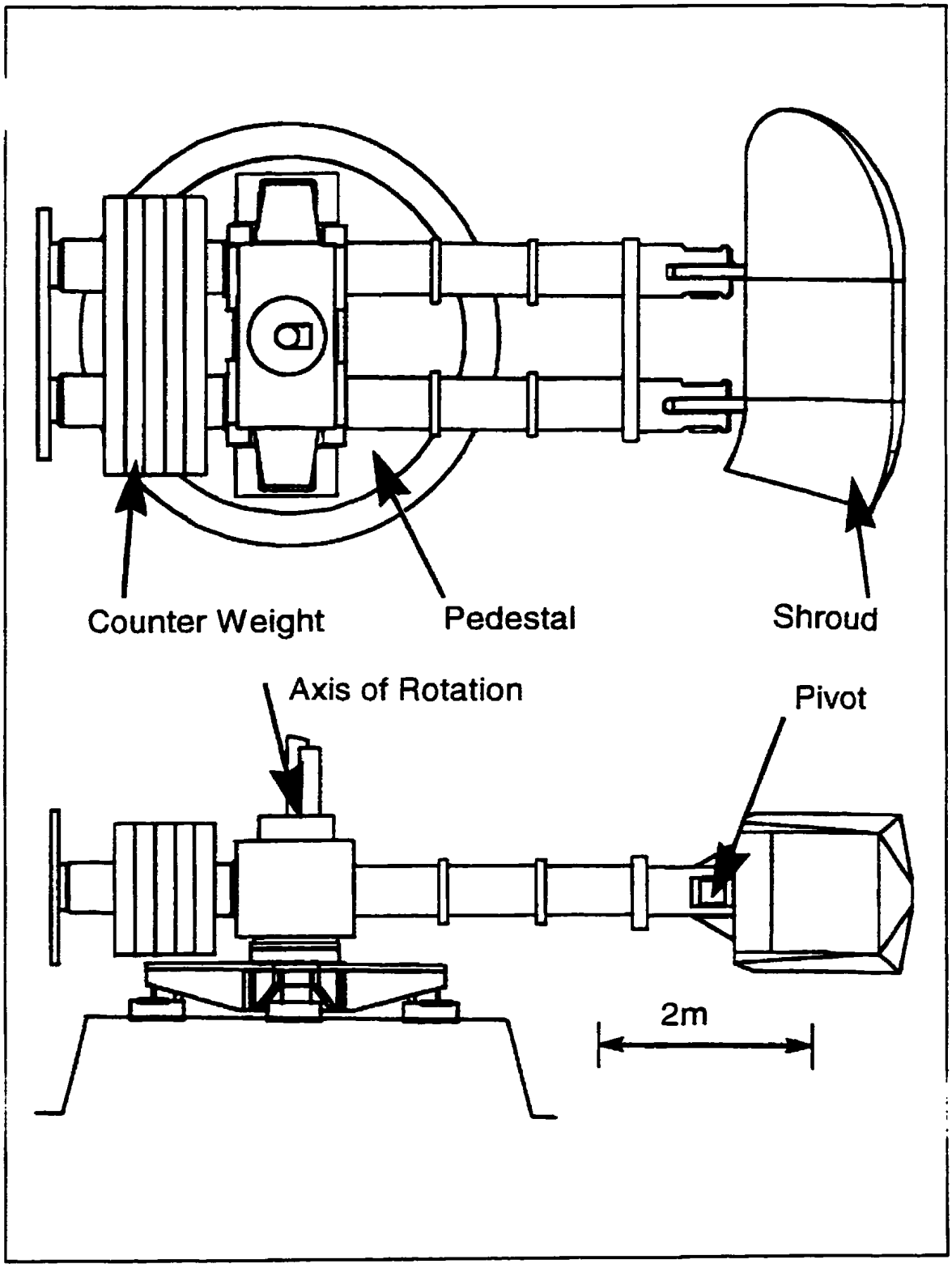

Figure 5.7 - Acutronic 680 centrifuge.

The centrifuge drive unit comprises a 450kW AC variable speed motor and a 9:1 gear reducer. The variable speed motor is energized through two 250kW invertors connected in parallel. Precision couplings and a hollow vertical drive shaft connect the hollow output shaft of the gear reducer to the central drive box. Two rotary joints are attached beneath the output shaft of the gearbox which contains 6 passages and is described below.

The power consumption is due mainly to aerodynamic drag within the centrifuge chamber. The centrifuge and the chamber are cooled by forced air ventilation. Air is drawn into the chamber through a ceiling vent around the central axis of the centrifuge. Air is drawn out of the chamber through a floor vent by an exhaust fan located in the lower level.

5.5.3 Centrifuge Services

Rotary Joints

The Acutronic 680-2 centrifuge is equipped with two rotary joints which permit fluids to flow through the central axis of the machine to the platform. These rotary joints contain a total of six passages; two are designed to accept high pressure hydraulic fluid; two are connected to the refrigeration unit (glycol refrigerant); and the remaining two can carry either air or water.

Refrigeration Unit

To enable cooling of the experimental package, the C-CORE Centrifuge Centre has been furnished with a refrigeration system. The refrigeration system is designed to deliver 7kW

of cooling to the platform. Cooling of the package can be accomplished by pumping a cold fluid through the rotary joint to the end of the boom. The refrigeration unit can deliver 10 litres/min. of glycol refrigerant and achieve temperatures as low as -25°C.

Ancillary Equipment

Ancillary equipment is constantly being developed to support operations within the centrifuge centre. These essential items include strongboxes, consolidometers, an in-flight cone penetrometer, and a refrigerated strongbox used to house experiments which require temperature control. The design of these devices is complicated by the level of stresses experienced in the centrifuge and by restrictions on size and weight. Additionally, mechanical or electrical systems must be controlled remotely.

5.6 Description of Equipment

5.6.1 Clay Mixer

The clay mixer used in preparation of the clay samples was a 5HP Bowers horizontal paste mixer. This mixer has a capacity of 200 litres, uses plough-type mixing blades, and is capable of mixing at blade speeds ranging from 13 to 60 RPM. The mixer was designed to accept a vacuum and, when connected to the C-CORE laboratory supply, 60-70kPa of vacuum could be achieved during mixing.

5.6.2 Soil/Model Containment

Primarily, the strongboxes or tubs act as containment structures for all experiments which are to be conducted on the centrifuge and provide bases to which experimental apparatus can be secured during flight. The existing rectangular strongboxes used in the current study have an internal working area of 1.18m x 0.94m and a depth of 0.4m (Figure 5.1). The strongbox walls are 80mm in thickness and of sufficient strength to carry a cone penetrometer or other necessary equipment during centrifuge flight.

5.6.3 Consolidometer

A consolidometer is a large hydraulic press which is used in sample preparation. The consolidometers are designed to apply consolidation pressures of up to 400kPa onto samples contained in the existing rectangular strongbox. The load is delivered by a 200mm diameter hydraulic cylinder with a working pressure of 17MPa, which equates to approximately 50 tonnes of static thrust.

5.6.4 Model Preparation Tools

The one-dimensional consolidation levels used in the current test series were sufficient to provide a clay which was sufficiently stiff to be carved with a cheese wire or a sharp knife. The model was prepared using vertical and horizontal cutters similar to those depicted in Figure 5.8. These cutters were machined from mild steel. Various widths of horizontal cutters were used to accommodate various trench widths. The cutters were connected to a support strut which was held in place over the clay surface using a strut clamp as shown

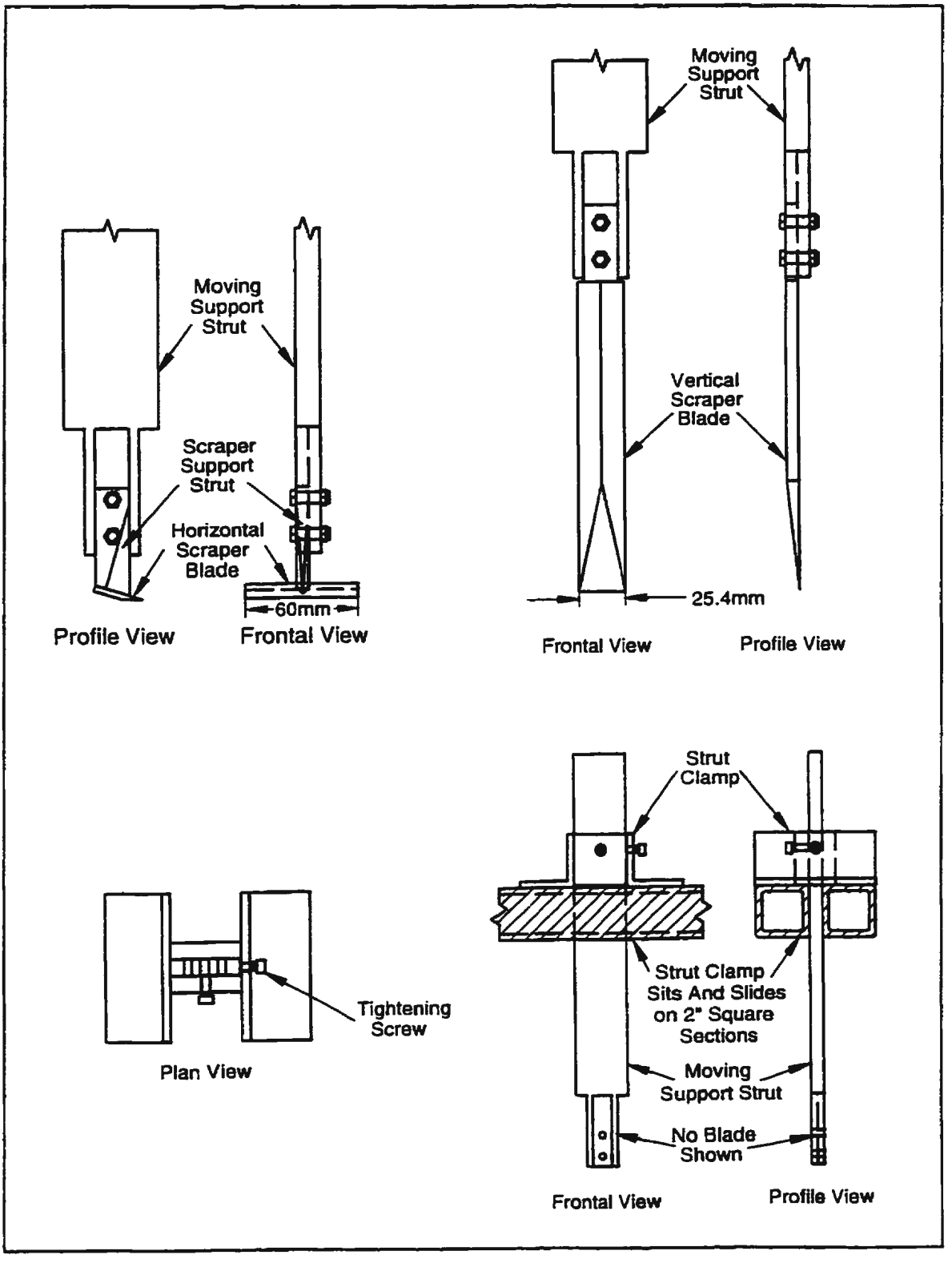

Figure 5.8 - Vertical and horizontal clay cutters as well as interface of support strut to strut clamp.

in the figure. This strut clamp sat on two parallel beams spanning the strongbox as shown in the figure and could be manually moved creating the desired cuts in the clay. Other model preparation tools included standard soils lab accessories such as spatulas, cheese wire soil cutters, etc.

5.6.5 Pipeline Loading System

As depicted in Figure 5.2, each of four pipelines are buried in the clay at predetermined depths below the surface and are pulled through the clay by a pair of tension cables (Figure 5.1). These tension cables are connected to the pipeline pulley depicted in Figure 5.1. Connected to the same shaft as the pipeline pulleys is a drive pulley which is also shown in the figure. This drive pulley is then connected to the prime mover, a DC variable speed motor, by means of a drive cable connected to the motor capstan. A typical drive system is depicted in Figure 5.9. During Test 01 through Test 06, the driven pulley and motor capstan were connected by a flexible braided stainless steel cable. To minimize potential backlash effects in the drive system for Tests 07 through 09, this cable was replaced by a chain drive system. The gearing of the various pulleys used in this configuration stepped down the motor speed to the extent that the pipelines were displaced at nominal speeds of 0.5-1.5mm/s. For slower speeds, an additional gearbox was incorporated into the drive system. With this gearbox, pipeline speeds as low as 0.001mm/s could be achieved.

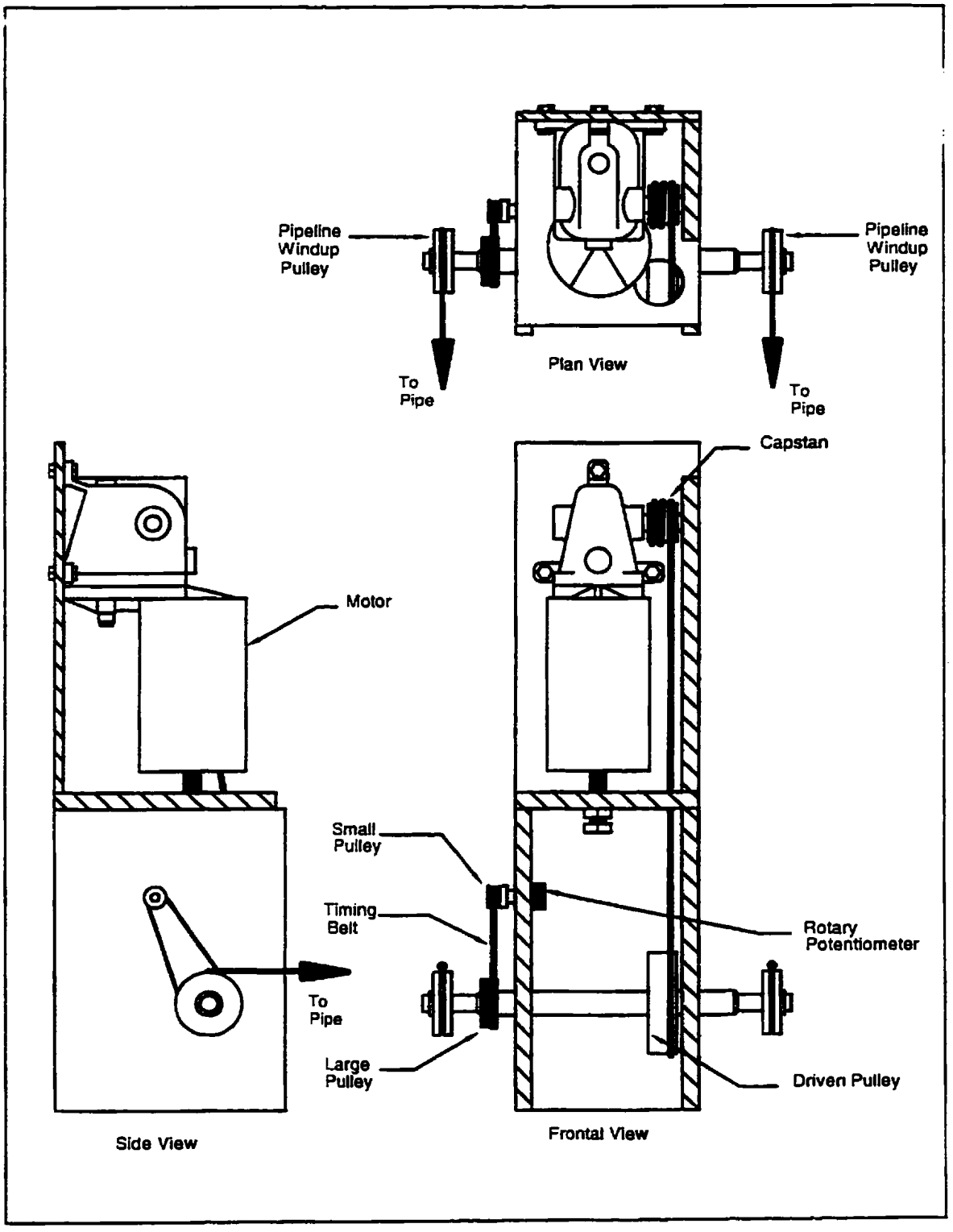

Figure 5.9 - Typical pipeline loading system.

5.7 Description of Instrumentation

Sensors and instrumentation were incorporated into each model to measure various parameters. A number of data acquisition channels was also dedicated to monitoring the instrumentation excitation voltages. The instrumentation used during testing is described in general below.

5.7.1 Model Pipelines

The 1:50 scale pipelines used in Test 01 through Test 04 consisted of a core encased in a (sectioned) sleeve as shown in Figure 5.10; the net result was a heavy rigid pipeline. The solid core had two reduced cross sections which were strain gauged. These four strain gauges measured the bending moment at the reduced sections. Because of the arrangement of the strain gauges, any load which was applied between the reduced sections was measured. Calibrations were conducted with a point loading at the centre of the pipeline only. An analysis of the pipelines shows that a uniformly distributed load of 1.23F induces the same pipeline response as a central point load of F. Therefore, a further calibration constant of 1.23 had to be applied on top of the experimentally derived calibration constants.

The 25 and 100g pipelines used in Test 05 and Test 06 were designed to measure shear directly and thus no further calibration factors needed to be applied on top of the experimentally derived calibration constants. Again these pipelines were essentially rigid

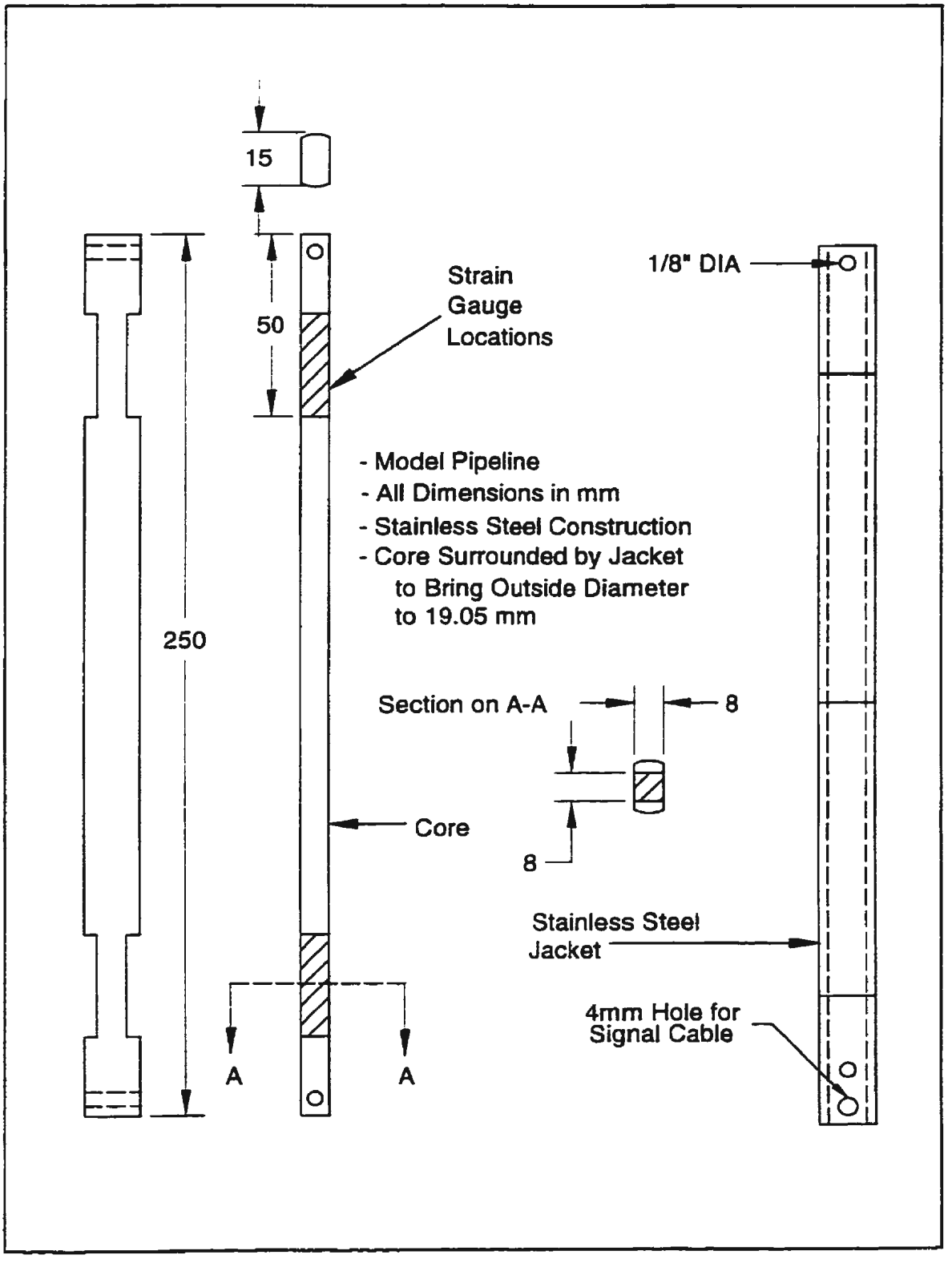

Figure 5.10 - 1:50 scale pipeline used in Test 01 through 04.

and calibration constants were derived by direct application of a shear force across the shear cell.

As mentioned earlier, the pipelines used in Tests 07 through 09 were redesigned to incorporate a pressure transducer to measure the suction conditions behind the pipe during pipeline displacement. The pipelines consisted of a core encased in a (sectioned) sleeve as shown in Figure 5.11. The net result again was a heavy rigid pipeline. The solid core has two reduced cross sections which are strain gauged. These 4 strain gauges measure the shear at the reduced sections. Because of the arrangement of the strain gauges, any load which is applied between the reduced sections is measured; this length was 180mm. Calibration constants were derived by direct application of a shear force across the shear cell. Pore pressure transducers were incorporated into the rear of the pipeline as indicated in Figure 5.11 to measure pipeline/soil interface pressures/suctions during testing. These pore pressure transducers are described in Subsection 5.7.5.

5.7.2 Torque Cells

Strain gauges were attached to the pipeline pulley shafts of Tests 01 through 04. As the pipeline pulleys reeled in the pipelines, torque was transmitted to the shaft and these strain gauges were arranged in such a manner that this torque could be measured. The torque measured was the result of the pipeline resistance plus friction along the pipeline tension cables. Pipeline loading can only be measured through an assumption as to the amount of

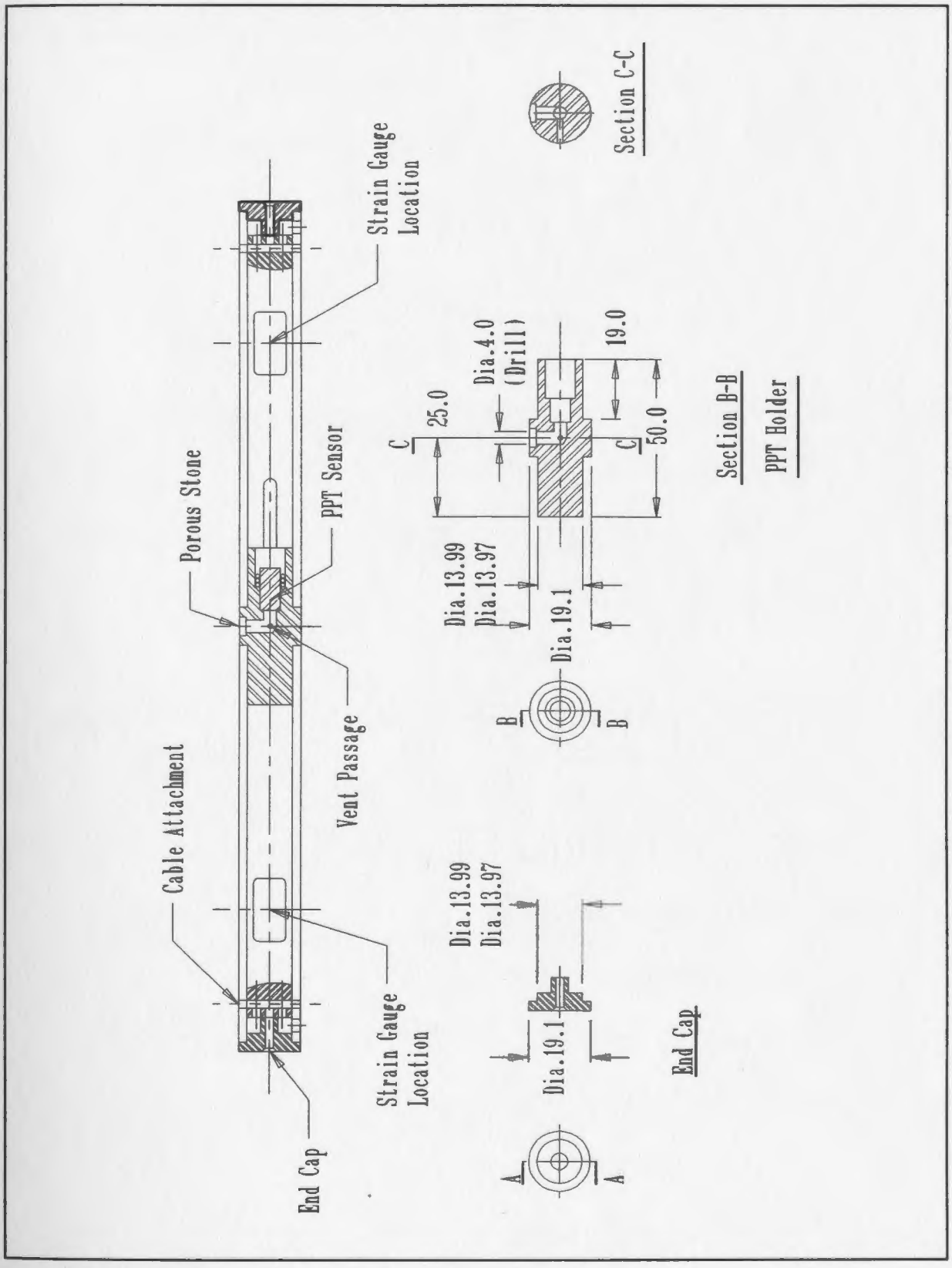

Figure 5.11 - 1:50 scale pipeline used in Test 07 through 09 into which pore pressure transducers had been incorporated.

the total load which could be attributed to the cable friction. These cells were built into the experiment so that in the event of a pipeline failure during testing, useful data could still be obtained.

5.7.3 Rotary Potentiometers

A rotary potentiometer was connected to the shaft of each pipeline pulley as depicted in Figure 5.9. This potentiometer measured the rotation of the pipeline reeling pulley attached to the tension cable pulling the pipeline. This rotation was then translated to a pipeline displacement using experimentally derived calibration constants.

5.7.4 Linear Displacement Transducers

During Tests 01 through 06, an arrangement of twenty linear displacement transducers (LDTs) was used to measure the soil surface movement surrounding the region of two of the buried pipelines designated Pipeline #1 and Pipeline #2. These transducers were attached to a frame which spanned the strongbox and bolted to the top edge. The measuring shafts of the LDTs rested upon plexiglass pads. As the soil heaved in front of the moving pipeline, the LDTs should have risen with the soil. However, because of friction in the LDTs and lateral forces due to the moving soil, LDT movement was affected and the pads became embedded, giving a lower bound to surface movement.

5.7.5 Pore Pressure Transducers

Pore pressures within the sample were measured by means of Druck PDCR81 miniature

pore pressure transducers (PPTs). These were used to monitor the state of equilibrium of the clay and were also placed along the pipeline displacement path during some of the tests to assess soil drainage conditions under various pipeline displacement rates. These PPTs were also used to monitor the depth of water in the sample in order to determine the position of the water table.

5.7.6 Cone Penetrometer

In-flight mechanical properties of test samples are required during centrifuge modelling. One means of acquiring these data is through the use of a cone penetrometer as shown in Figure 5.12. This device consists of an instrumented shaft capable of measuring tip resistance and two linear actuators. The horizontal actuator to move the cone penetrometer across the package is not shown in the figure. The cone is made from stainless steel and comprises a 60° cone tip attached to a 100mm^2 circular rod. The cone penetration velocity during the current test series was 3 mm/sec. but penetration rates up to 20 mm/sec. can be achieved. One actuator drives the instrumented shaft into the sample while the second actuator (not shown) is used to position the cone within the test package. Shear strength can be interpreted from the tip resistance of the cone (q_c).

5.7.7 Visual Markers

Where necessary, the backfill material used during testing was dyed so that any displacement of the backfill with the pipeline (e.g. caused by suction) could be observed during post-test excavation. Strands of painted spaghetti were introduced into the clay.

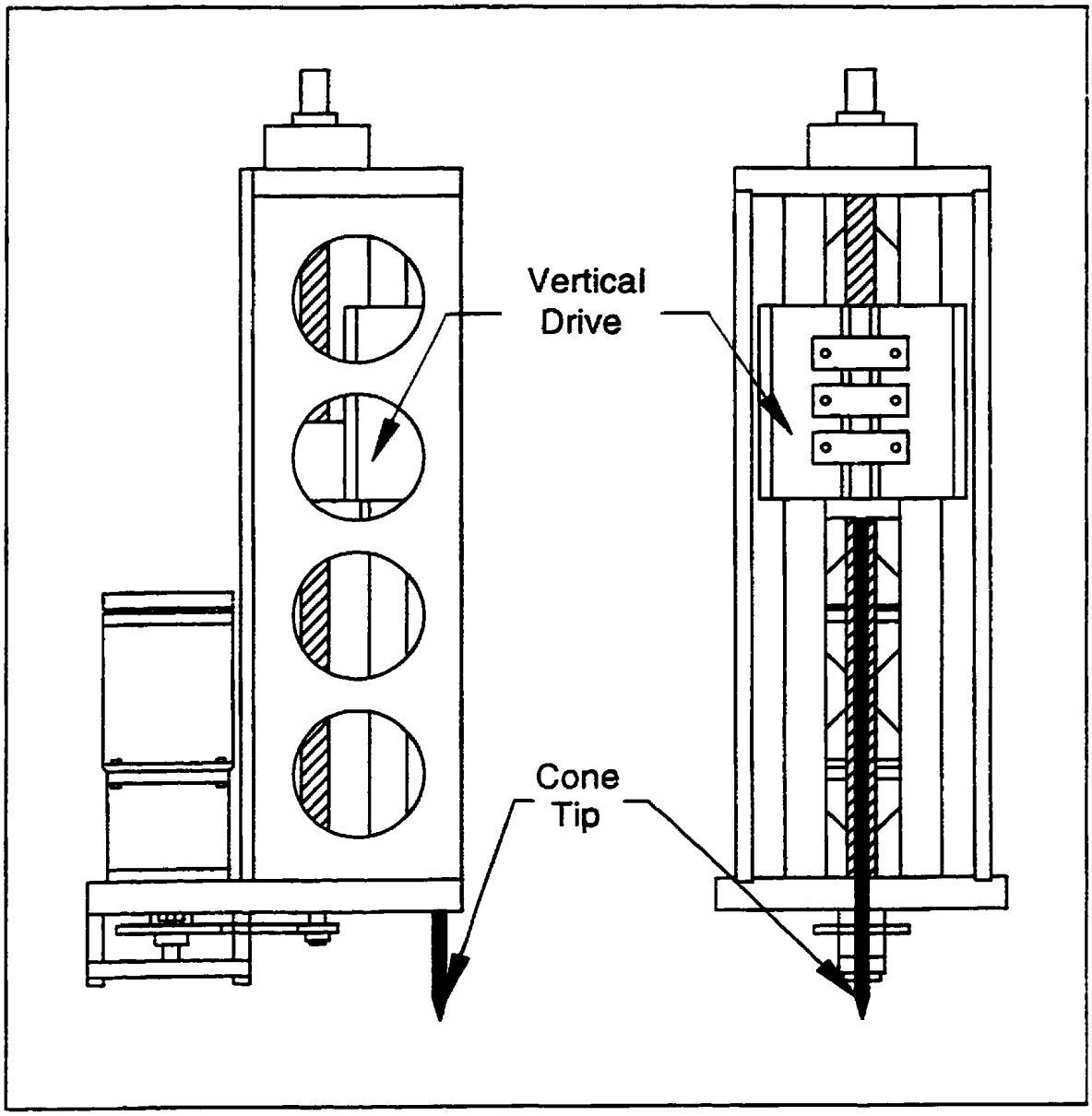

Figure 5.12 - Vertical drive of the cone penetrometer. Horizontal drive not shown.

The strands were inserted vertically into the clay and softened under prolonged exposure to water. The strands then deformed with the clay. They were used only to give a qualitative indication of the displacement field surrounding the moving pipeline and an indication of plastic zones of influence.

5.8 Data Acquisition and Processing

5.8.1 Data Acquisition

The electrical sliprings are located above the centrifuge in two capsules. An Aeroflyte capsule contains the necessary sliprings for machine functions and presents for research usage: 64 @ 1 amp individually shielded signal lines; 8 @ 15 amp shielded power lines; and 6 coaxial channels. The other slipring capsule contains a full 3-phase, 5 line, 380V, 80 amp power service, part of which is used to energize the counterweight motor.

The data acquisition system includes a high quality custom designed signal conditioning (S/C) sub-system mounted on the strongbox. The individual S/C modules are dual channel printed circuit cards and are mounted in a 12 card chassis. Each chassis provides on-board regulated excitation supplies for the attached instrumentation. Each individual channel /instrument is fed via a six pin Circular-Mil connector; the card/connector can be configured on the S/C card for a wide variety of instruments. The bulk power for the S/C cards and instrumentation is fed from a high quality power supply via a bulk power umbilical. The power supplies are fed from a 120V single phase, 3-wire connection through the sliprings.

The signals from each chassis are fed back through the 2 x 32 channel arrangement of the signal sliprings. On the far side of the sliprings the signals run into a shielded cabinet and are attached to a 64 channel multiplexer, which then feeds a PC based ANALOGIC

HSDAS-16 (16 bit A/D convertor). The slipring data acquisition PC runs SNAPMASTER data acquisition software. Data acquisition was conducted at rates ranging from 1 to 50Hz depending on the test activity. This PC is connected via a thinwire ethernet to the Control Room Data Acquisition PC, and logs all data to the CRDAS PC's Magneto-Optical drive. The various coaxial rings are rated to carry data-communications and high bandwidth analog signals.

5.8.2 Data Processing

Data processing for the current test series was achieved through the use of Matlab software which is a high-performance interactive software package for scientific and engineering numeric computations. Digital filtering of the data, as required, has been achieved using the Matlab filter FILTFILT with zero-phase shift. For example, Y = FILTFILT(B,A,X) filters the data in vector X with the filter described by vectors A and B to create the filtered data Y. After filtering in the forward direction, the filtered sequence is then reversed and run back through the filter. The resulting sequence has precisely zero-phase distortion and double the filter order. Care is taken to minimize startup and ending transients by matching initial conditions (MathWorks, 1991).

The vectors A and B are generated through a recursive filter design (YULEWALK) using a least-squares method. For example, [B,A] = YULEWALK(N,F,M) finds the N^{th} order recursive filter coefficients B and A such that the filter matches the magnitude frequency response given by the vectors F and M. Vectors F and M specify the frequency and

magnitude breakpoints for the filter such that a plot of M versus F would show a plot of the desired frequency response. During the filtering of the data, the following vectors were used in the filter design; F=[0.0, 0.05, 0.1, 1.0] and M = [1, 1, 0.00001, 0.0].

Chapter 6

Experimental Procedure and Testing

6.1 Introduction

The previous chapter presented a general overview of the physical model program plus facilities, equipment, and instrumentation available. In this chapter, experimental procedures and testing details are presented including: soil sample preparation; model preparation installation of instrumentation; model testing; and post-test investigation. Selected test details, observations, and experimental data associated with each test are contained in the *Test Data* appendices. Where necessary, modifications were made to improve the experimental set up and test conduct as the experimental program progressed.

6.2 Soil Sample Preparation

Preparation of the sample started by placing a layer of geotextile on the base of the tub over the base drainage channels. An extrusion plate, 9.5mm thick, was then placed into the tub (see Figure 5.1) to allow for extrusion and excavation of the sample subsequent to testing. This plate was covered by another layer of geotextile which was in turn covered by approximately 10mm of type 0 silica sand which would provide base drainage during consolidation. This sand was capped by a final layer of geotextile and the whole drainage

blanket carefully saturated. A layer of Whatman 2 filter paper was placed on top of the drainage blanket to prevent clogging of the geotextile by the slurry. Wet paper towels were rolled and placed along the wall of the tub on top of the geotextile to act as a seal. The walls of the tub were greased with Vaseline to minimize sidewall friction during consolidation and to assist in sample extrusion.

The silty clay being used during this test series was a mixture by weight of speswhite kaolin clay (50%) and Sil-Co-Sil silt (50%). This material has been described in detail in the previous chapter. The slurry for each test was mixed in two batches; both batches were mixed to a nominal water content of 70%. Mixes were prepared and then permitted to soak for at least one hour before mixing started. Mixing was conducted under a vacuum of 60-70kPa. As the mixes were poured into the strongboxes, water content measurements of the slurry were taken. During all tests, mixtures were generally observed to be homogenous during pouring and free from any lumps.

The thickness of the slurry after pouring and smoothing was measured. A layer of the filter paper was placed on top of the sample followed by a layer of wet geotextile. A 10mm drainage layer of silica sand was then carefully placed on the geotextile which immediately became saturated under capillary suction. A final layer of wet geotextile was placed over the sand and sealed to the sides of the tub using a rolled paper towel seal. This seal prevented slurry from leaking out along the sides of the strongbox. The consolidometer piston was then placed on the slurry mixture imparting a bearing pressure of 3.6kPa and

the strongbox was placed in the consolidometer as shown in Figure 6.1. Drainage was permitted from the top and bottom of the sample during consolidation. The total load imparted by the consolidometer was measured directly from a load cell located between the clay piston and the hydraulic loading cylinder. Consolidation to the desired effective stress level was conducted over several days using set, predetermined load increments.

During unloading of the sample below approximately 140kPa, flow of water into the sample was restricted by closing the base drain and removing excess water at the sample surface. After unloading, the strongbox was removed from the consolidometer and the piston removed. The geotextile and sand drainage layer were then removed and the Vaseline cleaned from around the exposed sides of the tub. The final thickness of the sample was then measured and recorded and the density of the soil calculated.

6.3 Model Preparation

Assembly of the model started by shaving the surface of the soil using the horizontal cutters as shown in Figure 6.2 and 6.3. The average water content of the shavings was measured and recorded. Because of the commonality of the equipment, the springline of each pipeline was maintained at 110mm above the extrusion plate as indicated in Figure 5.1 regardless of the model scale or pipeline cover. After this shaving was completed, the edges of the sample along the strongbox wall were pressed down to ensure contact between

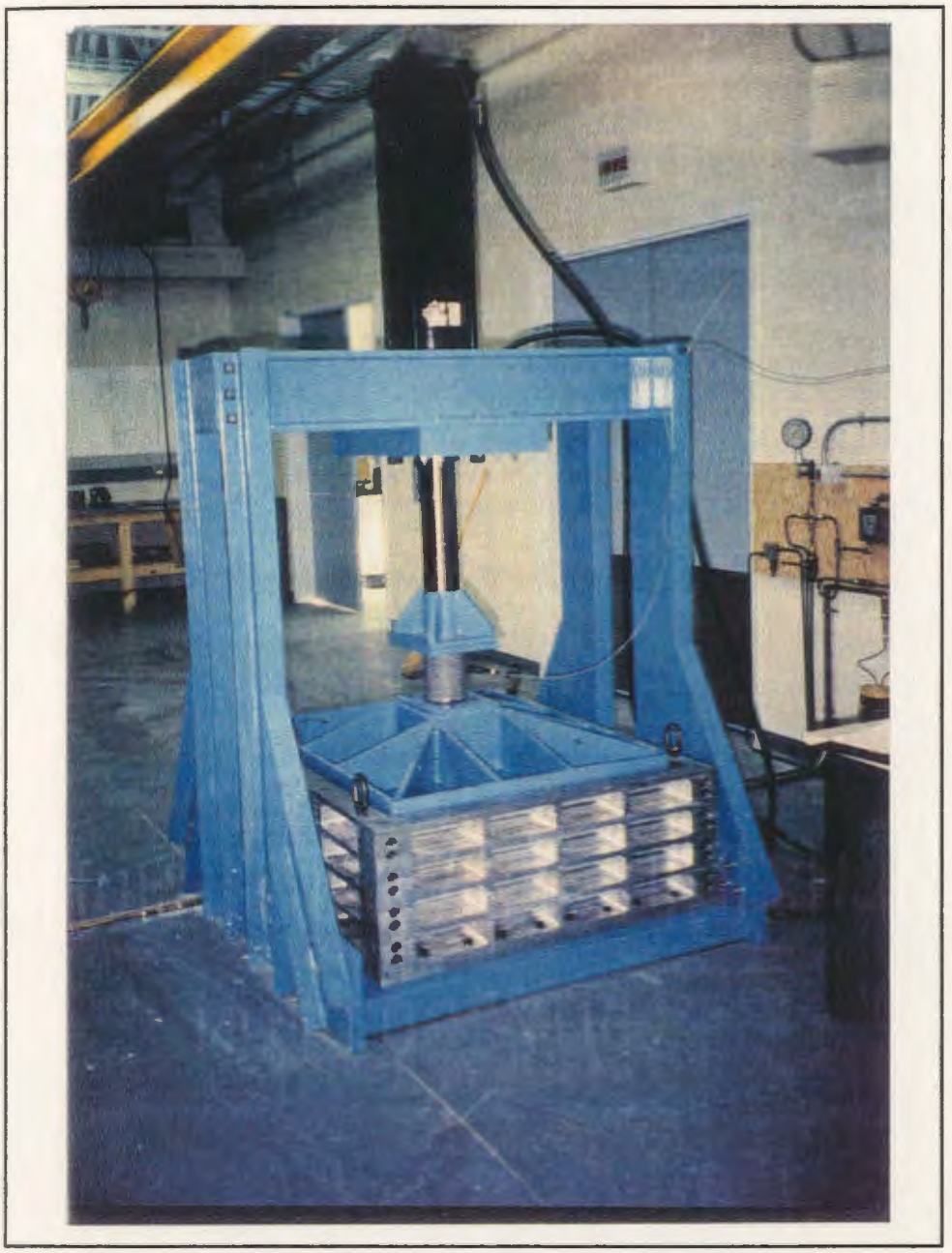

Figure 6.1 - Strongbox in the consolidometer.

the soil and the wall and thus minimize desiccation of the soil along the tub wall.

In cases where each pipeline of a particular test had a different cover (see, for example, Figure 5.2), each of the four quadrants in which the pipelines were located had to be

Figure 6.2 - Shaving of the soil surface.

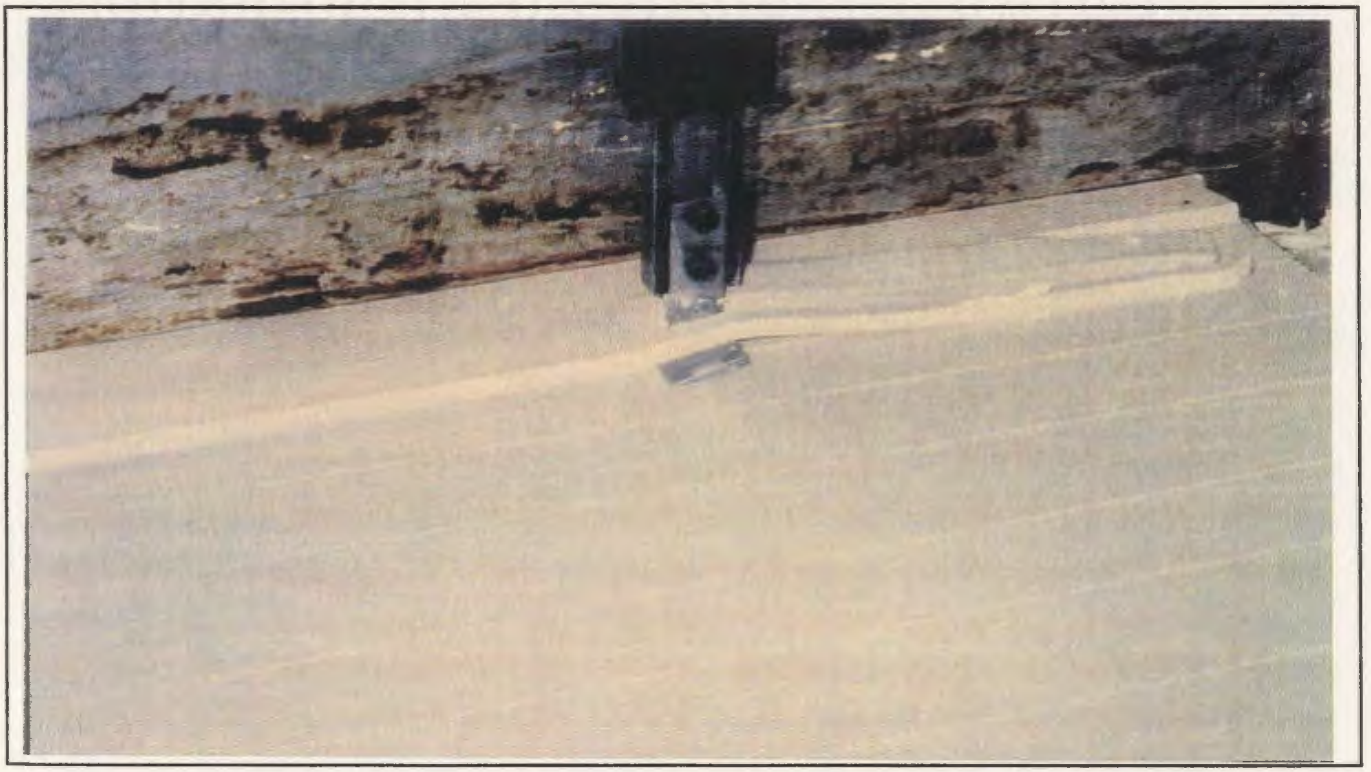

Figure 6.3 - Shaving of the soil surface.

shaved to a different final elevation. Once the surface of each pipeline quadrant had been shaved to the correct height, 15mm wide trenches were carved into the sample for the pipeline tension cables as indicated on Figure 5.1. When cutting trenches, vertical cuts were first made in the soil along the trench perimeter so that the trenches could be excavated "cleanly" with dimensions as close as possible to those specified.

Model preparation continued with installation of the bulkheads. Free water was prevented from entering the sample while the soil was unloaded from the consolidometer creating a state of pore suction in the clay. For this reason, water was introduced to the base of the sample prior to cutting through the soil into the base drain. Vertical cuts were first made down to the geotextile and clay was removed between the cut and end wall of the tub. The two layers of geotextile in the base drain were cut flush with the soil face and the exposed drainage sand vacuumed away. The bulkheads were then put in place and positioned by means of adjuster bolts at the rear of the assembly (Figure 5.1). A piece of stainless steel plate was located between the adjuster bolts and the strongbox to protect the end wall from damage. Figure 6.4 shows a model after installation of the bulkheads.

The pipeline trenches were then cut in the soil sample. Vertical cuts were made around each trench perimeter prior to excavation with the horizontal cutters. Figure 6.4 shows the completed trenches. As indicated in Figures 5.1 and 5.2, a cone test pit was excavated between the pipeline trenches in the centre of the sample which was filled with backfill. This test pit was necessary to determine the strength of the backfill during centrifuge

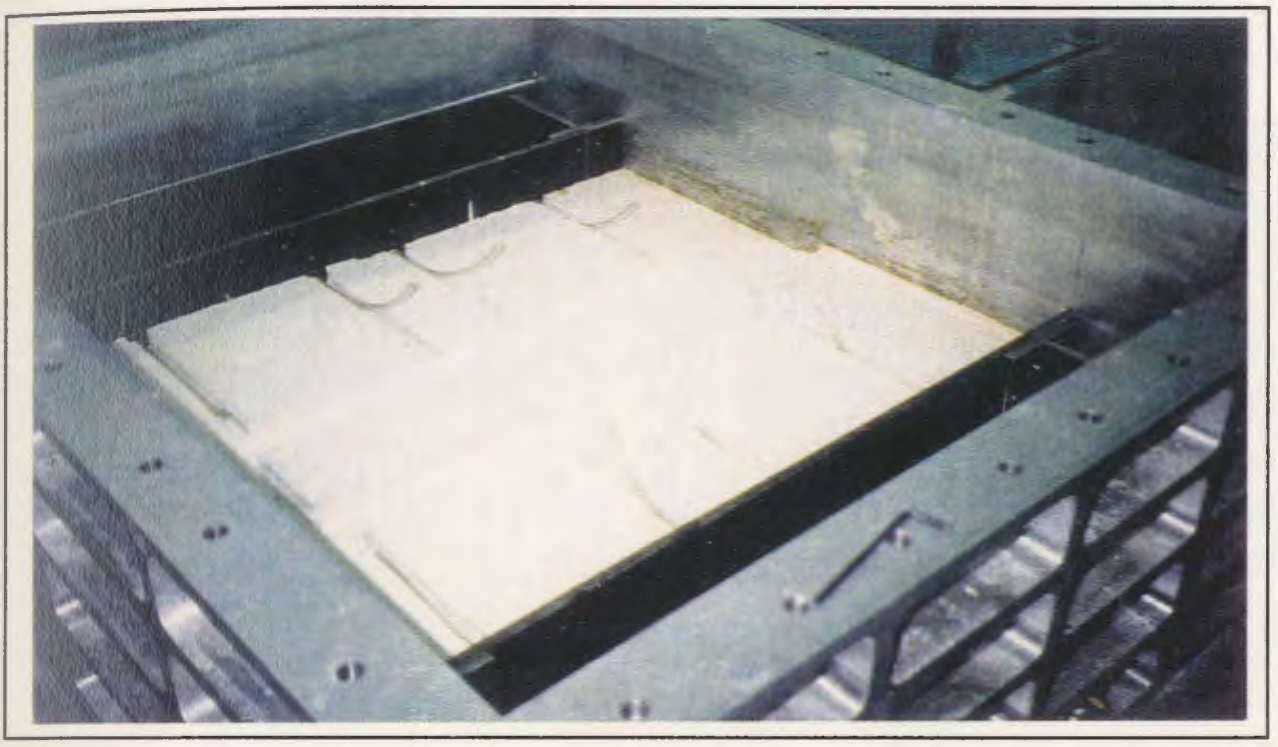

Figure 6.4 - Test sample after installation of bulkheads.

testing as movement of the cone was limited to the single transect between and parallel to the pipelines. The cone could then complete a transect between the pipelines and test the penetration resistance of both the native and backfill materials.

After the carving of the soil was completed, the entire surface of the sample was covered in Vaseline as shown in Figure 6.5. This practice was adopted to prevent migration of pore fluid from the backfill material into the native material and to prevent desiccation of the soil surface.

The pipelines were then placed in the trenches as shown in Figure 6.5 and the pipeline

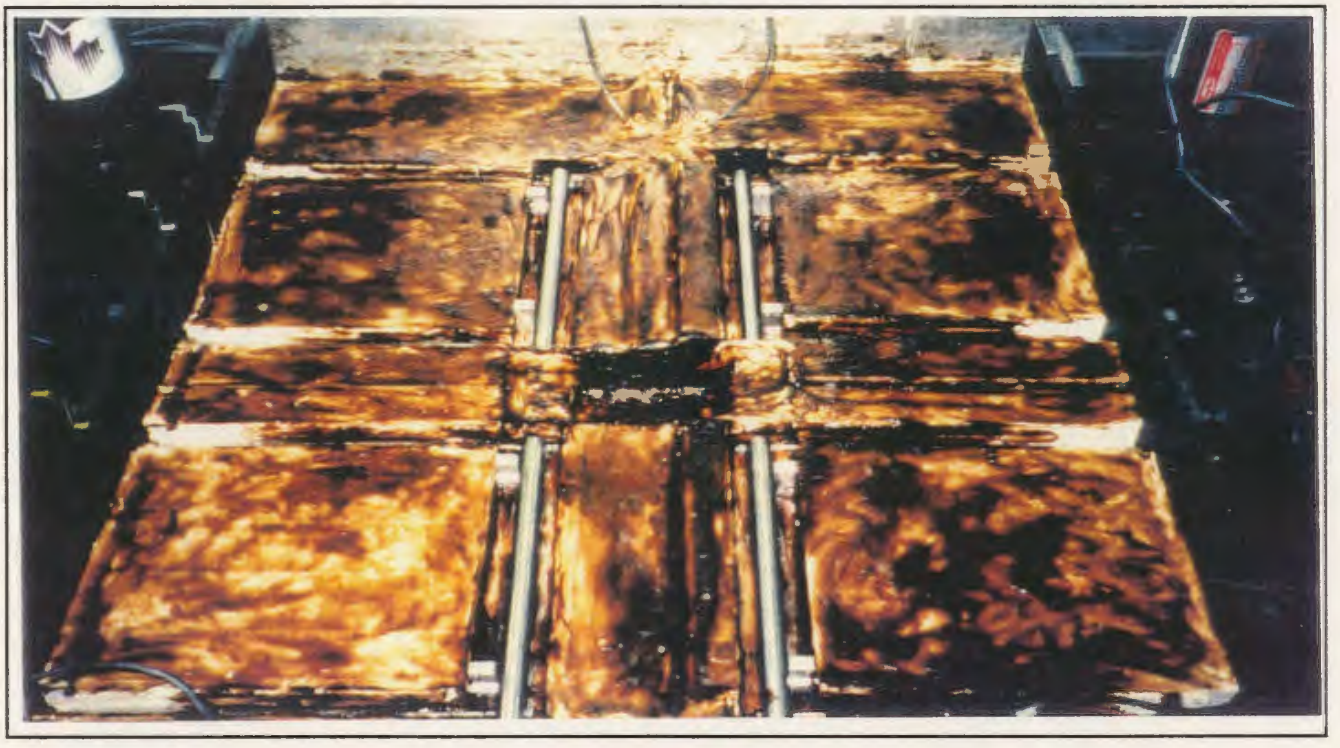

Figure 6.5 - Pipelines in position prior to backfilling of trenches.

displacement cables were run through the bulkhead and connected to the drive unit as was shown in Figure 5.1. Positioning blocks were used to locate the leading edge of the pipeline from the trench wall as shown in Figure 6.5 and small trenches were carved behind the pipelines for the passage of signal cable channels. These channels were lengths of tygon tubing approximately 150mm in length which provided a passageway from the pipeline to the soil surface for the pipeline instrumentation cables. Where testing was conducted at 1:50 scale, the model pipelines were 19mm in diameter; at 1:25 scale, the model pipelines were 38mm in diameter; at 1:100 scale, the model pipelines were 9.5mm in diameter.

During Test 01 through Test 08, the backfill used consisted of the same material as the native material but was a slurry mixed to approximately 65%. The trenches were then backfilled as shown in Figure 6.6. During Test 09, a variety of backfills were studied as shown in Figure 6.7. When backfilling was almost complete, the pipeline positioning blocks were removed. This backfill was roached immediately prior to centrifuge testing, allowed to consolidate and settle under high gravity, and then re-roached. In this manner, a backfill was obtained which was made of the same material as the native (with the exception of the fine sand backfill), but with differing properties due to a different stress history. During placement of the backfill into the trenches, samples were taken and the water content of the backfill was measured. Prior to testing, the trenches were covered with thin plastic film to prevent desiccation and thus ensure differences between the properties of the backfill and the native or surrounding material.

A standpipe was connected to the strongbox as depicted in Figure 5.1. An overflow was attached to this standpipe to establish a water table within the model. The interpreted position of the water table from each test is presented in Section 6.5.

6.4 Installation of Instrumentation

Once the model was prepared, the pipeline load cells were in position. If pore suction transducers were to be used for a particular test, then the pipelines in which they were incorporated were used. Additional sensors and instrumentation described below were

Figure 6.6 - Backfilling of 50g trenches.

Figure 6.7a - Slurry (left) and fine sand (right) backfills.

Figure 6.7b - Remoulded (left) and chunky (right) backfills.

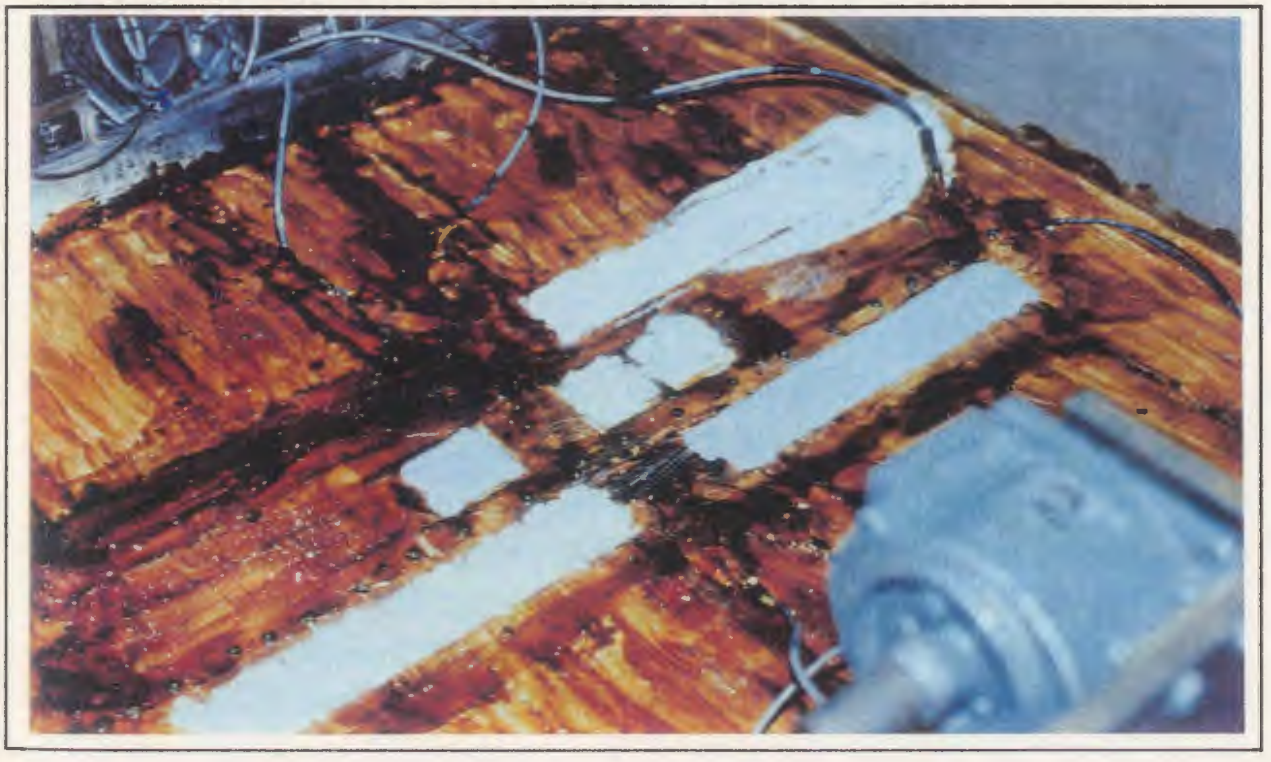

Figure 6.7c - Remoulded, sand, slurry, and chunky backfills clockwise from upper left.

then incorporated into the model to measure soil pore pressures, internal plastic deformation of the soil, soil surface movement, and to observe the overall experiment conduct.

Druck pore pressure transducers, PPTs, were inserted generally at midheight of the soil sample as shown in Figure 5.2. The PPTs were boiled prior to testing to ensure saturation of the porous stone and the void between the stone and the PPT membrane. The PPTs were inserted into the sample by drilling a 7mm diameter hole with a standard extended drill bit and inserting the PPT. The PPT was pushed approximately 5mm into virgin material past the end of the hole and the hole backfilled with slurry.

Spaghetti markers were inserted along the pipelines path. The insertion, shown in Figure 6.8, was aided by a special jig to keep the spaghetti vertical during the insertion process. The cone penetrometer could then be attached to the model and linear displacement transducers (LDTs) were attached to the model package. CCD cameras were also positioned to monitor and record the experiment progress. Just prior to centrifuge flight, when water was being added the model, the PPTs used to monitor water levels in the model were positioned. A photograph of a completed model package is presented in Figure 6.9.

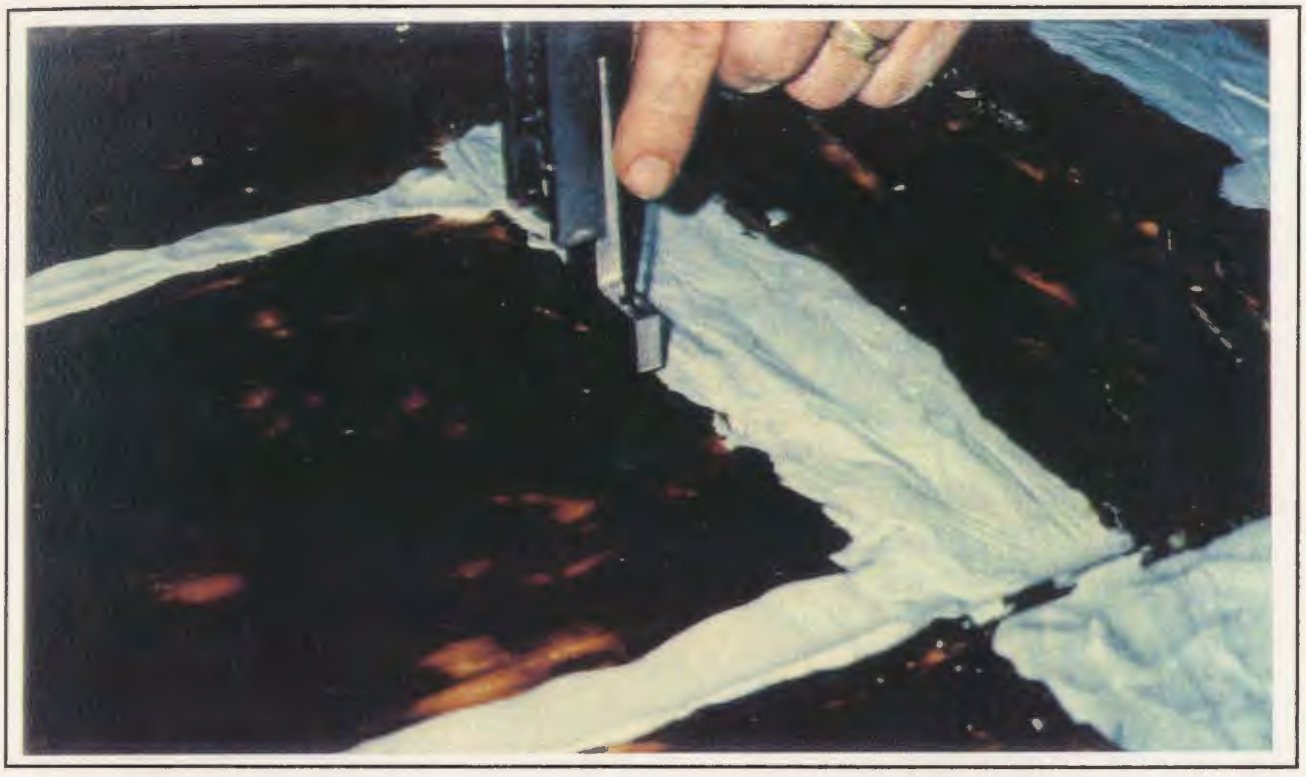

Figure 6.8 - Spaghetti marker being inserted in front of trench.

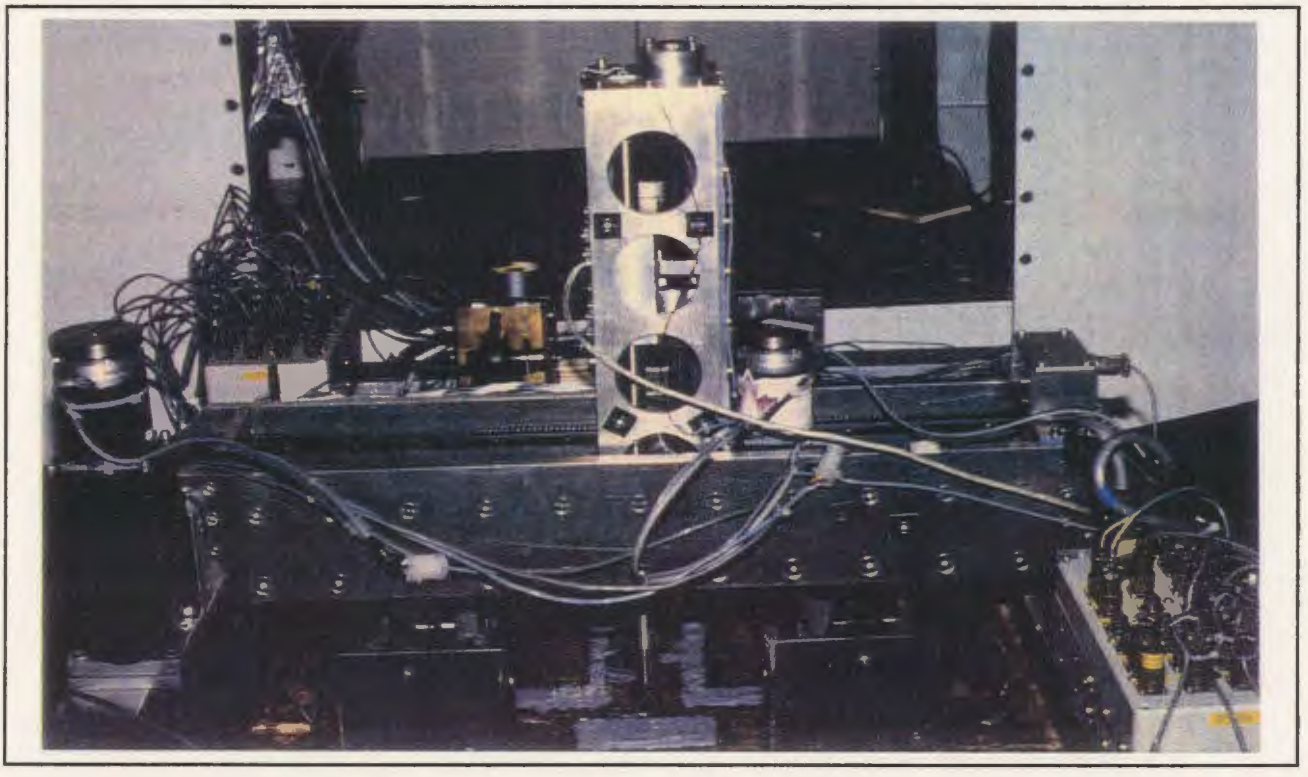

Figure 6.9 - Completed model package.

6.5 Model Testing Procedure

6.5.1 General Procedure

The general procedures of model preparation worked generally well and models were constructed within three days. Model configurations are presented in Appendices B through J; the *Test Data* appendices. At least 24 hours prior to testing, the coloured spaghetti markers were inserted at 5-10mm intervals along the pipelines path. Druck pore pressure transducers were inserted at approximately midheight of the soil sample at locations shown in the *Test Data* appendices. Once preparation was complete, the entire clay surface was covered and sealed with plastic film and the strongbox transported to the centrifuge. Linear displacement transducers were positioned over the soil surface of the model if required. The cone assembly was then mounted on the strongbox if it had not been mounted prior to model transport. Instrumentation and sensors were then connected to the two on-board signal conditioning boxes. The data acquisition system was then turned on and all wiring was secured for centrifuge flight. CCD cameras were mounted on the package and positioned to observe and record the pipeline displacements.

Prior to beginning centrifuge testing, the pipeline trenches and cone test pit were roached. The trenches and cone test pit were then covered with very thin plastic film (i.e. Saran Wrap) to prevent desiccation of the backfill material (as this material was too soft to be covered with Vaseline). Each piece of plastic film was specifically fitted to a trench and once positioned, thumbtacks were used to secure the plastic film in place and Vaseline used

to seal the edges. Care was taken to ensure that at no time during pipeline displacement would the pipeline come in contact with the thumbtacks. This method appeared to work well; the plastic film remained in place during testing and it could be removed and replaced to allow roaching of the trenches.

Immediately prior to the start of centrifuge testing, water was introduced to the soil sample to establish a water table within the model. During testing, control was maintained over the position of the water table in the sample. The clay sample was freely drained at the base of the bulkhead interface and along the base as the extrusion plate was porous. Through the use of a continuous water feed and a standpipe/weir system, the water level was maintained at a constant elevation within the sample. The water level was constantly monitored by two pore pressure transducers in the motor box area and one pore pressure transducer at the bottom of the standpipe.

The model package was then accelerated to the appropriate gravitational level with respect to the pipeline's springline. Pore pressure response within the soil model during centrifuge swingup to the appropriate acceleration level and during sample consolidation was monitored. After approximately one hour of flight, the centrifuge was stopped and the trenches roached. Centrifuge testing then resumed and the model soil allowed to consolidate under enhanced self-weight until 90% consolidation had been achieved. Cone testing and pipe displacements were then completed.

After all in-flight activities had been completed, the centrifuge was stopped and free water in the strongbox was removed immediately. After water content samples had been taken, the model soil was covered with plastic film until the strongbox could be unloaded from the centrifuge and extrusion of the sample could take place.

6.5.2 Test 01 - Effect of Shallow Cover Depth

The objective of Test 01 was to investigate the effect of shallow trench depth on the resulting pipeline/soil interaction. The model configuration is presented in Appendix B. This model was made at 1:50 scale in soil which had been preconsolidated to approximately 400kPa and thus tested at 50 gravities in the centrifuge. Cover depths investigated were 16, 10, 5, and 0mm (model-scale) which correspond to prototype values of 0.8, 0.5, 0.25, and 0m respectively. The model trench width during testing was 50mm (2.5m prototype-scale). The pipelines were to be displaced at a nominal speed of 0.5 to 0.7 mm/sec.

It was determined after completion of the pipeline trenches, that the soft backfill might flow from the deepest cover trench to the shallowest as there was a difference in elevation of 16mm. This potential flow of backfill was prevented by blocking the ends of each trench with a 3mm plexiglass sheet as shown in Figure B.1. These bulkheads were arranged in such a manner that the test pit could be filled with slurry to a height equivalent to 8mm of pipeline cover. In subsequent tests, this problem was remedied by ensuring that the four pipeline trenches and the test pit were not interconnected but rather were carved

independently.

A short delay was experienced during the first attempt to accelerate the experimental package to 10g; the second attempt was successful. During all tests, Taylor's Construction (Holtz and Kovacs, 1981) was used to determine when at least 90% consolidation of the soil had occurred; pipeline and cone testing was then permitted to proceed. The pore pressure transducers in the motor box area measured a total depth of approximately 49mm of water during testing. All water elevations were measured with respect to the extrusion plate and along centerline.

6.5.3 Test 02 - Effect of Deep Cover Depth

The objective of Test 02 was to investigate the effect of deep trench depth on the resulting pipeline/soil interaction. Presented in Figure C.1 is the model configuration used for this test. This model was made at 1:50 scale in soil which had been preconsolidated to approximately 400kPa and thus tested at 50 gravities in the centrifuge. Cover depths investigated were 65, 50, 38, and 27mm (model-scale) which correspond to prototype values of 3.25, 2.5, 1.9 and 1.35m respectively. The model trench width during testing was 50mm (2.5m prototype-scale). The pipelines were to be displaced at a nominal rate of 0.5 to 0.7 mm/sec.

Just prior to swingdown to roach the pipeline trenches, a crack was noticed to have developed between the test pit and the trench of Pipeline #4. The centrifuge was then

stopped and the test pit and pipeline trench were repaired using plexiglass and wire anchors as reinforcement. Because the cracking and subsequent reinforcement had occurred to the rear of the pipeline, it was felt that after it was repaired and the trenches roached that it should not seriously affect the pipeline/soil interaction in front of the pipeline. When centrifuge testing resumed, the crack was carefully monitored. The pore pressure transducers in the motor box area measured a total depth of approximately 74mm of water during testing.

6.5.4 Test 03 - Effect of Trench Width

The objective of Test 03 was to investigate the effect of trench width on the resulting pipeline/soil interaction. The model configuration used for this test is shown in Figure D.1. This model was made at 1:50 scale in soil which had been preconsolidated to approximately 400kPa and thus tested to 50 gravities in the centrifuge. Trench widths investigated were 30, 40, 50, and 60mm (model-scale) which correspond to prototype values of 1.5, 2.0, 2.5 and 3m. The model cover depth during testing was 16mm (0.8m prototype-scale). A nominal speed of 0.5 to 0.7 mm/sec. was to be used for the pipeline displacement. The pore pressure transducers in the motor box area measured a water depth of approximately 54mm during testing.

6.5.5 Test 04 - Effect of Interaction Rate

The objective of Test 04 was to investigate the effect of displacement rate on the resulting pipeline/soil interaction under constant trench geometry (model cover depth = 16mm and

model trench width = 50mm). Figure E.1 of Appendix E presents the model configuration used for Test 04. This model was made at 1:50 scale in soil which had been preconsolidated to approximately 400kPa and thus tested at 50 gravities in the centrifuge. Nominal displacement rates of 0.0008, 0.005, 0.05 and 1.0 mm/sec. (model-scale) were to be investigated. The reasoning behind the location of the PPTs shown in Figure E.1 was that an assessment of the drainage conditions in front of the pipelines could be made for different interaction rates. The reason that PPT #2 is shown twice in Figure E.1 is explained later.

The pore pressure transducers in the motor box area measured a total water depth of approximately 65mm during testing. Cone testing and the start of testing Pipeline #1 began without problem. When the attempt was made to pull Pipeline #2, it could not be displaced due to a malfunction with the drive system. It was decided to complete the displacement of Pipelines #1, 3, and 4 and to rerun the following day to displace Pipeline #2 (once the drive had been repaired).

The following day, the drive system for Pipeline #2 was repaired and PPT #2 moved in front of Pipeline #2 to assess drainage during testing. The pore pressure transducers in the motor box area measured a total water depth of approximately 68.5mm during testing. This time, the attempt to displace Pipeline #2 was successful as no problems were experienced during testing.

6.5.6 Test 05 - Modelling of Models at 1:25 Scale

The objective of Test 05 was to conduct a modelling of models investigation of Test 01 which investigated the effect of trench depth on the resulting pipeline/soil interaction. The model configuration used for this test is shown in Figure F.1 of Appendix F. This model was made at 1:25 scale in soil which had been consolidated to approximately 400kPa and thus tested at 25 gravities in the centrifuge. Cover depths investigated were 32, 20, 10, and 0mm (model-scale) which correspond to prototype values of 0.8, 0.5, 0.25, and 0m respectively. The model trench width during testing was 100mm (2.5m prototype-scale). The pipelines were to be displaced at a nominal speed of 0.25 mm/sec. (which was approximately half the displacement rate used in Test 01). The pore pressure transducers in the motor box area measured a depth of approximately 17mm of water during testing.

6.5.7 Test 06 - Modelling of Models at 1:100 Scale

The objective of Test 06 was to conduct a modelling of models investigation of Test 01 which investigated the effect of trench depth on the resulting pipeline/soil interaction. Figure G.1 of Appendix G presents the model configuration used for this test. This model was made at 1:100 scale in soil which had been consolidated to 400kPa and thus tested at 100 gravities in the centrifuge. Cover depths investigated were 8, 5, 2.5, and 0mm (model-scale) which correspond to prototype values of 0.8, 0.5, 0.25, and 0m respectively. The model trench width during testing was 25mm (2.5m prototype-scale). A pipeline displacement rate of 1.0 to 1.4 mm/sec. was strived for (which was approximately twice the displacement rate in Test 01). Pore pressure transducers in the motor box area

measured a depth of approximately 89mm of water during testing.

6.5.8 Test 07 - Effect of Interaction Rate

The objective of Test 07 was the same as for Test 04; to investigate the effect of displacement rate on the resulting interaction factors with constant trench geometry (model cover depth = 16mm and model trench width = 50mm). The model configuration used for Test 07 is shown in Figure H.1 of Appendix H. This 1:50 scale test in clay which had been consolidated to 400kPa was essentially a repeat of Test 04. Nominal displacement rates of 0.0005, 0.005, 0.05 and 0.5 mm/sec. (model-scale) were to be investigated. As with Test 04, the PPTs were located to assess the drainage conditions in front of the pipelines during pipeline displacement at different interaction rates.

The pore pressure transducers in the motor box area measured an average water depth of approximately 76mm during testing. A cone test was attempted after completion of the pipeline tests; however, control problems prevented completion of Cone Test #8 at 50g.

6.5.9 Test 08 - Effect of Soil Preconsolidation Stress

The objective of Test 08 was to assess the effect that variation in soil preconsolidation stress would have on the resulting pipeline/soil interaction as well as to investigate the effect of displacement rate on the interaction under constant trench geometry (model cover depth = 16mm and model trench width = 50mm). The model configuration used for Test 08 is shown in Figure I.1 of Appendix I. This 1:50 scale test was similar to Test 07 except

the preconsolidation pressure in the soil was reduced to 160kPa to determine if stress history has any effect on experimentally determined interaction factors. Nominal displacement rates of 0.0005, 0.005, 0.05 and 0.5 mm/sec. (model-scale) were to be investigated. PPTs were located to assess the drainage conditions in front of the pipelines during pipeline displacement. Pore pressure transducers in the motor box area measured an average water depth of approximately 68mm during testing.

6.5.10 Test 09 - Effect of Backfill Type

The objective of Test 09 was to investigate the effect of backfill type on the resulting pipeline/soil interaction under constant trench geometry (model cover depth = 16mm and model trench width = 50mm). Figure J.1 of Appendix J presents the model configuration used for Test 09. This model was made at 1:50 scale in soil preconsolidated to 400kPa and thus tested at 50 gravities in the centrifuge. A nominal displacement rate of 0.0005 mm/sec. (model-scale) was to be used.

Four different types of backfills were used in Test 09. During assembly of the model, The cone test pit was then subdivided as shown in Figure J.1 to accommodate the different types of backfills being used in the test. The backfills used during testing were as follows: Pipeline #1 - baseline slurry as used in previous tests; Pipeline #2 - grated native material patted into place; Pipeline #3 - remoulded native material pushed into place; Pipeline #4 - loose fine sand. Photographs of these backfills are presented as Figure 6.7. Each of the four subdivisions of the cone test pit were filled with the different backfill types. The

backfill of Pipeline #3 and associated test pit was levelled with respect to the native material surface and the surface covered with Vaseline. PPTs were located to assess of the drainage conditions in front of the pipelines during pipeline displacement. The cone test pit containing the slurry and chunky backfill was covered with plastic film to prevent desiccation of the backfill material.

Shortly after beginning testing of the pipelines, it was noticed that Drive #3 was not functioning. Therefore, the decision was made to stop the pipeline displacement, to swingdown, and to check out the drive. A broken electrical connection was repaired and centrifuge testing resumed. The pore pressure transducers in the motor box area measured an average water depth of approximately 66mm during testing.

Once 90% consolidation had been achieved, all drives were restarted. During testing it was observed that Pipeline #2 was travelling very slowly and eventually stopped after approximately 5mm of displacement. It was decided to continue with the testing of Pipelines #1, #3 and #4 and to retest Pipeline #2 once the drive could be repaired. It was observed after approximately 11 hours that Drive #4 appeared to have stalled so power to the drive was cut to allow the motor to rest and the pipeline was successfully restarted approximately 2 hours later. Testing of Pipelines #1, #3, #4 was then finished without incident, the centrifuge stopped, and the model covered.

Four days later, testing of Drive #2 indicated that it was functioning satisfactorily and

centrifuge testing recommenced. Cone testing and displacement of Pipeline #2 were then successfully completed. The pore pressure transducers in the motor box area measured an average water depth of approximately 60mm during this phase of testing.

6.6 Post-Test Investigation

Several post-test investigations were undertaken upon completion of the centrifuge portion of the testing. Immediately after testing, after free water in the strongbox was removed, water content samples were taken from both the native material and the backfill. These samples were taken in the native material using a one-inch diameter coring tube while the samples were taken from the backfill using a spatula. During excavation, water content measurements were also made between the trenches to provide an indication of backfill porewater (from consolidation) migration into the native material.

Following the majority of tests, hand and/or mechanical vane tests and torvane tests were conducted in the sample. After the model had been transported to the main lab floor, the model testbed surface was profiled either by hand or by using a laser profiler. The sample was then extruded from the strongbox using the extrusion plate and sectioned on the lab floor. Photographs were taken and sketches made at various predetermined positions along the pipeline length. Additional care was taken at the cross-section containing the spaghetti strands as these would provide the most information about internal deformations and displacement patterns within the soil.

Chapter 7

Experimental Results

7.1 Introduction

The previous chapter outlined the experimental procedures and testing details. This chapter details the relevant experimental results obtained from the centrifuge testing. Details are presented for Test 01 and as for the most part these details were the same for following tests, they have not been repeated; only deviations from the norm are presented. Selected test results and observations are presented in the *Test Data* appendices (Appendices B through J). Results will be analysed and compared in the following chapter.

7.2 Test 01 - Effect of Shallow Cover Depth

Eight cone penetrometer tests (CPTs) were conducted during the course of displacing the pipelines. Details are presented in Table B.1 of Appendix B. Figures B.2 and B.3 present the results of the tests as well as the location of the pipe springlines relative to each CPT. The bulge in the CPT data in the test trench appears to have been caused by the plastic film. However, once the cone punctured the film, there appears to have been no further effect on the penetration resistance. Penetration resistances were determined by extending the straight line portion (below 40mm depth) of the CPT data up to the relevant springline

as indicated in Figure 7.1. This procedure was followed for all tests. The interpreted penetration resistances at the original pipe springlines are summarized in Table B.2.

The pipelines were pulled by the stainless steel cables at the lowest possible rate on the existing motor system. Pipeline test details are presented in Table B.3 where it can be seen that the velocities were all relatively close. Model-scale force-displacement records from the four pipelines are presented in Figures B.4 through B.7. Figure B.8 compares the model pipeline responses from all four tests.

The combination of Vaseline and plastic film prevented desiccation of the soil sample during flight in the centrifuge. Immediately after testing, water content samples were taken in both the native and backfill materials using a coring tube. Comparing results indicated that a minimal amount of porewater from the backfill had migrated into the native material for this and all tests. During excavation of the sample, water content measurements were made between the trenches. The purpose of these tests was to determine if there was any significant change in the water content between the trenches; this might indicate migration of backfill porewater into the native material. Comparing results indicated that there appeared to have been a minimal migration of porewater into the native material for this and all tests.

Subsequent to centrifuge testing, the sample was extruded from the strongbox and

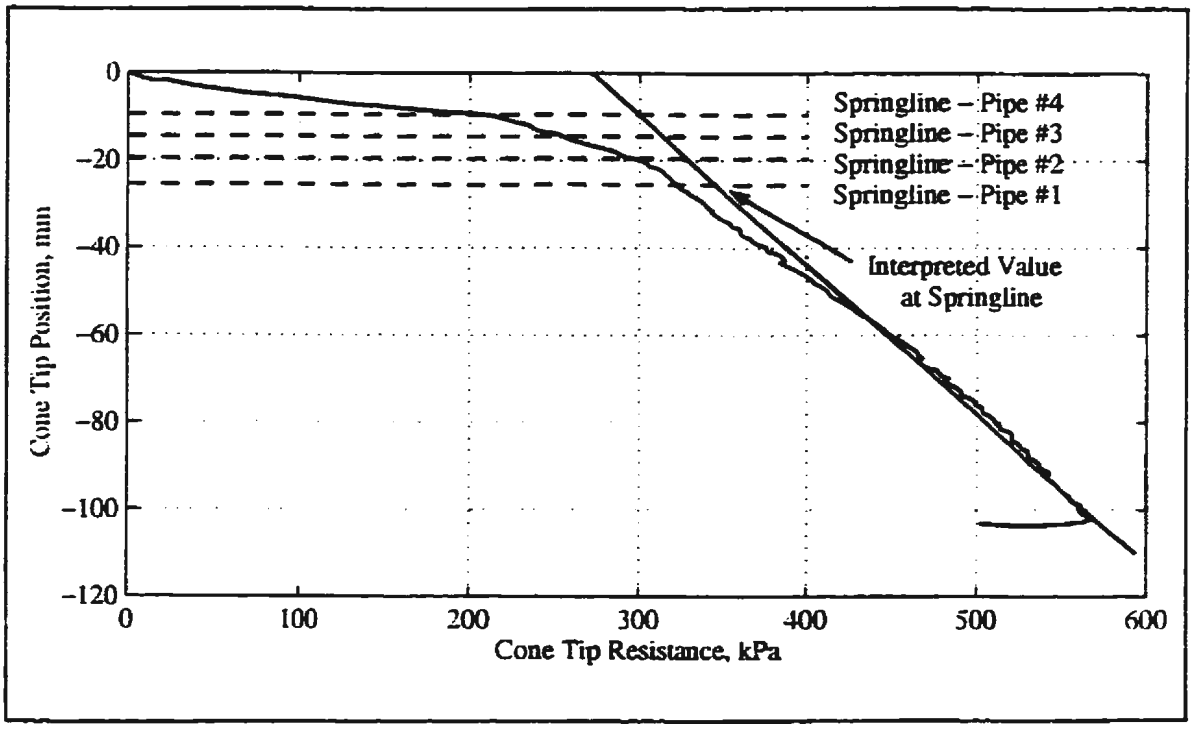

Figure 7.1 - Method of interpreting cone penetration resistances at pipe springlines.

sectioned at one gravity on the lab floor. Photographs were taken and sketches made and internal deformations noted to determine displacement patterns within the soil. Photographs of the deformations are presented in Figures B.9 through B.12 where the cross-sections are approximately halfway along the pipeline length. Sketches of the cross-sections are presented in Figures B.13 through B.16. In subsequent tests, additional spaghetti strands were used in front of the pipeline.

7.3 Test 02 - Effect of Deep Cover Depth

Selected data obtained from Test 02 are presented in Appendix C. During testing, it had been planned to conduct more cone tests but problems were experienced with the cone

vertical drive system and it was decided to conduct only the required cone tests.

Post-test analysis of the Pipeline #1 test data revealed that no displacement data had been collected by the data acquisition system. Therefore, the time-displacement relationship for the pipeline was estimated by measuring the post test output of the rotary potentiometer connected to the drive system.

After the model had been transported to the main lab floor, a series of five shear vane tests was conducted. Midheight of the vane was located at a depth of 61mm and measured undrained shear strengths ranged from 19.6 to 26.4kPa with an average of 24.3kPa.

7.4 Test 03 - Effect of Trench Width

Selected Test 03 test data and observations are presented in Appendix D. As can be seen from Figure D.5, there was a problem with data acquisition during the pulling of Pipeline #2. As soon as it was realized that data acquisition had stopped, pipeline movement was stopped. Data acquisition was started again as soon as possible and the pipeline permitted to continue moving. It is believed that because the pipeline stopped, excess pore pressures in the soil in front of the pipeline would have had time to dissipate (consolidation took place). Loads measured after starting the pipeline again would be higher due to the consolidation in front of the pipeline.

Four shear vane tests were conducted with a mechanized laboratory vane after model transport to the lab floor. Midheight of the vane was located at a depth of 61mm and undrained shear strengths ranged from 24.6 to 27.3kPa with an average of 26.4kPa.

7.5 Test 04 - Effect of Interaction Rate

Selected data collected and observations made during the course of Test 04 are presented in Appendix E. The force-displacement curves of Pipelines #1 and #2 have been corrected for any long-term electronic drift effects of the pipelines under load. As can be seen from the data, Pipeline #1 stopped before it reached the desired 80mm of travel. This occurred because the pipeline displacement system failed. The system was designed to handle a load equivalent to twice the measured undrained pipeline loading. However, this design load was exceeded and the drive system failed. Testing of Pipeline #2 was permitted to continue until the maximum travel of the drive system had been reached. Problems were encountered during the testing of Pipeline #3; the output shifted off scale due to electronic problems with the pipeline. The test continued using the windup-pulley torque cell output as a measure of the pipeline loading. Examination of the data from Pipeline #2 and Pipeline #4 indicated that the resulting torque load was, on average, 1.25 times the measured pipeline load. With this information, the load on Pipeline #3 could be estimated. Figure E.8 indicated that the estimated load was reasonable. Pore pressure transducers were positioned in front of the pipelines to assess the drainage conditions associated with the different interaction rates. The PPT locations were presented in Figure E.1.

Immediately after testing, eight Pilcon hand vane and six torvane tests were conducted. Midheight of the hand vane was located at depths of 44, 63, and 102mm during testing and resulting average undrained shear strengths were 15.5, 18, and 17kPa respectively. From the torvane, measured surface undrained shear strengths ranged from 17.2 to 19.6kPa with an average of 18.1kPa.

7.6 Test 05 - Modelling of Models 1:25 Scale

Selected Test 05 results are presented in Appendix F. The pipelines were pulled by the stainless steel cables at the lowest possible rate on a modified motor system. A velocity rate of 0.25 mm/sec. was targeted but the rate was a bit higher which is attributed to the lower "g" level forces acting on the motors and systems for this particular test. As can be seen from Figure F.5, there was a problem with the pulling of Pipeline #2. After approximately 45mm of displacement, the pipeline stopped moving because of a jam in the drive system. By reversing the motor several times, the jam was eliminated and pulling continued as shown in the figure. The spikes during the latter part of the force-displacement curve were believed to have been the result of noise picked up by the pipeline displacement transducer. Because the pipeline stopped, excess pore pressures in the soil in front of the pipeline would have had time to partially dissipate (consolidation took place). Figure F.8 compares the model pipeline responses from all four tests; loads measured from Pipeline #2 were higher than expected due to this consolidation.

After testing, five torvane and numerous Pilcon hand vane tests were conducted. Measured undrained shear strengths at approximately midheight of the sample from the hand vane ranged from 12 to 15kPa while the torvane indicated a surface shear strength ranging from 9.8 to 14.7kPa with an average of 12.2kPa.

7.7 Test 06 - Modelling of Models 1:100 Scale

Appendix G contains selected data and observations from Test 06. Variation in displacement rate is attributed to the responses of the individual motors to the higher "g" levels. During testing of Pipeline #2 and Pipeline #3, it was discovered that there were problems with the right shear cells of each of these pipelines. Based on comparisons of the left and right shear cell response of Pipelines #1 and #4, it was discovered that the ratio of the shear cell loads (left load/right load) at peak ranged from 0.9 to 1.1. Taking the mean of the two values, it is reasonable to assume that the missing right shear cell load would be approximately equal to the left shear cell load. This procedure was used in the analysis of Pipeline #2 and Pipeline #3. Figure G.8 compares the model pipeline responses from all four tests; while the above procedure is reasonable, it appears that it may have resulted in an overestimation of the load on Pipeline #2 and a slight underestimation of the load on Pipeline #3 as shown by the close proximity between the curves of Pipelines #1 and #2 and between the curves of Pipeline #3 and #4.

Measured undrained shear strengths from post-test hand vane testing ranged from 12 to

16kPa with an average of 14.6kPa for vane midheight depths ranging from 29 to 67mm. The torvane indicated a surface shear strength ranging from 17.7 to 21.6kPa with an average of 19.5kPa.

7.8 Test 07 - Effect of Interaction Rate

Selected Test 07 data and observations are presented in Appendix H. Model-scale force-displacement records are discontinuous in some of the traces as the data acquisition program had to be stopped and the program changed to accommodate other test activities such as cone tests. During analysis of the data from Pipeline #1, a problem with the data from one of the two pipeline load cells was discovered. Analysis of the load cell data from Pipeline #2 through #4 indicated that the ratio of load cell loads ranged from 0.768 to 1.334. Therefore, these two values, and a value of 1 (assuming the load is equally distributed between the two load cells) were used to reinterpret the Pipeline #1 data as shown in Figure H.4. The force-displacement curves of Pipelines #1 and #2 have also been evaluated for any long-term drift effects of the pipelines under load. Pipeline #1 was stopped after approximately 40mm of travel due to the very slow interaction rate. The drop in the trace of Pipeline #3 has been analysed and it appears to be the result of some mechanical slippage in the system although this cannot be confirmed.

Again, pore pressure transducers were incorporated in the model to assess the drainage conditions in front of the pipe. Transducer locations are presented in Figure H.1. As

mentioned previously, pressure transducers had also been incorporated into the rear of the pipe to assess the soil suction to the rear of the pipeline during testing.

Immediately after testing, four Pilcon hand vane and four torvane tests were conducted. Midheight of the hand vane was located at a depth of 44mm below the surface during testing and resulting undrained shear strengths ranged from 22 to 24kPa. From the torvane, measured surface undrained shear strengths averaged 22kPa.

7.9 Test 08 - Effect of Soil Preconsolidation Stress

Test 08 selected data and observations are presented in Appendix I. Figure I.8 compares the model pipeline responses from all four tests. During analysis of the data from Pipeline #2, a problem with the data from one of the pipeline load cells was discovered. Analysis of the load cell data from Pipeline #1, #3 and #4 indicated that the ratio of load cell loads could range from 0.859 to 1.170. Therefore, the two values, and a value of 1 (assuming the load is equally distributed between the two load cells) were used to interpret the Pipeline #2 data as shown in Figure I.5. The force-displacement curves of Pipelines #1 and #2 have also been evaluated for any long-term drift effects of the pipelines under load. Pipeline #1 was stopped after approximately 50mm of travel due to the very slow interaction rate.

Midheight of the hand vane during testing was located at a depth of 43mm below the

surface during testing and resulting average undrained shear strengths ranged from 9.0 to 11.0kPa with an average of 10.0kPa. From the torvane, measured surface undrained shear strengths ranged from 8.8 to 13.7kPa with an average of 11.0kPa.

7.10 Test 09 - Effect of Backfill Type

Appendix J contains selected data and observations collected during Test 09. With the exception of Pipeline #2, the model pipeline velocities were close to the desired values. The data of Figure J.5 (Pipeline #2) does not start at the point 0,0 due to the slight displacement and loading of the pipeline during testing before the drive unit malfunctioned during the first centrifuge flight. The response of Pipeline #3 falls off at a displacement of approximately 36mm due to slippage of the pipeline tension cable. The data are discontinuous in some of the traces as the data acquisition program had to be stopped and the program changed to accommodate other test activities such as cone tests. The force-displacement curves of the pipelines have been evaluated for any long-term drift effects of the pipelines under load. Pipelines were only displaced slightly more than two pipeline diameters due to the slow interaction rate.

Midheight of the hand vane was located at a depth of 44mm below the surface during testing and resulting undrained shear strengths ranged from 17.5 to 20.0kPa with an average of 18.9kPa. From the torvane, measured surface undrained shear strengths ranged from 16.7 to 19.6kPa with an average of 17.9kPa.

Chapter 8

Analysis and Comparison of Experimental Results

8.1 Analysis of Experimental Data

8.1.1 Introduction

The experimental data are analysed to undertake a parametric study and compared with accepted and proposed methods of pipeline/soil interaction analyses. This section presents these analyses of the experimental data. It consists of: a description of prototype conditions for each test; a description of internal soil deformations along the pipeline's displacement path; an explanation of how the undrained shear strengths were derived; prototype-scale force-displacement curves; a derivation of interaction factors; a determination of normalized loads at predetermined displacements; and a bilinear analysis of the force-displacement curves. These results will then be used in Section 8.2 for parametric analyses.

8.1.2 Description of Prototype Conditions

The prototype equivalent for each of the models described in a previous chapter is a system of four pipeline segments buried in overconsolidated clay. This clay has a stress history consisting of one-dimensional consolidation to the vertical effective stress indicated in

Chapter 6 followed by a complete removal of vertical boundary stress. Following unloading and prior to pipeline testing, the models had one or more excursions from one gravity to their appropriate increased gravity level before being maintained at the appropriate test acceleration for consolidation.

For Tests 01 through 04, the equivalent prototype pipelines are 0.95m in diameter and 12.5m long. They are pulled by stainless steel cables 0.158m in diameter. At one end of each pipeline, an electrical cable approximately 0.25m in diameter is dragged through a lubricated plastic channel. The equivalent prototype pipelines from Test 05 are 0.95m in diameter, 6.25m long, and are dragged by stainless steel cables 0.079m in diameter. An electrical cable approximately 0.125m in diameter is located at one end of each pipeline and is dragged through a lubricated plastic channel during pipeline displacement. For Test 06, the equivalent prototype pipelines are 0.95m in diameter and 17.5m long. Stainless steel cables, 0.316m in diameter, are used to drag the pipelines. A lubricated plastic channel provides a conduit from the soil surface for a 0.5m electrical cable which is attached to one end of each pipeline. The equivalent prototype pipelines for Test 07 through Test 09 are 0.95m in diameter, 14.1m long, and are pulled by stainless steel cables 0.125m in diameter. At each end of each pipeline, an electrical cable approximately 0.15m in diameter is dragged through a lubricated plastic channel. The pipelines are excited by a horizontal force but they are free to move vertically. The movements at each end of the pipeline are assumed to be equal. The prototype pipeline parameters and relevant geometries from the tests are summarized in Table 8.1 and Table 4 in the *Test Data*

Table 8.1 - Prototype test parameters

Test	Pipeline	Trench Width (m)	Cover Depth (m)	Embedment Ratio H/D	Pipeline Velocity (m/day)
01	1	2.5	0.80 → 0.80	1.842 → 1.842	0.86
01	2	2.5	0.50 → 0.70	1.526 → 1.737	0.98
01	3	2.5	0.25 → 0.40	1.263 → 1.421	1.16
01	4	2.5	0.00 → 0.20	1.000 → 1.211	1.05
02	1	2.5	3.25 → 3.25	4.421 → 4.421	0.90
02	2	2.5	2.50 → 2.55	3.632 → 3.684	0.95
02	3	2.5	1.90 → 1.90	3.000 → 3.000	1.12
02	4	2.5	1.35 → 1.35	2.421 → 2.421	0.81
03	1	3.0	0.80 → 0.80	1.842 → 1.842	0.74
03	2	2.5	0.80 → 0.80	1.842 → 1.842	0.95
03	3	2.0	0.80 → 0.90	1.842 → 1.947	1.19
03	4	1.5	0.80 → 0.90	1.842 → 1.947	0.92
04	1	2.5	0.80 → 0.80	1.842 → 1.842	0.0014
04	2	2.5	0.80 → 1.10	1.842 → 2.158	0.0078
04	3	2.5	0.80 → 0.90	1.842 → 1.947	0.075
04	4	2.5	0.80 → 1.05	1.842 → 2.105	1.60
05	1	2.5	0.80 → 0.725	1.842 → 1.763	1.76
05	2	2.5	0.50 → 0.375	1.526 → 1.395	1.80
05	3	2.5	0.25 → 0.25	1.263 → 1.263	1.66
05	4	2.5	0.00 → -0.025	1.000 → 0.947	1.66
06	1	2.5	0.80 → 1.95	1.842 → 3.053	1.22
06	2	2.5	0.50 → 1.75	1.526 → 2.842	0.86
06	3	2.5	0.25 → 1.55	1.263 → 2.632	0.93
06	4	2.5	0.00 → 1.45	1.000 → 2.526	0.93
07	1	2.5	0.80 → 0.925	1.842 → 1.974	0.0012
07	2	2.5	0.80 → 1.025	1.842 → 2.079	0.0092
07	3	2.5	0.80 → 0.925	1.842 → 1.974	0.083
07	4	2.5	0.80 → 1.075	1.842 → 2.132	0.74
08	1	2.5	0.80 → 0.825	1.842 → 1.868	0.00095
08	2	2.5	0.80 → 0.875	1.842 → 1.921	0.0092
08	3	2.5	0.80 → 1.175	1.842 → 2.237	0.083
08	4	2.5	0.80 → 1.225	1.842 → 2.289	0.74
09	1	2.5	0.80 → 0.825	1.842 → 1.868	0.00092
09	2	2.5	0.80 → 0.625	1.842 → 1.658	0.0024
09	3	2.5	0.80 → 0.925	1.842 → 1.974	0.00092
09	4	2.5	0.80 → 0.775	1.842 → 1.816	0.00079

appendices. The range in cover depth and thus embedment ratio (H/D) is explained later in this section.

The corresponding prototype pipeline/soil interaction rates (velocities) are also presented in Table 8.1. In these tests, drainage effects were important and therefore the velocity relationship $v_m = N*v_p$ was utilized in the test series to determine the prototype velocity where N is the model scaling factor.

8.1.3 Internal Deformations

Cross-sectional excavations, sketches, and slides were studied to make general comments on the pipeline/soil interaction during testing. These observations are semi-quantitative in nature but indicate trends in behaviour. During an undrained interaction of the pipeline with the soil, there should be no volume change within the soil mass. For shallow pipelines, the material in front of the pipeline takes the path of least resistance and flows up and over the top of the pipeline (Figure 8.1a). If the pipeline has moved truly horizontal, one would expect the final cover over the pipeline to equal the initial cover plus the diameter of the pipeline for undrained interaction. For deeper pipelines, the mechanism would be expected to be similar to soil flow around a laterally loaded pile with depth where the gravity influence is less; half of the material would be expected to flow up and over the top of the pipeline while the other half would be expected to flow down and under the base of the pipeline (see Figure 8.1b). For the drained case, for a pipeline which has moved truly horizontal, one would expect the final cover to be different than that of the undrained

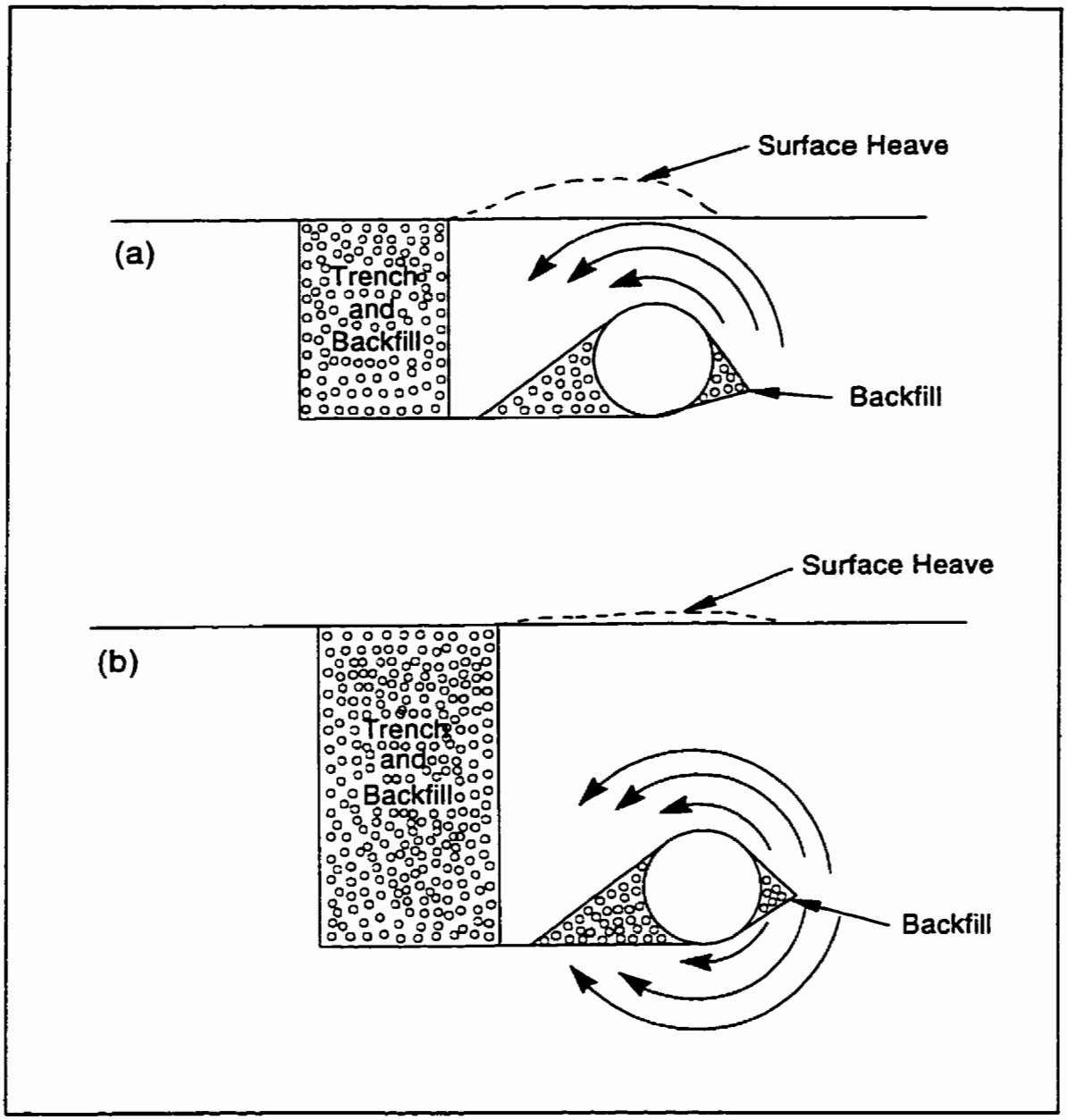

Figure 8.1 - Assumed mechanisms of soil deformation - (a) for a shallowly buried pipeline; (b) for deeply buried pipeline.

case; the actual amount depends on the amount of consolidation which has taken place in front and above the pipeline, the amount of swelling which has taken place during unloading in the centrifuge, and on whether or not dilation or compression has taken place

during shear. Certainly, if the pipeline does not move truly horizontal, vertical movement upwards by the pipeline will affect the amount of soil cover observed following pipeline displacement. Photos and sketches depicting the internal deformations are presented in the appendices containing the test data. Comments on the internal deformations for each pipeline are presented in Appendix K.

8.1.4 Determination of Undrained Shear Strength, c_u

Table 5 in each *Test Data* appendix presents the data used in the calculation of undrained shear strength at the original pipeline springline. In these tables, q_c is the cone tip resistance at the appropriate pipe springline. For Tests 01, 02, 03, 05, and 06, q_c (from the native and backfill materials) was calculated from the average of all the cone tests; because the duration of the tests was relatively short, it has been assumed there was no significant, temporal or spatial variation in tip resistance and an average tip resistance was taken. For tests of longer duration, the temporal variation in cone tip resistance was considered. The tables also present the individual cone tests used to derive an average cone tip resistance corresponding to that particular pipeline test.

Cone penetration tests conducted as part of proof activities leading up to this test series (Paulin *et al.*, 1993) indicated that CPT resistances measured between the pipeline trenches (in the CPT test area) were, on average, 87% of the CPT resistance away from the trench. Therefore, the CPT values obtained in the native material have been multiplied by 1.15 (*Interpreted* q_c, in the *Test Data* appendices) to give a measure of the soil strength of the

native material as the pipeline moved into the trench wall.

The saturated unit weights, γ_{sat}, for the native material shown in *Test Data* appendices (at the appropriate gravity level) were calculated from the densities measured prior to each test and are presented in the respective *Test Data* appendices. For the backfill, γ_{sat} was calculated from

$$\gamma = [\frac{G_s + e}{1 + e}] * \gamma_w \qquad [8\text{-}1]$$

where

$$e = w * G_s \qquad [8\text{-}2]$$

and the post-test water content used for calculations was from the test pit.

In order to calculate the effective stress in the native material at the pipe springline, an indication of the springline pore pressure, u, at the time of testing was estimated based on pore pressure transducer response.

The undrained shear strength of the native material was calculated using the equation

$$q_c = (N_c * c_u) + (\gamma * h) \qquad [8\text{-}3]$$

where c_u is the undrained shear strength of the soil, h is the depth to the springline (in

metres), and N_c has been calculated experimentally as part of proof activities leading up to the current test series for the kaolin-silt mixture. Two values for N_c in the native material at the pipe springline are presented in the *Test Data* appendices because measured strength depends on the method of testing. The first value corresponds to a correlation between cone tip resistance and the undrained shear strength obtained using the shear vane while the second corresponds to a correlation between cone tip resistance and the undrained shear strength obtained using the shear box. The cone factor, N_c, has been determined experimentally (Lin, 1995) to be

$$N_c = 10.1 - [0.94 * \ln(OCR)] \qquad [8\text{-}4]$$

from the vane test results, and

$$N_c = 7.2 + [1.9 * \ln(OCR)] \qquad [8\text{-}5]$$

from the direct shear results.

These relationships have been developed based on an OCR of 5 to 8; most of the current OCRs range from approximately 4 to 14 with variation up to approximately 20. It is assumed in the analysis that Equations [8-4] and [8-5] are valid for these OCR levels. Because two methods of obtaining shear strength profiles were utilized, a range of shear strengths for the native material is presented in the *Test Data* appendices. The first value corresponds to the correlation of cone tip resistance with undrained shear strength profiles derived from shear box data while the second value corresponds to the correlation of cone

tip resistance with undrained shear strength profiles derived from shear vane data. Figure 8.2 compares prototype shear strength profiles from Test 01 as a result of the two methods of correlation where the solid lines represent profiles obtained with the correlation with shear box data.

The backfill material during testing may not have been fully consolidated and the use of Equation [8-3] assuming OCR=1 can lead to negative values of c_u. No pore pressure measurements were taken in the backfill during testing and therefore the degree of consolidation of the backfill is unknown. Begemann (1974) states that the undrained shear strength for normally consolidated soil can be obtained from

$$c_u = q_c / A \qquad \textbf{[8-6]}$$

where A is taken to average 15. Due to lack of a correlation to estimate the shear strength of the backfill material, the undrained shear strength of the backfill material was calculated using this equation. The parameter "A" is more commonly known as N_k and the value of 15 is used in the *Test Data* appendices for the backfill material.

8.1.5 Prototype-Scale Force-Displacement Curves

Prototype-scale force-displacement records corresponding to each of the nine tests are presented in Figures 8.3 through 8.11. These data were obtained by applying the appropriate scaling factors (Table 4.1) to the model-scale data. In the figures, each pipeline's displacement has been normalized with respect to the pipeline diameter.

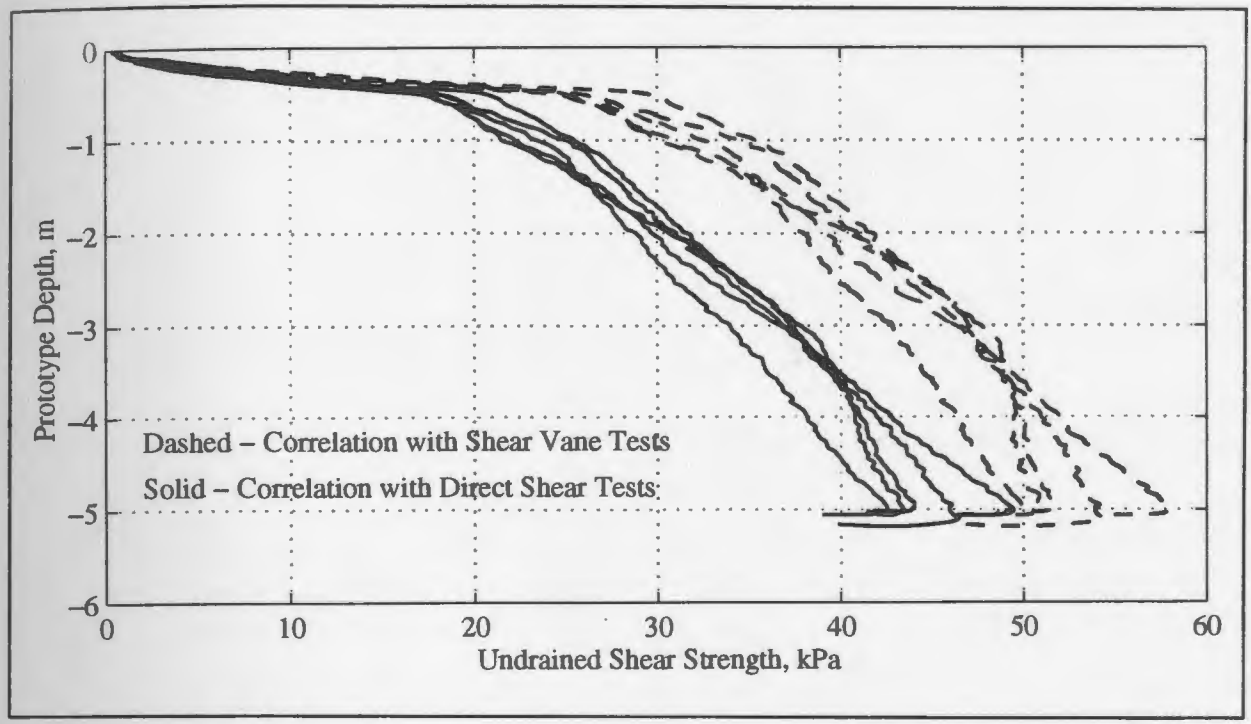

Figure 8.2 - Comparison of derived methods of determining undrained shear strength; dashed lines are from correlation with shear vane tests, solid lines are from correlation with direct shear tests.

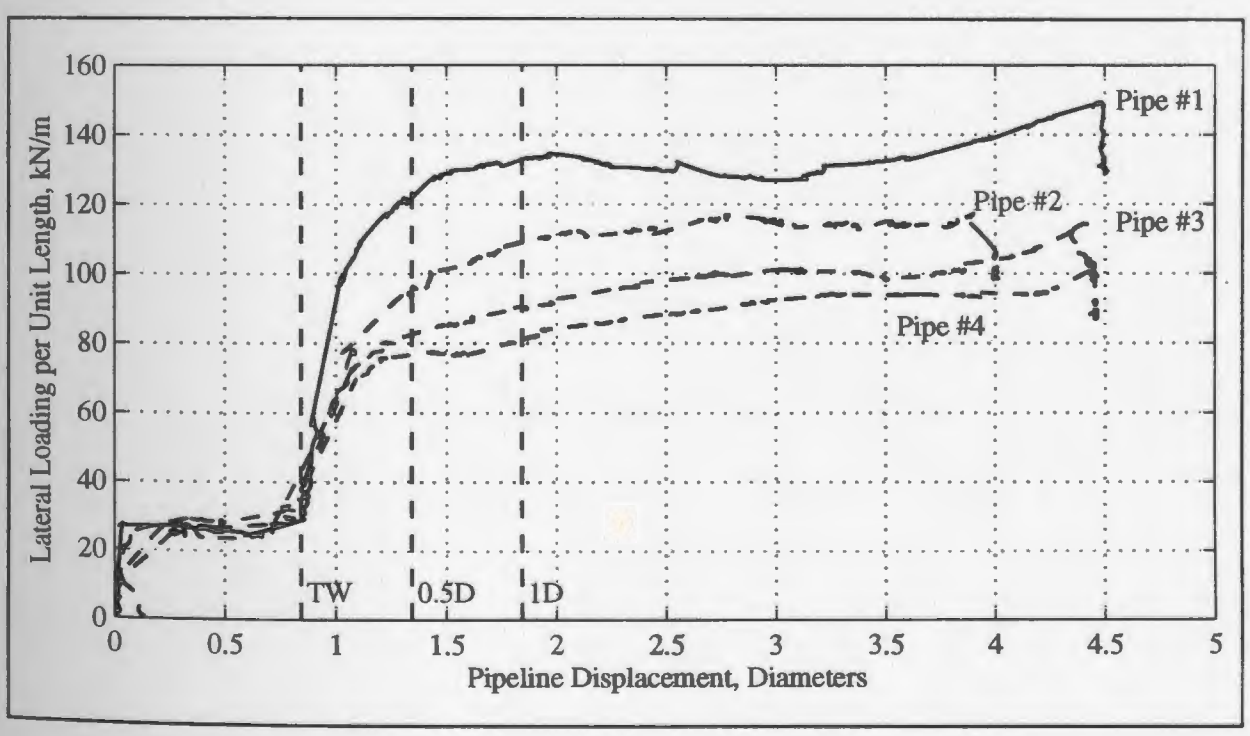

Figure 8.3 - Prototype-scale force-displacement curves from Test 01.

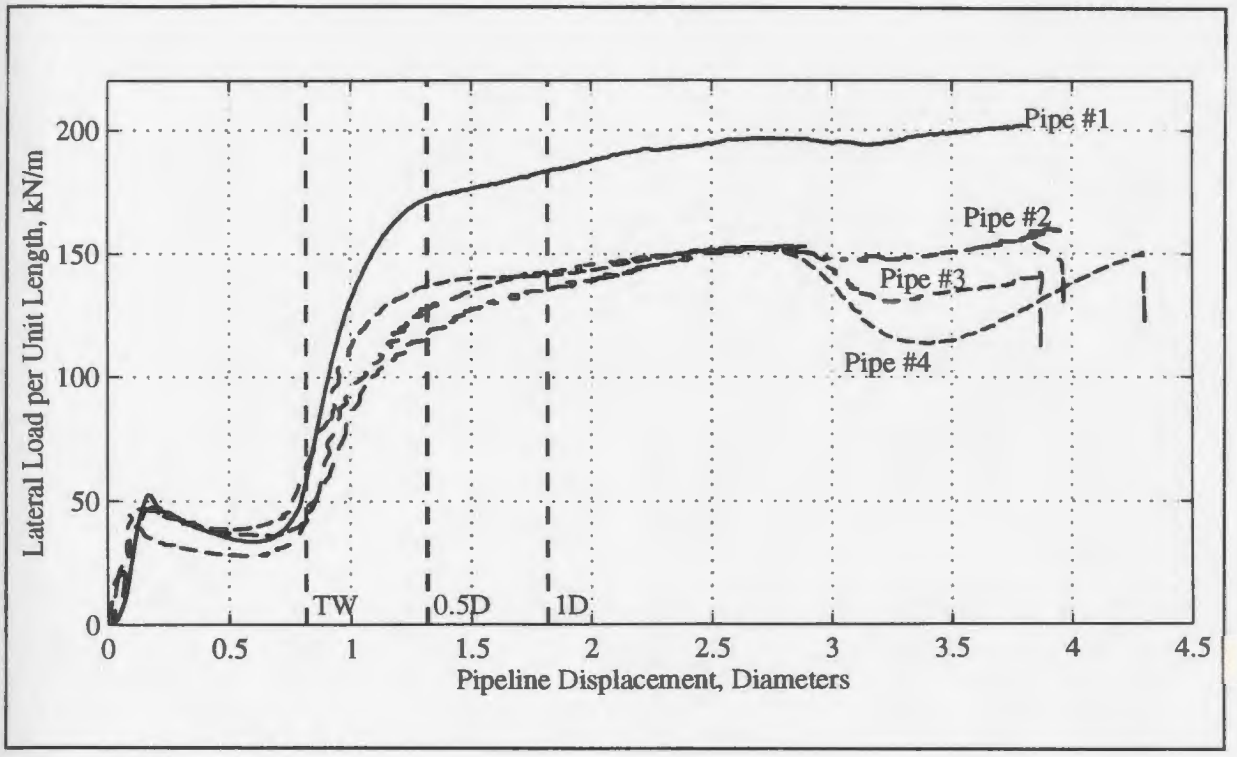

Figure 8.4 - Prototype-scale force-displacement curves from Test 02.

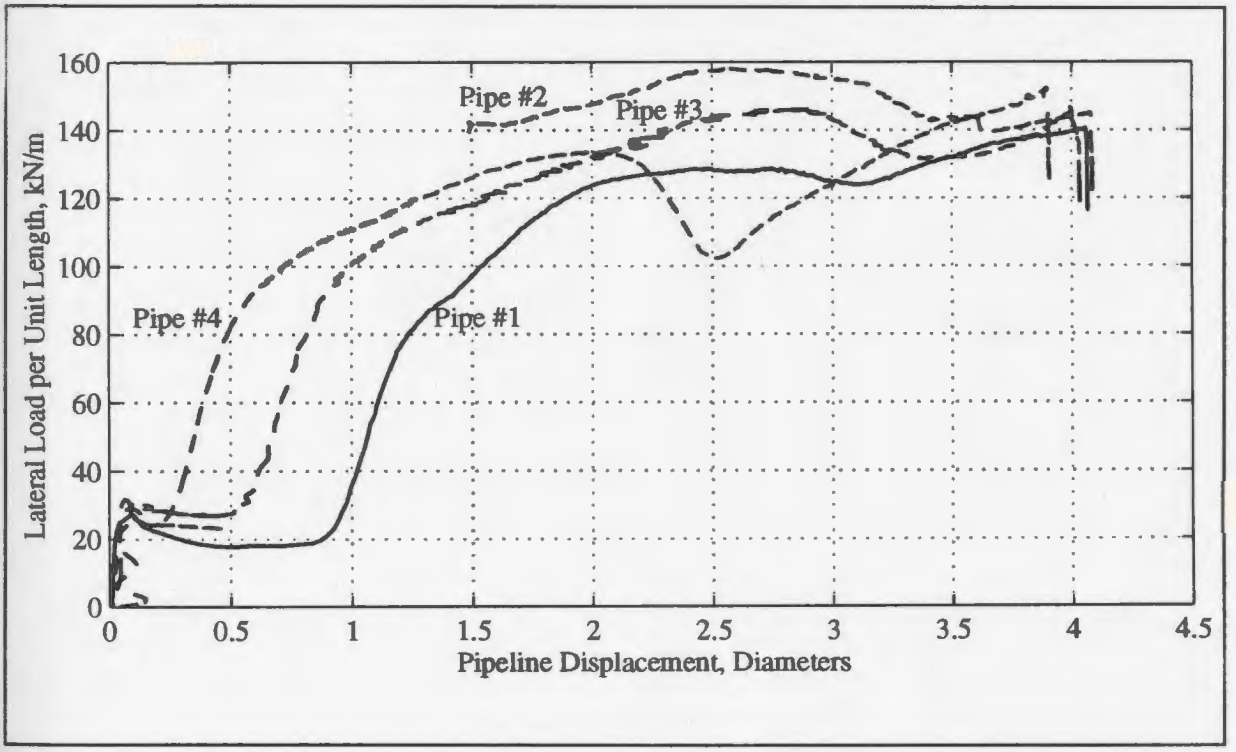

Figure 8.5 - Prototype-scale force-displacement curves from Test 03.

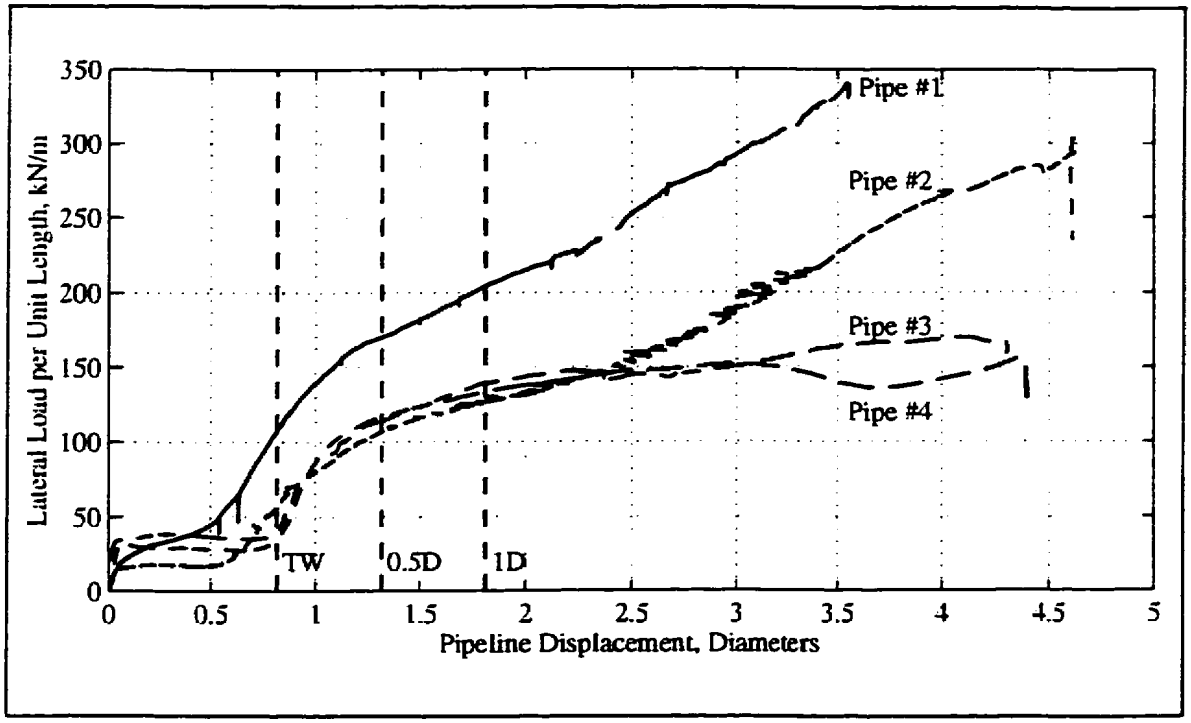

Figure 8.6 - Prototype-scale force-displacement curves from Test 04.

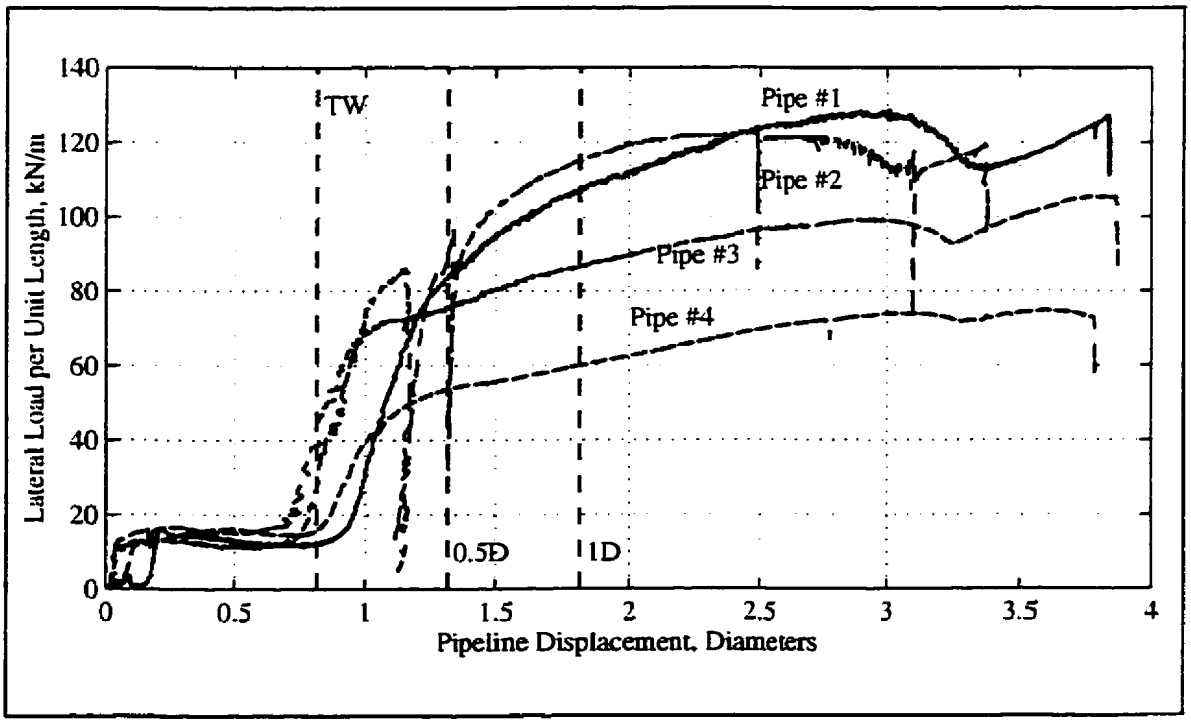

Figure 8.7 - Prototype-scale force-displacement curves from Test 05.

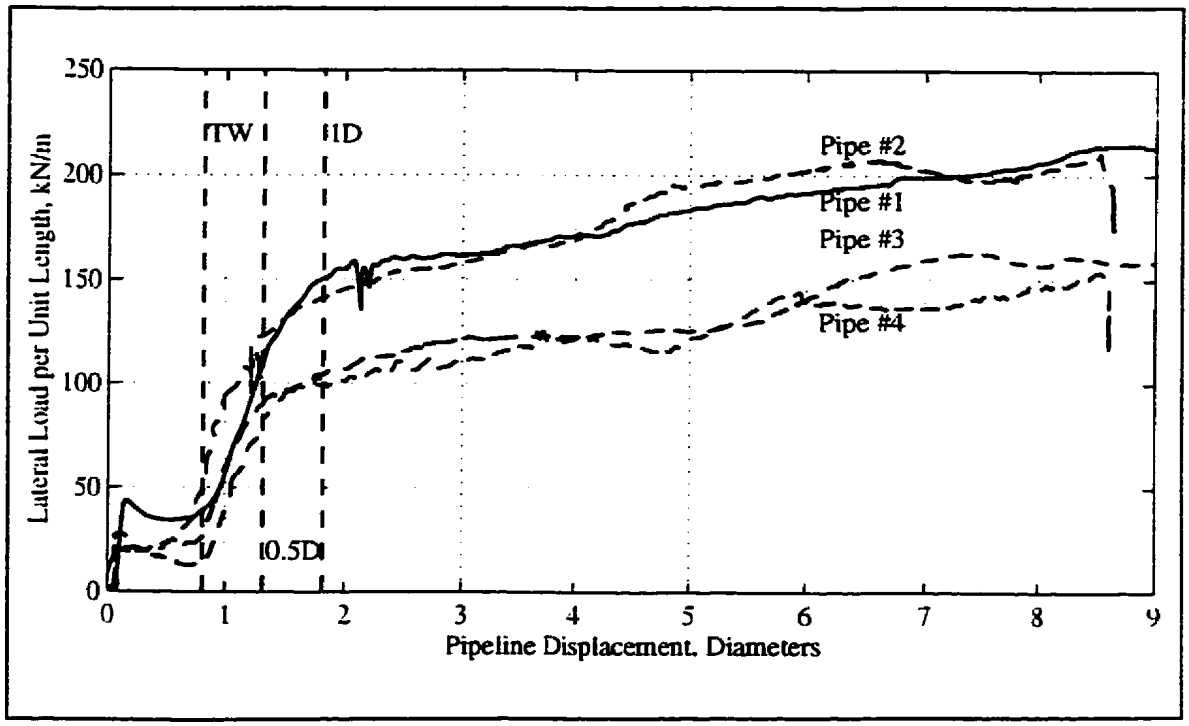

Figure 8.8 - Prototype-scale force-displacement curves from Test 06.

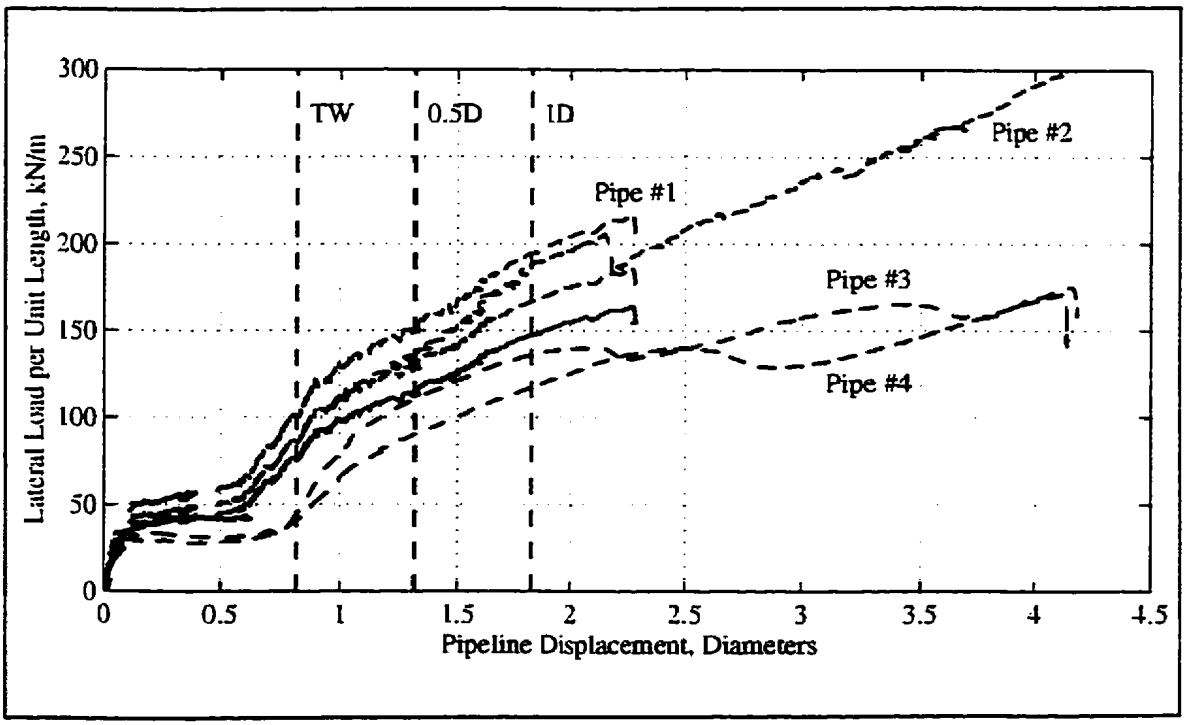

Figure 8.9 - Prototype-scale force-displacement curves from Test 07.

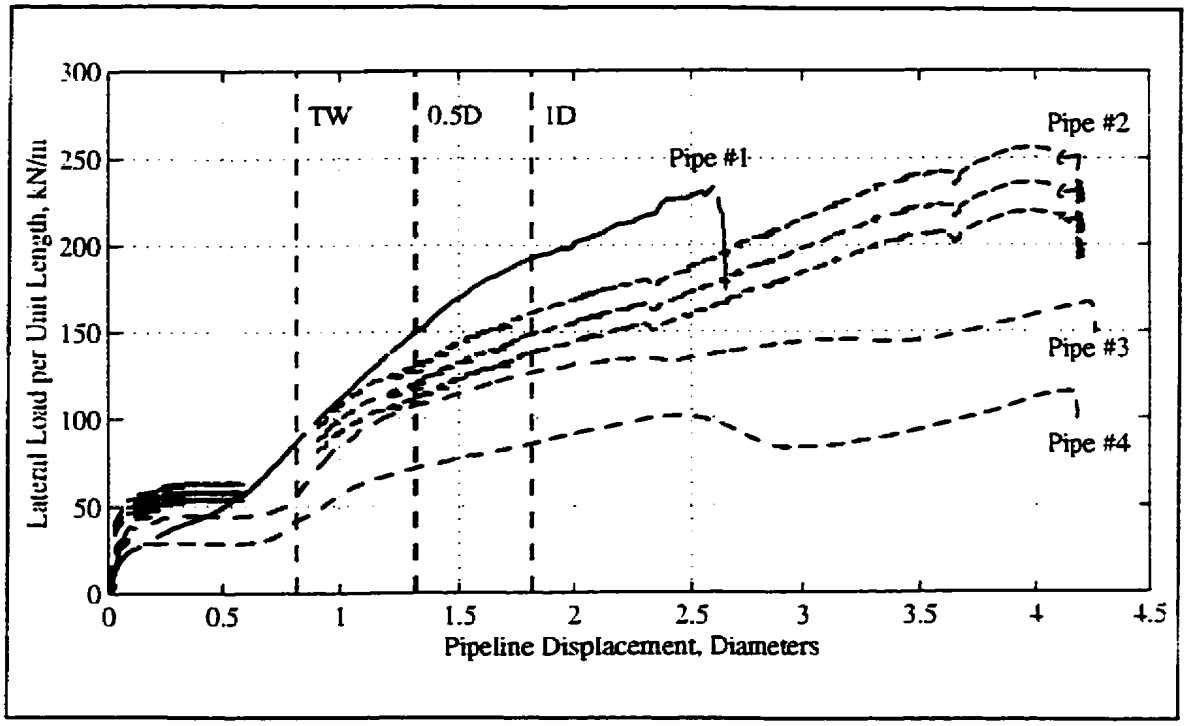

Figure 8.10 - Prototype-scale force-displacement curves from Test 08.

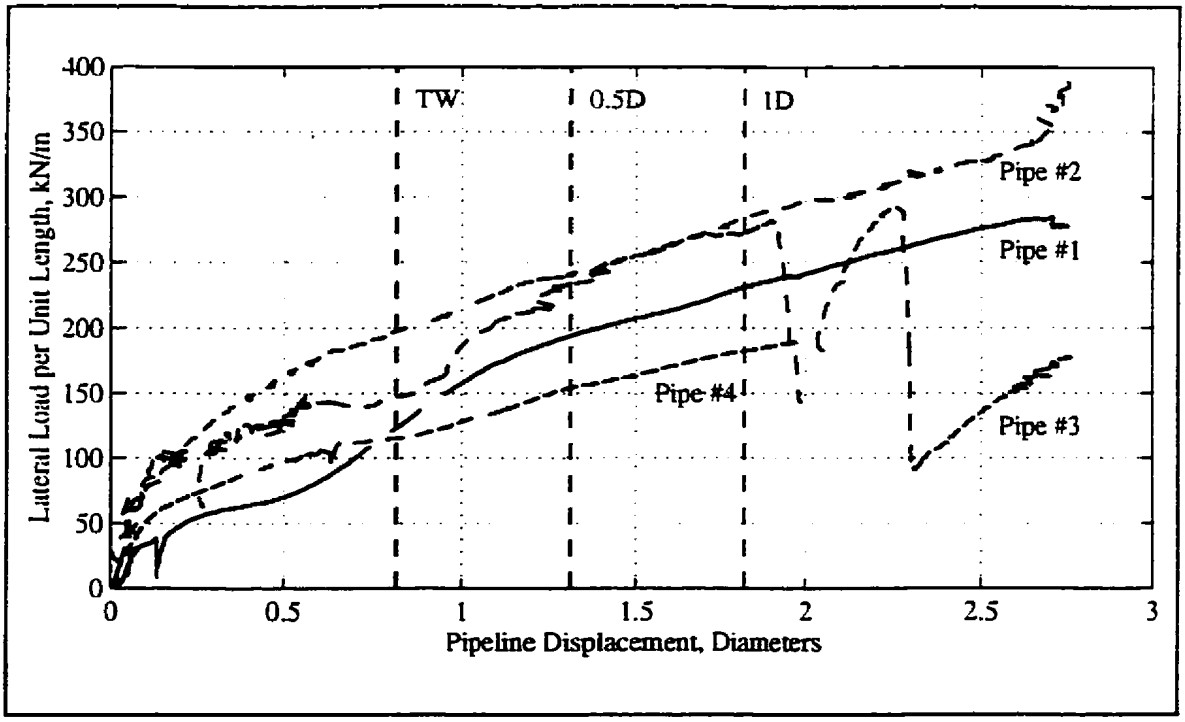

Figure 8.11 - Prototype-scale force-displacement curves from Test 09.

The general trend of the force-displacement curves for the rapidly displaced pipelines with slurry backfill is as follows (see Figure 8.3 for an example curve): the initial response is one of increasing force with displacement until the resistance is fully mobilized in the backfill; as the pipeline enters the native material, the response is again one of increasing force with displacement until a peak force is achieved; after the peak, there is a decrease in loading followed by a slight increase just prior to termination of the test. The approximate displacement to peak ranges from 1.15 to 3 pipe diameters after initial interaction with the trench wall. The vertical lines on the figures labelled TW, 0.5D, and 1D correspond to pipeline displacements where the pipe contacts the trench wall, where the pipe has been embedded 0.5 diameters into the trench wall, and where the pipe has been embedded 1 diameter into the trench wall. In some cases, the load on the pipelines is observed to have significantly increased before interacting with the trench wall (TW). This is believed to have been the result of minor pipeline displacement during model preparation and swingup so that the pipeline was closer to the trench wall than thought at the start of pipeline displacement. In an attempt to remedy this problem, modifications were made to the drive system after Test 06 so that it utilized a chain drive rather than a cable drive.

The general trend of the force-displacement curves for the pipelines subjected to a very slow pipeline displacement rate is as follows (see Figure 8.6 for an example curve): the initial response is one of increasing force with displacement but the resistance in the backfill does not appear to peak. Rather, the resistance to pipeline movement increases

with increased pipeline displacement and the interaction with the trench wall is somewhat masked.

With respect to the prototype-scale force-displacement curves, at this stage no consideration has been given to an increase or decrease in soil cover with increased pipeline displacement. No correction factor been applied to the prototype force-displacement curves presented above for the variation in undrained shear strength with depth. These corrections will be accounted for in the development of the normalized force-displacement curves and derivation of interaction factors as described in the following subsections.

8.1.6 Correction of Prototype-Scale Force-Displacement Curves

Where there was apparent significant vertical movement of the pipelines with horizontal displacement, corrections factors were applied to the prototype force-displacement curves to account for increased or decreased burial depth. The criteria for applying the correction factors was based on the post-test evaluation of the elevation of the base of the pipeline compared to the elevation at the start of the test. Any change in the basal elevation can be interpreted as a change in apparent or effective embedment ratio. As explained previously, during an undrained displacement of the pipeline, no volume change in the soil would be expected. If the pipeline moves with a constant cover depth, the final cover over the pipeline would be equal to the initial cover plus the diameter of the pipeline. If the embedment ratio changes, then the expected equivalent cover would also change. The

"expected cover" and "equivalent cover" were then compared and where there was a deviation of 3% (arbitrarily chosen) from the expected value, a correction factor was applied to the data to account for the increase or decrease in burial depth. For example, consider Pipeline #2, Test 01; the "expected cover" at the end of interaction would be 29mm (19mm pipeline diameter + 10mm cover). However, the base of the pipeline moved vertically downward 4mm during horizontal displacement which implies an "equivalent cover" of 29mm + 4mm = 33mm. The equivalent H/D ratio (where H=depth to base of pipeline and D=diameter) during displacement has not remained constant but has increased and should reflect an increase in load. This increase is 4mm, that is 14% of the expected cover. It is assumed that this increase occurred linearly from the point where the pipeline began to interact with the trench wall to the point where the pipeline came to rest. Therefore a correction (by division) is applied linearly (with displacement of the pipeline) to the force-displacement curve ranging from a value of 1.0 where the pipeline interacts with the trench wall to a value of 1.14 where the pipeline comes to rest. The pipelines and tests to which the corrections factors have been applied are summarized in Appendix L. The corrected prototype-scale force-displacement curves are presented in Figures 8.12 through 8.19 (note that no corrections were needed for Test 02). It should also be noted that the upper force-displacement curve was chosen as the representative data set for Pipeline #1, Test 07, and the median trace for Pipeline #2, Test 08, as these seemed to be most internally consistent with the other pipeline test data of the same test.

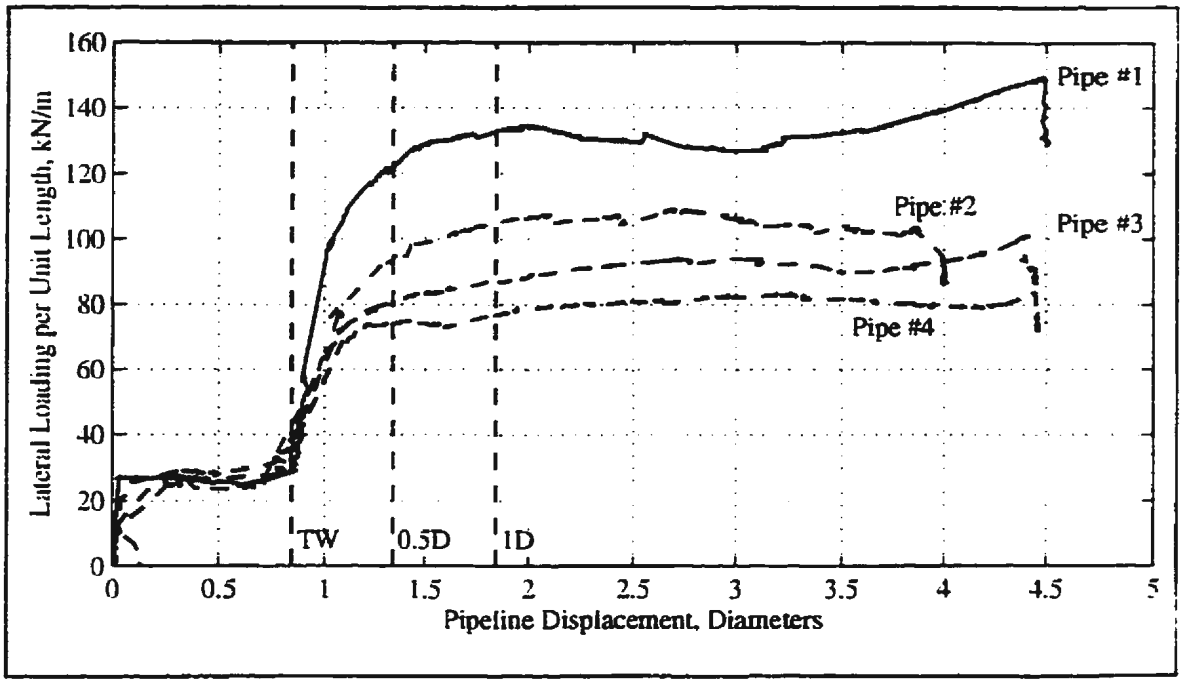

Figure 8.12 - Prototype-scale force-displacement curves from Test 01 corrected where necessary for change in embedment ratio with pipe displacement.

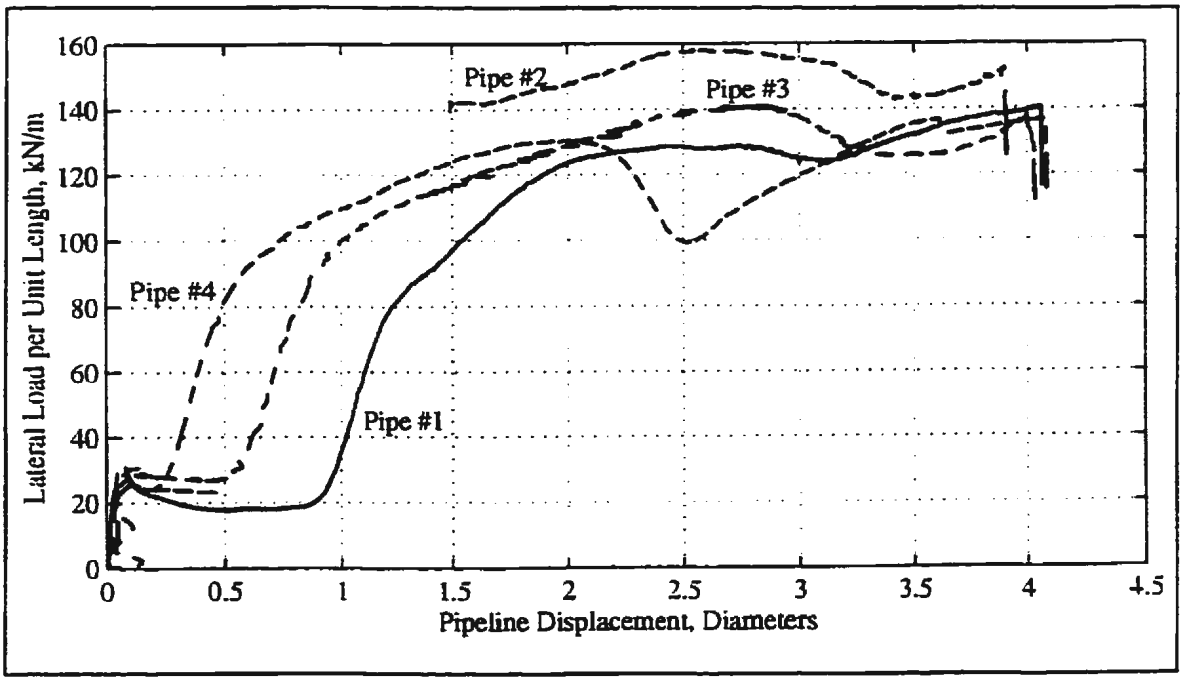

Figure 8.13 - Prototype-scale force-displacement curves from Test 03 corrected where necessary for change in embedment ratio with pipe displacement.

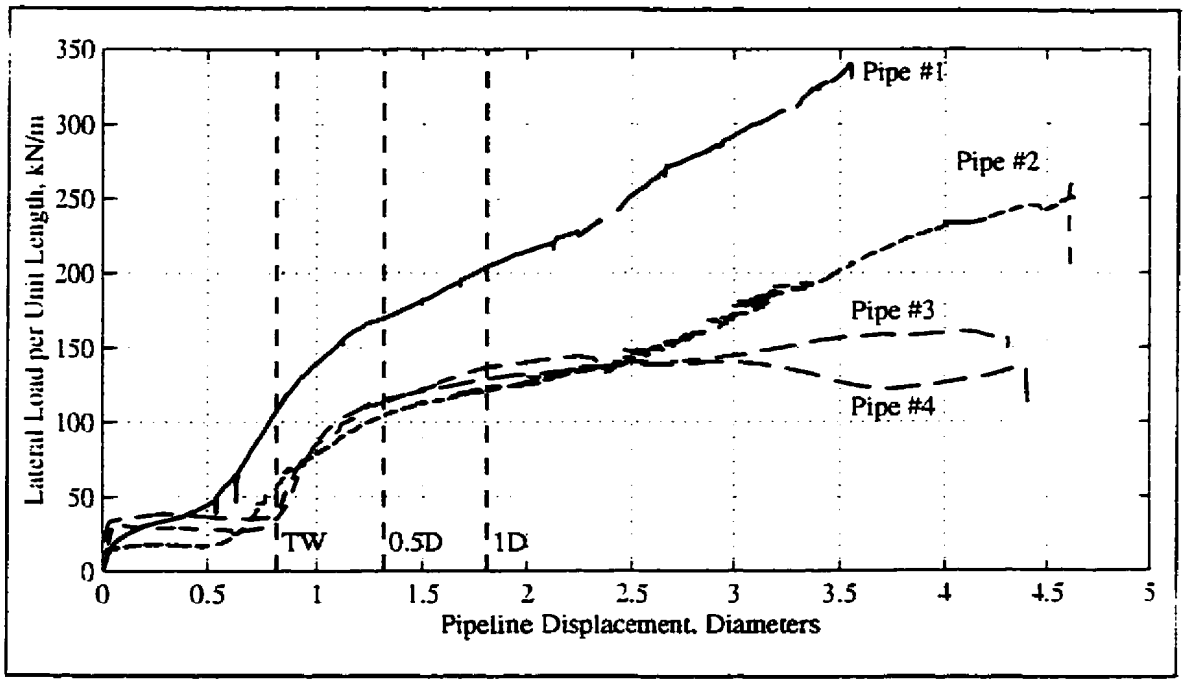

Figure 8.14 - Prototype-scale force-displacement curves from Test 04 corrected where necessary for change in embedment ratio with pipe displacement.

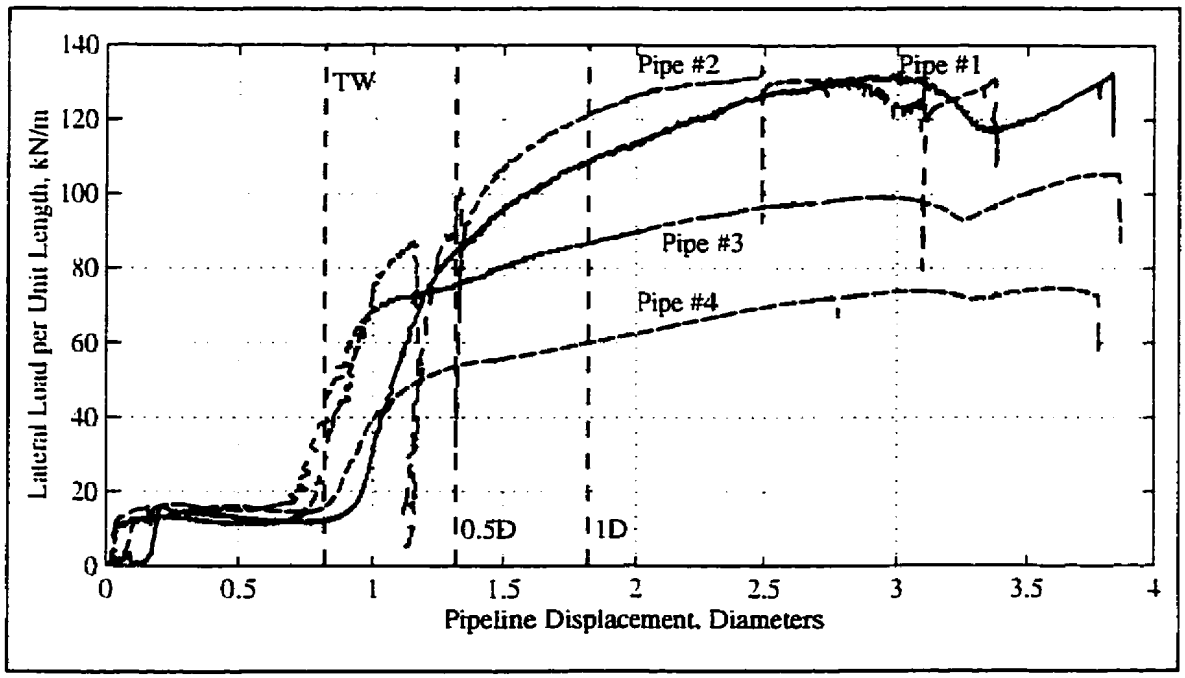

Figure 8.15 - Prototype-scale force-displacement curves from Test 05 corrected where necessary for change in embedment ratio with pipe displacement.

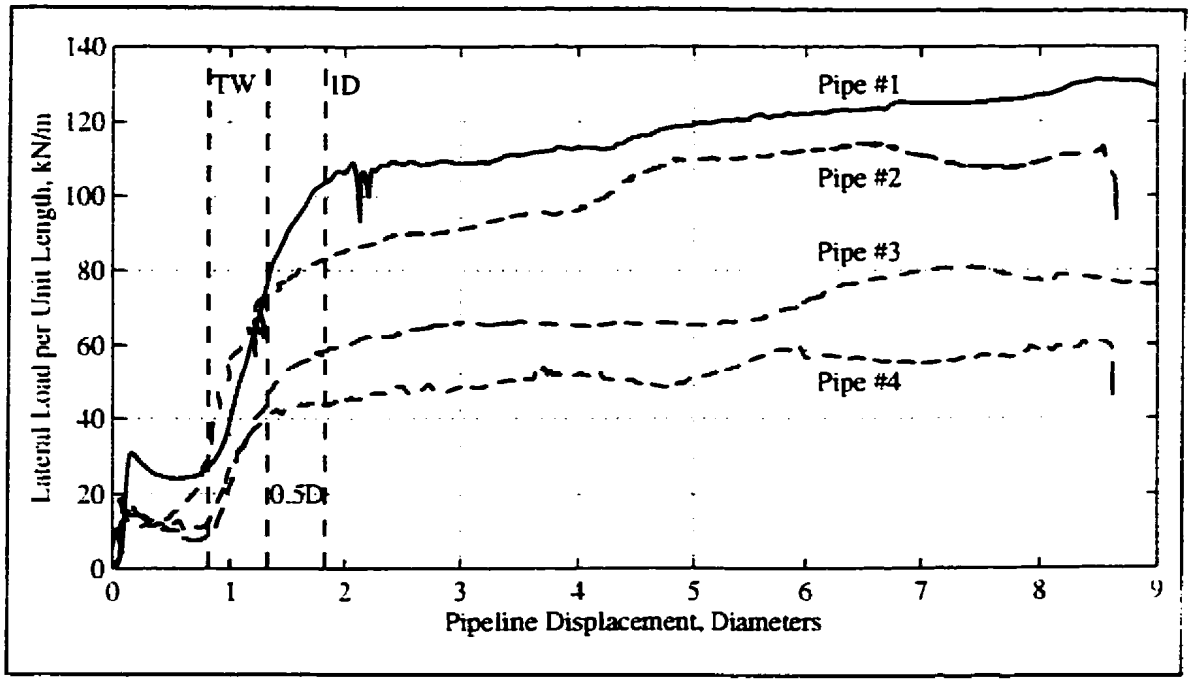

Figure 8.16 - Prototype-scale force-displacement curves from Test 06 corrected where necessary for change in embedment ratio with pipe displacement.

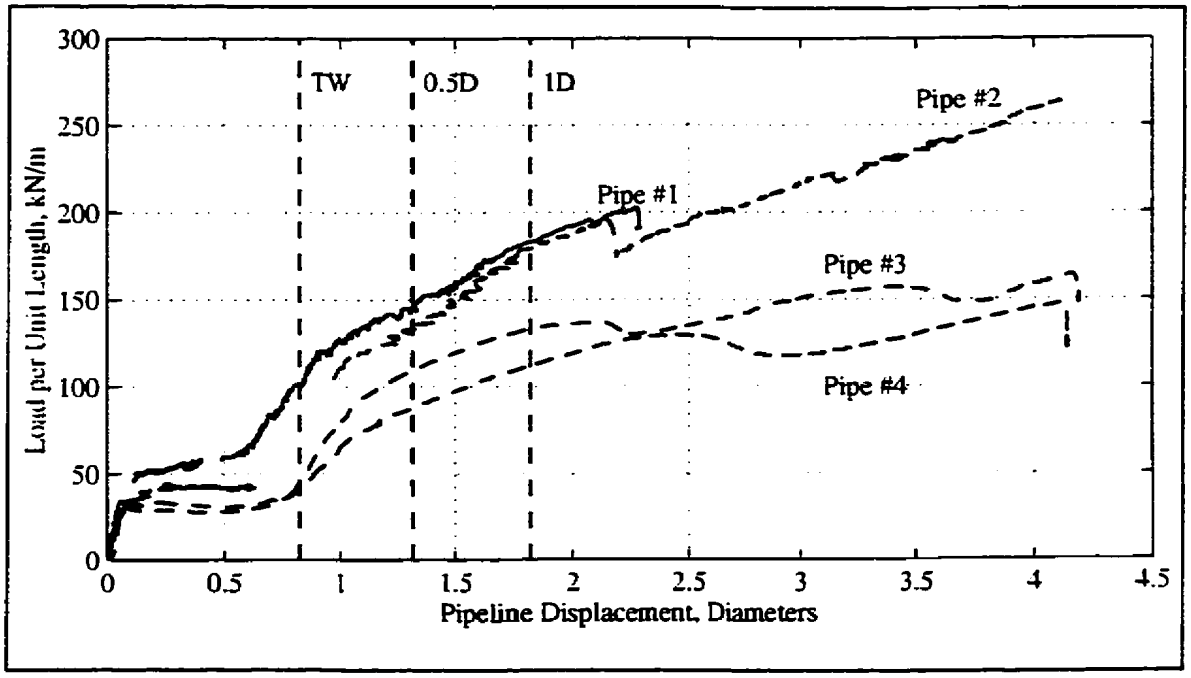

Figure 8.17 - Prototype-scale force-displacement curves from Test 07 corrected where necessary for change in embedment ratio with pipe displacement.

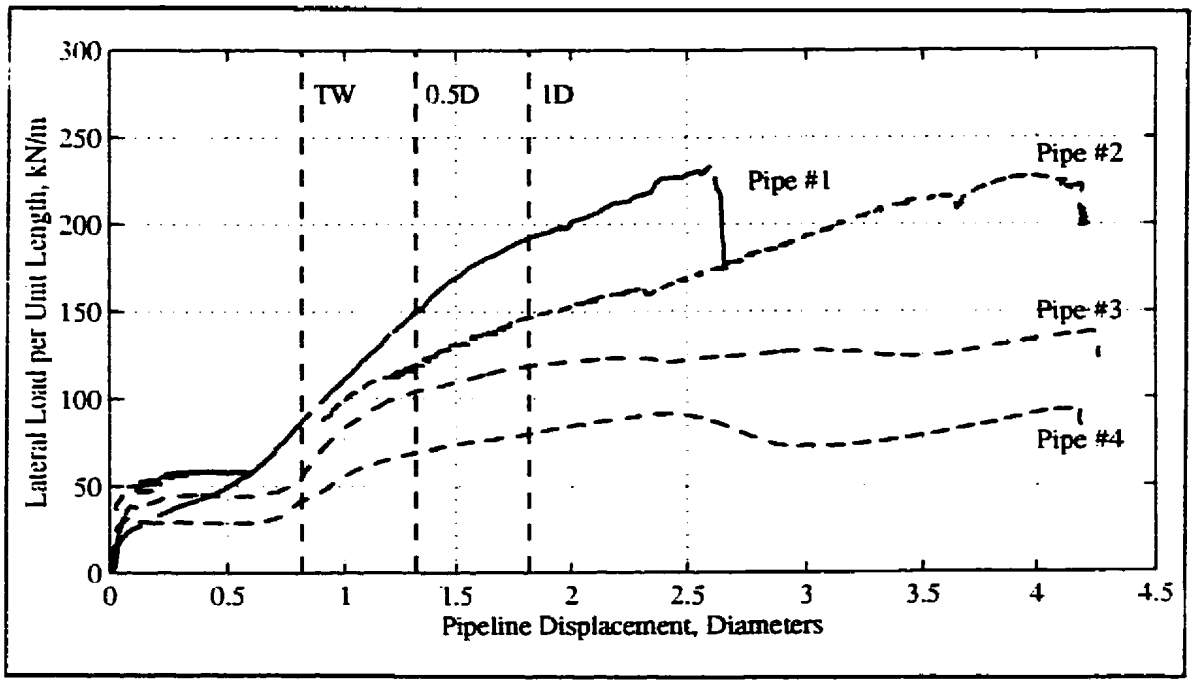

Figure 8.18 - Prototype-scale force-displacement curves from Test 08 corrected where necessary for change in embedment ratio with pipe displacement.

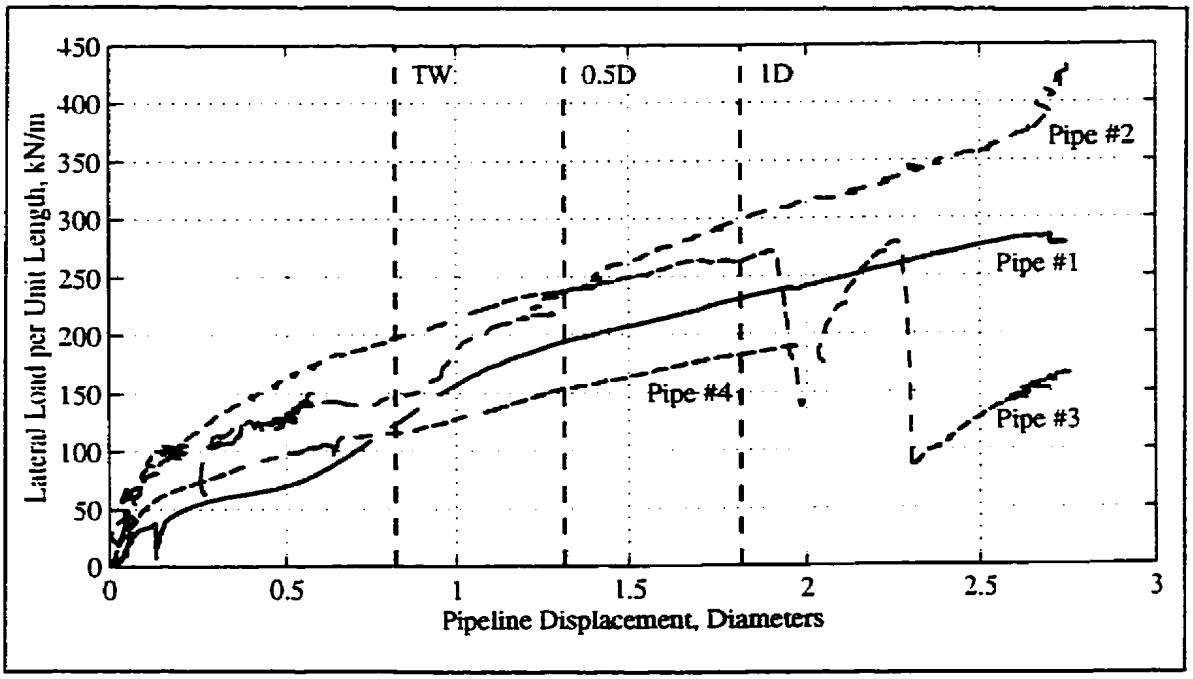

Figure 8.19 - Prototype-scale force-displacement curves from Test 09 corrected where necessary for change in embedment ratio with pipe displacement.

8.1.7 Derivation of Interaction Factors

If the prototype-scale force-displacement curves are normalized with respect to the pipeline diameter and undrained shear strength, then the first interpreted peak of normalized load is defined as the interaction factor, N. The average undrained shear strength measurement at each springline is shown in Table 6 of each *Test Data* appendix. This value is the average of the range provided by correlation with shear box and shear vane data. Normalization of the data has been carried out using this average undrained shear strength measurement. In the table, no range is presented for cover depths or embedment ratios as, where applicable, the force-displacement data has been corrected in the previous section for changes in pipeline elevation during displacement. Normalized force-displacement curves are presented in Figure 8.20 through Figure 8.28. As in most instances, the backfill was very soft (the consistency of toothpaste), no consideration has been given to normalization of the interaction in the backfill: the resistance in the backfill has simply been adjusted using the native material undrained shear strength. Where applicable, the undrained shear strength of the soil was adjusted with pipeline displacement to account for any vertical pipeline movement. The criteria for the application of a shear strength correction factor was the same as for the effect of cover depth described previously and thus was only applied to those tests where displacement corrections were also used.

Table 6 of each *Test Data* appendix presents the ultimate resistance (first interpreted peak) and the distance after interaction with the trench wall to peak. These points are indicated on Figures 8.20 through 8.28. One way in which to examine the ultimate load and the

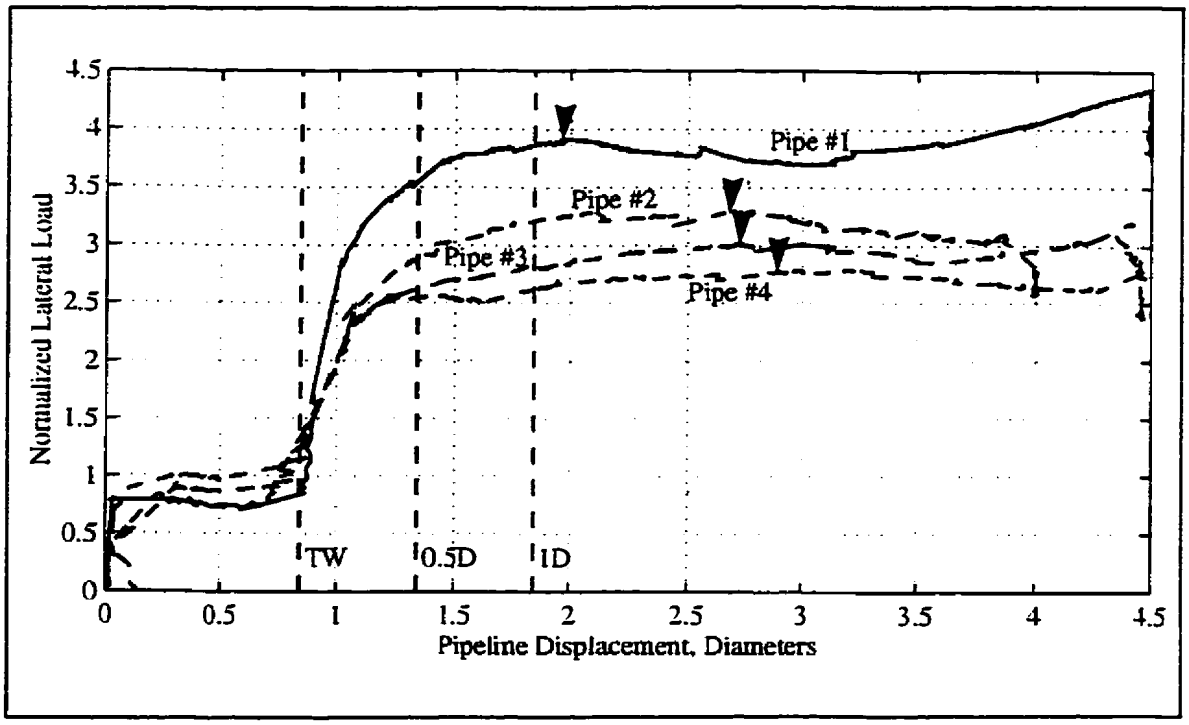

Figure 8.20 - Normalized prototype-scale force-displacement curves from Test 01.

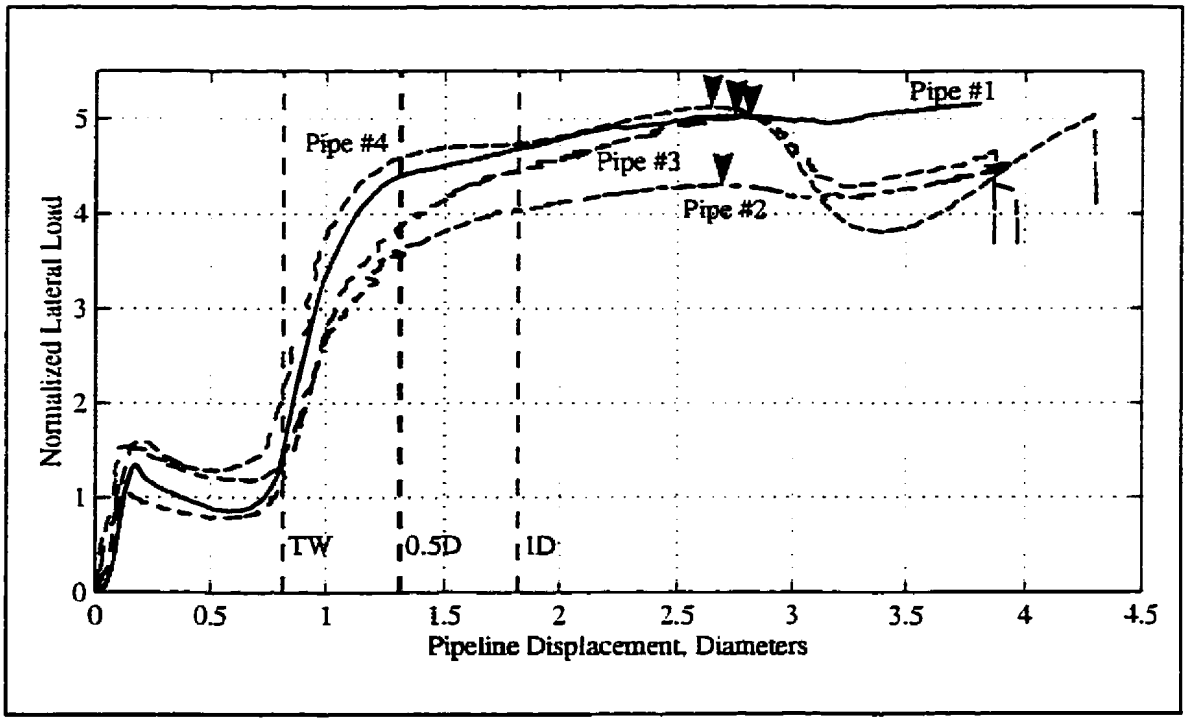

Figure 8.21 - Normalized prototype-scale force-displacement curves from Test 02.

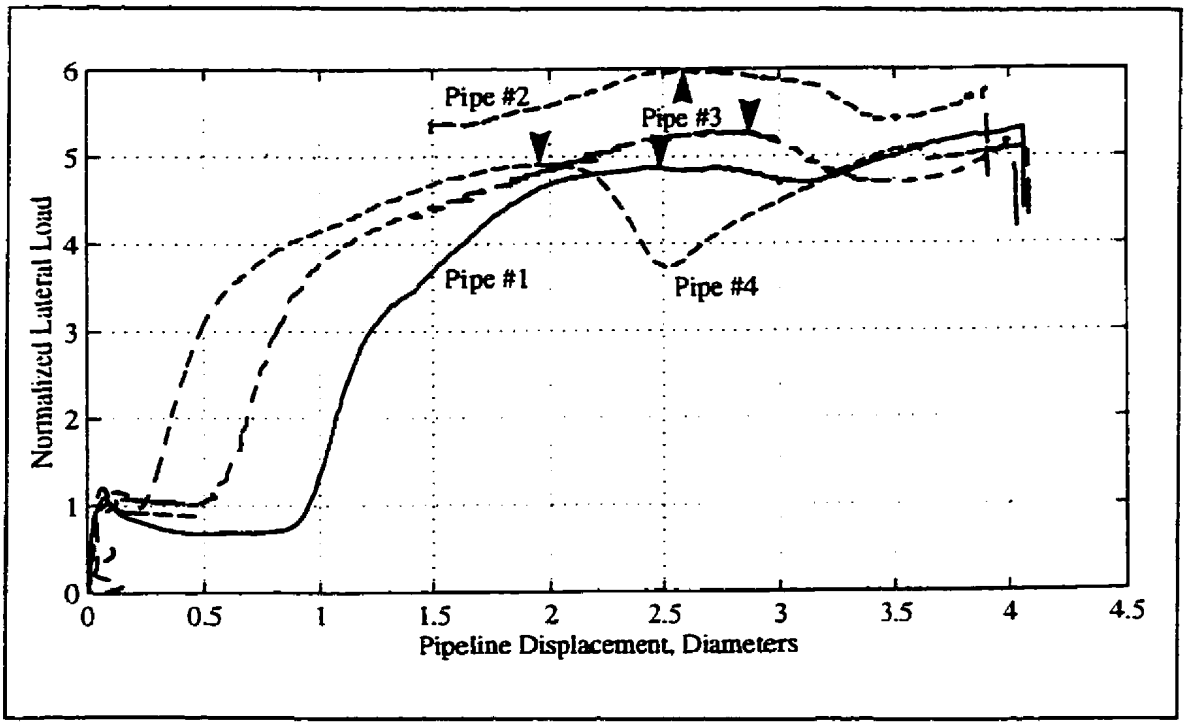

Figure 8.22 - Normalized prototype-scale force-displacement curves from Test 03.

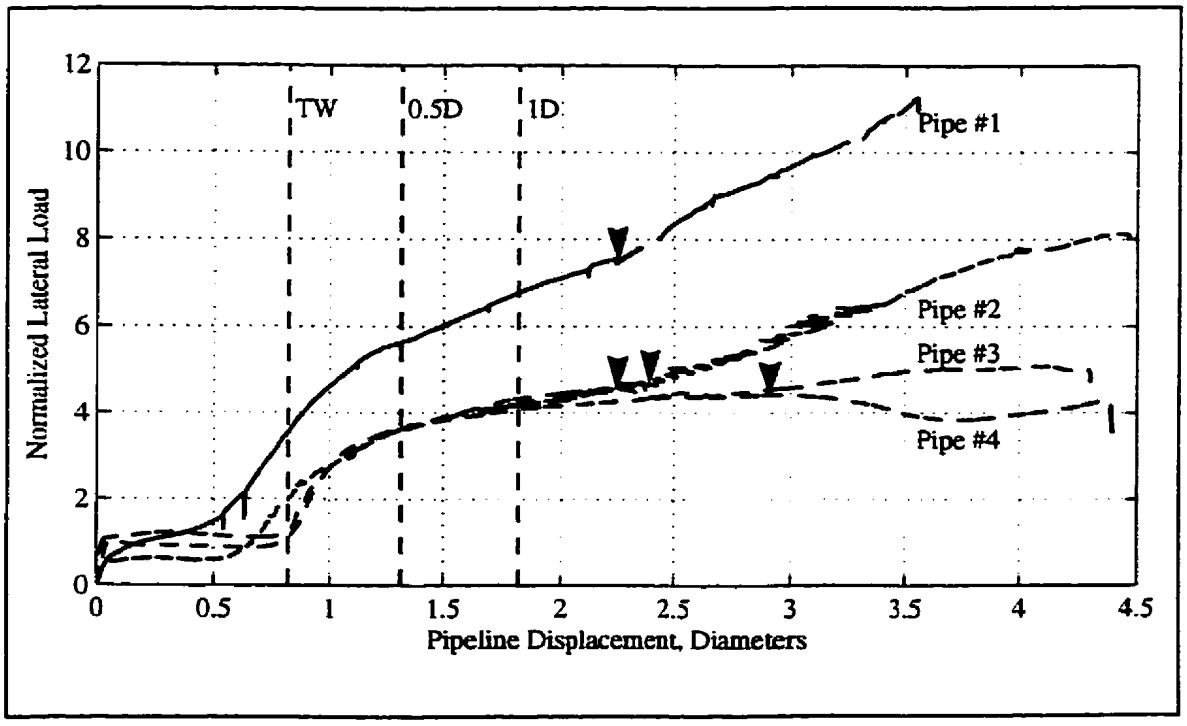

Figure 8.23 - Normalized prototype-scale force-displacement curves from Test 04.

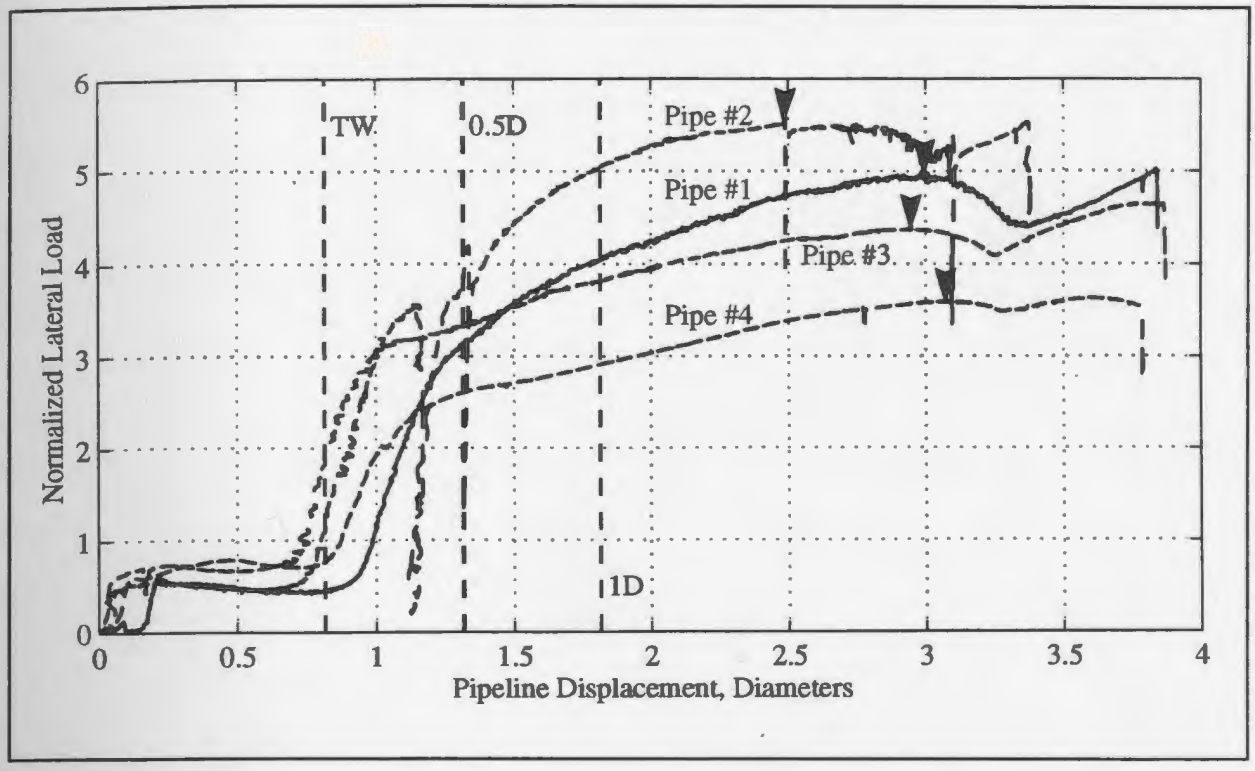

Figure 8.24 - Normalized prototype-scale force-displacement curves from Test 05.

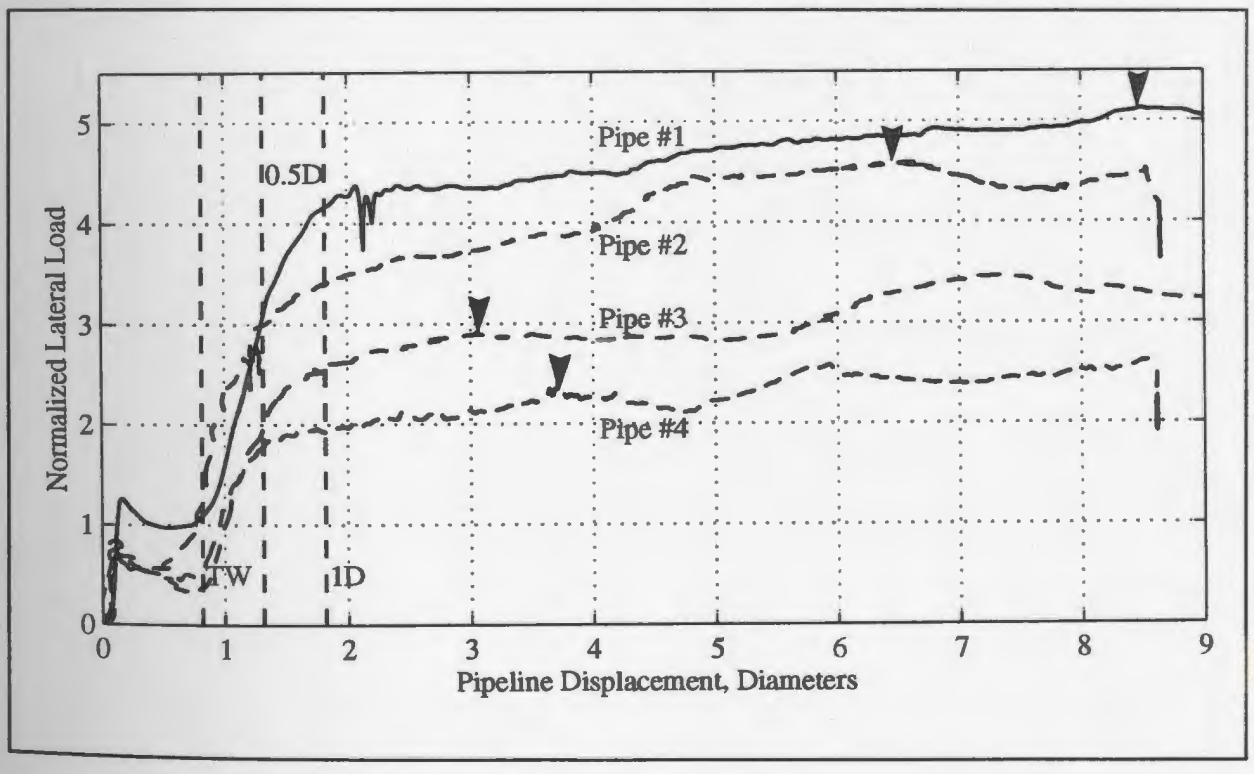

Figure 8.25 - Normalized prototype-scale force-displacement curves from Test 06.

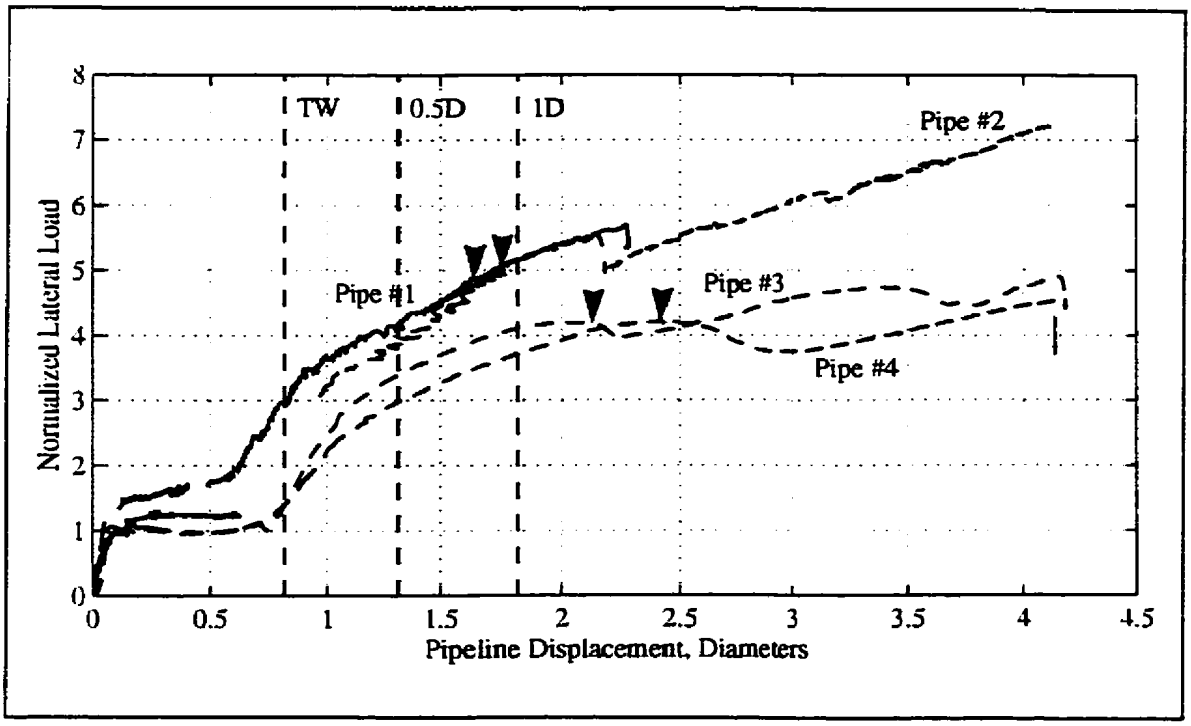

Figure 8.26 - Normalized prototype-scale force-displacement curves from Test 07.

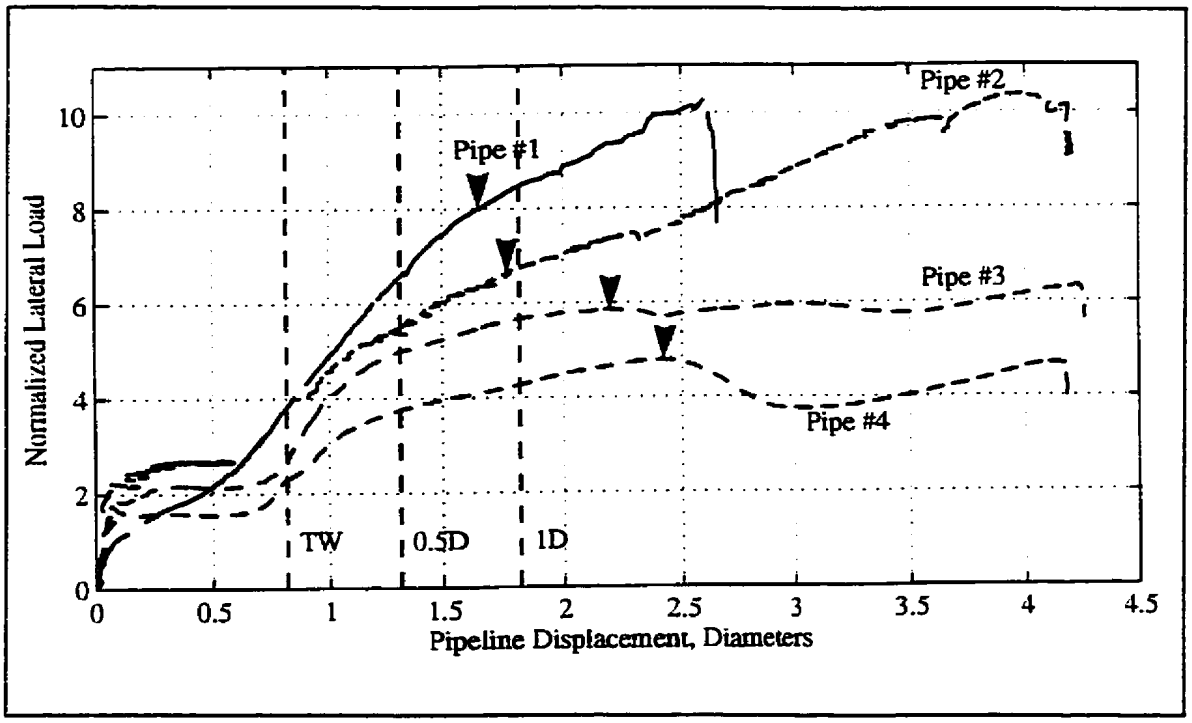

Figure 8.27 - Normalized prototype-scale force-displacement curves from Test 08.

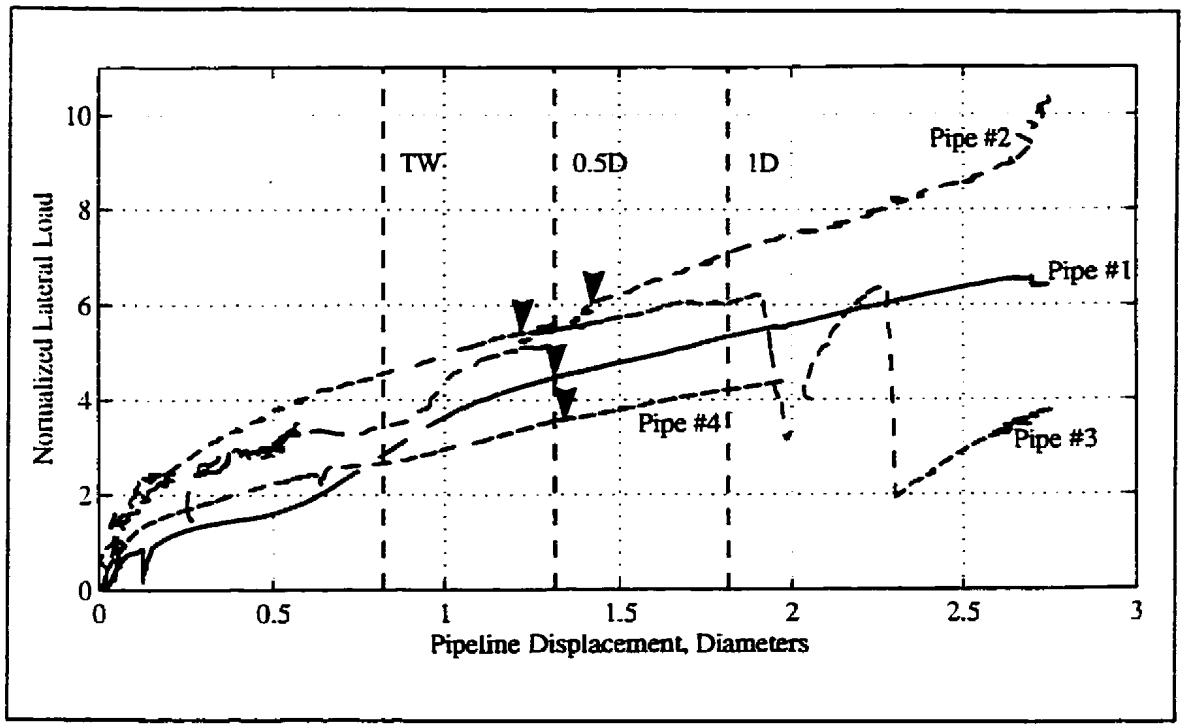

Figure 8.28 - Normalized prototype-scale force-displacement curves from Test 09.

required displacement to this ultimate load combined, is to look at a secant modulus from the plot origin to the interpreted ultimate resistance to lateral movement. This is depicted as an example in Figure 8.29 and test values are presented in Table 6 of the *Test Data* appendices. One drawback using this analysis method is that the choice of the ultimate normalized load can be subjective. Especially in partially-drained and drained cases, it was difficult to determine an ultimate load on the pipeline segment; this value has often been interpreted as the point where the test was terminated.

However, as documented in the literature for anchor plates, foundations, and pipelines, it can be difficult to interpret the ultimate load of a force-displacement curve in loose

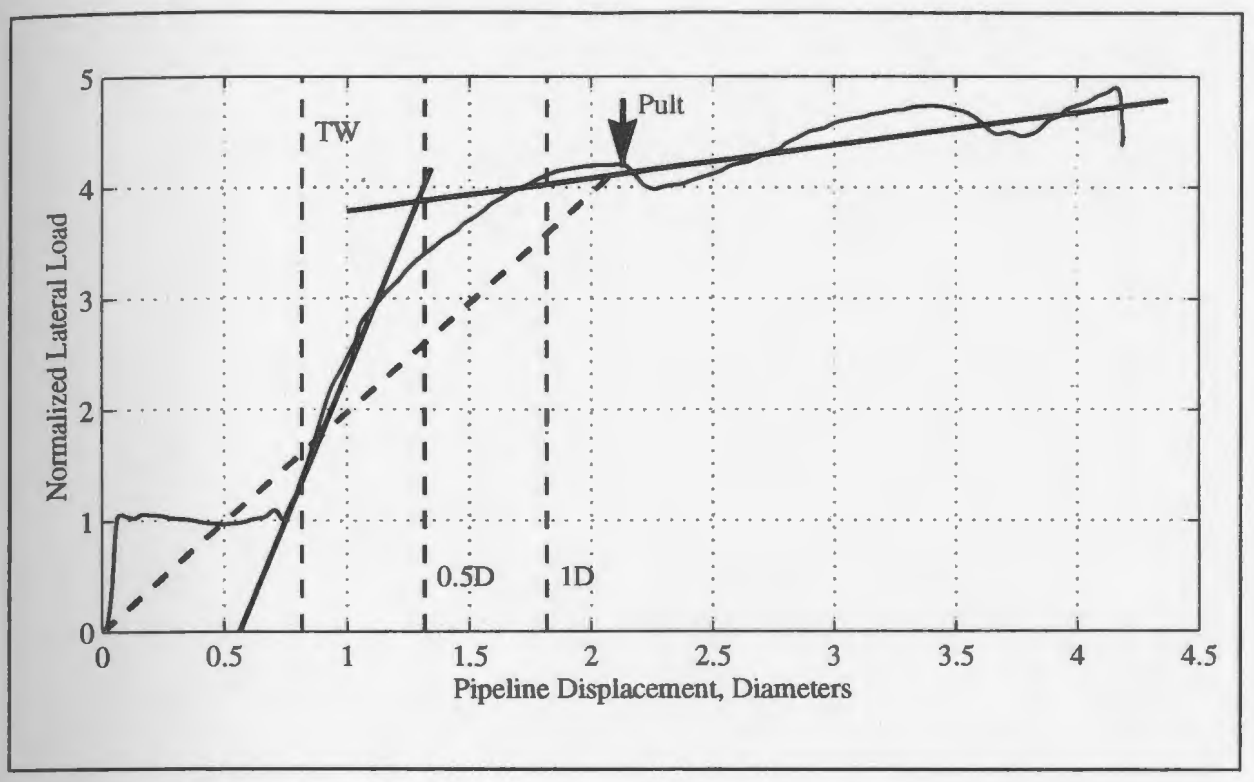

Figure 8.29 - Secant modulus and bilinear representation of force-displacement curve, Pipeline #3, Test 07.

cohesionless material. Often this load is taken as the point where the force-displacement response becomes linear corresponding to a buildup of surcharge in front of the displacing object (Trautmann and O'Rourke, 1985; Das *et al.*, 1985; Vesic, 1973). Such an interpreted point is indicated by the vertical arrows on the drained and partially-drained tests of Figures 8.23, 8.26, 8.27, and 8.28. Parameters associated with these points are presented in Table 6 of the *Test Data* appendices. It could be argued that this position should be at an alternative point on the force-displacement response and the placement is open to interpretation; in cases, the interaction of the pipe with the trench wall and/or the variable force-displacement response makes it difficult to locate where a linear portion of the curve should begin.

8.1.8 Determination of Normalized Loads at Specified Displacements

In the previous section, normalized ultimate loads were obtained from the prototype force-displacement curves by dividing the corrected lateral load per unit length (p) by the pipe diameter (D) and the average corrected undrained shear strength of the soil (c_u) at the pipe springline.

Little consideration was given to the displacement required to achieve these ultimate loads. In most cases of lateral loading in the field, it would probably not be reasonable to assume that there would be a relative pipeline/soil displacement equivalent to several pipeline diameters before the pipeline would fail or remediation measures would be initiated. It may be appropriate to analyse the data by considering a normalized load after a predetermined displacement so that direct comparison between tests can be made rather than use the ultimate normalized loads which might be somewhat subjectively chosen. As the pipeline moves into the trench wall, the projected area of the pipe embedded into the native material increases until a displacement of 0.5D. Therefore, intuitively, the shape of the force-displacement response of the pipelines should change once the pipeline has been embedded 0.5 diameters into the trench wall; this point would be called the "breakover point". Observation of the prototype-scale force-displacement records indicates that this assumption is reasonable. Therefore, the normalized force on the pipeline at a displacement of 0.5 diameters into the trench wall as well as at a displacement in which the pipeline has been embedded 1 diameter into the trench wall are considered to be two benchmarks which can be compared between tests. Also, strain hardening effects can be considered by

comparing the pipeline loads at embedment of 0.5 and 1.0 pipeline diameters. Table 6 of each *Test Data* appendix presents the normalized lateral loads interpreted from the tests at the trench wall (TW), at a displacement of 0.5 diameters (0.5D), and at a displacement of 1 diameter (1D) penetration into the trench wall.

8.1.9 Bilinear Analysis of Normalized Force-Displacement Curves

Current analysis methods define an ultimate limit state by the load, P_{ult}, on the pipeline but little consideration has been given to the serviceability limit state, including the displacement required to achieve these loads. As mentioned in the previous section, in the analysis of the experimental data, it may be difficult to interpret where the first peak in the prototype-scale force-displacement curves should be designated. A serviceability limit state corresponding to a relative pipeline/soil displacement equivalent to many pipeline diameters may be unreasonable. Observation of all of the normalized data indicate that the interaction curves can be approximately defined by two straight line segments as shown in Figure 8.29. Therefore, it may be appropriate to analyse the data by considering the loading to have a bilinear response with a measured stiffness up to a certain point (breakover point) followed by an interaction with a different measured stiffness as the slopes of the interaction curves generally appear to change dramatically after a certain penetration into the trench wall. This yield point is typically observed at a pipeline embedment of approximately 0.5 pipeline diameters into the trench wall. The interpreted slopes of the two linear portions of the curves, the values of the normalized lateral load at the intersection of the two curves (or the breakover point), and the pipeline displacement

into the trench wall to the breakover point are presented in Table 6 of the *Test Data* appendices. Again, no consideration has been given to normalization of the interaction in the backfill.

8.2 Parametric Analysis

8.2.1 Introduction

This section presents an analysis of the parametric effects examined during the experimental program. The parameters include pipeline burial depth, trench width, interaction rate, soil preconsolidation pressure, backfill type and model scale. The influence of each of these parameters are examined (at least) in terms of normalized prototype-scale force-displacement curves, associated interaction factors, normalized loads at specified displacements and a bilinear representation of the normalized force-displacement curves. In analysis of the data, consideration must be given to the tests where equipment malfunctioned, trends in missing data were estimated or there were anomalies in the testing procedure. Where most parameters are easily quantifiable, some such as drainage conditions due to interaction rate and characterization of backfill type are not as easily quantified. It should be noted that trends in the data presented in this section are based on a limited number of data points. This section also looks at curve fitting the normalized experimental data to develop general equations for the force-displacement response of laterally loaded pipelines. Analyses developed in this section will be evaluated in the following section.

8.2.2 Effect of Burial Depth - Undrained Conditions

Comparison of Normalized Prototype Force-Displacement Curves

Figure 8.30 presents the normalized force-displacement curves from Test 01 and Test 02. These two tests are considered to be representative of data sets from different cover depths but for similar drainage conditions[1], similar backfill (slurry), similar preconsolidation effective stress (≈ 400kPa), and a similar trench width (2.5m). The embedment ratios, H/D, are presented on the figure. This has been defined previously as the depth to the trench base divided by the pipe diameter. This figure clearly shows the influence of cover depth; as the H/D ratio increases from 1 to 1.842, the normalized peak lateral load increases. However, for higher H/D ratios, the effect of burial depth on lateral loading is not as obvious.

Interaction Factors

Table 6 of the *Test Data* appendices presented the interpreted interaction factors from all of the tests and these are presented again in Table 8.2 where they will be compared to accepted values in a later section. To analyse the effect of the variation in cover depth on undrained interaction, the following have been plotted in Figures 8.31 through 8.33: the ultimate normalized resistance or interaction factor (N_c); the normalized distance into the trench wall to the ultimate normalized resistance; and the secant modulus to the ultimate

---

1 As will be defined later, an interaction which is considered undrained is a prototype pipeline displacement rate greater than or equal to 0.075 m/day; drained is at a rate equal to or less than 0.0012 m/day.

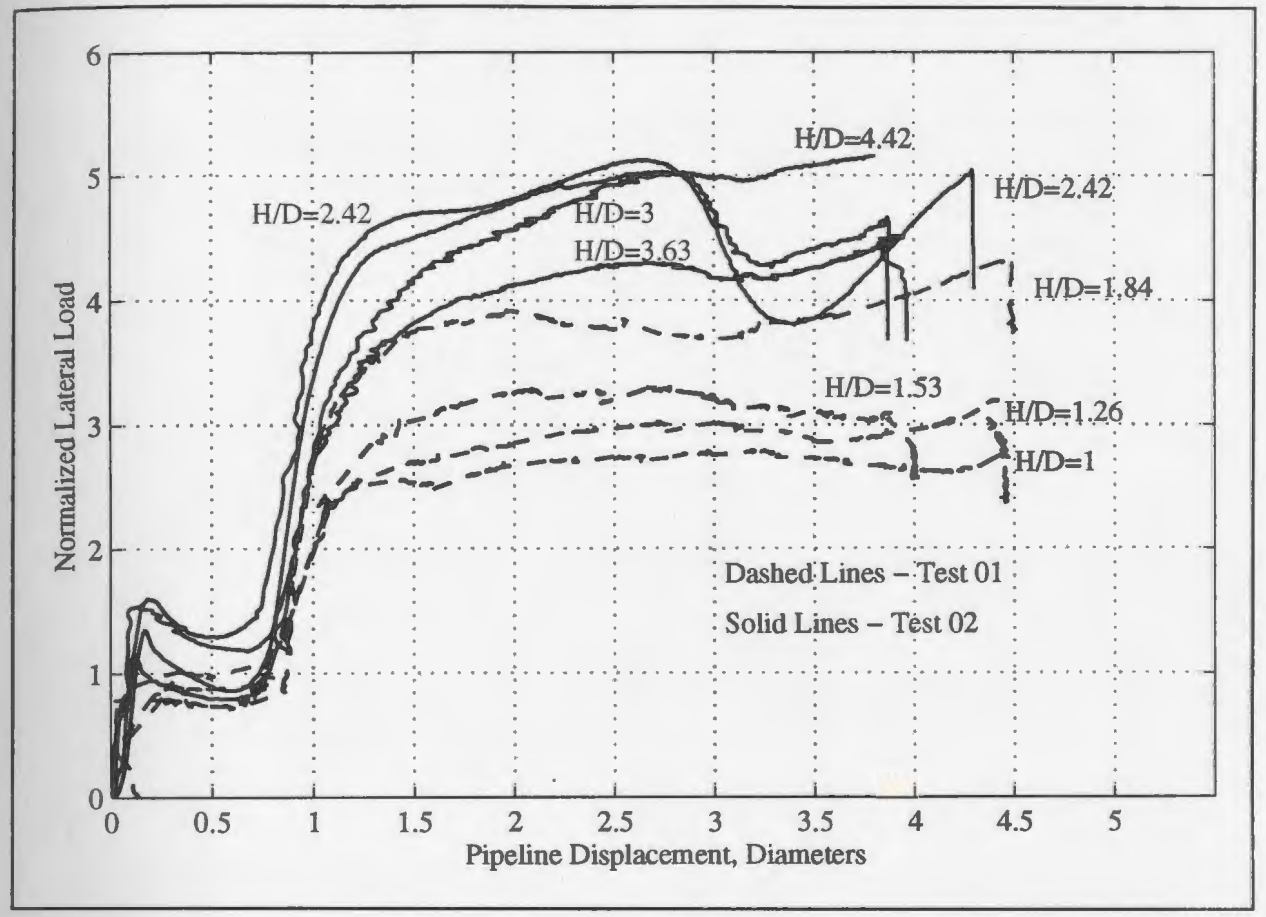

Figure 8.30 - Corrected normalized lateral load versus displacement - Test 01 and 02.

normalized resistance. To augment the data of Test 01 and Test 02, data from other pipeline displacements conducted under similar conditions (Pipelines #3 and #4, Test 04; Pipeline #3 and Pipeline #4, Test 07) have been included in analyses of this subsection.

Observation of Figure 8.31 indicates that a data trend similar to that suggested by Rowe and Davis (1982a) or Hansen (1961) can be fit to the data. A second order polynomial has been fit to a portion of the data as shown in the figure. Intuitively, and as suggested by the trend in the data, at higher H/D ratios the ultimate normalized resistance should maintain

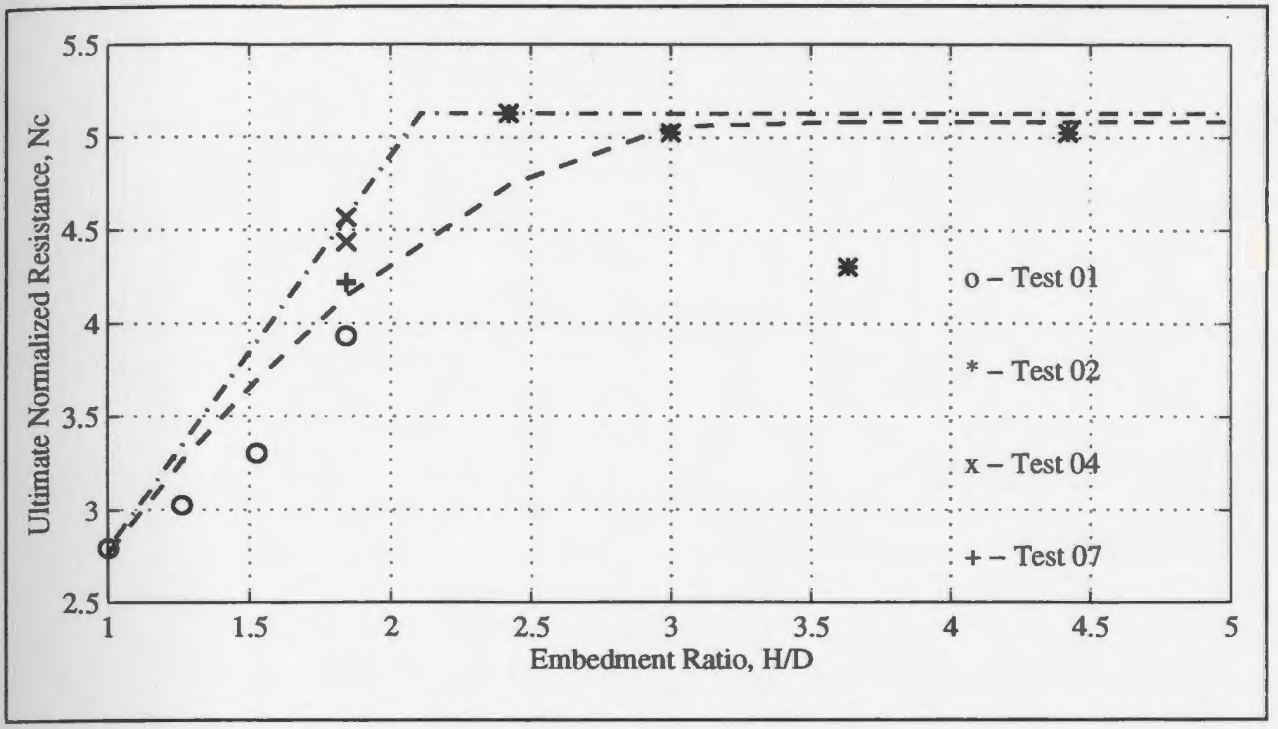

Figure 8.31 - Ultimate normalized resistance, N_c, versus embedment ratio, undrained tests.

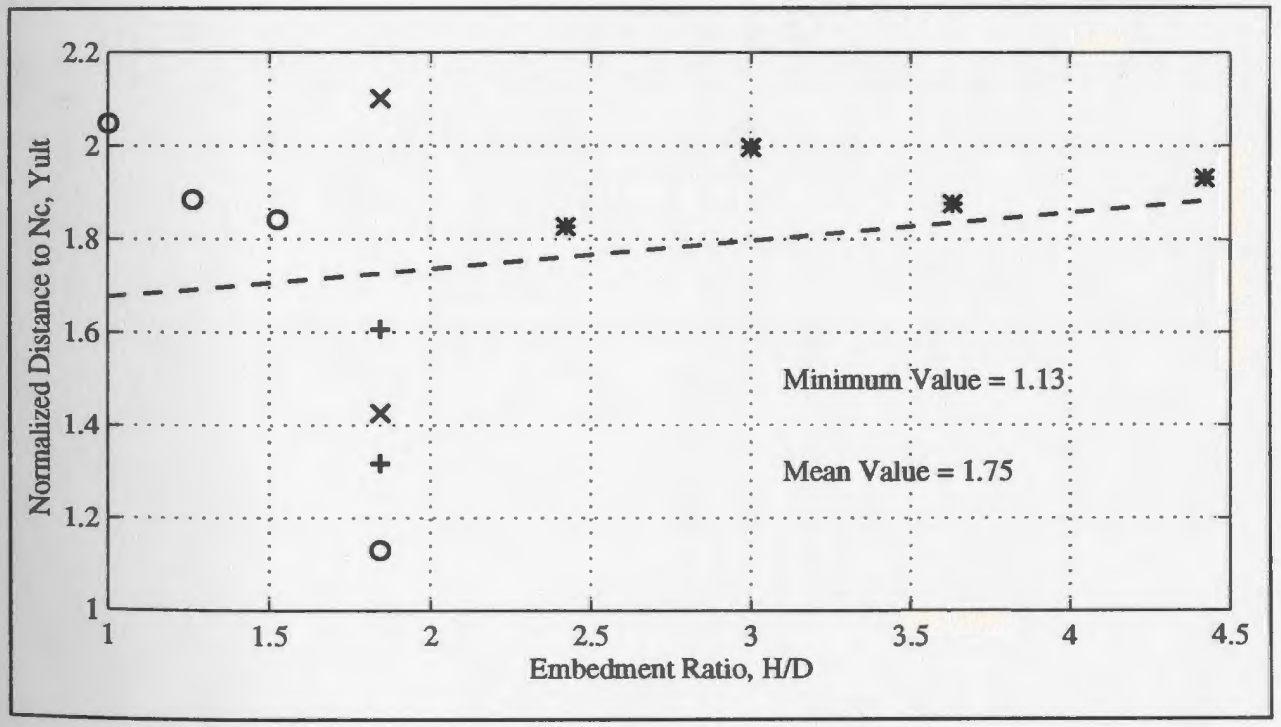

Figure 8.32 - Normalized distance to peak load, Y_{ult}, versus embedment ratio, undrained tests.

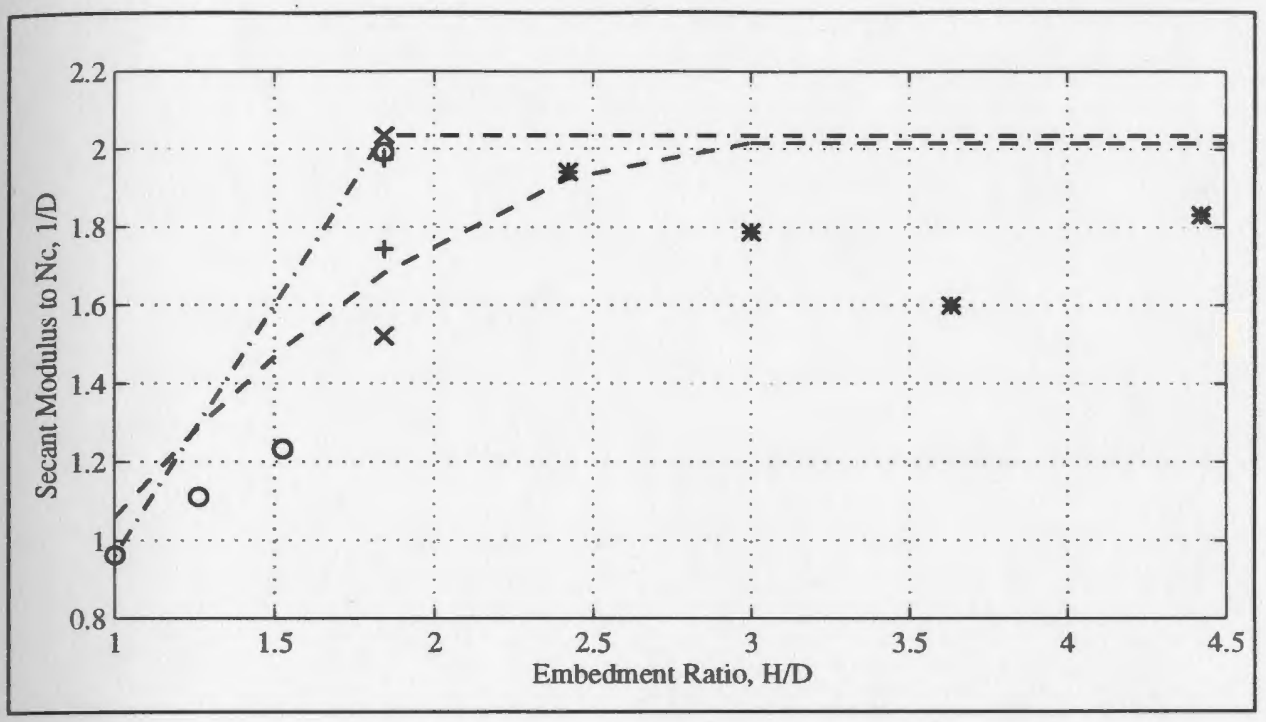

Figure 8.33 - Secant modulus to N_c versus embedment ratio, undrained tests.

a constant value or increase slightly. Alternatively, to be conservative, the data can be bounded by the bilinear dash-dot curve shown. From Figure 8.31, for the ultimate normalized resistance, N_c, the mean approach yields

$$N_c = -0.420\left(\frac{H}{D}\right)^2 + 2.83\left(\frac{H}{D}\right) - 0.360 \quad \textit{for } H/D \leq 3.632 \qquad \textbf{[8-7a]}$$

and

$$N_c = 5.09 \quad \textit{for } H/D > 3.632 \qquad \textbf{[8-7b]}$$

and the conservative approach yields

Table 8.2 - Summary of undrained interaction factors, existing analysis methods

Test	Pipe	Prototype Interaction Rate (m/day)	H/D	Distance Into Trench Wall to P_{ult} (D)*	Experimental Interaction Factor, N**	Rowe & Davis (1982b) Immediate/No Separation[1,2]	Hansen (1961)[3]	Edgers and Karlsrud (1982)[4]	Wantland *et al.* (1979)[5]	Mackenzie (1955)[6]	Tschec-botar-ioff (1973)[7]
01	1	0.86	1.842	1.13	3.98	4.0 / 8.7	5.4	5.35	3.43	3.34	2.99
01	2	0.98	1.526	1.84	3.31	3.5 / 7.3	4.9	4.80	3.13	2.98	2.53
01	3	1.16	1.263	1.88	3.03	2.9 / 5.6	4.5	4.34	2.96	2.65	2.23
01	4	1.05	1.000	2.05	2.79	2.0 / 4.0	4.0	3.88	2.59	2.30	1.66
02	1	0.90	4.421	1.93	5.03	4.9 / 11.4	6.7	9.86	4.83	6.24	5.58
02	2	0.95	3.632	1.88	4.31	4.9 / 11.4	6.5	8.47	4.47	5.49	4.84
02	3	1.12	3.000	2.00	5.03	4.9 / 11.4	6.3	7.38	4.15	4.92	4.32
02	4	0.81	2.421	1.83	5.13	4.6 / 10.6	5.9	6.36	3.81	4.19	3.57
03	1	0.74	1.842	1.40	4.89	4.0 / 8.7	5.4	5.35	3.43	3.52	2.99
03	2	0.95	1.842	1.78	5.98	4.0 / 8.7	5.4	5.35	3.43	3.52	2.99
03	3	1.19	1.842	2.32	5.28	4.0 / 8.7	5.4	5.35	3.43	3.52	2.99
03	4	0.92	1.842	1.66	4.91	4.0 / 8.7	5.4	5.35	3.43	3.52	2.99
04	1	0.0014	1.842	2.72/1.43	11.26 / 7.54	4.0 / 8.7	5.4	5.35	3.43	3.43	2.99
04	2	0.0078	1.842	3.60/1.57	8.15 / 4.76	4.0 / 8.7	5.4	5.35	3.43	3.47	2.99
04	3	0.075	1.842	1.43	4.57	4.0 / 8.7	5.4	5.35	3.43	3.40	2.99
04	4	1.60	1.842	2.10	4.44	4.0 / 8.7	5.4	5.35	3.43	3.40	2.99
05	1	1.76	1.842	2.18	4.98	4.0 / 8.7	5.4	5.35	3.43	3.50	2.99
05	2	1.80	1.526	1.67	5.52	3.5 / 7.3	4.9	4.80	3.13	3.13	2.53
05	3	1.66	1.263	2.13	4.37	2.9 / 5.6	4.5	4.34	2.96	2.78	2.23
05	4	1.66	1.000	2.26	3.60	2.0 / 4.0	4.0	3.88	2.59	2.41	1.66

Table 8.2, cont... - Summary of undrained interaction factors, existing analysis methods

Test	Pipe	Prototype Interaction Rate (m/day)	H/D	Distance Into Trench Wall to P_{ult} (D)*	Experimental Interaction Factor, N**	Rowe & Davis (1982b) Immediate/No Separation[1,2]	Hansen (1961)[3]	Edgers and Karlsrud (1982)[4]	Wantland *et al.* (1979)[5]	Mackenzie (1955)[6]	Tschec-botar-ioff (1973)[7]
06	1	1.22	1.842	7.66	5.12	4.0 / 8.7	5.4	5.35	3.43	3.76	2.99
06	2	0.86	1.526	5.64	4.60	3.5 / 7.3	4.9	4.80	3.13	3.33	2.53
06	3	0.93	1.263	2.24	2.91	2.9 / 5.6	4.5	4.34	2.96	2.94	2.23
06	4	0.93	1.000	2.89	2.36	2.0 / 4.0	4.0	3.88	2.59	2.53	1.66
07	1	0.0012	1.842	1.46/0.820	5.69 / 4.84	4.0 / 8.7	5.4	5.35	3.43	3.34	2.99
07	2	0.092	1.842	1.33/0.926	5.57 / 4.95	4.0 / 8.7	5.4	5.35	3.43	3.34	2.99
07	3	0.083	1.842	1.32	4.21	4.0 / 8.7	5.4	5.35	3.43	3.38	2.99
07	4	0.74	1.842	1.61	4.22	4.0 / 8.7	5.4	5.35	3.43	3.44	2.99
08	1	0.00095	1.842	1.78/0.835	10.28 / 7.97	4.0 / 8.7	5.4	5.35	3.43	3.63	2.99
08	2	0.0092	1.842	3.15/0.943	10.37 / 6.52	4.0 / 8.7	5.4	5.35	3.43	3.67	2.99
08	3	0.083	1.842	1.39	5.86	4.0 / 8.7	5.4	5.35	3.43	3.72	2.99
08	4	0.74	1.842	1.61	4.81	4.0 / 8.7	5.4	5.35	3.43	3.86	2.99
09	1	0.00092	1.842	1.85/0.497	6.54 / 4.42	4.0 / 8.7	5.4	5.35	3.43	3.21	2.99
09	2	0.0024	1.842	1.83/0.605	8.98 / 6.00	4.0 / 8.7	5.4	5.35	3.43	3.26	2.99
09	3	0.00092	1.842	1.44/0.402	6.38 / 5.44	4.0 / 8.7	5.4	5.35	3.43	3.21	2.99
09	4	0.00079	1.842	1.15/0.526	4.39 / 3.55	4.0 / 8.7	5.4	5.35	3.43	3.21	2.99

Notes: * Second distance for tests which were drained or partially drained corresponds to the point where the force-displacement curve became linear; ** Second interaction factor for tests which were drained or partially drained corresponds to the point where the force-displacement curve became linear; (1) Rowe and Davis (1982b) theoretical undrained "immediate separation" interaction factor; (2) Rowe and Davis (1982b) theoretical undrained "no separation" interaction factor; (3) Hansen (1961) theoretical undrained interaction factor; (4) Edgers and Karlsrud (1982) theoretical undrained interaction factor; (5) Wantland *et al.* (1979) theoretical undrained interaction factor; (6) Undrained interaction factor back-calculated from Mackenzie (1955) formulation; (7) Tschebotarioff (1973) theoretical undrained interaction factor.

$$N_c = 2.11\left(\frac{H}{D}\right) - 0.684 \leq 5.13. \qquad [8\text{-}8]$$

In Figure 8.32, a linear regression line has been fit through the data and distances have been normalized with respect to pipeline diameter. There is considerable variation in the data at an embedment ratio of 1.842. The distance into the trench wall to reach the normalized peak resistance generally ranges from 1.6 to 2.1 pipe diameters with a minimum value of 1.13 and an overall mean of approximately 1.75. The minimum value will be conservative as load will be transferred to the pipeline more rapidly. The linear regression presented in Figure 8.32 is expressed by

$$Y_{ult} = 0.060\left(\frac{H}{D}\right) + 1.62. \qquad [8\text{-}9]$$

A second order polynomial has been fit to the secant modulus data at lower H/D ratios as indicated on Figure 8.33. Again it is thought that the slope to ultimate normalized resistance should not decrease with increased burial depth; it should remain constant or increase slightly at some limiting embedment ratio. The conservative approach can alternatively be taken by utilizing the bounding bilinear dash-dot representation shown on the figure. The mean approach to determine the slope to ultimate normalized resistance, from Figure 8.33, yields

$$SM = -0.226\left(\frac{H}{D}\right)^2 + 1.38\left(\frac{H}{D}\right) - 0.094 \quad for\ H/D \leq 3 \qquad [8\text{-}10a]$$

and

$$SM = 2.02 \quad for\ H/D > 3 \qquad [8\text{-}10b]$$

and the conservative approach yields

$$SM = 1.27\left(\frac{H}{D}\right) - 0.312 \leq 2.04. \qquad [8\text{-}11]$$

Normalized Loads at Predetermined Displacements

The above analysis defined an ultimate normalized load on the pipeline. However, as mentioned previously, the choice of this ultimate load from the data sets may be somewhat subjective. The force on the pipeline at the trench wall, at a displacement of 0.5D into the trench wall, and at a displacement in which the pipeline has been embedded 1 diameter into the trench wall are considered to be benchmarks at which the normalized loads can be compared between tests. These data are presented in 6 of the *Test Data* appendices as well as in Figures 8.34 through 8.36 as a function of embedment ratio. Again, the select data of Test 04 and Test 07 has been included.

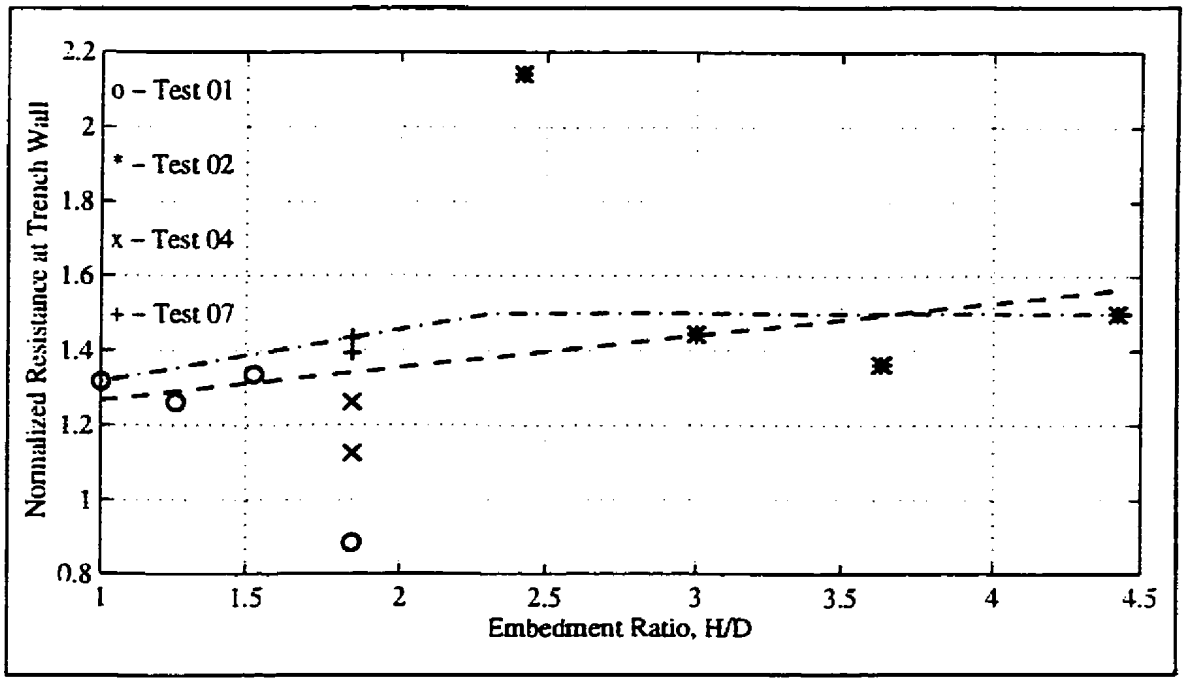

Figure 8.34 - Normalized resistance at the trench wall, N_{TW}, versus embedment ratio, undrained tests.

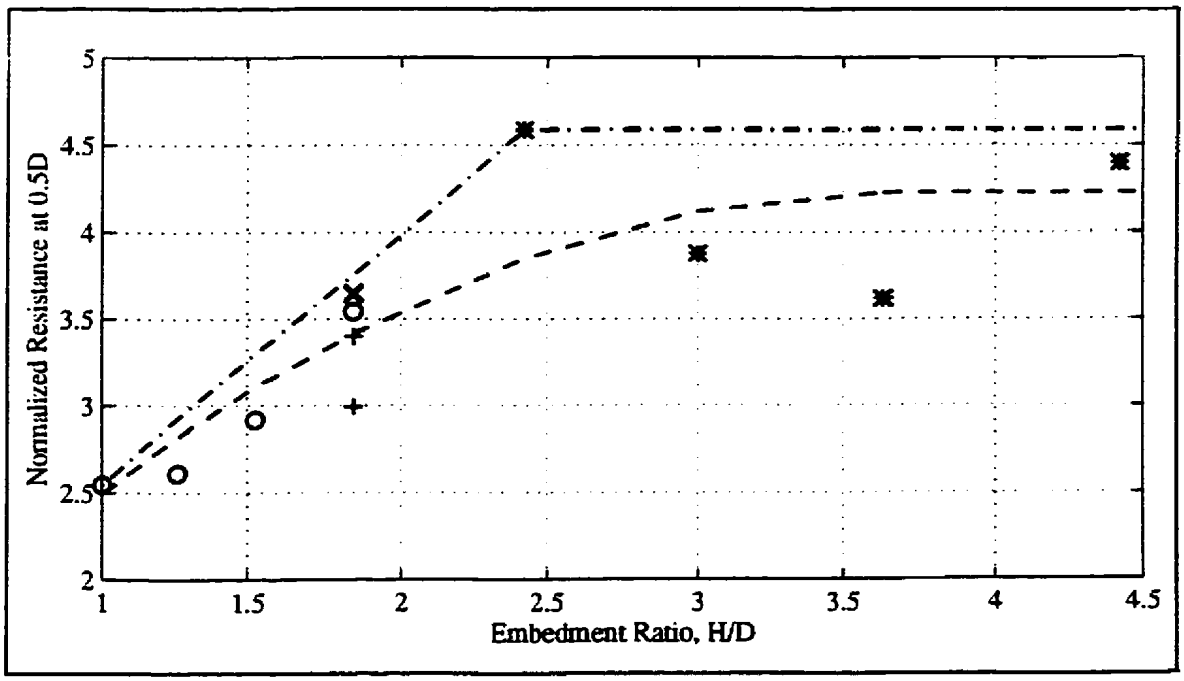

Figure 8.35 - Normalized resistance at 0.5D penetration into the trench wall, $N_{0.5D}$, versus embedment ratio, undrained tests.

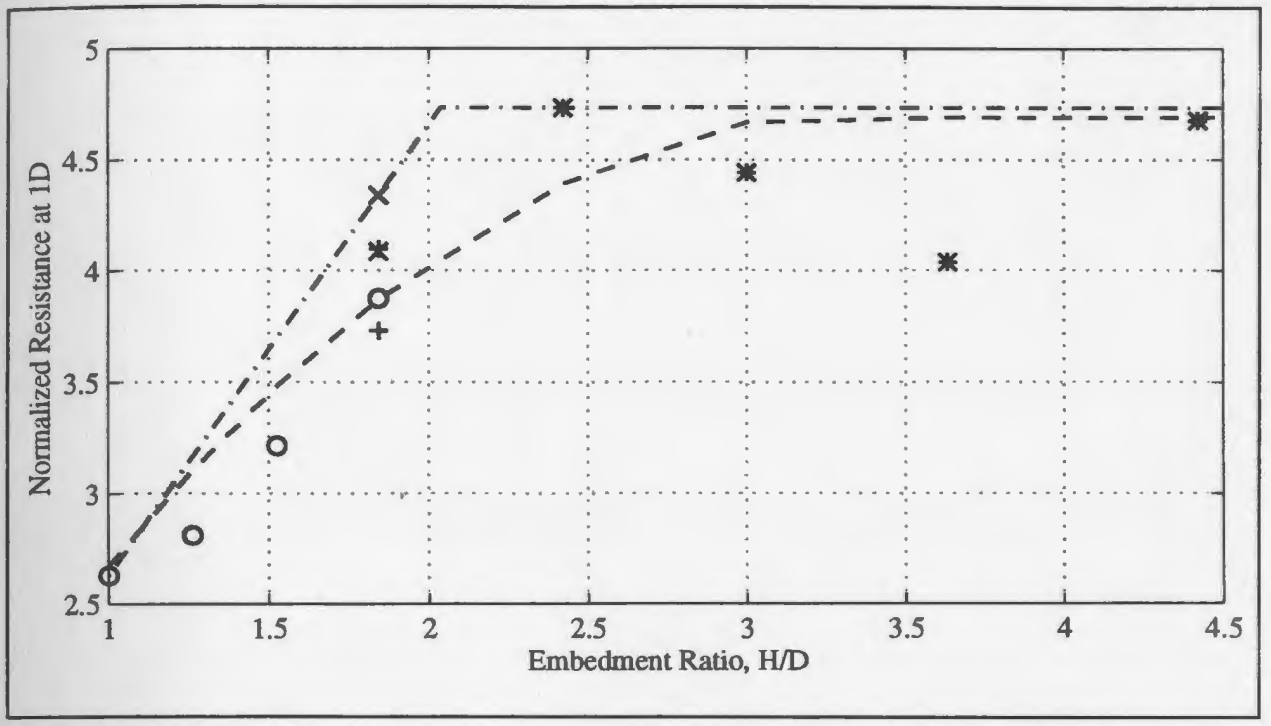

Figure 8.36 - Normalized resistance at 1D penetration into the trench wall, N_{1D}, versus embedment ratio, undrained tests.

The normalized resistance at the trench wall is presented in Figure 8.34. The high data point at an embedment ratio of 2.421 comes from Pipeline #4, Test 02 (see Figure 8.21). During this test there was some cracking around the trench and it is possible that this might have had some influence on the load transfer. A linear regression has been fit to the data which seems to provide a decent representation of the data trend as indicated by Figure 8.34. The normalized resistance generally ranges from approximately 1.2 to 1.6 with a mean of approximately 1.37. A conservative boundary to the data is shown in the figure by the bilinear dash-dot boundary. However, it should be pointed out that the resistance at the trench wall is predominantly controlled by the shear resistance of the backfill and the basal shear resistance of the pipe as the pipe has not yet contacted (laterally) the native

material. Therefore, the normalization of the resistance in Figure 8.34 does not take this fully into account. From Figure 8.34, for the normalized resistance at the trench wall yields

$$N_{TW} = 0.087\left(\frac{H}{D}\right) + 1.18 \qquad [8\text{-}12]$$

and the conservative approach yields

$$N_{TW} = 0.140\left(\frac{H}{D}\right) + 1.18 \leq 1.50. \qquad [8\text{-}13]$$

A regression line has been fit to the normalized resistance data at 0.5D penetration as shown in Figure 8.35. Again, it is thought that the resistance should not decrease at the higher H/D ratios but rather remain constant or increase slightly. Alternatively, a conservative interpretation would be to base values on the bilinear dash-dot boundary superimposed on the data. For the normalized resistance, the mean approach yields

$$N_{0.5D} = -0.245\left(\frac{H}{D}\right)^2 + 1.79\left(\frac{H}{D}\right) + 0.944 \qquad for\ H/D \leq 3.632 \qquad [8\text{-}14a]$$

and

$$N_{0.5D} = 4.23 \qquad for\ H/D > 3.632 \qquad [8\text{-}14b]$$

and the conservative approach yields

$$N_{0.5D} = 1.44(\frac{H}{D}) + 1.11 \leq 4.59. \qquad [8\text{-}15]$$

A similar exercise can be conducted with the 1D normalized resistances presented in Figure 8.36 to yield

$$N_{1D} = -0.365(\frac{H}{D})^2 + 2.46(\frac{H}{D}) + 0.580 \qquad for\ H/D \leq 3.632 \qquad [8\text{-}16a]$$

and

$$N_{1D} = 4.69 \qquad for\ H/D > 3.632 \qquad [8\text{-}16b]$$

while for the conservative approach

$$N_{1D} = 2.03(\frac{H}{D}) + 0.603 \leq 4.73. \qquad [8\text{-}17]$$

Bilinear Analysis

To investigate the effect of the variation in cover depth on undrained interaction, the following have been plotted as a function of H/D in Figures 8.37 through 8.40: the slope

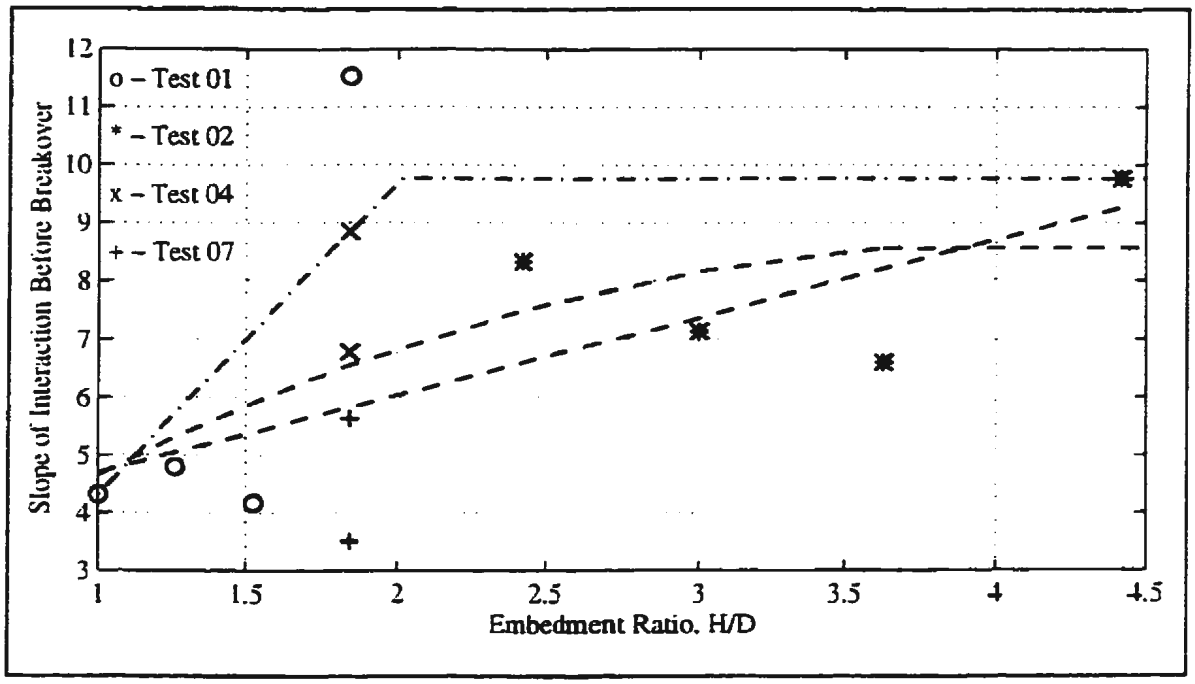

Figure 8.37 - Slope of interaction before breakover, S_{BB}, versus embedment ratio, undrained tests.

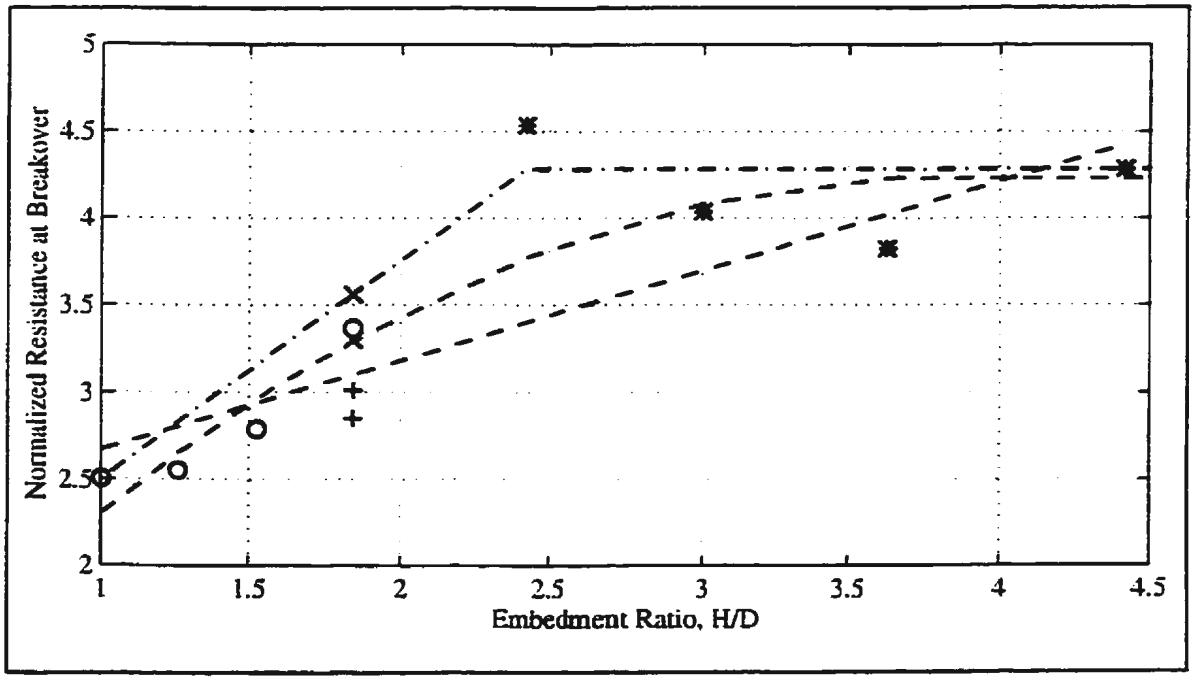

Figure 8.38 - Normalized resistance at breakover, N_{BO}, versus embedment ratio, undrained tests.

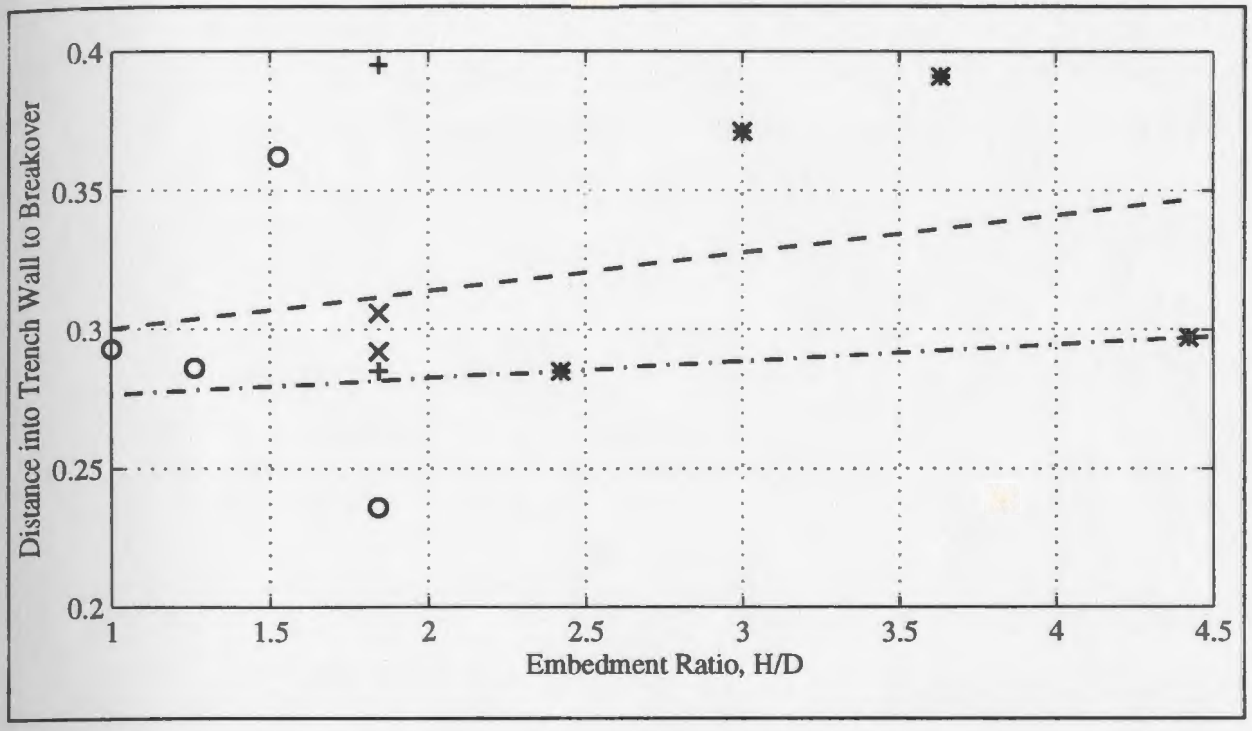

Figure 8.39 - Distance into the trench wall to breakover, D_{BO}, versus embedment ratio, undrained tests.

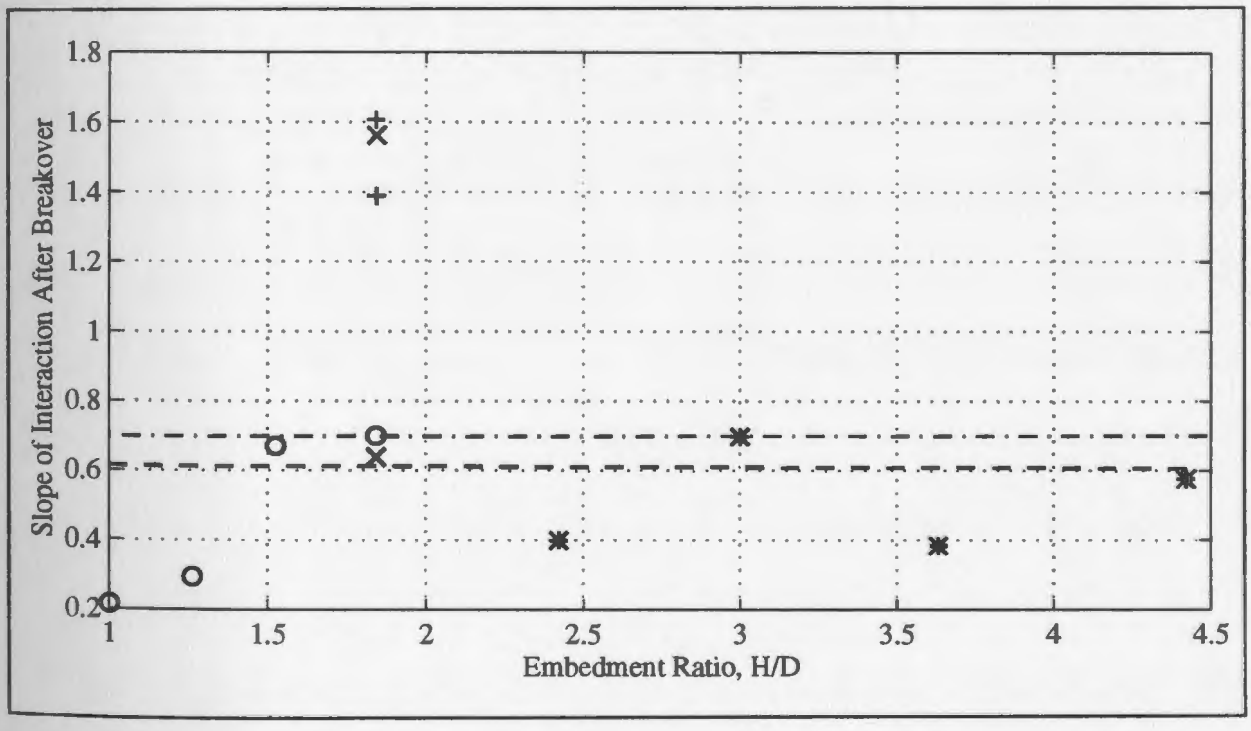

Figure 8.40 - Slope of interaction after breakover, S_{AB}, versus embedment ratio, undrained tests.

of the interaction between the trench wall and the breakover point; the normalized lateral load at breakover; the distance into the trench wall to breakover; and the slope of the interaction after breakover. As in the other analyses of this subsection, the data used in this analysis was taken from Test 01 and Test 02 augmented with select data from Test 04 and Test 07. If the parameter being studied is a distance, then it has been normalized with respect to the pipeline diameter.

The variation in the slope of the interaction between the trench wall and the breakover point as a function of H/D is presented in Figure 8.37. A second order polynomial has been fit to the initial portion of the data set which suggests that the slope increases with embedment ratio at least to an embedment ratio of 3.632 after which it has been represented as a constant. This may suggest the influence of a change in mode of soil deformation with increasing depth. If the extreme data point at an embedment ratio of 1.842 is discounted, the data appears to have a roughly linear trend increasing with increasing embedment ratio; however, there is no solid basis for excluding that data point other than the fact that it appears to be an outlier. It might be argued that the value of the slope associated with Pipeline #1, Test 01, is high and is an anomaly. Certainly, if the value of 11.538 (Pipeline #1, Test 01) is compared with undrained values of slope from Test 04 (6.8 - 8.8) and Test 07 (3.5 - 5.6), then the high value might be considered anomalous. Based on this assumption, a conservative estimate of the slope of the interaction before the breakover is presented as a dash-dot bilinear line in the figure. From the figure, the mean approach yields

$$S_{BB} = -0.427\left(\frac{H}{D}\right)^2 + 3.46\left(\frac{H}{D}\right) + 1.62 \qquad for\ H/D \leq 3.632 \qquad [8\text{-}18a]$$

and

$$S_{BB} = 8.56 \qquad for\ H/D > 3.632 \qquad [8\text{-}18b]$$

from the second order polynomial while the conservative approach yields

$$S_{BB} = 5.37\left(\frac{H}{D}\right) - 1.06 \leq 9.77. \qquad [8\text{-}19]$$

Normalized resistances at the breakover point as a function of embedment ratio are presented in Figure 8.38. A second order polynomial has again been fit to the data set which again suggests an increase in normalized resistance to at least an embedment ratio of 3.632 after which it has been represented as a constant value. The outlier in this particular data set is from Pipeline #4, Test 02. No explanation is apparent for this high value other than the fact that this was the pipeline which experienced trench cracking during testing. As indicated on the plot, a linear regression appears to give a reasonable fit to the data if the outlier is disregarded. A conservative representation of these data is presented as a dash-dot line on the plot. The second order polynomial representation is described by

$$N_{BO} = -0.250(\frac{H}{D})^2 + 1.89(\frac{H}{D}) + 0.663 \qquad for\ H/D \leq 3.632 \qquad [8\text{-}20a]$$

and

$$N_{BO} = 4.23 \qquad for\ H/D > 3.632 \qquad [8\text{-}20b]$$

for the mean approach while the conservative approach suggests

$$N_{BO} = 1.26(\frac{H}{D}) + 1.25 \leq 4.28. \qquad [8\text{-}21]$$

Figure 8.39 presents the distance into the trench wall to breakover as a function of embedment ratio. Although there is considerable scatter in the data, a linear regression indicates a slightly increasing trend with increasing embedment ratio. The data values range from approximately 0.28D to 0.40D with an approximate mean of 0.32D. A conservative bound to the data is also indicated on the plot by a dash-dot line and which discounts the Test 01 outlier at an embedment ratio of 1.842. The linear regression is expressed by

$$D_{BO} = 0.014(\frac{H}{D}) + 0.287 \qquad [8\text{-}22]$$

and the conservative approach by

$$D_{BO} = 0.006(\frac{H}{D}) + 0.271. \qquad [8\text{-}23]$$

The slope of the interaction after breakover is presented in Figure 8.40 as a function of embedment ratio. The majority of the data fall between a value of 0.2 and 0.7. Three outliers suggest a value between approximately 1.4 and 1.6. No definite conclusion can be made as to why the three outliers exist; however, the outliers came from the only tests (of the data presented in this subsection) where the displacement rate of the pipes was less than 0.75 m/day (prototype-scale). If the outliers are discounted, the data have a fairly constant linear trend as shown with a mean value of approximately 0.61. It is suggested a conservative approach would be to assume a value of 0.7 (dash-dot) line for the slope of the interaction after the breakover. The linear regression presented by the dashed line is expressed by

$$S_{AB} = -0.002(\frac{H}{D}) + 0.615. \qquad [8\text{-}24]$$

Internal Deformations

As mentioned previously, for an undrained shallow interaction, it would be expected that the soil in front of the pipeline would take the path of least resistance and would therefore

flow over the top of the pipe adding to the original soil cover. Visual observations made during post-test excavation were in acceptable agreement with this theory. During an undrained deep interaction, it would also be expected that the material in front of the pipeline would take the path of least resistance but half of the material would be expected to flow up and over the top of the pipeline while the other half would be expected to flow down and under the base of the pipeline. Therefore, one half a diameter of soil would be added to the original soil cover. Post-test visual observations were in acceptable agreement with this theory.

In both Test 01 and Test 02, the principal form of soil deformation was flow of soil around the pipeline. However, observation of internal deformations during soil excavation indicated potential differences in deformation. Above the pipeline, in the shallow tests, the spaghetti markers appeared to be distorted to the soil surface while in the deeper tests, the major distortion was restricted to approximately one diameter above the pipe. Below the pipe, the shallow tests exhibited very limited significant deformation of the spaghetti markers whereas under the deeper pipelines, the extent of significant deformation appeared to be greater (see Appendix K for details).

8.2.3 Effect of Trench Width - Undrained Conditions

Comparison of Normalized Prototype Force-Displacement Curves

Test 03 was conducted to investigate the effect of trench width on undrained lateral pipeline/soil interaction. Figure 8.22 presented the normalized corrected force-

displacement curves from the test. The curves can be better compared if they are offset so that interaction with the trench wall corresponds to the same point as shown in Figure 8.41. Here the curves of Pipelines #2 through #4 have been adjusted so that the position of the trench wall coincides with that of Pipeline #1. Pipeline #2 (2.5m trench width) exhibits higher values because of the problems with data acquisition described in Section 7.4 and the fact that some consolidation in front of the pipeline probably occurred when the pipeline was stopped. Up until a displacement of 2.5 pipeline diameters on the plot, the curves are obviously quite similar and there appears to have been no significant effect of varying the trench width.

Interaction Factors

Interpreted ultimate normalized resistances or interaction factors are presented in Table 8.2 for Test 03. With the exception of the interaction factor of Pipeline #2, all of the interaction factors are reasonably close. Observation of the data presented in the Table D.6 indicates that there appears to be no apparent relation between trench width and the distance into the trench wall to the ultimate normalized resistance or the secant modulus to that point.

Normalized Loads at Predetermined Displacements

Normalized resistances at benchmark displacements which were previously defined are presented in Table D.6. There appears to be no obvious correlation between the normalized resistance at the trench wall and trench width. Excluding the data of Pipeline

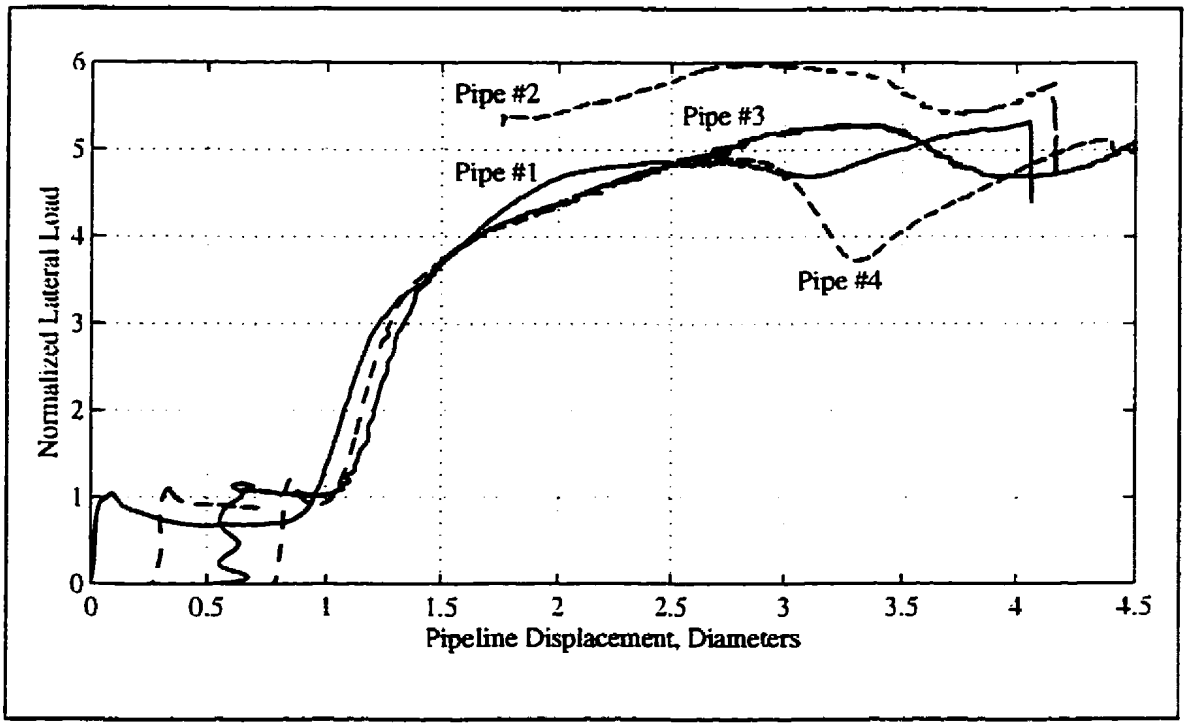

Figure 8.41 - Normalized prototype-scale force-displacement curves from Test 03 adjusted for differences in trench widths.

#2, observation of the normalized resistances at 0.5D and 1D penetration suggests that there is no effect of varying trench width on these data, at least for the range of trench widths studied.

Bilinear Analysis

Study of the bilinear parameters presented in Table D.6 reveals no obvious relations between the variation in trench width and values associated with the various parameters.

Internal Deformations

As in Test 01 and Test 02 described in the previous subsection, deformation of the soil

during Test 03 was primarily flow of soil around the pipeline. Any influence of trench width on the soil internal deformation was not apparent during post-test excavation (see also Appendix K).

8.2.4 Effect of Interaction Rate

Comparison of Normalized Prototype Force-Displacement Curves

Normalized prototype-scale force-displacement curves from Test 04, Test 07, and Test 08 were presented in Figures 8.23, 8.26, and 8.27. It appears that rate strongly influences the loads transferred to the pipe.

The first time Test 04 was run, it had to be terminated due to a problem with the centrifuge. However, ten hours of Pipeline #1 data (≈38mm of displacement) were collected prior to test termination. No useful data were collected for Pipelines #2 through #4. As there were limited useful data collected from this test, they are only used in selected parts of this thesis and a general test description and results section have not been presented. Figure 8.42 presents normalized force-displacement curves from Test 01, Test 04, and Test F4 where F4 designates the failed Test #4. The tests were conducted with similar burial depths, trench widths, and backfill types and in soil which had been preconsolidated to similar stress levels; the only difference were interaction velocities. The two tests conducted at prototype velocities of 0.0014 m/day yielded remarkably similar interaction curves up until the time when Test F4 was terminated. The remainder of the

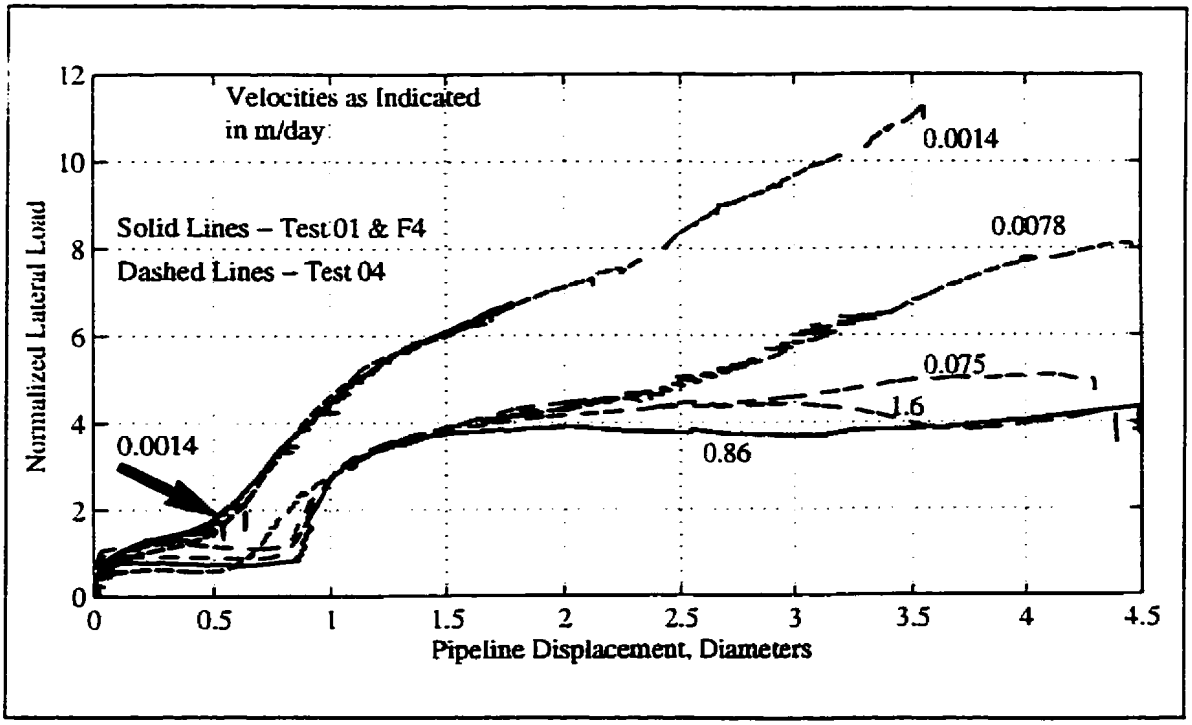

Figure 8.42 - Normalized prototype-scale force-displacement curves from Test 01, Test 04, and Test F4.

curves were quite similar up to a pipeline displacement of approximately 2 diameters (approximately 1D into the trench wall) after which Pipeline #2, Test 04, continued to increase in load while the other interaction curves remained relatively constant.

Figure 8.43 presents normalized prototype-scale force-displacement curves from Test 04 and Test 07. Again, the only difference between tests was the interaction velocities. In this case, the two slowest interaction curves from Test 07 fell between the two slowest from Test 04. The reader is reminded that there was a problem with Pipeline #1, Test 07. The curves from both Pipeline #2s appear to be comparable to a displacement of 1.5 pipeline diameters after which the load from the Test 07 pipeline increases more rapidly.

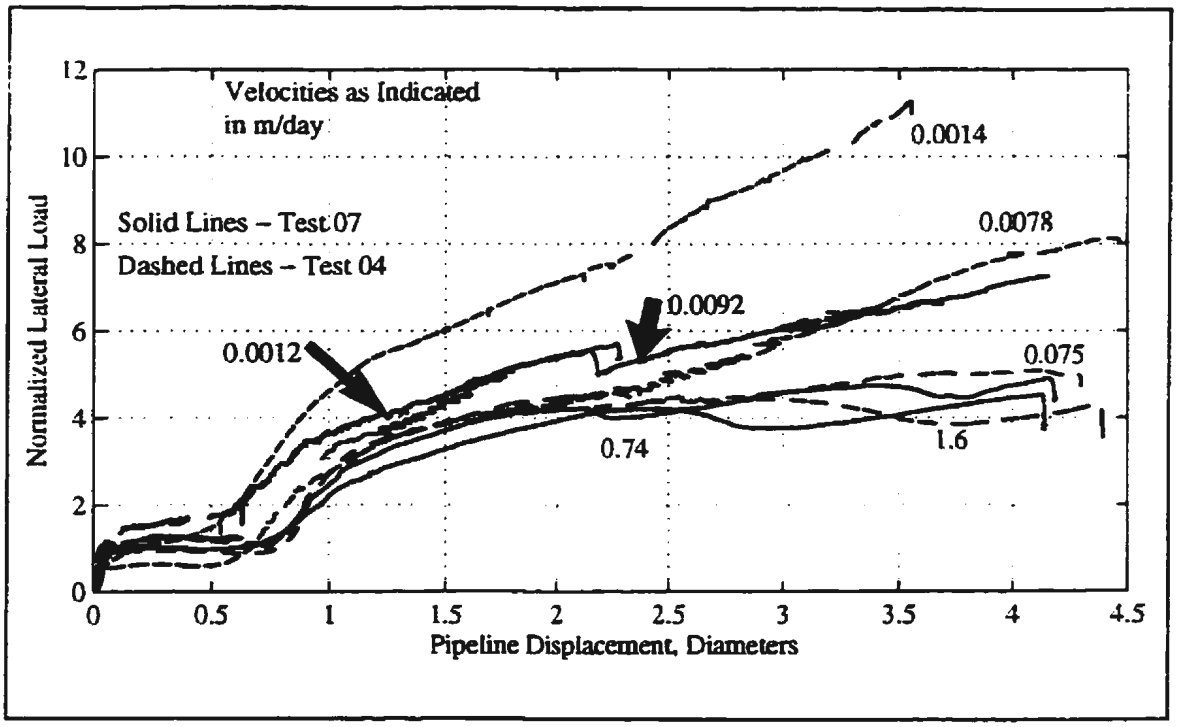

Figure 8.43 - Normalized prototype-scale force-displacement curves from Test 04 and Test 07.

At a displacement of approximately 2.2D, the output from the Test 07 pipeline dropped and the two curves were again in reasonable proximity. The curves from Pipeline #3 and Pipeline #4 from both tests were in reasonable proximity to each other throughout the displacement.

The data suggests that as the interaction velocity decreased or tended towards a drained loading condition, the loads experienced by the pipeline were greater than those experienced by a pipeline during an undrained loading condition for these soil conditions. During the drained test, the backfill became more of a factor in the interaction. In the undrained tests, the interaction curves remained relatively horizontal while the pipeline was

interacting with the backfill but during the drained test, the interaction curve increased significantly.

Observation of the data suggested three separate loading conditions; drained, partially-drained and undrained. For analysis purposes, the data have been divided into three drainage conditions for this particular soil/backfill system based on observations of the interactions described above: undrained - prototype velocity equal to or greater than 0.075 m/day; drained - prototype velocity equal to or less than 0.0012 m/day; partially-drained - prototype velocity between drained and undrained velocities. This criteria is in agreement with Head's (1986) method for calculating the shearing rate for drained triaxial compression; this value was calculated to be 0.002 m/day but yielded what was interpreted to be only a partially-drained sample.

Interaction Factors

Table 8.2 presented the interpreted interaction factors from all of the centrifuge tests. The drained and partially-drained interaction curves exhibited no clearly defined peak and may have continued to increase if the tests had not been terminated. Therefore, for these tests, the peak or interaction factor may be taken where the test terminated and should be considered a possible lower bound to the interaction factor (according to its formal definition). Also, an alternative interaction factor for the drained and partially-drained tests has been taken at the point where the force-displacement response had gone linear as discussed in the previous section. Interaction factors derived using both methods are

presented in Table 8.2.

Similar patterns of behaviour were found in the data of Test 04, 07, and 08. To augment the data from these tests, data from a similar pipeline test (Test 09, Pipeline #1) has been included in the analyses of this subsection. To analyse the effect of variation in interaction rate or drainage conditions on the interaction, the following have been plotted in Figures 8.44 through 8.46: interpreted ultimate normalized resistance or interaction factor (N_c); the normalized distance into the trench wall to the ultimate normalized resistance; and the secant modulus to the ultimate normalized resistance. Because the interaction velocities cover several orders of magnitude, the data have also been plotted in semilog space.

The data of Figure 8.44 indicates a slightly decreasing trend as indicated on the figure. Again it is emphasized that slower interaction rates exhibited no clearly defined peak and therefore the definition of the interaction factor may not be significant when comparing data from drained and undrained tests. The same argument can be put forth for the data of Figures 8.45 and 8.46. There is a slightly decreasing trend to the data sets but the trend of this line might have been different if the slower tests had been permitted to continue. Nonetheless, the normalized distance to the peak normalized load ranges from approximately 1.32 to 3.60 pipeline diameters with a mean distance of 1.95D. Conservative bounds have also been placed on the data sets as shown by the dash-dot lines.

In summary, the following representations have been derived from analysis of the

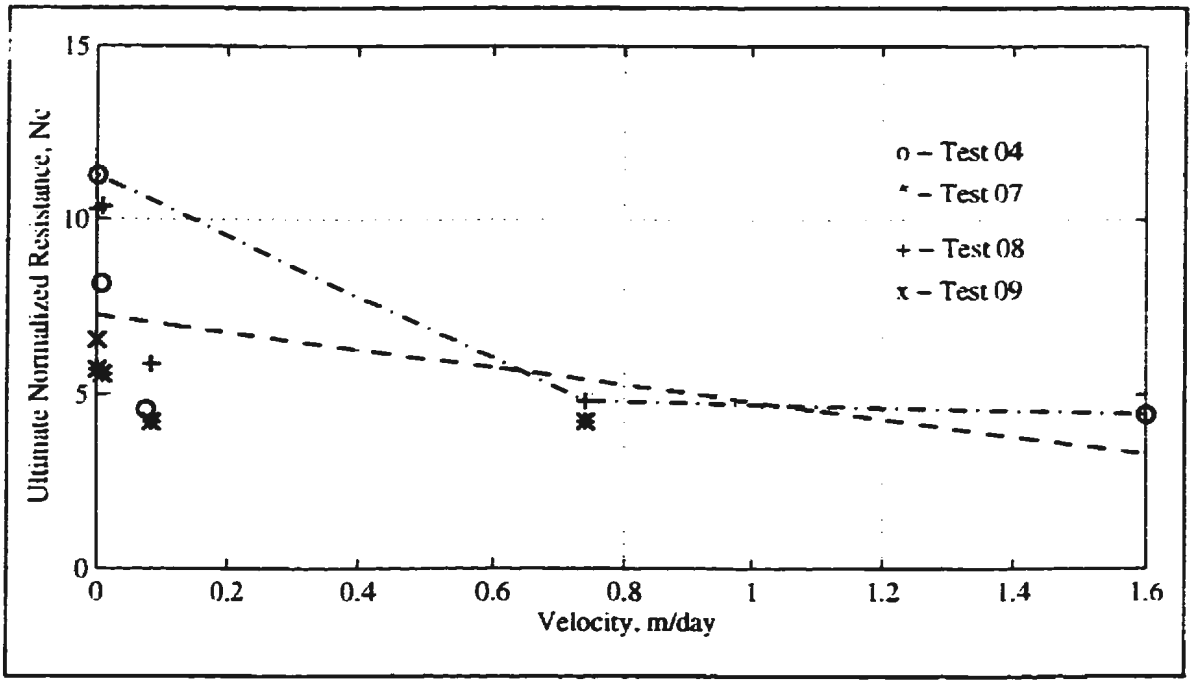

Figure 8.44a - Ultimate normalized resistance, N_c, versus interaction velocity.

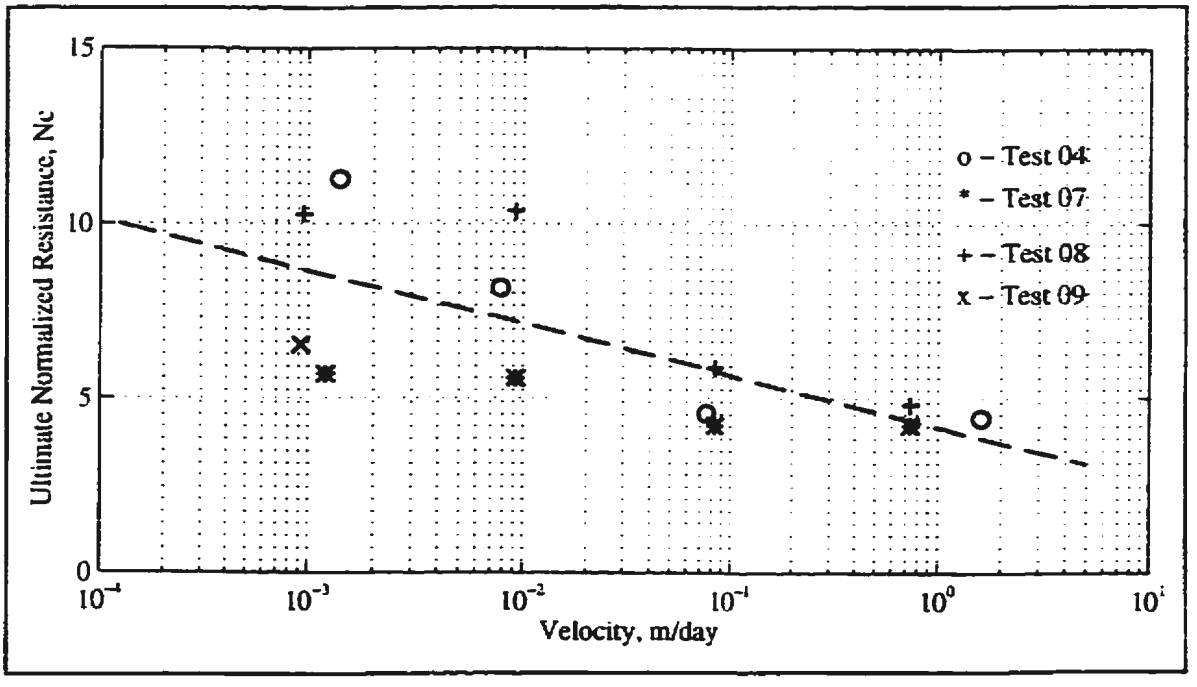

Figure 8.44b - *Ultimate normalized resistance, N_c, versus interaction velocity, semilog plot.*

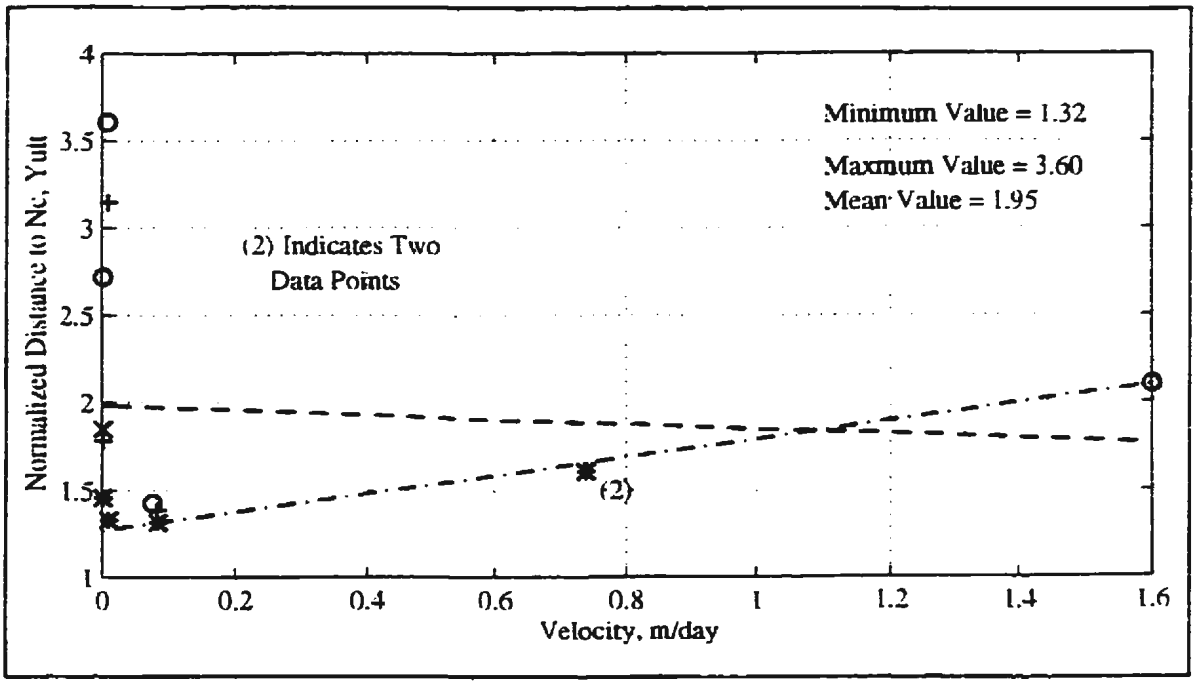

Figure 8.45a - Normalized distance to peak load, Y_{ult}, versus interaction velocity.

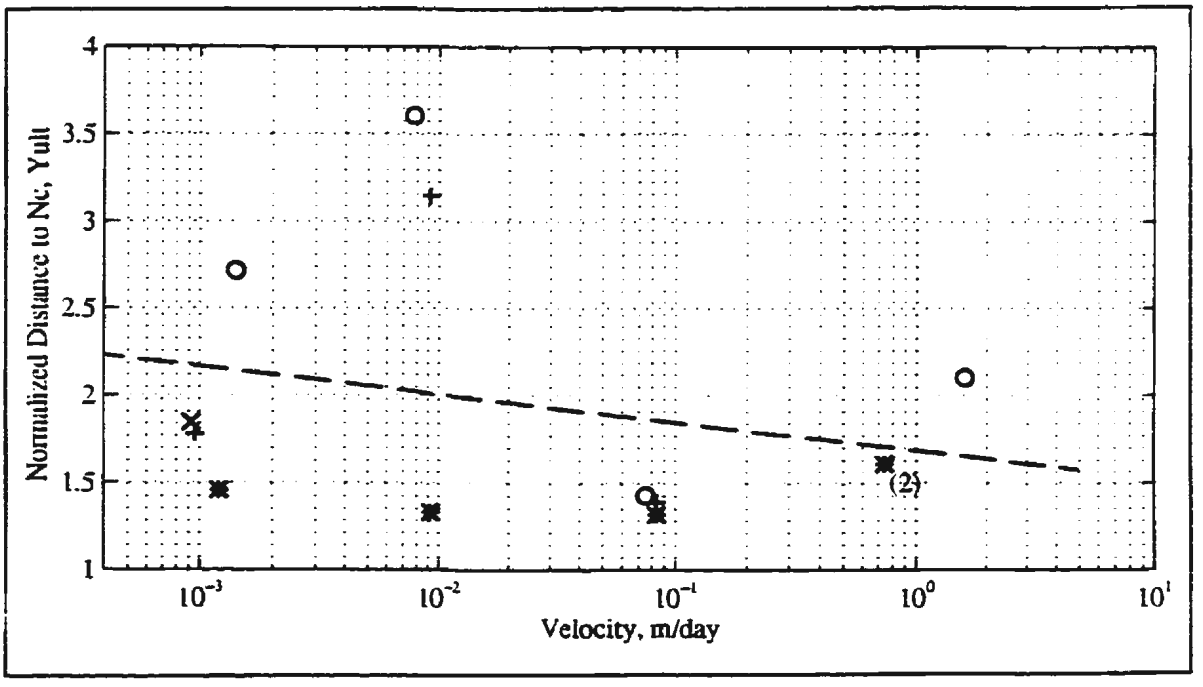

Figure 8.45b - Normalized distance to peak load, Y_{ult}, versus interaction velocity, semilog plot.

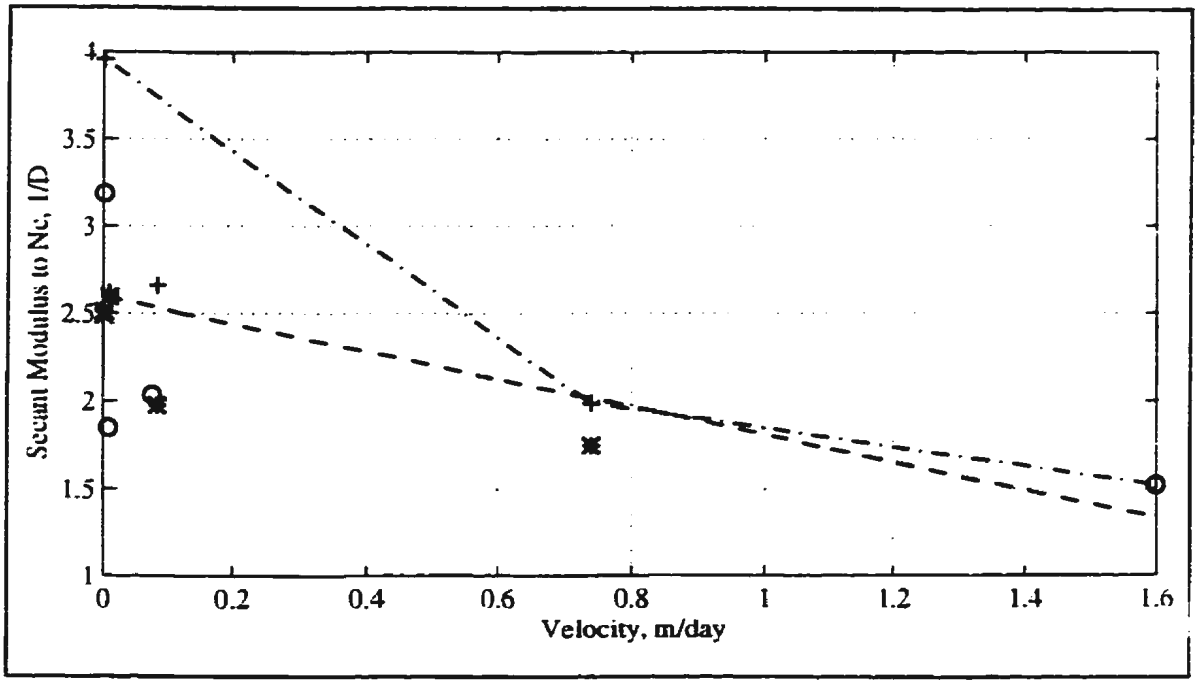

Figure 8.46a - Secant modulus to N_c versus interaction velocity.

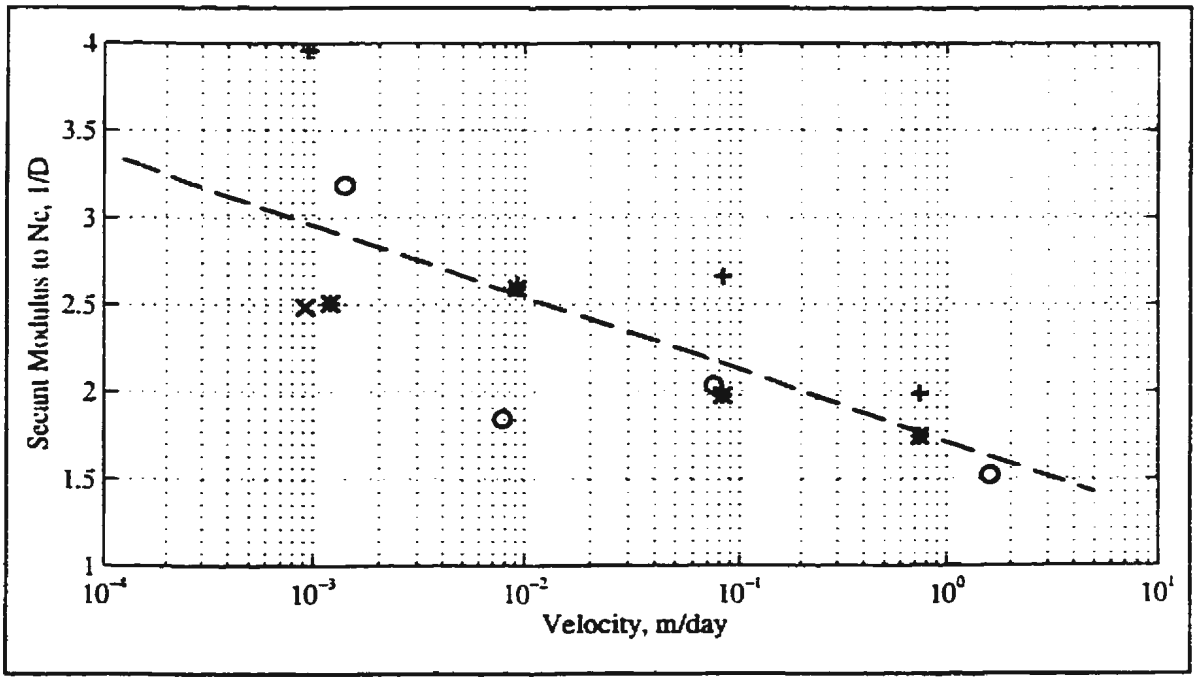

Figure 8.46b - *Secant modulus to N_c versus interaction velocity, semilog plot.*

interaction factors, the distance to the peak normalized force, and the secant modulus to ultimate load. From Figure 8.44, 8.45, and 8.46, the mean approach from the data in semilog space yields

$$N_c = -0.648 \ (\ln \ v) + 4.16 \qquad [8\text{-}25]$$

and

$$Y_{ult} = -0.070 \ (\ln \ v) + 1.69 \qquad [8\text{-}26]$$

and

$$SM = -0.176 \ (\ln \ v) + 1.73. \qquad [8\text{-}27]$$

Examination of the conservative representations presented in Figures 8.44a, 8.45a, and 8.46a suggests

$$N_c = 11.3 - 8.74\,v \qquad for \ v \leq 0.74 \ m/day \qquad [8\text{-}28a]$$

and

$$N_c = 5.12 - 0.430\,v \qquad for\ v > 0.74\ m/day; \qquad [8\text{-}28b]$$

while

$$Y_{ult} = 1.27 + 0.517\,v; \qquad [8\text{-}29]$$

finally,

$$SM = 3.96 - 2.67\,v \qquad for\ v \leq 0.74\ m/day \qquad [8\text{-}30a]$$

and

$$SM = 2.38 - 0.540\,v \qquad for\ v > 0.74\ m/day \qquad [8\text{-}30b]$$

Normalized Loads at Predetermined Displacements

As the choice of peak force from the data sets may be somewhat arbitrary, the load on the pipeline at the trench wall, at a penetration of 0.5D into the trench wall, and at a 1 diameter penetration are considered to be benchmarks for comparison purposes. These data are presented in Figures 8.47 through 8.49 as well as in the *Test Data* appendices. Again, data from Test 09, Pipeline #1 has been included. Referring to Figure 8.47, during the slower tests the backfill between the trench wall would have had more time for self-

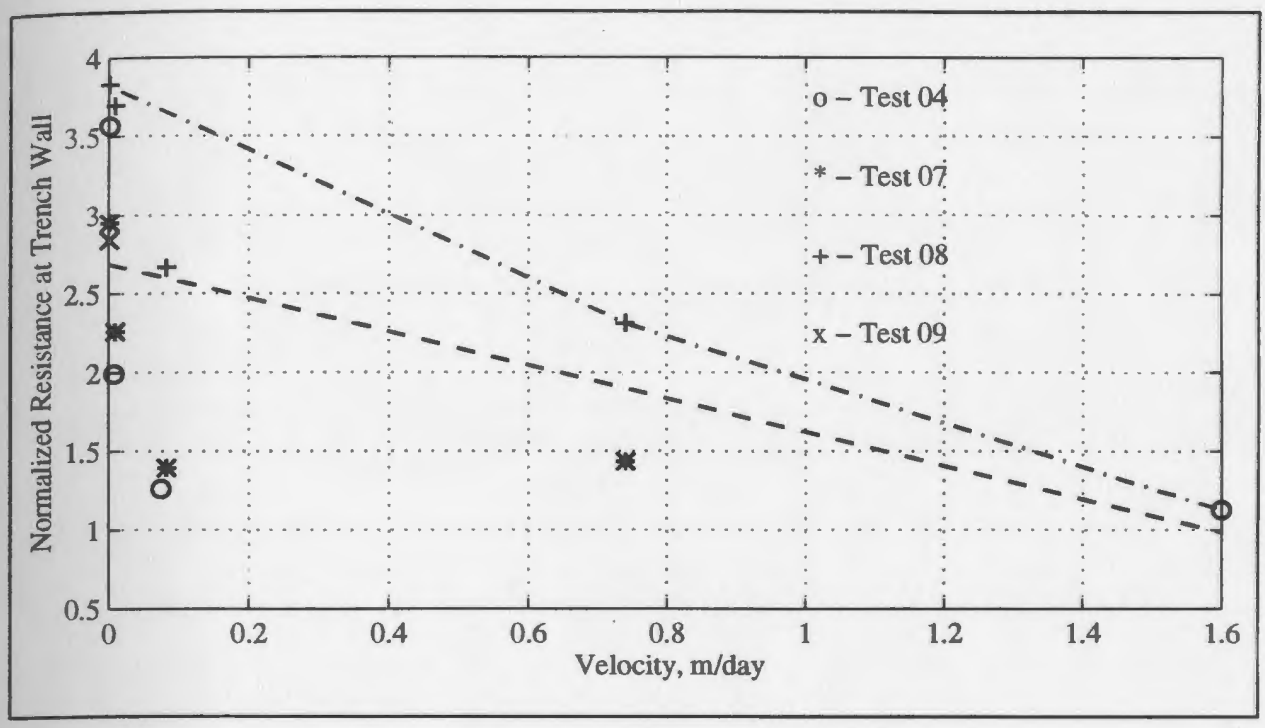

Figure 8.47a - Normalized resistance at the trench wall, N_{TW}, versus interaction velocity.

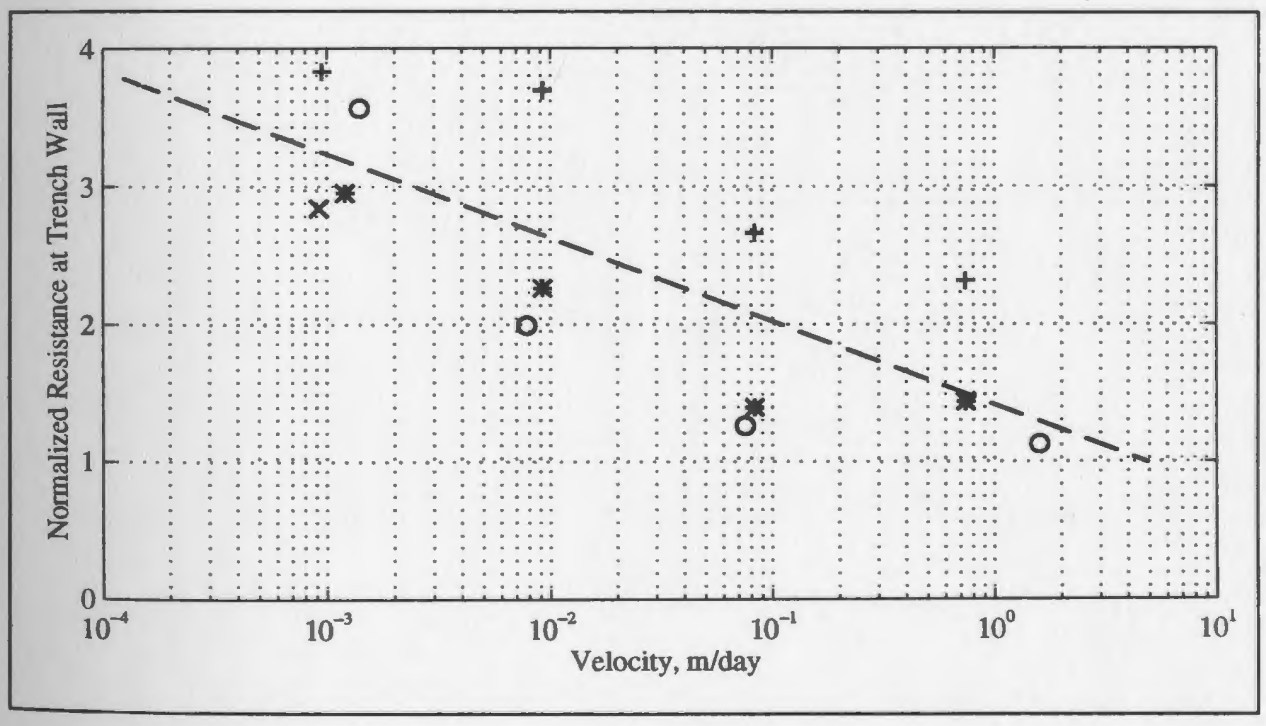

Figure 8.47b - Normalized resistance at the trench wall, N_{TW}, versus interaction velocity, semilog plot.

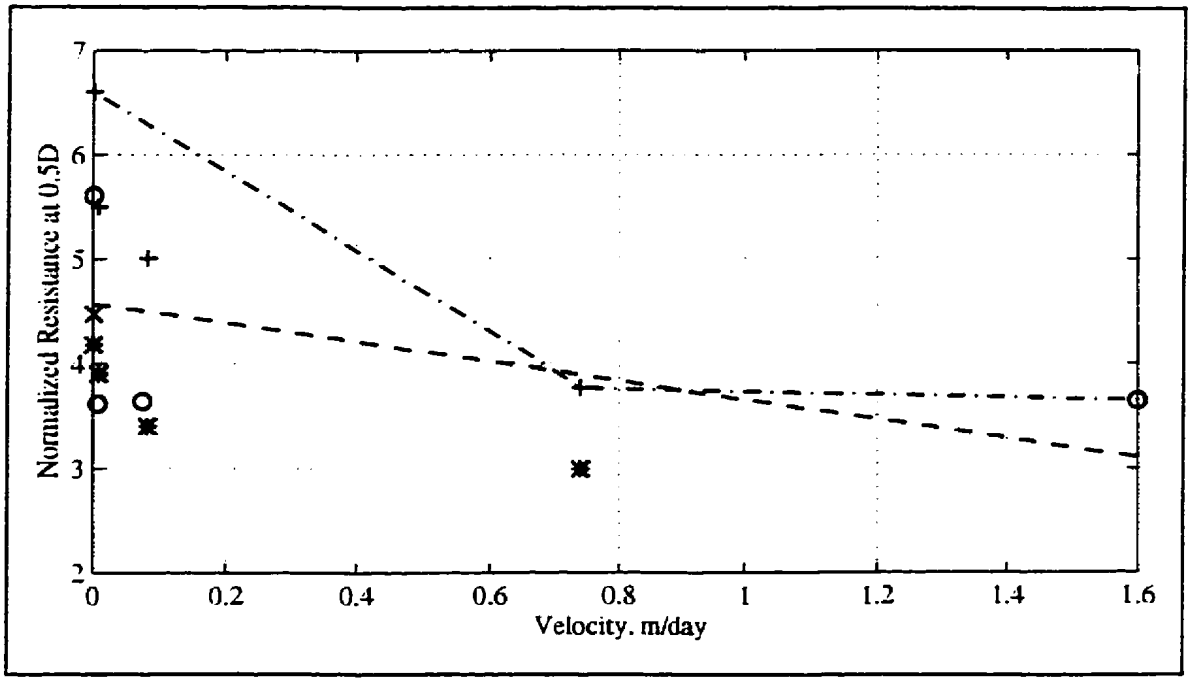

Figure 8.48a - Normalized resistance at 0.5D penetration into the trench wall, $N_{0.5D}$, versus interaction velocity.

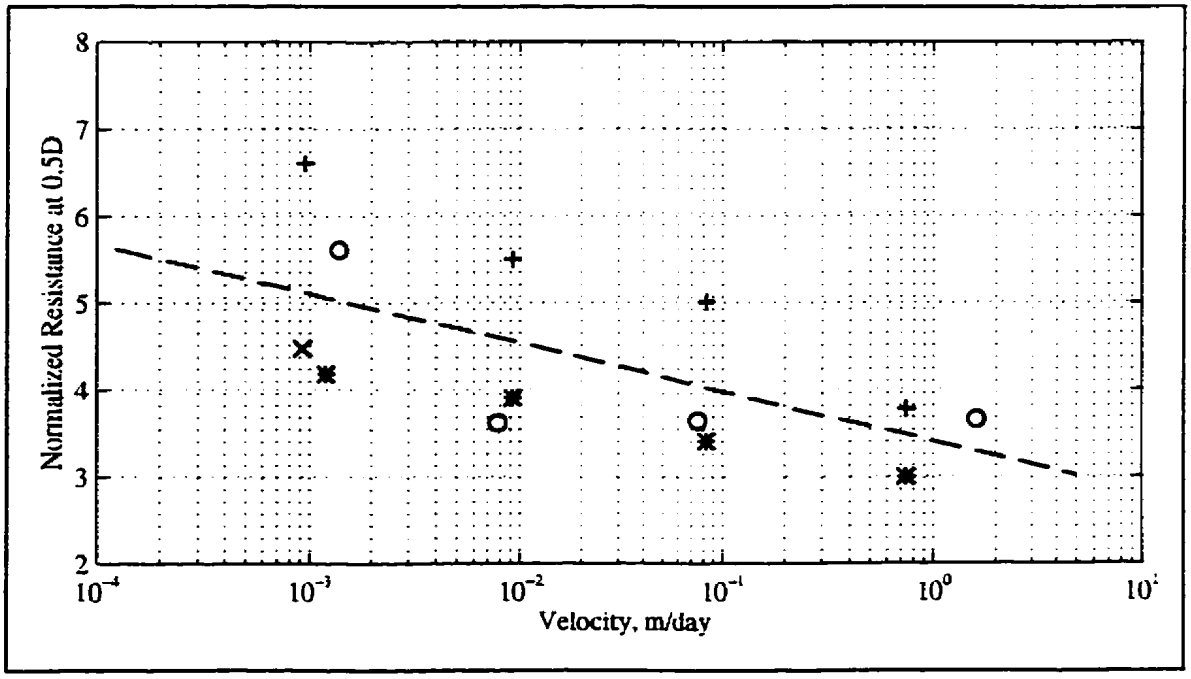

Figure 8.48b - Normalized resistance at 0.5D penetration into the trench wall, $N_{0.5D}$, versus interaction velocity, semilog plot.

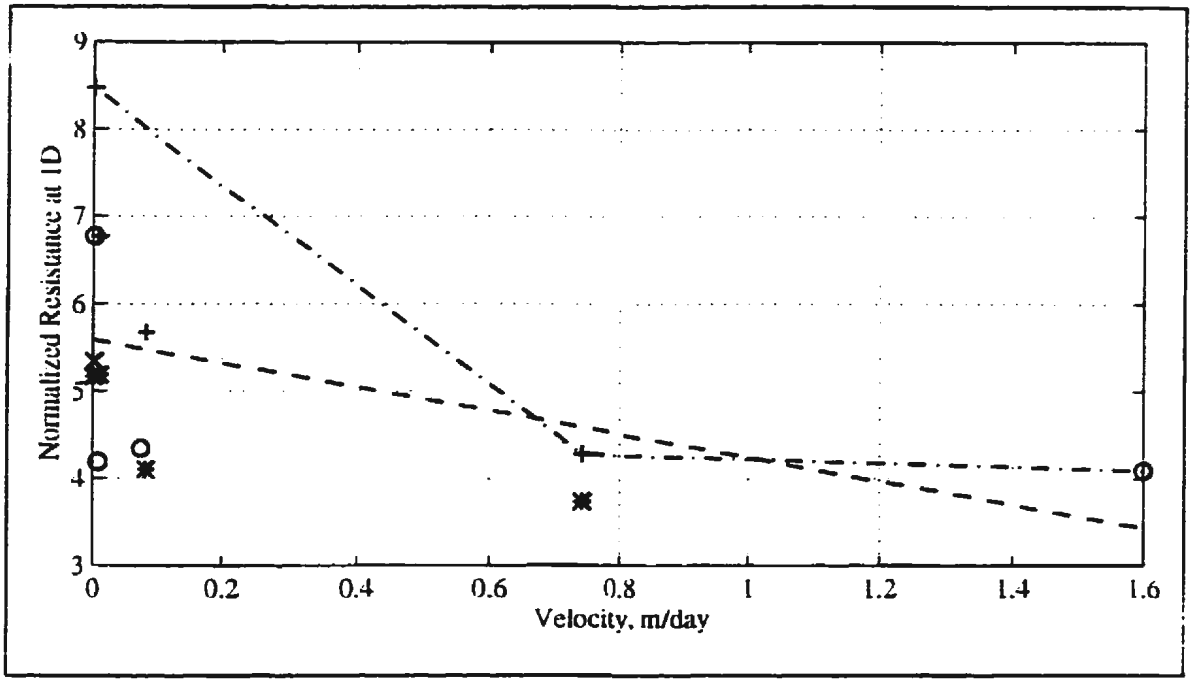

Figure 8.49a - Normalized resistance at 1D penetration into the trench wall, N_{1D}, versus interaction velocity.

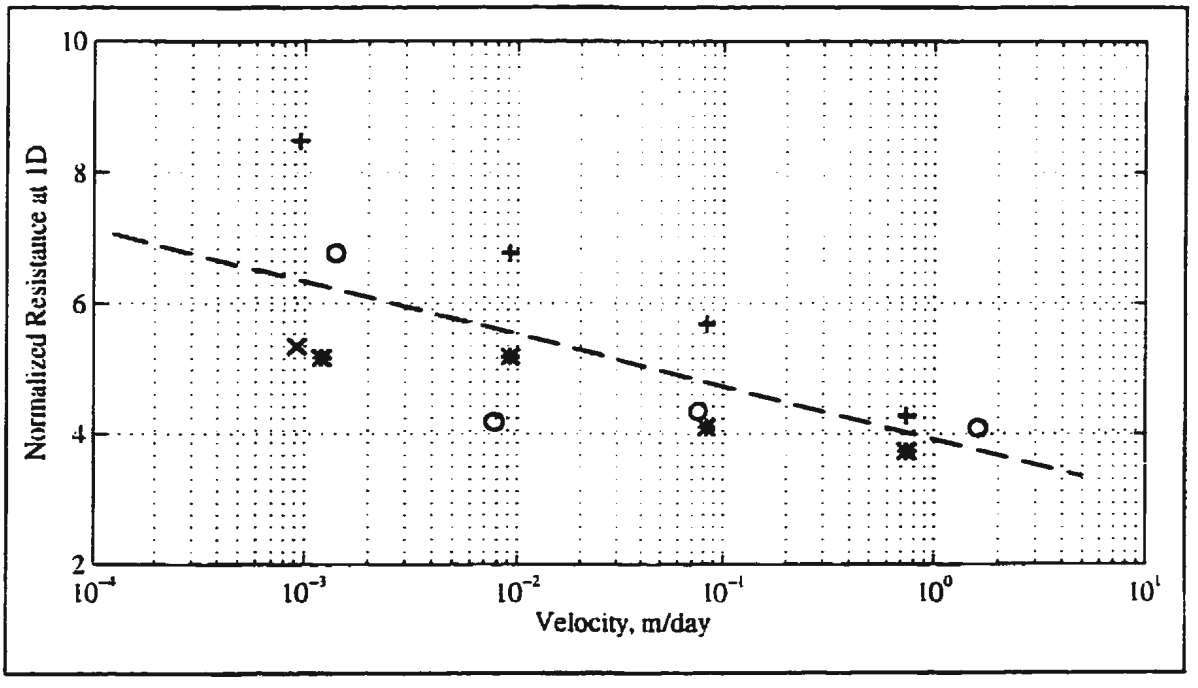

Figure 8.49b - Normalized resistance at 1D penetration into the trench wall, N_{1D}, versus interaction velocity, semilog plot.

weight consolidation and consolidation as a result of pipeline compression to occur. The other component contributing to the resistance at the trench wall is pipeline basal shear. The trend in the data of all three plots indicate a decrease in normalized resistance with increasing interaction velocity. Alternatively, a conservative interpretation would be to base values on the bilinear dash-dot boundary superimposed on the data. For Figures 8.47b, 8.48b, and 8.49b, the mean fits to the data are represented respectively by

$$N_{TW} = -0.263\ (\ln\ v) + 1.41, \qquad [8\text{-}31]$$

$$N_{0.5D} = -0.463\ (\ln\ v) + 3.40, \qquad [8\text{-}32]$$

and

$$N_{1D} = -0.350\ (\ln\ v) + 3.91. \qquad [8\text{-}33]$$

Examination of the conservative representations presented in Figures 8.47a, 8.48a, and 8.49a suggests for interaction rates less than or equal to 0.74 m/day

$$N_{TW} = 3.82 - 2.31\,v, \qquad [8\text{-}34a]$$

$$N_{0.5D} = 6.64 - 3.88\,v, \qquad [8\text{-}35a]$$

and

$$N_{1D} = 8.48 - 5.69v; \qquad \text{[8-36a]}$$

while for interaction rates greater than 0.74 m/day

$$N_{TW} = 3.34 - 1.39v, \qquad \text{[8-34b]}$$

$$N_{0.5D} = 3.87 - 0.137v, \qquad \text{[8-35b]}$$

and

$$N_{1D} = 4.44 - 0.219v. \qquad \text{[8-36b]}$$

Bilinear Analysis

To investigate the effect of variation in pipeline displacement rate on the bilinear analysis parameters, Figures 8.50 through 8.53 present the following parameters as a function of interaction velocity: the slope of the interaction between the trench wall and the breakover point; the normalized resistance at breakover; the distance into the trench wall to the breakover point; and the slope of the interaction after breakover. Linear regressions have been fit to the data as presented on the figures. Data used for analysis was taken from Tests 04, 07, and 08. Distances have been normalized with respect to pipeline diameter.

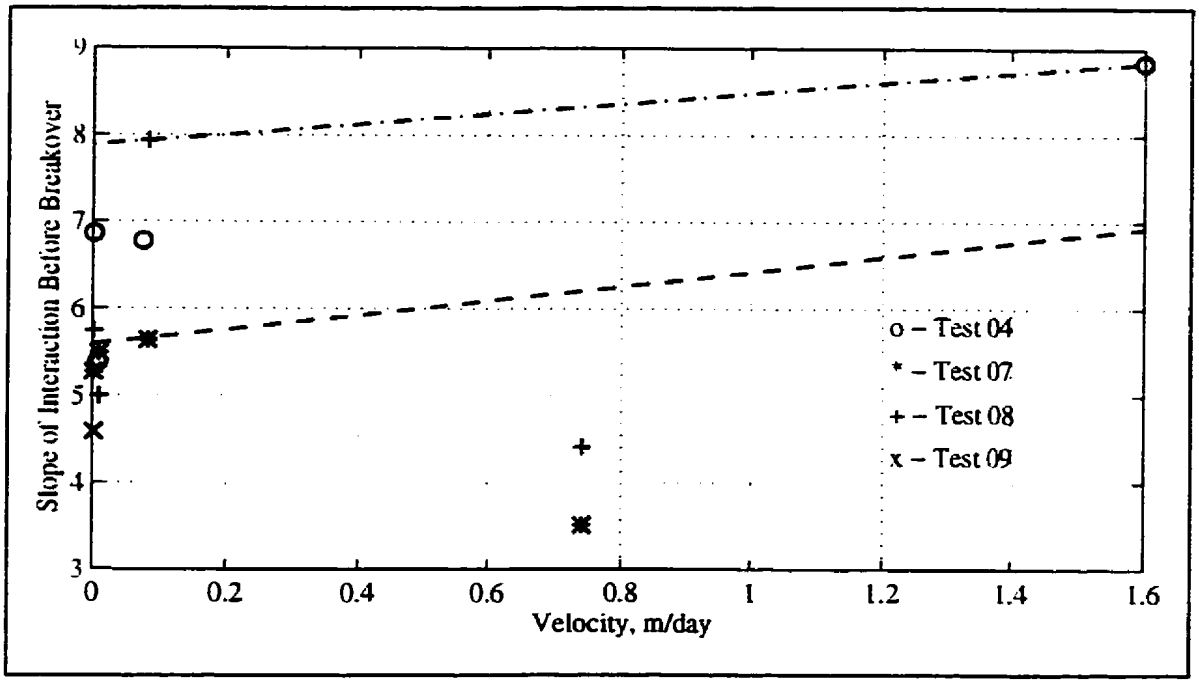

Figure 8.50a - Slope of interaction before breakover, S_{BB}, versus interaction velocity.

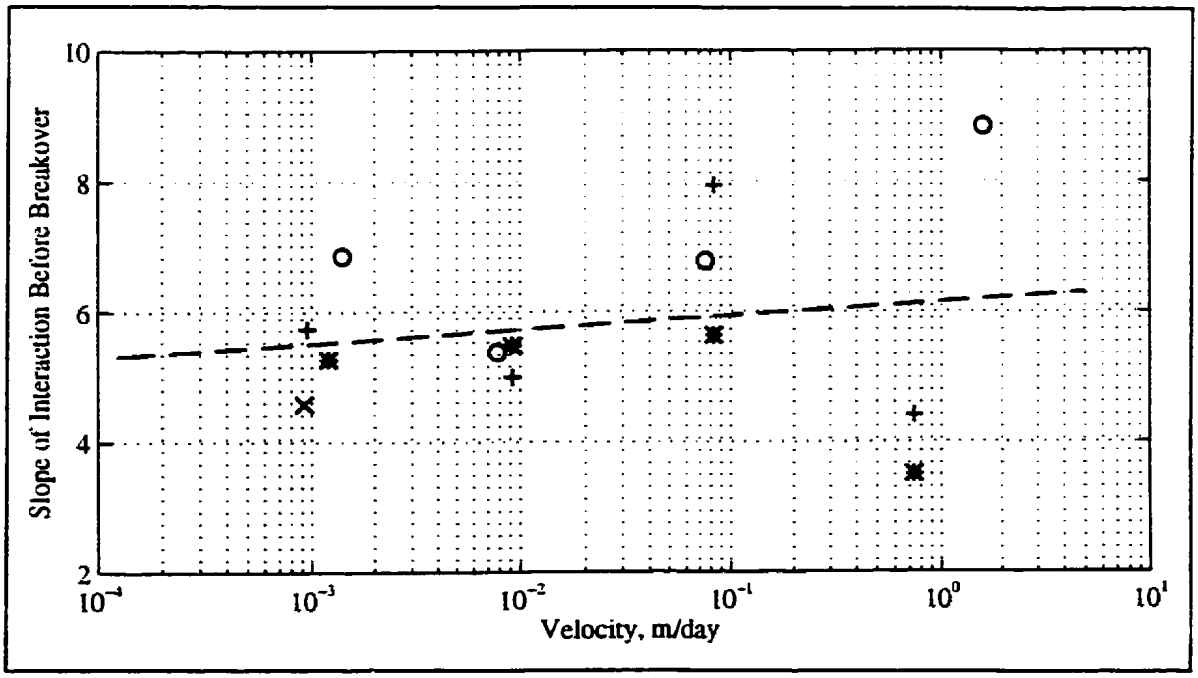

Figure 8.50b - *Slope of interaction before breakover, S_{BB}, versus interaction velocity, semilog plot.*

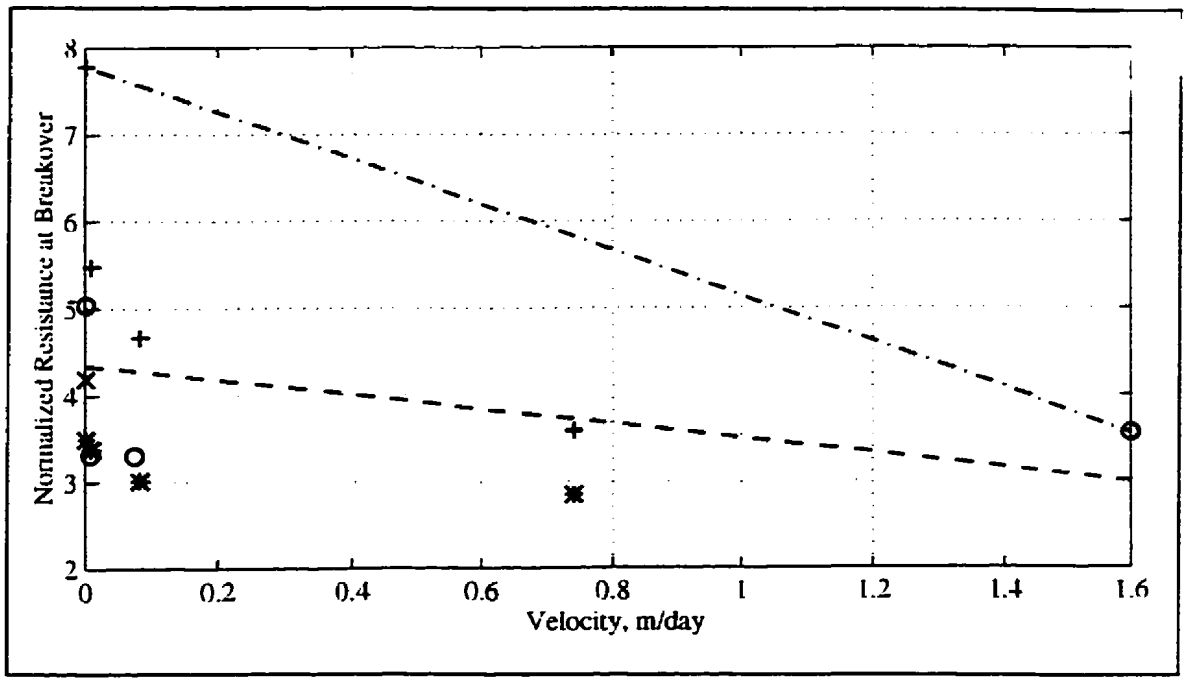

Figure 8.51a - Normalized resistance at breakover, N_{BO}, versus interaction velocity.

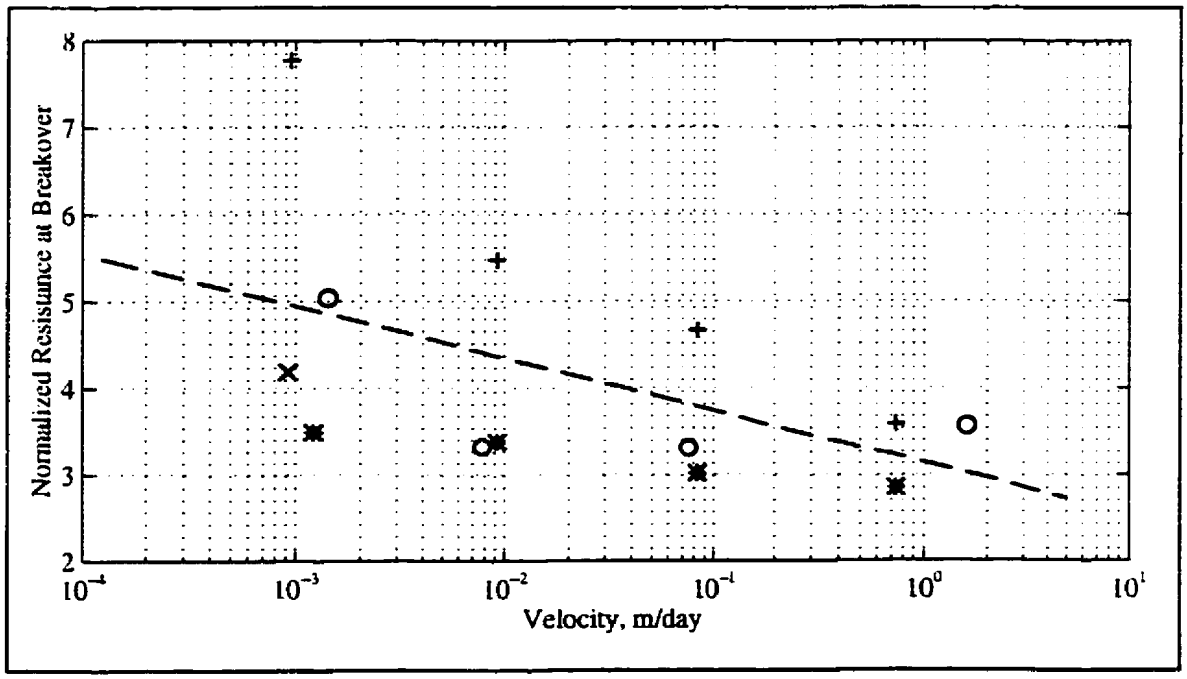

Figure 8.51b - Normalized resistance at breakover, N_{BO}, versus interaction velocity, semilog plot.

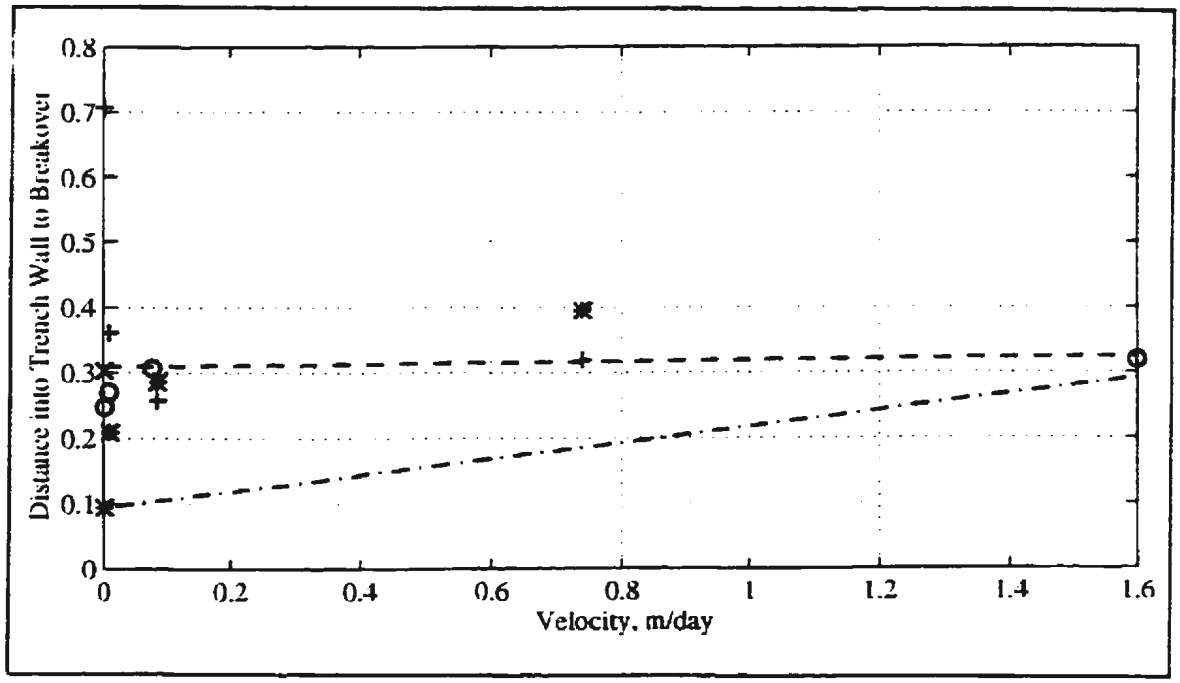

Figure 8.52a - Distance into the trench wall to breakover, D_{BO}, versus interaction velocity.

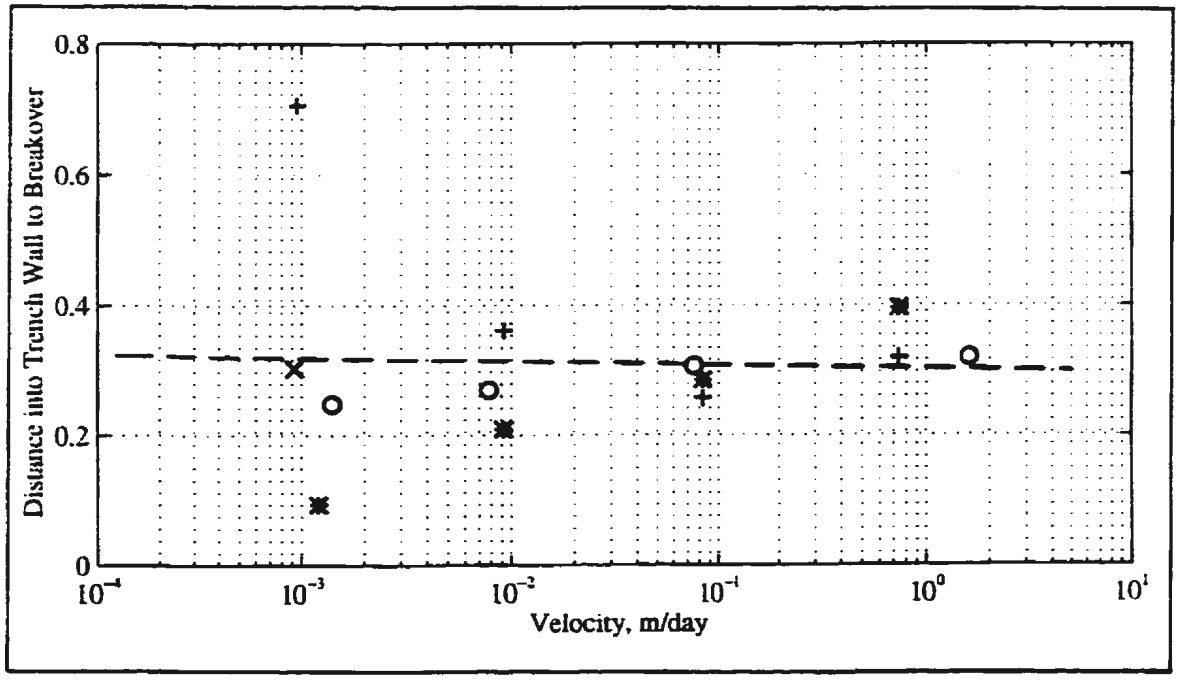

Figure 8.52b - Distance into the trench wall to breakover, D_{BO}, versus interaction velocity, semilog plot.

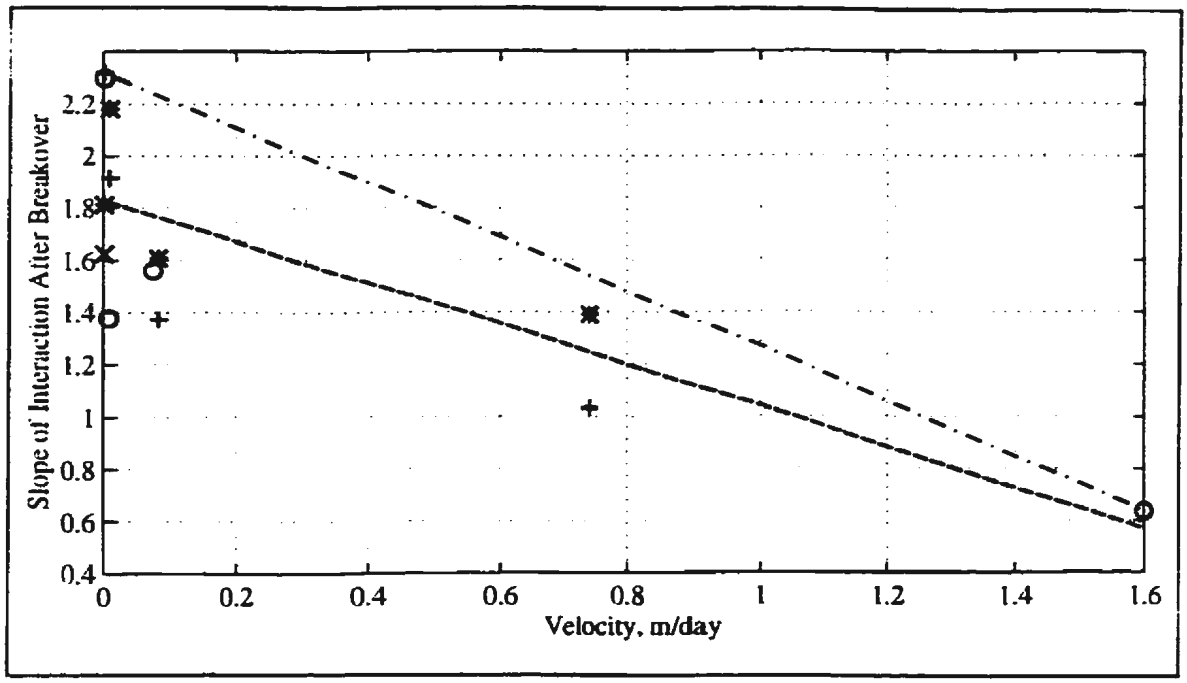

Figure 8.53a - Slope of interaction after breakover, S_{AB}, versus interaction velocity.

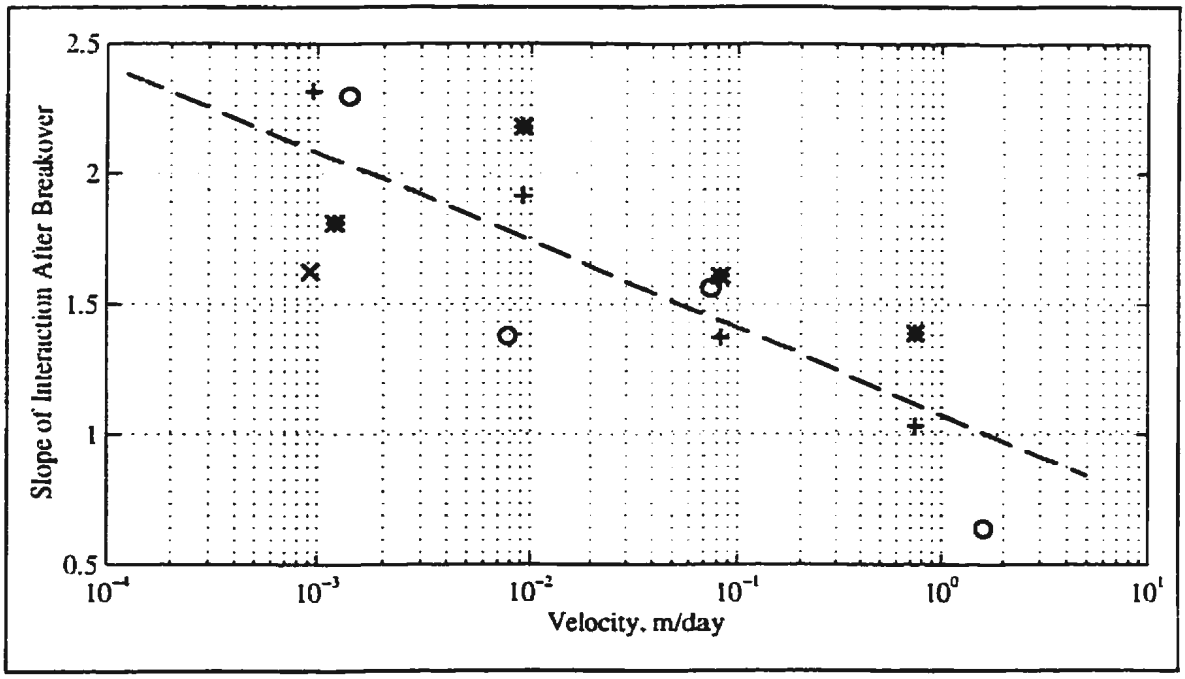

Figure 8.53b - Slope of interaction after breakover, S_{AB}, versus interaction velocity, semilog plot.

The variation in the slope of the interaction before breakover as a function of interaction rate is presented in Figure 8.50. The trend in the data suggests that this parameter increases slightly with increasing pipeline displacement rate. The low values at a velocity of approximately 0.75 m/day are thought to be associated with experimental variation as Pipeline #1 of Test 01 (velocity = 0.86 m/day) yielded a parameter value greater than 11 (which, as discussed in Subsection 8.2.2, may or may not be an anomaly in itself). Intuitively, the slope of the interaction between the trench wall and the breakover point should increase with increasing velocity up to a point as the effect of interacting with the trench wall was masked during the slower tests. A conservative estimate of the slope of the interaction before the breakover point is presented as a dash-dot line in the figure. From the figure, the mean approach yields

$$S_{BB} = 0.092 \ (\ln \ v) + 6.15 \qquad \text{[8-37]}$$

while the conservative approach yields

$$S_{BB} = 7.89 + 0.596 v. \qquad \text{[8-38]}$$

The normalized resistances at breakover as a function of interaction rate are presented in Figure 8.51. The linear regression appears to give a reasonable fit to the data as indicated on the plot. One point of exception is the Pipeline #1 resistance for Test 08. A conservative

representation of these data is presented as a dash-dot line on the plot. The linear regression on the semilog plot is described by

$$N_{BO} = -0.261 \ (\ln v) + 3.14 \qquad [8\text{-}39]$$

while the conservative approach suggests

$$N_{BO} = 7.78 - 2.64v. \qquad [8\text{-}40]$$

Figure 8.52 presents the distance into the trench wall to breakover as a function of pipeline displacement velocity. Again, with the exception of the Pipeline #1, Test 08 outlier, the data ranges from approximately 0.1 to 0.4 with a mean of 0.31. A conservative bound to the data is also indicated on the plot. The linear regression is expressed by

$$D_{BO} = -0.002 \ (\ln v) + 0.303 \qquad [8\text{-}41]$$

and the conservative approach by

$$D_{BO} = 0.093 + 0.124v. \qquad [8\text{-}42]$$

The slope of the interaction after the breakover point is presented in Figure 8.53 as a

function of interaction rate. A linear regression line fit to the data indicates a decrease in the slope of the interaction after breakover as the interaction velocity increases. A conservative approach would be to assume the upper bound relationship indicated on the figure. From the figure, the mean approach yields

$$S_{AB} = -0.146\ (\ln v) + 1.07 \qquad [8\text{-}43]$$

while the conservative approach yields

$$S_{AB} = 2.32 - 1.05v. \qquad [8\text{-}44]$$

Drained Versus Undrained Conditions

An assessment of soil drainage conditions in front of the pipeline during testing has been attempted. As an example, the response of the PPTs buried in the soil during Test 08 are presented in Figure 8.54 where the PPT designation number corresponds to the respective pipeline. The PPTs were buried at a position 63mm below the soil surface, 90mm from the forward trench wall and 30mm off centerline towards the tub wall (see Figure I.1). The pore pressure value at the start of pipeline displacement has been zeroed for ease of comparison between traces. The differences in the response of the PPTs are obvious. During testing, excess pore pressure at PPT #1 (drained interaction) continues to dissipate with time and is only slightly affected by the pipe interaction with the trench wall (at an approximate displacement of 16mm). During the displacement of Pipeline #2 (partially-

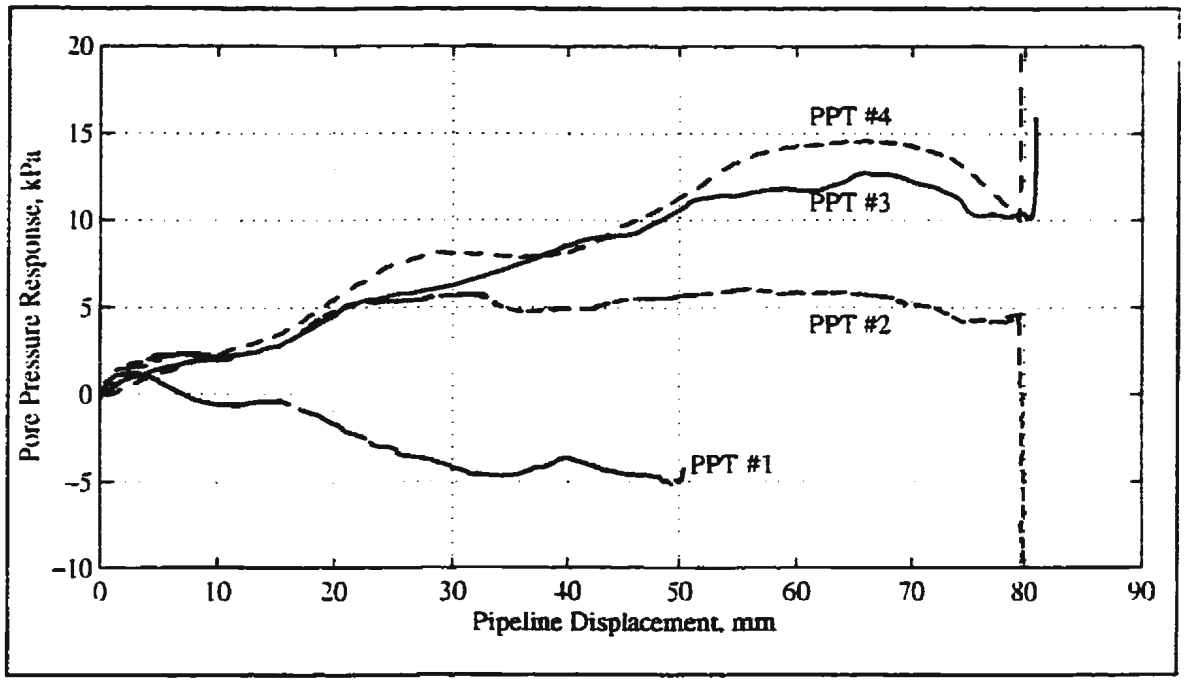

Figure 8.54 - Response of all PPTs during pipeline displacements, Test 08.

drained), there is a slight (≈5kPa) increase in the pore pressure at PPT #2. Similar responses were exhibited by PPT #3 and PPT #4 (undrained interaction) as indicated in the figure; both exhibited an increase of approximately 14kPa during the test and began to decrease after a pipeline displacement of approximately 70mm (which may have been the result of shear-induced strain). Overall, the effect of pipeline displacement rate on the excess pore pressure response was similar during Tests F4, 04, 07, and 08.

Separation Conditions Behind the Pipeline

As mentioned previously, pore pressure transducers had been incorporated into the rear of the pipelines midway between the two pipeline displacement cables. The purpose of the sensor was to assess the suction to the rear of the pipeline which would in turn give an

indication of the separation condition behind the pipeline.

A representative response of the pipeline pressure/suction transducers embedded at the rear of the pipelines during testing is presented in Figure 8.55 where the data has been taken from Test 08. The trends in the data generally indicate an initial increase in pore pressure followed by what appears to be the development of suction. However, as the Pipeline #1 and Pipeline #2 tests were conducted over relatively long periods of time, consolidation effects in the backfill (dissipation of excess pore pressures) would have been a factor. Therefore, it is probable that the decrease in P1PPT and P2PPT was the result of dissipation of excess pore pressures in the backfill. For Pipelines #3 and #4, there appears to have been little or no suction developed at the soil interface to the rear of the pipeline.

Internal Deformations

As mentioned previously, for a shallow interaction, it would be expected that the soil in front of the pipeline would take the path of least resistance and would therefore flow over the top of the pipe. If the pipeline has moved horizontally, one would expect the final cover over the pipeline to equal the initial cover plus the diameter of the pipe for an undrained interaction. For the drained case, one would expect the final cover to be different than that of the undrained case. Because the slow interaction is considered to be essentially drained, the final cover would be expected to be less than that experienced during undrained loading. Visual observations made during excavation were in agreement with this hypothesis.

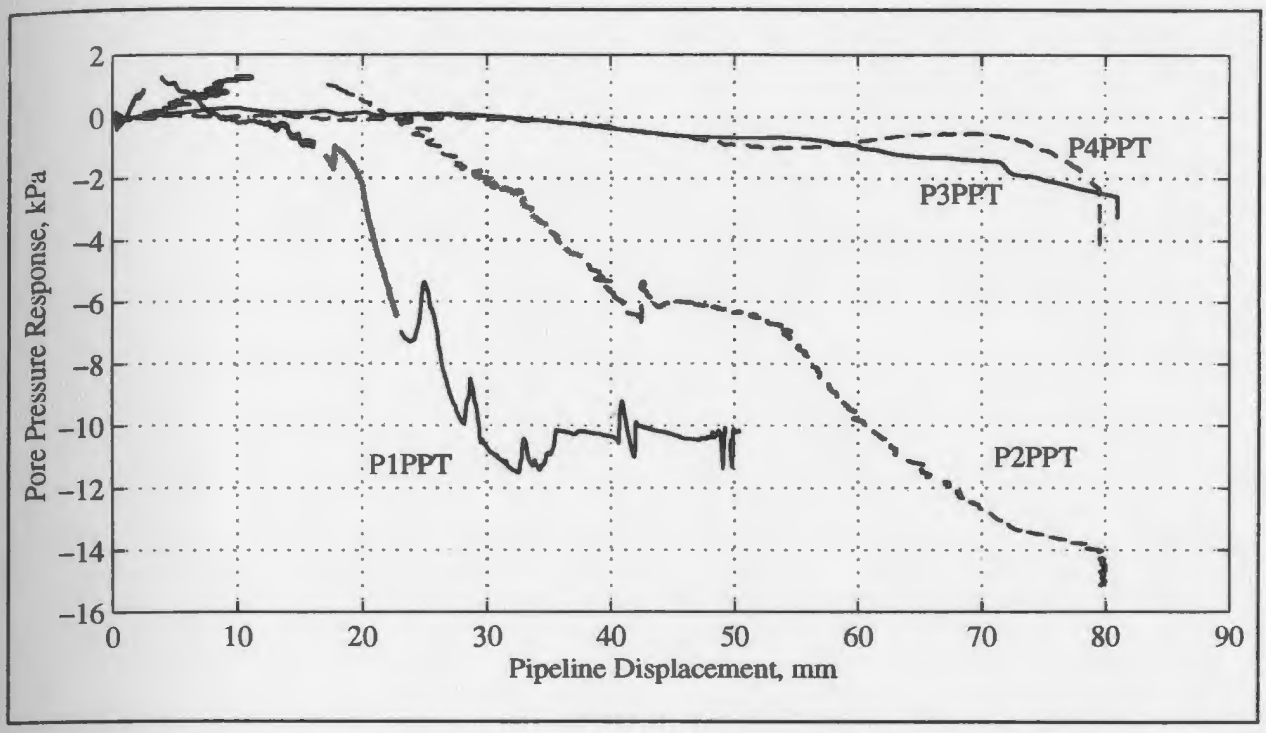

Figure 8.55 - Response of all pipeline pressure/suction transducers during pipeline displacements, Test 08.

The difference in drained and undrained behaviour is also evident from the internal deformations of the tests. Photographs in Appendices E, H, and I indicate these internal deformations. Failure mechanisms associated with soil displacement in front of Pipeline #1 and Pipeline #2 were similar. Distinct failure surfaces were observed in front of the pipeline extending from the toe of the pipeline to the soil surface at an angle ranging from 25-44° with the horizontal. Conditions during these tests are assumed to have been essentially drained to somewhat drained. Failure mechanisms associated with soil displacement in front of and above Pipeline #3 and Pipeline #4 were similar indicating plastic flow around the pipeline. The spaghetti strands below the pipeline indicated a well-defined zone of shear deformation extending approximately 0.5 to 0.75 pipeline diameters

below the base of the pipeline. Conditions during these tests are assumed to have been essentially undrained.

8.2.5 Effect of Soil Preconsolidation Pressure

Comparison of Normalized Prototype Force-Displacement Curves

Test 08 was conducted to investigate the effect of soil preconsolidation pressure on both drained and undrained lateral pipeline/soil interaction. Figure 8.56 presents the normalized corrected force-displacement curves from Test 04 and Test 08. These tests were similar with the exception that the Test 04 soil sample had been preconsolidated to approximately 400kPa while the Test 08 soil sample had been preconsolidated to an effective stress level of approximately 160kPa. Figure 8.57 presents the normalized corrected force-displacement curves of Test 07 and Test 08 where the preconsolidation stress of Test 07 was approximately 400kPa.

From Figure 8.56, it appears that the response of Pipeline #1 during both tests was similar up to a displacement of approximately 1.1D after which the Test 08 trace increases more rapidly than that of Test 04. In addition to soil preconsolidation stress level, another difference between the two Pipeline #1 tests (traces #1 and #2) was that the displacement rate during Test 04 was on average 47% greater than its counterpart of Test 08. A significant difference between tests is observed comparing data of Pipeline #2 (traces #3 and #4) as well as comparing data of Pipeline #3 (traces #5 and #6). Differences between the Pipeline #4 traces (#7 and #8) are minor up until a pipeline displacement of 2D.

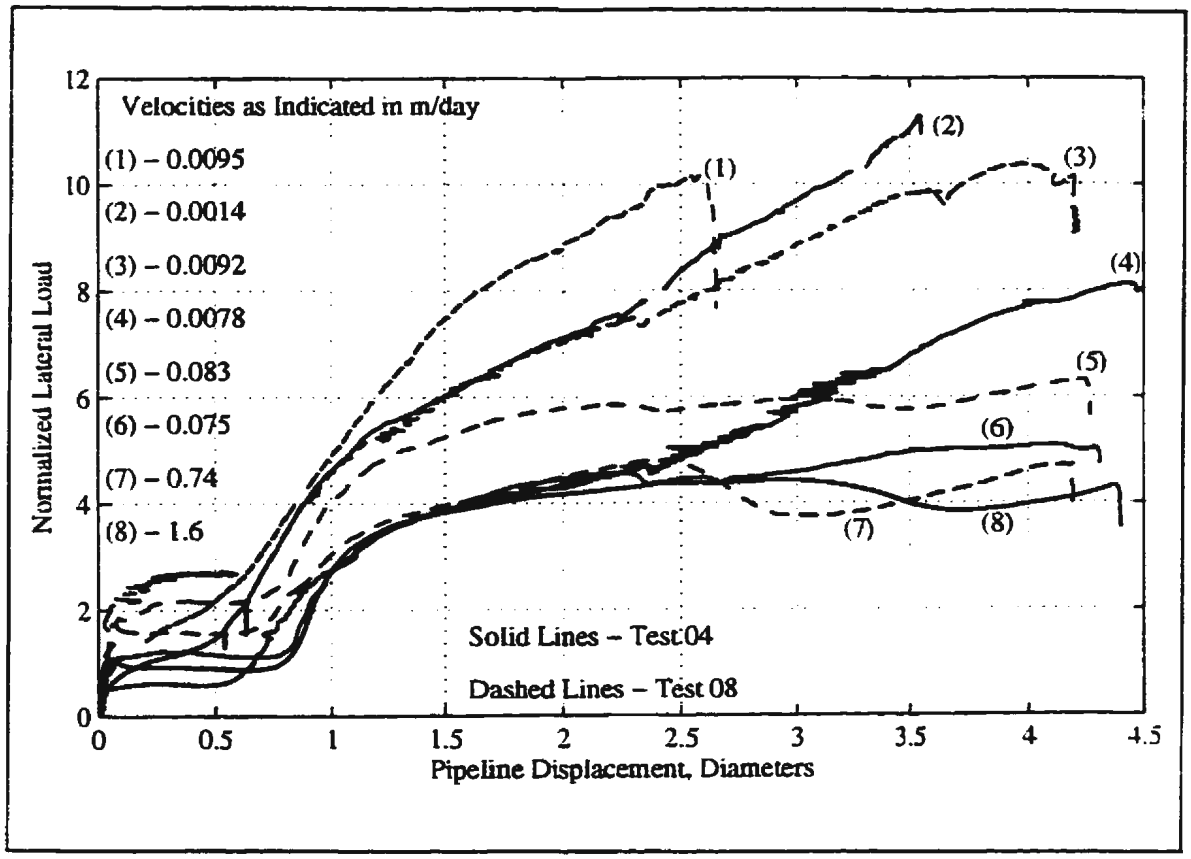

Figure 8.56 - Comparison of prototype-scale force-displacement curves from Test 04 and Test 08.

A variation in the responses of Pipeline #1 of Tests 07 and 08 (traces #1 and #2) is observed from Figure 8.57. Here the velocities were within 26% for Pipeline #1 and the same for the other pipes. The difference between traces continues to increase with increasing pipeline displacement. Again, a significant difference between tests is seen in the traces of Pipeline #2 (traces #3 and #4) and Pipeline #3 (traces #5 and #6). Differences between the Pipeline #4 traces (#7 and #8) were substantially less than differences for the other pipelines.

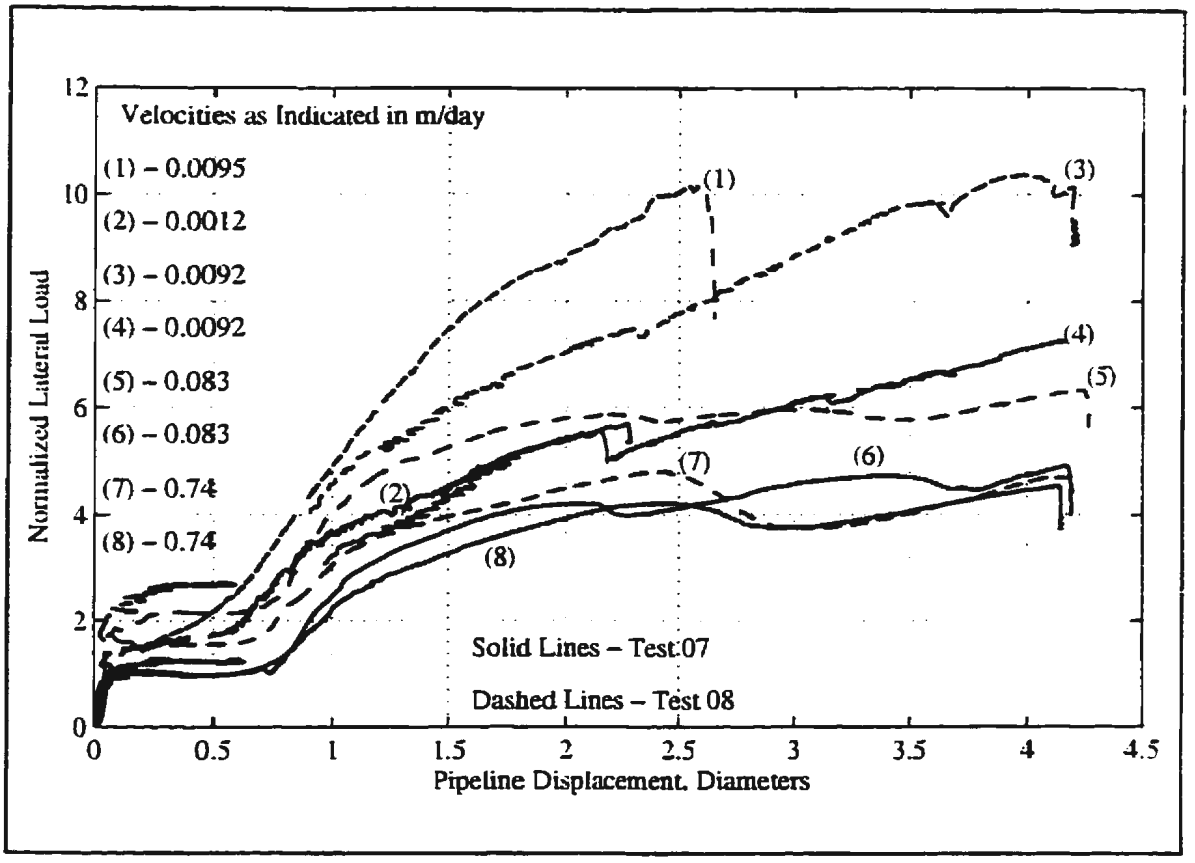

Figure 8.57 - Comparison of prototype-scale force-displacement curves from Test 07 and Test 08.

Overall, the prototype-scale force-displacement curves presented in Figure 8.56 and Figure 8.57 indicate higher normalized curves for drained to partially-drained interaction rates in the soil with the lower preconsolidation pressure. For undrained conditions, the differences appear to be minor. However, it must be stressed that these observations are based on a limited amount of data (one test with a lower preconsolidation stress).

Interaction Factors

As mentioned above, the clay used in Test 04 and Test 07 had been preconsolidated to an

effective stress of approximately 400kPa while the clay of Test 08 had been subjected to a preconsolidation stress of approximately 160kPa. Interpreted ultimate normalized resistances or interaction factors for these three tests are presented in Table 6 of the *Test Data* appendices. Observation of the data suggests slightly higher normalized interaction loads for the lower preconsolidation pressure. However, as discussed previously, the determination of the point of ultimate normalized load can be subjective and can be taken at the end of the pipeline pull for the slower interaction rates. For the faster interaction rates (Pipeline #3 and Pipeline #4), it appears that the ultimate normalized resistances are slightly higher. No meaningful interpretation is derived from the distances to ultimate resistance but the secant modulus to the ultimate resistance for the drained to partially-drained tests indicate a slightly higher value for those pipeline displacements in the soil with the lower preconsolidation pressure.

Normalized Loads at Predetermined Displacements

As the interaction factor for the slower interaction rate can be subjective, it may be more appropriate to look at normalized loads at benchmark displacements. Table 6 of the *Test Data* appendices presents normalized resistances at previously defined displacements. In all cases, for all pipelines, the normalized resistances determined from Test 08 were higher than those from corresponding cases of Test 04 or Test 07. Again, it should be emphasized that this conclusion is based on the data of one test at a lower preconsolidation pressure.

Bilinear Analysis

Little can be concluded with regards to the effect of preconsolidation stress levels on the various bilinear analysis parameters of Table E.6, H.6 and I.6 of the *Test Data* appendices. However, as might be expected based on observation of normalized loads at benchmark penetrations, it appears that the test with the lower preconsolidation stress yielded higher normalized resistances at breakover points for comparable tests.

Soil Pore Pressure Response

The soil pore pressure response during Test 07 and Test 08 have been analysed in an attempt to distinguish differences as a result of the different soil consolidation levels. For the drained and partially-drained tests, the pore pressure responses were not identical but were similar. During testing of the undrained interaction, the response of the PPTs in the more heavily consolidated soil peaks after a displacement of 25-35mm while the peak in Test 08 occurs much later; after 60-70mm of travel. The average peak response of the PPTs in Test 08 was observed to be slightly higher than in Test 07. Therefore, it appears that the soil preconsolidation stress has had little effect on the soil pore pressure response during the drained and partially-drained tests and has had a minor effect on the soil pore pressure during the undrained tests.

Separation Conditions Behind the Pipeline

The Test 07 and Test 08 responses of the pore pressure transducers incorporated into the rear of the pipelines have been analysed. For all interaction rates, the initial part of the

curves indicate that the pore response at the rear of the pipe increased or remained constant for a period of displacement. This may have been the result of excess pore pressure developed in front of the pipeline being transferred through the backfill to the rear of the pipe. It appears that preconsolidation stress influences the apparent pore suction developed at the rear of the pipe; lower preconsolidation levels resulted in apparent lower interface suctions.

Internal Deformations

Observation of internal deformations from Tests 04, 07, and 08 indicated that for the soil with the lower consolidation pressure, there was a greater extent of soil deformation in front of the displaced position of the pipe (below any shear plane that existed). For the soils preconsolidated to a higher stress level, it generally appeared that a greater number of rupture surfaces were discovered running from the toe of the pipeline to the soil surface. In most cases, the angle that these rupture surfaces made with the horizontal was 40°+ for the higher preconsolidation stress and less than 40° for the lower preconsolidation pressure. Rate effects on the internal deformations especially as they relate to the "end of test" measured soil cover were consistent with what was reported in the previous subsection (see Appendix K).

8.2.6 Effect of Backfill Type - Drained Conditions

Comparison of Normalized Prototype Force-Displacement Curves

Figure 8.28 presented the normalized prototype-scale force-displacement curves of Test

09 where the effect of different backfills during drained loading was investigated. The backfills used during testing were as follows: Pipeline #1 - baseline slurry; Pipeline #2 - chunks of (grated) native material; Pipeline #3 - remoulded native material; Pipeline #4 - loose fine sand. The response of Pipeline #3 falls off at a displacement of approximately 1.9D due to slippage of the pipeline tension cable. The greatest load at one point in the backfill was mobilized by Pipeline #2 which might have been partially the result of desiccation between the large voids of the backfill. The largest overall normalized lateral load was exhibited on Pipeline #2. Problems associated with the drive system of Pipeline #2 precluded pulling it more than approximately 0.2D during the first centrifuge run and the majority of the testing of Pipeline #2 did not take place until several days after the other pipelines had been tested. As might be expected, the tamped-in-place remoulded material generally offered the greatest initial resistance to pipeline movement within the confines of the trench. The pipeline which was buried in the loose sand mobilized the least amount of load as it transverses the trench and interacted with the native material. Comparing the response of Pipeline #1 and Pipeline #3, as expected, the normalized loading experienced by the pipeline increases with increased strength of the backfill. After a displacement of approximately 2D, it appears that the two curves are tending to approximately the same value. Perhaps somewhat surprising, the pipeline with the loose sand backfill offered the least resistance to movement after interaction with the trench wall. Intuitively, as the sand offered the greatest cone penetration resistance, the interaction in the backfill and beyond might have been expected to be greatest for Pipeline #4. Post-test excavation of Pipeline #4 indicated that the loose sand backfill had been pushed in front

of the pipeline. After penetration into the trench wall, the load experienced by this pipeline was considerably less (up to a third less) than the loads experienced by the other pipelines. This suggests that the loose sand may have acted as a wedge in front of the pipeline shedding load from in front of the pipeline.

Interaction Factors

Interaction factors interpreted from the ultimate normalized resistances of Figure 8.28 are presented in Table J.6. Again, with the slower interaction rate, determination of the interaction factor for any of the tests is open to interpretation. Again, these data will not be as meaningful as normalized resistances at specified benchmark displacements.

Normalized Loads at Predetermined Displacements

Normalized loads at benchmark displacements are presented in Table J.6. As to be expected, resistances increase with increasing penetration for each pipeline. With the exception of Pipeline #1 and Pipeline #3, there appears to be no obvious correlation between the normalized resistances at the benchmarks and the backfill type (or its penetration resistance). Again, intuitively, as the sand offered the greatest cone penetration resistance, the interaction of Pipeline #4 at the trench wall might have been expected to offer the greatest resistance of any of the pipelines at that point. That was not the case; at that point and at 0.5D and 1D penetration, the pipeline was subjected to the lowest lateral load.

Bilinear Analysis

A study of the bilinear parameters presented in Table J.6 reveals little in the way of obvious relations between the variation of backfill type (penetration resistance) and the various bilinear parameters. However, the slope of the interaction between the trench wall and breakover seems to decrease with increasing backfill CPT resistance.

Effect of Backfill Type on Pore Pressure Response

PPTs in Test 09 were buried at a position 63mm below the soil surface, 90mm from the forward trench wall, and 30mm off centerline towards the wall. Figure 8.58 presents the response of all four PPTs where the PPT designation number corresponds to the respective pipeline. In the figure, the pore pressure response at the start of pipeline displacement has been zeroed for ease of comparison between traces. The only major difference in the traces as the result of differences in backfill types is that the pore pressure at PPT #3 goes slightly positive at the beginning of displacement which might have been due to competence of the backfill. The response of this PPT goes negative after about 7mm of pipeline displacement but the data trace remains slightly higher than the other traces.

Separation Conditions Behind the Pipeline

The response of the pipeline pressure/suction transducers embedded in the rear of the pipelines during Test 09 is presented in Figure 8.59. In this figure, the pore pressure response at the start of pipeline displacement has been zeroed for ease of comparison between traces. As might be expected for similar displacements, the pore suction

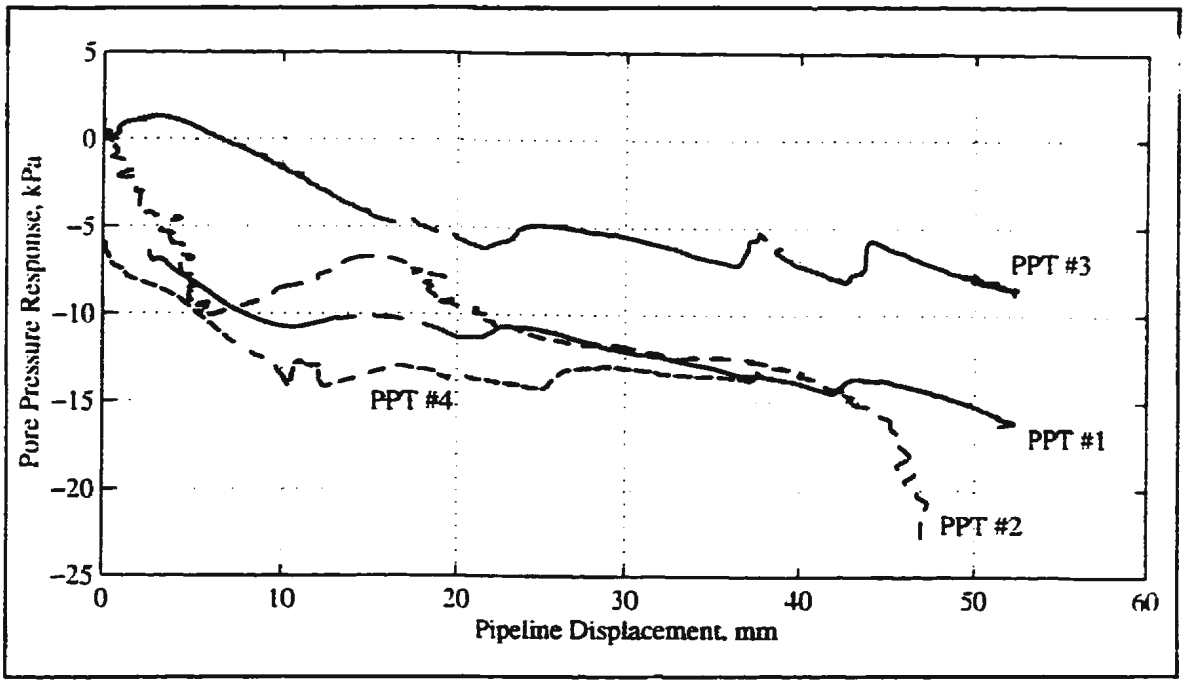

Figure 8.58 - Response of all PPTs during pipeline displacements, Test 09.

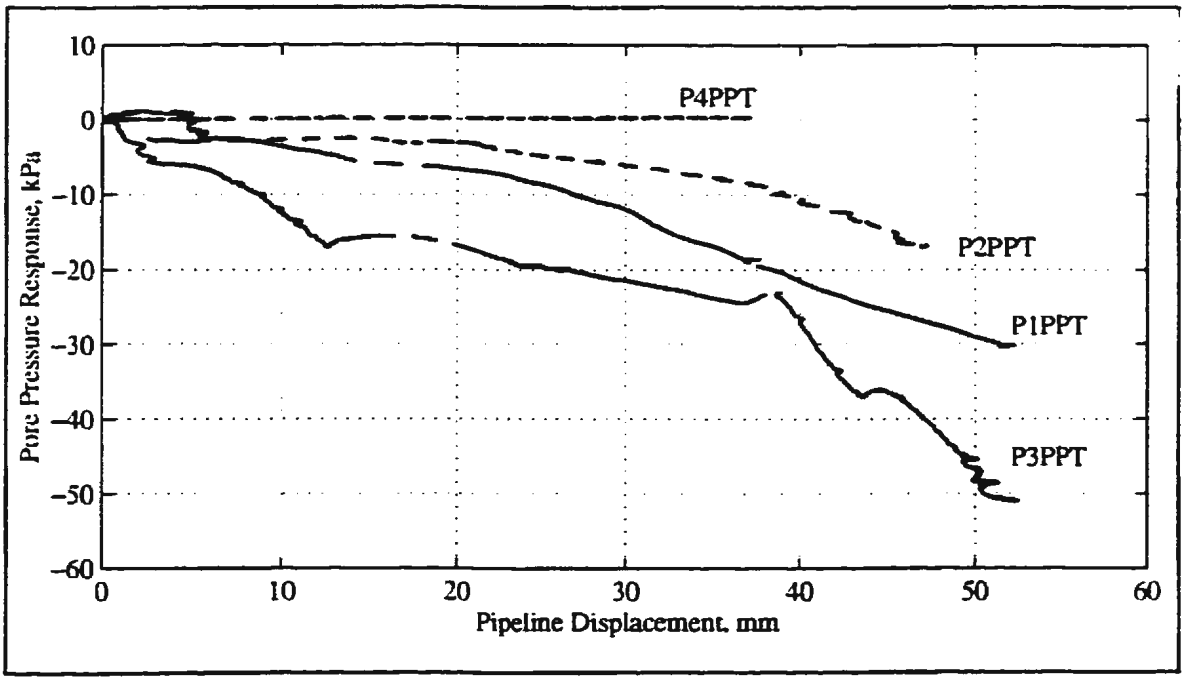

Figure 8.59 - Response of all pipeline pressure/suction transducers during pipeline displacements, Test 09.

developed behind the pipeline was the greatest in the remoulded backfill and least in the dry sand.

Stiffness of Backfill

The stiffness of the backfill has been evaluated from the tangent modulus of the prototype-scale force-displacement curves. Values for initial stiffness in pipeline order are as follows: 472kN/m^2; 906kN/m^2; 1230kN/m^2; and 662kN/m^2. The tamped in place remoulded backfill provided the greatest initial stiffness while the value from the slurry backfill provided the least. However, as described earlier, problems had been experienced during the Pipeline #2 displacement which might have affected the initial stiffness measurement of that particular backfill. The overall stiffness to the trench wall was measured as the slope of a line joining the plot origin and the intersection of the force-displacement curve with the trench wall. Values for average stiffness to the trench wall are as follows: 162kN/m^2; 190kN/m^2; 254kN/m^2; and 149kN/m^2. The values from Pipelines #1, #2, and #3 increase in the order expected. Again, surprisingly, the sand backfill offered the least average stiffness to the trench wall.

Internal Deformations

Upon study of internal deformations during post-test excavations, a wedge of slurry was observed in front of Pipeline #1, a wedge of remoulded material in front of Pipeline #3, and a bulb of sand in front of Pipeline #4. No backfill material was distinguished in front of Pipeline #2 but the backfill might have been remoulded with the native material. No

other features observed could be attributed to the backfill type. Rupture surfaces were observed to extend to the soil surface at an angle of 32-38° with the horizontal. Soil deformations extended at least one diameter in front of the pipeline. Final soil cover measurements were consistent with what was expected.

8.2.7 Effect of Model Scale - Undrained Conditions

Comparison of Normalized Prototype Force-Displacement Curves

Modelling of models is a technique whereby the applicability and accuracy of centrifuge modelling can be tested. Tests 01, 05 and 06 attempted to model the same prototype condition at 1:50, 1:25 and 1:100 scales. As mentioned earlier in this report, if the results correspond, then the modeller can be assured that the scaling has been correctly undertaken (at least within the range of gravitational accelerations chosen) and that the results should be applicable to the full-scale.

Figure 8.60 presents the prototype-scale cone penetration test results from the native material. The traces extending to approximately -3m are from Test 05; the traces extending to approximately -5m are from Test 01; and the traces extending to approximately -9m are from Test 06. Figure 8.61 and Figure 8.62 present the interpreted undrained shear strengths from the three tests. It is obvious that before the prototype force-displacement pipeline curves from different tests can be compared, they should be normalized with respect to the undrained shear strength of the material to account for variation between tests. Since it is necessary to normalize force-displacement curves with respect to

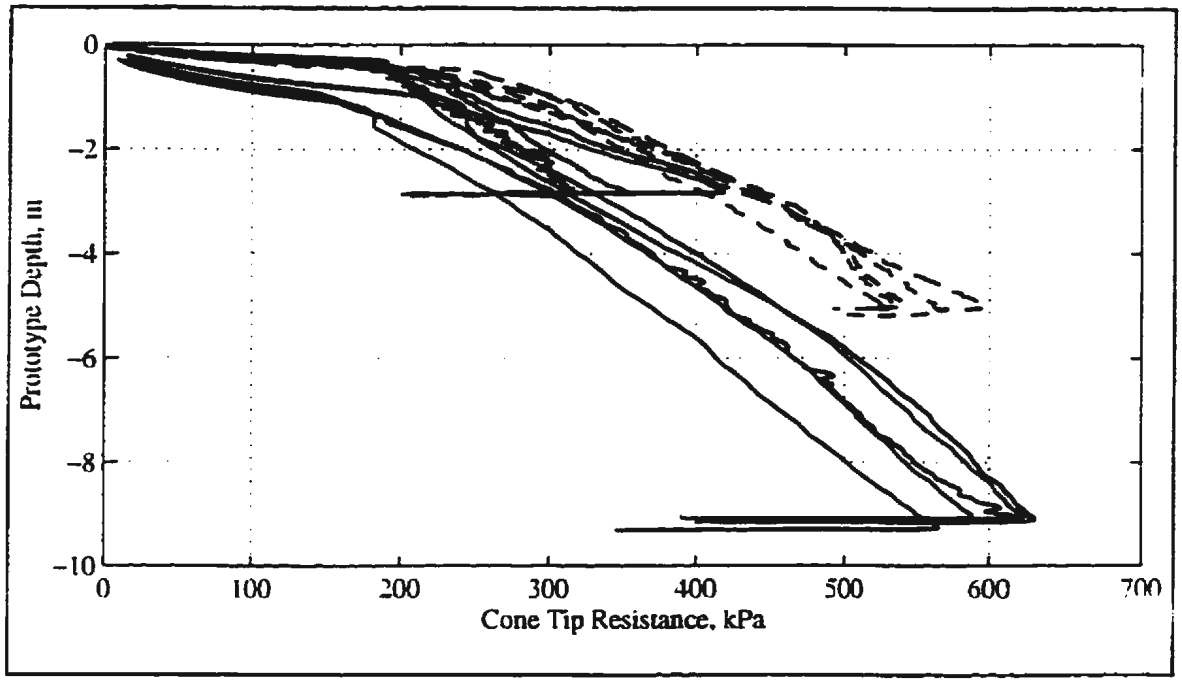

Figure 8.60 - All prototype cone tests, native material, Test 01, 05, and 06.

undrained shear strength and pipeline diameter to obtain interaction factors, then these normalized curves should then be compared to assess the suitability of the technique.

The normalized prototype-scale force-displacement curves from the four H/D ratios studied are presented in Figures 8.63 through 8.66. Agreement between the curves of Figure 8.63 is good (H/D=1.842). As explained earlier, the normalized lateral load measured during the displacement of Pipeline #2, Test 05, as shown in Figure 8.64 (H/D=1.526) is higher than expected due to the fact that the pipeline stopped several times during the interaction and consolidation would have occurred in front of the pipeline. However, there is decent agreement between Test 01 and Test 06. If there had not been problems associated with the Pipeline #2 displacement, it is anticipated that the peak normalized lateral load would

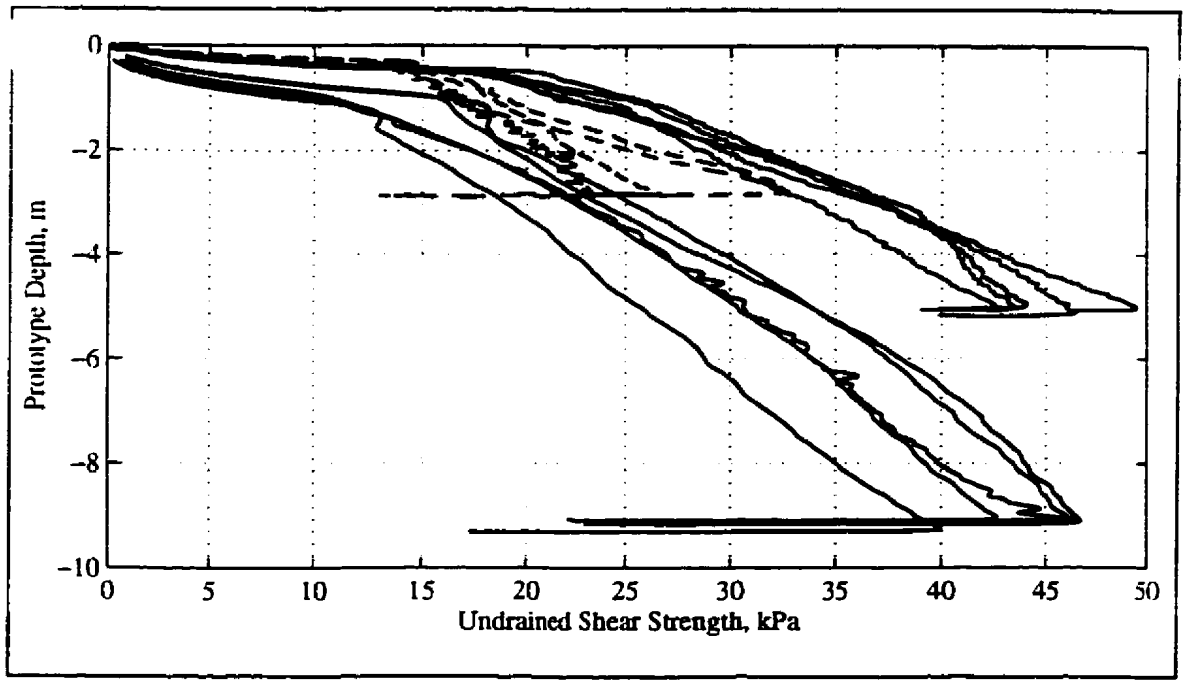

Figure 8.61 - Shear strength based on direct shear strength correlations, native material, Test 01, 05, and 06.

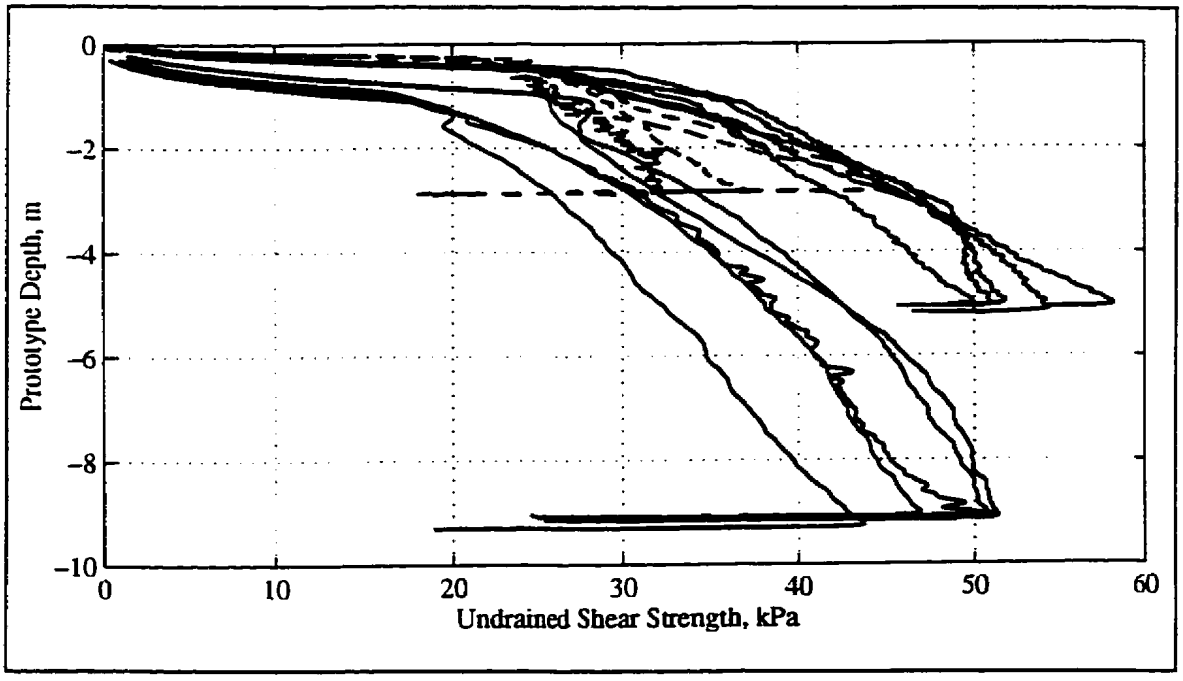

Figure 8.62 - Shear strength based on shear vane correlations, native material, Test 01, 05, and 06.

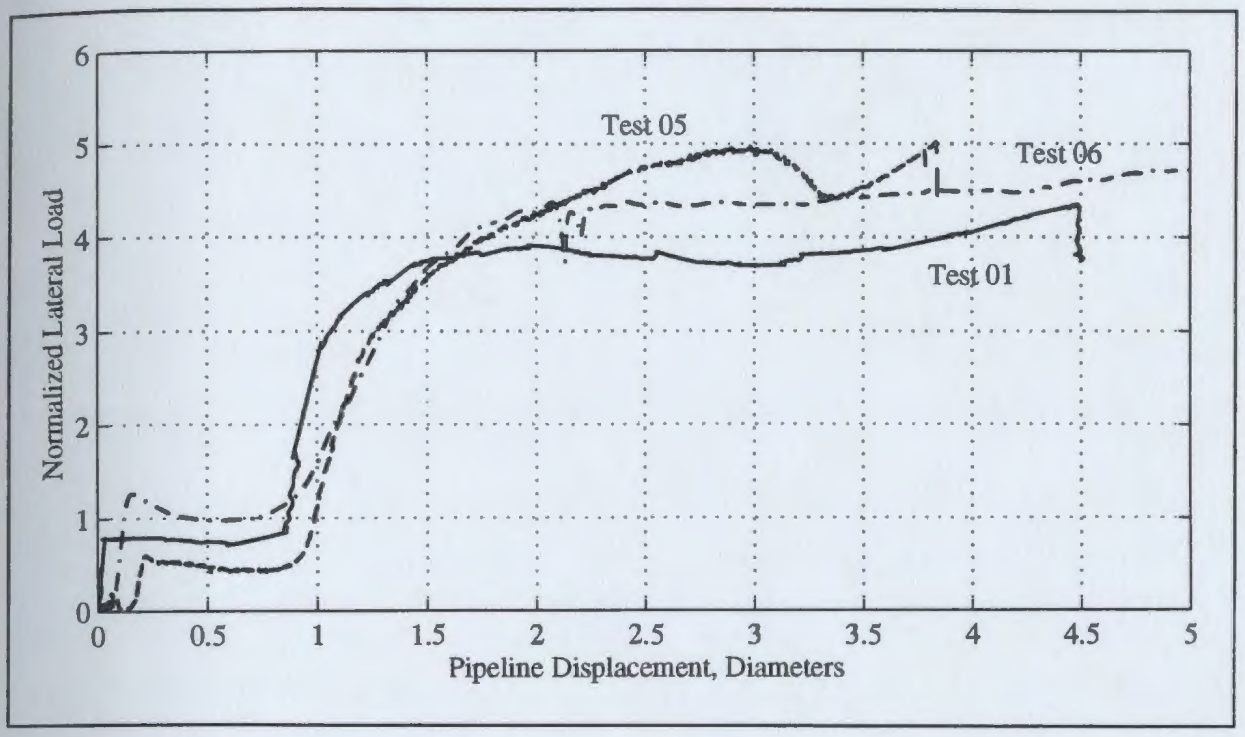

Figure 8.63 - Modelling of models, 0.8m cover.

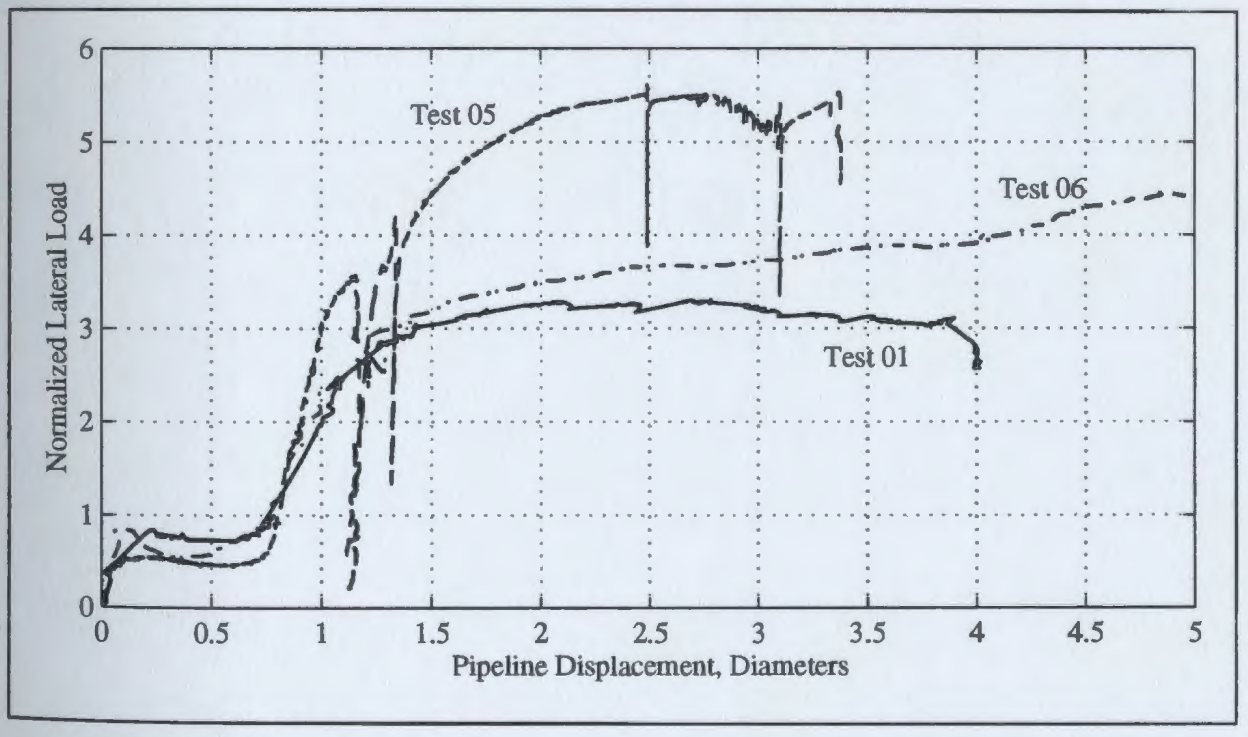

Figure 8.64 - Modelling of models, 0.5m cover.

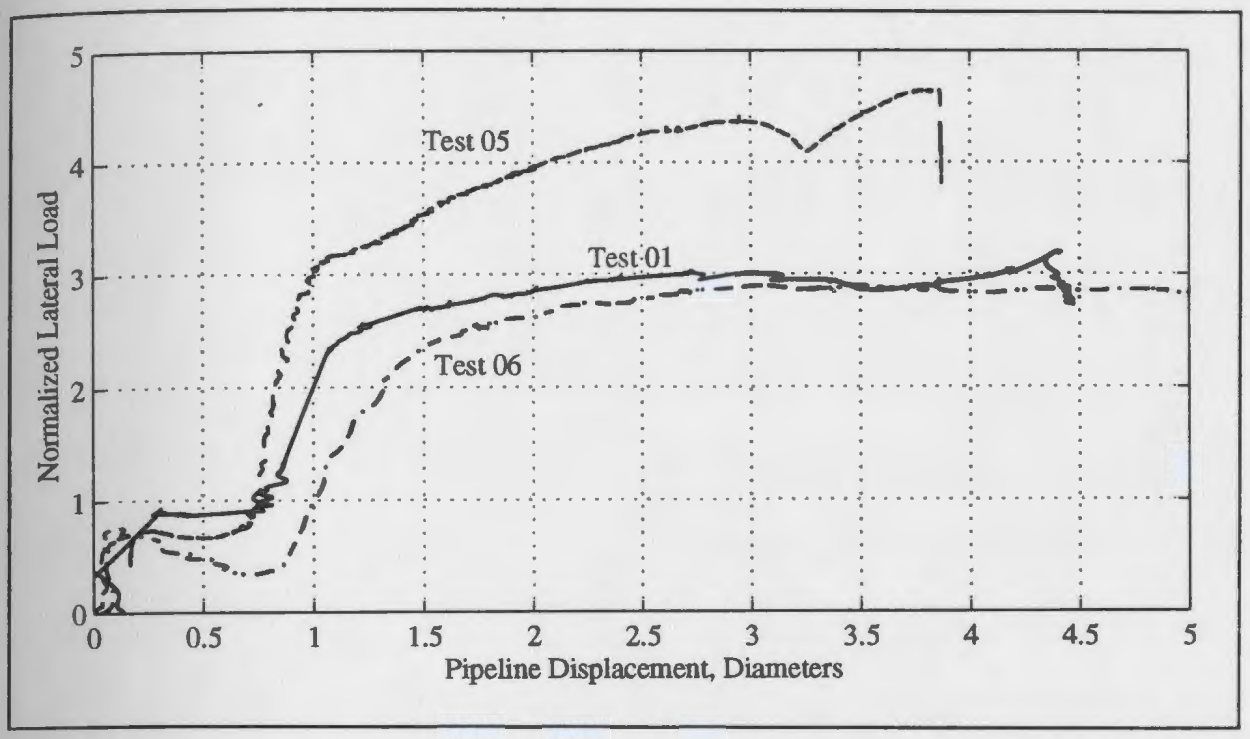

Figure 8.65 - Modelling of models, 0.25m cover.

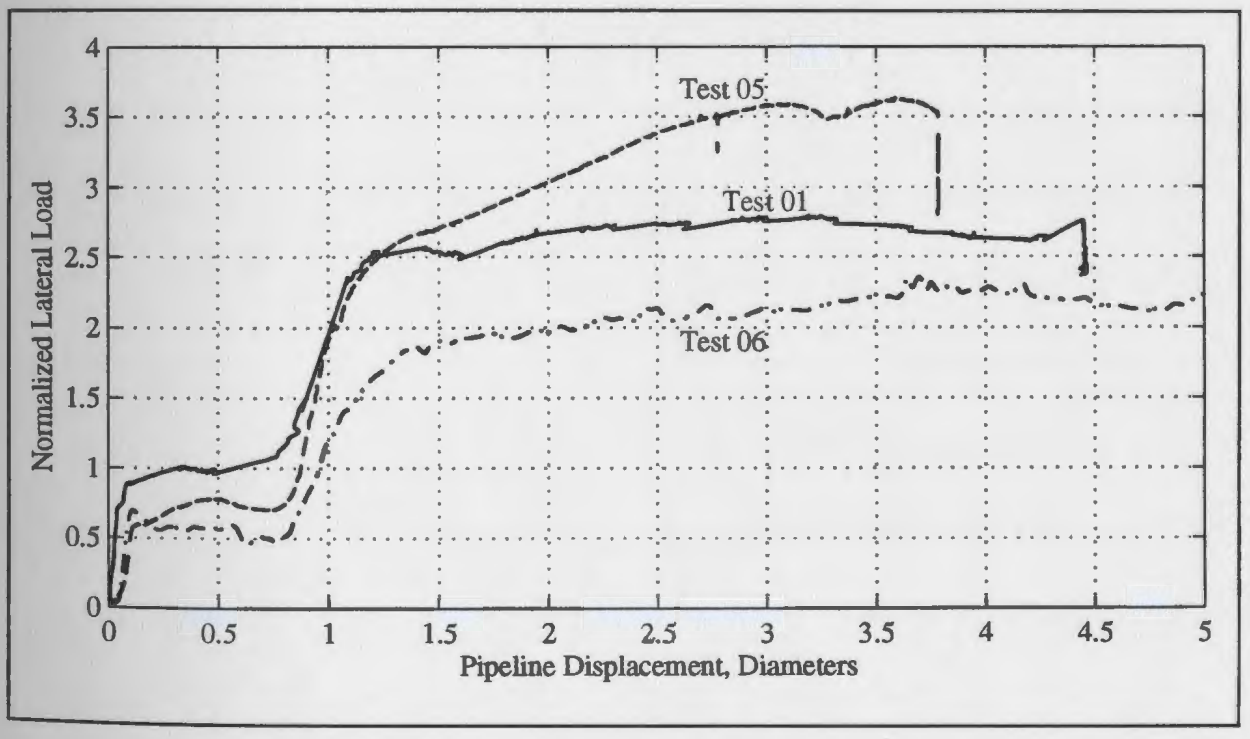

Figure 8.66 - Modelling of models, 0m cover.

have been in the range of 4-4.5. There is good agreement between the Test 01 and Test 06 pipeline data of Figure 8.65 (H/D=1.263). However, the data from Test 05 is considerably higher than the other two traces. Observation of Figure 8.66 (H/D=1.000) indicates reasonable agreement between Test 01 and Test 05 until a displacement of 1.5 pipe diameters is reached. However, beyond that point, there is increasing separation of the curves. The Test 06 data trace falls short of the other two traces over the entire pipeline displacement. It is suspected that because of the decreased burial depth, the pipe self-weight may have played a more significant role during the interaction. In general, the modelling of models yielded acceptable results; most of the interaction curves were within a bandwidth of 0.5-1 normalized lateral loads.

Interaction Factors

Interaction factors from Tests 01, 05, and 06 are presented in Table 8.2. To analyse what effect model scale might have had on interpretation of the data, the following have been plotted in Figure 8.67 through Figure 8.69: the ultimate normalized resistance; the normalized distance into the trench wall to the ultimate normalized resistance; and the secant modulus to the ultimate normalized load. Linear trend lines have been superimposed on the plots. There is considerable deviation of the data from the trend lines and between tests. The only apparently consistent comment that can be made is that it appears that the secant modulus to ultimate load decreased with increasing model scale.

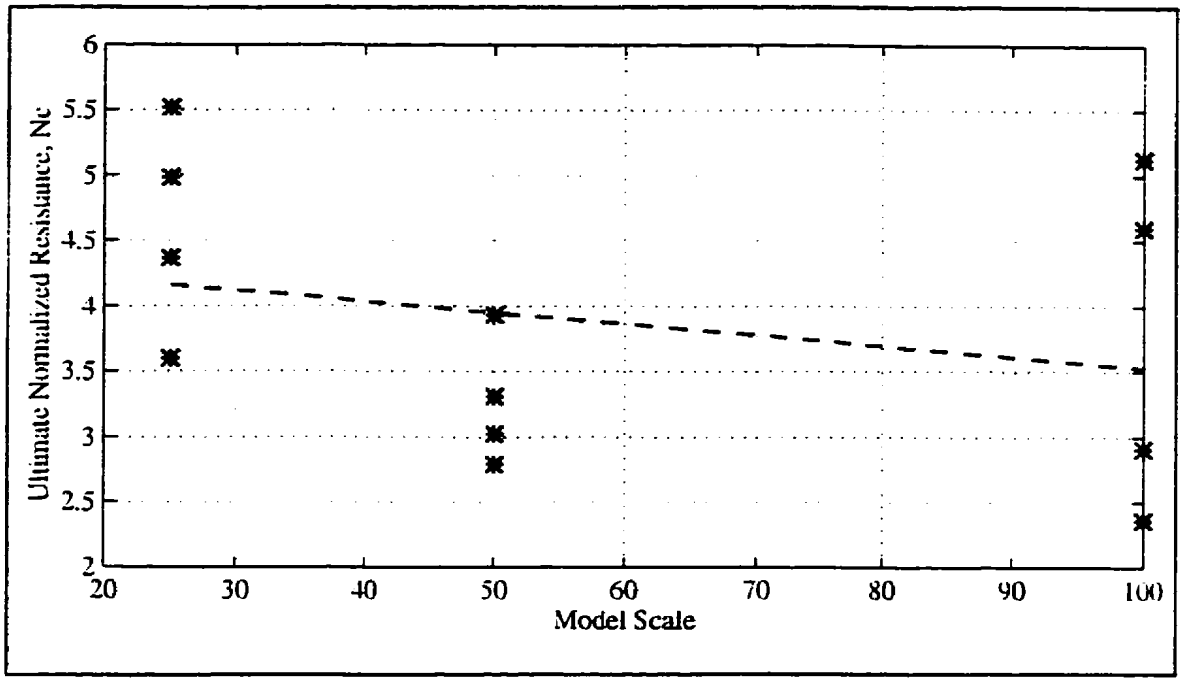

Figure 8.67 - Ultimate normalized resistance, N_c, versus model scale, undrained tests.

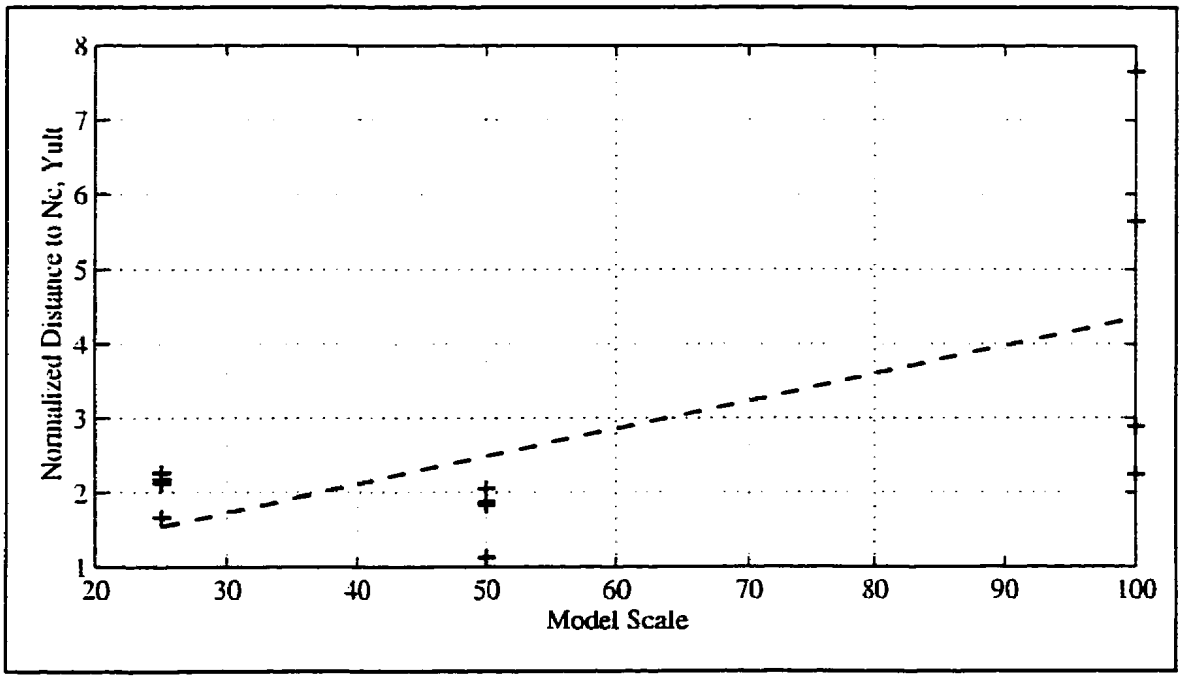

Figure 8.68 - Normalized distance to peak load, Y_{ult}, versus model scale, undrained tests.

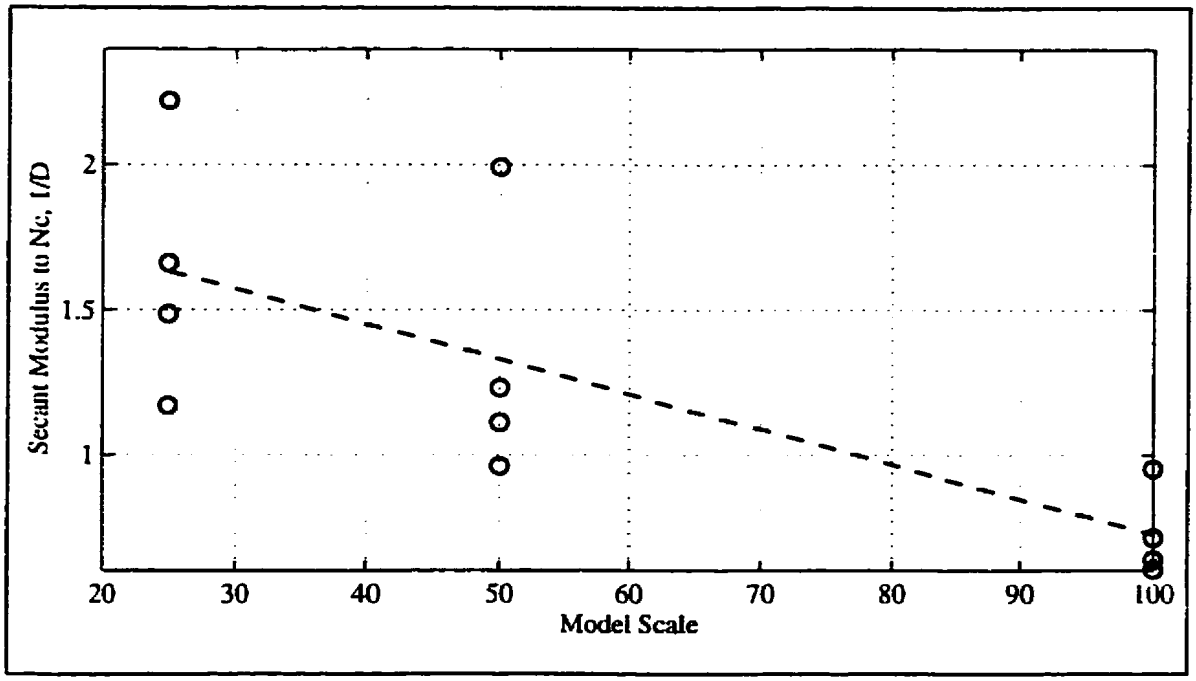

Figure 8.69 - Secant modulus to N_c versus model scale, undrained tests.

Normalized Loads at Predetermined Displacements

The above analysis again required the choice of a somewhat subjective ultimate load from the data sets. Therefore, the normalized lateral load on the pipeline at the trench wall, at a displacement of 0.5D into the trench wall, and at a displacement of 1 diameter into the trench wall are presented in Figure 8.70 through Figure 8.72. There is considerable variation of the data about the trend lines and none of the data sets indicate a consistent decrease in any single parameter with model scale.

Bilinear Analysis

Experimental parameters associated with the bilinear analyses of Tests 01, 05, and 06 are plotted as a function of model scale in Figures 8.73 through 8.76. Linear regression trends

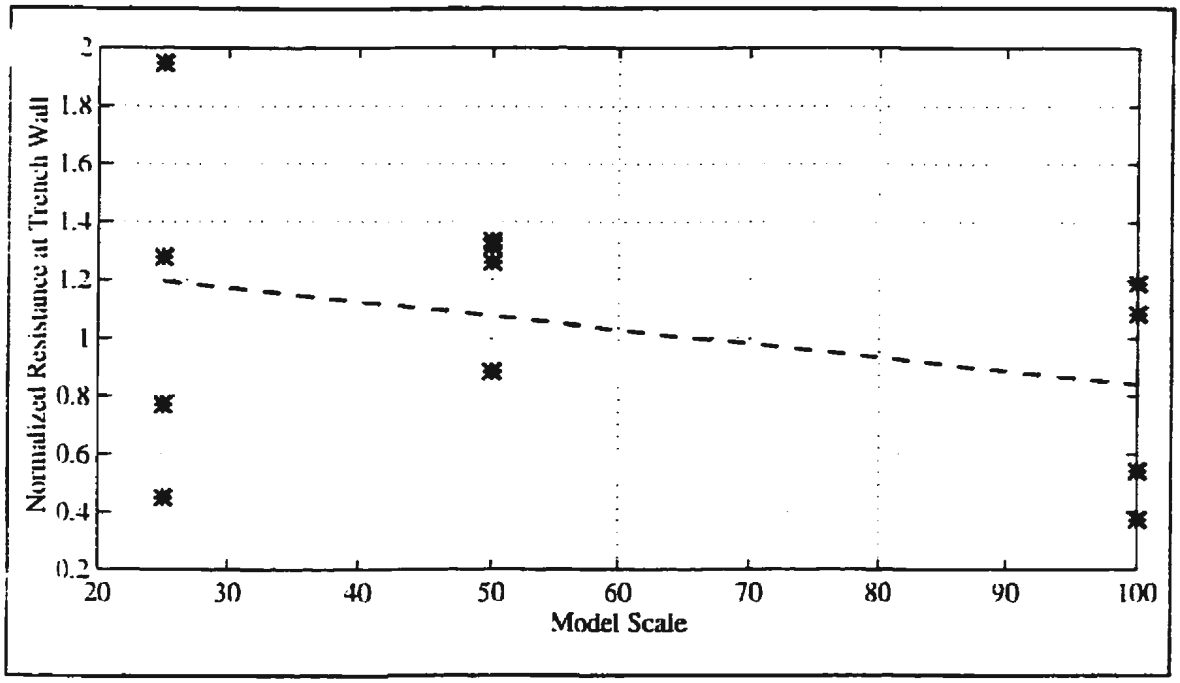

Figure 8.70 - Normalized resistance at the trench wall, N_{TW}, versus model scale, undrained tests.

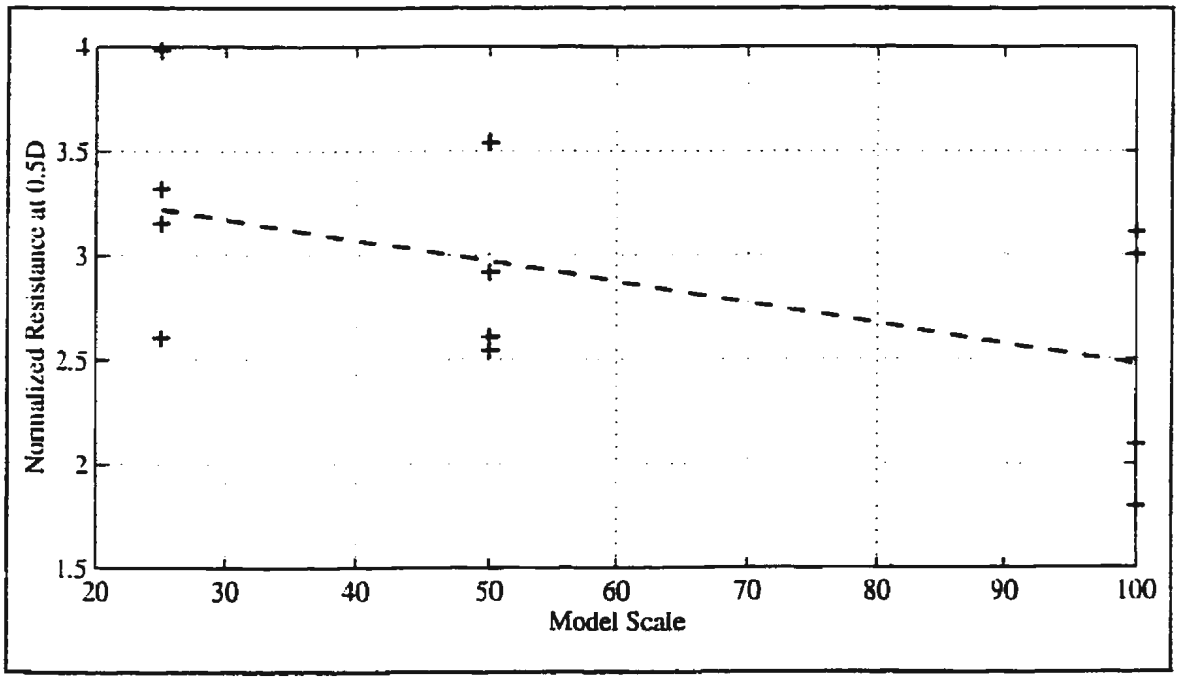

Figure 8.71 - Normalized resistance at 0.5D penetration into the trench wall, $N_{0.5D}$, versus model scale, undrained tests.

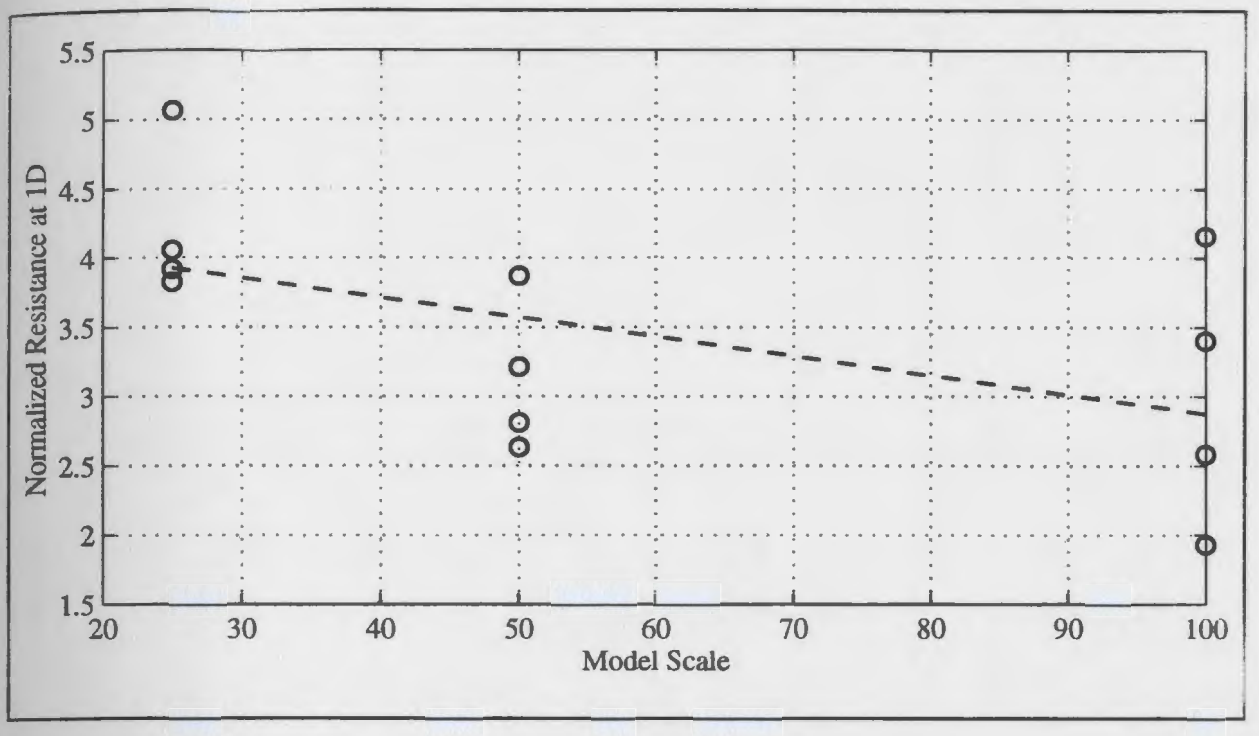

Figure 8.72 - Normalized resistance at 1D penetration into the trench wall, N_{1D}, versus model scale, undrained tests.

are also plotted on the graphs. As in other analyses of this subsection, for the most part no consistent variation in the data (for respective pipelines) was observed. However, it does appear that model scale may have had an influence on the slope of the interaction before and after the breakover point.

Internal Deformations

Observations made during excavation of the samples of Tests 01, 05, and 06 provided little in the way of differences in internal deformations. The general mode of soil deformation was flow of soil around the pipe. Observation of the Test 05 excavation indicated deformation of soil extending about 1D in front of the displaced position of the pipe while

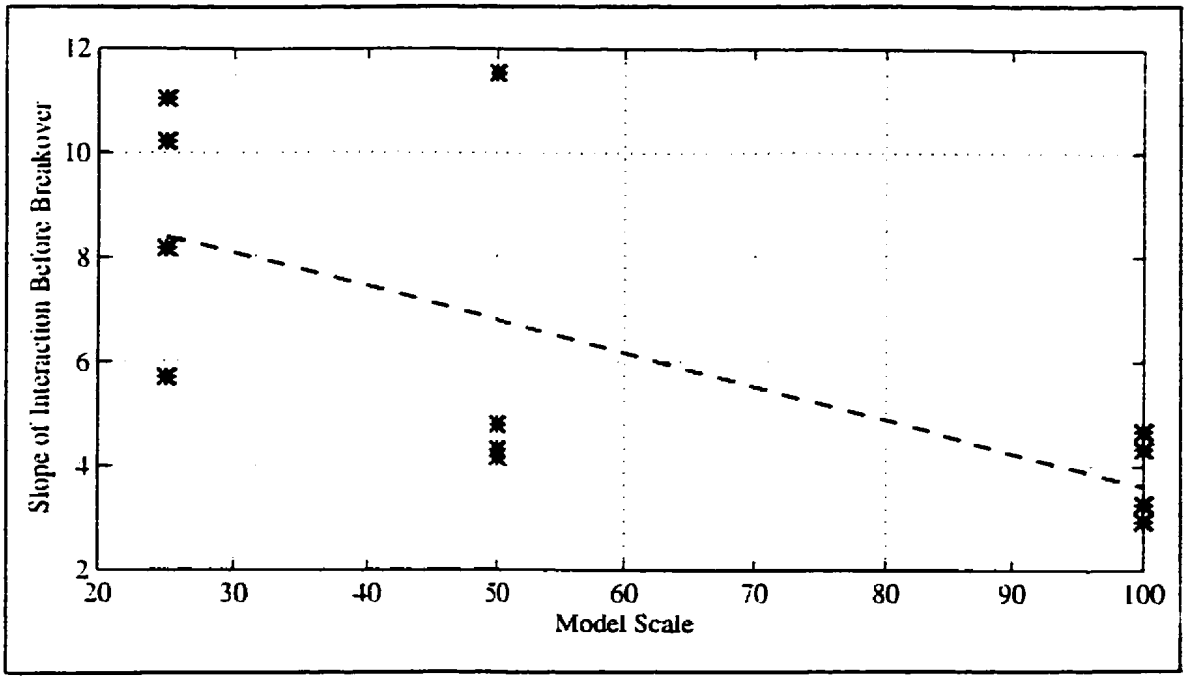

Figure 8.73 - Slope of interaction before breakover, S_{BB}, versus model scale, undrained tests.

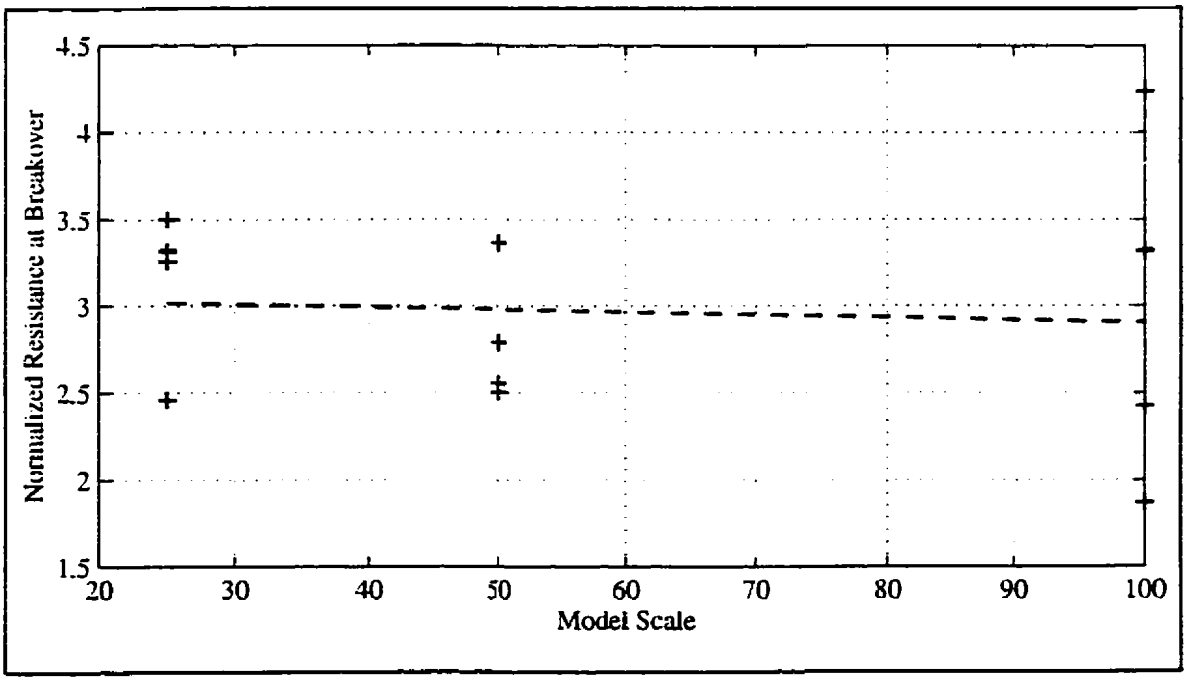

Figure 8.74 - Normalized resistance at breakover, N_{BO}, versus model scale, undrained tests.

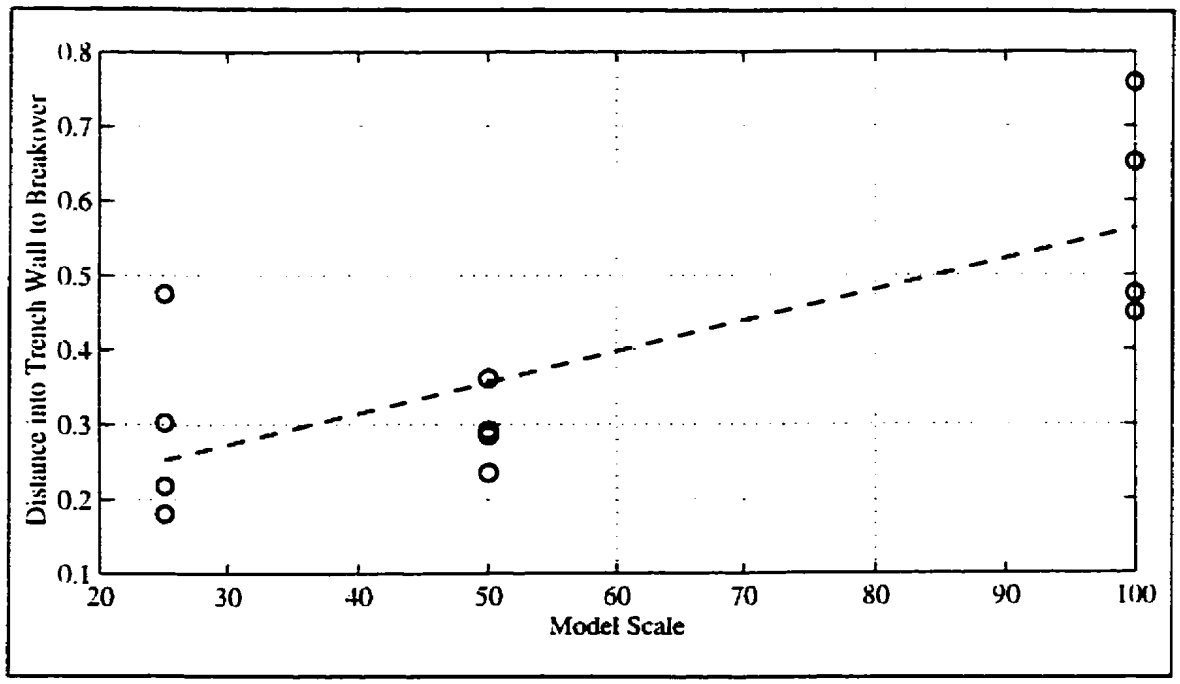

Figure 8.75 - Distance into the trench wall to breakover, D_{BO}, versus model scale, undrained tests.

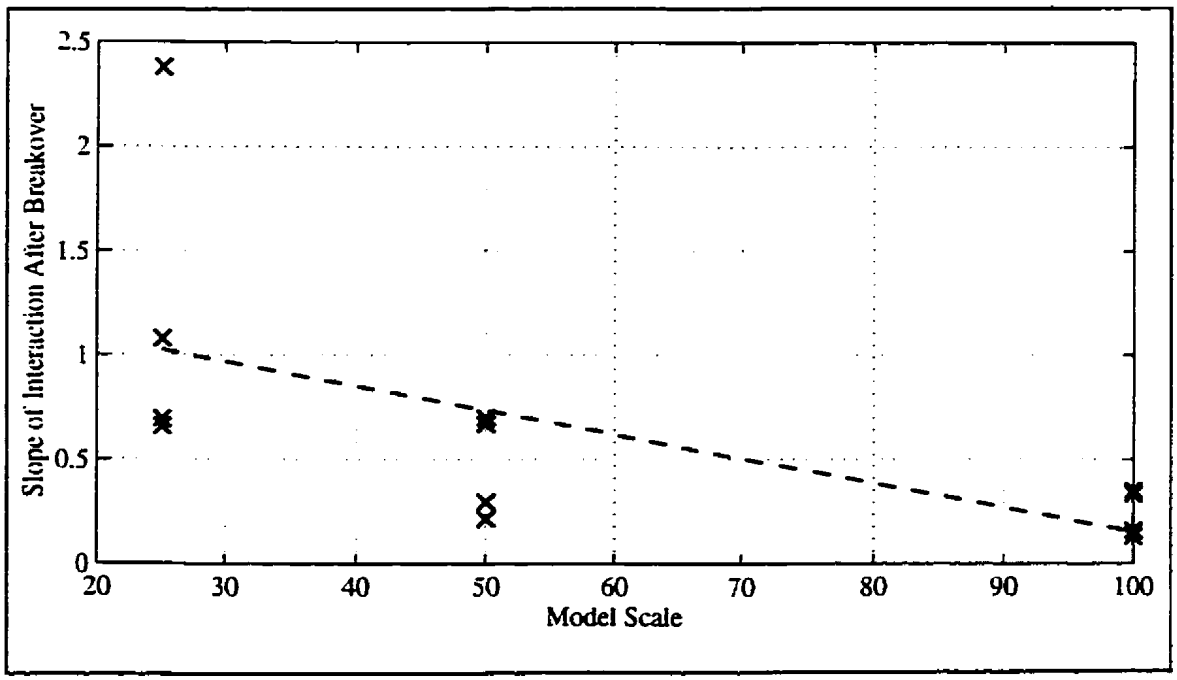

Figure 8.76 - Slope of interaction after breakover, S_{AB}, versus model scale, undrained tests.

excavation of the Test 06 sample suggested less than this. Deformations in front of the pipelines following Test 01 were hard to assess as the amount of spaghetti markers used had been limited. With Test 05, it was observed that as the overburden was transferred up and over the top of the pipe, it primarily cracked and fell behind the pipe while it appeared that during Test 06, the soil flowed more smoothly over the pipeline without cracking and the void simply closed behind the pipe (see *Test Data* appendices for photographs). The behaviour of the soil passing over the pipelines in Test 01 appeared to be somewhat between the behaviour observed upon excavation of Tests 05 and 06.

8.2.8 Curve Fitting of Normalized Data

Curve fitting of the normalized data was undertaken to provide relationships between normalized force (p") and normalized displacement (y") where these are defined as

$$p'' = \frac{p}{c_u D} / \frac{P_{ult}}{c_u D} \qquad [8\text{-}45]$$

and

$$y'' = \frac{y}{D} / \frac{Y_{ult}}{D} \qquad [8\text{-}46]$$

and where p is the force measured at each increment of displacement, y. Three types of curves have been fit to the data including simple bilinear relationships, hyperbolic curves, and polynomial functions.

The bilinear representations have been constructed with the origin at the start of interaction with the trench wall as depicted in Figure 8.77. The slope of the elastic portion of the bilinear relationship has been taken as the secant slope defined at 70% of the maximum normalized force. For the hyperbolic and polynomial fits (Figures 8.78 and 8.79), Y_{ult} has also been measured with respect to the trench wall. For the drained test analyses, Y_{ult} has been taken as the load at a penetration of 1.5 pipe diameters into the trench wall because there was no apparent peaks. No consideration has been given to curve fitting within the trench walls. An approach to estimating resistance within the trench walls is introduced in the next subsection.

Test 01 has been taken as being representative of an undrained test. Curve fitting was conducted on all four pipeline data collectively and results are presented in Table 8.3. Figures 8.80 and 8.81 present the overall fit of the hyperbolic and polynomial curves respectively. Drained tests have been represented by Test 04, Pipeline #1, and Test 08, Pipeline #1. Analysis results are presented in Table 8.3. Figures 8.82 and 8.83 indicate fits to the drained data.

8.2.9 Analysis of Interaction in the Backfill

The baseline backfill used in the current study was relatively soft as far as backfills might be concerned in order to yield the necessary difference between backfill and native soils. It is believed that resistance within the trench walls for the undrained tests and the initial resistance within the trench walls for the drained tests, for the particular backfill system

Table 8.3 - Summary of Fitted Curve Details

Analysis Method	Undrained Tests	Drained Tests[1]
Bilinear Fit	P_{ult} @ 15.7% of Y_{ult}	P_{ult} @ 43.7% of Y_{ult}
Hyperbolic Fit	$\frac{p}{P_{ult}} = \frac{\frac{y}{Y_{ult}} - (-0.0481)}{0.8742(\frac{y}{Y_{ult}} - (-0.0481)) + 0.1008}$	$\frac{p}{P_{ult}} = \frac{\frac{y}{Y_{ult}} - (-0.2246)}{0.7216(\frac{y}{Y_{ult}} - (-0.2246)) + 0.3710}$
Polynomial Fit	$\frac{p}{P_{ult}} = 8.8556x^5 - 26.6495x^4 + 30.7780x^3 - 17.2181x^2 + 4.8984x + 0.3359$ *where* $x = \frac{y}{Y_{ult}}$	$\frac{p}{P_{ult}} = 2.5620x^5 - 7.1354x^4 + 7.5275x^3 - 3.9765x^2 + 1.0649x + 0.4188$ *where* $x = \frac{y}{Y_{ult}}$

Note: (1) Y_{ult} considered to be at a penetration of 1.5 pipeline diameters into the trench wall for drained and partly-drained tests for hyperbolic and polynomial fits.

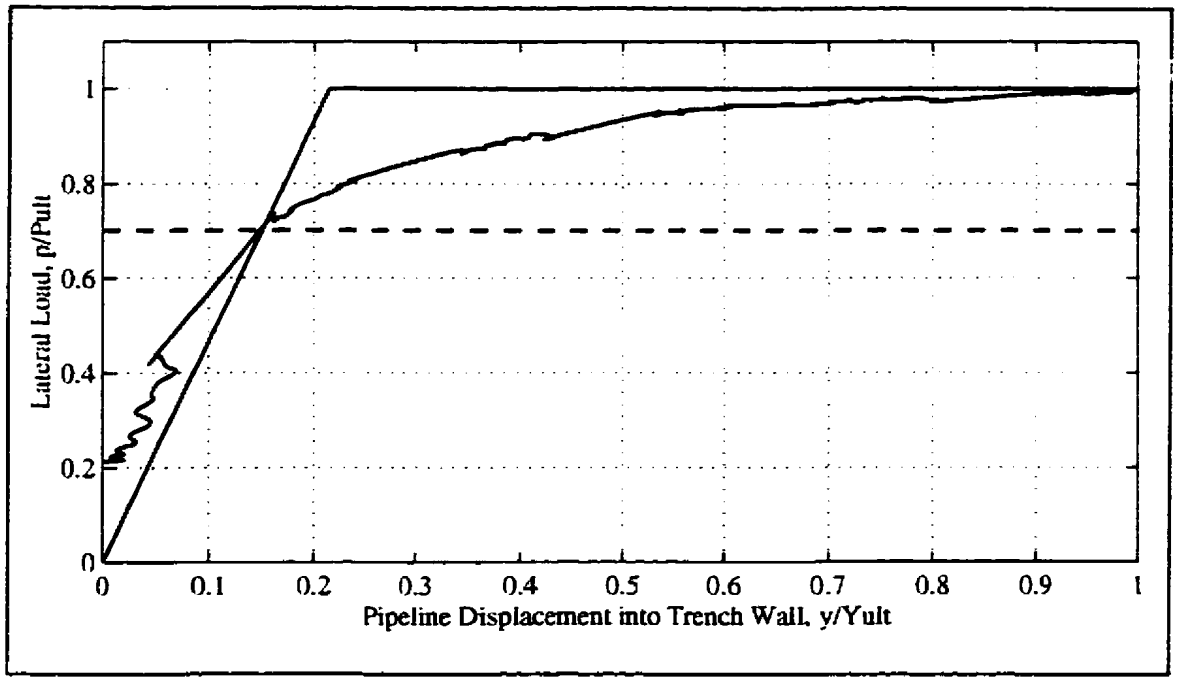

Figure 8.77 - Bilinear representation of normalized force-displacement response with representation starting at the beginning of interaction with the trench wall, Pipeline #1, Test 01.

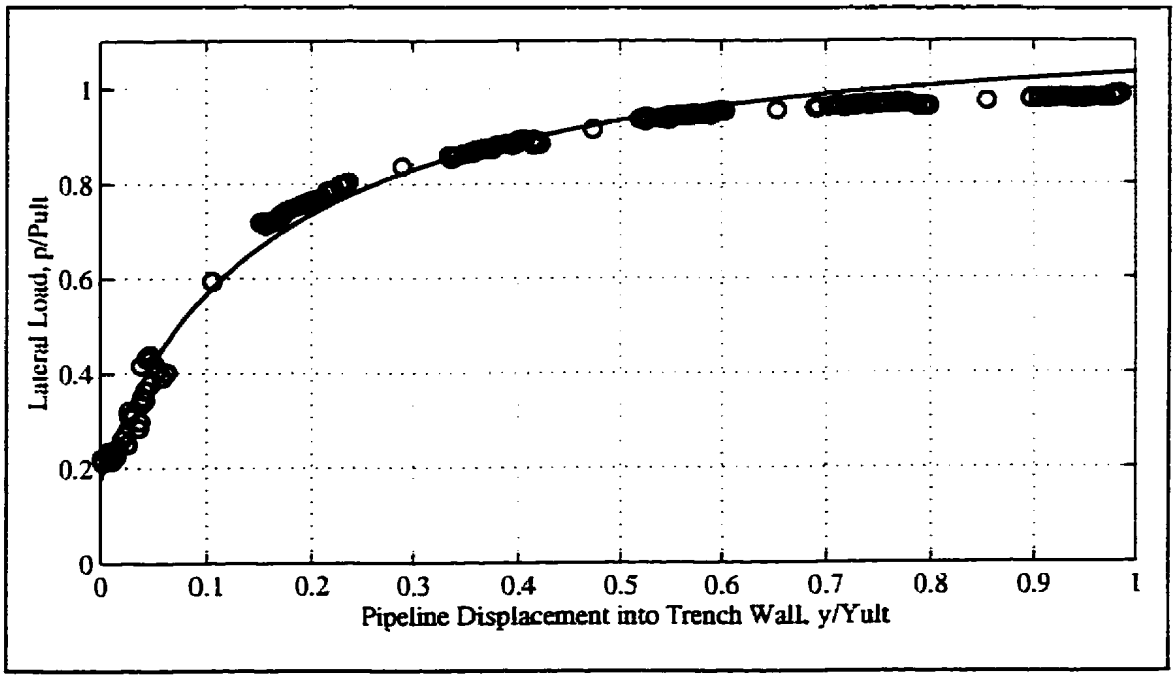

Figure 8.78 - Hyperbolic fit to normalized force-displacement data where data considered extends from the trench wall to ultimate load, Pipeline #1, Test 01.

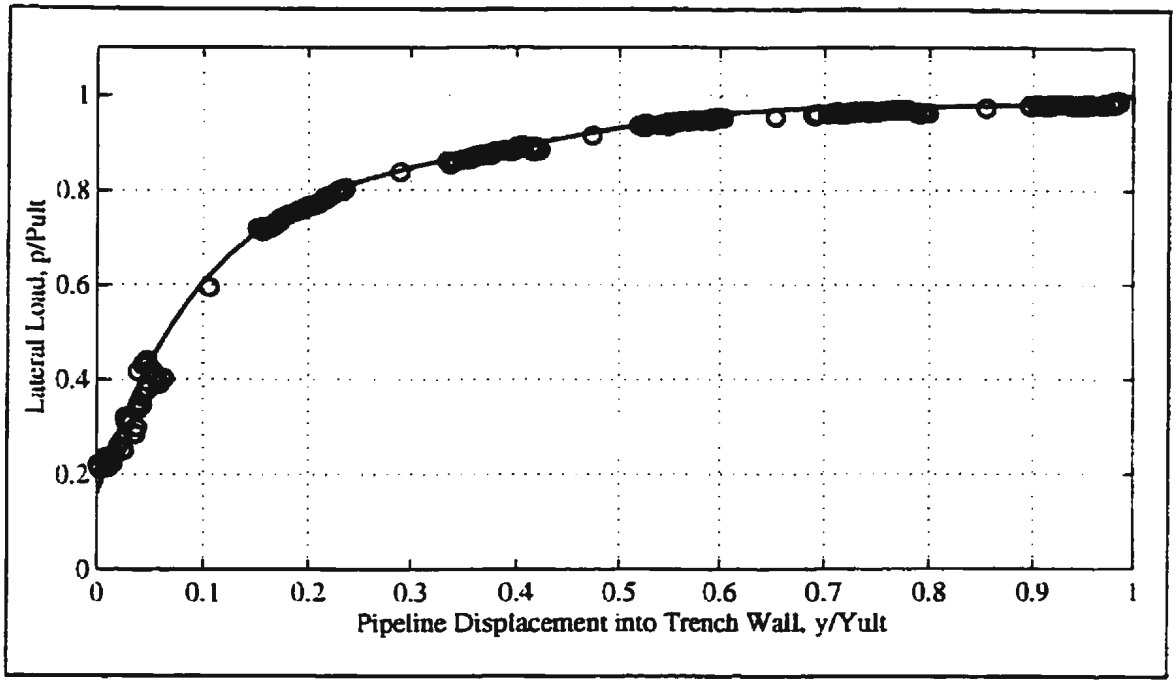

Figure 8.79 - Polynomial fit to normalized force-displacement data where data considered extends from the trench wall to ultimate load, Pipeline #1, Test 01.

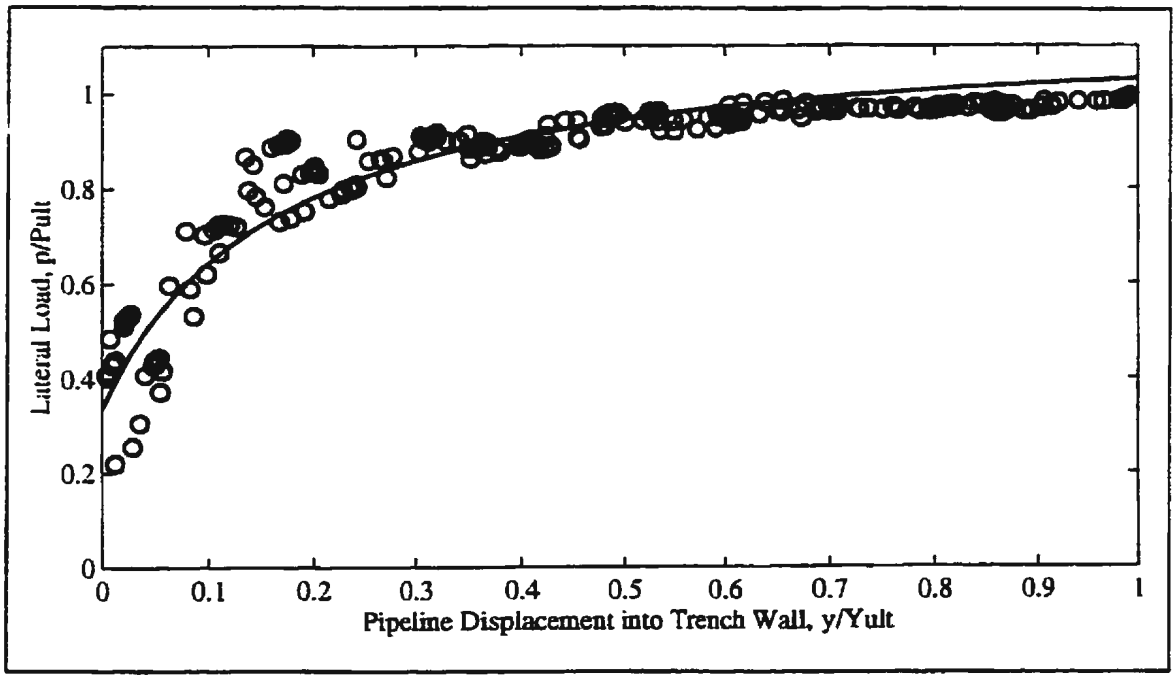

Figure 8.80 - Hyperbolic fit to normalized force-displacement data where data considered extends from the trench wall to ultimate load, for all pipelines of Test 01.

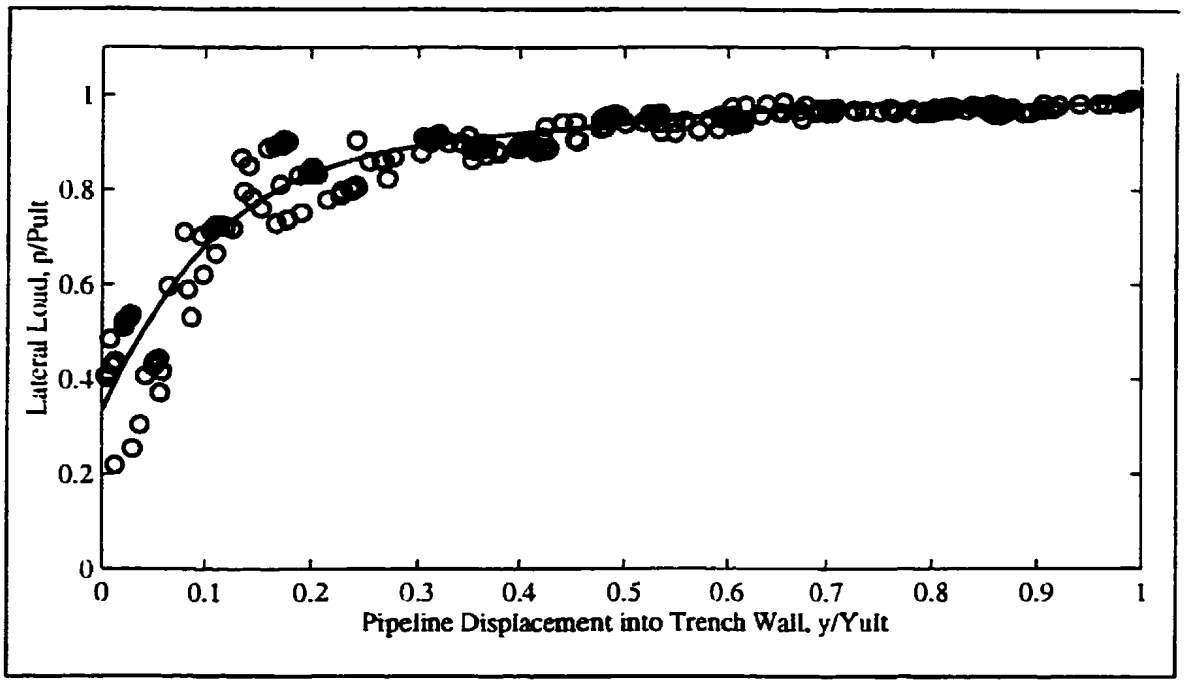

Figure 8.81 - Polynomial fit to normalized force-displacement data where data considered extends from the trench wall to ultimate load, for all pipelines of Test 01.

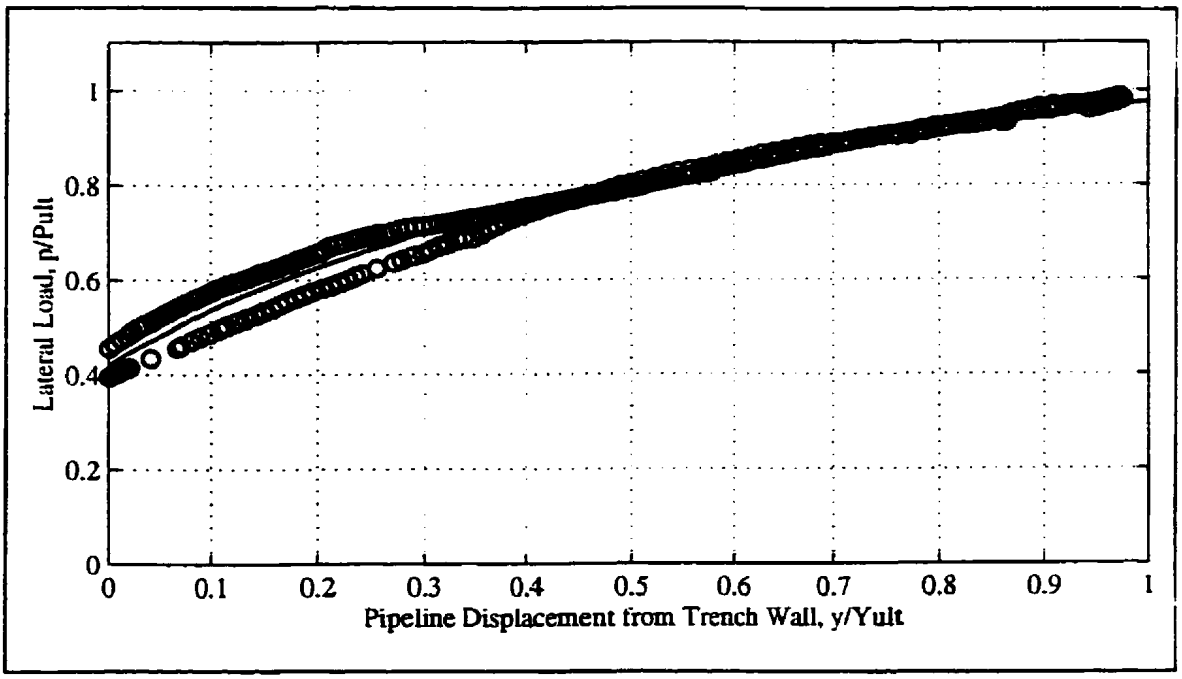

Figure 8.82 - Hyperbolic fit to normalized force-displacement data where data considered extends from the trench wall to ultimate load, Pipeline #1, Tests 04 and 08.

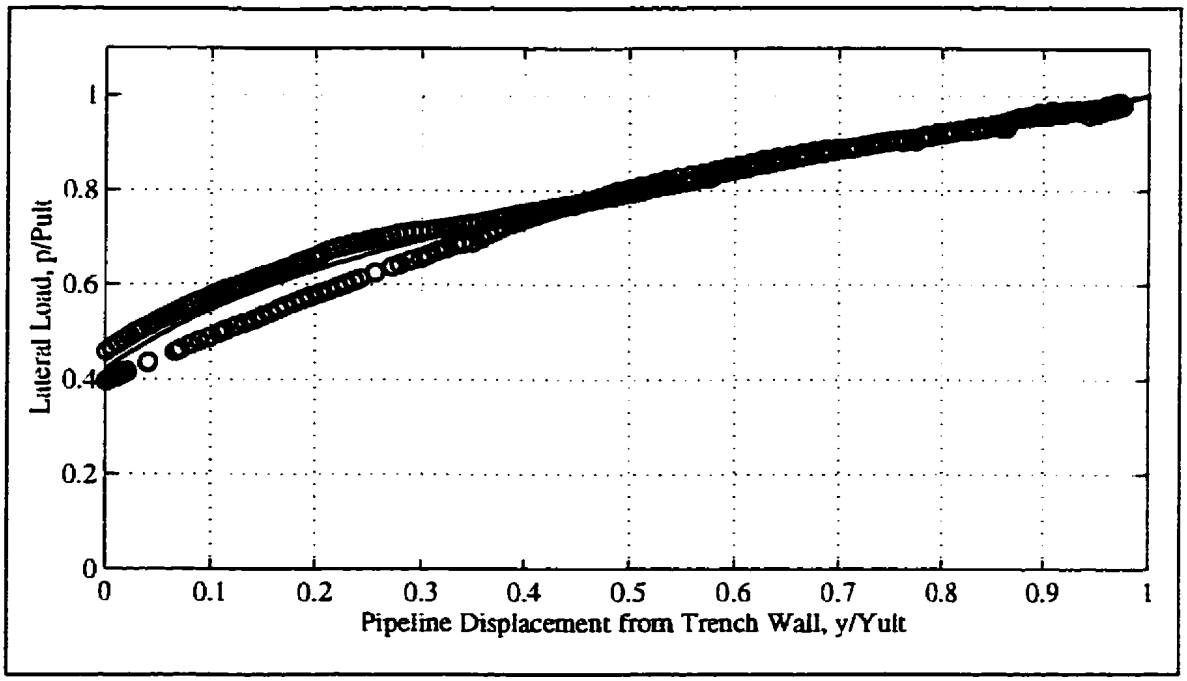

Figure 8.83 - Polynomial fit to normalized force-displacement data where data considered extends from the trench wall to ultimate load, Pipeline #1, Tests 04 and 08.

of this study, was governed primarily by the pipeline basal shear resistance and not by the resistance of the backfill itself. This basal shear resistance would be dependant on at least three factors: (1) the initial vertical pipeline embedment (which would be dependant on the bearing capacity of the soil and the mass of the pipeline); (2) the shear strength of the material at the base of the trench (native material); and, (3) any suction forces developed between the pipeline and the base of the trench.

As different pipelines may have embedded to different depths depending on the factors presented above, it would be impractical to attempt to look at the factors surrounding each pipe displacement. However, observation of the normalized (with respect to native soil

undrained shear strength) load-displacement curves suggests that the resistance within the trench walls for the undrained tests and the initial resistance within the trench walls for the drained tests generally ranged from approximately 0.5 to 1.5 with a mean of 0.885. There does not appear to be any direct correlation of this parameter with burial depth or native soil undrained shear strength.

8.3 Evaluation of Existing Methods of Interaction Analysis

8.3.1 Introduction

A review of current methods of analysis and design for laterally loaded pipelines, previous research into pipeline/soil interaction, and relevant literature applicable to the analysis of lateral pipeline/soil interaction was presented in Chapter 2. That information has been used in this section to compare experimental results with existing methods of pipeline/soil interaction analysis. The section is subdivided into three major subsections which look at undrained interaction, drained interaction, and an assessment of the experimentally derived analysis methods developed in the last subsection.

8.3.2 Undrained Interaction

Interaction Factors

Table 8.2 presents prototype interaction rates, H/D values and interaction factors from all of the centrifuge tests. The experimental data from Test 01 and Test 02 clearly showed the influence of cover depth; as the H/D ratio increases from 1 to 1.84, the interaction factor

or normalized lateral load becomes greater. However, for higher H/D ratios, the effect of burial depth on the factor was not as obvious. This is as expected; for higher H/D ratios, the interaction factor might be expected to reach a limiting value. The interaction factors from Test 01 and Test 02 are presented in Figure 8.84 along with the interpreted interaction factor curves from existing methods of pipeline/soil interaction analysis explored including those of Hansen (ASCE, 1984), Rowe and Davis (1982a), Edgers and Karlsrud (1982), Wantland *et al.* (1979), Mackenzie (1955), and Tschebotarioff (1973) for comparison purposes. Interaction factors from each of the existing methods of analysis are also presented in Table 8.2. In the figure, the embedment ratio defined by Hansen (1961) is different from that presented by Rowe and Davis (1982a) but the curve has been adjusted so that the Hansen interaction curve can be compared on the same plot with the Rowe and Davis (1982a) and other interaction curves.

The experimental interaction factors presented in Figure 8.84 have been calculated using Equation [2-12]. Rizkalla *et al.* (1992) suggest that this equation can utilize the interaction factors suggested by Rowe and Davis (1982a) to obtain the ultimate lateral load on a pipeline. However, in its true form, the method of Rowe and Davis (1982a) to obtain the lateral capacity of vertical anchors accounts for overburden pressure as indicated by Equation [2-41]. If this equation were applied to the experimental data, the result would be slightly lower experimental interaction factors than those shown in Figure 8.84.

The Edgers and Karlsrud (1982) curve was constructed based on an interaction factor

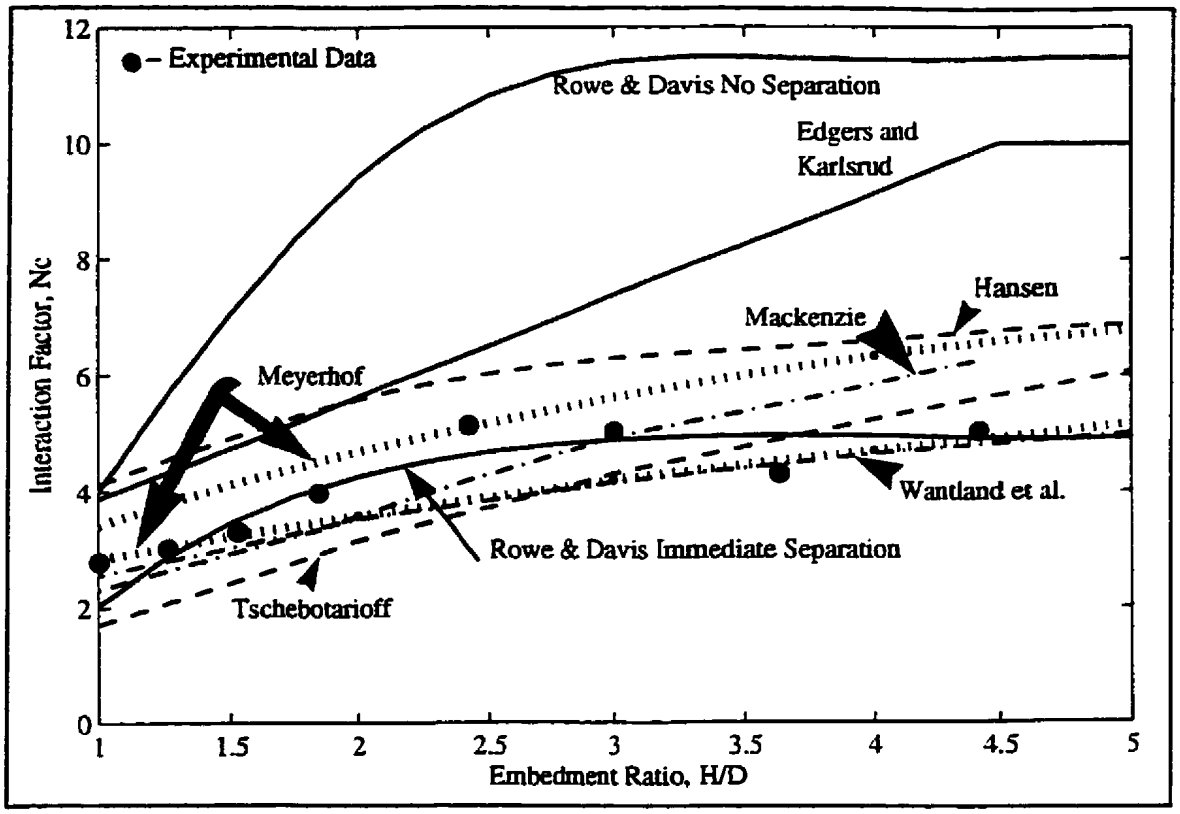

Figure 8.84 - Test 01 and Test 02 interaction factors presented as a function of embedment along with interpreted interaction factors trends from existing methods of pipeline/soil interaction analysis.

ranging from 3 at the mudline, H/D=0.5, to 10 at a depth equivalent to 4 pipe diameters, H/D=4.5 (as suggested by Bea *et al.* (1975)). It might be noted that the analysis method of Wantland *et al.* (1982) does not use an undrained shear strength at the springline but rather the average strength over a distance 2D above the pipeline invert. If the current experimental data were analysed in this fashion, slightly higher interaction factors than those shown would result. Mackenzie (1955) did not define an interaction factor but the curve shown in the figure has been back-calculated using the data of Test 01 and Test 02 and Equation [2-37]. As mentioned in Chapter 2, Tschebotarioff (1973) reanalysed the data

of Mackenzie (1955) and plotted it in non-dimensionalized form as shown in the figure. The method of Ng (1994) is not indicated on the figure because this method is more applicable to an interaction in which the pipeline does not leave the backfill after which the author's analysis considers the interaction factors provided by Hansen (1961) to be suitable. The Meyerhof references, based on laterally loaded piles, are discussed later.

The interaction factors of Test 01 and Test 02 presented in Figure 8.84 support the hypothesis that after a certain H/D value, the stress level at the springline has less influence on the interaction factor and a deep-seated displacement mechanism occurs. Overall, there is some experimental scatter in the data but generally the trend is quite similar to the Rowe and Davis (1982a) "Immediate Separation" curve.

Interpreted interaction factors derived from all of the tests are presented in Figure 8.85. For the tests which were considered to be undrained, the experimental interaction factors generally appear to be bounded by the Rowe and Davis (1982a) and Hansen (1961) interaction curves for an embedment ratio less than approximately 2. Beyond this embedment ratio, only the data described in the previous paragraph are available.

Displacement to Ultimate Load

It should be noted that ASCE (1984) suggests a displacement to ultimate load, Y_{ult}, equivalent to approximately 3 to 5% of H. This would typically be less than 0.1D for prototype pipelines scaled from the experimental program. Observation of the data of

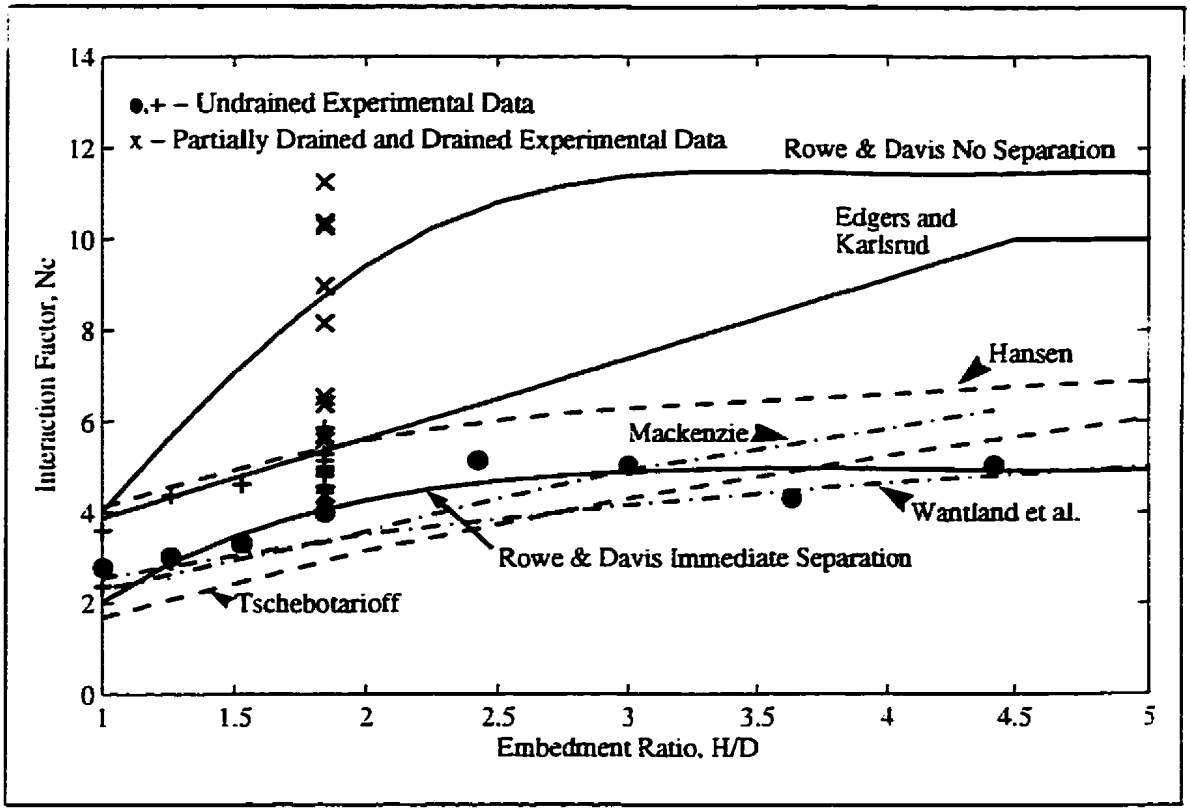

Figure 8.85 - All interaction factors presented as a function of embedment ratio along with interpreted interaction factors trends from existing methods of pipeline/soil interaction analysis.

Table 8.2 indicates displacements greater than 1D into the trench wall to achieve the interpreted ultimate load on the pipeline.

Experimental Results, Developed p-y Curves, and Predicted Ultimate Loads

The Committee on Gas and Liquid Fuel Lifelines (ASCE, 1984) guidelines suggested that the p-y relationship for pipeline/soil interaction in cohesive soils can be expressed by Equations [2-4], [2-5], and [2-6] with Y_{ult} as defined above. These equations were used to develop the prototype-scale p-y curves presented in Figure 8.86 using input parameters

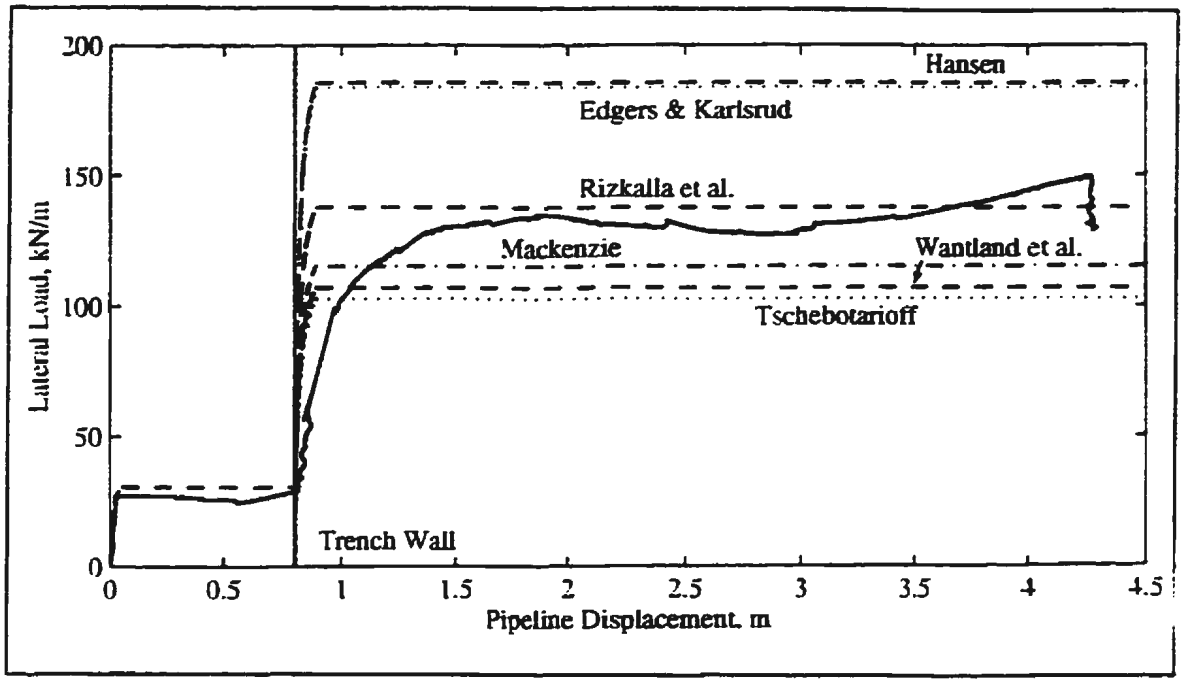

Figure 8.86a - Predicted undrained ultimate loads and p-y curves based on existing methods of analysis compared with Pipeline #1, Test 01, data.

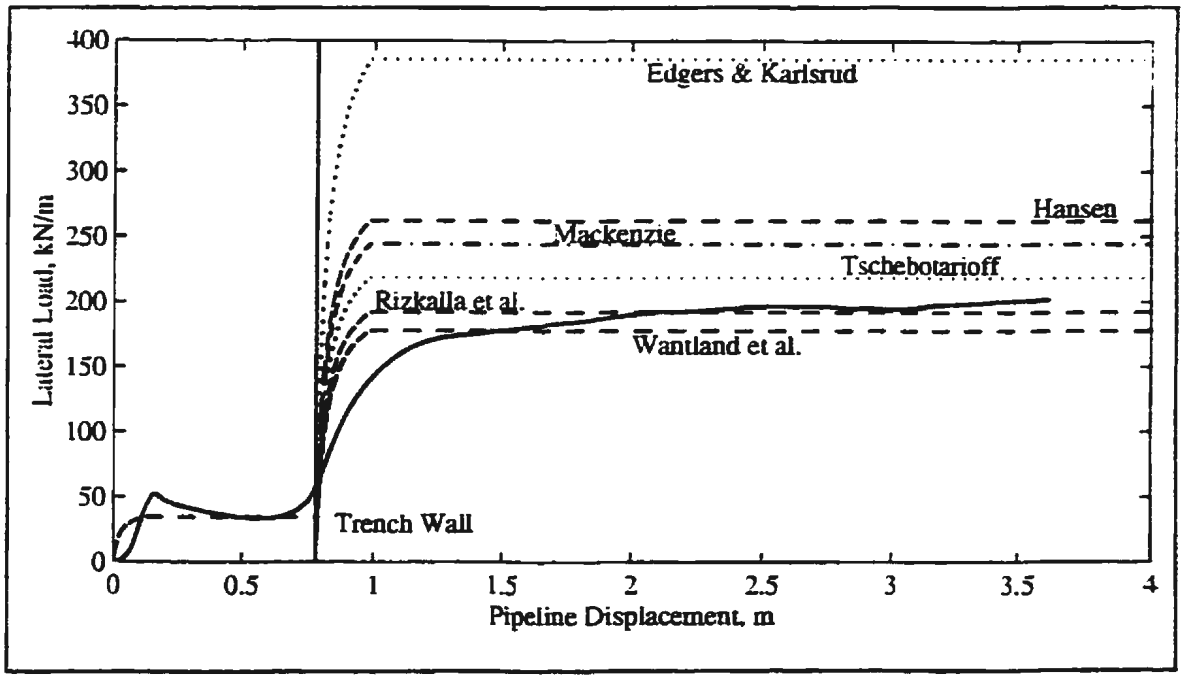

Figure 8.86b - Predicted undrained ultimate loads and p-y curves based on existing methods of analysis compared with Pipeline #1, Test 02, data.

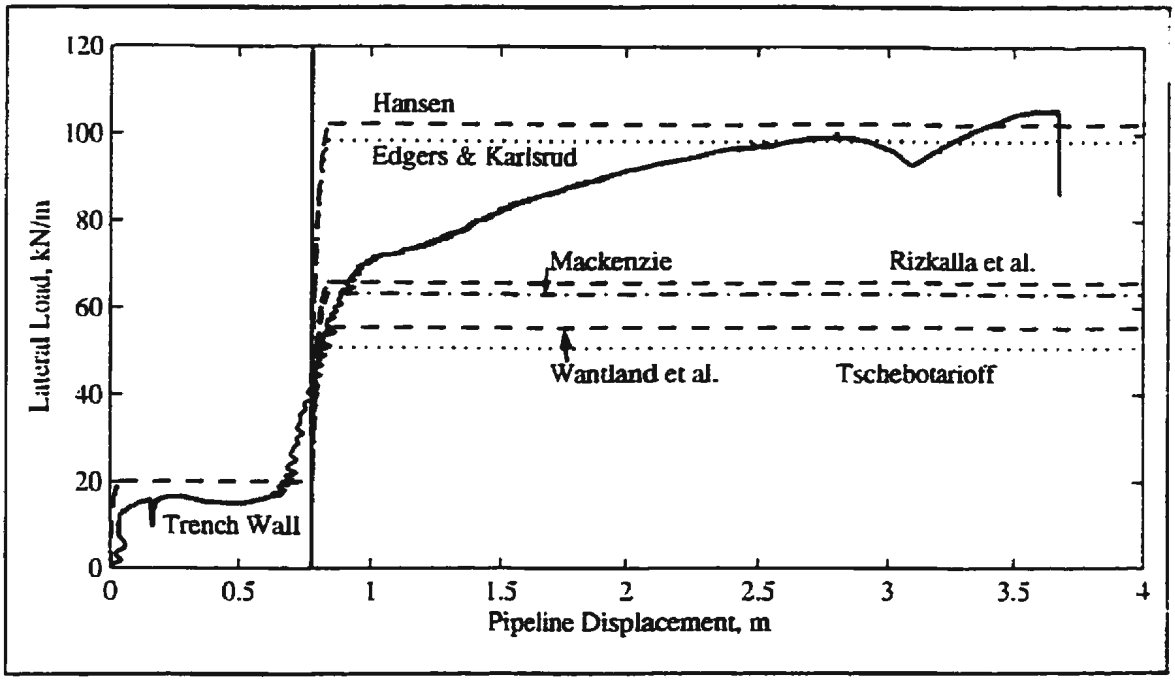

Figure 8.86c - Predicted undrained ultimate loads and p-y curves based on existing methods of analysis compared with Pipeline #3, Test 05, data.

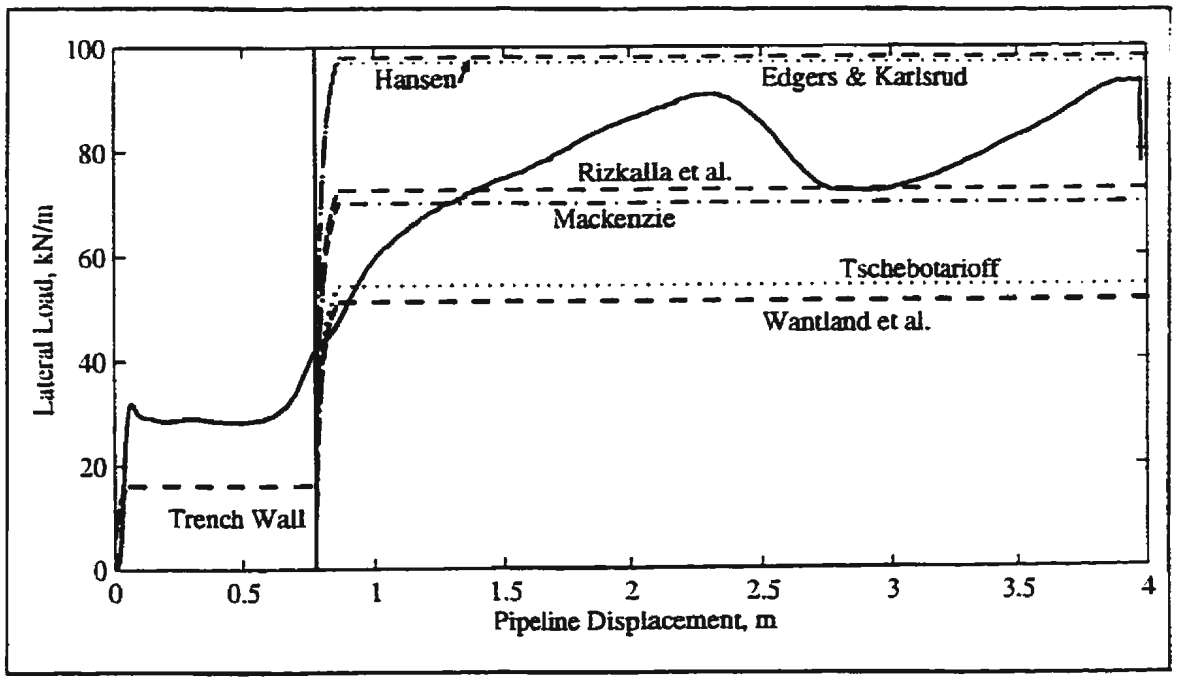

Figure 8.86d - Predicted undrained ultimate loads and p-y curves based on existing methods of analysis compared with Pipeline #4, Test 08, data.

from: Pipeline #1, Test 01; Pipeline #1, Test 02; Pipeline #3, Test 05; and Pipeline #4, Test 08. These four pipeline tests were chosen randomly from the undrained tests conducted. The prototype-scale experimentally derived force-displacement curves from the pipeline tests are also plotted on the figures.

Six theoretical p-y curves are shown on each of the figures. These were based on existing methods of ultimate load interaction analysis from: ASCE (1984)/Hansen (1961); Rizkalla *et al.* (1992); Edgers and Karlsrud (1982); Wantland *et al.* (1979); Mackenzie (1955); and, Tschebotarioff (1973). The method suggested by Rizkalla *et al.* (1992) uses Equation [2-12] and interaction factors of Rowe and Davis (1982a); however, the actual method of Rowe and Davis (1982a) also includes a term to account for surcharge pressure. Results from this method will be compared to experimental data in Section 8.4. The pipeline displacement to ultimate load was taken as 5% of H. The origin of the theoretical p-y curves has been set with respect to the beginning of interaction with the trench wall. Interaction in the backfill has been calculated as defined in Subsection 8.2.9 with peak taken to occur at 3% of H.

With the exception of Pipeline #4, Test 08, all estimations of the resistance of the pipeline displacement in the backfill was adequate. If, in the softer soil of Test 08, the pipeline had embedded itself more deeply due to self-weight, then the resistance within the trench walls might be higher than in the other tests with higher strength native soil. Comparison of the theoretical results in the hyperbolic portion of the curves indicates that the suggested

construction (ASCE, 1984) overpredicts the rate at which load is transferred to the pipeline. The ultimate resistance of the Test 01 and Test 02 pipelines were best estimated after a displacement of 1.5m using the Rowe and Davis (1982a) interaction factors as suggested by Rizkalla *et al.* (1992). The Edgers and Karlsrud (1982) and Hansen (1961) methods provided reasonable estimates for the Test 05 pipeline after a displacement of approximately 2m. The mean of the trace of Figure 8.86d from Pipeline #4, Test 08 (after a displacement of 1.5m), falls between the curves constructed using the Hansen (1961) and Rowe and Davis (1982a) interaction factors (as suggested by Rizkalla *et al.*, 1992). Curves using the Mackenzie (1955), Wantland *et al.* (1979), and Tschebotarioff (1973) suggestions were almost consistently off the mark. Using an average interaction factor from Rowe and Davis (1982a) and Hansen (1961) yields an ultimate lateral load within $\pm 20\%$ of that found experimentally based on the four tests presented above.

8.3.3 Drained Interaction

Interaction Factors

Test data and interaction factors from all of the tests which were considered drained or partially-drained are presented in Table 8.4. In most cases, drained interaction has yielded factors significantly higher than those from undrained interaction. As mentioned previously, often the load on the pipeline continued to increase and, in cases, the peak load was simply taken as the point where the test was terminated. As indicated by Figure 8.85, interaction factors from tests which were considered to be drained or partially-drained ranged from the Hansen (1961) interaction curve to beyond the Rowe and Davis (1982a)

"No Separation" interaction curve.

Also, as mentioned earlier in this thesis, it is difficult to interpret the ultimate load of a drained or partially-drained force-displacement response. An alternative means of determining where this occurs, is to take the point where the force-displacement response becomes linear. The relevant data pertaining to this interpretation for the drained and partially-drained tests are also presented in Table 8.4.

Displacement to Ultimate Load

ASCE (1984) suggests a displacement to ultimate load of 2 to 10% of H for frictional material. Other suggested necessary displacements for pipelines in frictional soil from the literature include 1.5 to 2% of h from Audibert and Nyman (1977) and 3 to 13% of h from Trautmann and O'Rourke (1985) where h is the depth to the pipe springline. This would translate to less than 0.2D for prototype pipelines with a H/D ratio of 1.842 scaled from the experimental program. Displacements greater than 1D into the trench wall were required to achieve the peak load on the pipeline interpreted as the point where the test was terminated. If the peak load is interpreted as the point where the force-displacement response went linear, then a displacement of approximately 0.5 to 1.5D into the trench wall would be needed to reach this point.

Experimental Results, Developed p-y Curves, and Predicted Ultimate Loads

ASCE (1984) guidelines (Committee on Gas and Liquid Fuel Lifelines) present, for sand,

Table 8.4 - Summary of drained ultimate loads

Test	Pipe	Prototype Interaction Rate (m/day)	H/D	Distance Into Trench Wall to P_{ult} (D) *	Experimental Interaction Factor, N **	Experimental Ultimate Load (kN/m)	Hansen (1961) ϕ Analysis[1]	Hansen (1961) $c + \phi$ Analysis[2]	Luscher (1982)[4] ϕ Analysis[3]	Luscher (1982) ϕ Analysis + Hansen (1961) Cohesive Component [4]
04	1	0.0014	1.842	2.72 / 1.43	11.26 / 7.54	341	142	176	86	119
04	2	0.0078	1.842	3.60 / 1.57	8.15 / 4.76	246	142	176	86	119
07	1	0.0012	1.842	1.46 / 0.820	5.69 / 4.84	203	140	173	84	118
07	2	0.092	1.842	1.33 / 0.926	5.57 / 4.95	195	140	173	84	118
08	1	0.00095	1.842	1.78 / 0.835	10.28 / 7.97	229	137	170	82	116
08	2	0.0092	1.842	3.15 / 0.943	10.37 / 6.52	228	137	170	82	116
09	1	0.00092	1.842	1.85 / 0.497	6.54 / 4.42	285	143	176	86	119
09	2	0.0024	1.842	1.83 / 0.605	8.98 / 6.00	376	143	176	86	119
09	3	0.00092	1.842	1.44 / 0.402	6.38 / 5.44	279	143	176	86	119
09	4	0.00079	1.842	1.15 / 0.526	4.39 / 3.55	190	143	176	86	119

Notes: * Second distance to P_{ult} corresponds to the point where the force-displacement curve became linear.

** Second interaction factor corresponds to the point where the force-displacement curve became linear.

(1) Hansen's (1961) method for a purely frictional soil, Equation [2-7].

(2) Hansen's (1961) method to estimate the ultimate lateral load for a c-ϕ soil, Equation [2-56].

(3) Rankine's passive earth pressure for a purely frictional soil as suggested by Luscher (1982), Equation [2-1].

(4) Rankine pressure as suggested by Luscher (1982), Equation [2-1], plus a cohesive component from Hansen (1961), Equation [2-11].

Table 8.4, cont... - Summary of drained ultimate loads

Test	Pipe	Prototype Interaction Rate (m/day)	H/D	Distance Into Trench Wall to P_{ult} (D) *	Experimental Interaction Factor, N **	Experimental Ultimate Load (kN/m)	Ovesen and Stroman (1972) ϕ Analysis[5]	Ovesen and Stroman (1972) ϕ Analysis + Hansen (1961) Cohesive Component[6]	Ranjani *et al.* (1993) ϕ Analysis[7]	Ranjani *et al.* (1993) ϕ Analysis + Hansen (1961) Cohesive Component[8]
4	1	0.0014	1.842	2.72 / 1.43	11.26 / 7.54	341	93	126	69	103
4	2	0.0078	1.842	3.60 / 1.57	8.15 / 4.73	246	93	126	69	103
7	1	0.0012	1.842	1.46 / 0.820	5.69 / 4.84	203	91	124	68	102
7	2	0.092	1.842	1.33 / 0.926	5.57 / 4.95	195	91	124	67	102
8	1	0.00095	1.842	1.78 / 0.835	10.28 / 7.97	229	89	122	67	100
8	2	0.0092	1.842	3.15 / 0.943	10.37 / 6.52	228	89	122	70	100
9	1	0.00092	1.842	1.85 / 0.497	6.54 / 4.42	285	93	126	70	103
9	2	0.0024	1.842	1.83 / 0.605	8.98 / 6.00	376	93	126	70	103
9	3	0.00092	1.842	1.44 / 0.402	6.38 / 5.44	279	93	126	70	103
9	4	0.00079	1.842	1.15 / 0.526	4.39 / 3.55	190	93	126	70	103

Notes: * Second distance to P_{ult} corresponds to the point where the force-displacement curve became linear.

** Second interaction factor corresponds to the point where the force-displacement curve became linear.

(5) Ovesen and Strohman's (1972) method for a purely frictional soil, Equation [2-7].

(6) Ovesen and Strohman's (1972) method, Equation [2-7], plus a cohesive component from Hansen (1961), Equation [2-11].

(7) Ultimate resistance suggested by Ranjani *et al.* (1983), Equation [2-13], for a purely frictional soil.

(8) Ultimate resistance suggested by Ranjani et al. (1983), Equation [2-13], plus a cohesive component from Hansen (1961), Equation [2-11].

a hyperbolic p-y curve of the form derived from Equations [2-4], [2-5], and [2-6]. Audibert and Nyman (1977) suggested a p-y curve described by Equation [2-22] whereas Trautmann and O'Rourke (1985) suggested Equation [2-29] be used. Distances to ultimate loads were defined above.

As discussed previously, drained and partially-drained tests have exhibited higher interpreted interaction factors than their undrained counterparts. Therefore, ultimate soil resistance for the drained and partially-drained tests have been calculated using the following existing methods for both purely frictional and c-ϕ soils: (1) Hansen's (1961) method for a purely frictional soil, Equation [2-7]; (2) Hansen's (1961) method to estimate the ultimate lateral load for a c-ϕ soil, Equation [2-56]; (3) Rankine's passive earth pressure for a purely frictional soil as suggested by Luscher (1982), Equation [2-1]; (4) Rankine pressure as suggested by Luscher (1982), Equation [2-1], plus a cohesive component from Hansen (1961), Equation [2-11]; (5) Ovesen and Strohmen's (1972) method for a purely frictional soil, Equation [2-7]; (6) Ovesen and Strohman's (1972) method, Equation [2-7], plus a cohesive component from Hansen (1961), Equation [2-11]; (7) the ultimate resistance suggested by Ranjani *et al.* (1993), Equation [2-13], for a purely frictional soil; and (8) ultimate resistance suggested by Ranjani *et al.* (1993), Equation [2-13], plus a cohesive component from Hansen (1961), Equation [2-11]. The c-ϕ method of Rowe and Davis (1982a) for horizontally loaded vertical anchor plates will be compared to experimental data in Section 8.4. Ultimate lateral loads were calculated using effective stress or drained strength parameters ($c' \approx 6.5$kPa and $\phi' = 30°$) which were interpreted

from the undrained triaxial tests data presented in the q-p' plot of Figure 8.87. Interpreted experimental and calculated ultimate soil resistances are summarized in Table 8.4.

Using suggested constructions for p-y curves and the ultimate soil resistance results presented in Table 8.4, prototype-scale p-y curves are presented in Figure 8.88 for: Pipeline #1, Test 04; Pipeline #1, Test 07; Pipeline #1, Test 08; and Pipeline #1, Test 09. These four pipeline tests are considered representative of "drained" conditions. Interaction in the backfill has been calculated as in the previous subsection. As observation of Table 8.4 indicated that the ultimate resistance for a purely frictional soil were not representative of experimental values, only constructions for a c'-ϕ' soil have been presented in Figure 8.88. The prototype-scale experimentally derived force-displacement curves from the pipeline tests are also plotted on the figures as are the ultimate loads defined by the position where the force-displacement response went linear. The pipeline displacement to ultimate load as well as the suggested p-y curve formulation for the Hansen (1961) construction was that suggested by Audibert and Nyman (1977); for the Ovesen and Strohman (1972) construction was that suggested by Trautmann and O'Rourke (1985); the other two cases used the recommendations suggested by ASCE (1984). In all cases, the displacement was taken as the maximum of the range suggested.

The initial interaction in the backfill has been reasonably estimated using the method proposed in Subsection 8.2.9. However, due to the slow displacement rate, consolidation of the backfill does occur and lateral force quickly rises with displacement. All of the

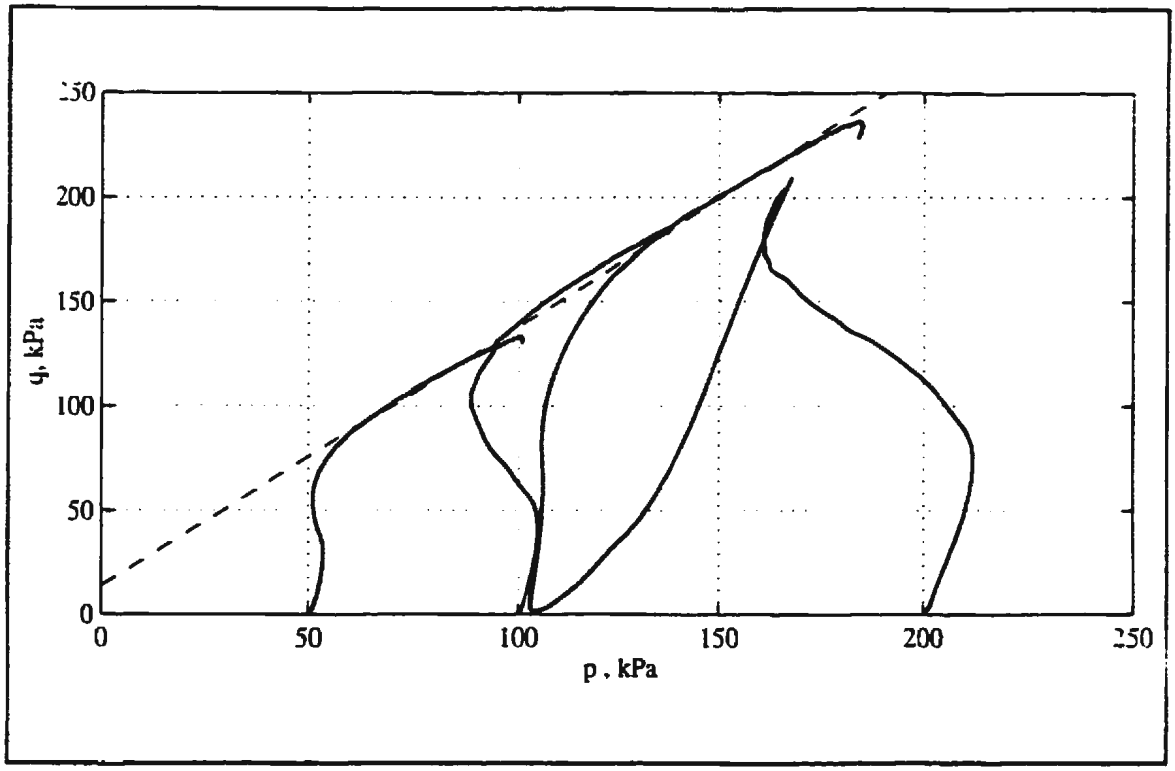

Figure 8.87 - Consolidated undrained triaxial compression test results plotted in p' - q space for consolidation pressures of 50, 100, and 200kPa.

suggested constructions for interaction in the native material overpredict the rate at which load is transferred to the pipeline. Ultimate resistances were sometimes underpredicted and sometimes overpredicted depending on when the tests were terminated which often dictated the measured ultimate load on the pipeline. Resistance curves obtained using these methods are not considered to be very representative of the actual loading on the pipeline. At best, the Hansen (1961) method can be said to be conservative up to a displacement of approximately 0.2 to 0.7 pipe diameters into the trench wall. Ultimate resistances suggested by the point where the force-displacement curves became linear were generally underpredicted by the suggested analysis methods. The Hansen (1961) method provided

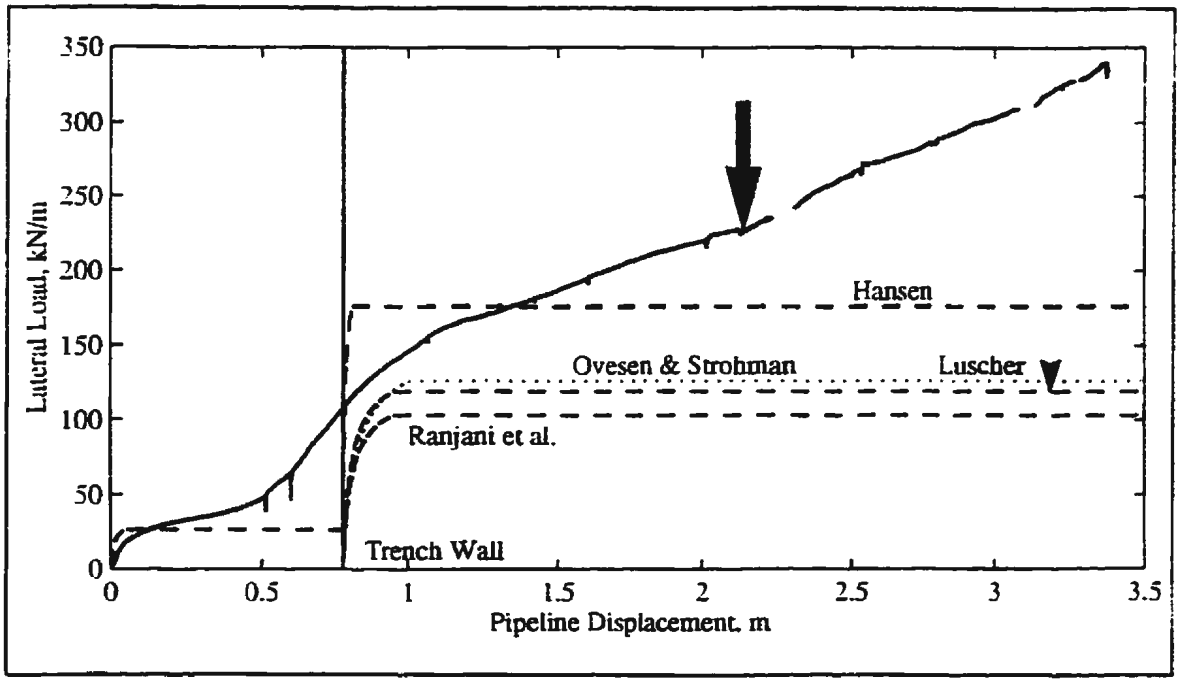

Figure 8.88a - Predicted undrained ultimate loads and p-y curve formulation based on the interaction factor approach and compared with Pipeline #1, Test 04, data.

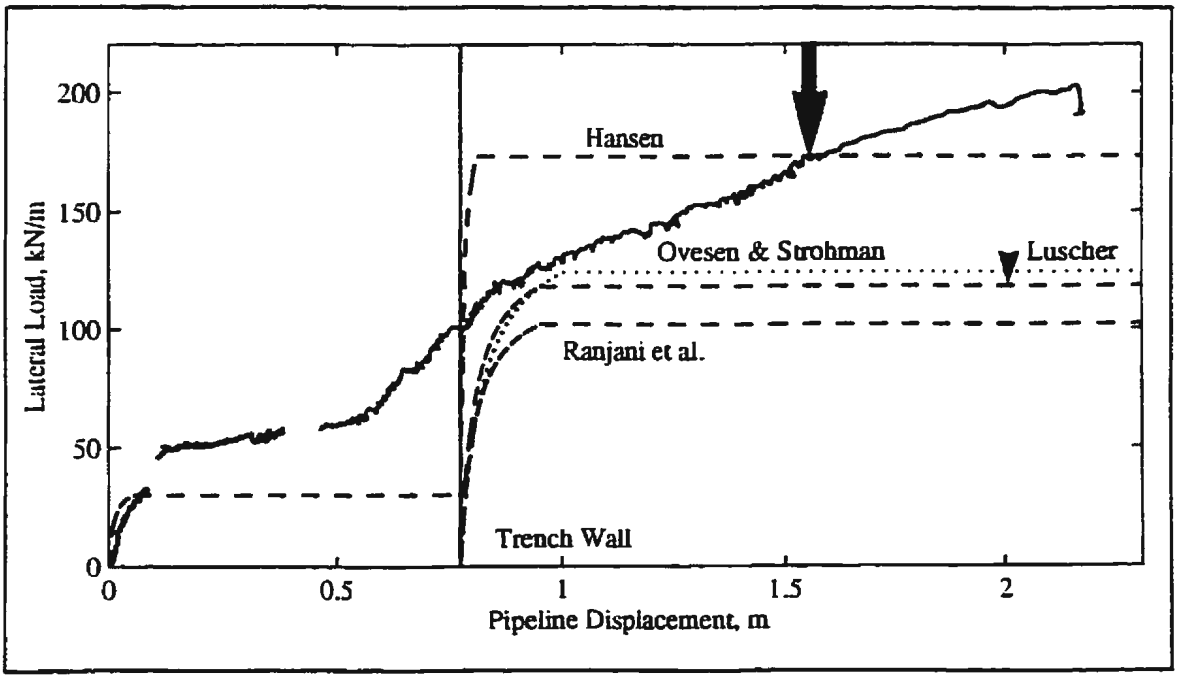

Figure 8.88b - Predicted undrained ultimate loads and p-y curve formulation based on the interaction factor approach and compared with Pipeline #1, Test 07, data.

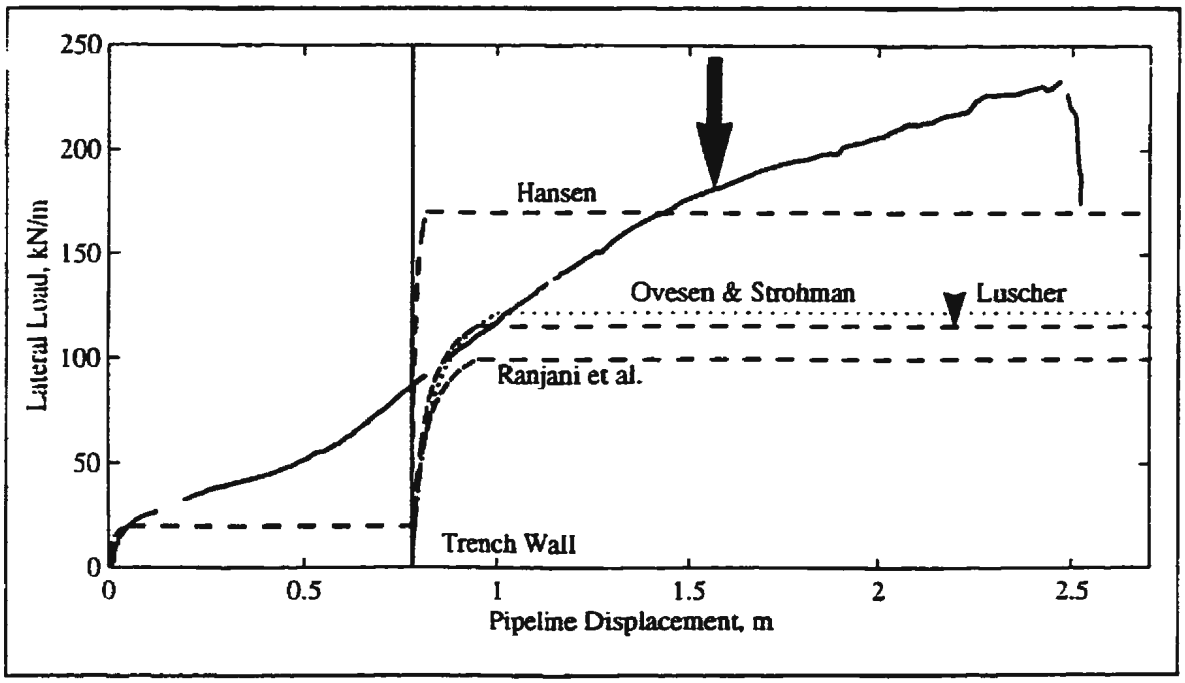

Figure 8.88c - Predicted drained ultimate loads and p-y curves based on existing methods of analysis compared with Pipeline #1, Test 08, data.

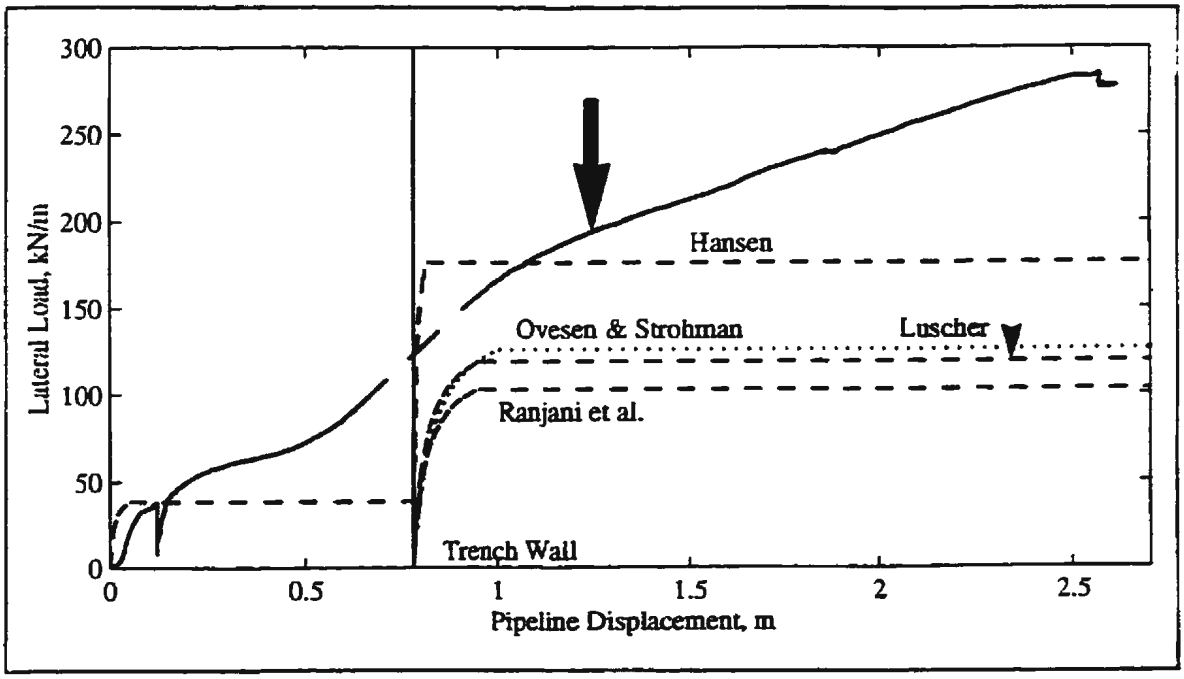

Figure 8.88d - Predicted ultimate loads and p-y curves based on existing methods of analysis compared with Pipeline #1, Test 09, data.

the best approximation to this ultimate load definition providing estimates ranging from essentially correct to underpredicting by as much as 20%.

8.3.4 Assessment of Experimentally Derived Analysis Methods

Interaction Factor Approach - Undrained Analysis

Initially, it was thought that the ultimate normalized resistance or interaction factors for undrained tests could be represented by the trends shown in Figure 8.31. However, examination of Figure 8.85 indicated a wider spread to the undrained interaction factor data. This data has been replotted in Figure 8.89. Superimposed on the data are reasonable fits to the data including: (1) a bilinear conservative bound; (2) a polynomial fit through all points but only plotted to an embedment ratio of 2.5 followed by a constant interaction factor value; (3) a polynomial fit through the Test 01 and Test 02 data; and (4) a bilinear regression made up of a linear regression through the Test 01 and Test 02 data up to and including the interaction factor at an embedment ratio of 2.5 followed by a constant interaction factor value.

Equations describing the four trends are as follows: for trend (1),

$$N_c = 1.57\frac{H}{D} + 2.38 \qquad for\ \frac{H}{D} \leq 1.842; \qquad [8\text{-}47]$$

for trend (2),

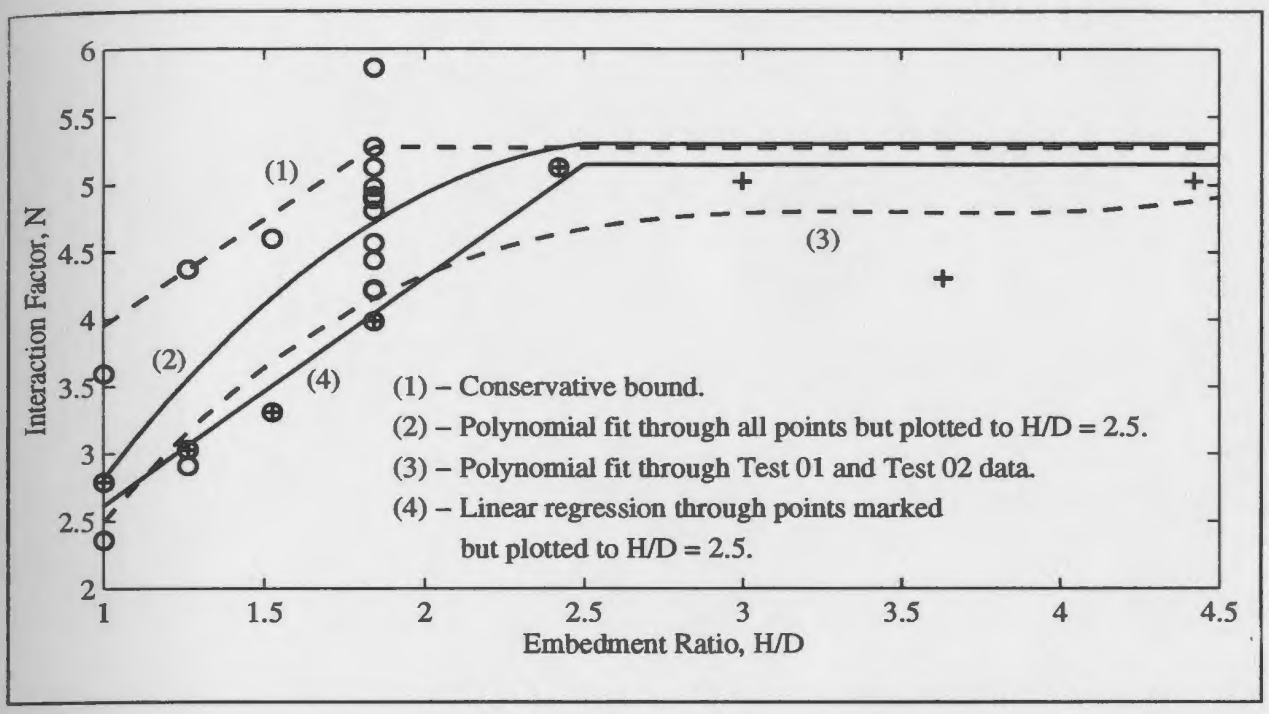

Figure 8.89 - Evaluated trends (as indicated on the figure) through undrained interaction factor data from all tests.

$$N_c = -0.915\left(\frac{H}{D}\right)^2 + 4.86\left(\frac{H}{D}\right) - 1.13 \qquad for\ \frac{H}{D} \le 2.5; \qquad [8\text{-}48]$$

for trend (3),

$$N_c = 0.150\left(\frac{H}{D}\right)^3 - 1.58\left(\frac{H}{D}\right)^2 + 5.51\left(\frac{H}{D}\right) - 1.59 \qquad for\ \frac{H}{D} \le 2.5; \qquad [8\text{-}49]$$

and, for trend (4)

$$N_c = 1.69\frac{H}{D} + 0.928 \qquad for\ \frac{H}{D} \le 2.5. \qquad [8\text{-}50]$$

These curves can be used along with the displacements to ultimate loads presented in Figure 8.32 to generate prototype-scale force-displacement curves. The hyperbolic form of the curve used was that presented in Equation [2-4] as suggested by the Committee on Gas and Liquid Fuel Lifelines (ASCE, 1984). Three theoretical force-displacement curves are presented in Figure 8.90 representing: (1) the mean displacement to ultimate load; (2) the conservative minimum displacement to ultimate load; and (3) the displacement to ultimate load suggested by the linear regression of Figure 8.32. Interaction in the backfill has again been represented using the method proposed in Subsection 8.2.9. Comparison of theoretical with experimental curves indicated that the representation which utilized the displacement to ultimate loads suggested by linear regression of Figure 8.32 (Equation [8-9]) generally provided the best fit to the undrained experimental data.

Curves constructed using the four trends suggested above are presented in Figure 8.91 along with the experimental data of the tests analysed in Subsection 8.3.2: Pipeline #1, Test 01; Pipeline #1, Test 02; Pipeline #3, Test 05; and Pipeline #4, Test 08. Interaction within the backfill has been commented on previously. The curves constructed using the polynomial fit through the selected points (curve 3) of Figure 8.89 appears to have provided the best overall fit to the force-displacement curves from the tests studied. This method yielded an ultimate lateral pipeline load within approximately -6% to +18% of that found experimentally based on an evaluation of the four tests presented above.

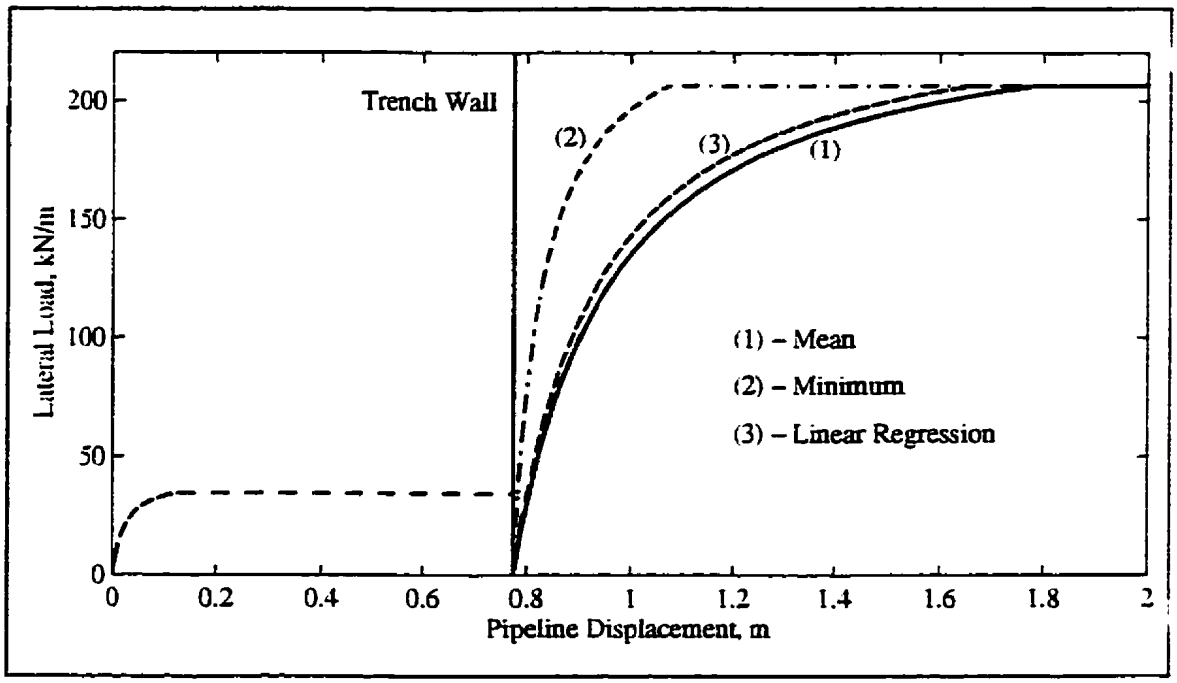

Figure 8.90 - Comparison of the three methods of predicting the distance to ultimate load, undrained tests.

Normalized Resistance Approach - Undrained Analysis

Figures 8.34, 8.35, and 8.36 presented data regarding the normalized resistance at specified displacements as both a regression and conservative bound. These data have been used to generate the theoretical prototype-scale force-displacement curves shown in Figure 8.92. Interaction in the backfill has again been represented using the method proposed in Subsection 8.2.9. The hyperbolic form of the curve between the trench wall and 0.5D penetration has been chosen to be represented by Equations [2-4], [2-5], and [2-6] for no other reason than the fact that by trial and error, this form of equation gave a reasonable approximation to the trend of the experimental data. Interaction between 0.5D and 1D of pipe penetration was represented as a straight line as indicated in Figure 8.92. Also

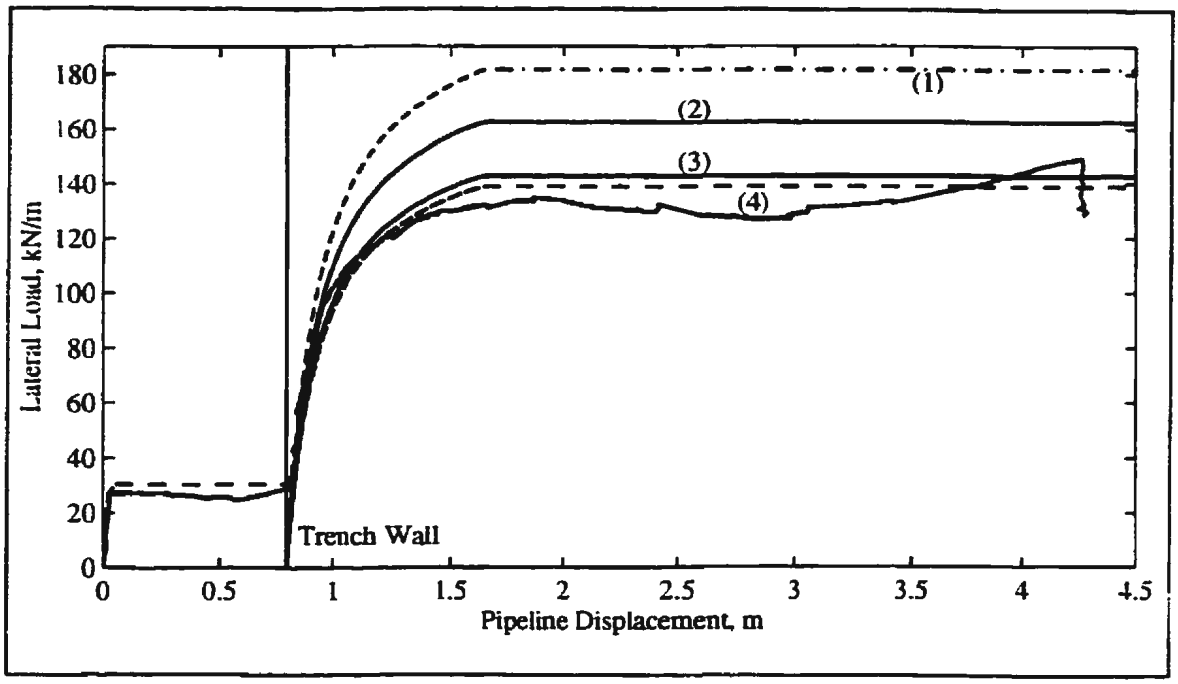

Figure 8.91a - Predicted undrained ultimate loads and p-y curve formulation based on the interaction factor approach and compared with Pipeline #1, Test 01, data.

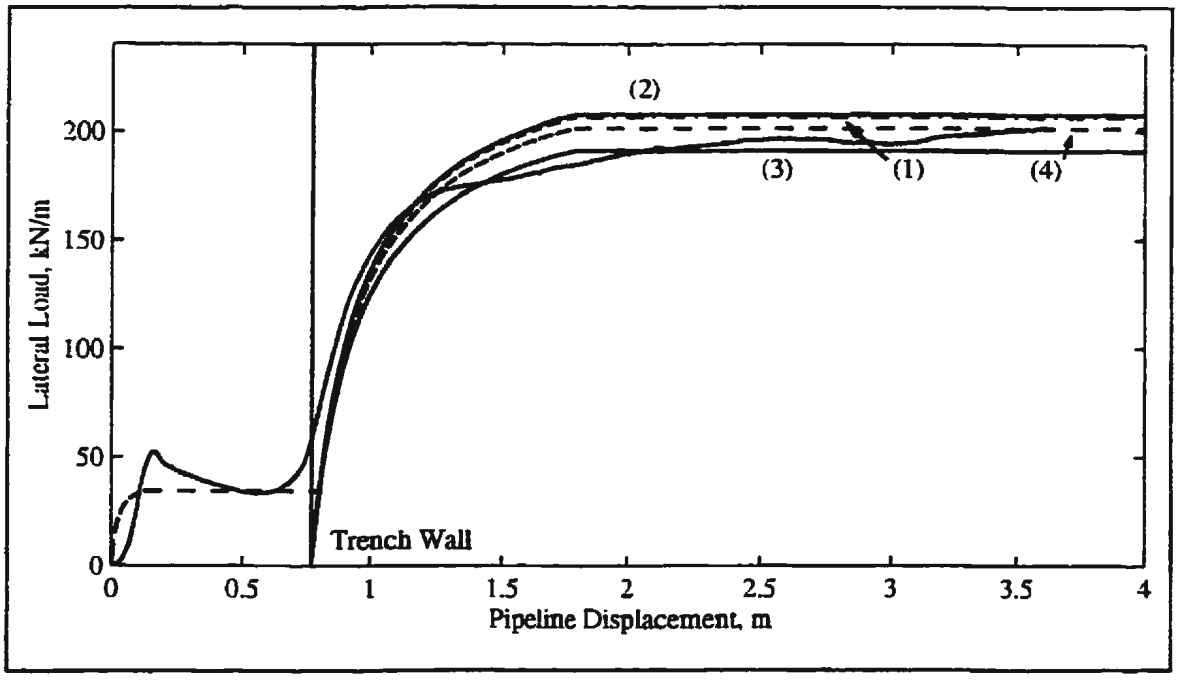

Figure 8.91b - Predicted undrained ultimate loads and p-y curve formulation based on the interaction factor approach and compared with Pipeline #1, Test 02, data.

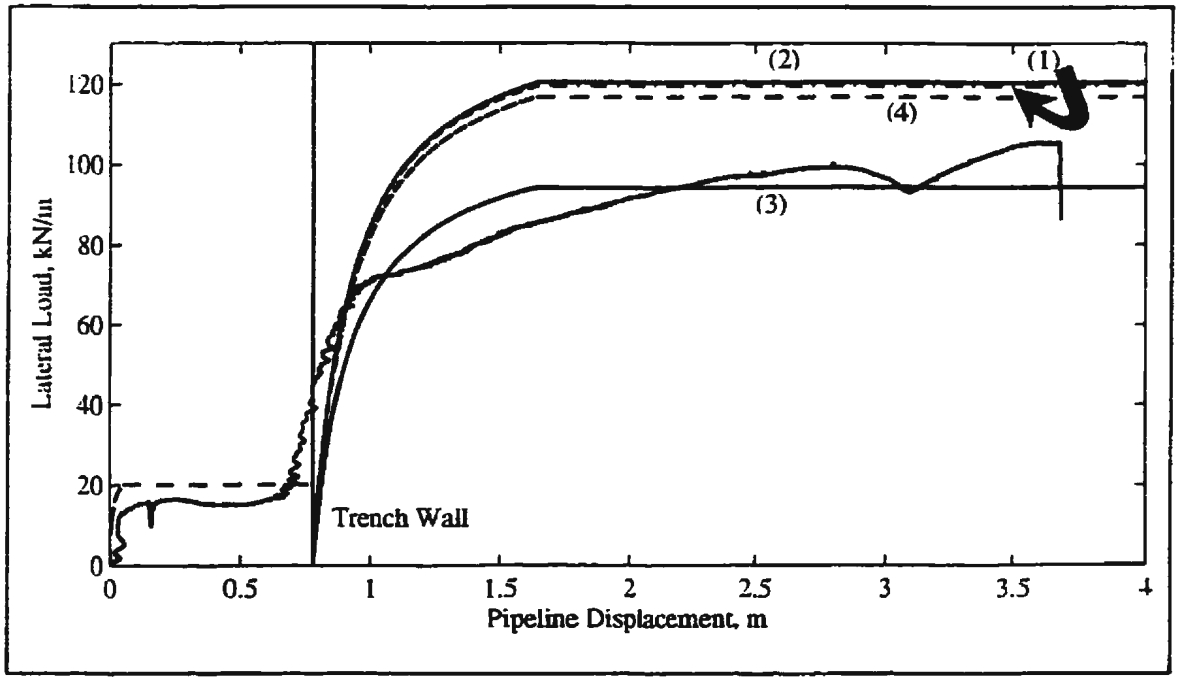

Figure 8.91c - Predicted undrained ultimate loads and p-y curve formulation based on the interaction factor approach and compared with Pipeline #3, Test 05, data.

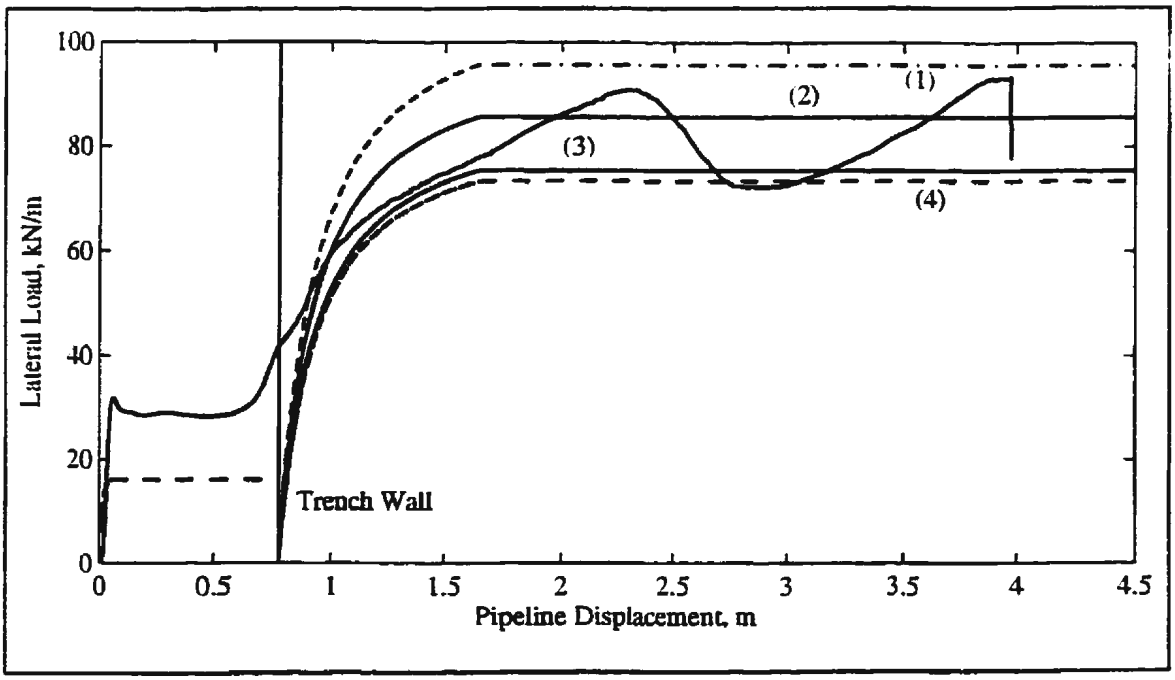

Figure 8.91d - Predicted undrained ultimate loads and p-y curve formulation based on the interaction factor approach and compared with Pipeline #4, Test 08, data.

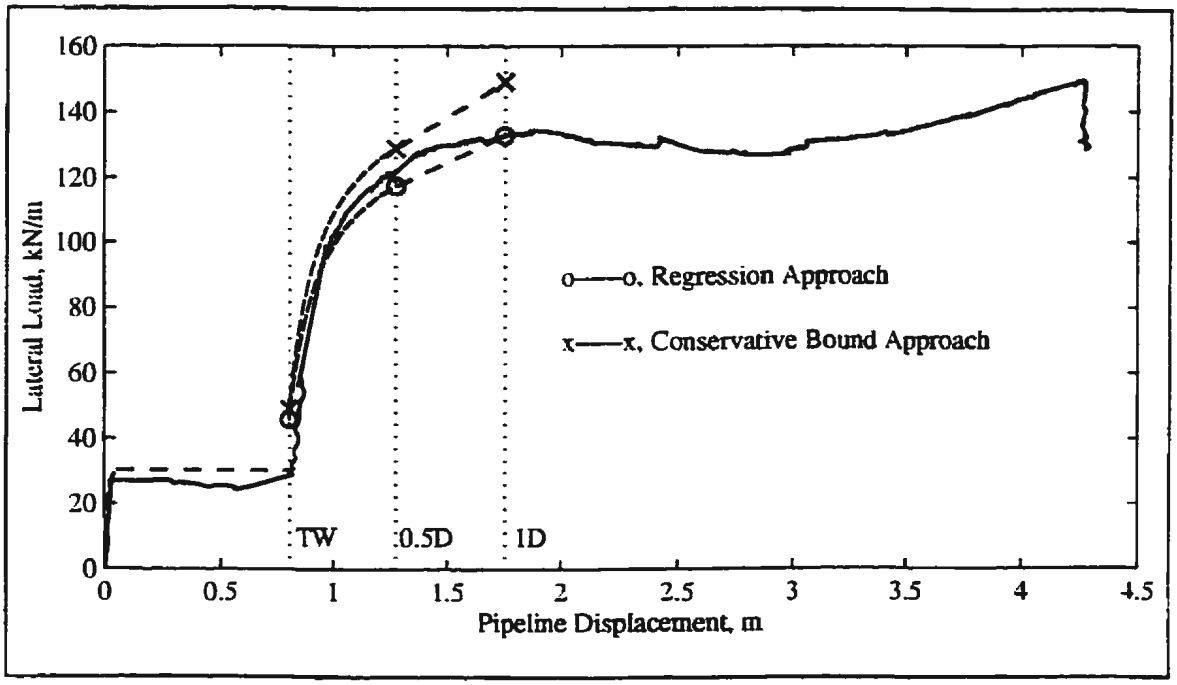

Figure 8.92a - Predicted undrained p-y curve forms based on the normalized resistance approach and compared with Pipeline #1, Test 01, data.

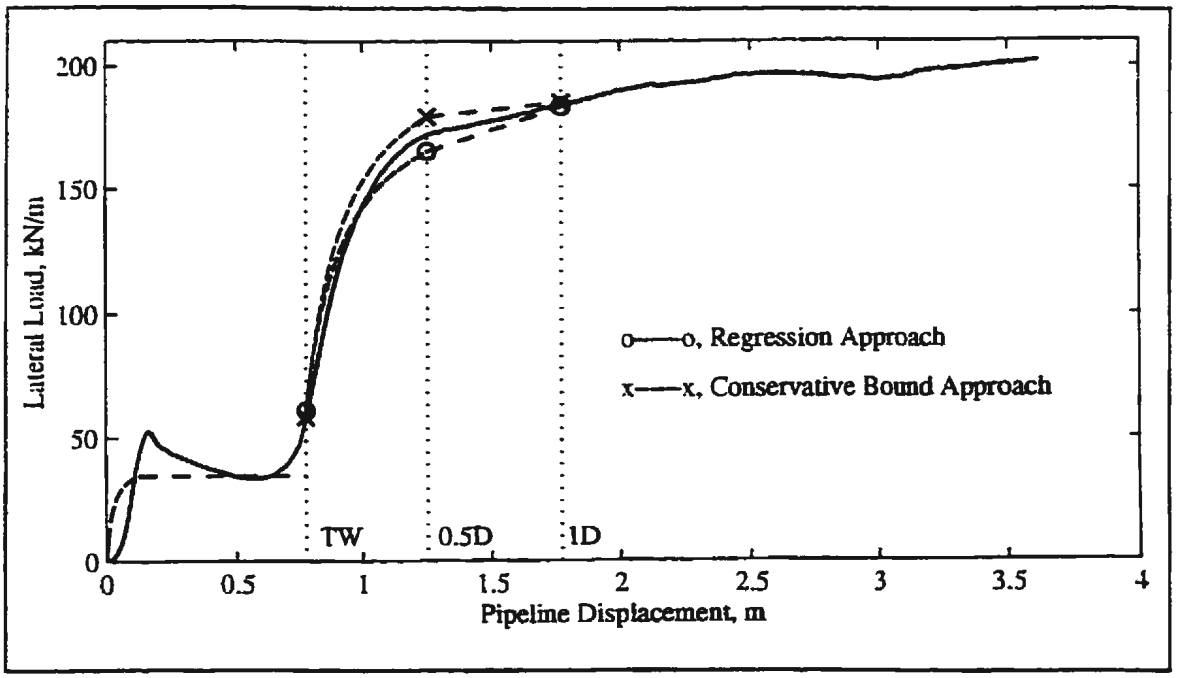

Figure 8.92b - Predicted undrained p-y curve forms based on the normalized resistance approach and compared with Pipeline #1, Test 02, data.

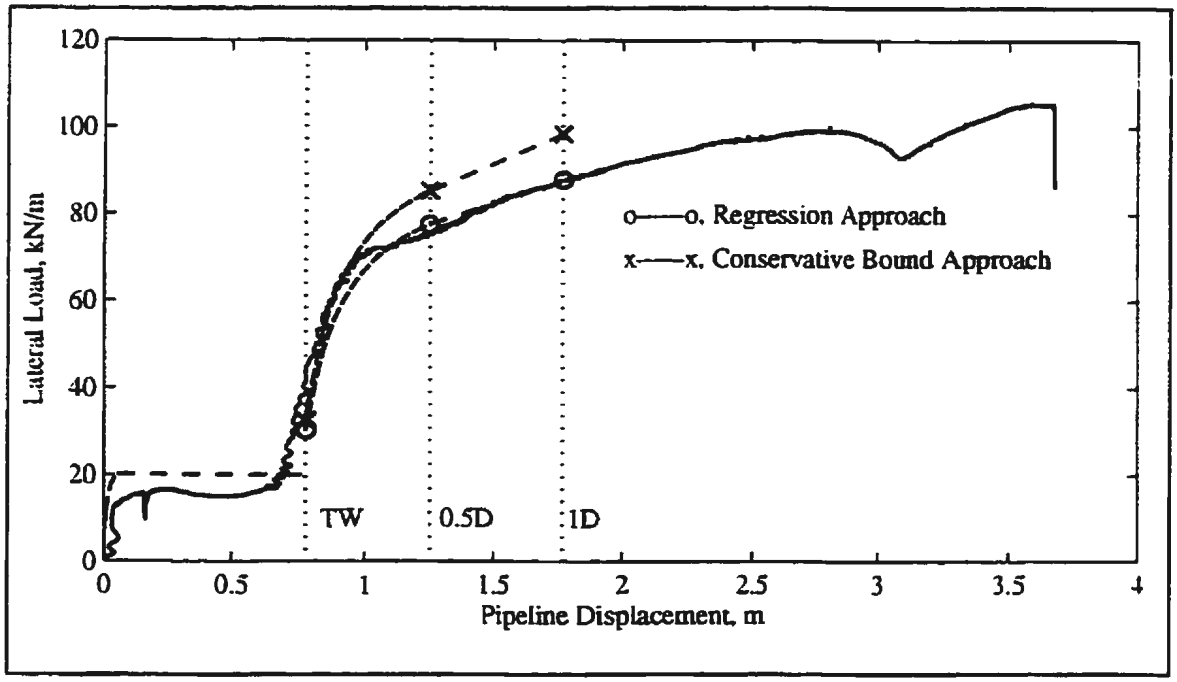

Figure 8.92c - Predicted undrained p-y curve forms based on the normalized resistance approach and compared with Pipeline #3, Test 05, data.

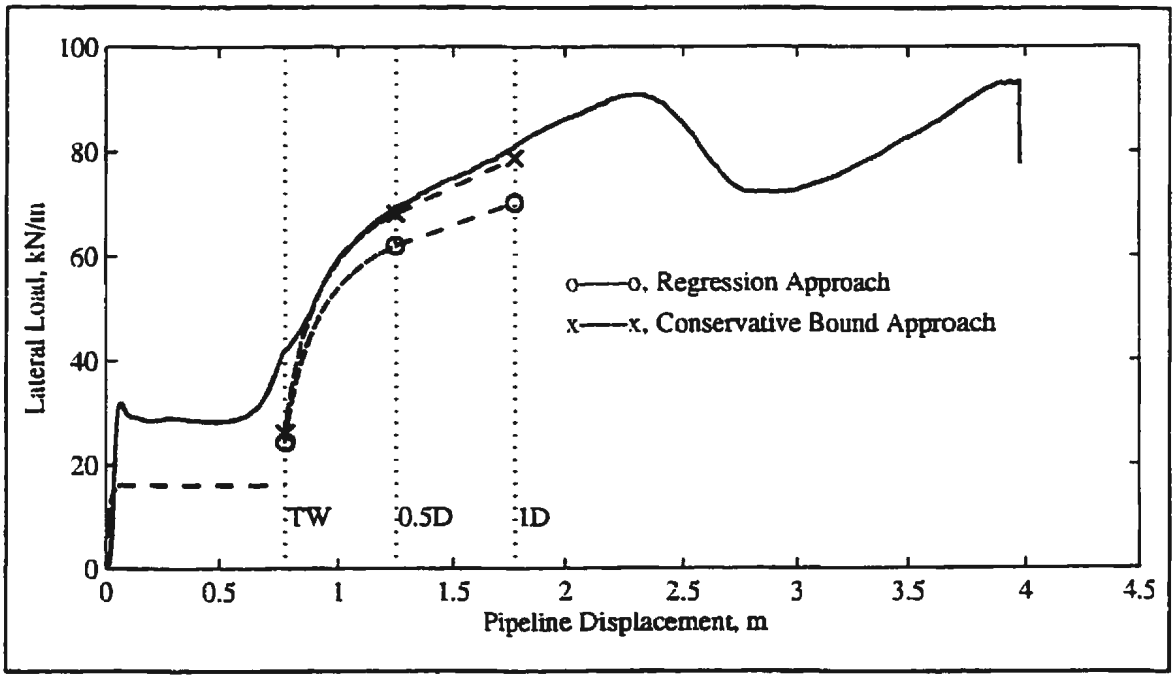

Figure 8.92d - Predicted undrained p-y curve forms based on the normalized resistance approach and compared with Pipeline #4, Test 08, data.

presented in Figure 8.92 are the experimental force-displacement data being compared in this subsection; Pipeline #1, Test 01; Pipeline #1, Test 02; Pipeline #3, Test 05; and Pipeline #4, Test 08. It appears for the most part that the experimental force-displacement data has been bounded by the two approaches at least up to a displacement equivalent to a penetration of 1 pipeline diameter.

Bilinear Analysis Approach - Undrained Analysis

Data pertaining to the bilinear analysis of normalized force-displacement curves were analysed in Subsection 8.1.9 and presented in Figure 8.37 through Figure 8.40. To the data, regression lines and conservative bounds were fitted as shown in the figures. Prototype-scale experimental force-displacement curves from the tests under consideration are presented in Figure 8.93. Superimposed on the experimental curves are the regressive and conservative results from Subsection 8.1.9 based on: the slope of the interaction before breakover; the normalized resistance at breakover; the distance into the trench wall to breakover; and the slope of the interaction after breakover. These data are only plotted to a pipeline displacement equivalent to 1 diameter into the trench wall as indicated on the figure. Interaction in the backfill is as before. For the most part, the theoretical predictions provide a reasonable approximation to the experimental data although the approach does not seem to provide as good an overall fit as the normalized resistance approach.

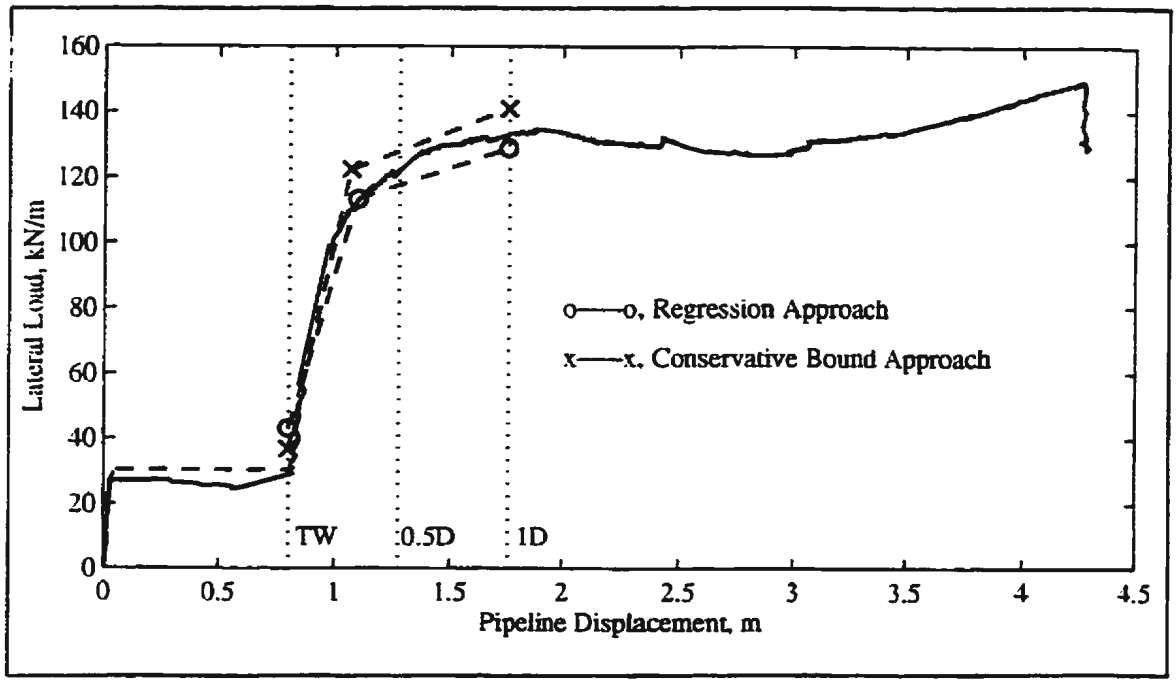

Figure 8.93a - Predicted undrained p-y curve forms based on the bilinear analysis approach and compared with Pipeline #1, Test 01, data.

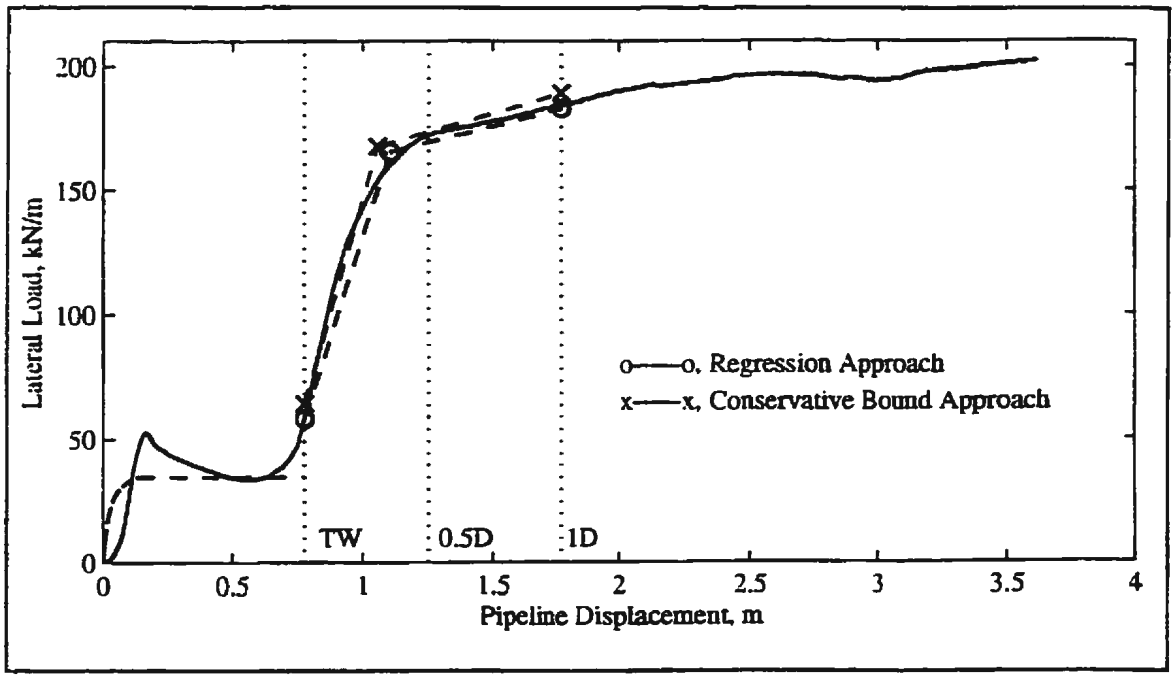

Figure 8.93b - Predicted undrained p-y curve forms based on the bilinear analysis approach and compared with Pipeline #1, Test 02, data.

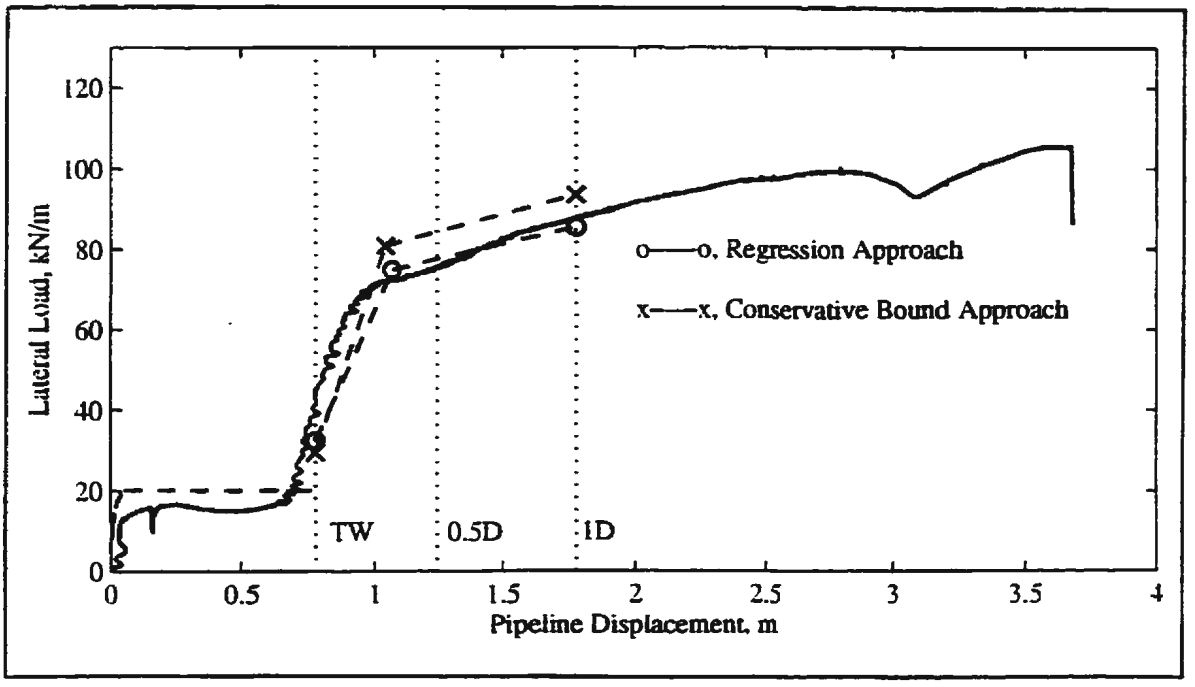

Figure 8.93c - Predicted undrained p-y curve forms based on the bilinear analysis approach and compared with Pipeline #3, Test 05, data.

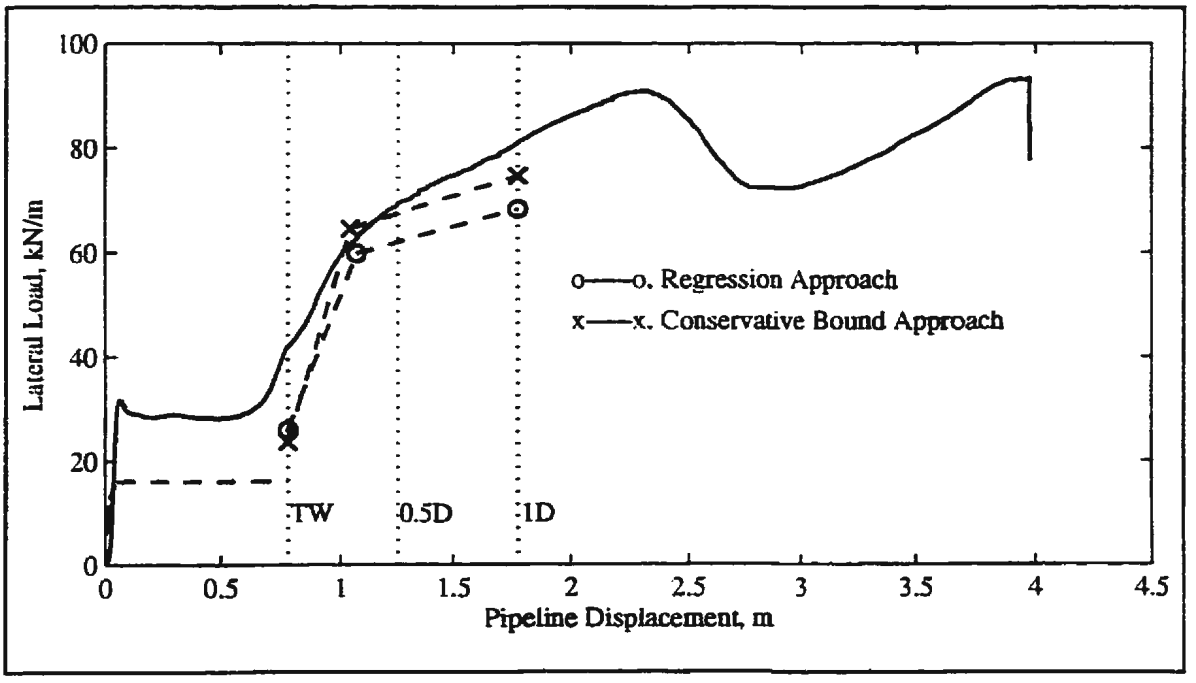

Figure 8.93d - Predicted undrained p-y curve forms based on the bilinear analysis approach and compared with Pipeline #4, Test 08, data.

Curve Fitting Approach - Undrained Analysis

In Subsection 8.2.8, curves were fit to selected normalized undrained data and typical results were demonstrated in Figures 8.77 through 8.81. These formulations have been used to generate the theoretical prototype-scale force-displacement curves shown in Figure 8.94. Interaction in the backfill is as before. Peak lateral resistance has been calculated based on Method 3 of the interaction factor approach (Equation [8-49]) above and a distance to ultimate load defined by the linear regression through the data of Figure 8.32 (Equation [8-9]). As to be expected, the bilinear curve fit gives a crude approximation to the experimental results. Overall, the developed hyperbolic and polynomial functions provide a reasonable approximation to the experimental force-displacement curves. Up to a displacement of 1D, the predictions are typically 90 to 110% of the experimentally-derived prototype-scale pipeline loading.

Rate Variation from Drained to Undrained Interaction

Analysis to this point has indicated that it is not possible to assess a drained interaction factor in its true form because tests which were considered drained exhibit no clearly defined peak in their force-displacement response. Therefore, it seems more appropriate to use a normalized resistance approach (or perhaps a bilinear analysis approach) as was done with selected undrained test results. Figures 8.47 through 8.49 present normalized resistances as a function of interaction rate at the trench wall, at 0.5D penetration, and at 1D penetration. The linear fit through the data in semilog space has been used for the regressive approach while the dash-dot line indicated on the upper plots indicates the

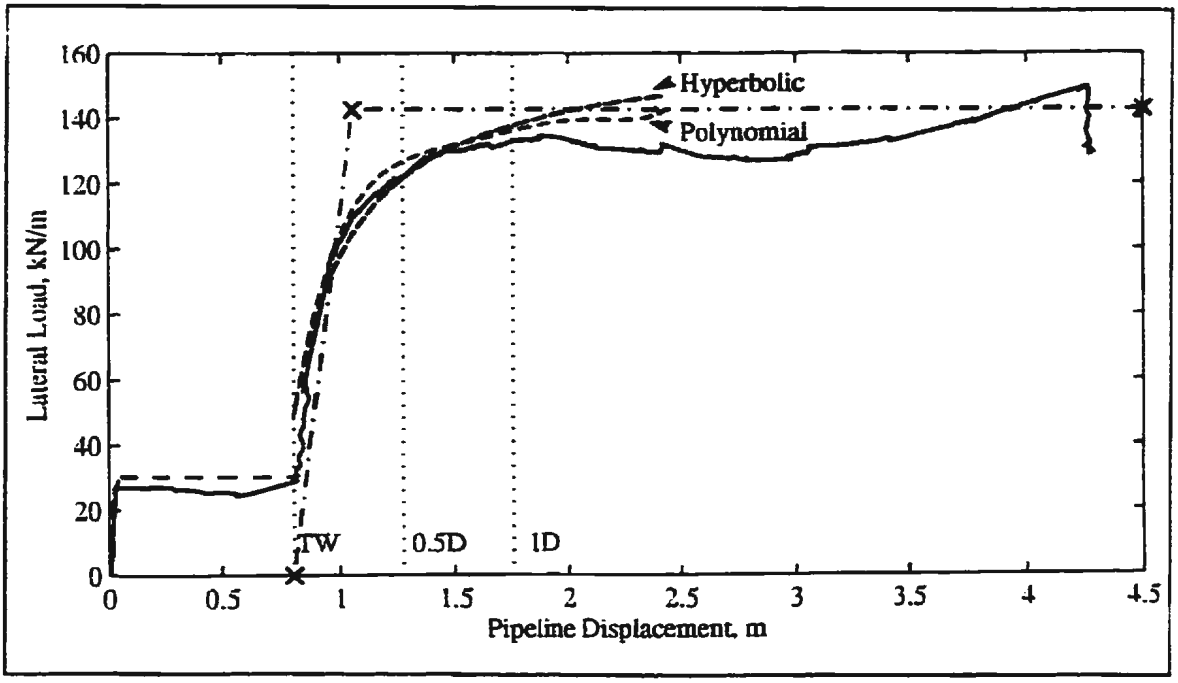

Figure 8.94a - Predicted undrained p-y curve forms based on the curve fitting approach and compared with Pipeline #1, Test 01, data.

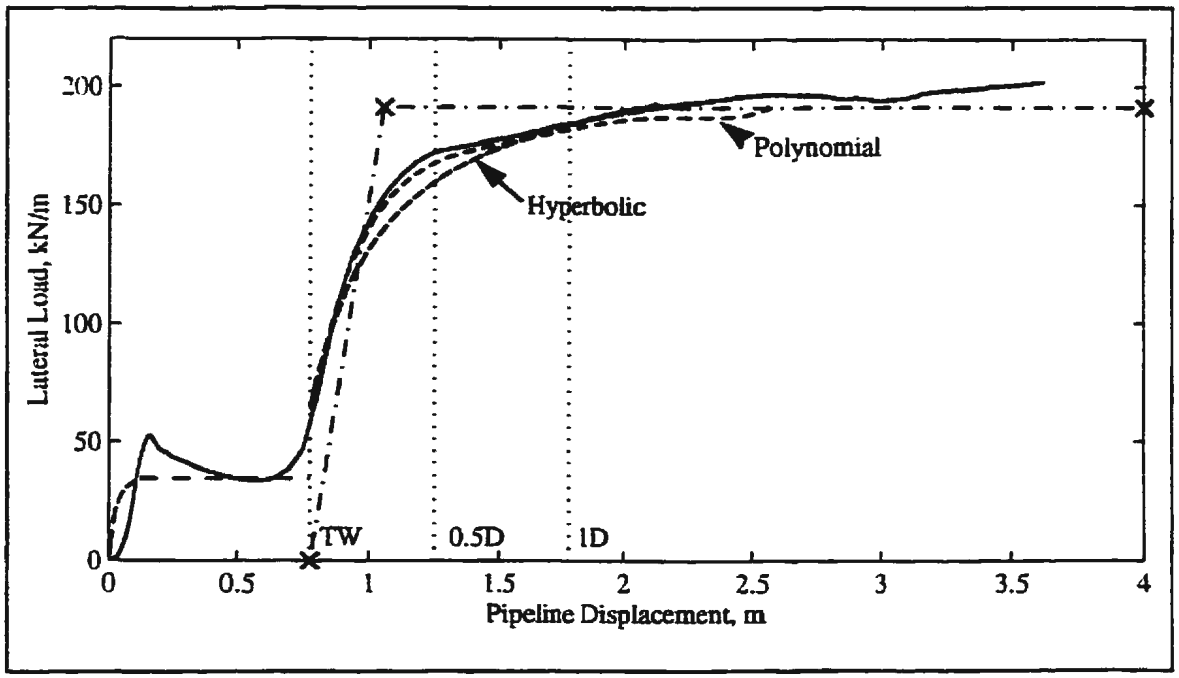

Figure 8.94b - Predicted undrained p-y curve forms based on the curve fitting approach and compared with Pipeline #1, Test 02, data.

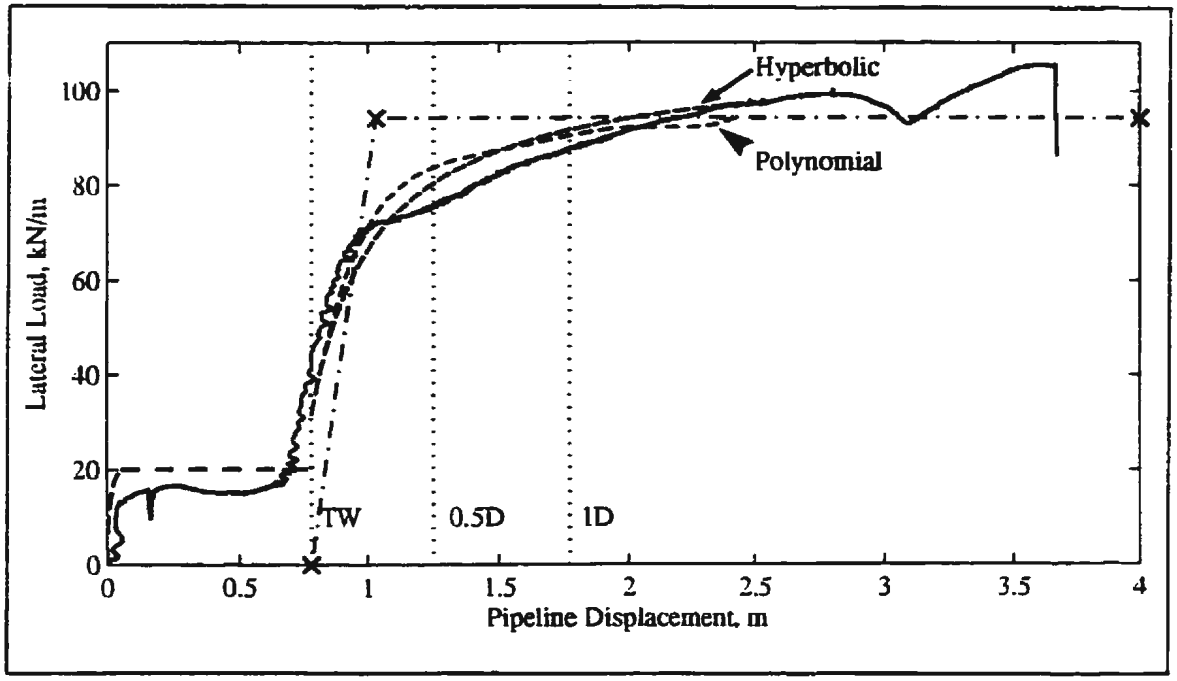

Figure 8.94c - Predicted undrained p-y curve forms based on the curve fitting approach and compared with Pipeline #3, Test 05, data.

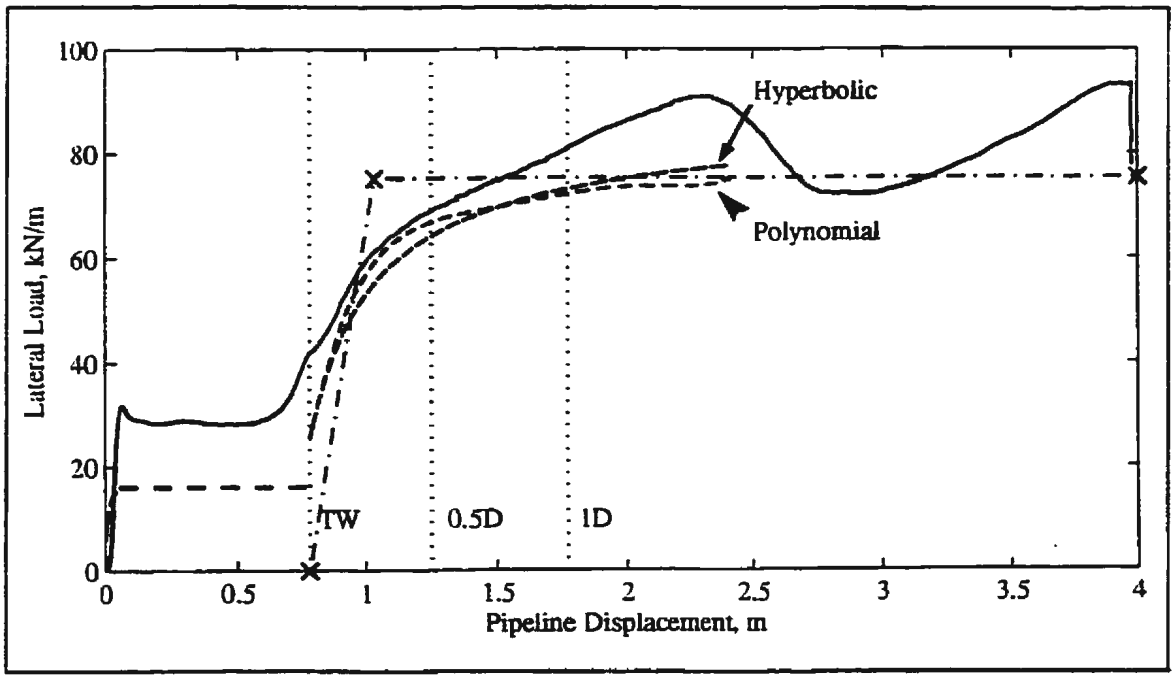

Figure 8.94d - Predicted undrained p-y curve forms based on the curve fitting approach and compared with Pipeline #4, Test 08, data.

conservative bound utilized. These relationships have been used to generate the theoretical prototype-scale force-displacement curves presented in Figure 8.95. In this case, input parameters from Test 04 (Pipelines #1 through #4) have been used as this test covered the range of interaction rates of interest; from drained to undrained conditions. Prototype-scale force-displacement curves derived from the experimental data are also presented with the theoretical predictions. Interaction in the backfill has been calculated as before but, for the tests which were considered drained, is only plotted in this form to a displacement of 0.1m after which the response is considered linear to the resulting load at the trench wall. For Pipeline #1, Pipeline #2 and the conservative prediction of Pipeline #3, the force-displacement responses have been presented as straight line segments. For the remainder of the predictions, the hyperbolic form of the curve between the trench wall and 0.5D penetration has been presented according to Equation [2-4]. With the exception of Pipeline #2, the regression analysis generally provided reasonable predictions to the experimental data; generally the predictions were 90 to 110% of the experimentally-derived values up to a displacement equivalent to a penetration of 1 pipeline diameter.

Curve Fitting Approach - Drained Analysis

Curves were fit to selected normalized drained data in Subsection 8.2.8 as demonstrated in Figures 8.82 and 8.83. Prototype-scale force-displacement curves from Test 04 (Pipeline #1), Test 07 (Pipeline #1), Test 08 (Pipeline #1) and Test 09 (Pipeline #1) are presented in Figure 8.96. Formulations from the curve fitting generated in Subsection 8.2.8 have been used to generate the theoretical prototype-scale force-displacement curves shown in

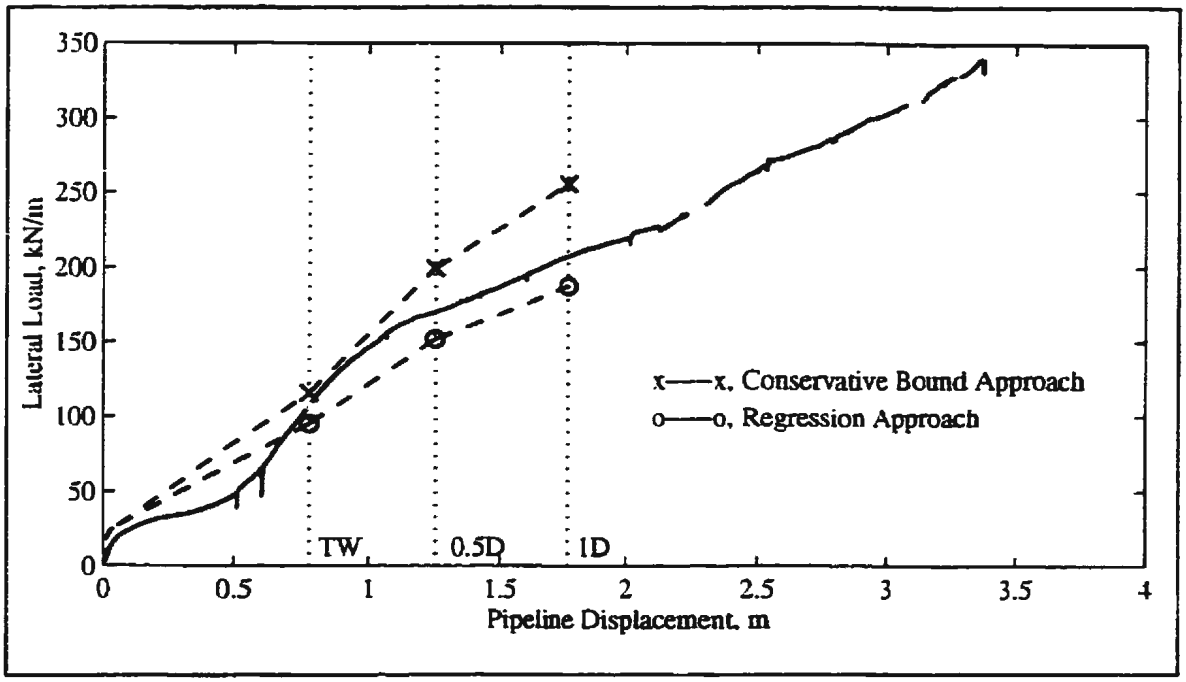

Figure 8.95a - Predicted p-y curves based on variation of normalized resistance with rate and compared with Pipeline #1, Test 04, data.

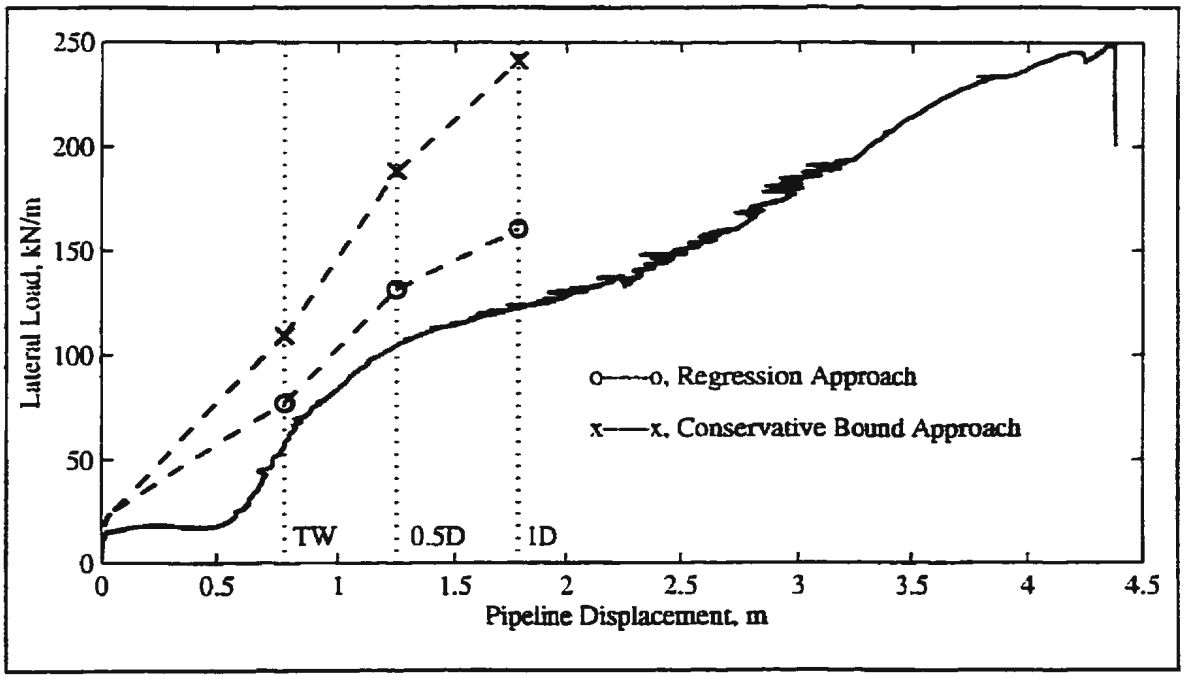

Figure 8.95b - Predicted p-y curves based on variation of normalized resistance with rate and compared with Pipeline #2, Test 04, data.

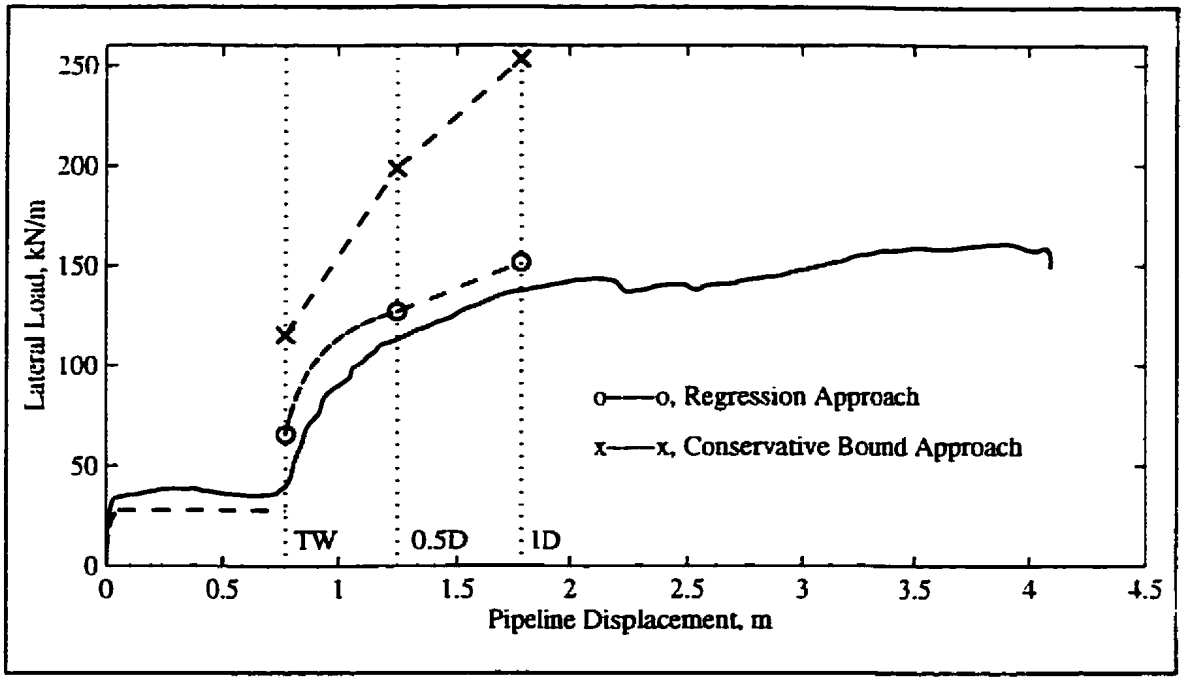

Figure 8.95c - Predicted p-y curves based on variation of normalized resistance with rate and compared with Pipeline #3, Test 04, data.

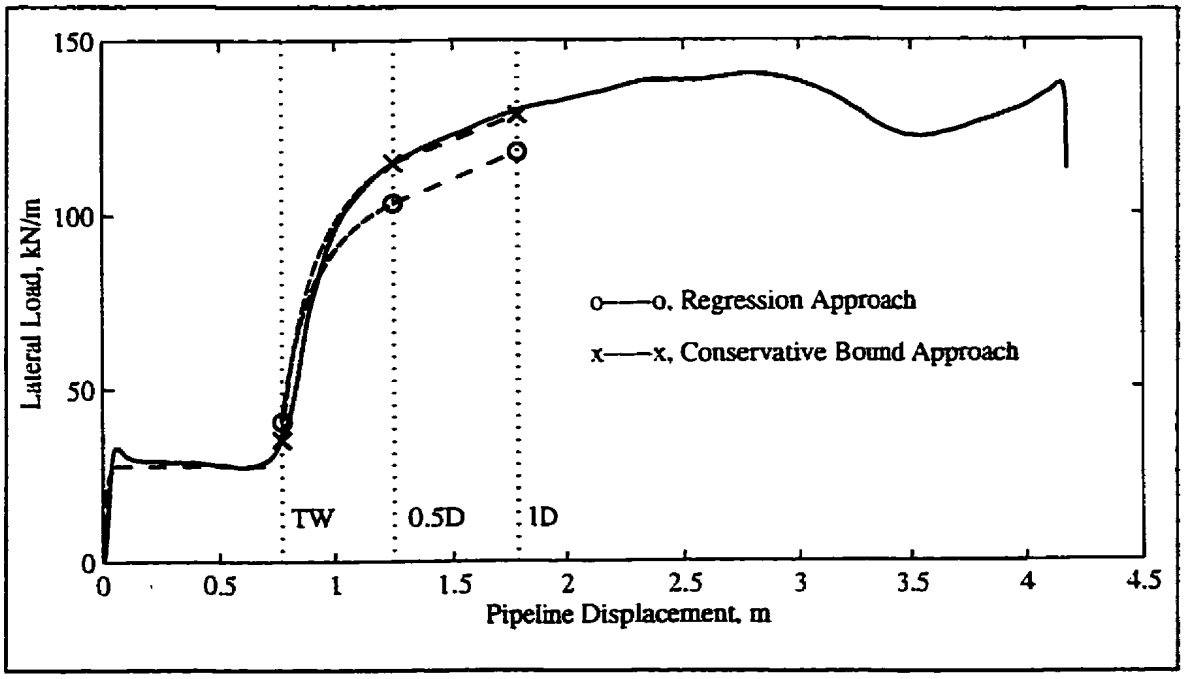

Figure 8.95d - Predicted p-y curves based on variation of normalized resistance with rate and compared with Pipeline #4, Test 04, data.

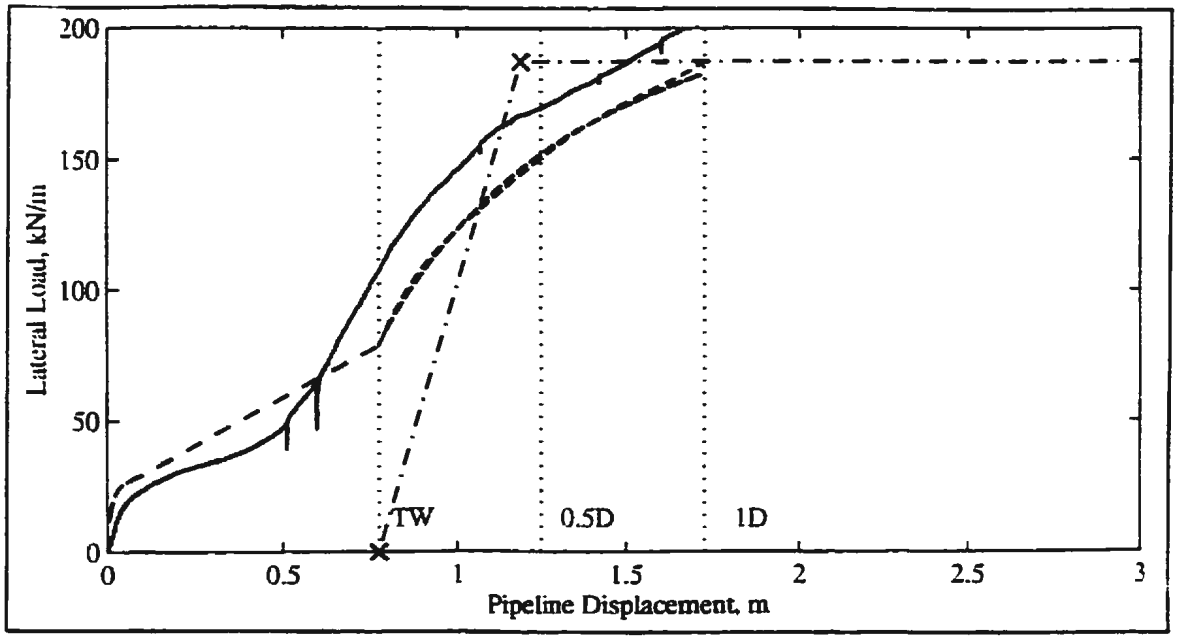

Figure 8.96a - Predicted drained p-y curve forms based on the curve fitting approach with load at 1D penetration based on the regression approach of Figure 8.49b and compared with Pipeline #1, Test 04, data.

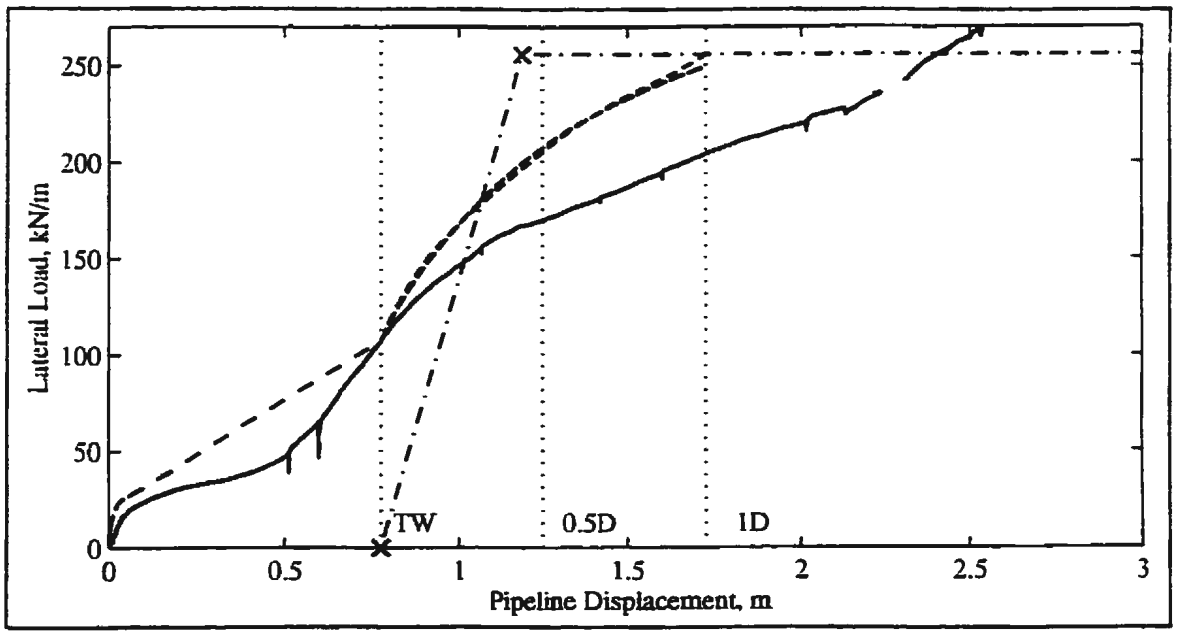

Figure 8.96b - Predicted drained p-y curve forms based on the curve fitting approach with load at 1D penetration based on the conservative approach of Figure 8.49a and compared with Pipeline #1, Test 04, data.

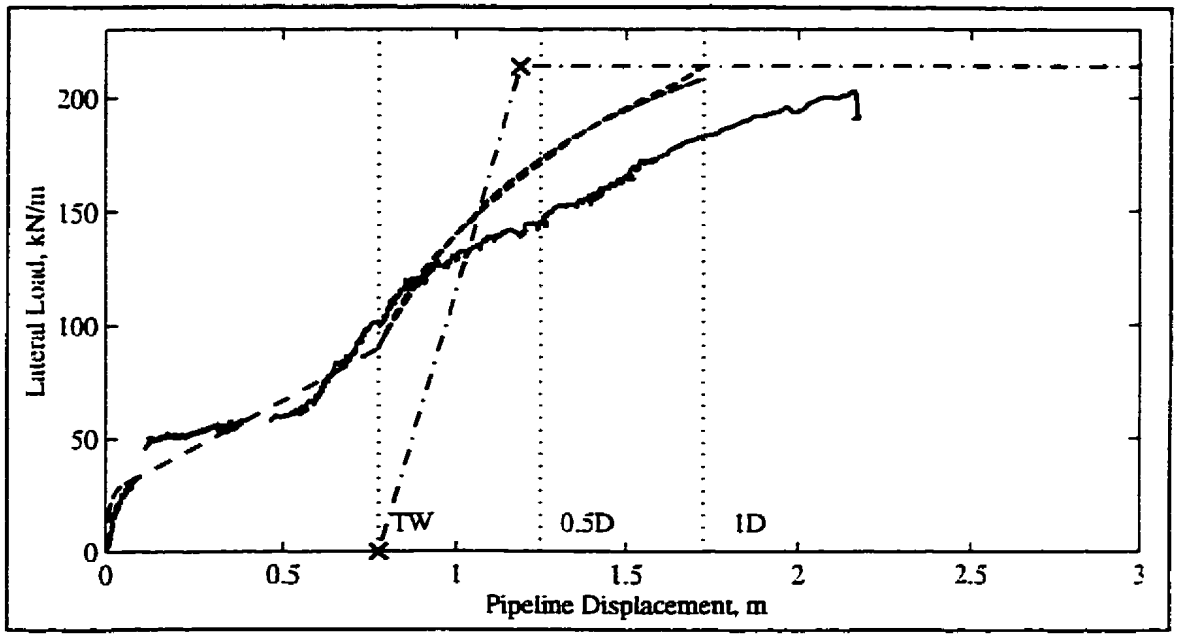

Figure 8.96c - Predicted drained p-y curve forms based on the curve fitting approach with load at 1D penetration based on the regression approach of Figure 8.49b and compared with Pipeline #1, Test 07, data.

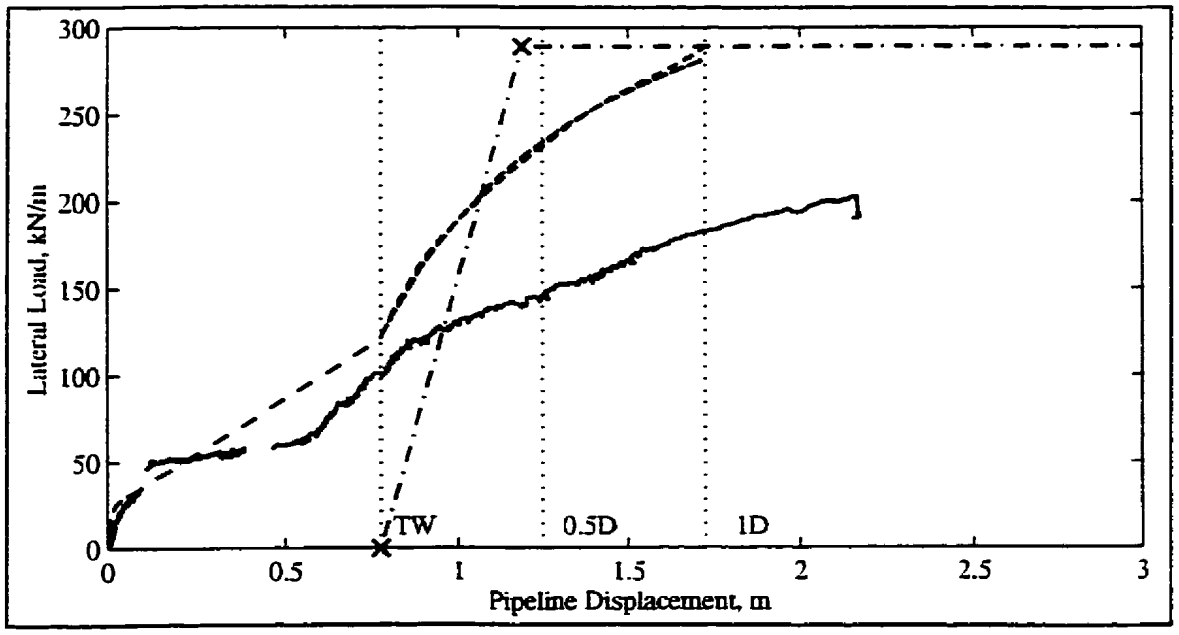

Figure 8.96d - Predicted drained p-y curve forms based on the curve fitting approach with load at 1D penetration based on the conservative approach of Figure 8.49a and compared with Pipeline #1, Test 07, data.

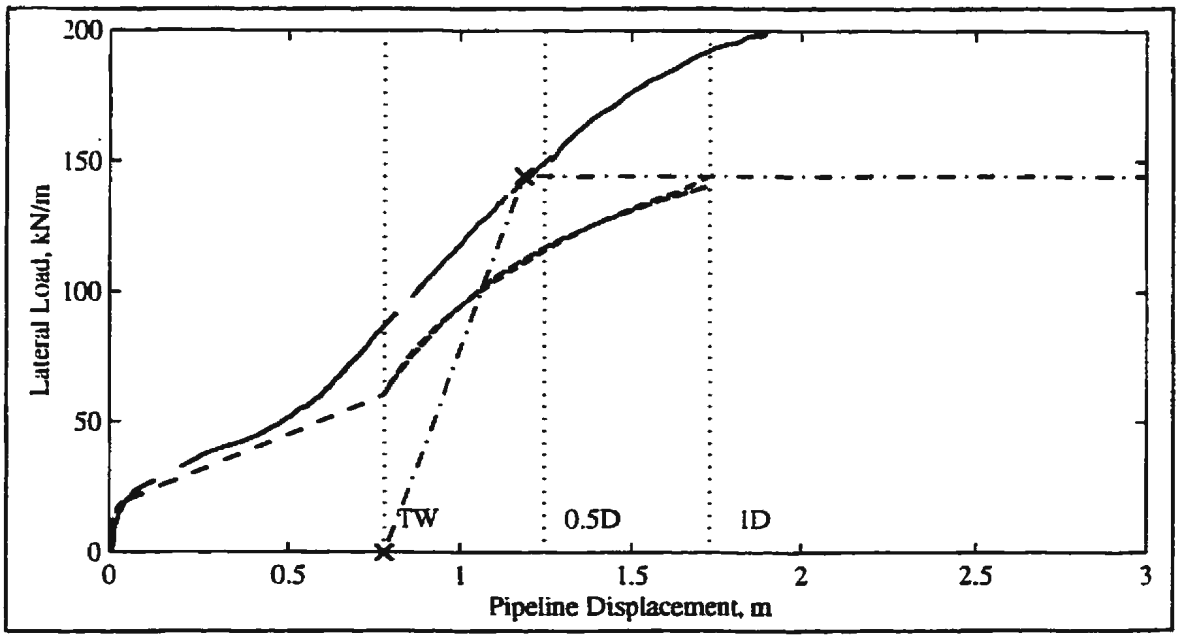

Figure 8.96e - Predicted drained p-y curve forms based on the curve fitting approach with load at 1D penetration based on the regression approach of Figure 8.49b and compared with Pipeline #1, Test 08, data.

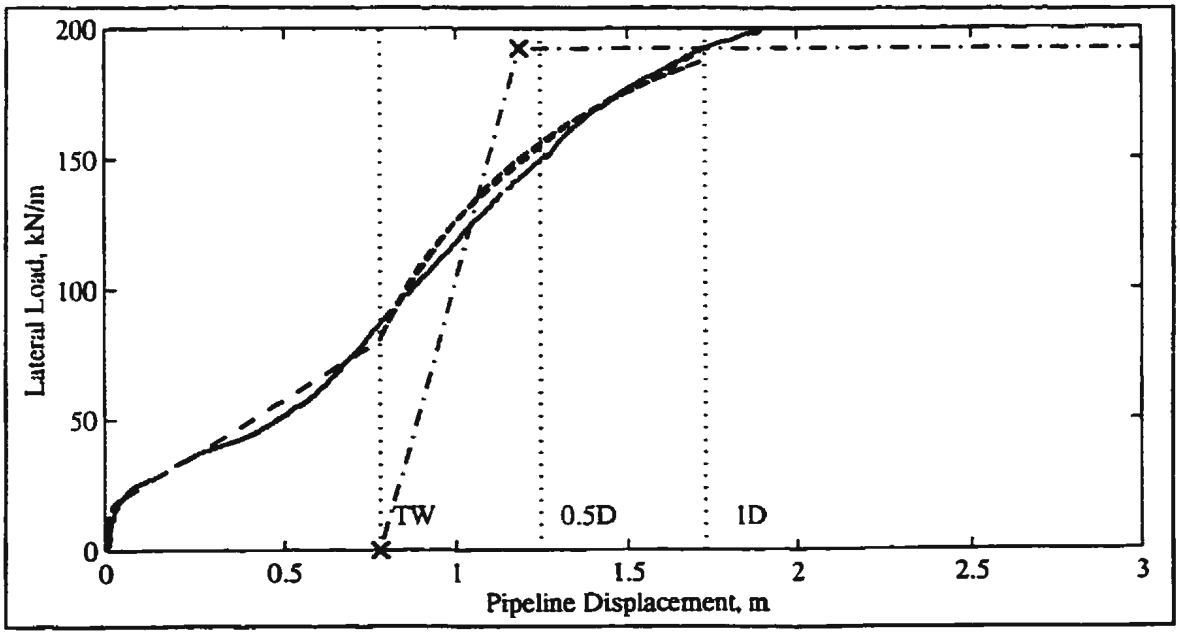

Figure 8.96f - Predicted drained p-y curve forms based on the curve fitting approach with load at 1D penetration based on the conservative approach of Figure 8.49a and compared with Pipeline #1, Test 08, data.

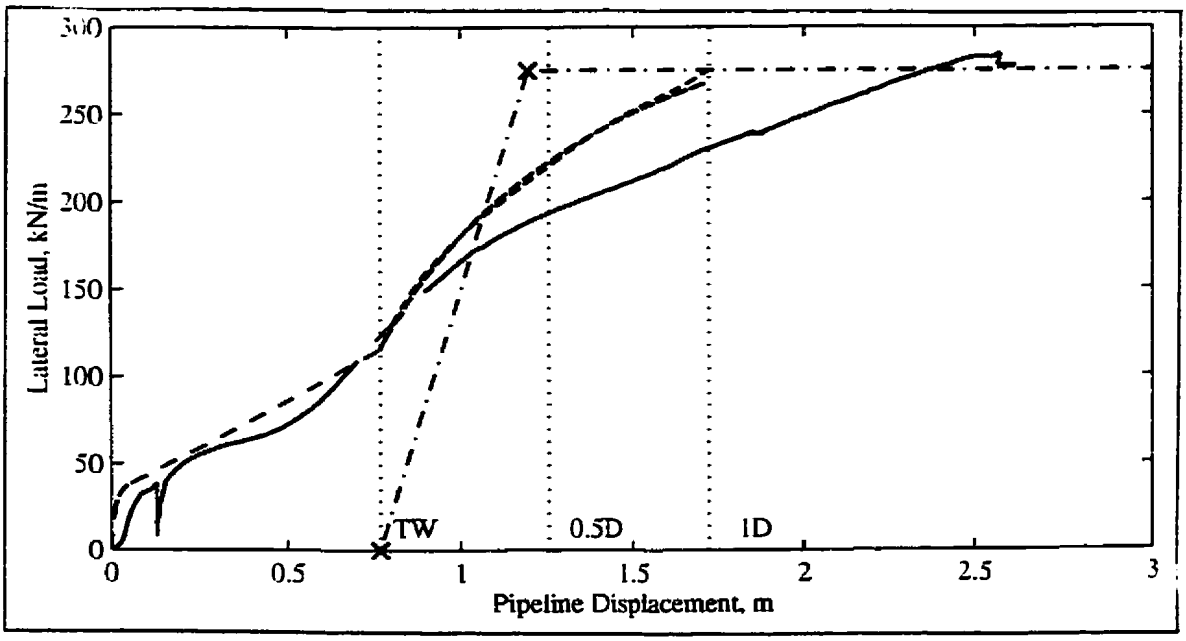

Figure 8.96g - Predicted drained p-y curve forms based on the curve fitting approach with load at 1D penetration based on the regression approach of Figure 8.49b and compared with Pipeline #1, Test 09, data.

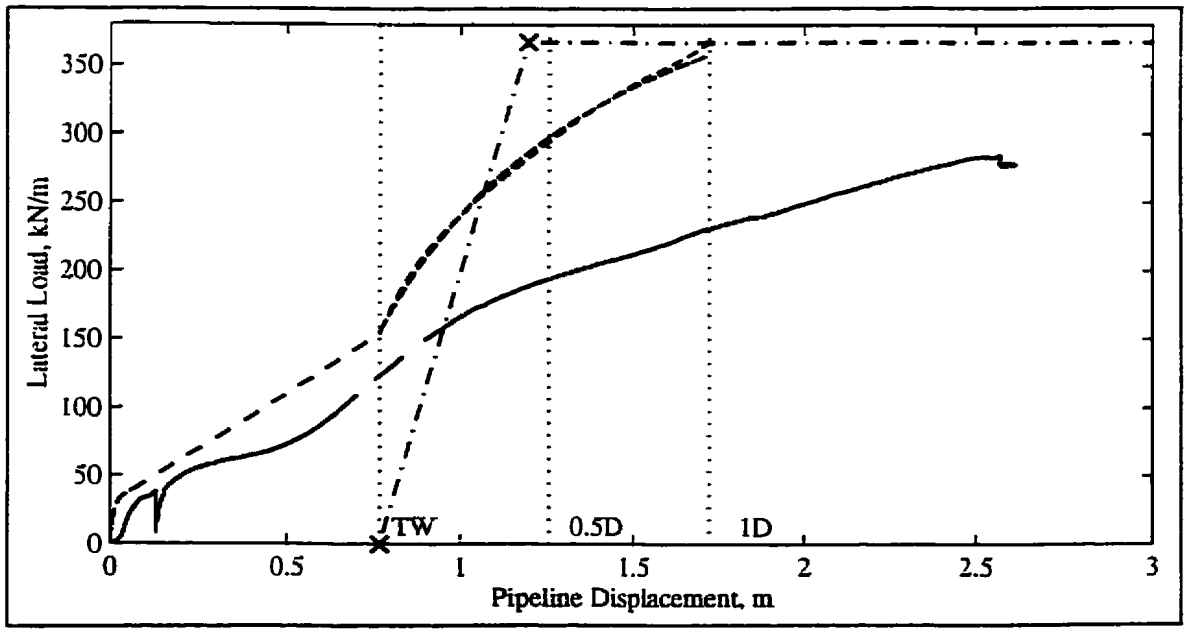

Figure 8.96h - Predicted drained p-y curve forms based on the curve fitting approach with load at 1D penetration based on the conservative approach of Figure 8.49a and compared with Pipeline #1, Test 09, data.

the figure. Interaction in the backfill has been generated as before for drained interaction. A peak lateral resistance has not been used rather the interaction has been calculated from the normalized resistance at a one diameter penetration from Figure 8.49. Both the regression approach from Figure 8.49b and the conservative approach from Figure 8.49a have been presented. The forms of the force-displacement curves have been presented in Table 8.3. In some cases, the regression approaches give the best fit to the data while in one case, the conservative approach yields the best fit. Overall, the hyperbolic or polynomial representations give the best fit to the data. At the trench wall, these representations yield values ranging from 70% to 94% of the values derived from the experimental data. At 0.5D, the theoretical curves are from 78 to 118% of the experimentally derived values and at 1D, this range is from 75 to 119% of the prototype-scale pipeline loading.

8.4 Analysis Based on Conventional Soil Mechanics Methods

8.4.1 Introduction

Specific theories (i.e. from anchors and piles) have been applied to the analysis of pipeline/soil interaction by a number of authors. It then stands to reason that other state-of-the-art solutions to the same type of problem should be assessed as to their suitability. From the experimental testing, it appears that the backfill generally does not add to the ultimate load that the pipeline is subjected. Therefore, analyses examined in this section are only applied where the pipeline moves through the stronger native material.

8.4.2 Subgrade Reaction Analysis Approach

The relationship between horizontal force and displacement is commonly known as the concept of subgrade reaction. The soil resistance against the horizontal movement of a pile, buried pipeline or conduit is generally called the coefficient of horizontal subgrade reaction, k_h. A limited review of current numerical formulations to estimate this coefficient is presented in this section and the applicability to the current problem assessed.

In the design of laterally loaded pile foundations, the governing criteria is often not the ultimate load a pile might be subjected to but rather the maximum deflection the pile will be subjected to at a working load (Poulos and Davis, 1980). One method to determine the load-deflection prediction within the elastic region for laterally loaded piles is the subgrade reaction approach (Poulos and Davis, 1980; Prakash and Sharma, 1990). As discussed previously, lateral pipeline/soil interaction might be considered to be analogous to a pile subjected to lateral soil movement.

In the subgrade reaction analysis, the pile may be modelled as a beam on an elastic foundation. It is assumed the soil surrounding the pile can be represented by a series of horizontal springs. As horizontal loading forces the pile against the soil, the soil deforms elastically and resists the movement of the pile. The elastic reaction of the soil is assumed to be equivalent to the force that would be generated by a spring representing the soil subjected to the same deformation. For a linear feature, the soil is modelled using a series of closely-spaced independent and linear elastic soil springs (Canadian Foundation

Engineering Manual, 1992). The modulus or coefficient of subgrade reaction is the equivalent spring constant and is expressed as

$$k_h = \frac{p}{y} \qquad [8\text{-}49]$$

where p is the soil reaction at a point on the pile (per unit length of pile) and y is the deflection at that point (Prakash and Sharma, 1990). The coefficient is considered somewhat difficult to evaluate (Canadian Foundation Engineering Manual, 1992); however, a number of empirical correlations are available for determining the modulus (Poulos and Davis, 1980).

A limited review of the literature has yielded a number of formulations to determine the coefficient of horizontal subgrade reaction primarily from laterally loaded pipelines and piles. These are summarized in Appendix M and include formulations for both cohesive and cohesionless soils. The cohesive soil formulations have been evaluated for Pipeline #1 of Test 01 and Pipeline #4 of Test 04 and selected suggested responses are presented in Figure 8.97. Selected cohesionless soil formulations are presented for Pipeline #1, Test 04, in Figure 8.98. In both cases, origins have been set with the start of interaction with the trench wall and responses not shown were as stiff or stiffer than those presented.

In the cohesive soil, the interaction is reasonably approximated by some of the subgrade reaction formulations up to approximately 50 to 60% of the ultimate resistance. In the cohesionless soil formulations, no reasonable approximations resulted.

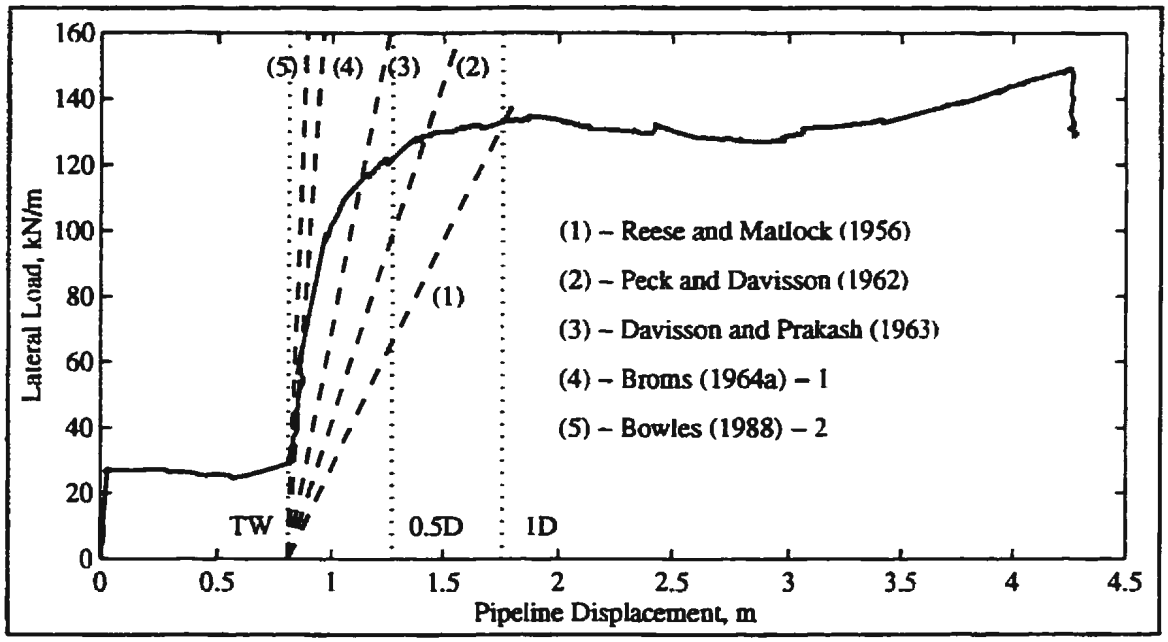

Figure 8.97a - Suggested subgrade reactions for cohesive soils which have been evaluated in terms of normalized force-displacement. Origins have been set with respect to the trench wall and results are compared with Pipeline #1, Test 01, data.

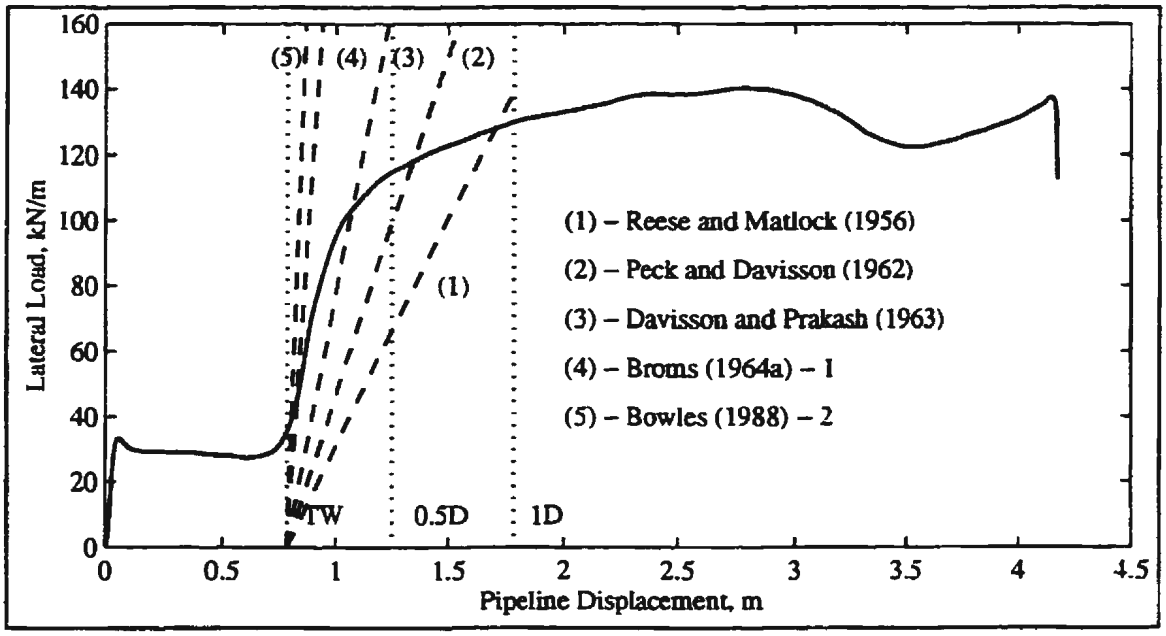

Figure 8.97b - Suggested subgrade reactions for cohesive soils which have been evaluated in terms of normalized force-displacement. Origins have been set with respect to the trench wall and results are compared with Pipeline #4, Test 04, data.

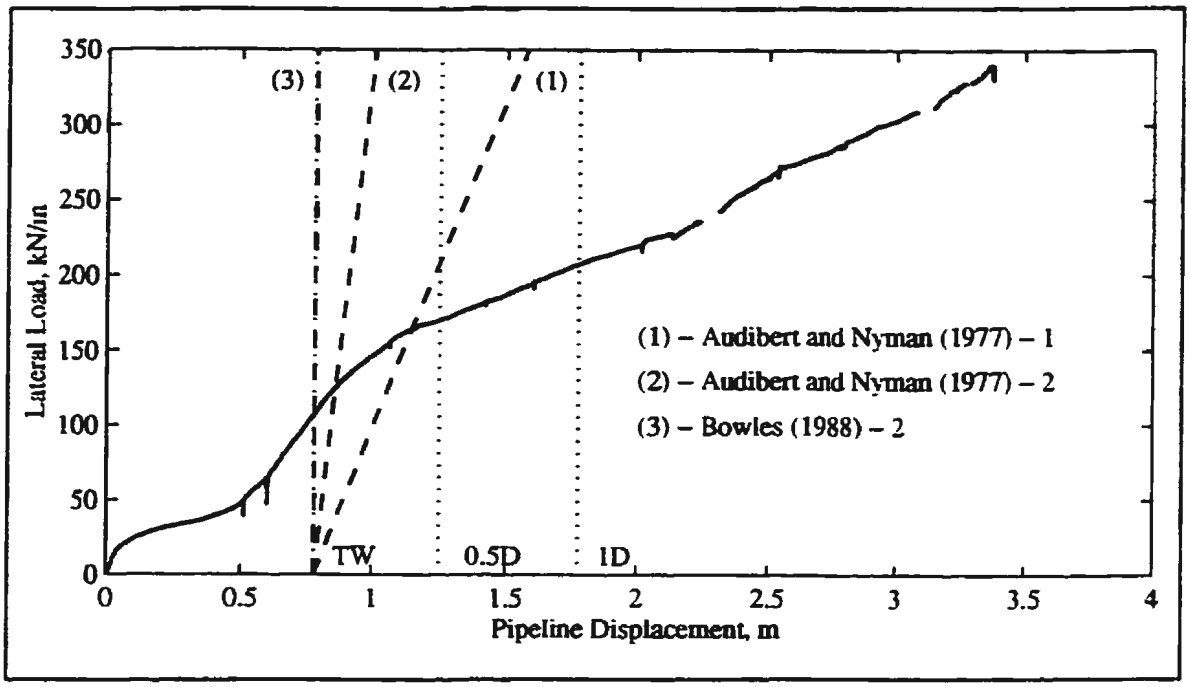

Figure 8.98 - Suggested subgrade reactions for cohesionless soils evaluated in terms of normalized force-displacement. Origins have been set with respect to the trench wall and results are compared with Pipeline #1, Test 04, data.

8.4.3 Anchor Plate/Soil Interaction

In Section 8.3, experimental undrained interaction factors and drained ultimate loads were compared to values determined using accepted pipeline/soil interaction methods from the literature. Some of these accepted methods were based on the interaction between horizontally loaded vertical anchor plates and the surrounding soil. If these methods are thought to apply, then other similar methods of anchor plate/soil interaction might also apply. A limited review of the literature has revealed formulations for undrained, frictional, and c-ϕ interactions. These formulations were obtained from the following authors for cohesive soils: Meyerhof (1973); Kovacs *et al.* (1975); Rowe and Davis (1982a); Das *et al.* (1985); and Das *et al.* (1987). Formulations for anchor plates

in cohesionless soils include: Teng (1962); Meyerhof (1973); Neely *et al.* (1973); and Rowe and Davis (1982b). The only method found for analysing horizontally loaded vertical anchor plates in a c-ϕ soil was provided by Rowe and Davis (1982b).

Ultimate lateral loads based on the cohesive soil formulations are presented in Figure 8.99 and summarized in Table 8.5a. The loads were calculated using input parameters from: Pipeline #1, Test 01; Pipeline #1, Test 02; Pipeline #3, Test 05; and Pipeline #4, Test 08. The corresponding prototype-scale experimentally derived force-displacement curves from the pipeline tests are also plotted on the figures. Overall, the ultimate resistance of the pipeline/soil interaction was best estimated using the Rowe and Davis (1982a) method. Using this method yields an ultimate lateral load within 20% for three of the four cases studied. However, for Pipeline #1, Test 02, the method overpredicted the experimental load by about 30%.

Prototype-scale experimentally derived force-displacement curves from tests which were considered drained are presented in Figure 8.100. These include: Pipeline #1, Test 04; Pipeline #1, Test 07; Pipeline #1, Test 08; and Pipeline #1, Test 09. Predicted ultimate lateral loads based on the cohesionless and c'-ϕ' soil formulations are also presented in the figures as well as in Table 8.5b. In the figures, the Rowe and Davis (1982b) method marked as #1 corresponds to that for cohesionless soils while that designated #2 is for c'-ϕ' soils. The loads were calculated using input parameters from the corresponding pipeline test. Overall, the highest estimated ultimate resistance was obtained using the

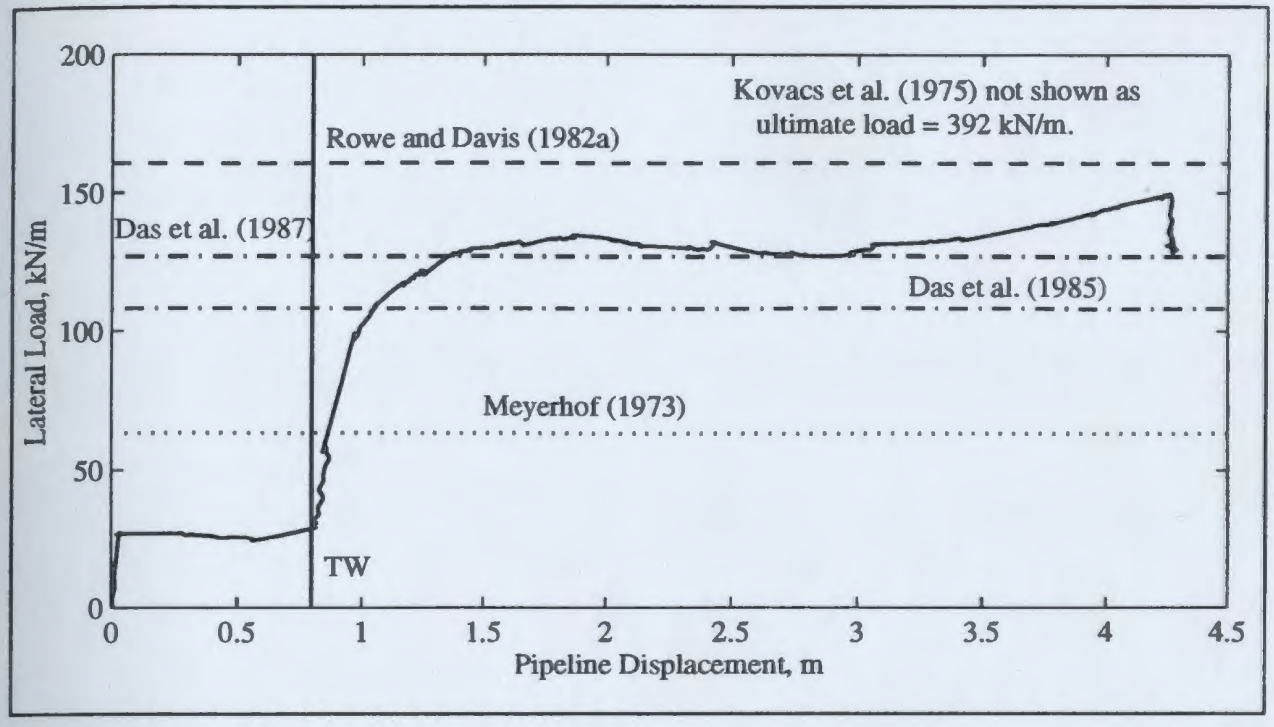

Figure 8.99a - Ultimate lateral loads based on anchor plate/soil interaction formulations for cohesive soil and comparison with Pipeline #1, Test 01, data.

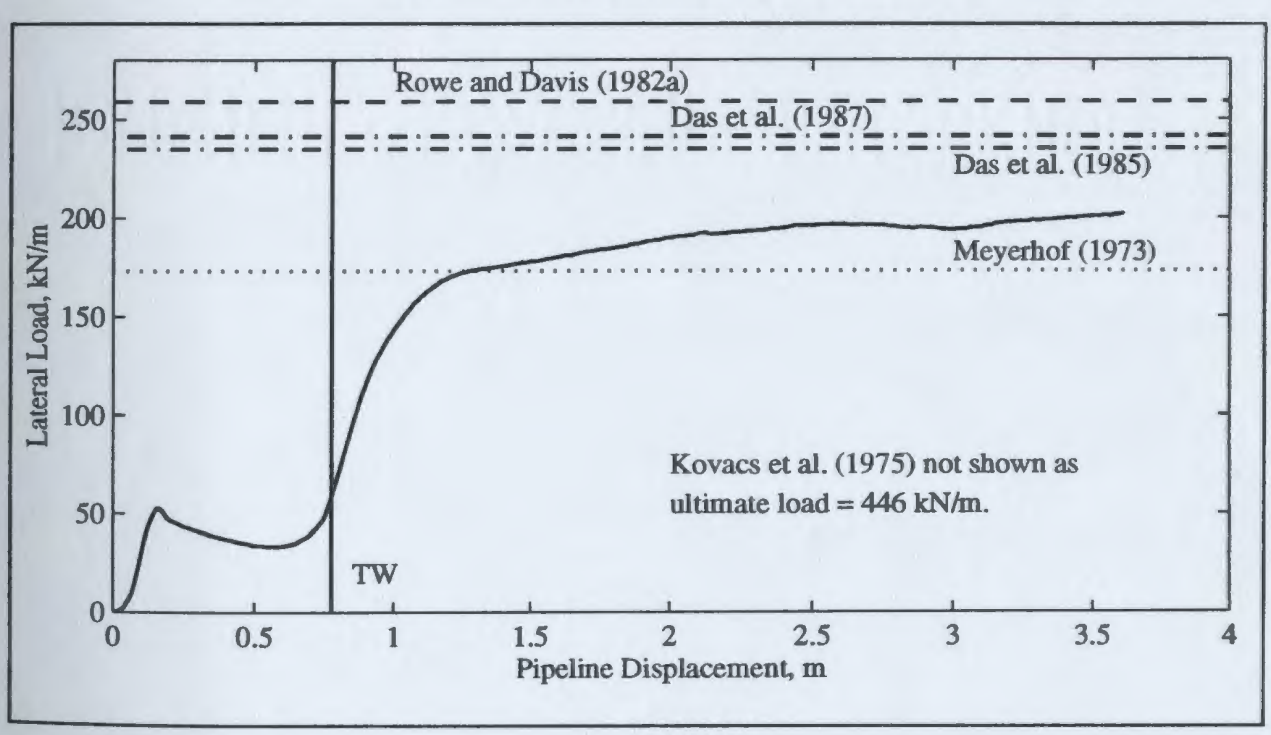

Figure 8.99b - Ultimate lateral loads based on anchor plate/soil interaction formulations for cohesive soil and comparison with Pipeline #1, Test 02, data.

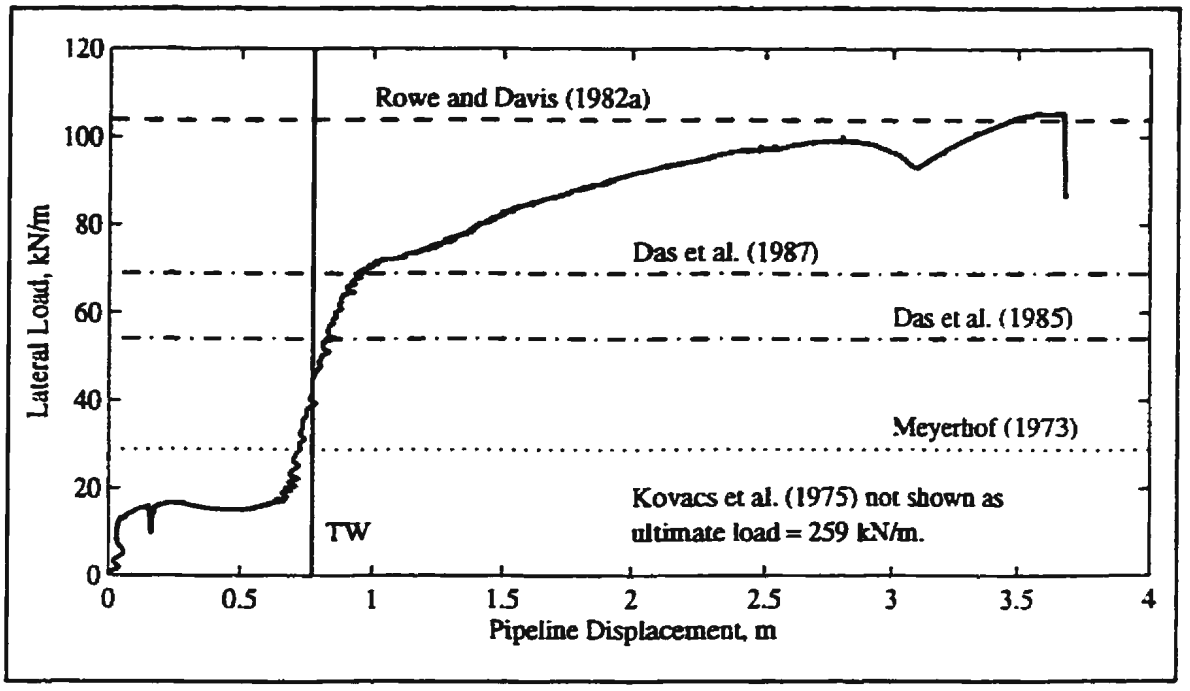

Figure 8.99c - Ultimate lateral loads based on anchor plate/soil interaction formulations for cohesive soil and comparison with Pipeline #3, Test 05, data.

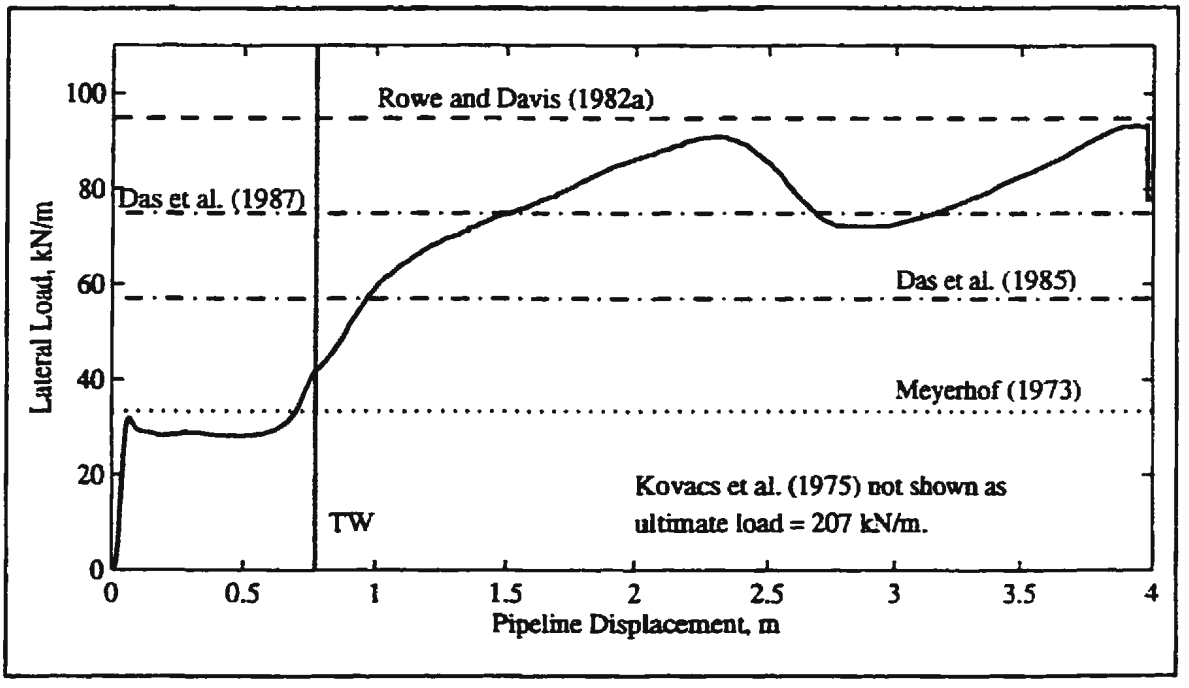

Figure 8.99d - Ultimate lateral loads based on anchor plate/soil interaction formulations for cohesive soil and comparison with Pipeline #4, Test 08, data.

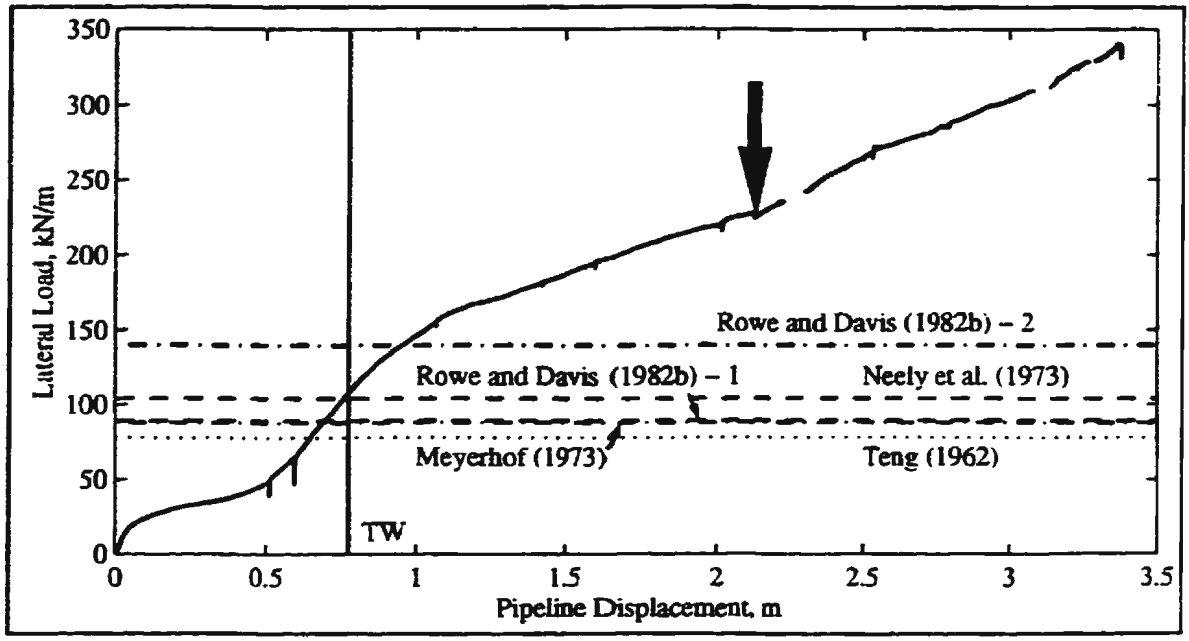

Figure 8.100a - Ultimate lateral loads based on anchor plate/soil interaction formulations for cohesionless and c'-φ' soils and comparison with Pipeline #1, Test 04, data.

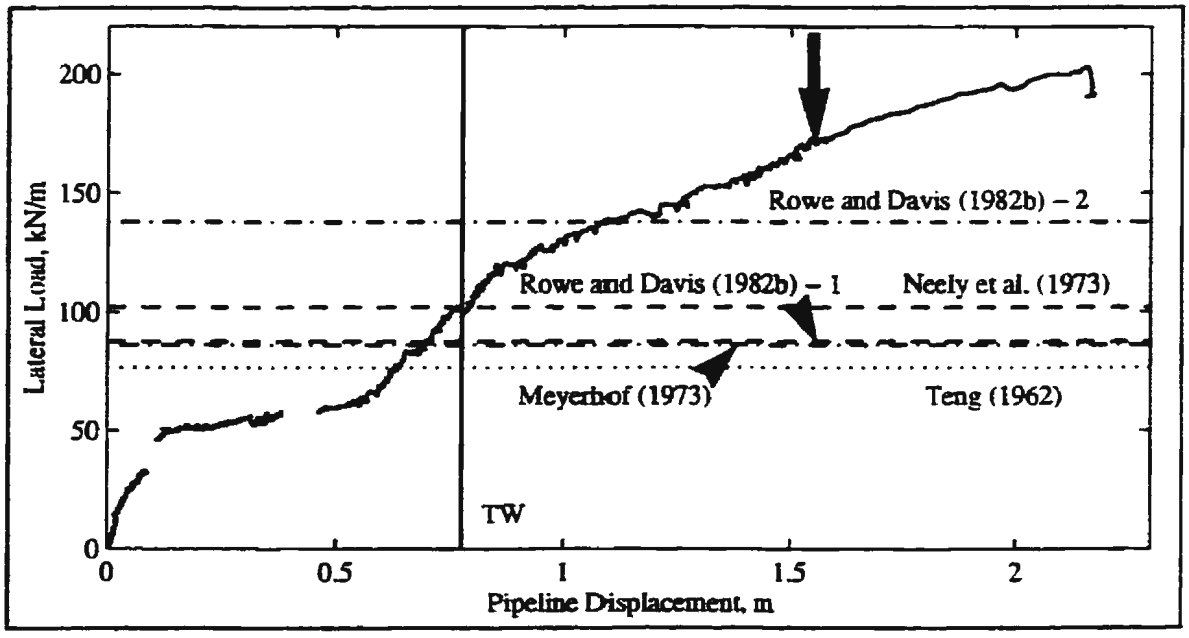

Figure 8.100b - Ultimate lateral loads based on anchor plate/soil interaction formulations for cohesionless and c'-φ' soils and comparison with Pipeline #1, Test 07, data.

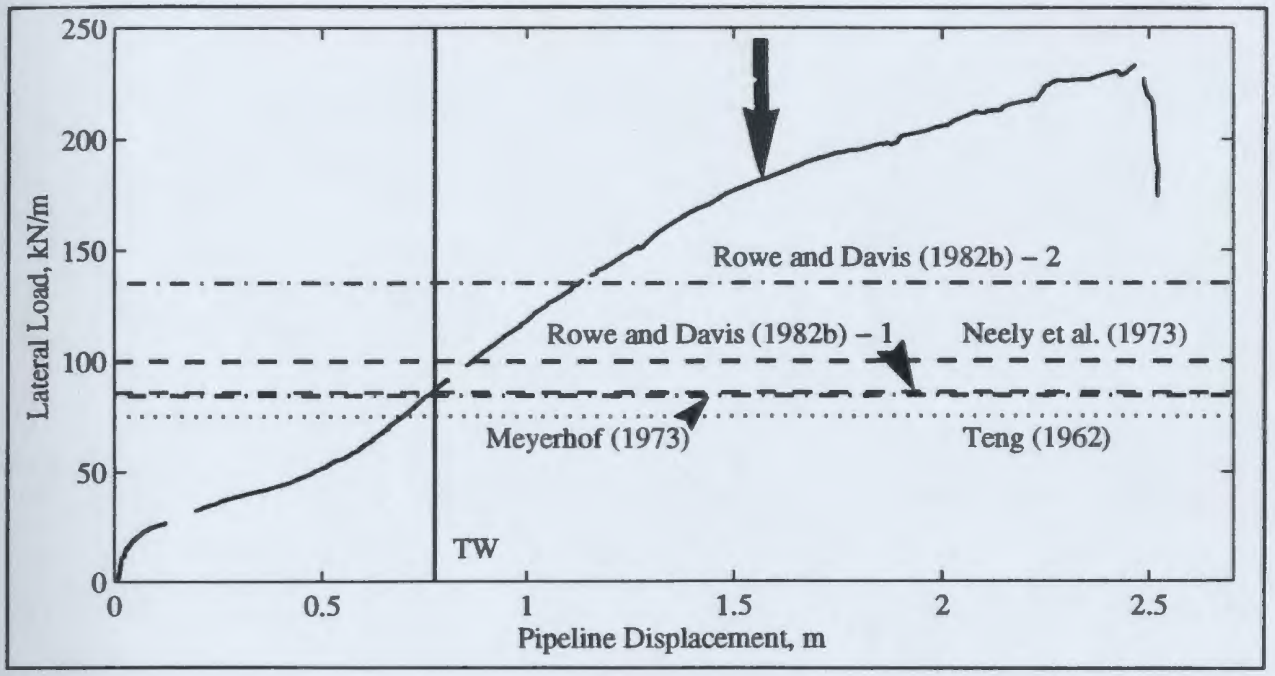

Figure 8.100c - Ultimate lateral loads based on anchor plate/soil interaction formulations for cohesionless and c'-ϕ' soils and comparison with Pipeline #1, Test 08, data.

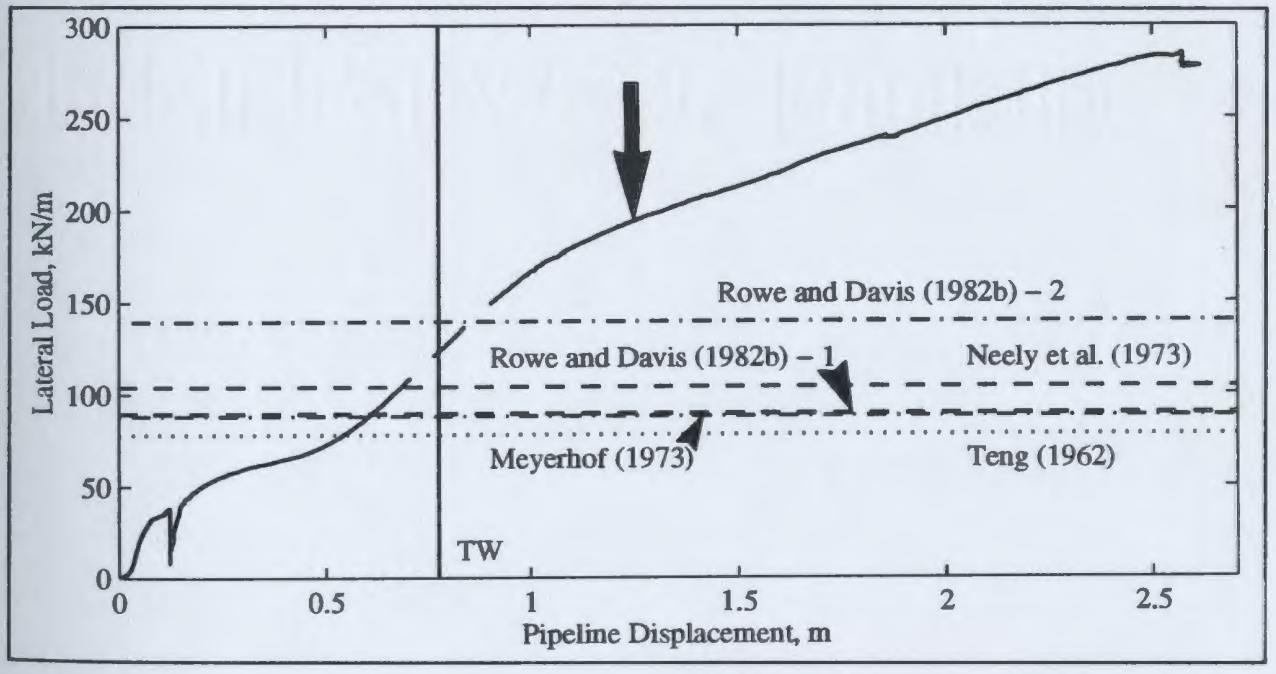

Figure 8.100d - Ultimate lateral loads based on anchor plate/soil interaction formulations for cohesionless and c'-ϕ' soils and comparison with Pipeline #1, Test 09, data.

Table 8.5a - Ultimate Loads Derived from Anchor Plate/Soil Interaction Methods - Cohesive Soil

Reference	Test 01 Pipeline #1 (kN/m)	Test 02 Pipeline #1 (kN/m)	Test 05 Pipeline #3 (kN/m)	Test 08 Pipeline #4 (kN/m)
Meyerhof (1973)	63	173	29	33
Kovacs *et al.* (1975)	392	446	259	207
Rowe and Davis (1982a)	161	259	104	95
Das *et al.* (1985)	108	235	54	57
Das *et al.* (1987)	127	242	69	75

Table 8.5b - Ultimate Loads Derived from Anchor Plate/Soil Interaction Methods - Cohesionless and c'-ϕ' Soils

Reference	Test 04 Pipeline #1 (kN/m)	Test 07 Pipeline #1 (kN/m)	Test 08 Pipeline #1 (kN/m)	Test 09 Pipeline #1 (kN/m)
Teng (1962)	78	77	75	78
Meyerhof (1973)	88	86	84	88
Neeley *et al.* (1973)	104	102	100	104
Rowe and Davis (1982b)[1]	89	88	86	89
Rowe and Davis (1982b)[2]	140	138	135	139

Notes: (1) Cohesionless soils.
(2) c'-ϕ' soils.

Rowe and Davis (1982b) c'-ϕ' soil formulation method. At best, this method provided a conservative estimate of the load transferred to the pipe up to an approximate overall displacement of 1m. It might also be noted that O'Brien (1997) compared lateral pipeline/soil interaction results from dry sand with suggested loadings in the literature and concluded that Teng (1962) provided the most accurate formulation when compared to full-scale data.

However, as documented in the literature for anchor plates and pipelines, it can be difficult to interpret the ultimate load of a force-displacement curve in loose cohesionless material. Often this load is taken as the point where the force-displacement response becomes linear corresponding to a buildup of surcharge in front of the displacing object (i.e Trautmann and O'Rourke, 1985; Das *et al.*, 1985; Vesic, 1973). Such an interpreted point is indicated by the vertical arrows on Figure 8.100. It could be argued that this position should be at an alternative point on the force-displacement response and its placement is open to interpretation. The effect of the interaction of the pipe with the trench wall makes it difficult to locate where a linear portion due to surcharge loading should be interpreted to begin. However, if it is assumed that the interpreted point is an ultimate, then the Rowe and Davis (1982b) method predicts to within 60 to 80% of that ultimate.

8.4.4 Pile/Soil Interaction

Ultimate Lateral Resistance

Some of the accepted methods of analysing pipeline/soil interaction presented in Section

8.3 from the literature were also based on the interaction between a laterally loaded pile and the surrounding soil. If these methods are thought to apply, then other similar methods of pile/soil interaction might be thought to apply as well. Table 8.6 presents references as the result of a limited review of the literature for undrained interaction in cohesive soil and interaction in cohesionless soil.

Meyerhof (1998) has suggested that the data of Figure 8.84 looks similar to the lateral soil pressure coefficients for rigid piles under lateral ultimate lateral load in clay presented by Meyerhof (1995). Meyerhof (1995) extended previous analyses of the ultimate resistance and displacements of rigid piles under lateral load to the general case of eccentric and inclined loads on flexible piles by using the concept of effective embedment depths of equivalent rigid piles. In doing so, the author presents a net lateral soil pressure coefficient, K_c, and a resultant net lateral soil pressure coefficient, K_{cr}, as a function of Z/D and L/D respectively where D is the diameter of the pile, L is the embedded length, and Z is the depth below the soil surface. These coefficients are multiplied by the soil cohesion to give the lateral soil pressure on the pile shaft and therefore are similar to the interaction factor used in an equation of the form presented in Equation [2-11]. The difference between the two is that K_{cr} represents an average value of K_c between the ground level and depth, L. These relations have been redrawn on Figure 8.84 where the upper line corresponds to the variation with K_c with embedment ratio while the lower line corresponds to the variation of K_{cr} with embedment ratio. Using the proposed analysis method, Meyerhof (1995) found reasonable agreement between observed and predicted

behaviour in model tests as well as good comparison with the results of a significant number of field case records of laterally loaded piles in clay.

The Meyerhof (1995) coefficients have been used to estimate the ultimate lateral load on a pipeline. These estimates are indicated on Figure 8.101 and in Table 8.6a and are designated Mc and Mcr representing values obtained using K_c and K_{cr} respectively. As expected from Figure 8.84, where the coefficient trends bracket the experimental interaction factors, the estimated ultimate lateral loads somewhat bracket the general undrained response (with the exception of Pipeline #3, Test 05).

Ultimate lateral loads based on the cohesive soil formulations are presented in Figure 8.101 and are summarized in Table 8.6a. The loads were calculated as using input parameters as in the previous section from: Pipeline #1, Test 01; Pipeline #1, Test 02; Pipeline #3, Test 05; and Pipeline #4, Test 08. The corresponding prototype-scale experimentally derived force-displacement curves from the pipeline tests are also plotted on the figures. Comparison of Figure 8.101 and Table 8.6a permits the various predictions to be identified. Four methods yielded reasonable predictions of the experimental data on multiple occasions. These were: (1) the method of Matlock (1970) using J=0.25; (2) the method of Matlock (1970) using J=0.5; (3) the method of Reese and Welch (1975); and (4) the first method suggested by Viggiani (1981). Overall, for the tests considered, the ultimate resistance of the pipeline/soil interaction was best estimated using the Matlock (1970) method with J=0.25. Using this method yielded a theoretical ultimate lateral load

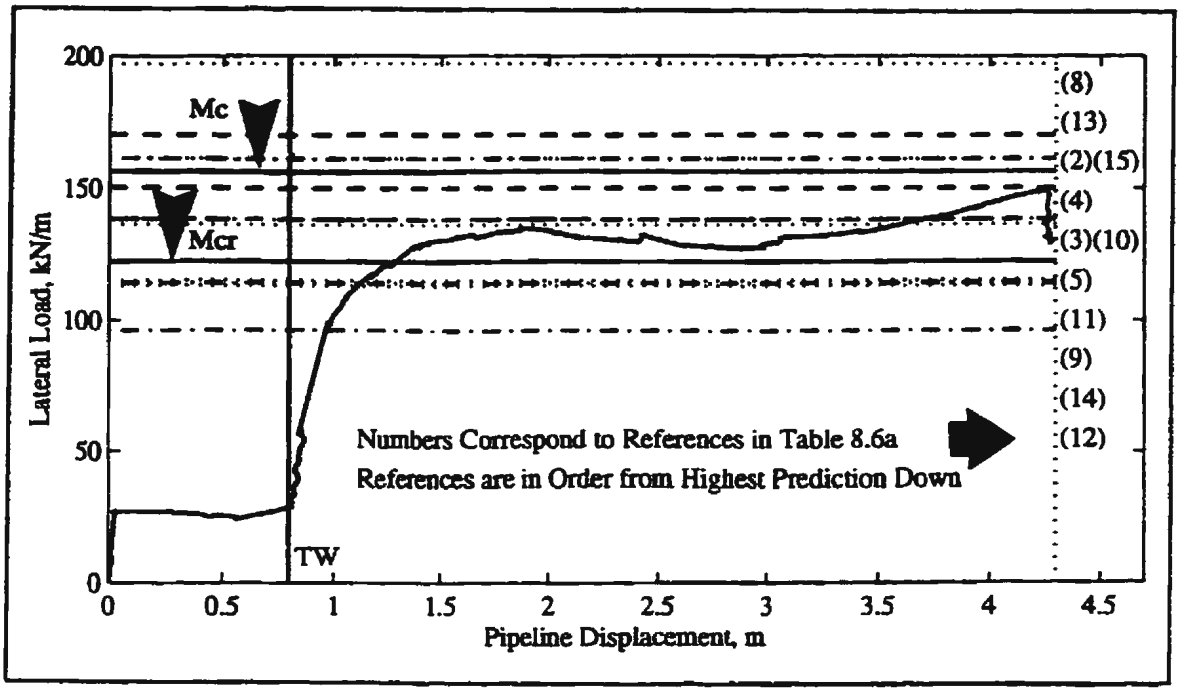

Figure 8.101a - Ultimate lateral loads based on pile/soil interaction formulations for cohesive soil and comparison with Pipeline #1, Test 01, data.

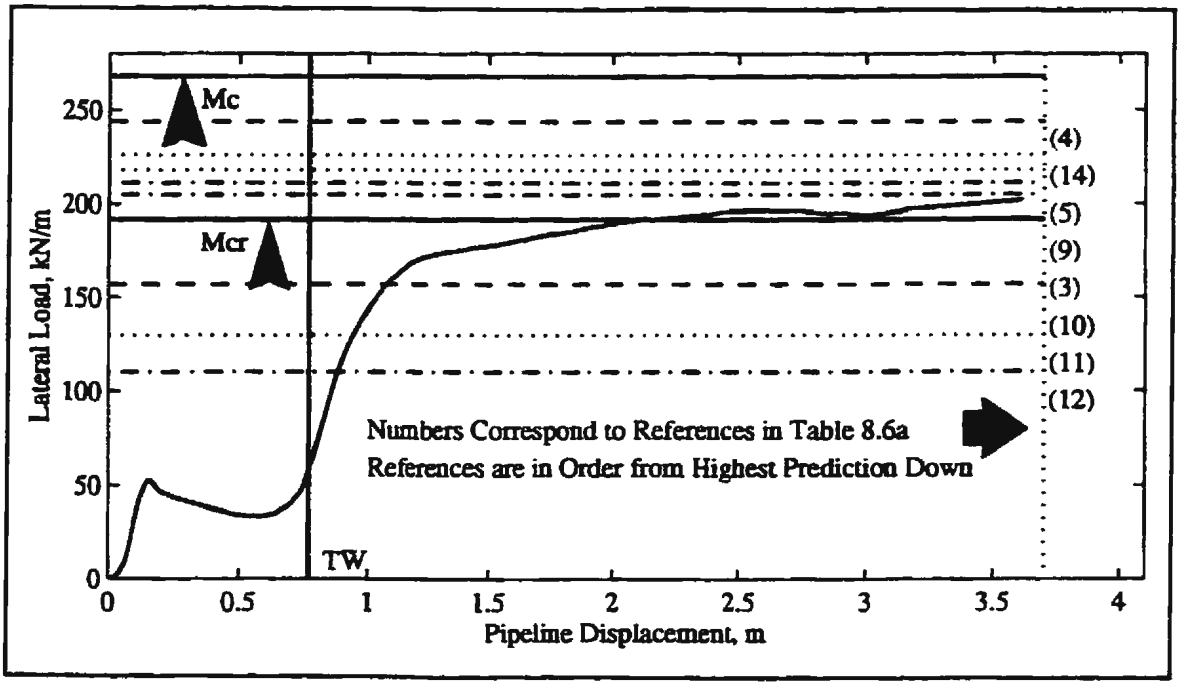

Figure 8.101b - Ultimate lateral loads based on pile/soil interaction formulations for cohesive soil and comparison with Pipeline #1, Test 02, data.

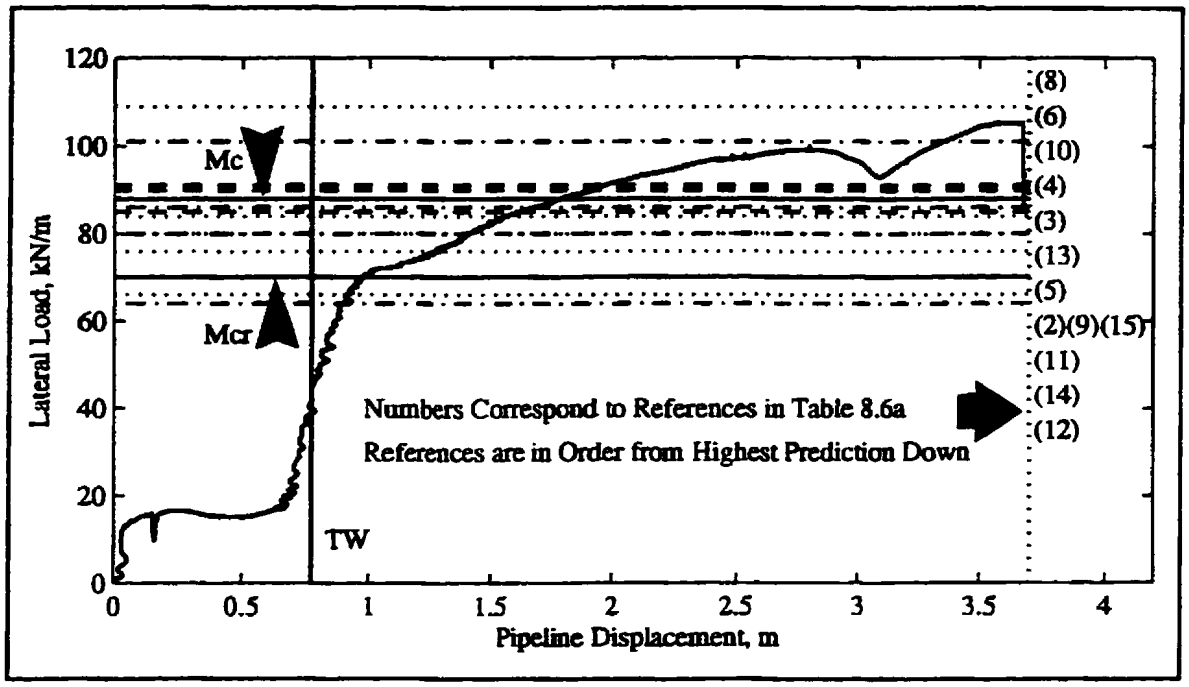

Figure 8.101c - Ultimate lateral loads based on pile/soil interaction formulations for cohesive soil and comparison with Pipeline #3, Test 05, data.

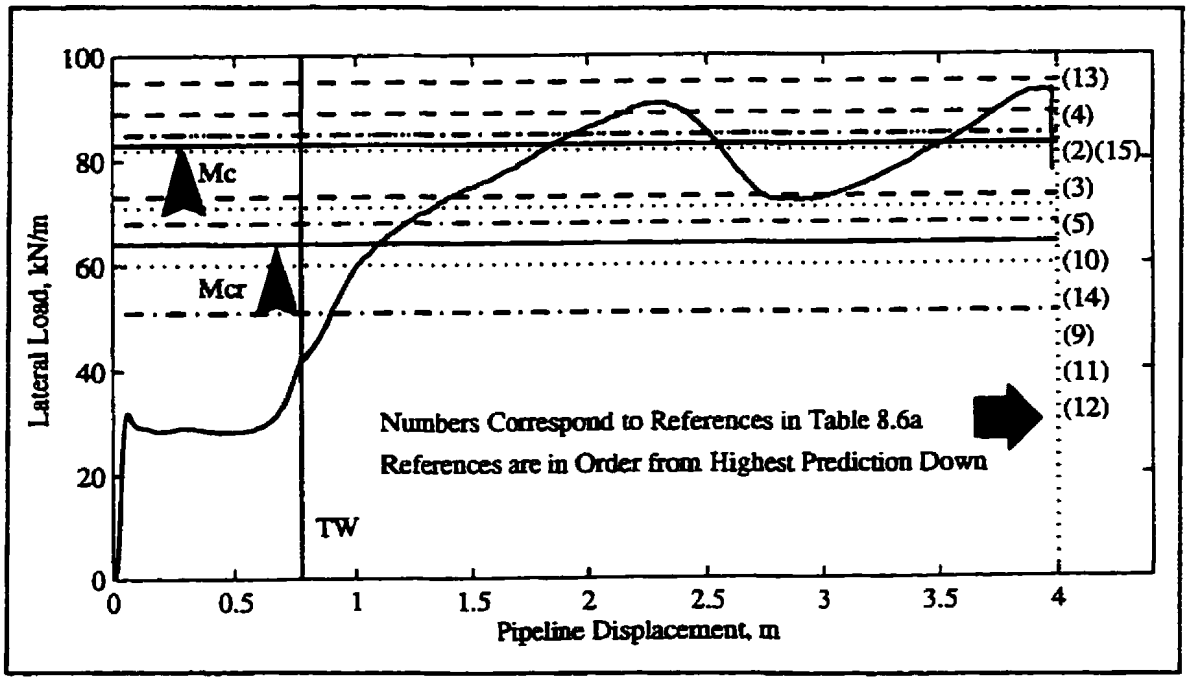

Figure 8.101d - Ultimate lateral loads based on pile/soil interaction formulations for cohesive soil and comparison with Pipeline #4, Test 08, data.

Table 8.6a - Ultimate Loads Derived from Pile/Soil Interaction Methods - Cohesive Soil.

Reference		Test 01 Pipeline #1 (kN/m)	Test 02 Pipeline #1 (kN/m)	Test 05 Pipeline #3 (kN/m)	Test 08 Pipeline #4 (kN/m)
Meyerhof (1995)	(Mc)	156	268	88	83
Meyerhof (1995)	(Mcr)	122	192	70	64
Hansen (1948)	(1)	285	325	189	151
Broms (1964a)	(2)	161	313	80	85
Matlock (1970)[1]	(3)	138	205	86	83
Matlock (1970)[2]	(4)	150	244	90	89
Reese and Welch (1975)	(5)	136	218	84	82
Reese *et al.* (1975)	(6)	201	431	101	116
Stevens and Audibert (1979)	(7)	299	470	164	158
Bhushan *et al.* (1979)	(8)	197	352	109	114
Sullivan *et al.* (1980)	(9)	114	211	80	68
Viggiani (1981)[3]	(10)	138	157	91	73
Viggiani (1981)[3]	(11)	115	130	76	60
Viggiani (1981)[3]	(12)	96	110	64	51
Randolph and Houlsby (1984)	(13)	170	376	85	95
O'Neil *et al.* (1990)	(14)	113	226	66	71
Poulos (1995)	(15)	161	385	80	85

Notes - (1) J = 0.25; (2) J = 0.50; (3) Three methods presented.

Table 8.6b - Ultimate Loads Derived from Pile/Soil Interaction Methods - Cohesionless Soil.

Reference	Test 04 Pipeline #1 (kN/m)	Test 07 Pipeline #1 (kN/m)	Test 08 Pipeline #1 (kN/m)	Test 09 Pipeline #1 (kN/m)
Broms (1964b)	208	205	200	209
Reese *et al.* (1974)	224	220	215	224
Murchinson and O'Neil (1984)	124	122	119	124
Randolph and Houlsby (1984)	208	205	200	209
Poulos (1995)	347	342	334	348

ranging from -14% to +4% of the experimental ultimate resistance for the four cases studied. The other three methods mentioned above respectively yielded theoretical values in the following ranges: (2) -24% to +11%; (3) -16% to +11%; and (4) -20% to +3%.

Force-displacement curves (prototype-scale) from tests which were considered drained are presented in Figure 8.102. These include: Pipeline #1, Test 04; Pipeline #1, Test 07; Pipeline #1, Test 08; and Pipeline #1, Test 09. Predicted ultimate lateral loads based on the cohesionless soil formulations listed in Table 8.6b have also been superimposed on the figures. Loads were calculated using input parameters from each corresponding pipeline test. The methods are hard to evaluate as there was no obvious peak loading on the pipes but rather the load achieved appeared to be dependant on the overall pipeline displacement. Overall, the highest estimated ultimate resistance was obtained using the Poulos (1995) formulation method. At best, this method provided a conservative estimate of the load transferred to the pipe up to overall displacements investigated in this study.

Interpreted ultimate loads based on the point where the force-displacement response becomes linear are again indicated by the vertical arrows in Figure 8.102. As in the previous section, it might be argued that these points could be positioned at alternative locations. If it is assumed that the interpreted point is reasonable, then the best overall predictions for the tests studied were from the method suggested by Broms (1964b) and Randolph and Houlsby (1984) which predicts within 93 to 119% of the interpreted ultimate load.

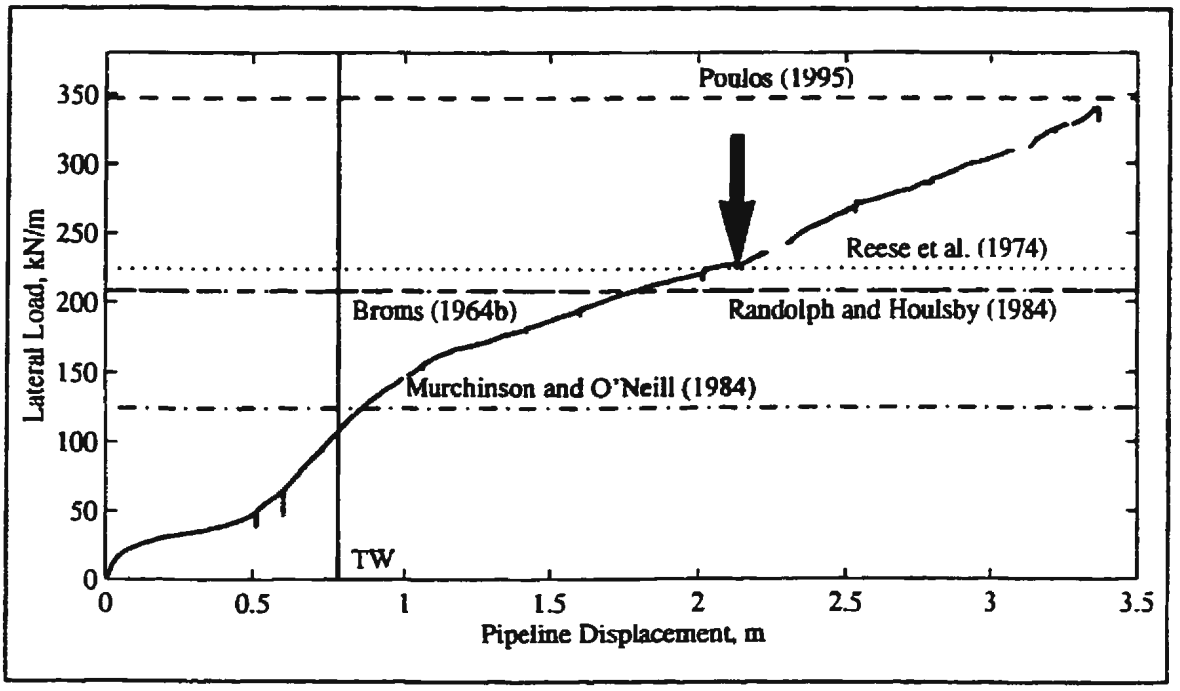

Figure 8.102a - Ultimate lateral loads based on pile/soil interaction formulations for cohesionless soils and comparison with Pipeline #1, Test 04, data.

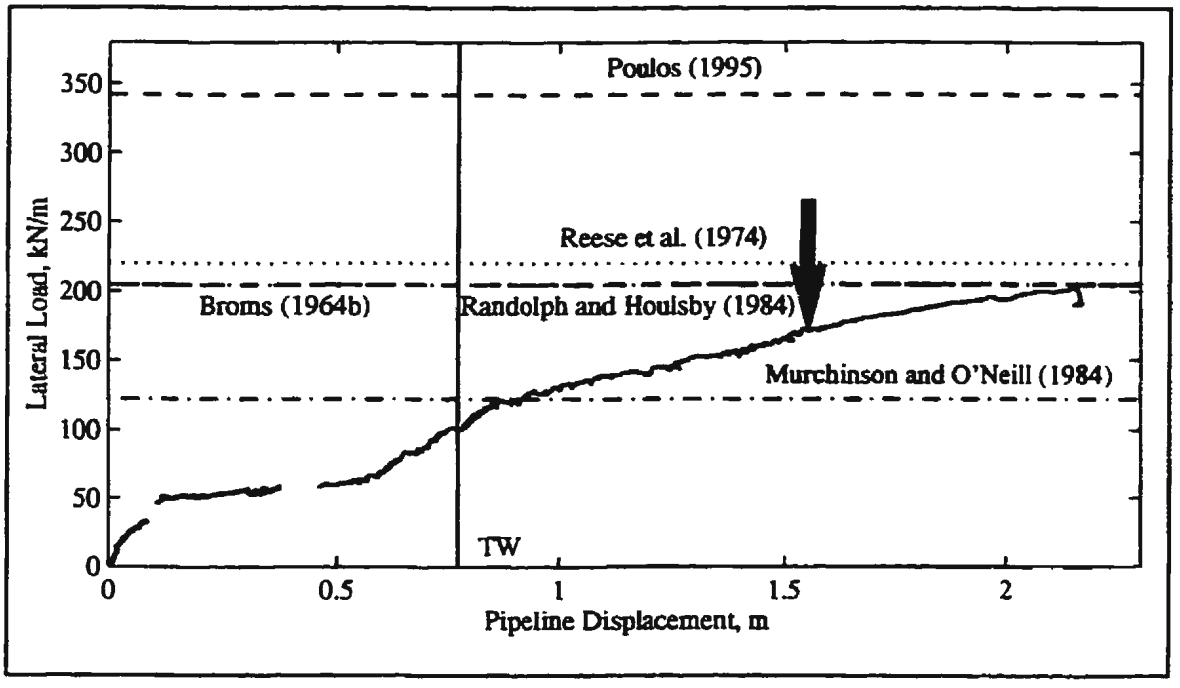

Figure 8.102b - Ultimate lateral loads based on pile/soil interaction formulations for cohesionless soils and comparison with Pipeline #1, Test 07, data.

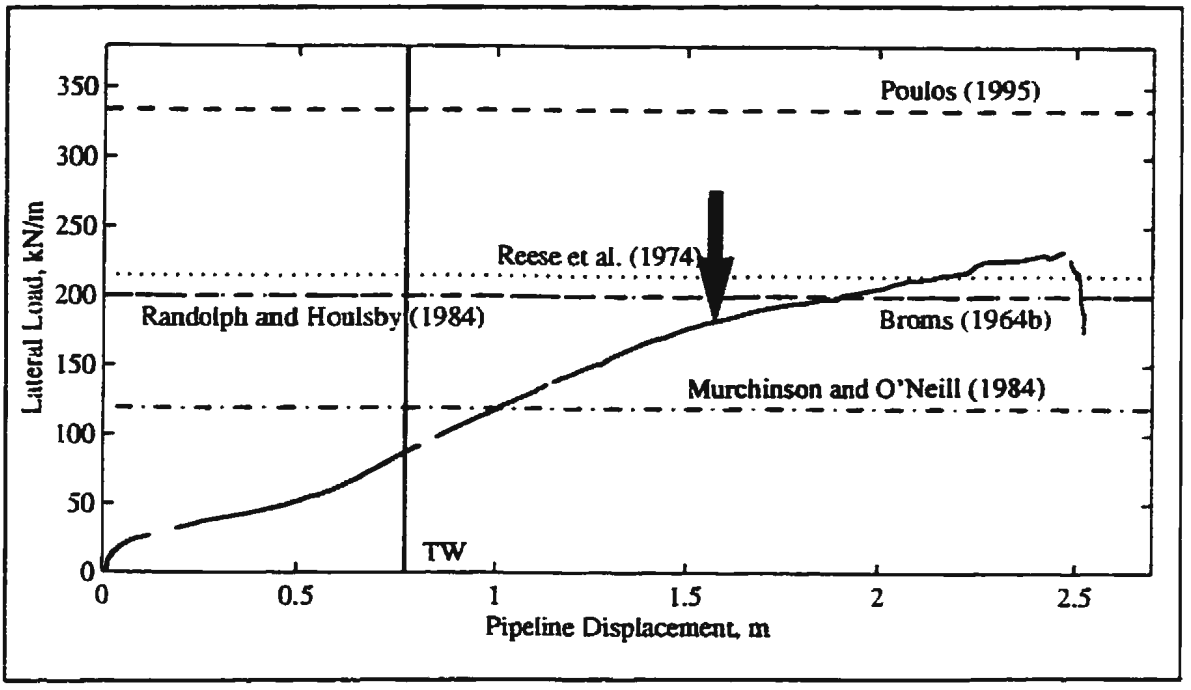

Figure 8.102c - Ultimate lateral loads based on pile/soil interaction formulations for cohesionless soils and comparison with Pipeline #1, Test 08, data.

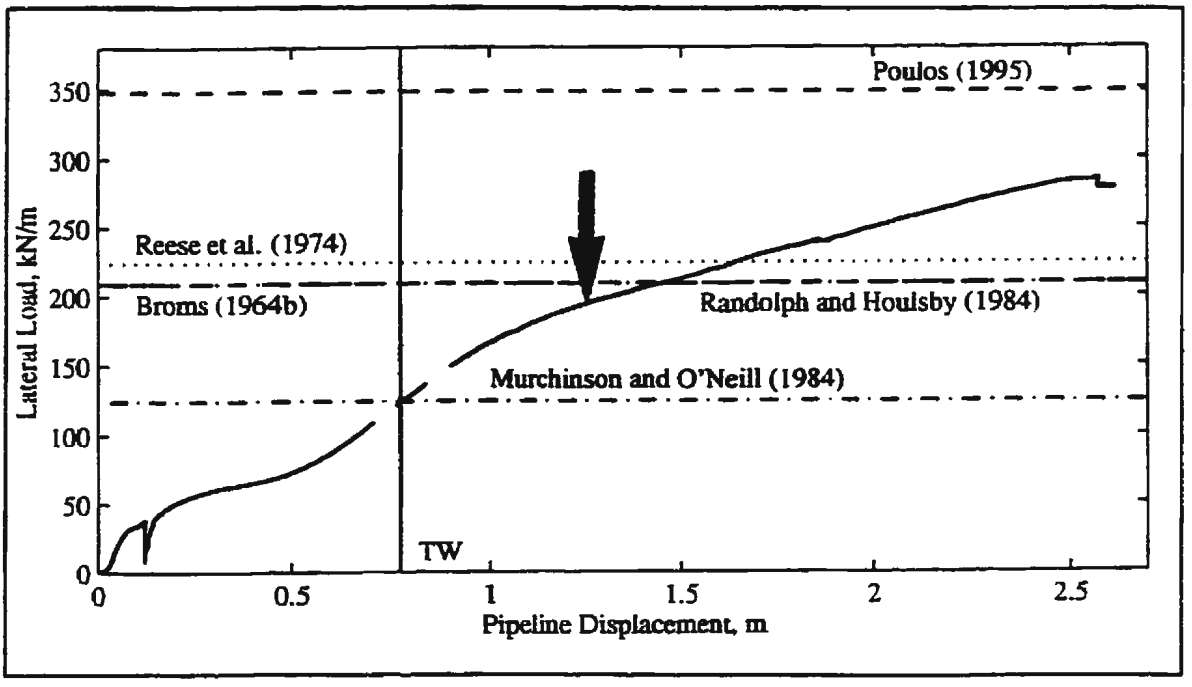

Figure 8.102d - Ultimate lateral loads based on pile/soil interaction formulations for cohesionless soils and comparison with Pipeline #1, Test 09, data.

p-y Curves

There are a number of suggested methods in the literature which can be used to construct an undrained p-y curve for a laterally loaded pile in clay. These include the methods of: Matlock (1970) for soft to firm clays; Reese and Welch (1975) for stiff clays; Bhushan *et al.* (1979) for stiff clays; Stevens and Audibert (1979) for clays in general; Reese *et al.* (1975) for stiff clays; and O'Neill *et al.* (1990) for overconsolidated clays. Triaxial test data presented in Chapter 5 were obtained from material which had been one-dimensionally preconsolidated to 400kPa and subjected to isotropic consolidation of 25kPa. These data have been used along with specific test parameters to construct undrained p-y curves which can be compared with pipeline force-displacement curves of selected centrifuge tests.

Experimental data from selected undrained pipeline tests and theoretically-derived p-y curves are presented in Figure 8.103 where the limits of the data plotted have been adjusted to maximize the pipeline displacement zone of interest. The origin of the theoretical curves has been set with respect to the start of interaction with the trench wall. In these figures, the ultimate load has been taken as the actual experimental ultimate load. The reasoning behind this was so that each method could be evaluated based on its p-y formulation which has been decoupled from its associated estimate of P_{ult} which, for some methods, has been analysed in the previous sub-section. The method of Reese *et al.* (1975) has been slightly modified in that the initial portion of the curve has not been modelled as a straight line. The method of O'Neill *et al.* (1990) requires an estimate of the pipe bending stiffness which has been made based on typical pipe material and geometry.

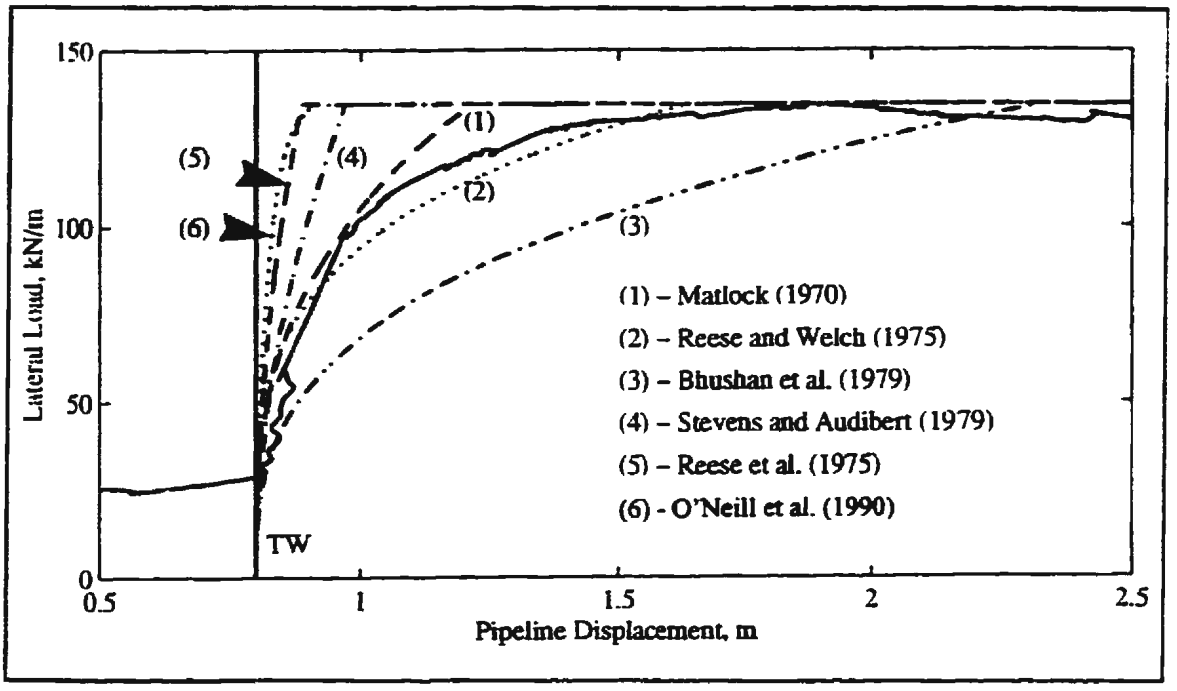

Figure 8.103a - Theoretical p-y curve formulations based on pile/soil interaction for cohesive soil and comparison with Pipeline #1, Test 01, data.

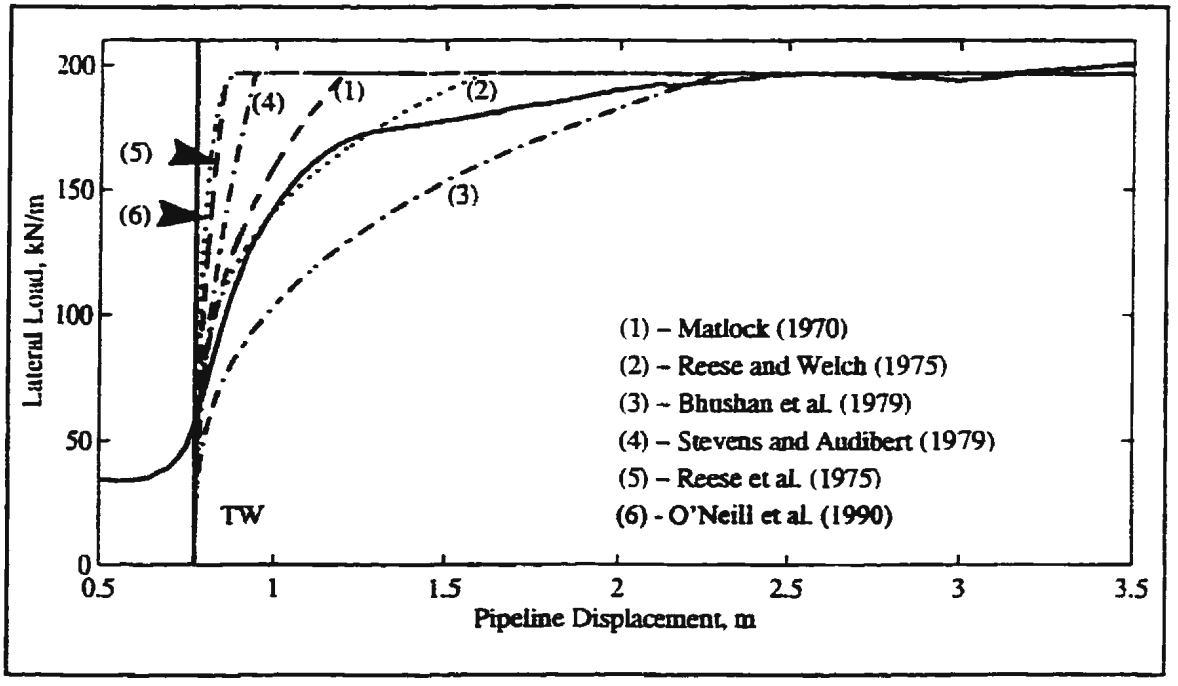

Figure 8.103b - Theoretical p-y curve formulations based on pile/soil interaction for cohesive soil and comparison with Pipeline #1, Test 02, data.

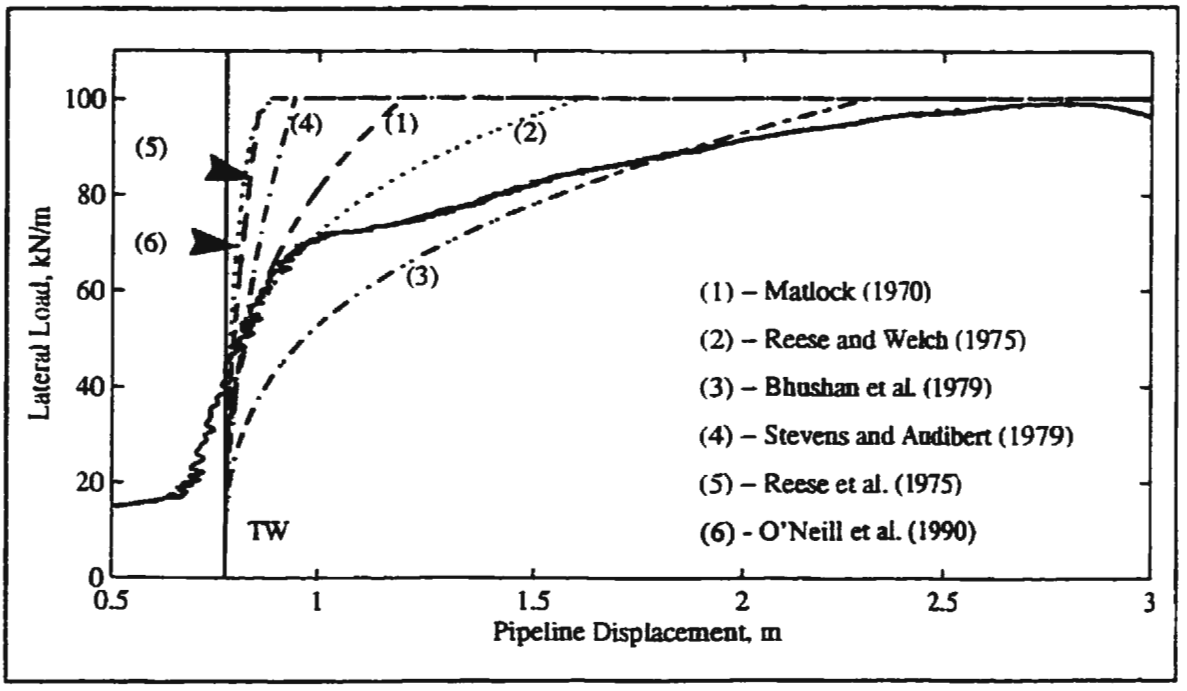

Figure 8.103c - Theoretical p-y curve formulations based on pile/soil interaction for cohesive soil and comparison with Pipeline #3, Test 05, data.

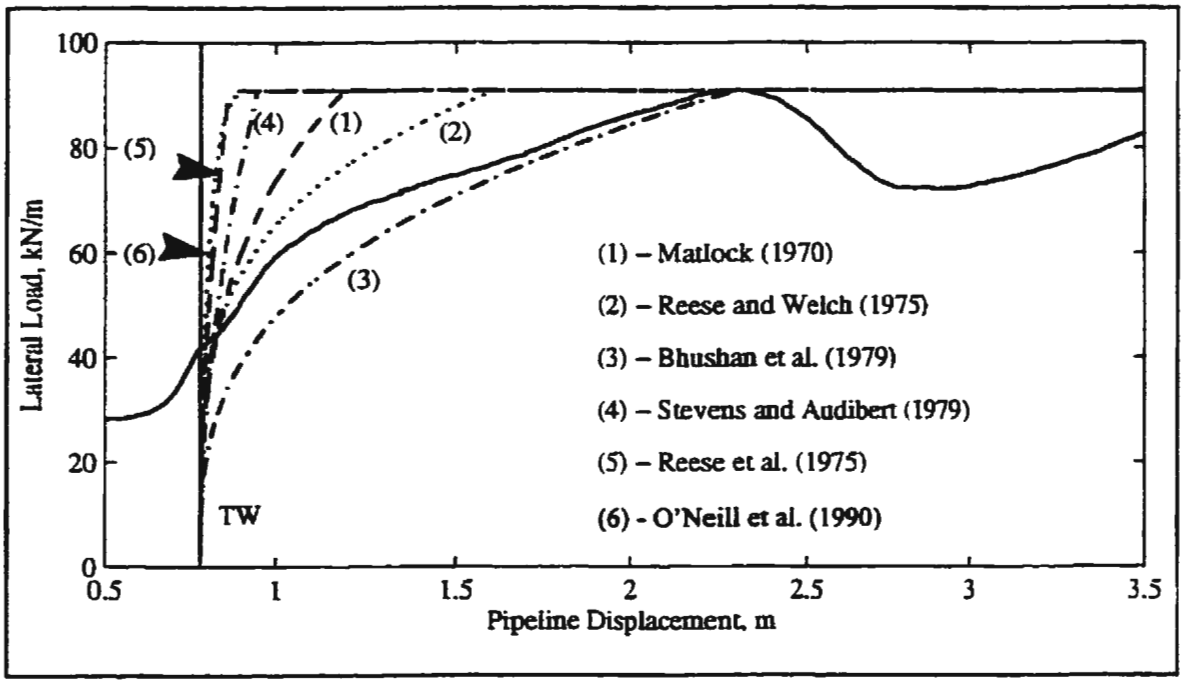

Figure 8.103d - Theoretical p-y curve formulations based on pile/soil interaction for cohesive soil and comparison with Pipeline #4, Test 08, data.

In Figures 8.103a and 8.103b, the best approximations of the experimental force-displacement curves comes from the methods of Matlock (1970) and Reese and Welch (1975). All methods of estimation require an estimate of ε_{50} which is the strain at one-half the principal stress difference in an undrained laboratory triaxial test. As pointed out above, the triaxial test from which the data was obtained had been isotropically consolidated to 25kPa. This consolidation stress level prior to shearing was similar to the effective vertical stress at the springline of Pipeline #1, Test 01 (24.4kPa), but considerably less than that at the springline of Pipeline #1, Test 02 (70.7kPa). This might account for some of the deviation of the Matlock (1970) formulation from the experimental data of Figure 8.103b. Similarly, in Figure 8.103c, the effective vertical stress at the springline of Pipeline #3, Test 05, was considerably less than that tested in the triaxial (13.7kPa) which may have resulted for some of the discrepancy between experimental data and theoretical formulation. The method of Bhushan *et al.*(1979) appears to provide the most reasonable estimate of the experimental data; however, in Test 08, the soil was only preconsolidated to 160kPa rather than the baseline 400kPa and even though the effective vertical stress at the springline was similar to that tested in the triaxial (23.4kPa), the strain to one-half of ultimate load might be expected to be underestimated resulting in an overestimate in the stiffness of the theoretical formulation.

There are a number of suggested methods in the literature which can be used to construct a p-y curve for piles in cohesionless material. Methods investigated here include those

suggested by Audibert and Nyman (1977), Murchison and O'Neill (1984), and Trautmann and O'Rourke (1985). These formulations are compared to the experimental data of selected tests in Figure 8.104. During the drained tests, significant load was transferred to the pipeline before interaction with the trench wall; therefore, the theoretical force-displacement curves have been originated at the start of pipe displacement. Again, the ultimate load used is the experimentally derived overall experimental load so that meaningful comparison between formulations can be made. As seen, the methods of Audibert and Nyman (1977) and Trautmann and O'Rourke (1985), while conservative, provide the closest approximations to the experimental curves. It appears that, if the trench was not present, these two formulations might provide a decent approximation to the shape of the force-displacement curve.

If, as before, the ultimate load is interpreted where the force-displacement response goes linear, the cohesionless approximations would be as shown in Figure 8.105. Again, the methods of Audibert and Nyman (1977) and Trautmann and O'Rourke (1985), while conservative, provide the closest approximations to the experimental curves. As above, it also appears that if the trench was not present, the two formulations might provide a decent approximation to the shape of the force-displacement curve.

8.4.5 Bearing Capacity Solutions

Bearing Capacity Solutions

Wantland *et al.* (1982) suggested that soil resistance to lateral pipeline movement is similar

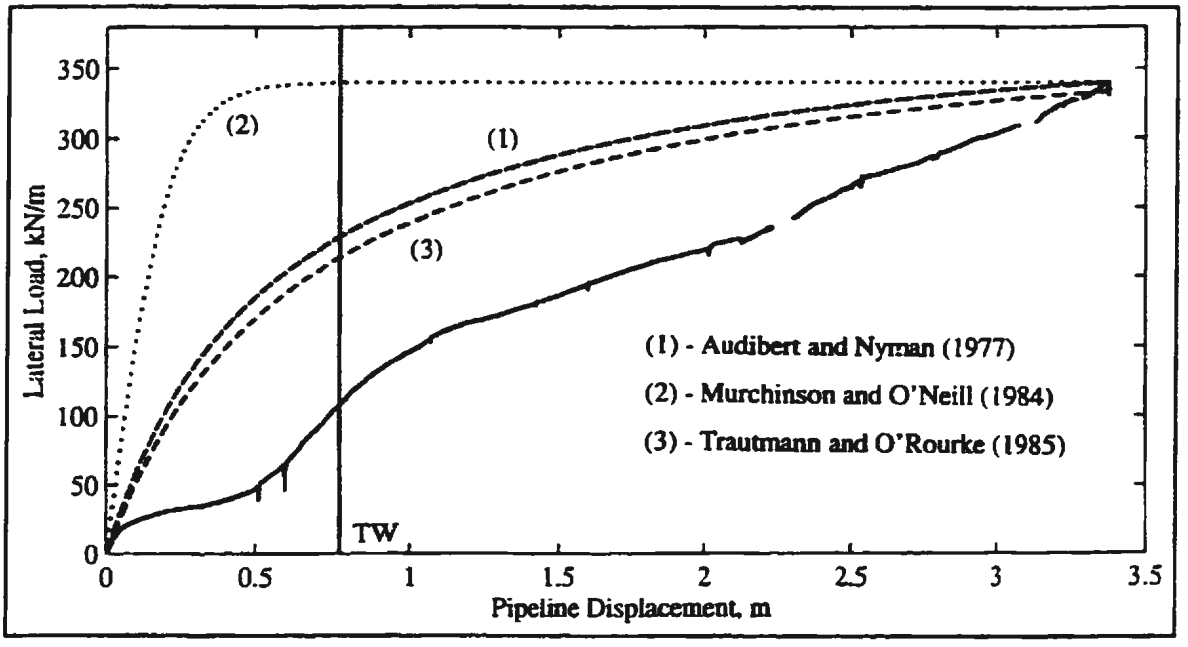

Figure 8.104a - Theoretical p-y curve formulations based on pile/soil interaction for cohesionless soil to overall ultimate load and comparison with Pipeline #1, Test 04, data.

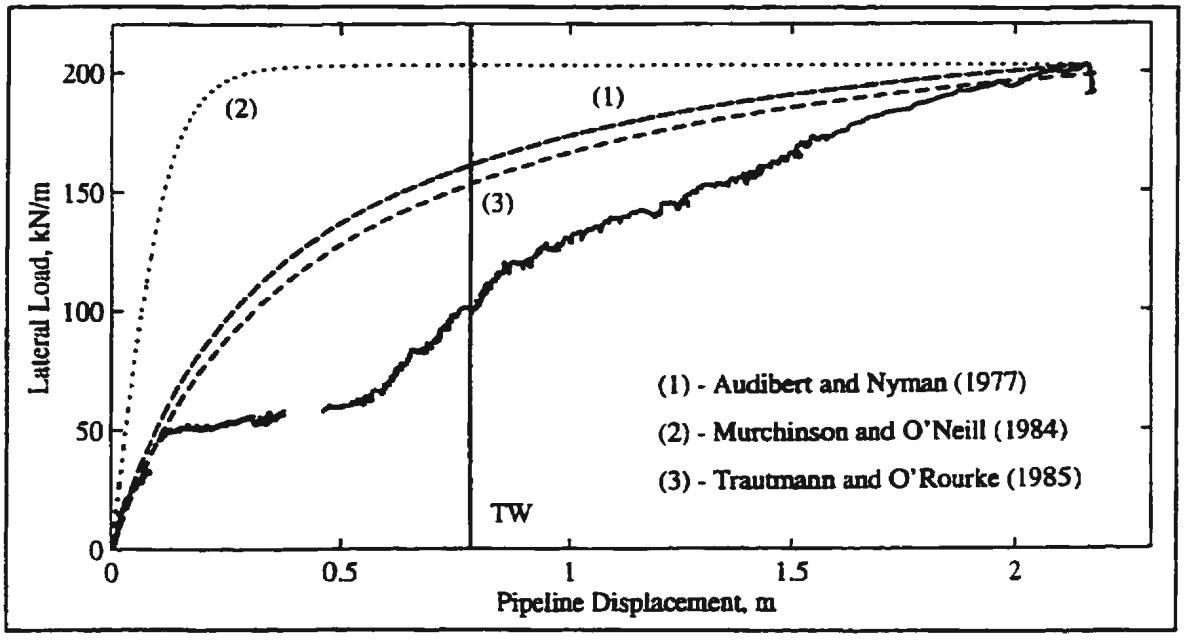

Figure 8.104b - Theoretical p-y curve formulations based on pile/soil interaction for cohesionless soil to overall ultimate load and comparison with Pipeline #1, Test 07, data.

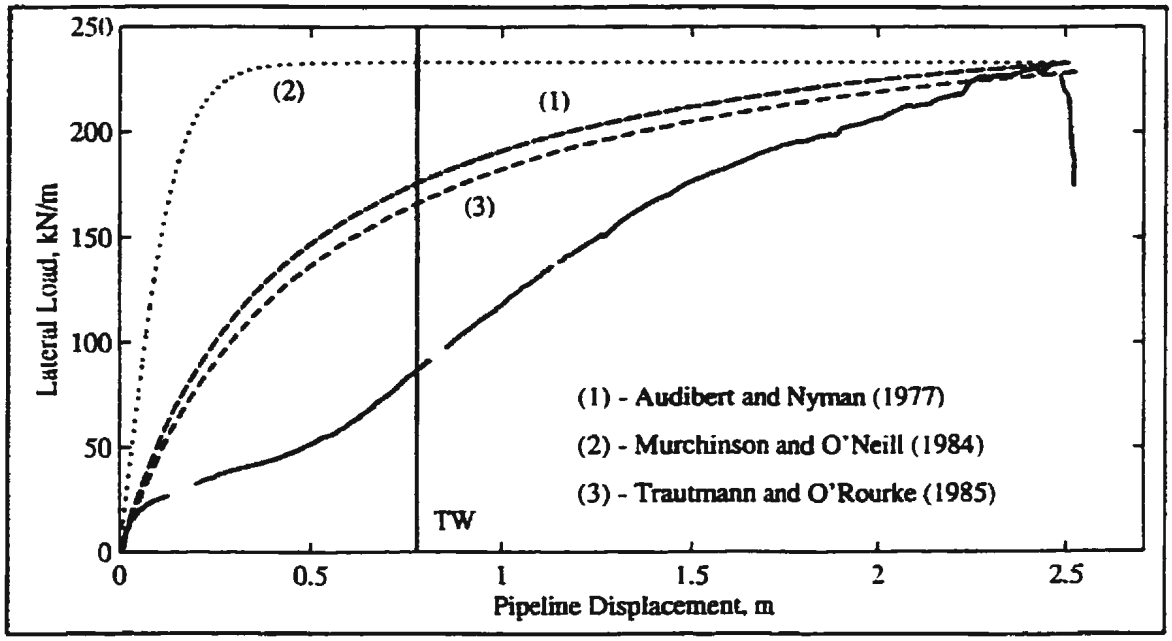

Figure 8.104c - Theoretical p-y curve formulations based on pile/soil interaction for cohesionless soil to overall ultimate load and comparison with Pipeline #1, Test 08, data.

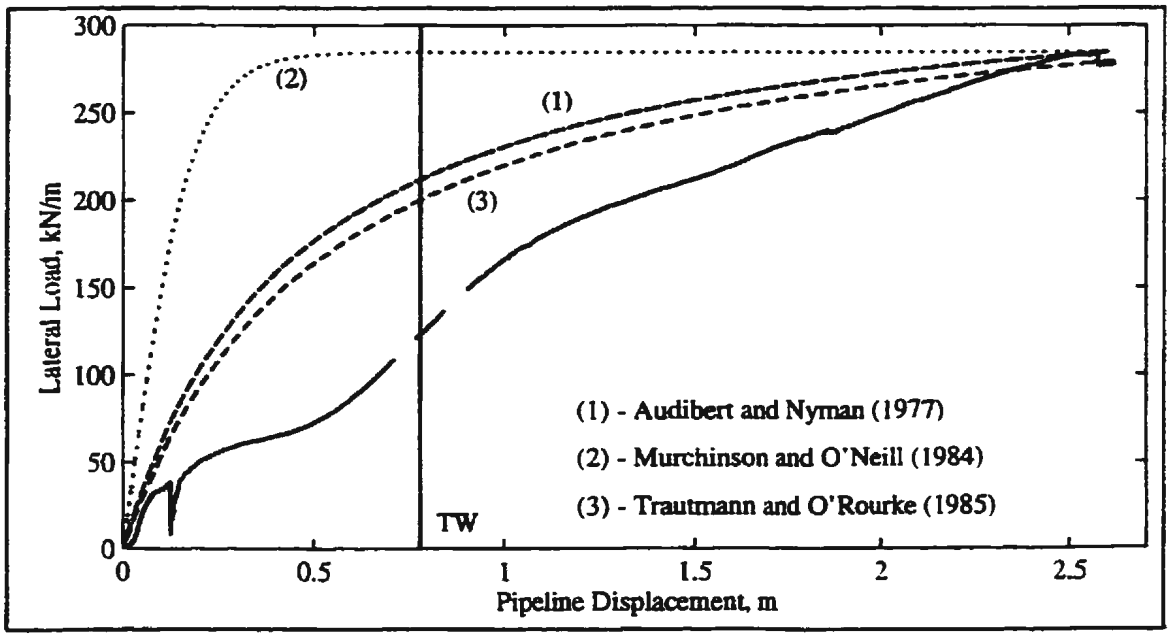

Figure 8.104d - Theoretical p-y curve formulations based on pile/soil interaction for cohesionless soil to overall ultimate load and comparison with Pipeline #1, Test 09, data.

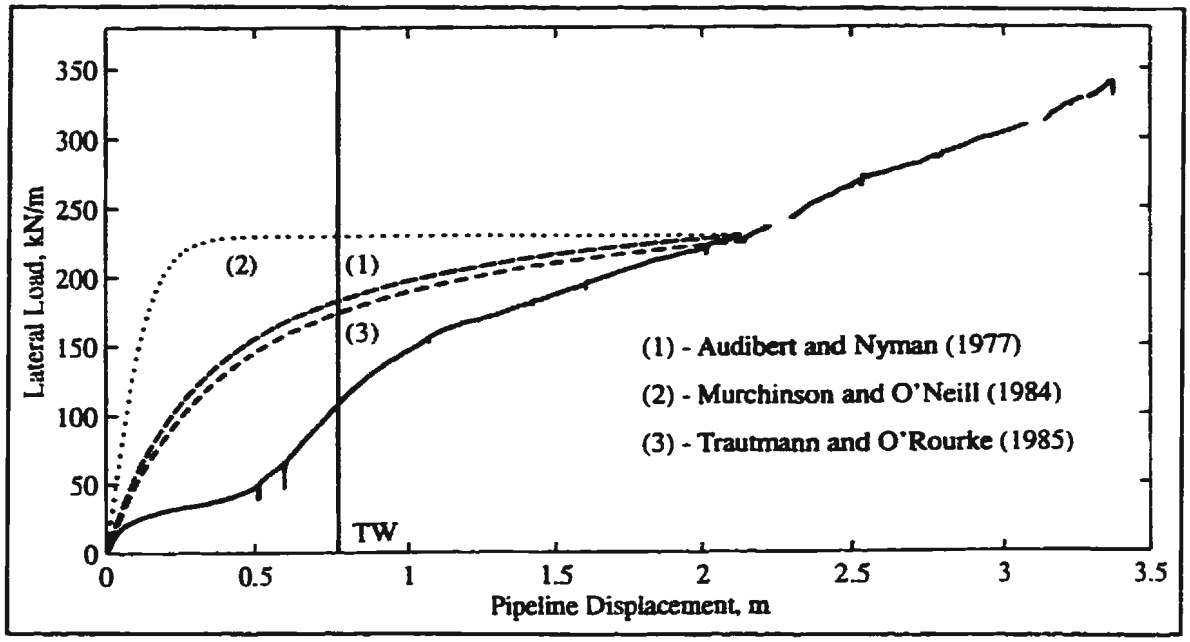

Figure 8.105a - Theoretical p-y curve formulations based on pile/soil interaction for cohesionless soil to interpreted ultimate load and comparison with Pipeline #1, Test 04, data.

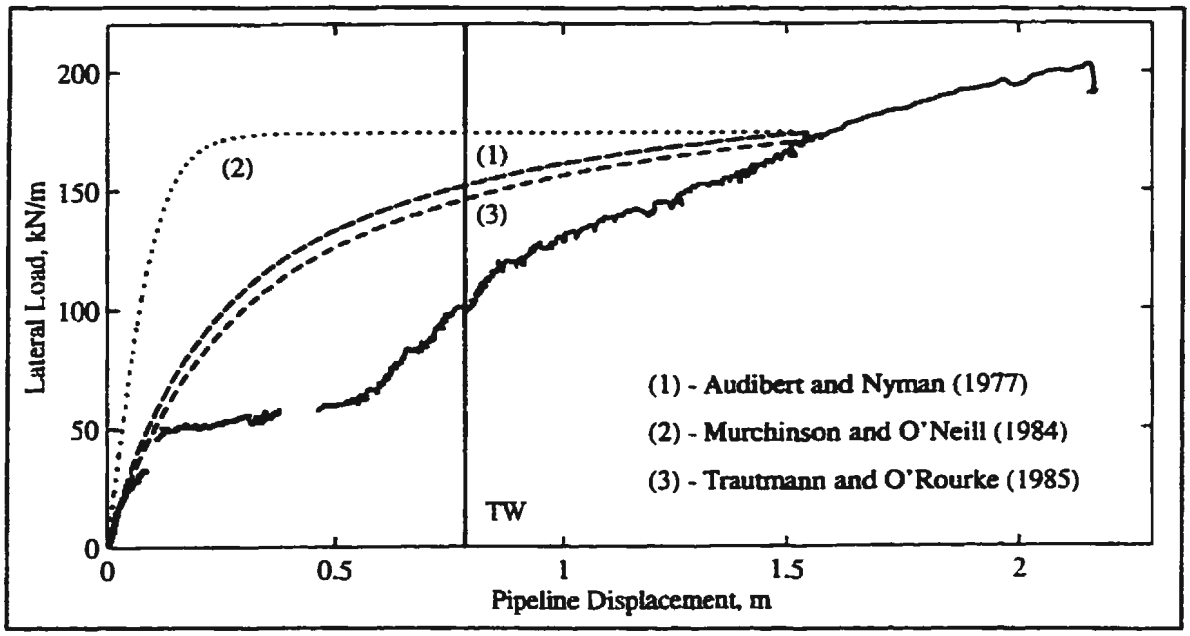

Figure 8.105b - Theoretical p-y curve formulations based on pile/soil interaction for cohesionless soil to interpreted ultimate load and comparison with Pipeline #1, Test 07, data.

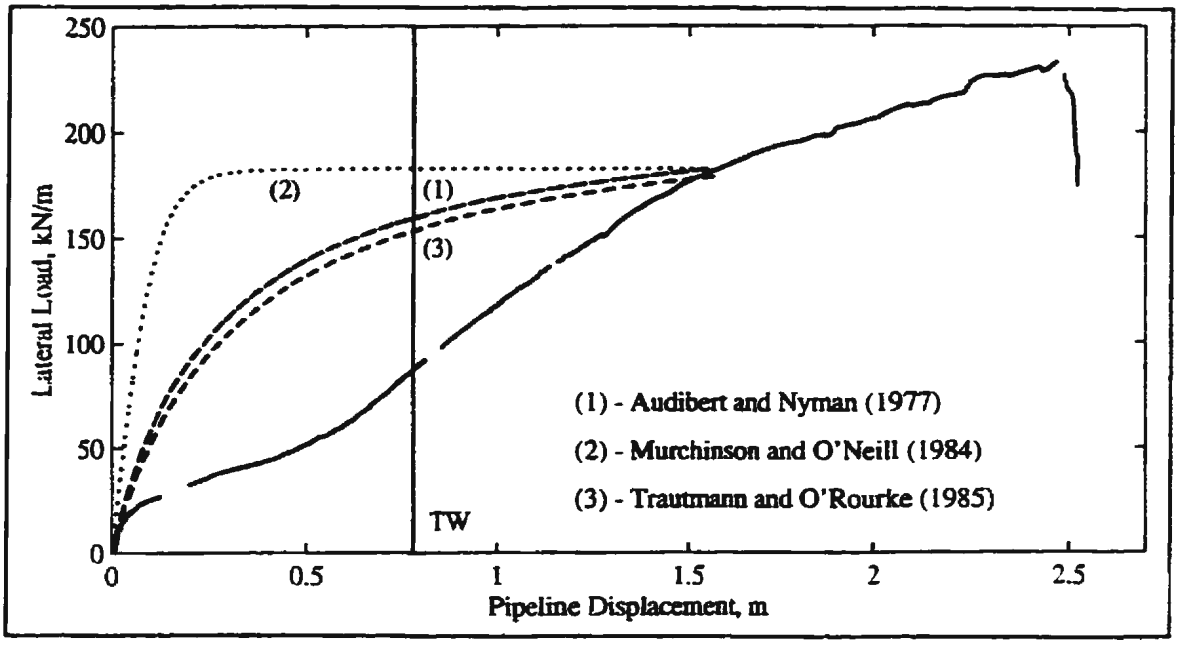

Figure 8.105c - Theoretical p-y curve formulations based on pile/soil interaction for cohesionless soil to interpreted ultimate load and comparison with Pipeline #1, Test 08, data.

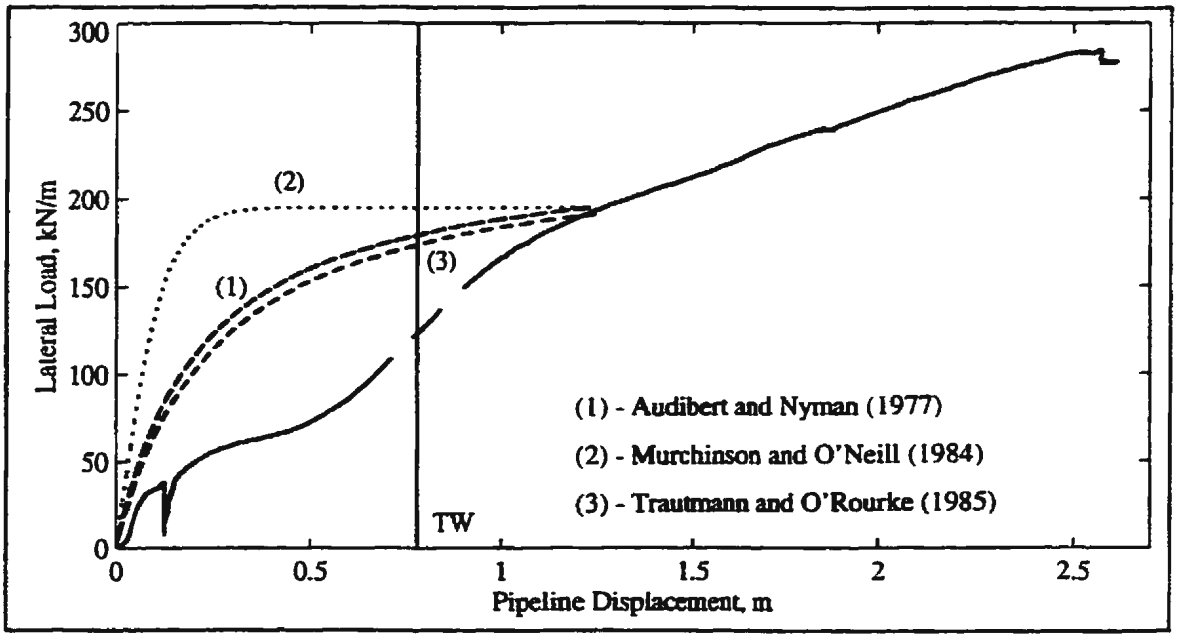

Figure 8.105d - Theoretical p-y curve formulations based on pile/soil interaction for cohesionless soil to interpreted ultimate load and comparison with Pipeline #1, Test 09, data.

to the bearing capacity of a foundation. If that is the case, an analysis can be conducted based on an assumed bearing capacity failure mechanism similar to that suggested by the authors and presented in Figure 8.106. For the analysis, it is assumed that the footing width is equivalent to the diameter of the pipeline, D, as shown in Figure 8.106a. The bearing capacity analysis is then carried out as depicted in Figure 8.106b. Terzaghi (1943) suggested that the force required to pull a deeply embedded anchor slab (similar to a pipeline) is approximately equal to the bearing capacity of a footing slab located at the depth of the springline. Similarly for piles at depths greater than four to six pile diameters below the ground surface, the lateral deflection of the pile is assumed to deform the soil in a mode similar to that for a deep two-dimensional footing.

Thus, analysis of the problem suggests three possible solutions: (1) the bearing capacity of a footing on a flat surface (ignoring backfill and soil surface); (2) considering the presence of the soil surface (top of trench) by assessing the bearing capacity of a footing on the edge of a slope where the slope is at an angle of 90° or vertical (ignoring backfill); and (3) the bearing capacity of a footing located at the depth of the springline as suggested by Terzaghi (1943). Results of this analysis and the appropriate references are presented in Table 8.7. Results are compared to experimental data in Figures 8.107 and 8.108. The notations BC and PP stand for bearing capacity and passive pressure respectively and correspond to methods presented in Table 8.7.

With regards to the undrained ($\phi = 0$) analysis presented in Figure 8.107, the bearing

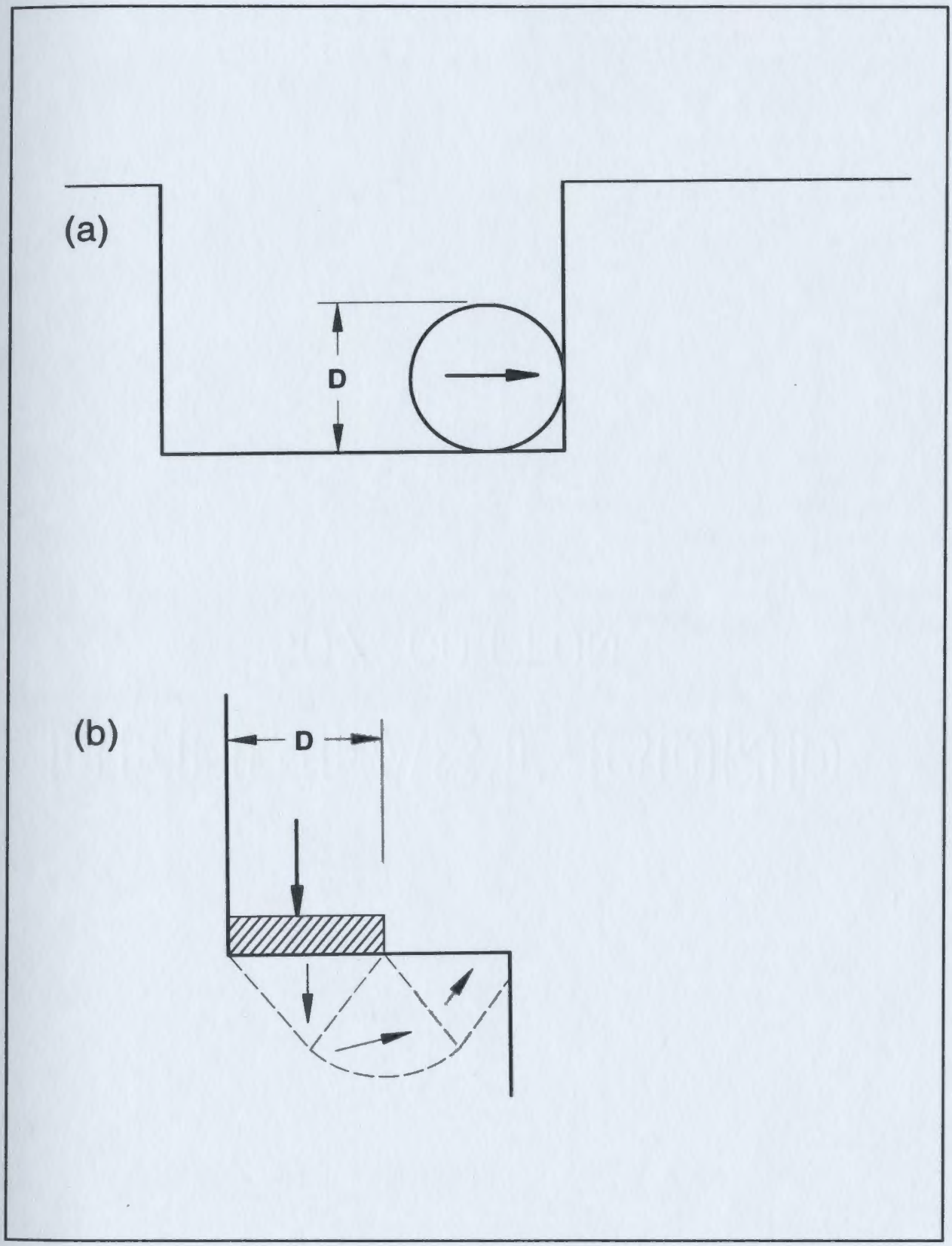

Figure 8.106 - Proposed analogy between interaction with the trench wall and bearing capacity failure.

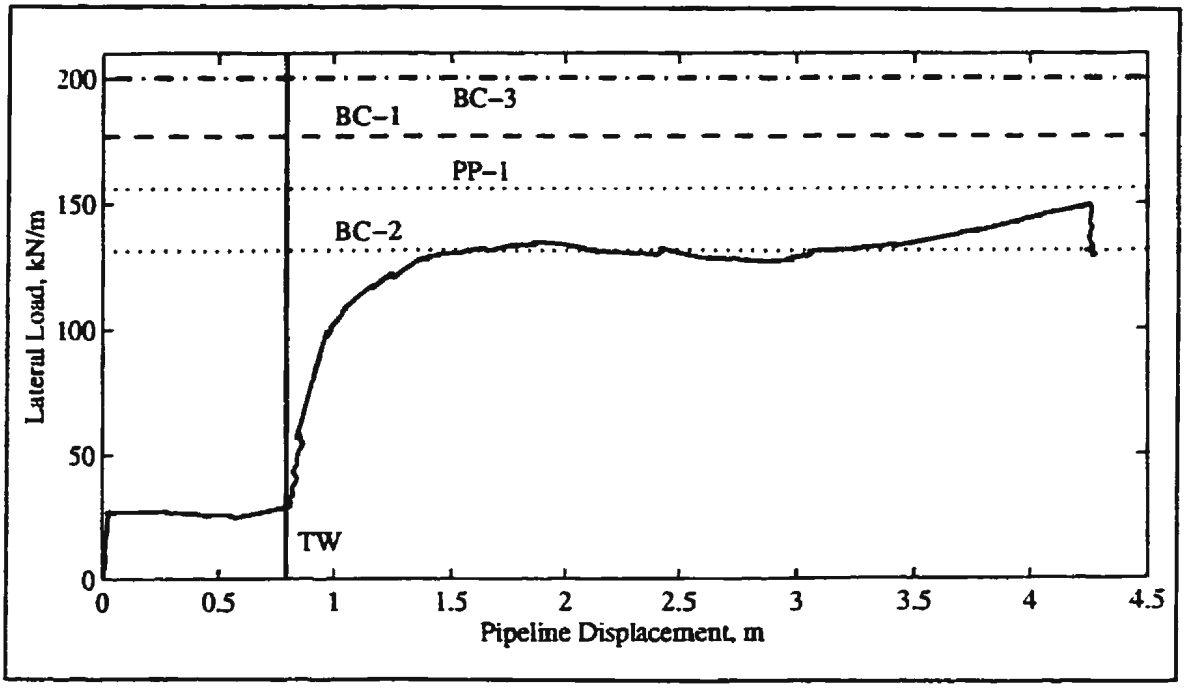

Figure 8.107a - Ultimate lateral loads based on bearing capacity and passive earth pressure formulations for cohesive soil and comparison with Pipeline #1, Test 01, data.

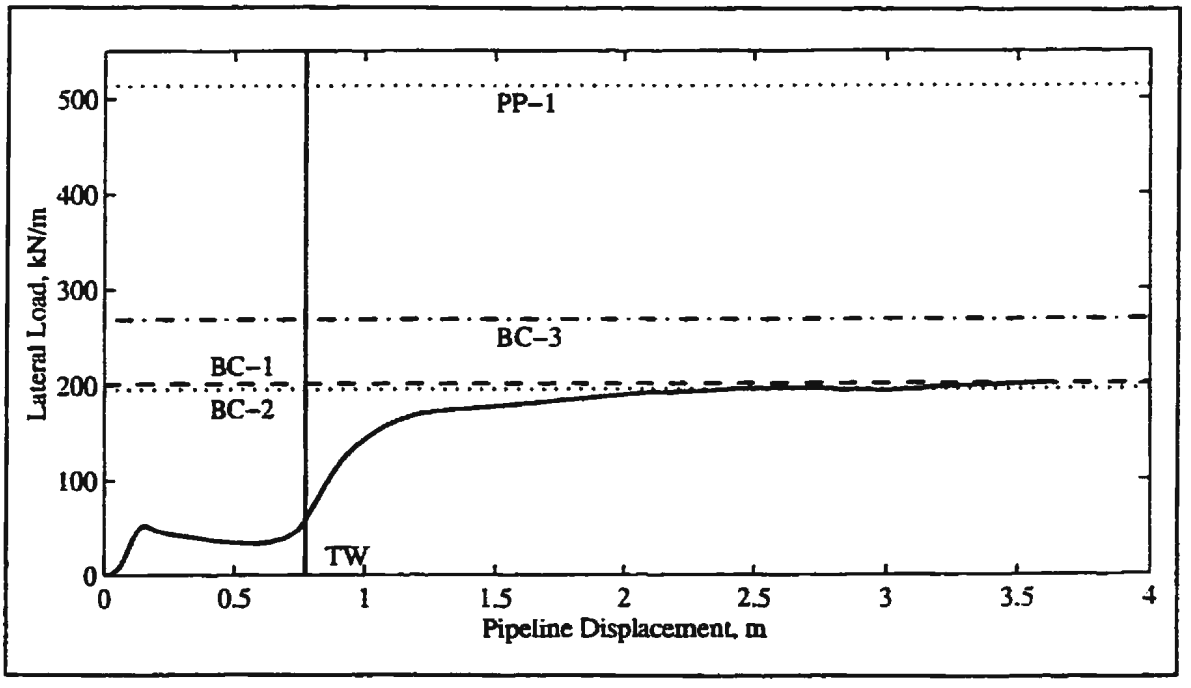

Figure 8.107b - Ultimate lateral loads based on bearing capacity and passive earth pressure formulations for cohesive soil and comparison with Pipeline #1, Test 02, data.

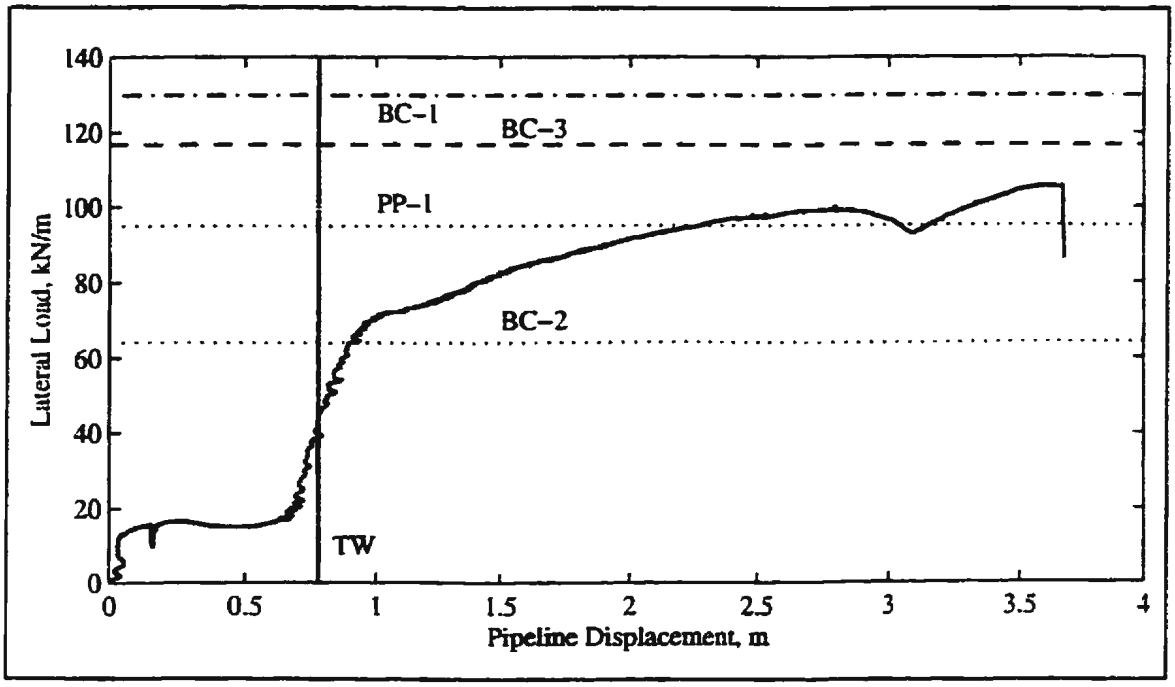

Figure 8.107c - Ultimate lateral loads based on bearing capacity and passive earth pressure formulations for cohesive soil and comparison with Pipeline #3, Test 05, data.

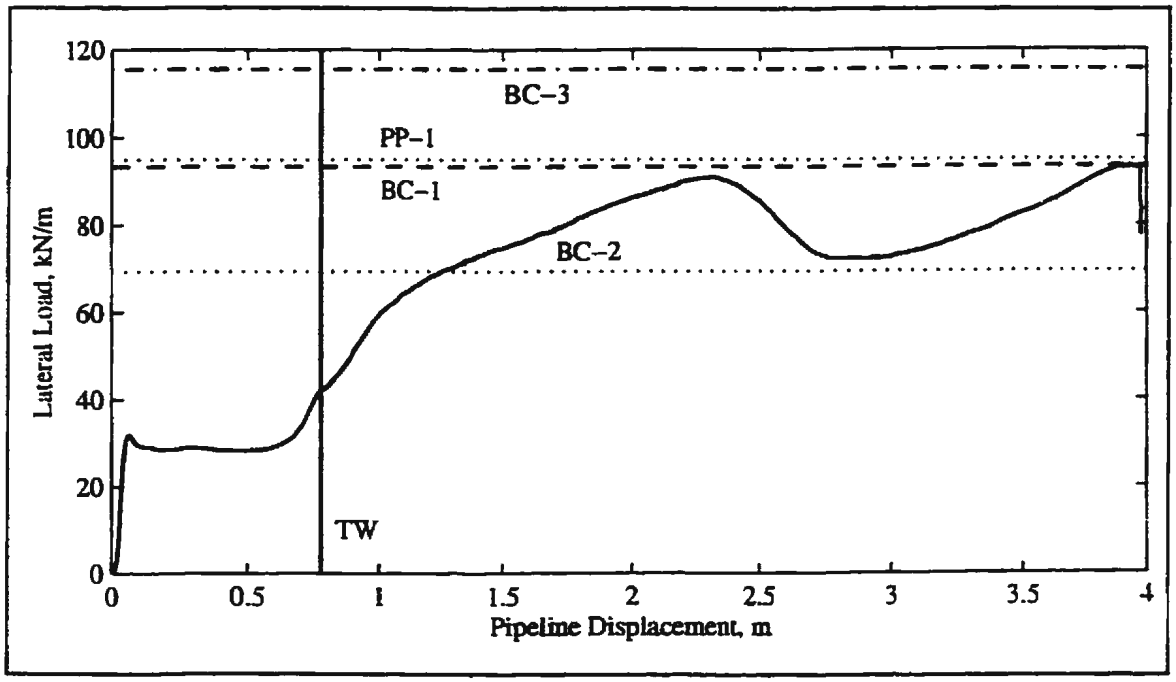

Figure 8.107d - Ultimate lateral loads based on bearing capacity and passive earth pressure formulations for cohesive soil and comparison with Pipeline #4, Test 08, data.

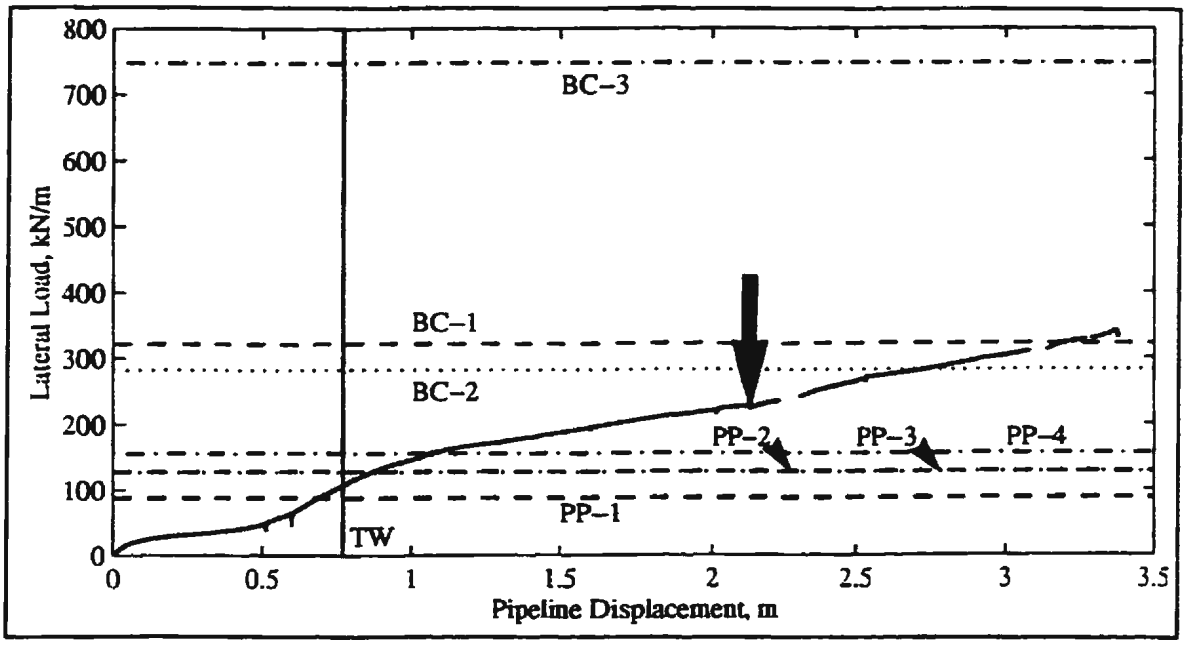

Figure 8.108a - Ultimate lateral loads based on bearing capacity and passive earth pressure formulations for cohesionless or c-ϕ soil and comparison with Pipeline #1, Test 04, data.

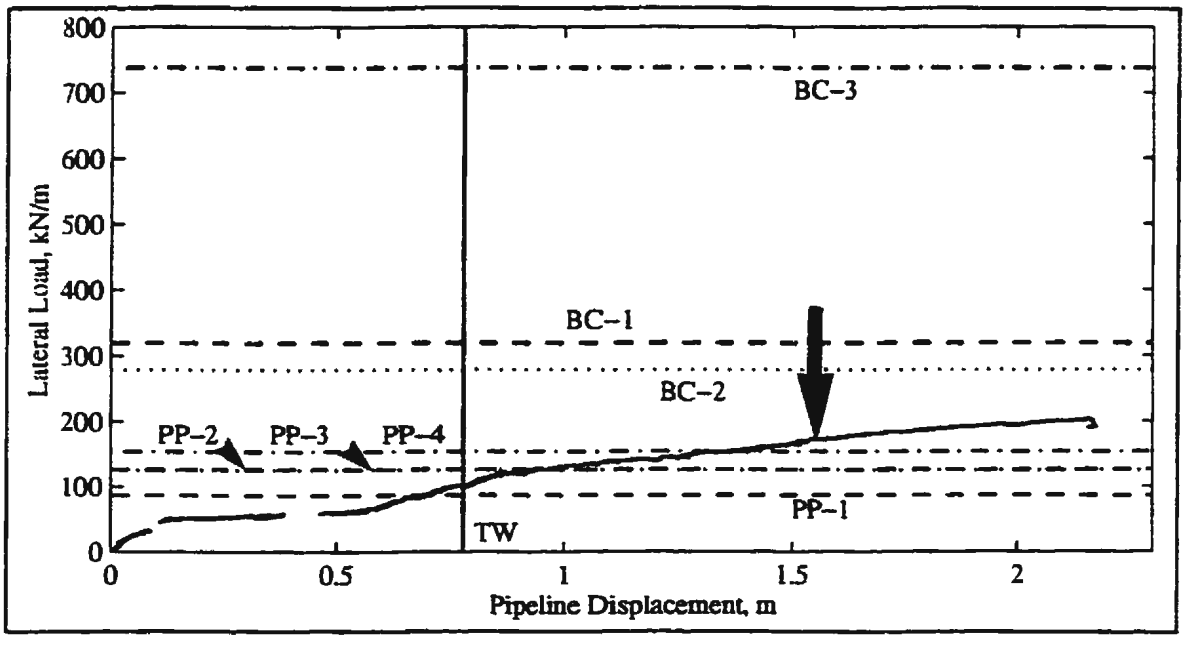

Figure 8.108b - Ultimate lateral loads based on bearing capacity and passive earth pressure formulations for cohesionless or c-ϕ soil and comparison with Pipeline #1, Test 07, data.

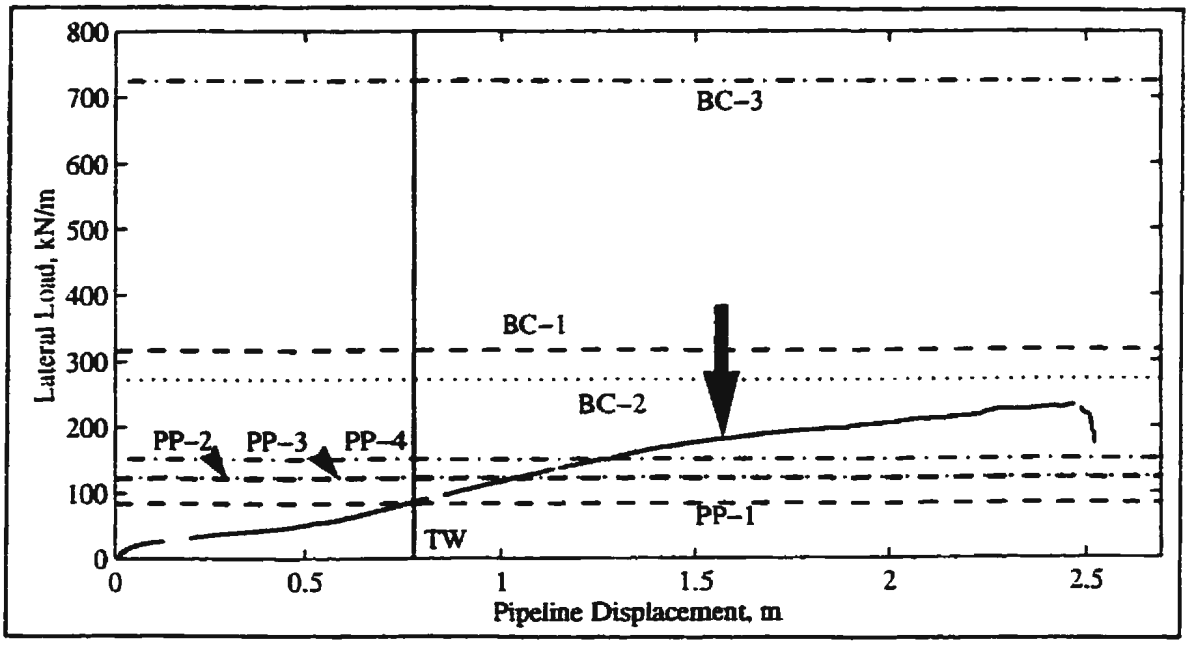

Figure 8.108c - Ultimate lateral loads based on bearing capacity and passive earth pressure formulations for cohesionless or c-ϕ soil and comparison with Pipeline #1, Test 08, data.

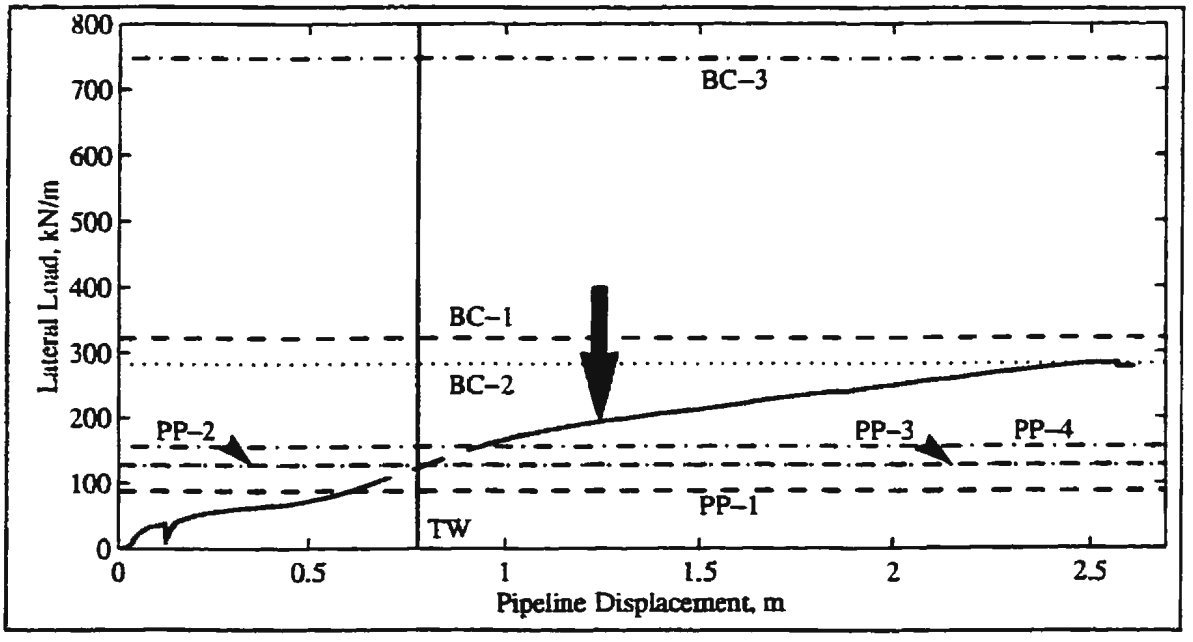

Figure 8.108d - Ultimate lateral loads based on bearing capacity and passive earth pressure formulations for cohesionless or c-ϕ soil and comparison with Pipeline #1, Test 09, data.

Table 8.7a - Bearing Capacity and Passive Earth Pressure Results - Cohesive Soil.

Method/Reference	Test 01 Pipeline #1 (kN/m)	Test 02 Pipeline #1 (kN/m)	Test 05 Pipeline #3 (kN/m)	Test 08 Pipeline #4 (kN/m)
BC-1: Bearing Capacity of a Footing on the Soil Surface (Meyerhof, 1951; Meyerhof, 1963)	177	201	117	93
BC-2: Bearing Capacity of a Footing on the Edge of a Slope (Das, 1987b)	131	196	64	69
BC-3: Bearing Capacity of a Footing Located at the Depth of the Springline (Meyerhof, 1951; Meyerhof, 1963)	200	268	130	116
PP-1: Passive Earth Pressure Solution (Atkinson, 1981)	156	514	71	95

Table 8.7b - Bearing Capacity and Passive Earth Pressure Results - c-ϕ Soil.

Method/Reference	Test 04 Pipeline #1 (kN/m)	Test 07 Pipeline #1 (kN/m)	Test 08 Pipeline #1 (kN/m)	Test 09 Pipeline #1 (kN/m)
BC-1: Bearing Capacity of a Footing on the Soil Surface (Meyerhof, 1951; Meyerhof, 1963)	322	319	316	322
BC-2: Bearing Capacity of a Footing on the Edge of a Slope (Das, 1987b)[1]	282	278	272	283
BC-3: Bearing Capacity of a Footing Located at the Depth of the Springline (Meyerhof, 1951; Meyerhof, 1963)	748	738	725	748
PP-1: Rankine Passive Earth Pressure Solution (Bowles, 1988)	88	86	84	88
PP-2: Coulomb Passive Earth Pressure Solution (Bowles, 1988)	128	125	123	128
PP-3: Passive Earth Pressure Solution for c-ϕ Soils (Terzaghi and Peck, 1967)	127	126	124	127
PP-4: Passive Earth Pressure Solution for c-ϕ Soils (Meyerhof, 1982)	156	154	151	156

Notes - (1) The maximum slope angle, β, available for this analysis ($\beta = 40°$) was used.

capacity analysis for a footing near a slope gives a good approximation to the ultimate lateral load for two of the tests studied. The bearing capacity of a footing on the soil surface also gives a good approximation to the experimental data of Figure 8.107b. The experimental results of Figures 8.107c and 8.107d are somewhere between that predicted by the two analyses. The loading predicted by the bearing capacity of a footing located at the depth of the springline consistently overestimates the ultimate experimental load. Overall, it appears an average value from a footing on the soil surface (BC-1) and a footing near a slope (BC-2) would provide a decent approximation to the measured load.

The data from the drained (c - ϕ) analysis is presented in Figure 8.108 along with the theoretical predictions. For two of the tests, the bearing capacity solutions provide good estimates to the measured peak in the experimental data. However, this may be considered a coincidence as these pipelines have not exhibited a peak but yet have been displaced large distances. If one considers the ultimate to be, as before, where the force-displacement response goes linear, then the bearing capacity methods significantly overestimate the interpreted ultimate lateral load.

Breakover Analysis

An undrained analysis can be conducted based on an assumed bearing capacity failure mechanism similar to that presented by Wantland *et al.* (1979) in Figure 8.109. For the analysis, it is assumed that the chord length of the pipeline/trench wall intersection is similar to the width of a strip footing, B, as shown in Figure 8.109a. The bearing capacity

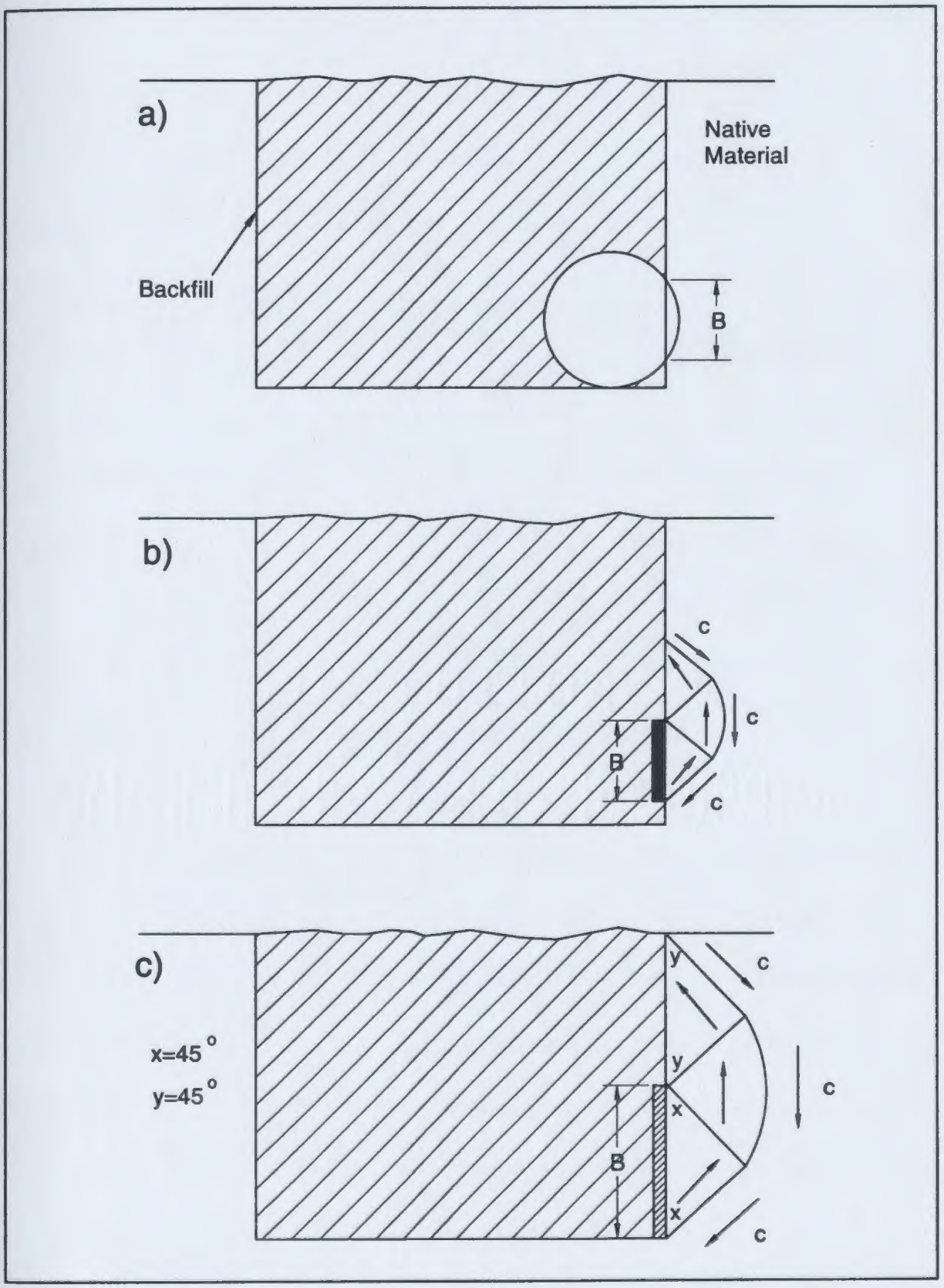

Figure 8.109 - Proposed failure mechanism; undrained analysis.

analysis is carried out as depicted in Figure 8.109b. At some point, the mechanism breaks out at the surface (Figure 8.109c) and this should be the breakover point - that is, the point where there is a noticeable change in the slope of the force-displacement curve. For the conditions investigated during the present test series, a distance to breakover of 0.5D would be expected for pipelines with an embedment ratio greater than 2; in these cases, the failure mechanism would not break out to the surface but rather B would increase with pipeline penetration to a maximum value of D at 0.5D penetration. The theoretical distance into the trench wall to breakover (for a 0.95m diameter pipeline) as a function of embedment ratio is presented in Figure 8.110 along with the experimental data points from Table 8.2. It must be stressed that this is only one possible failure mechanism and also that the mechanism could change with pipeline burial depth; other potential mechanisms could be investigated.

Drained and undrained analyses similar to those outlined above can be conducted to assess the effect of drainage conditions on the distance of penetration to breakover. Again, it should be emphasized that this is only one potential failure mechanism and that there are other potential mechanisms which could be investigated. For the analysis, a 0.95m diameter pipeline is considered to have 0.8m of cover (H/D = 1.842). Again, it is assumed that the chord length of the pipeline/trench wall intersection is similar to the width of a strip footing, B, as was shown in Figure 8.109a. The bearing capacity analysis is carried out as depicted in Figure 8.109c where x and y = 45° for an undrained analysis and $x = 45° + \phi/2$, $y = 45° - \phi/2$ for an drained analysis. At the breakover point, the

mechanism breaks out at the surface as was depicted in 8.109c. Analysis of these mechanisms indicates a penetration of 0.263m or 0.28D to undrained breakover and a penetration of 0.019m or 0.02D to drained breakover. The theoretical distance into the trench wall to breakover (for a 0.95m diameter pipeline with an embedment ratio of approximately 1.842) as a function of pipeline displacement rate is presented in Figure 8.111 along with the experimental data points from Table 8.2. It has been assumed that the distance to breakover varies linearly from the undrained condition to the drained condition at an interaction rate of 0.82 m/day.

8.4.6 Passive Earth Pressure Solutions

Theories of Terzaghi (1943) consider the lateral resistance of a vertical anchor plate (similar to a pipeline) similar to a passive earth pressure solution for shallow anchors to an embedment ratio of approximately 2. Thus passive earth pressure solutions should be investigated and compared to experimental results. In the analysis, it is assumed that the soil from the surface to the base of the pipeline is being displaced. Results of this analysis and the appropriate references are presented in Table 8.7. Results are compared to experimental data in Figures 8.107 and 8.108.

For the undrained tests (Figure 8.107), the passive pressure solution appears to have provided a good approximation to the ultimate lateral load for the test with the embedment ratio of 1.263 (Figure 8.107c), a reasonable approximation for the tests in which the embedment ratio equalled 1.842 (Figures 8.107a and 8.107d), and a poor estimate for the

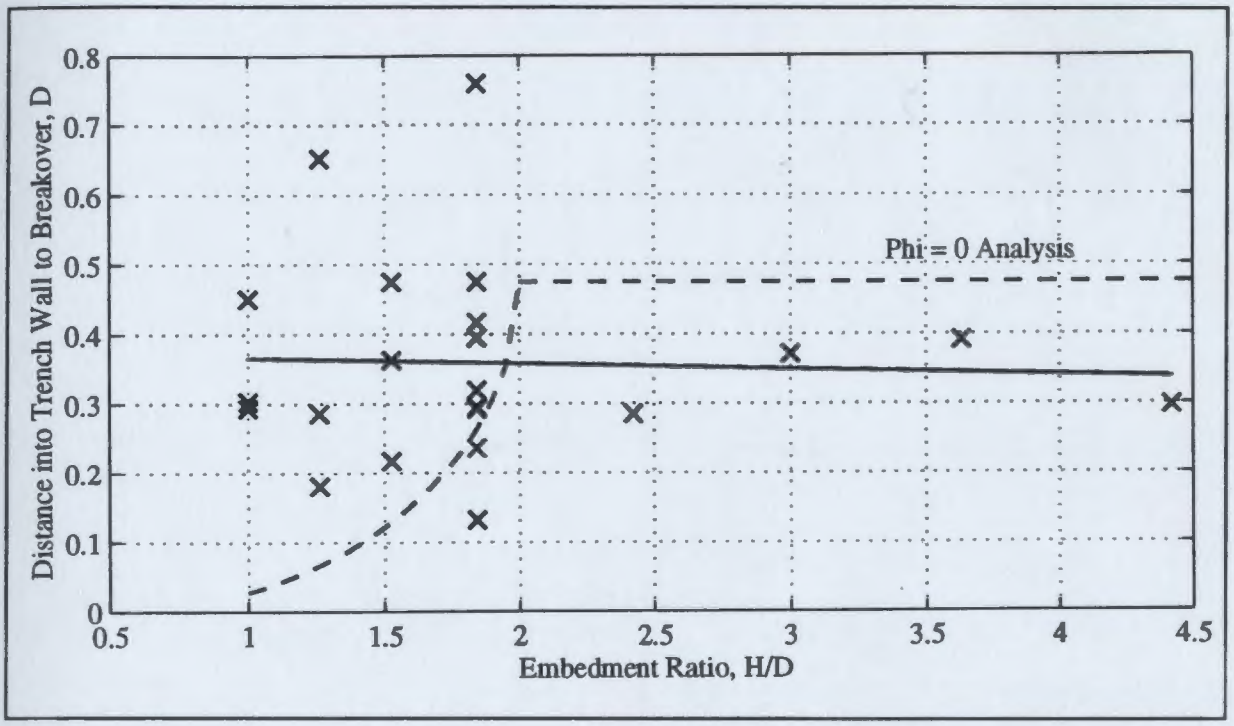

Figure 8.110 - Theoretical and experimental distances into the trench wall to breakover versus embedment ratio for undrained conditions.

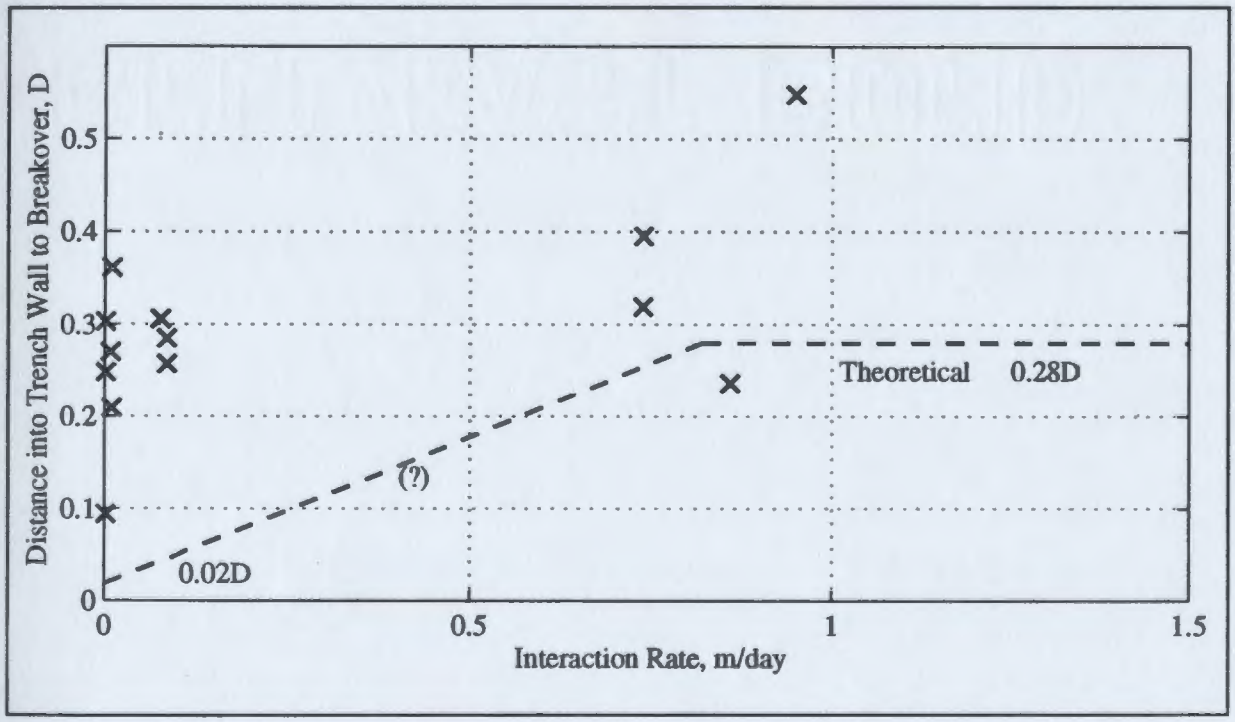

Figure 8.111 - Theoretical and experimental distances into the trench wall to breakover versus interaction rate for an embedment ratio of 1.842.

test with an embedment ratio of 4.421 (Figure 8.107b). This is consistent with the findings of Mackenzie (1955) who found that passive wedge theory yielded good predictions in cases of shallow anchor cover but deviated for deeper covers and a correction had to be used. Overall, this method provided estimates ranging from 95 to 256% of the measured experimental ultimate load while for the shallow cases (embedment ratio less than 2) the estimates ranged from 95 to 115%.

The results for the cohesionless and c-ϕ analyses are presented in Figure 8.108 and Table 8.7b. For all of the tests, the passive earth pressure solutions underpredict the measured ultimate lateral loads. Again, if the ultimate is considered to be where the force-displacement response goes linear as indicated by the vertical arrows in Figure 8.108, then the method suggested by Meyerhof (1982) provides the best estimate; between 69 to 87% of the interpreted ultimate experimental lateral load for the tests studied.

Chapter 9

Summary, Conclusions, and Recommendations

9.1 Summary

The work outlined in this thesis was conducted to examine lateral pipeline/soil interaction and to concentrate on objectives which were determined in consultation with an industry sponsor. This thesis has described the tests and results from the experimental program. Lateral pipeline/soil interaction was investigated for a 0.95m prototype pipeline under cover depths ranging from 0 to 3.25m and buried in a trench ranging from 1.5 to 3m in width. The objectives of the test program were to determine the effects of trench geometry, soil preconsolidation stress, pipeline displacement rate, and backfill type on the interaction. Prototype-scale pipeline displacement rates ranging from 0.00079 to 1.8 m/day were investigated in kaolin-silt testbed materials which had been preconsolidated to 140 and 400kPa. Trench backfill types included slurry, chunks of backfill, remoulded material and fine sand. Also presented in this thesis are an analysis of the experimental data, an investigation of the effects of the various parameters studied, an evaluation of existing methods of interaction analysis, and analyses derived from conventional soil mechanics methods.

9.2 Conclusions

The general procedures followed in this test series were adequate in the setting up and execution of the centrifuge experiments. All of the instruments generally operated without problem and the sample preparation and site investigation techniques proved to work well. Spaghetti strands excavated approximately halfway along the length of the pipeline indicate the potential failure mechanisms during the interaction. In the tests which were considered undrained, the spaghetti strands below the pipeline showed a well defined zone of shear deformation extending approximately 0.5D below the base of the pipeline. The spaghetti strands passing above the pipe indicated plastic flow around the pipe during displacement. In the tests which were considered drained or partially-drained, the spaghetti strands indicated a completely different failure mechanism. Distinct failure surfaces were observed in front of the pipeline extending from the toe of the pipeline to the soil surface at approximately 25 to 44°.

Results of Parametric Analyses of Experimental Data

The experimental data definitely demonstrated the effect of embedment or pipeline cover; as the H/D ratio increased from 1 to 1.84 the normalized lateral load became greater. However, for higher H/D ratios, the effect of burial depth on the lateral loading was not as obvious. Therefore, based on experimental data, it appears that the interaction or ultimate normalized resistance increases with increasing embedment ratio up to a point and that the normalized distance to peak load increases slightly with embedment ratio. Relationships have also been derived relating normalized loads at predetermined displacements versus

embedment ratio and parameters describing a bilinear analysis versus embedment ratio. Data from a test in which trench width was investigated indicated that this parameter had little or no effect on the interaction when the data was adjusted so that the trench wall corresponded to the same point along the force-displacement curve.

It is apparent from the analyses contained herein that as interaction velocity decreased or tended towards a drained loading condition, the loads experienced by the pipeline were greater than those experienced by a pipeline during an undrained loading condition for these soil conditions. The observed rate effect agrees well with the finite element study conducted by Altaee and Boivin (1995) which indicated that the faster the pipe displaced, the smaller the resulting lateral force against the pipe. As well, Karal (1983) suggests that decreasing loading rate results in increasing soil reaction, except for a rapid loading which allows development of suction as part of the soil resistance. It would also appear that during the drained test, the backfill becomes more of a factor in the interaction. During the undrained tests, the interaction curve remains relatively horizontal while the pipeline is still in the backfill but during the drained test, the interaction curve increases significantly. The drained and partially-drained interaction curves exhibited no clearly defined peak and might have continued to increase if the tests had not been terminated. However, this may have been the result of a surcharge buildup over and in front of the pipe. The rate effect is significant because if current state-of-practice is based on assuming an undrained interaction between pipe and soil, then it could significantly underestimate the load transferred to the pipeline.

As pointed out above, the difference in drained and undrained behaviour was also evident from the internal deformations of the tests. Failure mechanisms associated with soil displacement in front of the pipelines during drained to somewhat drained tests were similar (rupture formation - failure wedges extending in front of the pipeline). Failure mechanisms associated with soil displacement in front of the pipelines during essentially undrained interactions were similar (plastic flow around the pipeline).

Pore pressure transducers buried in the soil mass also give an indication of the effect of the pipeline displacement rate on the drainage conditions within the soil mass. Excess pore pressures in front of the slowly displaced pipelines continue to dissipate with time and are only slightly affected by the pipe interaction with the trench wall. Excess pore pressures in the soil in front of the rapidly displaced pipelines increased significantly during pipeline interaction with the trench wall. The largest deviation in pore pressure response at the pipeline/soil interface was recorded by the rapidly displaced pipelines.

It appears that soil preconsolidation stress level affects the lateral pipeline/soil interaction curves. Observation of the data suggests slightly higher normalized interaction loads for the a lower overconsolidation ratio. However, not enough tests were conducted to determine conclusively what effect, if any, soil preconsolidation stress had on the interaction.

The experimental data suggests that backfill properties could affect the overall normalized interaction between the pipeline and the soil. However, it has not been determined if this is

due to a change in failure mechanism (because of the different backfill being pushed in front of the pipe) or a change in the separation condition behind the pipeline. As might be expected, in the test where different backfills were used, it was observed that the pore pressure response at the pipeline/soil interface was greatest in the remoulded backfill and least in the dry sand. In any event, it might be expected that interaction factors might increase with increased suction at the rear pipeline/soil interface which has also been suggested by Karal (1983). Post-test observation during excavation indicated a small wedge of backfill was pushed in front of the pipe during the test involving soft backfill. During the test involving sand backfill, it appears that a bulb of sand was pushed in front of the pipe. This mode of failure is similar to that suggested by Meyerhof and Hanna (1978) for a footing which rests on a relatively thin strong layer above a weak deposit. The authors suggest that at ultimate load, a soil mass would be pushed in the underlying deposit in approximately the direction of applied load. In the case of a soft stratum overlying a stronger stratum, Meyerhof and Hanna (1978) show that the ultimate bearing capacity of the upper soil layer is much smaller than that of the soil below it and the weak soil may be squeezed out from between the footing and the strong soil layer. While differences in ultimate loads from the different backfills were observed, no definitive difference in failure mechanism could be discerned.

It is suggested that the modelling of models experiments provided an acceptable comparison of the results. However, there was some observed scatter in the data especially at the shallower burial depths. It is suspected that because of the decreased burial depth, the pipe

self weight may have played a more significant role during the interaction. Because the pipeline mass has not been scaled, some discrepancy in results might be expected. Also, undrained shear strength has been interpreted by extrapolating a shear strength profile at depth back to the pipe springline assuming a linear relationship. The springline of the shallow pipelines were located a very small distance below the soil surface (4-5mm in the 100g tests). Therefore, the method of interpreting shear strength might have some limitations.

Evaluation of Existing Methods of Interaction Analysis

The interaction factors presented in this thesis support the hypothesis that after a certain H/D value, the stress level at the springline has less influence on the interaction factor and a deep seated failure mechanism occurs. For the tests which were considered to be undrained, the experimentally derived interaction factors appear to be bounded by the Rowe and Davis (1982a) "Immediate Separation" and Hansen (1961) interaction curves for an embedment ratio less than approximately 2. For embedment ratios greater than 2, the trend in the experimentally derived interaction factors is quite similar to the Rowe and Davis (1982a) "Immediate Separation" curve. Therefore, undrained pipeline loads can be estimated from existing means using a form similar to Equation [2-11] along with Figure 8.85. Results indicate that what is used in sate-of-practice is reasonable. Differences between the experimental and theoretical interaction factors are attributed to the fact that the theories have been based on the horizontal movement of buried plates and piles and not on pipeline/soil interaction. Also these theories do not consider the construction aspects of the interaction

(i.e. the presence of a trench).

It is noted that ASCE (1984) suggests, for clays, a displacement to ultimate load equivalent to 3 to 5% of the depth to the base of the pipeline. This would typically be less than 0.1D for the prototype pipelines with a H/D ratio of 1.842 scaled from this experimental program. Observation of the experimental data indicates displacements greater than one pipe diameter were needed to achieve the interpreted ultimate load on the pipelines (see Equation [8-9]. Differences are partially attributed to the presence of a trench during the current tests (the pipe would not be as confined).

Comparison of the theoretical results in the hyperbolic portion of the curves indicates that the p-y curve construction suggested by ASCE (1984) overpredicts the rate at which the load was transferred to the pipeline. Again, this is attributed to the fact that these theories do not consider the construction aspects of the interaction.

The drained and partially-drained interaction curves exhibited no clearly defined peak and may have continued to increase if the tests had not been terminated. In one instance, the peak has been taken where the test terminated and should be considered a possible lower bound to the interaction factor. In another instance, the peak has been take at the point where the p-y curve goes linear as the result of the buildup of surcharge over and in front of the pipe. Actuator restraint may have also had an effect on the development of the curve; the pipeline may not have been able to follow the path of least resistance.

ASCE also provide suggestions for displacements to ultimate load in frictional material; 2 to 10% of the depth to the base of the pipeline. However, displacements greater than one pipe diameter were required during the drained tests to achieve the interpreted peak load on the pipeline (or the point where the test was terminated). Again, the presence of a trench likely played a part in the distance needed to the interpreted peak.

Existing theoretical formulations to estimate ultimate load on the pipeline in c-ϕ and cohesionless soils have been compared to experimental data. Ultimate resistances were sometimes underpredicted and sometimes overpredicted depending on where the ultimate load on the pipeline was interpreted. At best, the Hansen (1961) method can be said to be conservative up to a certain displacement.

Empirical formulations have been derived from the experimental data using common analysis procedures and back-compared to experimental force-displacement curves. For undrained response, these formulations were derived through analysis of ultimate normalized resistances (see Equation [8-47] through [8-50]), analysis of normalized resistances at specified displacements (see Equation [8-12] through [8-17]), bilinear analysis of the force-displacement curves (see Equation [8-18] through [8-24]), and curve fitting of the experimental data (see Table 8.3). These methods yielded ultimate lateral pipeline loads within approximately ±10%. For drained response, curve fitting of the experimental data has yielded empirical formulations predicting lateral pipeline loads within approximately ±25% (see Equation [8-33] through [8-36] and Table 8.3.

Evaluation of Conventional Soil Mechanics Methods

Other theories (i.e. from anchors and piles) have been assessed for application to the analysis of pipeline/soil interaction. Several potential methods have been analysed looking at: the suitability of subgrade reaction estimates to the initial portion of the force-displacement curve; the estimate of ultimate load using other anchor plate/soil and pile/soil interaction methods; the fit of pile/soil p-y curve formulation methods to the experimental data; and estimates of ultimate load using bearing capacity and passive earth pressure solutions.

The subgrade reaction analysis approach showed little promise to estimate the initial slope of the force-displacement response (see Appendix M). In cohesive soils, where the subgrade reaction was set at the start of pipeline interaction with the trench wall, the interaction was reasonably approximated by some of the subgrade reaction formulations up to approximately 50 to 60% of the ultimate resistance. No reasonable approximations resulted for interaction in cohesionless soil.

Analysis of anchor plate/soil interaction methods for cohesive soils suggest that the ultimate lateral loads were best estimated by the method of Rowe and Davis (1982a) which typically yielded an ultimate lateral load within $\pm 20\%$ of the experimental load (see Equation [2-40] and Figure 2.8). This method utilized all the components of the formulation while previously only the interaction factors were utilized (method of Rizkalla *et al.*, 1992). In cohesionless soil, if the ultimate load is taken to be the ultimate measured

due to no clearly defined peak, the best method (Rowe and Davis, 1982b) offered a conservative estimate to the load transferred to the pipe up to an approximate overall displacement of 1m (see Equation [2-43] and Figures 2.19 and 2.20). If the ultimate is interpreted as the point where the force-displacement curve went linear, then the Rowe and Davis (1982b) method predicts to within 60 to 80% of the ultimate.

A similar analysis for laterally loaded piles in cohesive soil indicated the ultimate resistance of the pipeline/soil interaction was best estimated using the method of Matlock (1970) with an empirical factor, J, equal to 0.25 (see Equations [2-58] through [2-63]). Using this method yielded a theoretical ultimate lateral load ranging from -14 to +4% of the experimental ultimate resistance for the cases studied. For the drained analyses (see appropriate references), the Poulos (1995) method provided a conservative estimate of the overall load transferred to the pipes while if the ultimate load is interpreted at the point where the force-displacement curve becomes linear, then the best estimate is provided by the formulations suggested by Broms (1964b) or Randolph and Houlsby (1984) which predicts within 93 to 119% of the interpreted ultimate load. Overall, the best estimates of the force-displacement curves in cohesive soil appear to be obtained from the p-y curve formulations of Matlock (1970) and Reese and Welch (1975) (see Equations [2-62], [2-63], and [2-66] through [2-68]). For cohesionless soils, the p-y curve formulations tend to overestimate the force-displacement response due mainly to the presence of a trench.

Bearing capacity analyses (see Subsection 8.4.5) conducted suggest that an average

capacity for a footing on the soil surface and a footing near a slope would provide a reasonable approximation to the undrained ultimate lateral load for a pipeline. The capacity predicted for a footing located at the depth of the springline consistently overestimated the ultimate experimental load. Under drained conditions, in some cases, the bearing capacity solutions provided decent estimates to the measured peak in the experimental data. If the ultimate is considered to be as before, where, the force-displacement response goes linear, then the bearing capacity methods significantly overestimate the interpreted ultimate load.

An undrained analysis was conducted based on an assumed bearing capacity failure mechanism where it was assumed that the chord length of the pipeline/trench wall intersection is similar to the width of a strip footing. The analysis was conducted for a number of embedment ratios and results compared to the experimental data. It was found the theoretical distance into the trench wall to breakover typically underestimates the actual experimental data points. Drained and undrained analyses were also conducted to assess the effect of drainage conditions on the distance of pipe (0.95m diameter and embedment ratio of 1.84) penetration to breakover. Comparison of the theoretical distance into the trench wall to breakover with experimental data points indicates that the theory generally significantly underestimates the experimental distances especially at low interaction rates.

Passive earth pressure theories (see Subsection 8.4.6) were also investigated for cohesive, cohesionless, and c-ϕ soils. For undrained tests, the passive earth pressure solution appears to have provided a good approximation to the ultimate lateral load for shallow

pipeline depths and a poor estimate to the ultimate lateral load for deep pipeline depths. The results for the cohesionless and c-ϕ analyses indicated the passive earth pressure solutions underpredicted the measured ultimate lateral loads. The c-ϕ analysis method suggested by Meyerhof (1982) provided the best estimate; between 69 and 87% of the ultimate experimental load (where the load goes linear) of the tests studied.

Finally, while several methods of estimating lateral pipeline/soil interaction have been presented in this thesis, no particular one is suggested as the definitive answer to a particular problem. Rather, several of the suggested analyses methods should be evaluated for that particular problem and the results of such a study compared and contrasted to arrive at a reasonable prediction for the force-displacement response of a laterally loaded pipeline.

9.3 Recommendations

This research program examined the problem of laterally displacing pipeline/soil interaction through the development of a high strength modelling soil and a series of centrifuge tests. These tests investigated the effects of burial depth, ditch width, displacement rate, soil preconsolidation stress, and backfill properties on the pipeline/soil interaction. The interaction was considered to be two-dimensional as the pipeline was essentially a rigid segment. Subsequent to testing, analysis indicated that: the trench width had little or no effect on the interaction; the load on a pipeline increased with increasing burial depth; and the

displacement rate had a significant effect on the loads transferred to the pipeline by the soil (for the particular soil/backfill system studied). The rate result is significant because if current state-of-practice is based on undrained interaction between pipe and soil, then it could significantly underestimate the load transferred to the pipeline. The data also suggest that backfill properties could affect the overall interaction curve. However, not enough tests were conducted to determine what effect, if any, soil preconsolidation stress has on pipeline/soil interaction. It was also noted that the displacements needed to mobilize ultimate resistance on the pipelines were considerably larger than those suggested by accepted theory based on anchor plates and piles.

It is often assumed that soils are isotropic; that is their strength and properties are the same in all directions. However, it has been proven that the material properties, stress-strain response, and undrained strength of many clays are directionally dependant; they are anisotropic. This, in cases, has resulted in an inclusion of anisotropic behaviour in analyses of soil response, and in particular the finite element method (Hansen and Clough, 1982). The implications of anisotropy on the current results have not been investigated. The soil strength and properties were determined from triaxial and cone penetrometer testing. The samples for triaxial testing was taken from vertical oriented cores through the sample. CPT testing was conducted vertically through the soil sample. However, the model pipeline was moved laterally and therefore loaded horizontally through interaction with the soil. Davis and Christian (1971) suggest that the undrained strength of undisturbed samples cut vertically may be as much as 170% greater than a sample cut with an axis 45° to the vertical. The

authors suggest that if anisotropic strength is though to be a concern, a correction factor. which the authors suggest, should be applied to the bearing capacity factor. It has been suggested in the literature by some authors that soil resistance to lateral pipe movement is similar to the bearing capacity of a foundation. Therefore, during analysis of the experimental data of this thesis, experimental interaction factors have been compared to an undrained bearing capacity factor as. It is therefore recommended that in future work the effects of anisotropy on the interpreted undrained shear strength be investigated.

It was apparent from the experimental research, that loads experienced during a slow interaction were significantly greater than those from a rapid, undrained interaction for the single burial depth (H/D approximately 1.84) and trench width (2.5m full-scale) investigated. The data from this research program were for an essentially rigid pipeline segment (two-dimensional) and large relative distances were needed to mobilize ultimate soil resistance. The effect of relative pipeline stiffness on the ultimate soil resistance and distance to mobilize this resistance can be investigated through three-dimensional testing.

Further research could be conducted to increase the size of the existing data base which would in turn reduce scatter in the experimental data. This could result in an improvement or refinement in the analytical methods presented herein and assist in selecting the most appropriate methods of analysis. It is also suggested that a research program be conducted to further examine slow lateral pipeline/soil interaction and to determine the sensitivity of a three-dimensional interaction to pipeline burial depth, trench width, pipeline relative

stiffness, and stress history of the soil. The effects of internal pressure on the response of the pipeline to loading, the effect of end conditions of the pipeline, and the effect of backfill properties could also be investigated. The results could be compared with predictions using available pipeline/soil interaction computer analysis software.

References

Adams, A. (1991). "U.K. Experience in Offshore Pipeline Management". Keynote Address, Proceedings, *International Workshop on Offshore Pipeline Safety*, D.V. Morris (ed.), New Orleans, LA, Dec. 4-6, pp. 34-43.

Altaee, A. and Boivin, R. (1996). "Laterally Displaced Pipelines: Finite Element Analysis". Proceedings, *15th Offshore Mechanics and Arctic Engineering Symposium*,Volume V, pp. 209-216.

API - American Petroleum Institute (1993). *Design, Construction, Operation, and Maintenance of Offshore Hydrocarbon Pipelines*. API Recommended Practice 1111, 2nd Edition, November.

ASCE (1984). *Guidelines for the Seismic Design of Oil and Gas Pipeline Systems*. Committee on Gas and Liquid Fuel Lifelines, Technical Council on Lifeline Earthquake Engineering, ASCE, New York.

Ashworth, B. (1994). "Integrity Management Methods". *Managing Pipeline Integrity - An Issues Workshop on Pipeline Lifecycle*. Sponsored by CANMET, NEB and ARC, Banff, Alberta, June 9-10.

ASME (1995). *Gas Transmission and Distribution Piping Systems*. ASME B31.8-1995 Edition, American Society of Mechanical Engineers, New York.

Atkinson, J.H. (1981). *Foundations and Slopes - An Introduction to Applications of Critical State Soil Mechanics*. John Wiley and Sons, New York, 382p.

Audibert, J.M.E. and Nyman, K.J. (1977). "Soil Restraint Against Horizontal Motion of Pipes". Journal of the Geotechnical Engineering Division, ASCE, Vol. 103, No. GT10, pp. 1119-1142.

Audibert, J.M.E., Lai, N.W., and Bea, R.G. (1978). "Design of Pipelines to Resist Seafloor Instabilities and Hydrodynamic Forces". Proceedings, *Energy Technology Conference and Exhibition*, Houston, Texas, Paper 78-PET-37, Nov. 5-9, 12p.

Audibert, J.M.E., Lai, N.W., and Bea, R.G. (1979). "Design of Pipelines - Sea Bottom Loads and Restraints". *Pipelines in Adverse Environments: A State of the Art*, ASCE, Vol. 1, pp. 187-203.

Audibert, J.M.E., Lai, N.W., and Bea, R.G. (1980). "Designing Subsea Pipelines to Resist Instabilities - Part 3". Pipeline & Gas Journal, Vol. 207, June, pp. 49-53.

Bea, R.G. (1985). "Geotechnical considerations in Submarine Pipeline Design". *Advances in Offshore Oil & Gas Pipeline Technology*, R.F. de La Mare (ed.), Gulf Publishing Company, Houston, pp. 1-13.

Bea, R.G. and Arnold, P. (1973). "Movements and Forces Developed by Wave-Induced Slides in Soft Clays". Proceedings, *5th Offshore Technology Conference*, ASME, Houston, Vol. 2, pp. 731-742.

Bea, R.G. and Bernard, H.A. (1973). "Movements of Bottom Soils in the Mississippi Delta Offshore". In, *Offshore Louisiana Oil and Gas Fields*, The New Orleans Geological Society, pp. 13-28.

Bea, R.G. and Audibert, J.M.E. (1980). "Geotechnical Problems in Design of Offshore Pipelines". Proceedings, *International Symposium on Marine Soil Mechanics*, Mexico City, pp. 139-154.

Bea, R.G. and Aurora, R.P. (1982). "Design of Pipelines in Mudslide Areas". Proceedings, *14th Offshore Technology Conference*, ASME, Houston, pp. 401-415.

Bea, R.G., Bernard, H.A., Arnold, P., and Doyle, E.H. (1975). "Soil Movements and Forces Developed by Wave Induced Slides in the Mississippi Delta". Journal of Petroleum Technology 27 (4), pp. 500-514.

Bea, R.G., Wright, S.G., Sircar, P., and Niedorada, A.W. (1980). "Wave Induced Slides in South Pass Block 70, Mississippi Delta". Proceedings, *ASCE Convention and Exposition*, October, Preprint 80-506.

Begemann, H. (1974). "General Report: Central and Western Europe", Proceedings, *European Symposium on Penetration Testing*, pp. 29-39.

Bellassai, S.J. (1995). "Comments on the NRC Marine Boards Report on Improving the Safety of Marine Pipelines - Special Written Contribution". Proceedings, *International Workshop on Damage to Underwater Pipelines*, New Orleans, Louisiana, February, pp. 206-216.

Bennett, B.A. (ed.) (1988). *Pipeline Infrastructure*. ASCE, ASCE Publication 662-9, New York, 475p.

Bhushan, K., Haley, S.C., and Fong, P.T. (1979). "Lateral Load Tests on Drilled Piers in Stiff Clays". Journal of the Geotechnical Engineering Division, ASCE, Vol. 105, No. GT8, pp. 969-985.

Boivin, R.P. and Cavanagh, P.C. (1992). "Remedial Action Required for Two Gas Pipelines Crossing an Unstable Slope". Proceedings, *11th Offshore Mechanics and Arctic Engineering Symposium*, Volume V-B, pp. 553-558.

Boizoni, G., Cuscuna, S. and Perego, U. (1993). "Physical and Mathematical Modelling of Pipeline Behaviour in Landslide Areas". Proceedings, *9th PRC/EPRG Biennial Joint Technical Meeting on Line Pipe Research*, Paper Number 5, Houston, May 11-14, pp. 5-1 - 5-17.

Boon, M.P. and Craig, W.H. (1978). "Model Ground Anchors Under Gravitational and Centrifugal Accelerations". Revue Francaise de Geotechnique, No. 3, pp. 18-23.

Bowles, J.E. (1977). *Foundation Analysis and Design*. 3rd Edition, McGraw-Hill Inc., New York, 1004p.

Bowles, J.E. (1988). *Foundation Analysis and Design*. 4th Edition, McGraw-Hill Inc., New York, 1004p.

Broms, B.B. (1964a). "Lateral Resistance of Piles in Cohesive Soils". Journal for Soil Mechanics and Foundation Engineering, ASCE, Vol. 90, SM3, pp. 27-64.

Broms, B.B. (1964b). "Lateral Resistance of Piles in Cohesionless Soils". Journal for Soil Mechanics and Foundation Engineering, ASCE, Vol. 90, SM3, pp. 123-156.

Bukovansky, M., Greenwood, J.H., and Major, G. (1985). "Maintaining a Natural Gas Pipeline in Active Landslides". Proceedings, *Advances in Underground Pipeline Engineering*, J.K. Jeyapalan (ed.), ASCE, pp. 438-448.

Canadian Foundation Engineering Manual (1992). Third Edition. Canadian Geotechnical Society, Technical Committee on Foundations, 512p.

CANMET, (1993). Report on the *Issues Workshop on Pipeline Lifetime*. R.W. Revie (ed.). Red Deer, Alberta, June 1-2.

Cavanagh, P.C. and Rizkalla, M. (1992). "The Development of an Alternative Approach for Pipeline Operation in Unstable Slopes: A Case History". Proceedings, *11th Offshore Mechanics and Arctic Engineering Symposium*, Volume V-B, pp. 543-551.

C-FER (1994). *Risk-Based Calibration of Reliability Levels for Limit States Design of Pipelines*. Final Report Submitted to National Energy Board, Centre for Frontier Engineering Research (C-FER), March.

C-FER (1995). *Development of Pipe-Soil Interaction Models for Frost Heave Analysis*. Final Report Submitted to National Energy Board, Centre for Frontier Engineering Research (C-FER), July.

Christian (1961). *Model Tests with Transversally Loaded Rigid Piles in Sand*. Bulletin 12, Danish Geotechnical Institute, Copenhagen, Denmark, pp. 10-16.

Chung, R. (ed.) (1996). *The January 17, 1995 Hyogoken-Nanbu (Kobe) Earthquake; Performance of Structures, Lifelines, and Fire Protection Systems*. National Institute of Standards and Technology Special Publication 901, July.

Clark, J.I., Paulin, M.J., Lach, P.R., Yang, Q.S., and Poorooshasb, H. (1994). "Development of a Design Methodology for Pipelines in Ice Scoured Seabeds". Proceedings, *13th Offshore Mechanics and Arctic Engineering Conference*, ASME, Houston, Vol. 5, pp. 107-125.

Corté, J-F. (ed.) (1988). *Centrifuge 88 - Proceedings of the International Conference on Geotechnical Centrifuge Modelling*, A.A. Balkema, Rotterdam, 610p.

Corté, J-F. (1989). "General Report/Discussion Session 11: Model Testing - Geotechnical Model Tests". Proceedings, *Twelfth International Conference on Soil Mechanics and Foundation Engineering*, Rio de Janeiro, Vol. 4, pp. 2553-2571.

Couperwaite, S.L. and Marshall, R.G. (1989). "Slope Monitoring Key to Maintaining Pipeline Integrity". Oil and Gas Journal, 87 (39), pp. 106-111.

Craig, W.H. (ed.) (1985). *Application of Centrifuge Modelling to Geotechnical Design*. A.A. Balkema, Rotterdam, 501p.

Crofts, J.E., Menzies, B.K., and Tarzi, A.I. (1977). "Lateral Displacement of Shallow Buried Pipelines Due to Adjacent Deep Trench Excavations". Geotechnique 27, No. 2, pp. 161-179.

CSA (1994). *Oil and Gas Pipeline Systems: Oil and Gas Industry Systems*. Canadian Standards Association, Standard Z662-94, September.

Das, B.M. (1987a). "Pullout Resistance of Vertical Strip Anchor Slab in Clay". Indian Geotechnical Conference (IGC87), Bangalore, December, pp. 383-386.

Das B.M. (1987b). *Theoretical Foundation Engineering*. Developments in Geotechnical Engineering 47. Elsevier Science Publishers, Amsterdam, 440p.

Das, B.M. (1990). *Earth Anchors*. Developments in Geotechnical Engineering Volume 50, Elsevier Science Publishers B.V., Amsterdam, 241p.

Das, B.M., Moreno, R., and Dallo, K.F. (1985). "Ultimate Pullout Capacity of Shallow Vertical Anchors in Clay". Soils and Foundations, Vol. 25, No. 2, pp. 148-152.

Das, B.M., Tarquin, A.J. and Marino, R. (1987). "Model Tests for Pullout Resistance of Vertical Anchors in Clay". Soils and Foundations, 17 (2), pp. 52-56.

Davis, E.H. and Christian, J.T. (1971). "Bearing Capacity of Anisotropic Cohesive Soil". Journal of the Soil Mechanics and Foundations Division, ASCE, Vol. 97, No. SM5, pp. 753-769.

Davisson, M.T. (1970). *Lateral Load Capacity of Piles*. Highway Research Record No. 333 Highway Research Board, Washington, D.C.,, pp. 104-112.

Davisson, M.T. and Prakash, S. (1963). *A Review of Soil-Pole Behaviour*. Highway Research Record, No. 39, 1963, pp. 25-48.

Dickin, E.A. (1988). "Stress-Displacement of Buried Plates and Pipes". *Centrifuge 88 - Proceedings of the International Conference on Geotechnical Centrifuge Modelling*, J.F. Corté (ed.), A.A. Balkema, Rotterdam, pp. 205-214.

Dickin, E.A. and Leung, C.F. (1983). "Centrifugal Model Tests on Vertical Anchor Plates". Journal of Geotechnical Engineering, Vol. 109, No. 12, pp. 1503-1525.

Dickin, E.A. and Leung, C.F. (1985). "Evaluation of Design Methods for Vertical Anchor Plates". Journal of Geotechnical Engineering, Vol. 111, No. 4, pp. 500-520.

Dixon, J.M. (1988). "Centrifuge Modelling of Fold-Thrust Mountain Belts: Thrust Ramp Nucleation". *Centrifuge 88 - Proceedings of the International Conference on Geotechnical Centrifuge Modelling*, J.F. Corté (ed.), A. A. Balkema, Rotterdam, pp. 553-562.

Edgers, L. and Karlsrud, K. (1982). "Soil Flows Generated by Submarine Slides - Case Studies and Consequences". Proceedings, *Third International Conference on the Behaviour of Off-Shore Structures*, C. Chryssotomidis and J.J. Connor (eds.), Cambridge, Massachusetts, pp. 425-437.

EERC (1995). *Seismological and Engineering Aspects of the 1995 Hyogoken-Nanbu (Kobe) Earthquake*. Earthquake Engineering Research Center, College of Engineering, University of California at Berkeley, Report No. UCB/EERC-95/10, November.

Eguchi, R.T. and Taylor, C.E. (1988). "Seismic Risk to Natural Gas and Oil Systems". Proceedings, *Seismic Design and Construction of Complex Civil Engineering Systems*, M.A. Cassaro and J.D. Cooper (eds.), ASCE, New York, pp. 30-46.

English, R.J. and Schofield, A.N. (1973). "Centrifuge Tests Buckle Rigid Pipes". New Civil Engineer, 8, February, p.23.

Garrison, L.E. and Bea, R.G. (1977). "Bottom Stability as a Factor in Platform Siting and Design". Proceedings, *9th Offshore Technology Conference*, ASME, Houston, Vol. 3, pp. 127-133.

Georgiadis, M., Anagnostopoulos, C. and Saflekou, S. (1992). "Centrifugal Testing of Laterally Loaded Piles in Sand". Canadian Geotechnical Journal 29 (2) pp. 208-216.

Hamilton, J.M., Dunnavant, T.W., Murff, J.D. and Phillips, R. (1991). "Centrifuge Study of Laterally Loaded Behavior in Clay". *Centrifuge 91 - Proceedings of the International Conference Centrifuge 1991*, H-Y. Ko and F.G. McLean (eds.), A.A. Balkema, Rotterdam, pp. 285-292.

Hansen, J.B. (1948). *The Stabilizing Effect of Piles in Clay*. CN Post No. 3, Christiani and Nielson, Copenhagen, Denmark, November, pp. 14-15

Hansen, J.B. (1961). *The Ultimate Resistance of Rigid Piles Against Transversal Forces*. Bulletin 12, Danish Geotechnical Institute, Copenhagen, Denmark, pp. 5-9.

Hansen, L.A. and Clough, G.W. (1982). "Characterization of the Undrained Anisotropy of Clays ". In Proceedings of the Symposium on Limit Equilibrium, Plasticity and Generalized Strain Applications in Geotechnical Engineering, R.N. Yong and E.T. Selig (Eds.), ASCE, Hollywood Florida, pp. 253-276.

Head, K.H. (1986). *Manual of Soil Laboratory Testing*. Pentech Press, London, Volume 3, 1238p.

Hmadi, K.E. and O'Rourke, M.J. (1988). "Soil Springs for Buried Pipeline Axial Motion". Journal of Geotechnical Engineering, Vol. 114, No. 11, pp. 1335-1339.

Holtz, R.D. and Kovacs, W.D. (1981). An Introduction to Geotechnical Engineering. Prentice-Hall, Englewood Cliffs, New Jersey, 733p.

Itzkovitch, I. (1993). Opening Address. *Issues Workshop on Pipeline Lifetime*. R.W. Revie (ed.), Red Deer, Alberta, June 1-2, pp. 3-6.

Itzkovitch, I. (1994). Opening Address. *Managing Pipeline Integrity - An Issues Workshop on Pipeline Lifecycle*. Sponsored by CANMET, NEB and ARC, Banff, Alberta, June 9-10.

Karal, K. (1983). "Time Effect on the Lateral Soil Resistance to Pipeline Movement". Proceedings, *2nd Offshore Mechanics and Arctic Engineering Conference*, ASME, pp. 504-509.

Kettle, R.J. (1984). "Soil-Pipeline Interaction: A Review of the Problem". *Pipelines and Frost Heave*, Proceedings of a Seminar at Caen, France, April, pp. 35-37.

Ko, H-Y. and McLean, F.G. (eds.) (1991). *Centrifuge 91 - Proceedings of the International Conference Centrifuge 91*. A.A. Balkema, Rotterdam, 616p.

Kovacs, A., Bouin, S., McKelvy, B., and Colligan, H. (1975). *On the Theory of Ground Anchors*. CRREL Technical Report 258, Cold Regions Research and Engineering Laboratory, Hanover, New Hampshire, 68p.

Krstelj, I. (1996). *Behavior of Laterally loaded Pipes in Dry and Saturated Sand (Centrifuge Testing)*. Ph.D. Thesis, Department of Civil Engineering and Operations Research, Princeton University, Princeton, New Jersey, U.S., January.

Kusakabe, O. (1984). "Centrifuge Model Tests on the Influence of an Axisymetric Excavation on Buried Pipes". Proceedings, *International Symposium on Geotechnical Centrifuge Model Testing*, T. Kimura (ed.), Tokyo, pp. 87-93.

Kyrou, K. and Kalteziotis, N.A. (1985). "The Effect of Trenching on Adjacent Pipelines". Proceedings, Proceedings, *11th International Conference on Soil Mechanics and Foundation Engineering*, San Francisco, pp. 1657-1660.

Laine, E.P., Damuth, J.E., and Jacobi, R. (1986). "Surficial Sedimentary Processes Revealed by Echo Character Mapping in the Western North Atlantic Ocean". *The Geology of North America*, P.R. Vogt and B.E. Tucholke (eds.), The Western North Atlantic Region: Geological Society of America, Volume M, pp. 427-436.

Lin, L. (1995). *The Strength Characteristics of a Modelling Silty Clay*. M.Eng. Thesis, Memorial University of Newfoundland, St. John's, Newfoundland, Canada.

Lovell, S. and Schofield, A.N. (1986). "Centrifugal Modelling of Sea Ice". Proceedings, *1st International Conference on Ice Technology*, Springer-Verlag, Berlin, pp. 105-113.

Luscher, U., Thomas, H.P., and Maple, J.A. (1979). "Pipe-Soil Interaction, Trans-Alaska Pipeline". Proceedings, *Pipelines in Adverse Environments: A State of the Art*, ASCE, Vol. 2, pp. 486-502.

Mackenzie, T.R. (1955). *Strength of Deadman Anchors in Clay*. M.Sc. Thesis, Princeton University, Princeton, USA.

Mandke, J. (1995). "Pipeline Failure Data for Hurricane Andrew". Keynote Presentation, *International Workshop on Damage to Underwater Pipelines*, New Orleans, Louisiana, February, pp. 110-123.

MathWorks (1991). *MATLAB - Users Guide*. The MathWorks, Inc., Natick, MA.

Matlock, H. (1970). "Correlations for Design of Laterally Loaded Piles in Soft Clay". Proceedings, *2nd Offshore Technology Conference*, Houston, Paper No. OTC 1204, pp. 577-594.

McCaffrey, M. And O'Rourke, T.D. (1983). "Buried Pipeline Response to Reverse Faulting During the 1971 San Fernando Earthquake". Proceedings, *Earthquake Behavior and Safety of Oil and Gas Storage Facilities, Buried Pipelines and Equipment*, T. Ariman (ed.), ASME PVP - Vol. 77, June, pp. 151-159.

McCarthy, J. (1994). "Risk Assessment Guidelines". *Managing Pipeline Integrity - An Issues Workshop on Pipeline Lifecycle*. Sponsored by CANMET, NEB and ARC, Banff, Alberta, June 9-10.

McVay, M.C., Papadopoulos, P., Bloomquist, D., and Townsend, F.C. (1994). "Long-Term Behaviour of Large-Span Culverts in Cohesive Soils". Proceedings, Transportation Research Board Annual Meeting, Paper No. 826, 25p.

Meyerhof, G.G. (1951). "The Ultimate Bearing Capacity of Foundations". Geotechnique, Vol. 2, pp. 301-332.

Meyerhof, G.G. (1953). "The Bearing Capacity of Foundations Under Eccentric and Inclined Loads". Proceedings, *3rd International Conference on Soil Mechanics and Foundation Engineering*, Vol. 1, pp. 440-445.

Meyerhof, G.G. (1963). "Some Recent Research on the Bearing Capacity of Foundations". Canadian Geotechnical Journal, Vol. 1, No. 1, pp. 16-26.

Meyerhof, G.G. (1973). "Uplift Resistance of Inclined Anchors and Piles". Proceedings, *8th International Conference on Soil Mechanics and Foundation Engineering*, Moscow, Vol. 2, pp. 167-172.

Meyerhof, G.G. (1982). "Limit Equilibrium Plasticity in Soil Mechanics". Proceedings, *Symposium on Limit Equilibrium, Plasticity and Generalized Stress Strain Applications in Geotechnical Engineering*, ASCE 1980 Annual Convention and Exposition, Hollywood, Florida, Oct 27-31, 1980, pp. 7-24.

Meyerhof, G.G. (1995). "Behaviour of Pile Foundations Under Special Loading Conditions: 1994 R.M. Hardy Keynote Address". Canadian Geotechnical Journal, Vol. 32, No. 2, pp. 204-222.

Meyerhof, G.G. (1998). Personal Communication. October, St. John's, Newfoundland.

Meyerhof, G.G. and Hanna, A.M. (1978). "Ultimate Bearing Capacity of Foundations on Layered Soils Under Inclined Load". Canadian Geotechnical Journal, Vol. 15, No. 4, pp. 565-572.

Milz, E.A. and Broussard, D.E. (1972). "Technical Capabilities in Offshore Operations to Maximize Safety". Proceedings, *4th Offshore Technology Conference*, ASME, Houston, Paper OTC 1711, pp. 809-820.

Murchison, J.M. and O'Neill, M.W. (1984). "Evaluation of p-y Relationships in Cohesionless Soils". *Analysis and Design of Pile Foundations*, Proceedings of a Symposium Sponsored by the Geotechnical Engineering Division, ASCE, San Francisco, October, pp. 174-192.

Murff, J.D. (1996). "The Geotechnical Centrifuge in Offshore Engineering". Proceedings, *28th Offshore Technology Conference*, ASME, Houston, Volume 1, pp. 675-689.

National Research Council (1994). *Improving the Safety of Marine Pipelines*. National Academy Press, Washington, D.C., 141p.

Ng, P.C.F. (1994). *Behaviour of Buried Pipelines Subjected to External Loading*. Ph.D. Thesis, University of Sheffield, Department of Civil and Structural Engineering, Sheffield, England, November.

Neely, W.J., Stuart, J.G. and Graham, J. (1973). "Failure Load of Vertical Anchor Plates in Sand". Journal of the Soil Mechanics and Foundations Division, ASCE, Vol. 99, No. SM9, pp. 669-685.

Norem, H. (1993). *Estimating Impact Pressure of Submarine Slides on Pipelines*. Norwegian Geotechnical Institute Report No. 524234-1, 17p.

Novacorp (1992). *Pembina Reroute Stress Analysis*. Novacorp International Consulting Inc., September.

Nunez, I.L., Phillips, R., Randolph, M.F., and Wesselink, B.D. (1988). "Modelling Laterally Loaded Piles in Calcareous Sand". *Centrifuge 88 - Proceedings of the International Conference on Geotechnical Centrifuge Modelling*, J.F. Corté (ed.), A.A. Balkema,

Nyman, K.J. (1984). "Soil Response Against Oblique Motion of Pipes". Journal of Transportation Engineering, ASCE, Vol. 110, No. 2, pp. 190-202.

O'Brien, S.R. (1997). *Soil-Pipeline Interaction in Dry Sand Under Lateral Loading Conditions*. M.Eng. Thesis, Faculty of Engineering and Applied Science, Memorial University of Newfoundland, St. John's, Newfoundland, Canada.

O'Neill, M.W., Reese, L.C. and Cox, W.R. (1990). "Soil Behaviour for Piles under Lateral Loading". Proceedings, *22nd Offshore Technology Conference*, ASME, Houston, Paper OTC 6377, pp. 279-287.

O'Rourke, T.D. and Tawfik, M.S. (1983). "Effects of Lateral Spreading on Buried Pipelines During the 1971 San Fernando Earthquake". Proceedings, *Earthquake Behavior and Safety of Oil and Gas Storage Facilities, Buried Pipelines and Equipment*, T. Ariman (ed.), ASME PVP - Vol. 77, June, pp. 124-132.

O'Rourke, T.D. and Ahmed, I. (1985). "Effect of Shallow Trench Construction on Cast Iron Pipelines". Proceedings, *International Conference on Advances in Underground Pipeline Engineering*, J.K. Jeyapalan (ed.), ASCE, Wisconsin, pp. 21-31.

O'Rourke, T.D. and Lane, P.A. (1989). *Liquefaction Hazards and Their Effects on Buried Pipelines*. National Center for Earthquake Engineering Research, Technical Report NCEER-89-0007, February.

Ovesen, N.K. (1964). *Anchor Slab Calculation Methods and Model Tests*. Bulletin 16, Danish Geotechnical Institute, Copenhagen, Denmark, 40p.

Ovesen, N.K. (1981). "Centrifuge Tests of the Uplift Capacity of Anchors". Proceedings, *10th International Conference on Soil Mechanics and Foundation Engineering*, Stockholm, Vol. 4, pp. 717-722.

Ovesen, N.K. and Stromann, H. (1972). "Design Methods for Vertical Anchor Slabs in Sand". Proceedings, *Specialty Conference on Performance of Earth and Earth-Supported Structures*, ASCE, Vol. 1, pp. 1481-1500.

Oynes C. (1995). Keynote Address. *International Workshop on Damage to Underwater Pipelines*, New Orleans, Louisiana, February, pp. 18-23.

Pamukcu, S., Poplin, J.K., Suhayda, J.N., and Tumay, M.T. (1983). "Dynamic Sediment Properties, Mississippi Delta". Proceedings, *Geotechnical Practice in Offshore Engineering*, S.G. Wright (ed.), ASCE, pp. 111-132.

Paulin, M.J. and Phillips, R. (1994). *Centrifuge Modelling Relevant to the Lateral Loading of Pipelines; Year 1 Summary Report*. Contract Report for NOVA Corporation of Alberta, C-CORE Contract Number 94-C16.

Paulin, M.J. and Phillips R. (1995). *Centrifuge Modelling Relevant to the Lateral Loading of Pipelines; Year 2 Summary Report*. Contract Report for NOVA Corporation of Alberta, C-CORE Contract Number 95-C7.

Paulin, M.J.and Phillips R. (1996). *Centrifuge Modelling Relevant to the Lateral Loading of Pipelines; Year 3 Summary Report*. Contract Report for NOVA Gas Transmission Limited, C-CORE Contract Number 96-C1.

Paulin, M.J., Phillips, R., and Lin, L. (1993). *Centrifuge Modelling Relevant to the Lateral Loading of Pipelines; Report on Proof Activities*. Contract Report for NOVA Corporation of Alberta, C-CORE Contract Number 93-C10.

Paulin, M.J., Clark, J.I., Poorooshasb, F. and Rizkalla, M. (1994). "Study of Pipelines Subjected to Landslide Conditions". *Centrifuge 94 - Proceedings of the International Conference Centrifuge 94*, C.F. Leung, F.H. Lee, and T.S. Tan (eds), A. A. Balkema, Rotterdam, pp. 739-744.

Paulin, M.J., Phillips, R., Clark, J.I., and Boivin, R. (1998). "An Experimental Investigation into Lateral Pipeline/Soil Interaction - Phase II". *Centrifuge 98 - Proceedings of the International Conference Centrifuge 98*, A. A. Balkema, Rotterdam, *in press*.

Peck, R.B. and Davisson, M.T. (1962). "Discussion". Transactions ASCE, Vol. 127, Pt. 4, p. 413.

Pelletier, B.R. (1979). "Review of Surficial Geology and Engineering Hazards in the Canadian Offshore". Maritime Sediments, Vol. 15, Nos. 2 and 3, August - December, pp. 55-91.

Peltzer, G. and Garnier, J. (1988). "Experimental Approach in a Centrifuge of Large Scale Continental Tectonics in Asia". *Centrifuge 88 - Proceedings of the International Conference on Geotechnical Centrifuge Modelling*, J.F. Corté (ed.), A.A. Balkema, Rotterdam, pp. 563-574.

Phillips, R. (1986). *Ground Deformation in the Vicinity of a Trench Heading*. Ph.D. Thesis, Cambridge University, Cambridge, England, December.

Poorooshasb, F. (1990). "On Centrifuge Use for Ocean Research". Marine Geotechnology, Volume 9, pp. 141-158.

Poulos, H.G. (1988). *Marine Geotechnics*. Unwin Hyman, London, 473p.

Poulos, H.G. (1995). "Design of Reinforcing Piles to Increase Slope Stability". Canadian Geotechnical Journal, Vol. 32, No. 5, pp. 808-818.

Poulos, H.G. and Davis, E.H. (1980). *Pile Foundation Analysis and Design*. John Wiley and Sons, New York, 397p.

Prakash, S. and Sharma, H.D. (1990). *Pile Foundations in Engineering Practice*. John Wiley and Sons, New York, 734p.

Pratson, L.F. and Laine, E.P. (1989). "The Relative Importance of Gravity- Induced Versus Current-Controlled Sedimentation During the Quaternary Along the Mideast U.S. Outer Continental Margin Revealed by 3.5 kHz Echo Character". Marine Geology, Volume 89, pp. 87-126.

Pyke, R. and Beikae, M. (1984). "A New Solution for the Resistance of Single Piles to Lateral Loading". Proceedings, *Laterally Loaded Deep Foundations: Analysis and Performance*, J.A. Langer, E.T. Mosley, and C.D. Thompson, (eds), ASTM STP 835, pp. 3-20.

Randolph, M.F. and Houlsby, G.T. (1984). "The Limiting Pressure on a Circular Pile Loaded Laterally in Cohesive Soil". Geotechnique, 34 (4), pp. 613-623.

Rajani, B.B., Robertson, P.K., and Morgenstern, N.R. (1993). "A Simplified Method for Pipelines Subject to Transverse Soil Movements". Proceedings, *12th Offshore Mechanics and Arctic Engineering Symposium*, Vol. V, pp. 157-165.

Ranjan, G. and Aurora, V.B. (1980). "Model Studies on Anchors Under Horizontal Pull in Clay". Proceedings, *3rd Australia, New Zealand Conference on Geomechanics*. Vol. 1, pp. 65-70.

Rawat, P.C. (1978). "State-of-the-Art Report on Geotechnical Aspects of Submarine Pipeline Design". Proceedings, *GEOCON-India Conference on Geotechnical Engineering*, Indian Geotechnical Society, New Delhi, pp. 148-153.

Reese, L.C. (1990). *Pile Foundations for Deep-Water Structures*. Geotechnical Engineering Group, Bureau of Engineering Research, College of Engineering, The University of Texas at Austin, October, 50p.

Reese, L.C. and Matlock, H. (1956). "Non-Dimensional Solutions for Laterally Loaded Piles with Soil Modulus Assumed Proportional to Depth". Proceedings, *8th Texas Conference on Soil Mechanics and Foundation Engineering*. Specialty Publication #29, Bureau of Engineering Research, University of Texas, Austin.

Reese, L.C., Cox, W.R., and Koop, F.D. (1974). "Analysis of Laterally Loaded Piles in Sand". Proceedings, *7th Offshore Technology Conference*, ASME, Houston, Paper No. OTC 2080, pp. 473-483.

Reese, L.C. and Welch, R.C. (1975). "Lateral Loading of Deep Foundations in Stiff Clay". Journal of the Geotechnical Engineering Division, ASCE, Vol. 101, No. GT7, pp. 633-649.

Reese, L.C., Cox, W.R., and Koop, F.D. (1975). "Field Testing and Analysis of Laterally Loaded Piles in Stiff Clay". Proceedings, *7th Offshore Technology Conference*, ASME, Houston, Paper No. OTC 2312, pp. 671-679.

Reifel, M.D. (1979). "Storm Related Damage to Pipelines, Gulf of Mexico". Proceedings *Pipelines in Adverse Environments: A State of the Art*, ASCE, Vol. 1, pp. 169-186.

Rizkalla, M. and McIntyre, M.B. (1991). "A Special Pipeline Design for Unstable Slopes". Proceedings, *Pipeline Engineering 1991*, 14th Annual Energy-Sources Technology Conference and Exhibition, Houston, ASME, PD-Vol. 34, pp. 69-74.

Rizkalla, M., Poorooshasb, F., and Clark, J.I. (1992). "Centrifuge Modelling of Lateral Pipeline/Soil Interaction". Proceedings, *11th Offshore Mechanics and Arctic Engineering Symposium*, 13p. insert.

Rizkalla, M., Turner, R.D., and Colquhoun, I.R. (1993). "State of Development of a Fibre Optic Technology-Based Pipeline Structural Integrity Monitoring System". Proceedings, *12th Offshore Mechanics and Offshore Engineering Symposium*, Volume V, pp. 295-302.

Rossato, G., Nicholas, N.L., and Jardine, R.J. (1992). "Properties of Some Kaolin Based Model Clay Soils". Geotechnical Testing Journal, Vol. 15, No. 2, pp. 166-179.

Rowe, R.K. (1984). "Centrifugal Model Tests on Vertical Anchor Plates - Discussion". Journal of Geotechnical Engineering, Vol. 110, No. 11, pp. 1693-1695.

Rowe, R.K. and Davis, E.H. (1982a). "The Behaviour of Anchor Plates in Clay". Geotechnique, Volume 32, No. 1, pp. 9-23.

Rowe, R.K. and Davis, E.H. (1982b). "The Behaviour of Anchor Plates in Sand". Geotechnique, Vol. 32, No. 1, pp. 25-41.

Sangrey, D.A. (1977). "Marine Geotechnology - State of the Art". Marine Geotechnology, Vol. 2, pp. 45-80.

Schofield, A.N. (1980). "Twentieth Rankine Lecture: Cambridge Geotechnical Centrifuge Operations". Geotechnique, Volume 30, Number 3, pp. 227-268.

Selig, E.T. and Nash, W.A. (1988). "Buried Pipeline Research Needs". Proceedings, *Pipeline Infrastructure*, Proceedings of a Conference Sponsored by the Pipeline Division of ASCE, B.A. Bennett (ed.), ASCE Publication 662-9, pp. 463-475.

Selvadurai, A.P.S. (1985). "Numerical Simulation of Soil-Pipeline Interaction in a Ground Subsidence Zone". Proceedings, *Advances in Underground Pipeline Engineering*, J.K. Jeyapalan (ed.), ASCE, pp. 311-319.

Selvadurai, A.P.S. (1992). "The Uplift Behaviour of a Rigid Pipe Embedded in a Creep Susceptible Frozen Soil". Proceedings, *12th Offshore Mechanics and Arctic Engineering Conference*, ASME, Vol. V-B, pp. 349-357.

Silva, A.J., Brandes, H.G., Sadd, M.H., Karamanlidis, D., Tian, W-M., and Laine, E.P. (1989). "Experimental and Analytical Study of Creep Deformations of Submarine Slopes". Proceedings, *Oceans '89*, Volume 5, pp. 1530-1535.

Silva, A.J., Tian, W-M., Sadd, M.H., and Brandes, H.G. (1991). "Creep Behaviour of Fine-Grained Ocean Sediments". Proceedings, *Computer Methods and Advances in Geomechanics*, G. Beer, J.R. Booker, and J.P Carter (eds.), A.A. Balkema, Rotterdam, pp. 683-688.

Skempton, A.W. (1951). "The Bearing Capacity of Clays". Proceedings, *Building Research Congress*, Institute of Civil Engineers, London, Div. 1, p. 180.

Smith, C.C. (1991). *Thaw Induced Settlement of Pipelines in Centrifuge Model Tests*. Ph.D. Thesis, Cambridge University, Cambridge, England, September.

Springman, S.M. (1993). "Centrifuge Modelling in Clay: Marine Applications". Proceedings, *4th Canadian Conference on Marine Geotechnical Engineering*, St. John's, Newfoundland, Vol. 3., pp. 853-895.

Stevens, J.B. and Audibert, J.M.E. (1979). "Re-Examination of P-Y Formulations". Proceedings, *11th Offshore Technology Conference*, ASME, Houston, Paper No. OTC 3402, Vol. 1, pp. 397-403.

Sullivan, W.R., Reese, L.C., and Fenske, C.W. (1980). "Unified Method for Analysis of Laterally Loaded Piles in Clay". Proceedings, *I[st] International Conference on Numerical Methods in Offshore Piling*, ICE, London, pp. 135-146.

Sylwester, R.E. and Holmes, M.L. (1989). "Marine Geophysical Evidence of a Recent Submarine Slope Failure in Puget Sound, Washington". Proceedings, *Oceans '89*, Volume 5, pp. 1524-1529.

Takada, N., Tohda, J., and Mikasa, M. (1985). "Bending Moment of Flexible Pipes in a Centrifuge". Proceedings, *International Conference on Advances in Underground Pipeline Engineering*, J.K. Jeyaplan (ed.), ASCE, Wisconsin, pp. 224-233.

Tawfik, M.S. and O'Rourke, T.D. (1986). *Analysis of Pipelines Under Large Soil Deformations*. Cornell Geotechnical Engineering Report 86-1, School of Civil and Environmental Engineering, Cornell University, Ithaca, N.Y., 244p.

Taylor, R.N. (1995). *Geotechnical Centrifuge Technology*. Blackie Academic & Professional, London, 296p.

Templeton, J.S., Murff, J.D., Goodwin, R.H., and Klejbuk, L.W. (1985). "Evaluating Soils and Hazards in the Mississippi Canyon". Proceedings, *17th Offshore Technology Conference*, ASME, Houston, Vol. 3, pp. 63-72.

Teng, W.C. (1962). *Foundation Design*. Prentice-Hall, Englewood Cliffs, New Jersey.
Terzaghi, K. (1943). *Theoretical Soil Mechanics*. John Wiley and Sons, New York, 510p.

Terzaghi, K. (1955). "Evaluation of Coefficient of Subgrade Reaction". Geotechnique, Vol. 5, No. 4, pp. 297-326.

Terzaghi, K. and Peck, R.B. (1967). *Soil Mechanics in Engineering Practice*. John Wiley and Sons, New York, 729p.

Tohda, J., Takada, N., and Mikasa, M. (1985). "Earth Pressure on Underground Rigid Pipe in a Centrifuge". Proceedings, *International Conference on Advances in Underground Pipeline Engineering*, J.K. Jeyapalan (ed.), ASCE, Wisconsin, pp. 567-575.

Trautmann, C.H. and O'Rourke, T.D. (1983). *Behaviour of Pipe in Dry Sand Under Lateral and Uplift Loading*. Geotechnical Engineering Report 83-6, Cornell University, Ithaca, New York.

Trautmann, C.H. and O'Rourke, T.D. (1985). "Lateral Force-Displacement Response of Buried Pipe". Journal of Geotechnical Engineering, Vol. 111, No. 9, pp. 1077-1092.

Trautmann, C.H., O'Rourke, T.D. and Kulhawy, F.H. (1985). "Uplift Force-Displacement Response of Buried Pipe". Journal of Geotechnical Engineering, Vol. 111, No. 9, pp. 1061-1076.

Tschebotarioff, G.P. (1973). *Foundations, Retaining and Earth Structures*. McGraw-Hill Book Company, New York, 642p.

Valsangkar, A.J. and Britto, A.M. (1979). *Centrifuge Tests of Flexible Circular Pipes Subjected to Surface Loading*. Transport and Road Research Laboratory Supplementary Report 530.

Venzi, S., Malacarne, C., and Cuscuna, S. (1993). "Development of an Expert System to Manage the Safety of Pipeline in Unstable Slopes". Proceedings, *12th Offshore Mechanics and Arctic Engineering Conference*, ASME, Volume V, pp. 127-134.

Vesic, A.S. (1971). "Breakout Resistance of Objects Embedded in Ocean Bottom". Journal of the Soil Mechanics and Foundations Division, ASCE, Vol. 97, No. SM9, pp. 1183-1205.

Vesic, A.S. (1973). "Analysis of Ultimate Loads of Shallow Foundations". Journal of the Soil Mechanics and Foundations Division, ASCE, Vol. 99, No. SM1, pp. 45-73.

Viggiani, C. (1981). "Ultimate Lateral Load on Piles Used to Stabilise Landslides". Proceedings, *10th International Conference on Soil Mechanics and Foundation Engineering*, Vol. 3, pp. 555-560.

Vinson, T.S. and Palmer, A.C. (1989). "Settlement of Arctic Submarine Pipelines: Theoretical Considerations and Physical Model Tests". Proceedings, *International Symposium on Geocryological Studies in Arctic Regions*, Nadium, USSR, August. 32p.

Wantland, G.P., O'Neill, M.B., Reese, L.C., and Coelogyne, E.H. (1979). "Lateral Stability of Pipelines in Clay". Proceedings, *11th Offshore Technology Conference*, ASME, Houston, pp. 1025-1034.

Wantland, G.P., O'Neill, M.B., Coelogyne, E.H. and Reese, L.C. (1982). "Pipeline Lateral Stability in Soft Clay". Journal of Petroleum Technology, Vol. 34, No. 1, pp. 217-220.

Wesselink, B.D., Murff, J.D., Randolph, M.F., Nunez, I.L., and Hyden A.M. (1988). "Analysis of Centrifuge Model Test Data from Laterally Loaded Piles in Calcareous Sand". Engineering for Calcareous Sediments, Proceedings, *International Conference on Calcareous Sediments*, Perth, March, pp. 1-10.

Williams, R.B. (1979). "Permitting for a Cross-Country Pipeline". Proceedings, *Pipelines in Adverse Environments: A State of the Art*, ASCE, Vol. 1, pp. 16-22.

Winterkorn, H.F. and Fang, H-Y. (1975). *Foundation Engineering Handbook.* Van Nostrand Reinhold Company, New York, 751p.

Wolters, J.G. (1973). "Lateral Load Carrying Capacity of Piles in Offshore Structures". Journal of Petroleum Technology, Vol. 25, No. 4, pp. 487-498.

Wong, M.Y.T. (1992). *Geotechnical Investigation NPS 30 Western Alberta Mainline Crossing and Unnamed Creek NE 1/4 8-47-9-5*. NOVA Corporation of Alberta, August.

Yeh, Y-H. (1988). "Landslide Effects to Buried Pipelines". Proceedings, *Numerical Methods in Geomechanics*, Swoboda (ed.), A.A. Balkema, Rotterdam, pp. 901-905.

Yeh, Y-H. and Lai, S-S. (1992). "Failure Analysis of Buried Pipeline Subjected to Landslide". Proceedings, *Seismic Ground Motions, Response, Repair, and Instrumentation of Pipes and Bridges*, 1992 Pressure Vessels and Piping Conference, ASME, New Orleans, PVP-Vol. 227, pp. 91-96.

Yungblut G.R. (1994). Luncheon Talk. *Managing Pipeline Integrity - An Issues Workshop on Pipeline Lifecycle*. Sponsored by CANMET, NEB and ARC, Banff, Alberta, June 9-10.
Zhou, Z. and Murray, D.W. (1993). "Behaviour of Buried Pipelines Subjected to Imposed Deformations". Proceedings, *12th Offshore Mechanics and Arctic Engineering Conference*, ASME, Volume V, pp. 115-122.

Zelikson, A. (1985). "Hydro-Geotechnical Modelling on Large Centrifuges". Proceedings, *Application of Centrifuge Modelling to Geotechnical Design*, W.H. Craig (ed.), A.A. Balkema, Rotterdam, pp. 155-170.

Appendix A

Triaxial Test Data

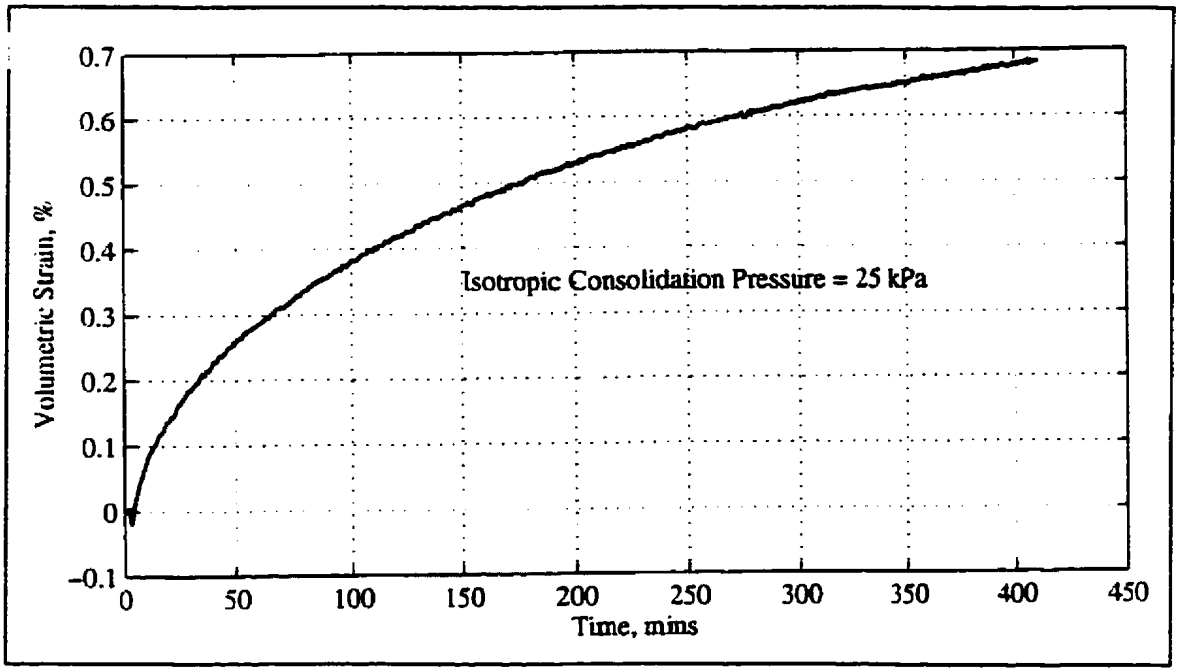

Figure A.1a - *Isotropic consolidation data, consolidated-undrained test.*

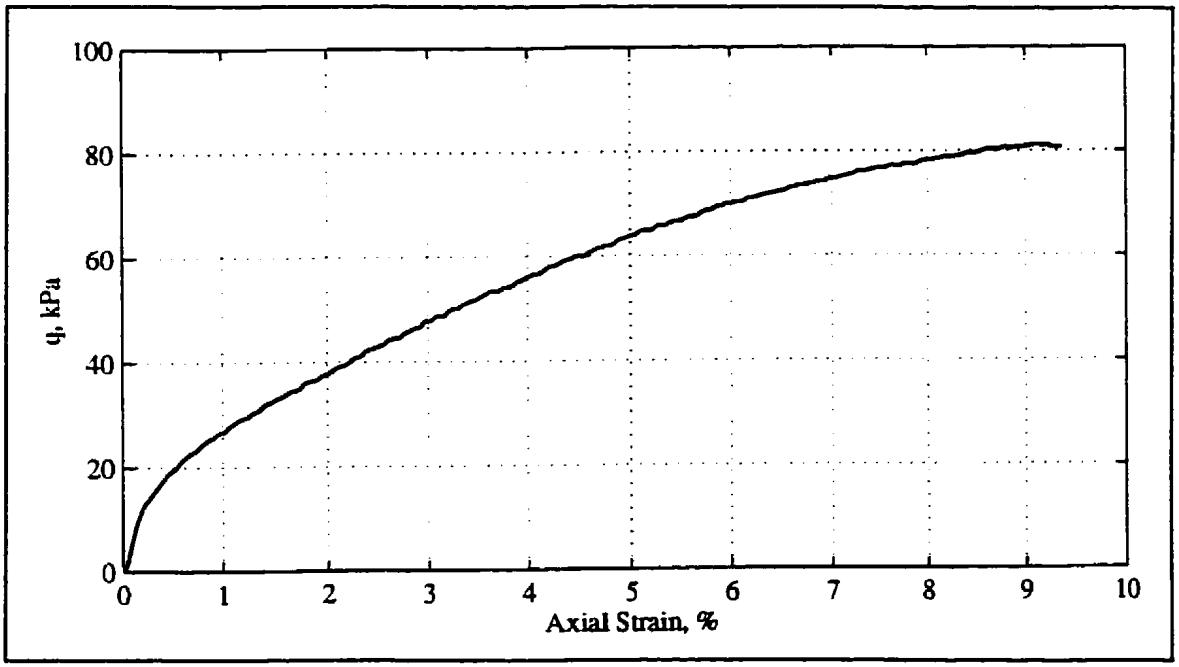

Figure A.1b - *Stress-strain data, consolidated-undrained test.*

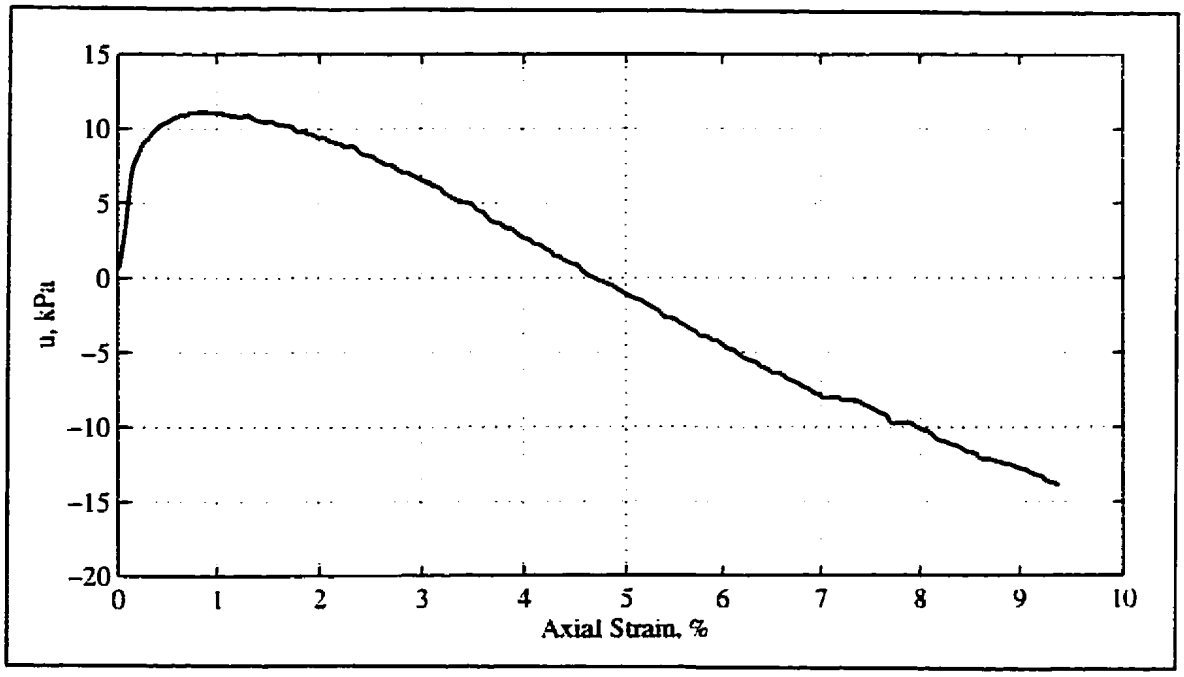

Figure A.1c - *Pore pressure change - strain data, consolidated-undrained test.*

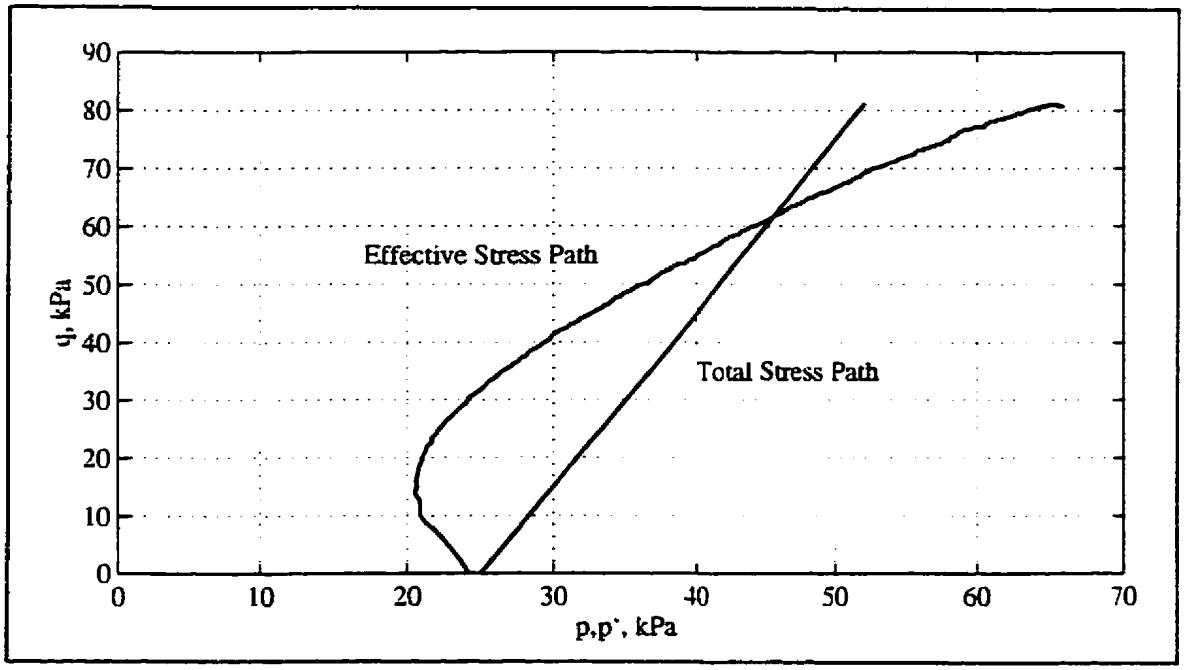

Figure A.1d - *Total and effective stress paths - consolidated-undrained test.*

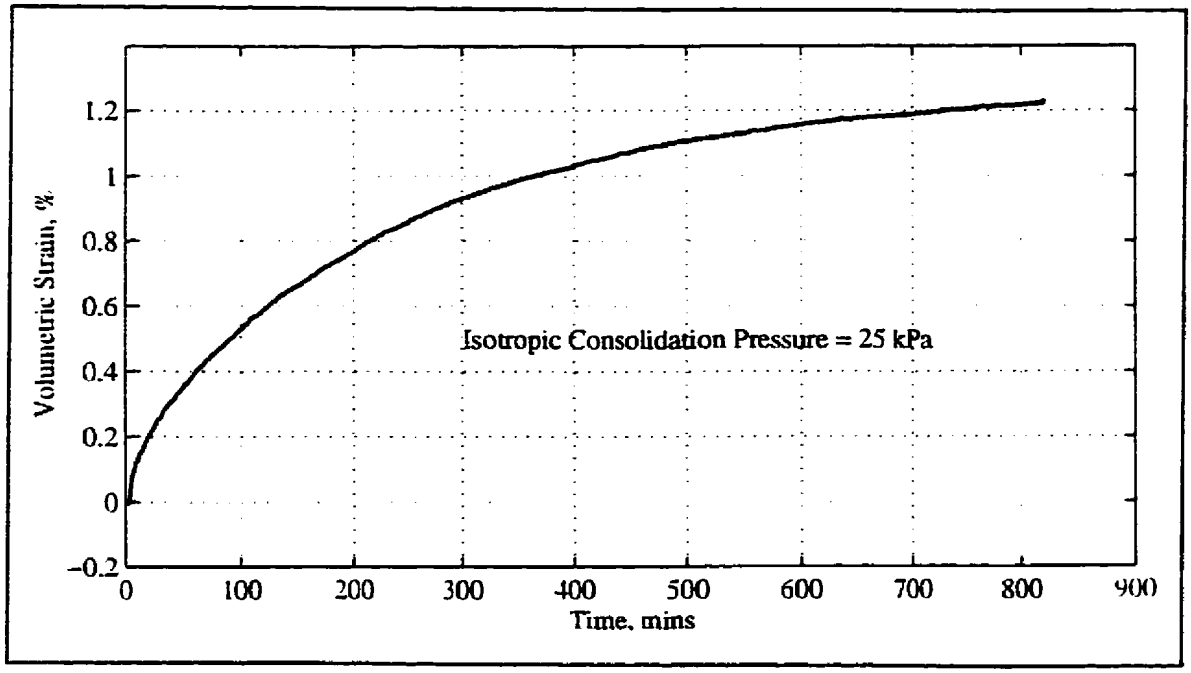

Figure A.2a - *Isotropic consolidation data, consolidated-drained test.*

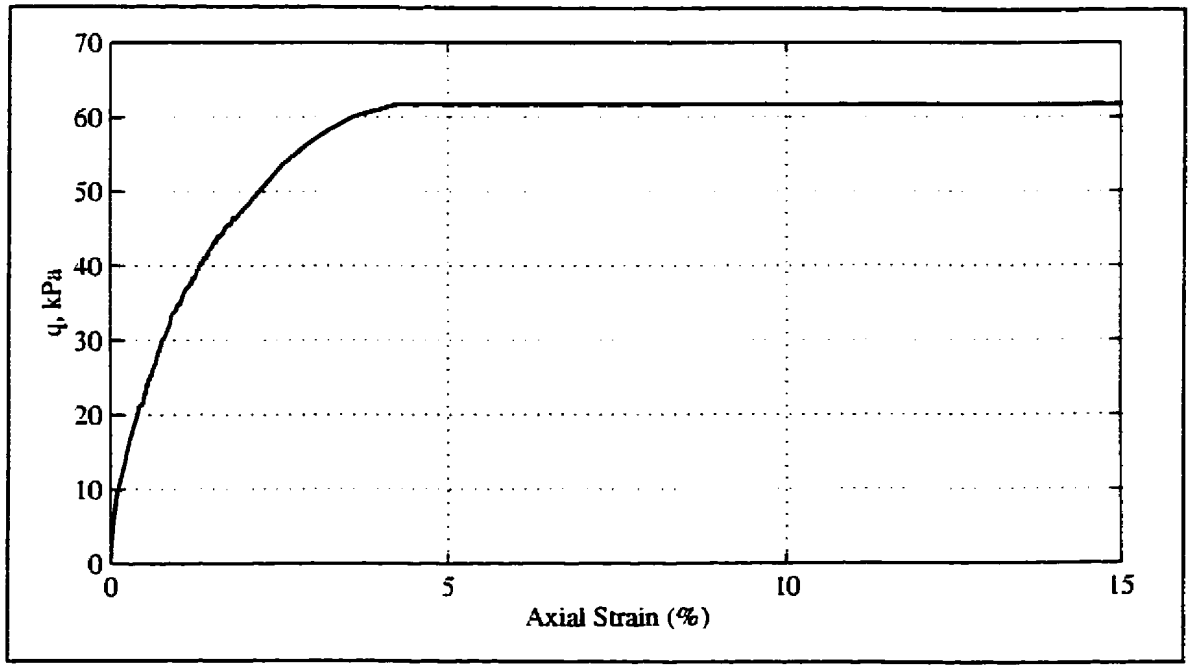

Figure A.2b - *Stress-strain data, consolidated-drained test.*

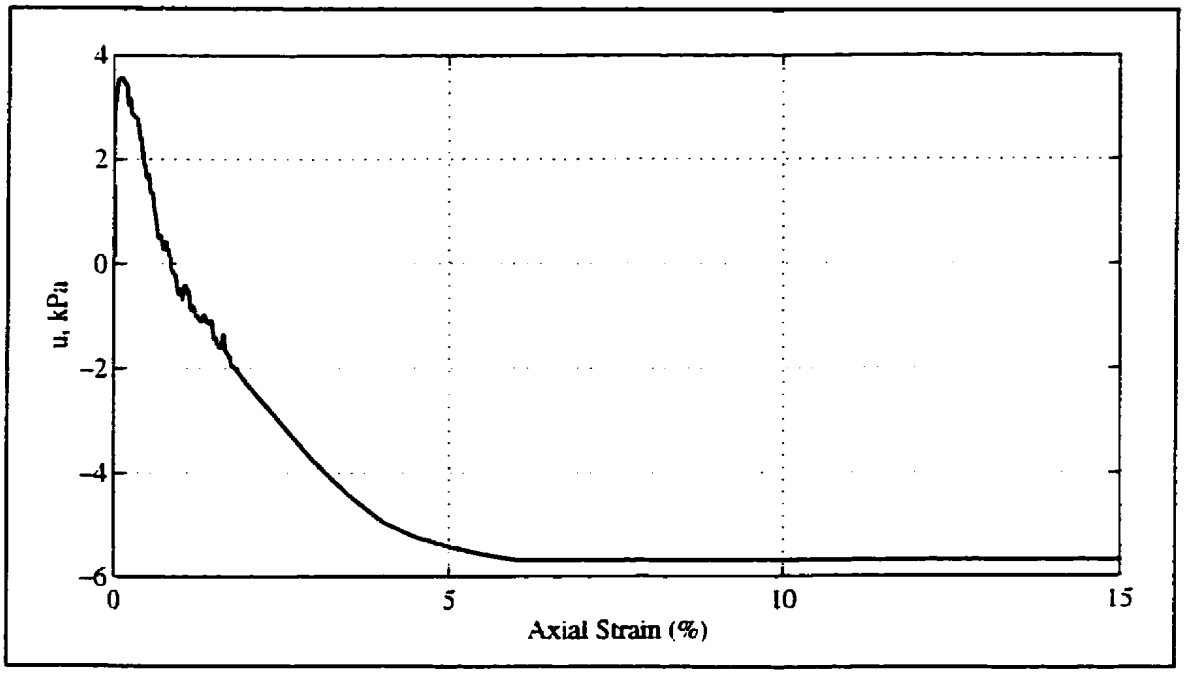

Figure A.2c - *Pore pressure change - strain data, consolidated-drained test.*

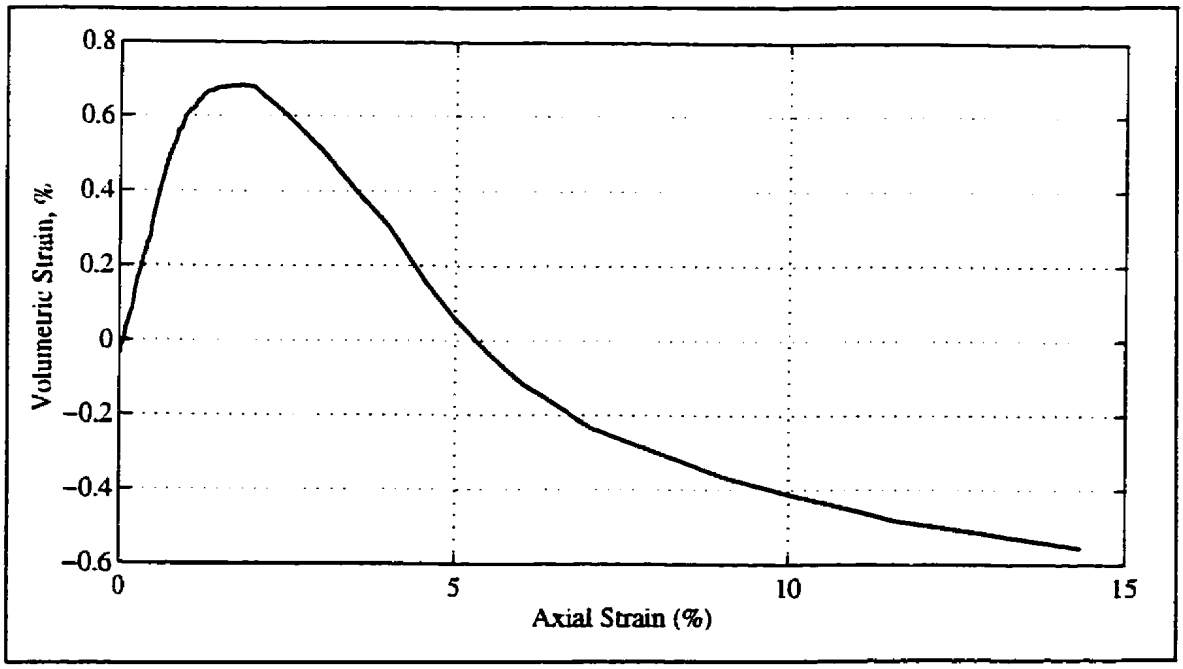

Figure A.2d - *Volumetric strain - axial strain data - consolidated-drained test.*

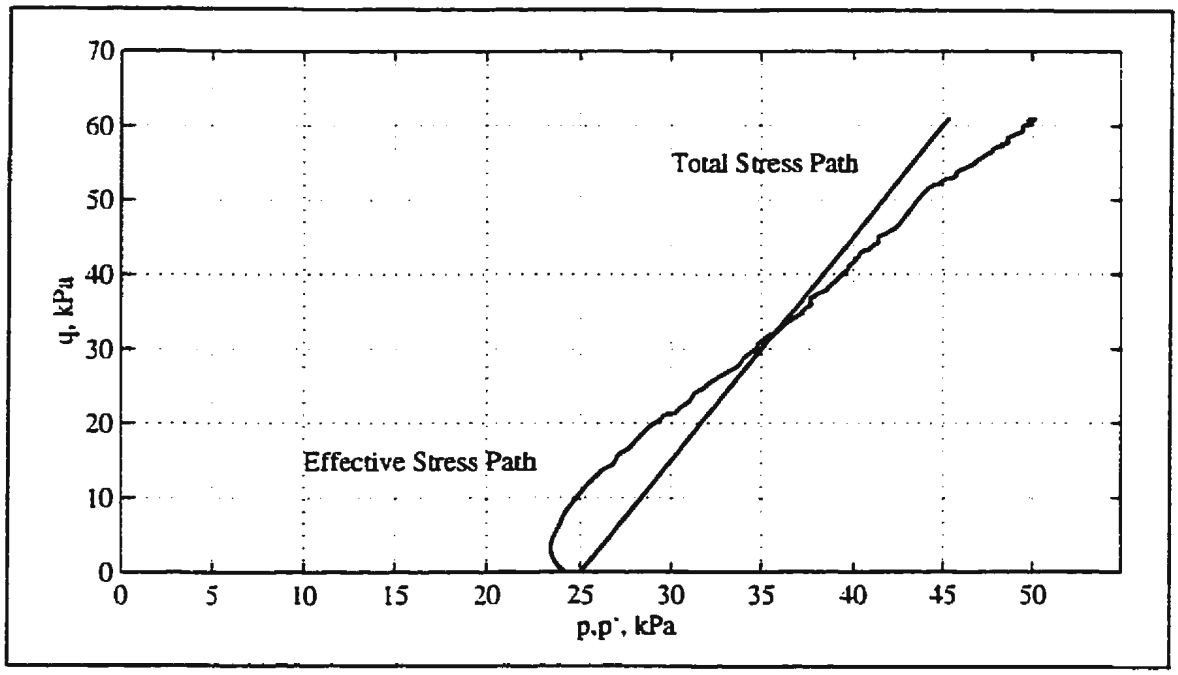

Figure A.2e - *Total and effective stress paths - consolidated-drained test.*

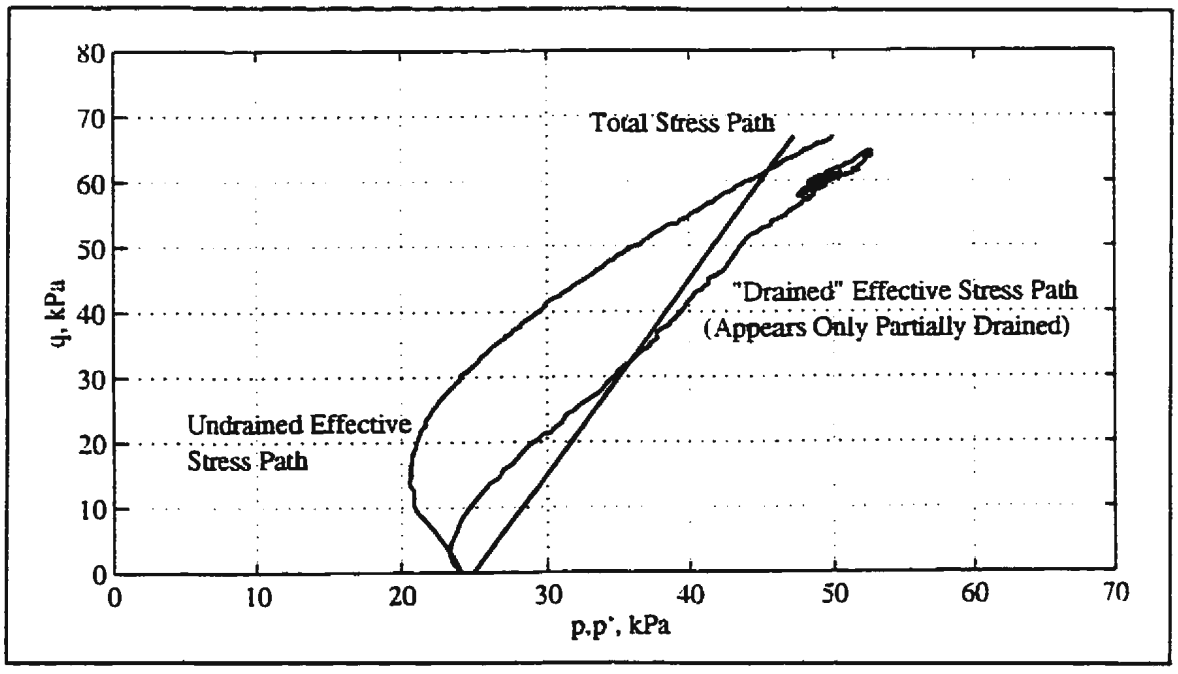

Figure A.3 - *Total and effective stress paths - drained and undrained tests.*

Appendix B

Test 01 - Selected Test Data

Table B.1 - Cone Penetration Test Details for Test 01

CPT No.	X[1] (mm)	Y[1] (mm)	Backfill or Native	Time Tested (hrs)
1	470	590	Backfill	0245
2	330	590	Native	0305
3	505	590	Backfill	0350
4	615	590	Native	0408
5	655	590	Native	0442
6	435	590	Backfill	0504
7	266	590	Native	0515
8	180	590	Native	0533

Notes: 1 - Coordinate convention shown on Figure B.1.

Table B.2 - Interpreted Cone Penetration Resistances for Test 01

Cone Test No.	Interpreted Penetration Resistance (kPa)			
	@ Initial Springline of Pipeline #1	@ Initial Springline of Pipeline #2	@ Initial Springline of Pipeline #3	@ Initial Springline of Pipeline #4
1	64	58	51	44
2	327	307	289	271
3	44	36	29	20
4	316	296	282	267
5	307	284	267	247
6	40	31	24	16
7	336	313	296	276
8	300	273	249	224

Table B.3 - Pipeline Test Details for Test 01

Pipeline No.	Trench Width (mm)	Cover Depth (mm)	X:Y Coordinates of Pipe Centre (mm)	Pipeline Velocity (mm/sec)	Time Tested (hrs)
1	50	16	290 : 505.5	0.50	0326
2	50	10	650 : 505.5	0.57	0417
3	50	5	650 : 674.5	0.67	0450
4	50	0	290 : 674.5	0.61	0528

Table B.4 - Prototype Test Geometries for Test 01

Pipeline	Distance to Trench Wall in the Direction of Travel (m)	Distance to Trench Wall Towards the Rear of the Pipeline (m)	Distance to a Stiff Retaining Wall in the Direction of Travel (m)	Distance to the Pipeline in the Direction Opposite to Travel (m)	Distance Laterally to a Stiff Retaining Wall (m)	Distance Laterally to the Edge of the Adjacent Pipeline (m)	Distance From Base of Pipeline to Rigid Base, i.e. Bedrock (m)	Water Level Above Rigid Base, i.e. Bedrock (m)	Water Level Below Base of Pipeline (m)
1	0.8	0.75	14.2	7.5	7.75	5.0	5.025	2.45	2.575
2	0.8	0.75	14.2	7.5	7.75	5.0	5.025	2.45	2.575
3	0.8	0.75	14.2	7.5	7.75	5.0	5.025	2.45	2.575
4	0.8	0.75	14.2	7.5	7.75	5.0	5.025	2.45	2.575

Table B.5 - Calculation of Undrained Shear Strength for Test 01

Pipeline	Soil Type	Cone Tests Used to Derive q_c	Interpreted Cone Tip Resistance at Springline, q_c (kPa)	Saturated Bulk Density, γ_{sat} (kN/m^3)	Pore Pressure at Springline, u (kPa)	Depth to Springline, h (m)	Cone Factor, N_c or N_k*	Undrained Shear Strength, c_u (kPa)
1	Native	2,4,5,7,8	364.8	958.4	-26.9	0.0255	8.2/11.1	30.6 - 41.7
1	Backfill	1,3,6	49.3	859.3	---	0.0255	15	3.3
2	Native	2,4,5,7,8	338.8	958.4	-26.9	0.0195	8.1/11.3	28.2 - 39.8
2	Backfill	1,3,6	41.6	859.3	---	0.0195	15	2.8
3	Native	2,4,5,7,8	318.1	958.4	-26.9	0.0145	7.9/11.6	26.3 - 38.3
3	Backfill	1,3,6	34.7	859.3	---	0.0145	15	2.3
4	Native	2,4,5,7,8	295.6	958.4	-26.9	0.0095	7.8/11.8	24.3 - 36.6
4	Backfill	1,3,6	26.7	859.3	---	0.0095	15	1.8

Notes: * - N_c range of values correspond to native material; N_k values correspond to backfill.

Table B.6 - Summary of Prototype Pipeline Data; Test 01

Pipeline →	Pipeline #1	Pipeline #2	Pipeline #3	Pipeline #4
Trench Width	2.5m	2.5m	2.5m	2.5m
Cover Depth	0.80m	0.50m	0.25m	0.00m
Embedment Ratio, H/D	1.842	1.526	1.263	1.000
Average Backfill Undrained Shear Strength @ Springline	3.3kPa	2.8kPa	2.3kPa	1.8kPa
Average Native Undrained Shear Strength @ Springline	36.2kPa	34.0kPa	32.3kPa	30.5kpa
Ultimate Normalized Resistance, N	3.928	3.306	3.027	2.791
Distance into Trench Wall to Ultimate Normalized Resistance	1.130D	1.841D	1.883D	2.048D
Slope to Ultimate Normalized Resistance	1.992	1.232	1.111	0.962
Normalized Resistance at Trench Wall	0.885	1.334	1.262	1.316
Normalized Resistance at 0.5D Penetration	3.541	2.919	2.611	2.545
Normalized Resistance at 1D Penetration	3.873	3.213	2.811	2.631
Slope of Interaction Between TW and Breakover	11.538	4.172	4.801	4.317
Normalized Resistance at Breakover	3.366	2.790	2.553	2.502
Distance into Trench Wall to Breakover	0.236D	0.362D	0.286D	0.293D
Slope of Interaction After Breakover	0.699	0.670	0.294	0.215

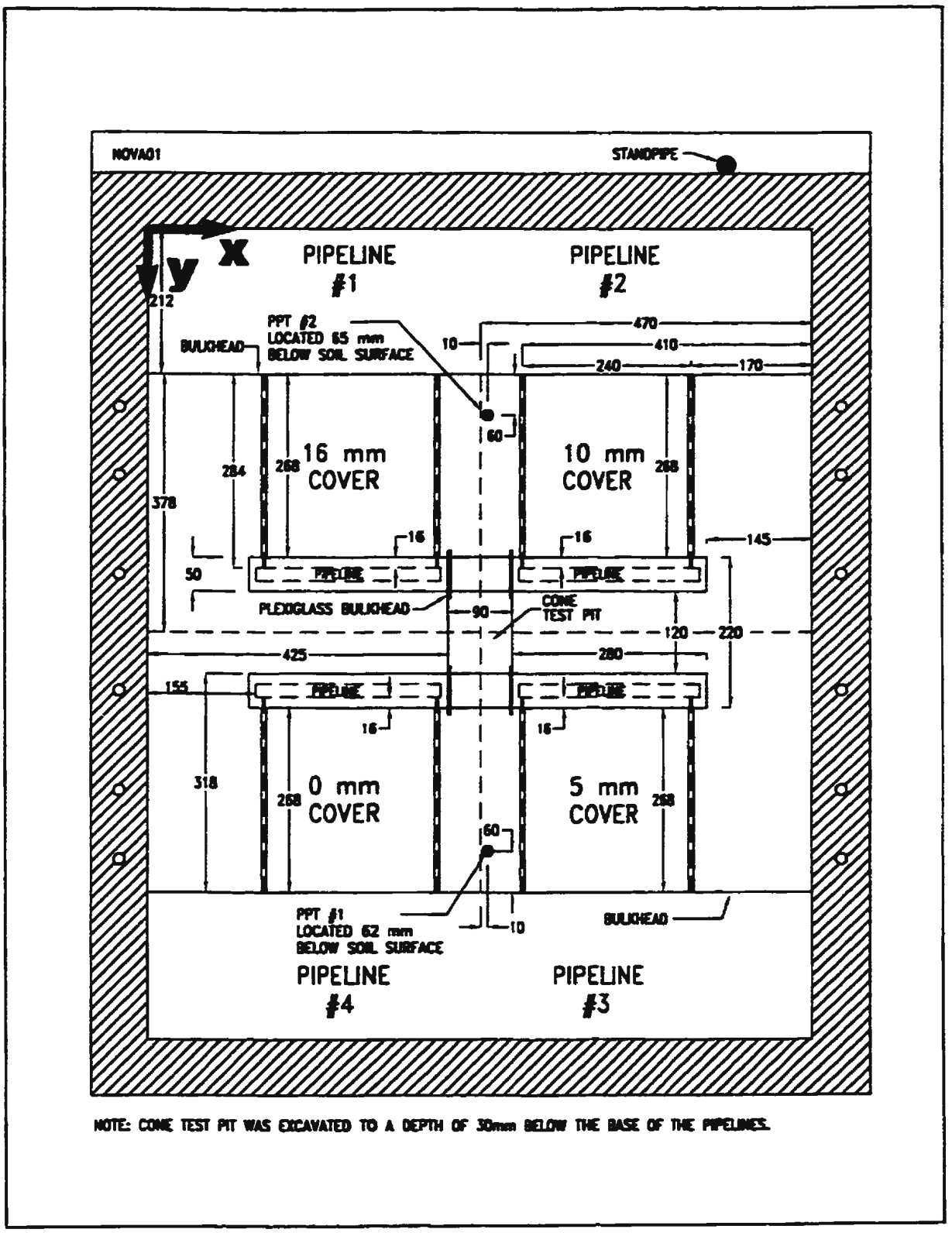

NOTE: CONE TEST PIT WAS EXCAVATED TO A DEPTH OF 30mm BELOW THE BASE OF THE PIPELINES.

Figure B.1 - *Model Test Geometry, Test 01.*

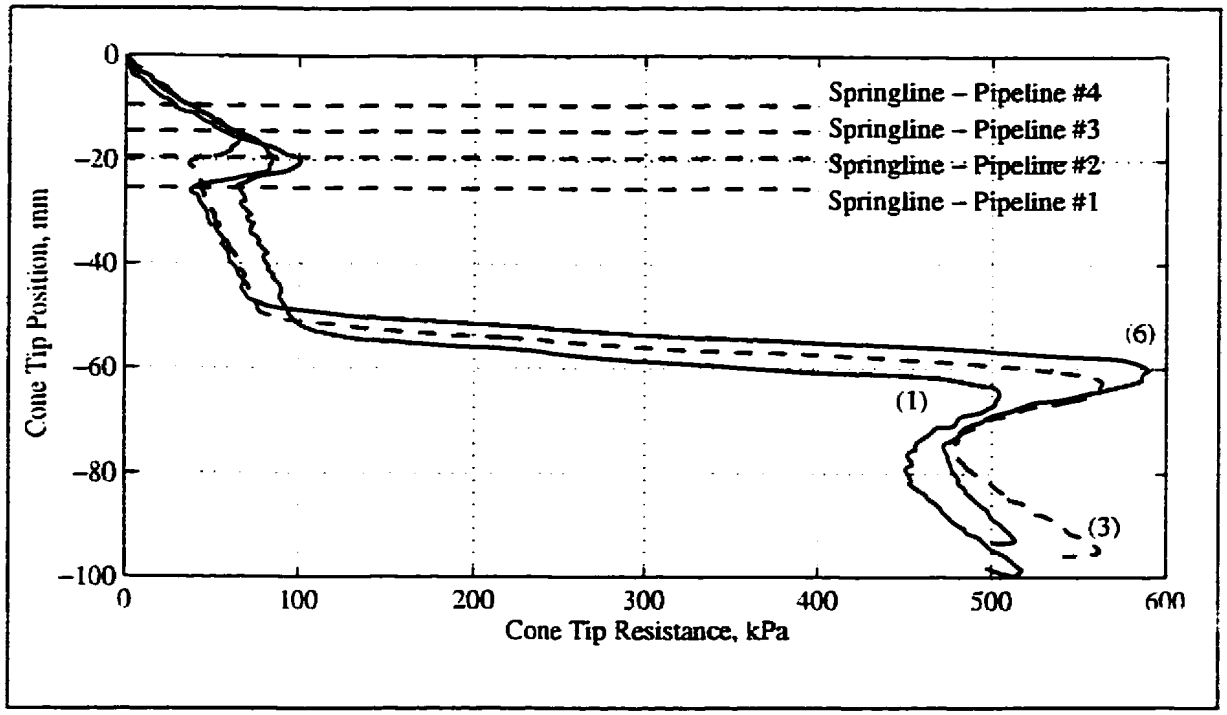

Figure B.2 - *All cone penetration tests. backfill material. Test 01.*

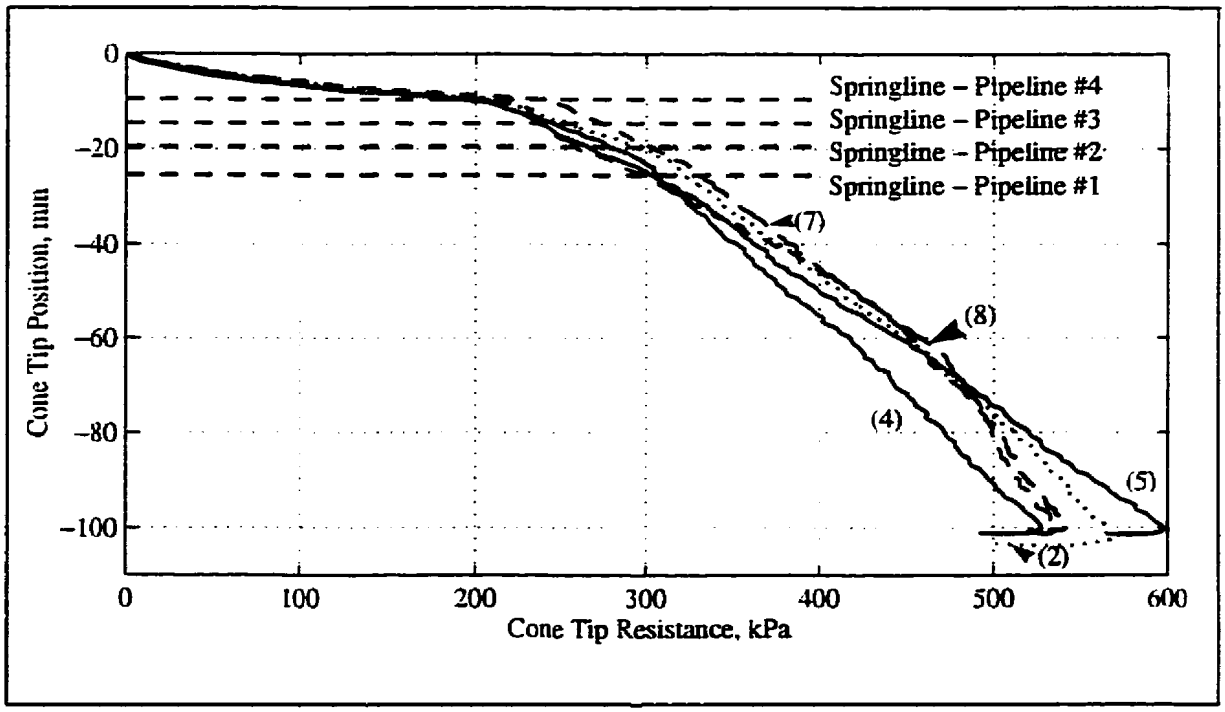

Figure B.3 - *All cone penetration tests, native material. Test 01.*

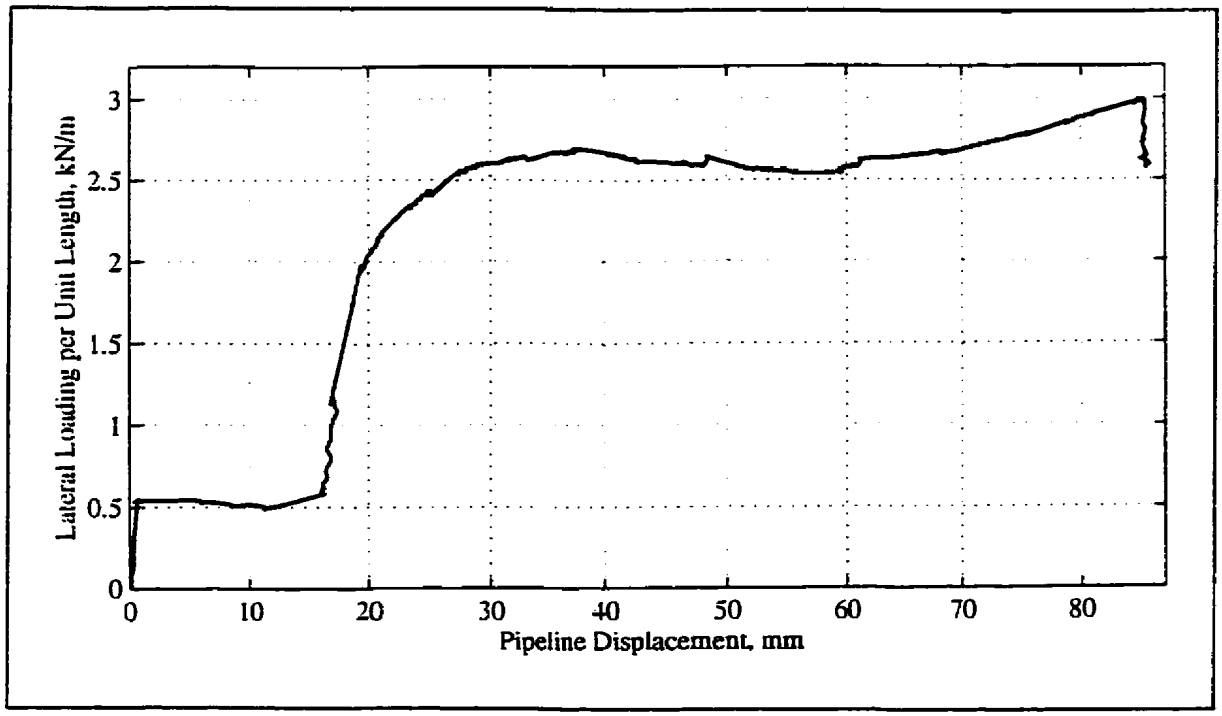

Figure B.4 - *Force-displacement response, model pipeline #1, 16mm cover, Test 01.*

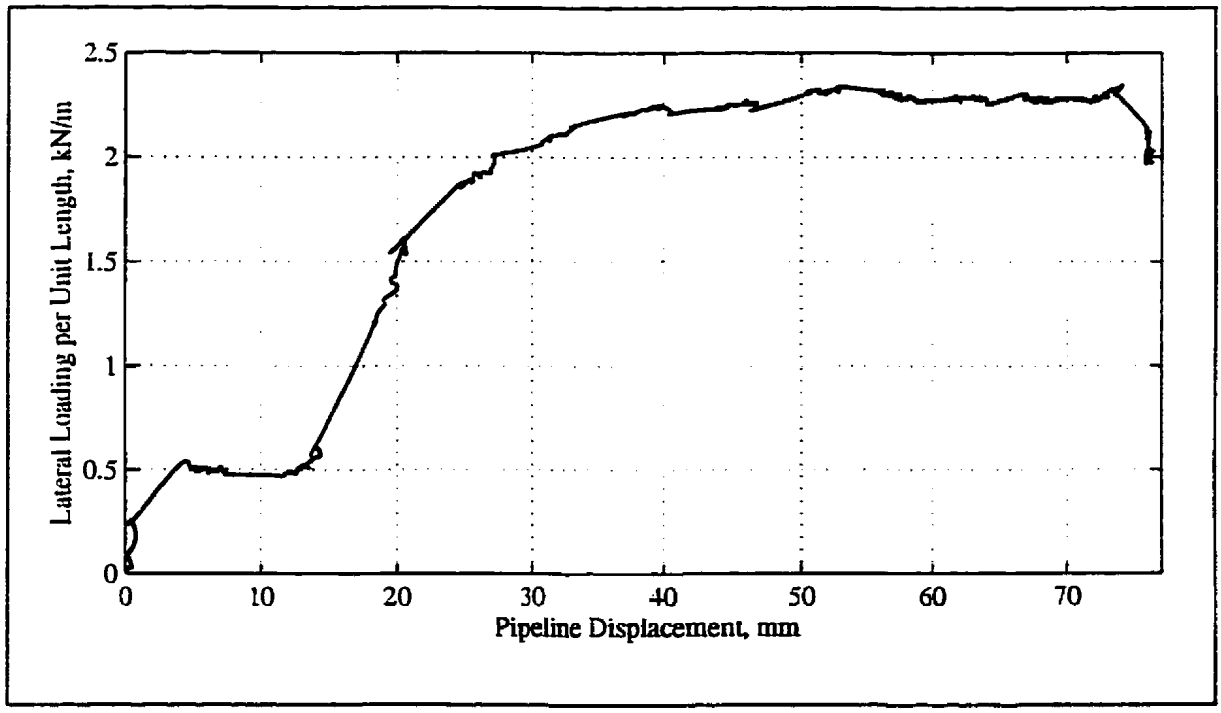

Figure B.5 - *Force-displacement response, model pipeline #2, 10mm cover, Test 01.*

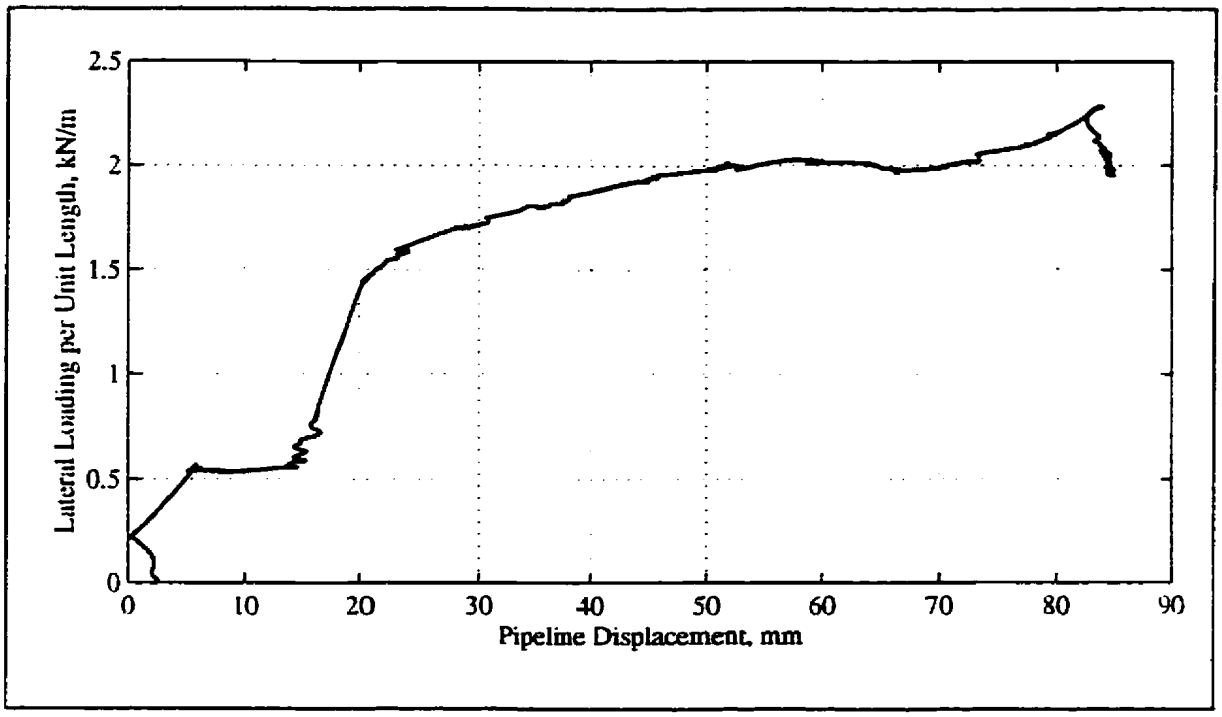

Figure B.6 - *Force-displacement response, model pipeline #3, 5mm cover, Test 01.*

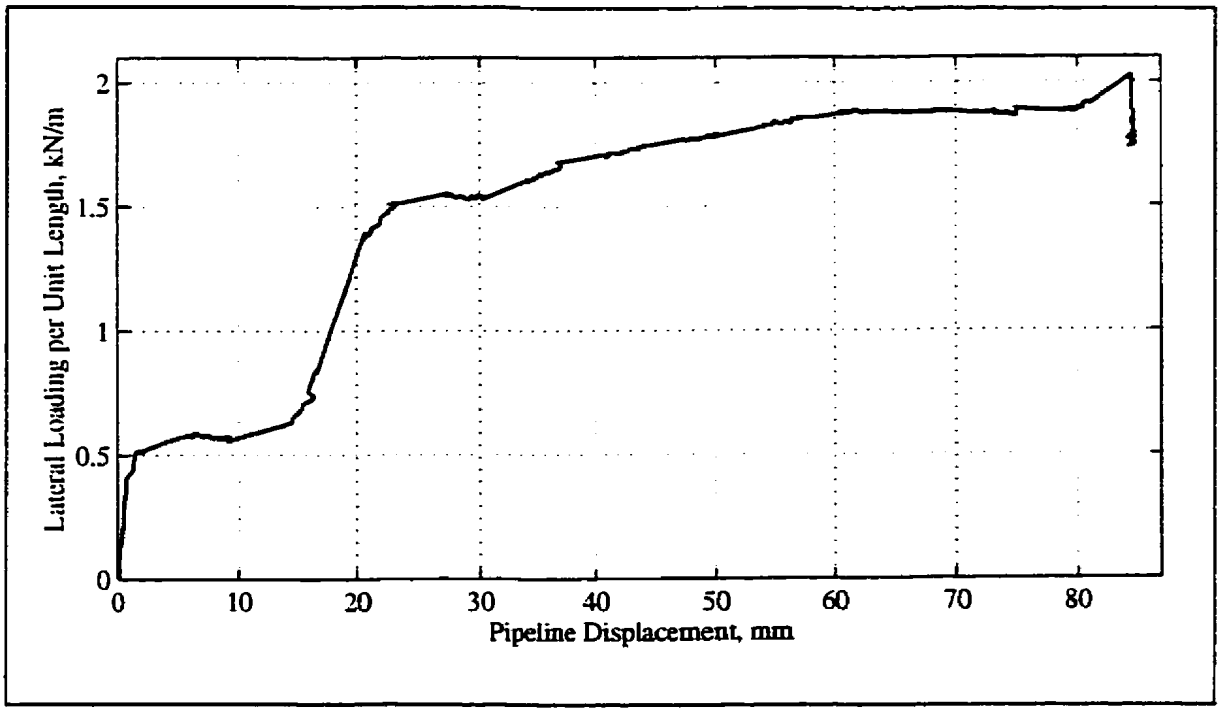

Figure B.7 - *Force-displacement response, model pipeline #4, 0mm cover, Test 01.*

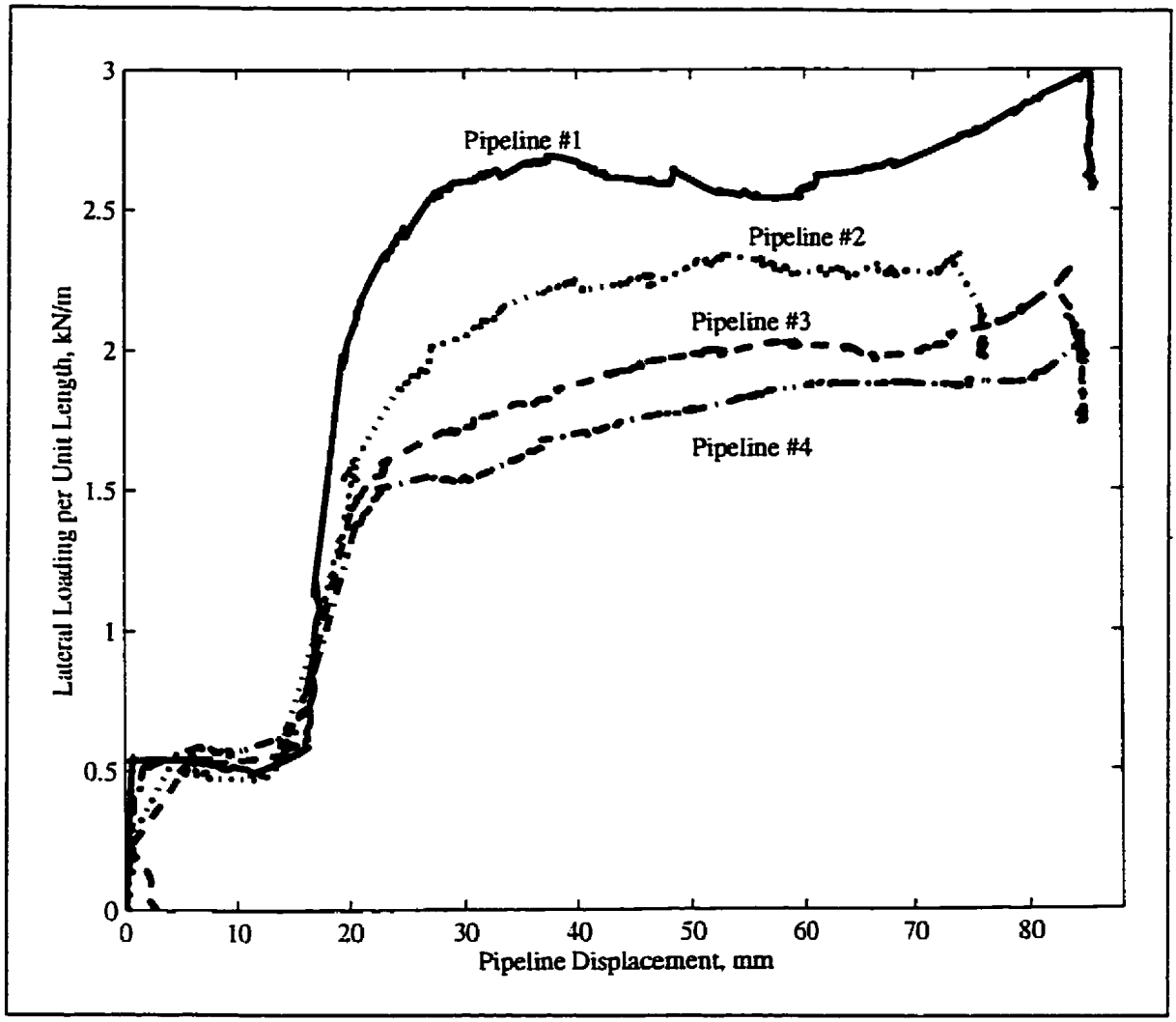

Figure B.8 - Force-displacement response, all model pipelines, Test 01.

Figure B.9 - *Photo of excavated cross-section along mid length of model pipeline #1, 16mm cover, Test 01.*

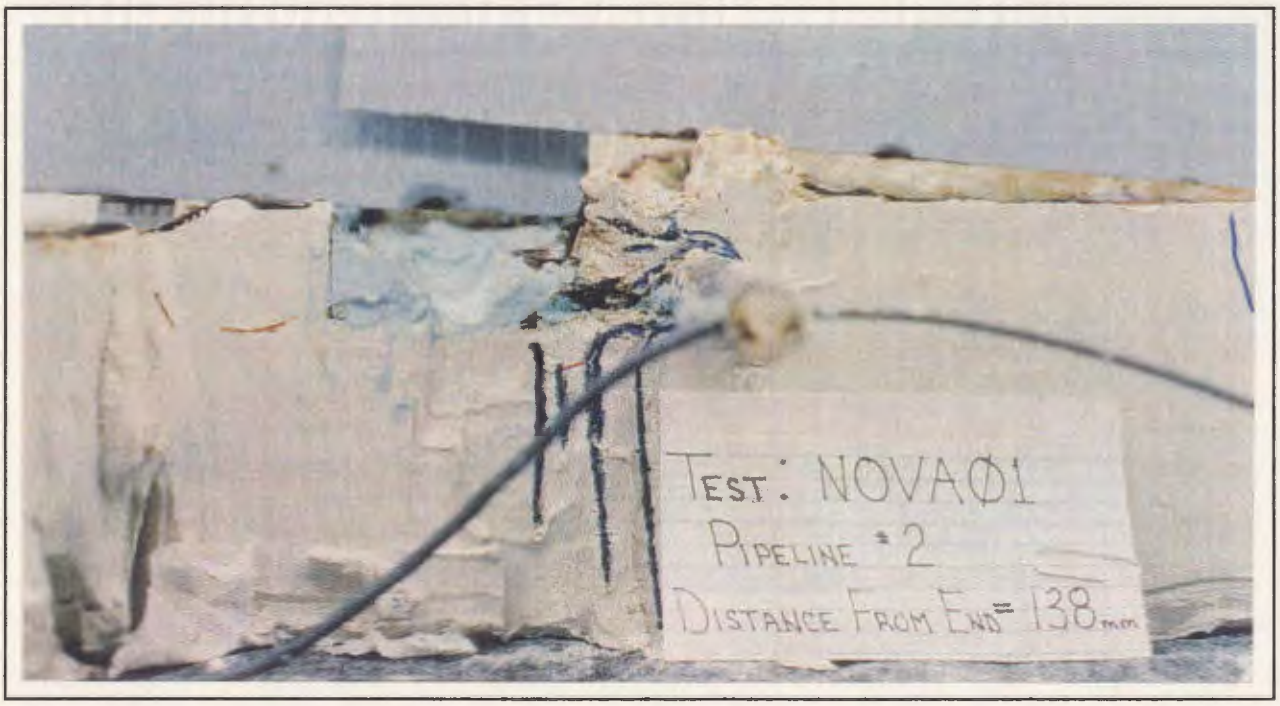

Figure B.10 - *Photo of excavated cross-section along mid length of model pipeline #2, 10mm cover, Test 01.*

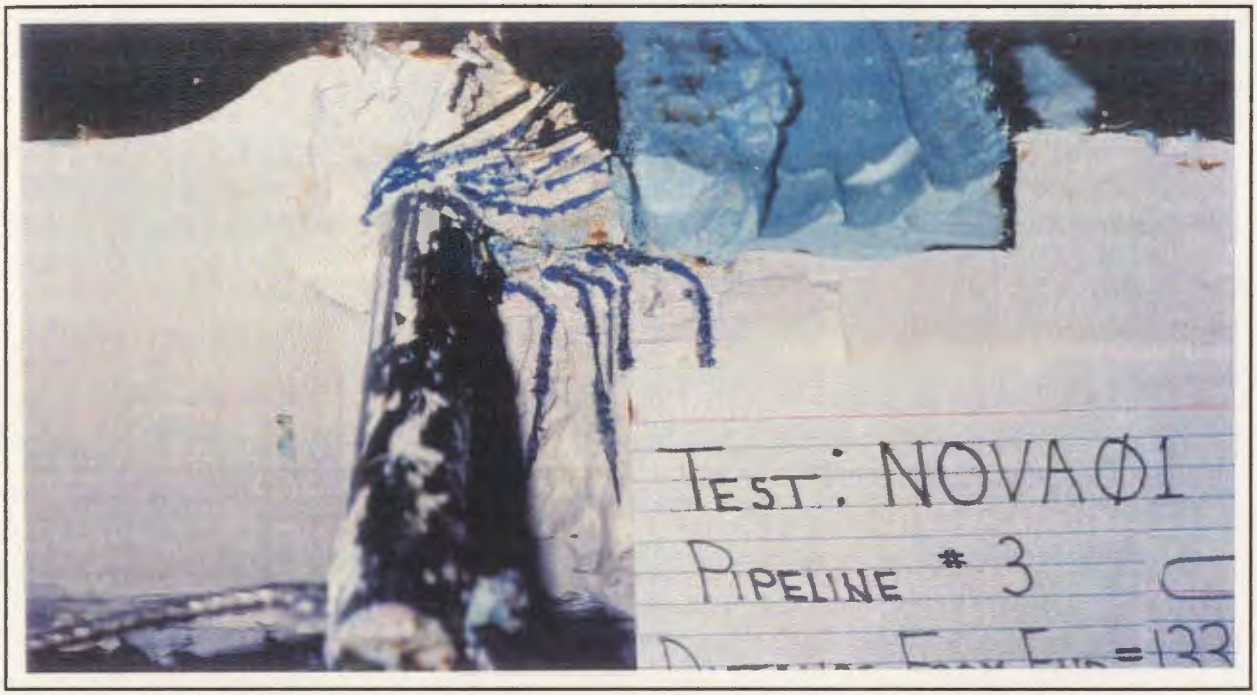

Figure B.11 - *Photo of excavated cross-section along mid length of model pipeline #3, 5mm cover, Test 01.*

Figure B.12 - *Photo of excavated cross-section along mid length of model pipeline #4, 0mm cover, Test 01.*

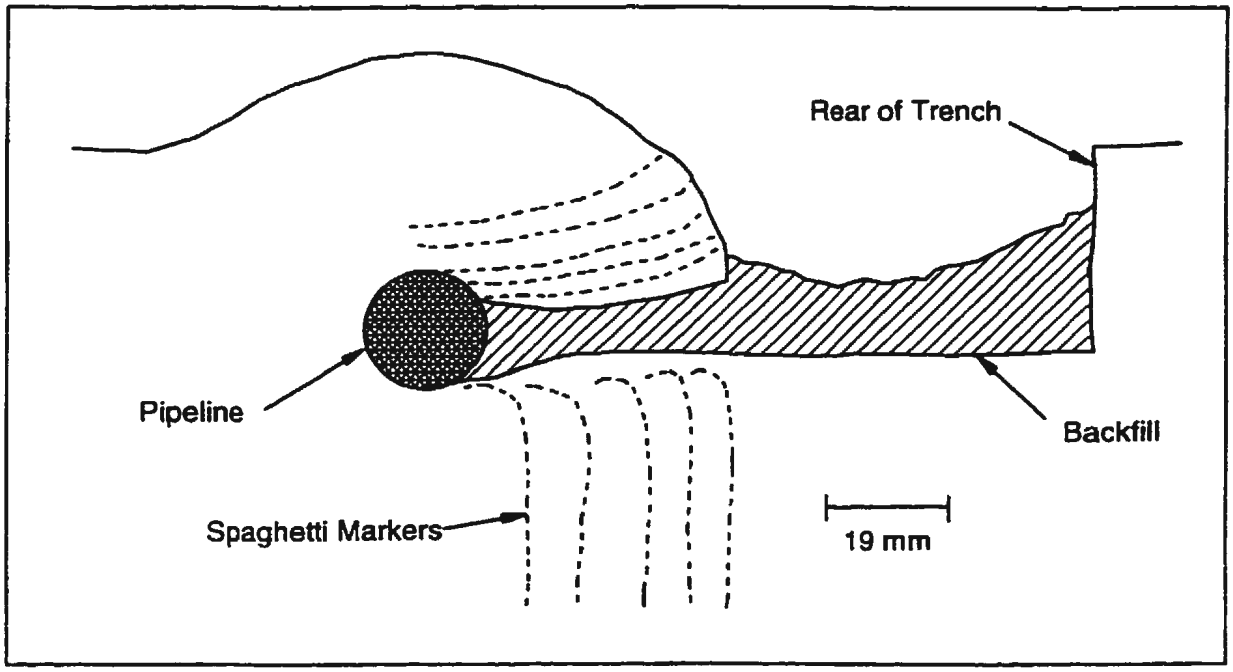

Figure B.13 - *Sketch of excavated cross-section along mid length of model pipeline #1, 16mm cover, Test 01.*

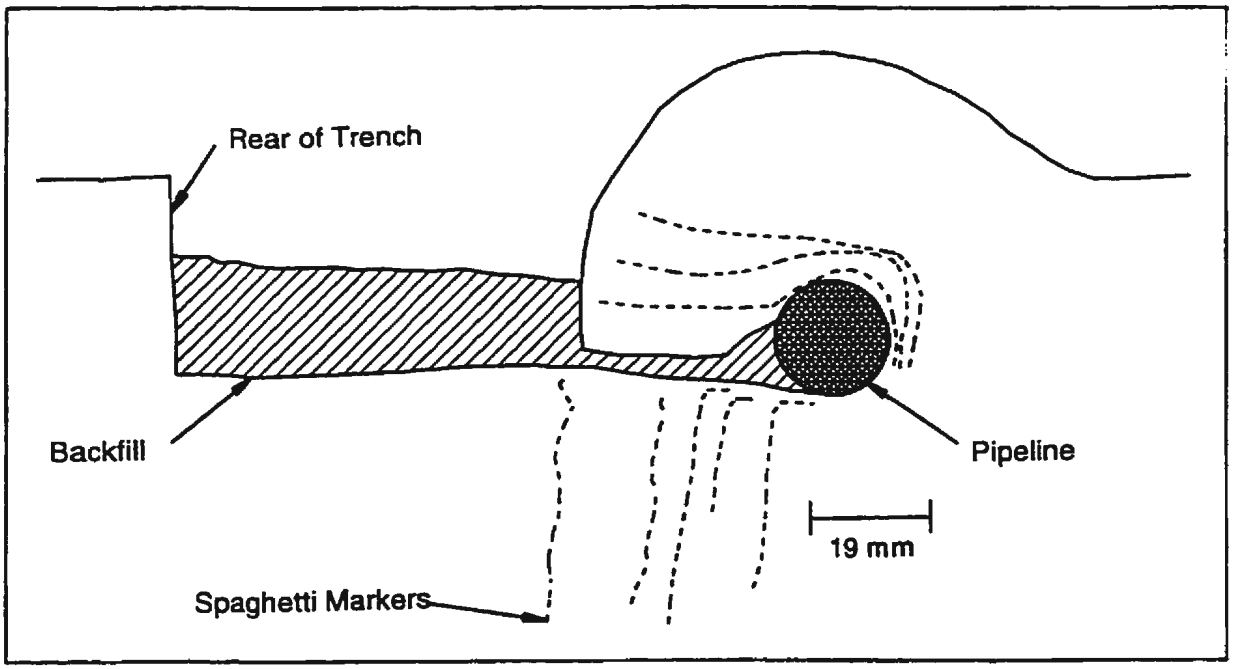

Figure B.14 - *Sketch of excavated cross-section along mid length of model pipeline #2, 10mm cover, Test 01.*

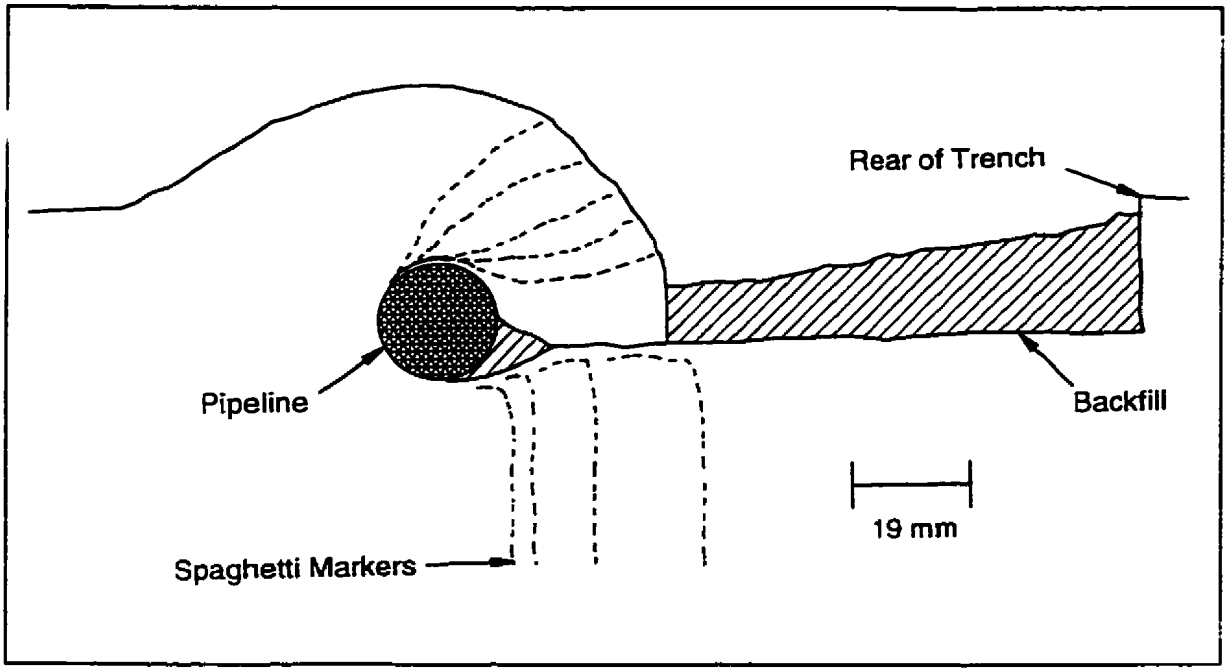

Figure B.15 - *Sketch of excavated cross-section along mid length of model pipeline #3, 5mm cover, Test 01.*

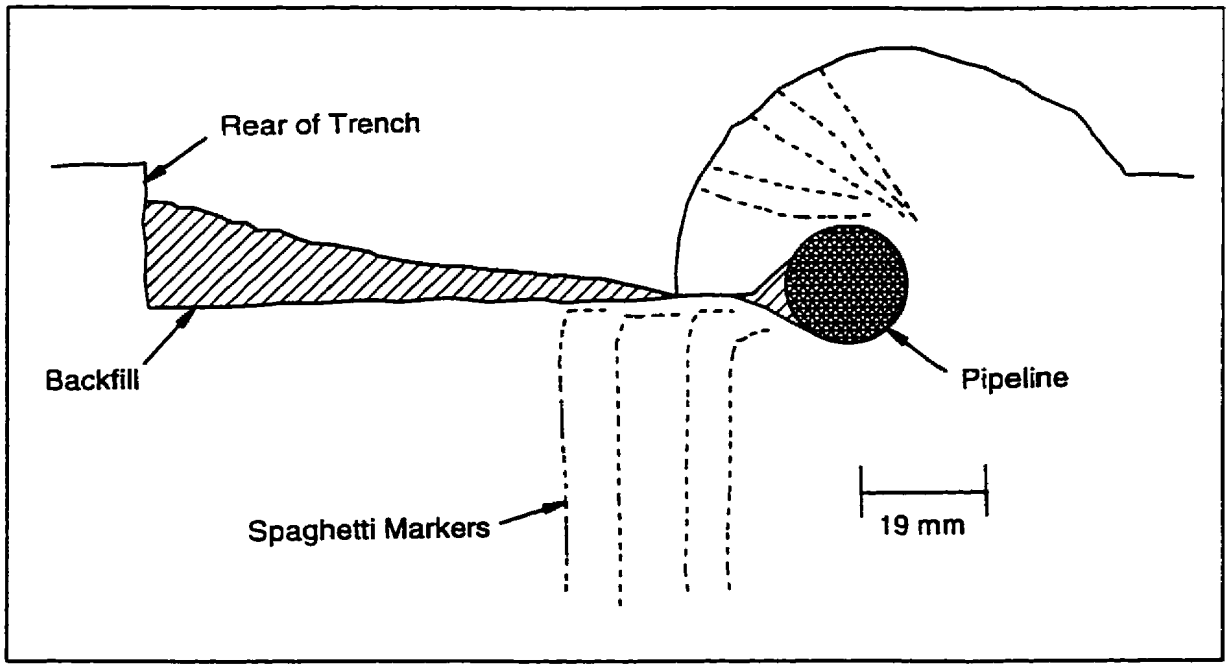

Figure B.16 - *Sketch of excavated cross-section along mid length of model pipeline #4, 0mm cover, Test 01.*

Appendix C

Test 02 - Selected Test Data

Table C.1 - Cone Penetration Test Details for Test 02

CPT No.	X[1] (mm)	Y[1] (mm)	Backfill or Native	Time Tested (hrs)
1	470	590	Backfill	1907
2	191	590	Native	1938
3	430	590	Backfill	2022
4	590	590	Native	2211

Notes: 1 - Coordinate convention shown on Figure C.1.

Table C.2 - Interpreted Cone Penetration Resistances for Test 02

Cone Test No.	Interpreted Penetration Resistance (kPa)			
	@ Initial Springline of Pipeline #1	@ Initial Springline of Pipeline #2	@ Initial Springline of Pipeline #3	@ Initial Springline of Pipeline #4
1	52	43	33	23
2	396	352	317	287
3	54	40	28	17
4	394	324	269	217

Table C.3 - Pipeline Test Details for Test 02

Pipeline No.	Trench Width (mm)	Cover Depth (mm)	X:Y Coordinates of Pipe Centre (mm)	Pipeline Velocity (mm/sec)	Time Tested (hrs)
1	50	65	290 : 505	0.52	1948
2	50	50	650 : 505	0.55	2058
3	50	38	650 : 675	0.65	2107
4	50	27	290 : 675	0.47	2006

Table C.4 - Prototype Test Geometries for Test 02

Pipeline	Distance to Trench Wall in the Direction of Travel (m)	Distance to Trench Wall Towards the Rear of the Pipeline (m)	Distance to a Stiff Retaining Wall in the Direction of Travel (m)	Distance to the Pipeline in the Direction Opposite to Travel (m)	Distance Laterally to a Stiff Retaining Wall (m)	Distance Laterally to the Edge of the Adjacent Pipeline (m)	Distance From Base of Pipeline to Rigid Base, i.e. Bedrock (m)	Water Level Above Rigid Base, i.e. Bedrock (m)	Water Level Below Base of Pipeline (m)
1	0.775	0.775	14.175	7.55	7.75	5.0	5.025	3.715	1.310
2	0.775	0.775	14.175	7.55	7.75	5.0	5.025	3.715	1.310
3	0.775	0.775	14.175	7.55	7.75	5.0	5.025	3.715	1.310
4	0.775	0.775	17.175	7.55	7.75	5.0	5.025	3.715	1.310

Table C.5 - Calculation of Undrained Shear Strength for Test 02

Pipeline	Soil Type	Cone Tests Used to Derive q_c	Interpreted Cone Tip Resistance at Springline, q_c (kPa)	Saturated Bulk Density, γ_{sat} (kN/m^3)	Pore Pressure at Springline, u (kPa)	Depth to Springline, h (m)	Cone Factor, N_c or N_k*	Undrained Shear Strength, c_u (kPa)
1	Native	2	455.4	949.1	-3.0	0.0745	8.5/10.4	37.0 - 45.3
1	Backfill	1,3	53	854.0	---	0.0745	15	3.5
2	Native	2	404.8	949.1	-3.0	0.0595	8.3/10.8	32.3 - 42.0
2	Backfill	1,3	41.5	854.0	---	0.0595	15	2.8
3	Native	2	364.6	949.1	-3.0	0.0475	8.1/11.2	26.9 - 37.2
3	Backfill	1,3	30.5	854.0	---	0.0475	15	2.0
4	Native	2	330.1	949.1	-3.0	0.0365	7.9/11.7	25.3 - 37.4
4	Backfill	1,3	20	854.0	---	0.0365	15	1.3

Notes: * - N_c range of values correspond to native material; N_k values correspond to backfill.

Table C.6 - Summary of Prototype Pipeline Data; Test 02

Pipeline →	Pipeline #1	Pipeline #2	Pipeline #3	Pipeline #4
Trench Width	2.5m	2.5m	2.5m	2.5m
Cover Depth	3.25m	2.50m	1.90m	1.35m
Embedment Ratio, H/D	4.421	3.632	3.000	2.421
Average Backfill Undrained Shear Strength @ Springline	3.5kPa	2.8kPa	2.0kPa	1.3kPa
Average Native Undrained Shear Strength @ Springline	41.2kPa	37.2kPa	32.1kPa	31.4kPa
Ultimate Normalized Resistance, N	5.027	4.303	5.027	5.128
Distance into Trench Wall to Ultimate Normalized Resistance	1.930D	1.875D	1.997D	1.826D
Slope to Ultimate Normalized Resistance	1.831	1.599	1.787	1.941
Normalized Resistance at Trench Wall	1.499	1.363	1.443	2.141
Normalized Resistance at 0.5D Penetration	4.395	3.617	3.877	4.587
Normalized Resistance at 1D Penetration	4.677	4.037	4.441	4.734
Slope of Interaction Between TW and Breakover	9.769	6.596	7.134	8.321
Normalized Resistance at Breakover	4.283	3.822	4.035	4.538
Distance into Trench Wall to Breakover	0.297D	0.391D	0.371D	0.285D
Slope of Interaction After Breakover	0.576	0.384	0.696	0.399

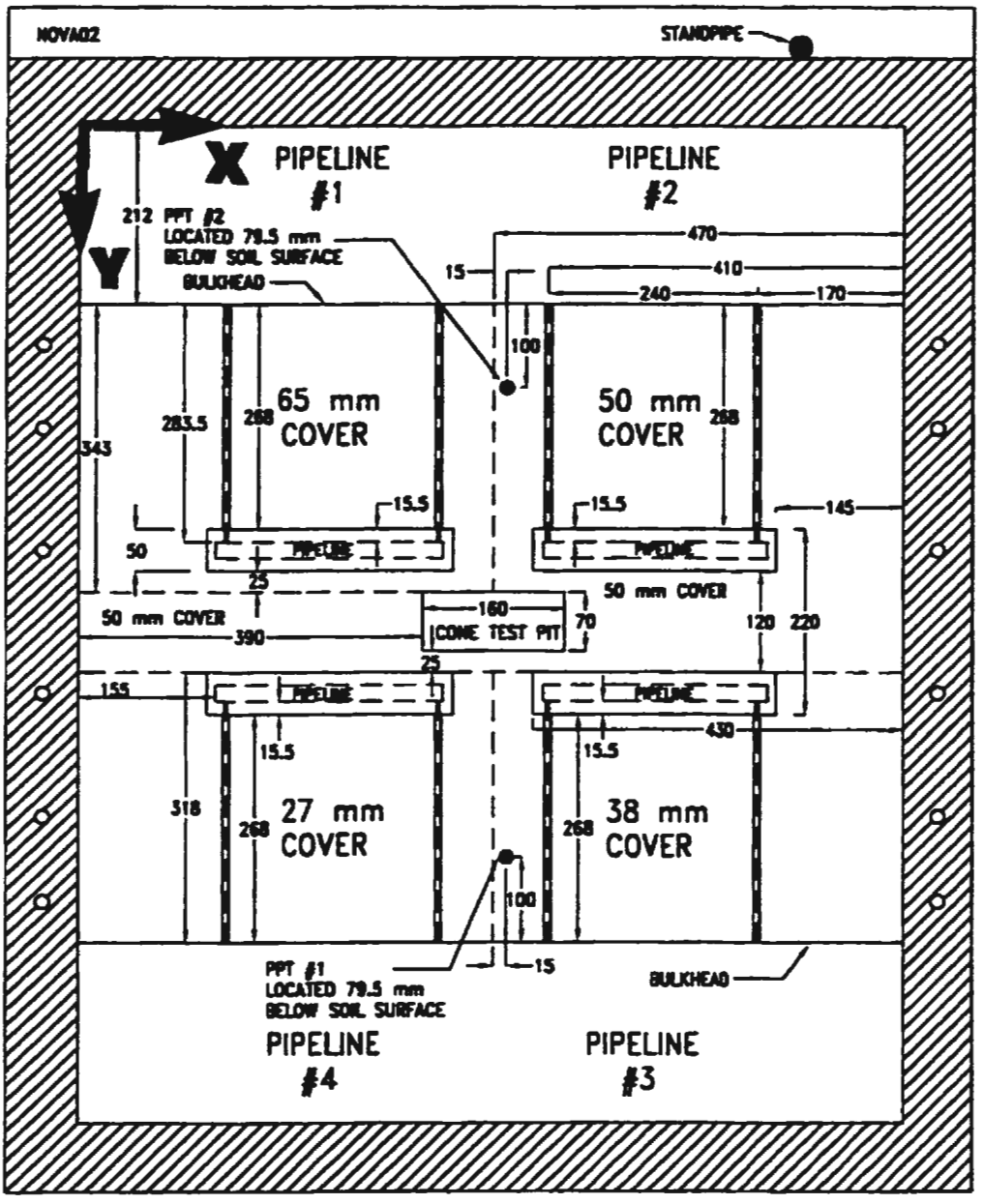

NOTE: CONE TEST PIT WAS EXCAVATED TO A DEPTH OF 20mm BELOW THE BASE OF THE PIPELINES

Figure C.1 - *Model Test Geometry, Test 02.*

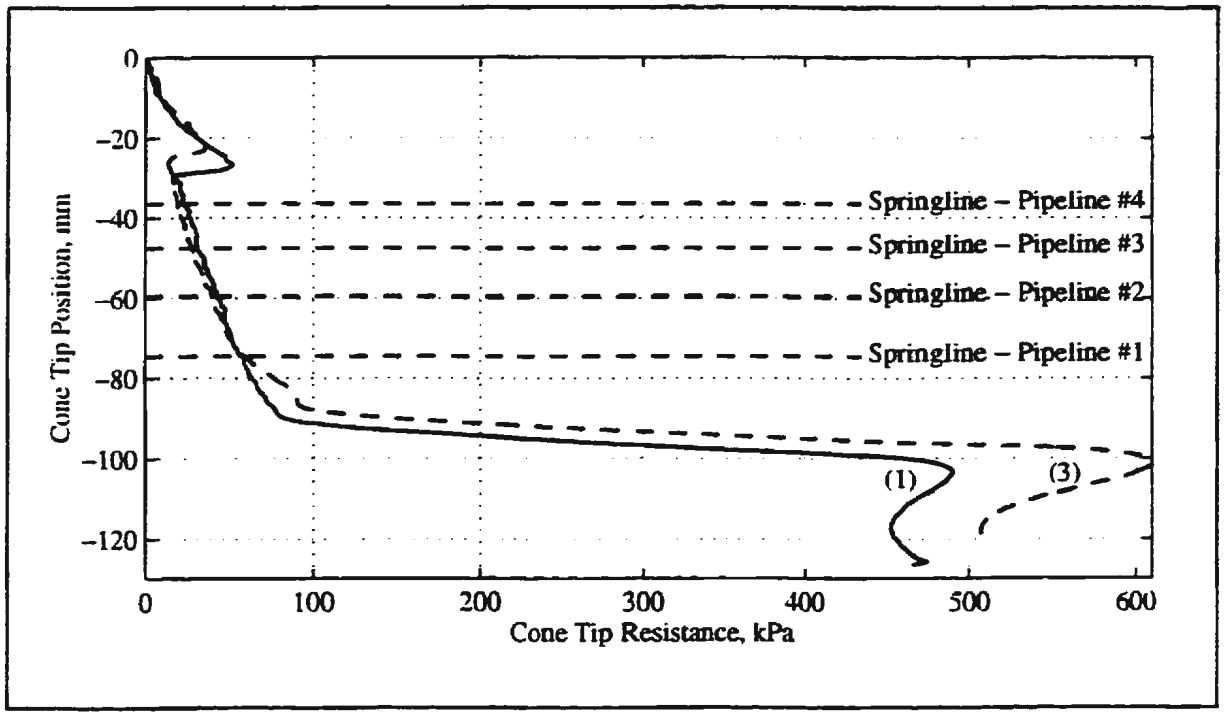

Figure C.2 - *All cone penetration tests, backfill material, Test 02.*

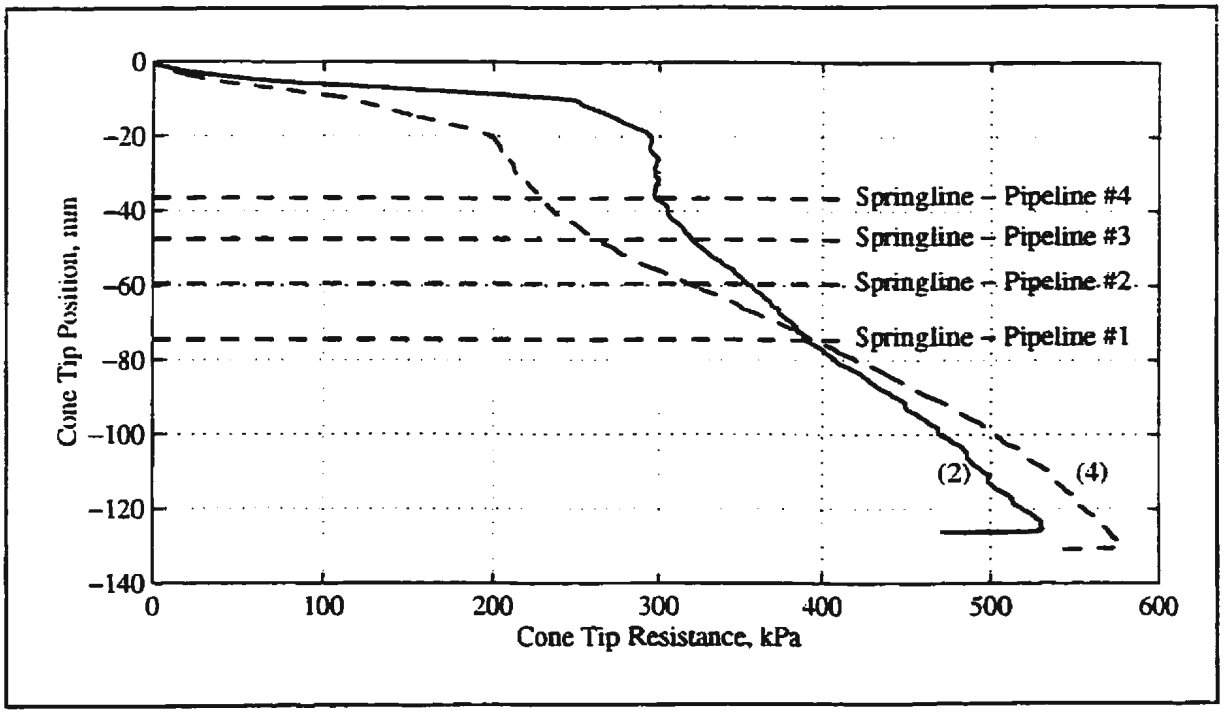

Figure C.3 - *All cone penetration tests, native material, Test 02.*

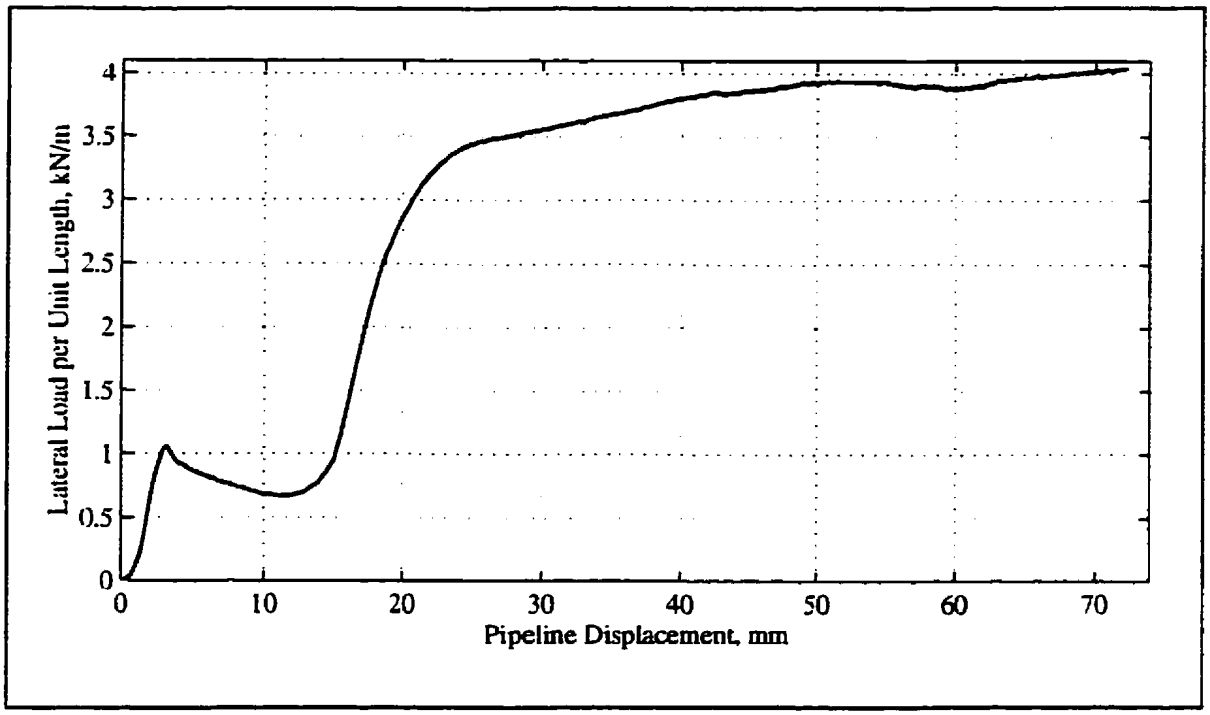

Figure C.4 - *Force-displacement response, model pipeline #1, 65mm cover, Test 02.*

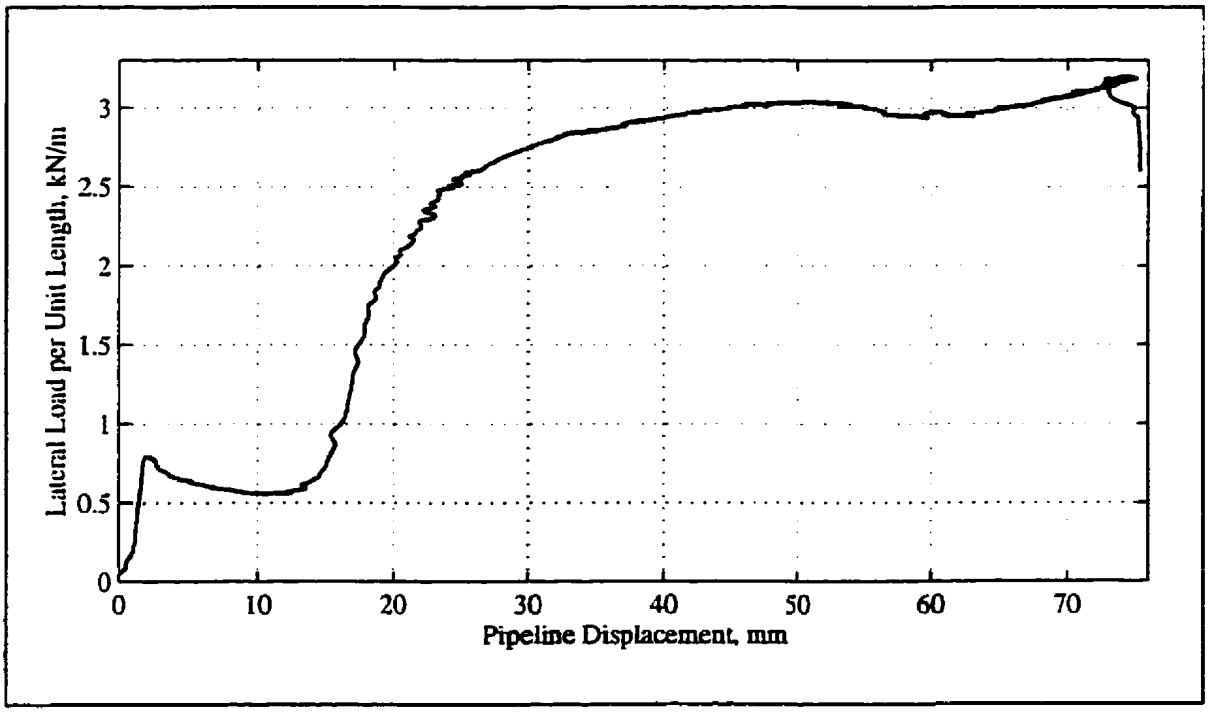

Figure C.5 - *Force-displacement response, model pipeline #2, 38mm cover, Test 02.*

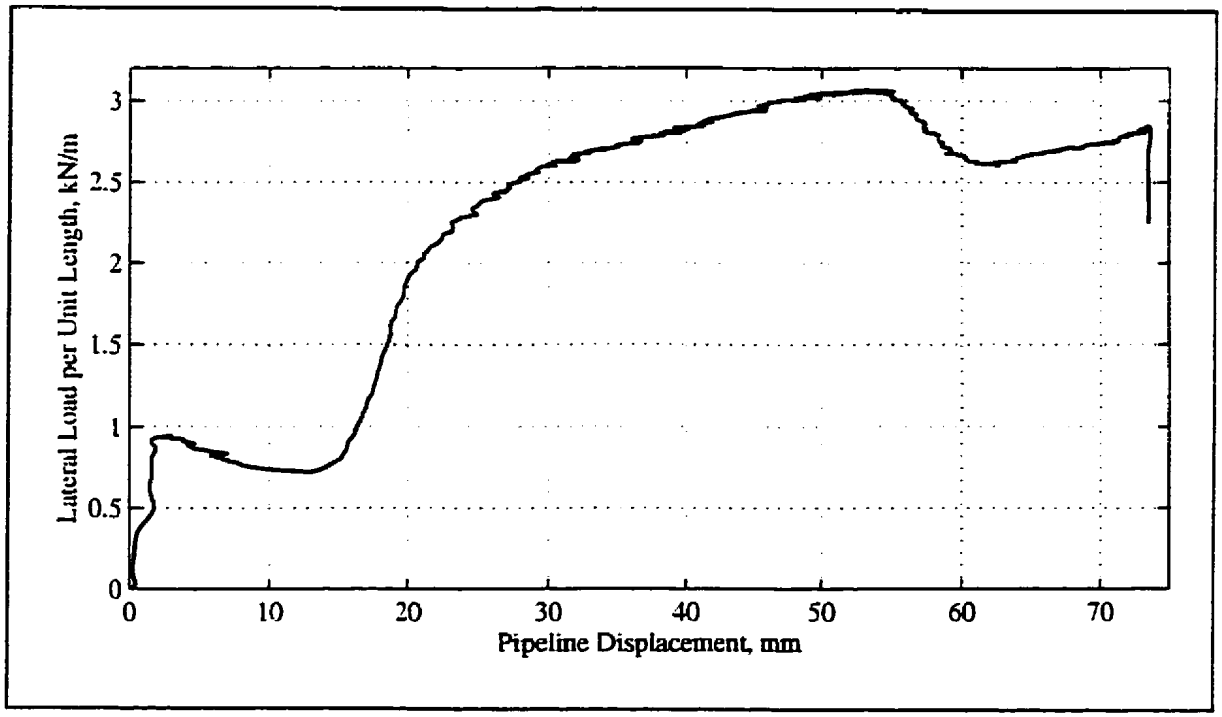

Figure C.6 - *Force-displacement response, model pipeline #3, 38mm cover, Test 02.*

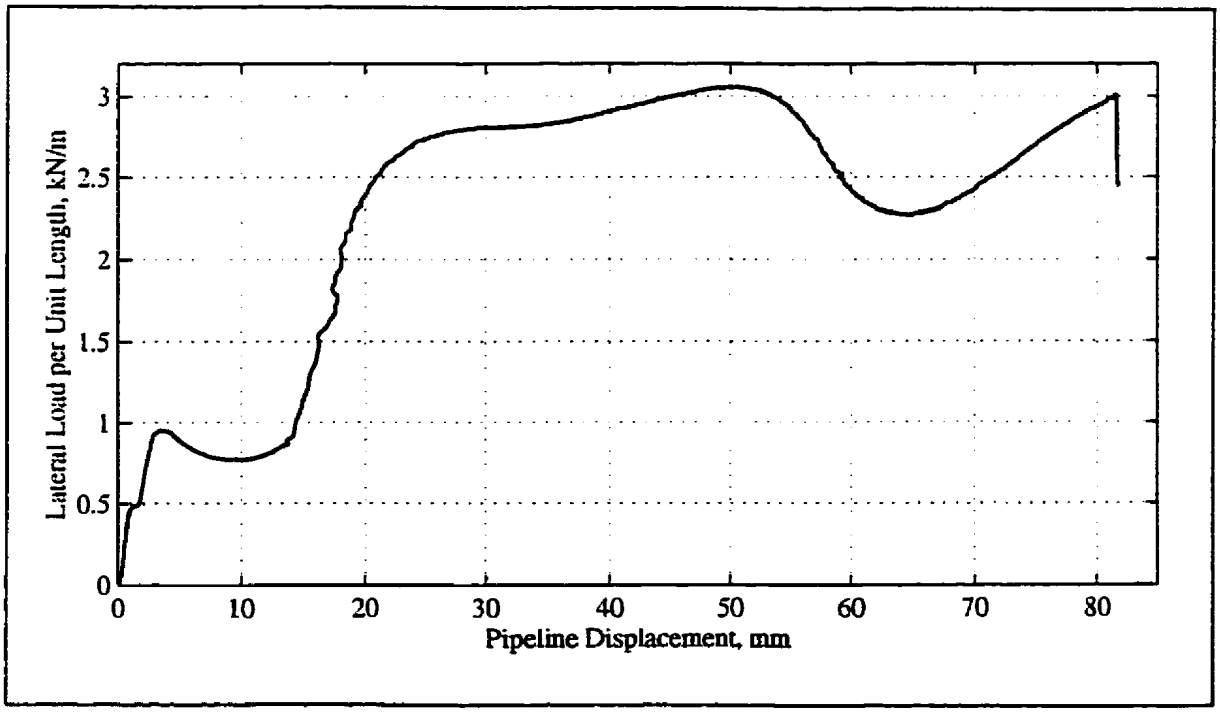

Figure C.7 - *Force-displacement response, model pipeline #4, 27mm cover, Test 02.*

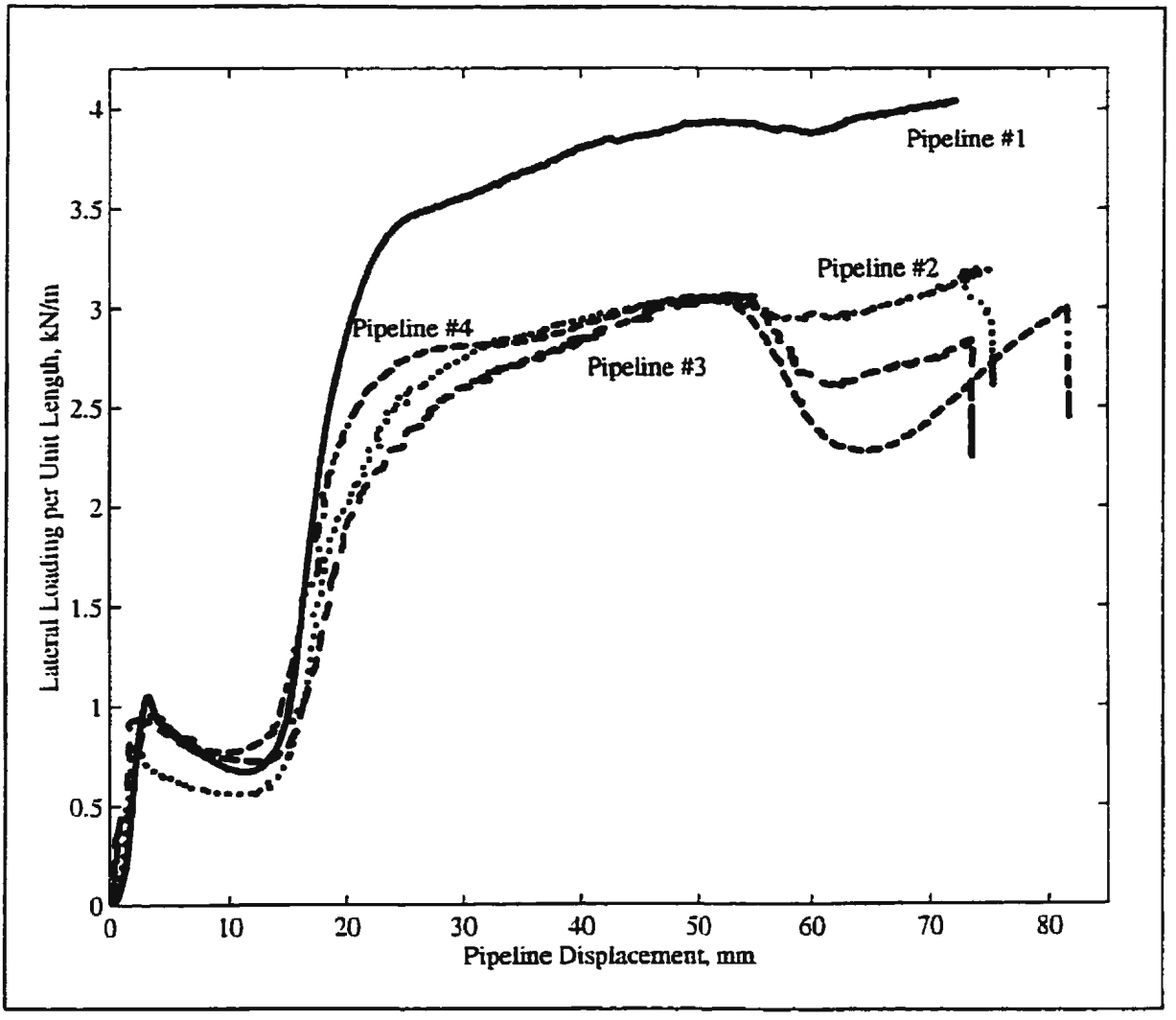

Figure C.8 - Force-displacement response, all model pipelines, Test 02.

Figure C.9 - *Photo of excavated cross-section along mid length of model pipeline #1, 65mm cover, Test 02.*

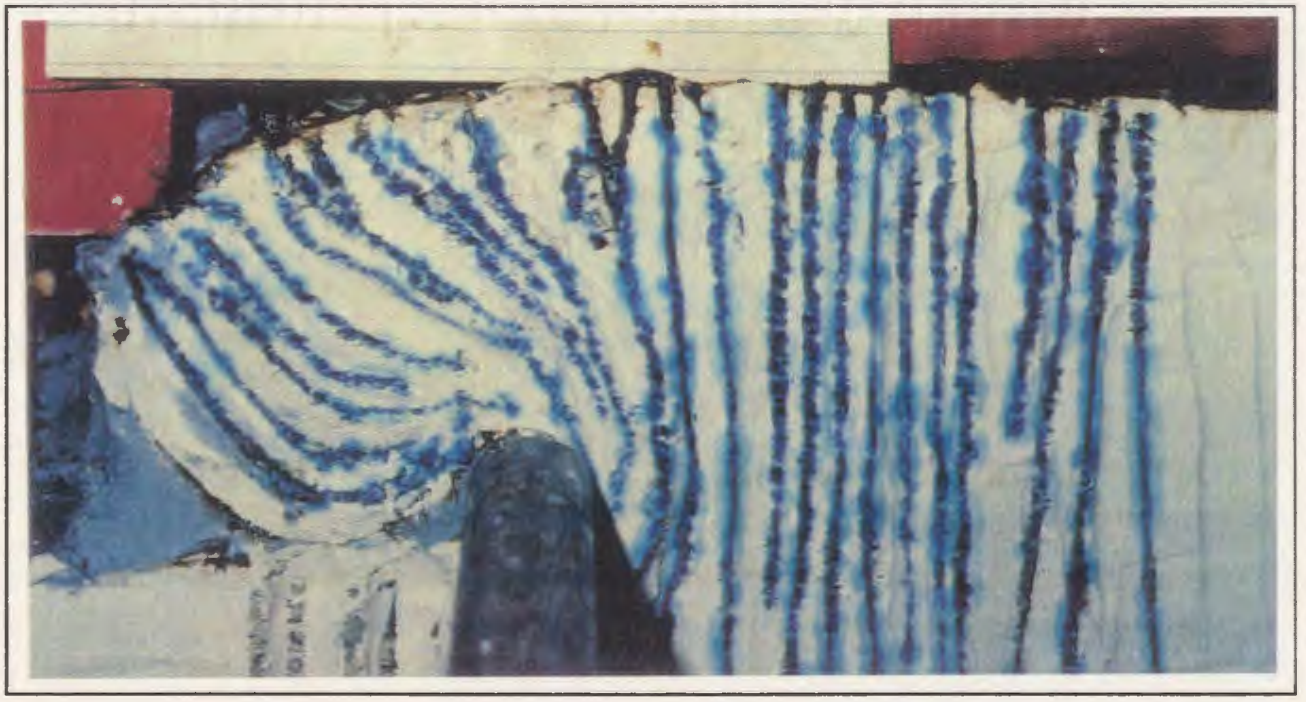

Figure C.10 - *Photo of excavated cross-section along mid length of model pipeline #2, 50mm cover, Test 02.*

Figure C.11 - *Photo of excavated cross-section along mid length of model pipeline #3, 38mm cover, Test 02.*

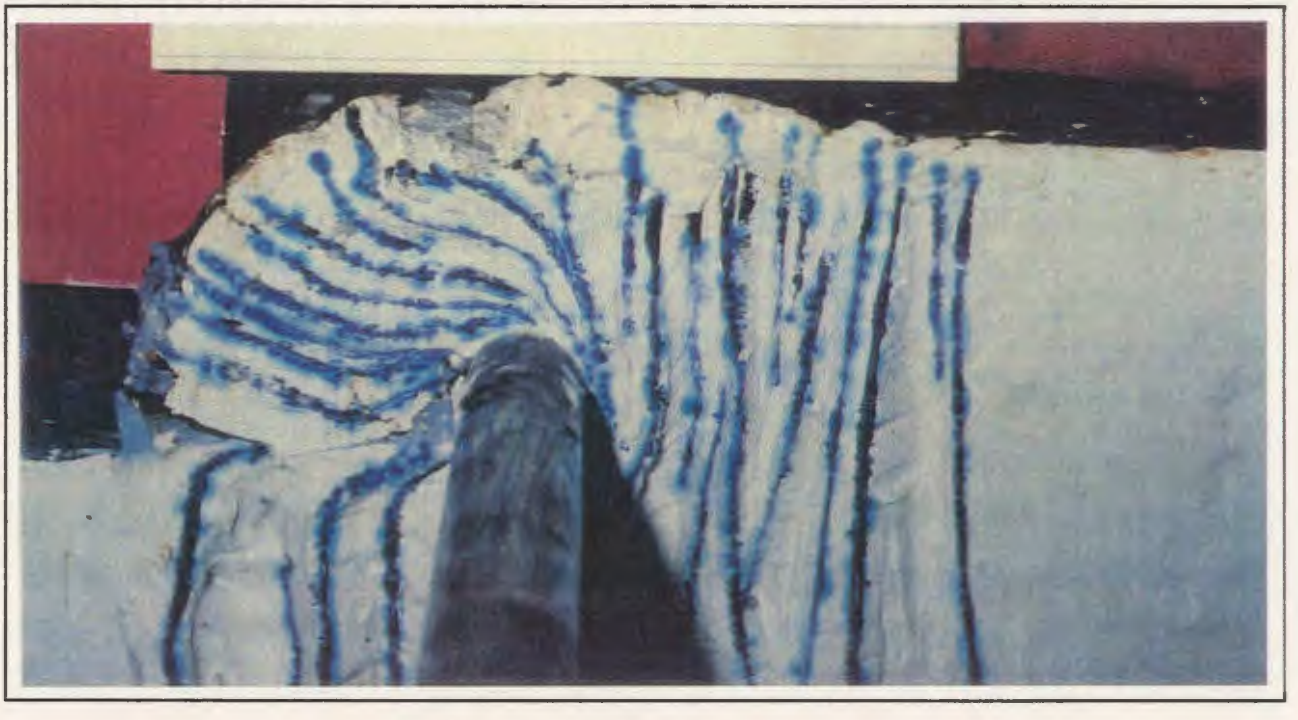

Figure C.12 - *Photo of excavated cross-section along mid length of model pipeline #4, 27mm cover, Test 02.*

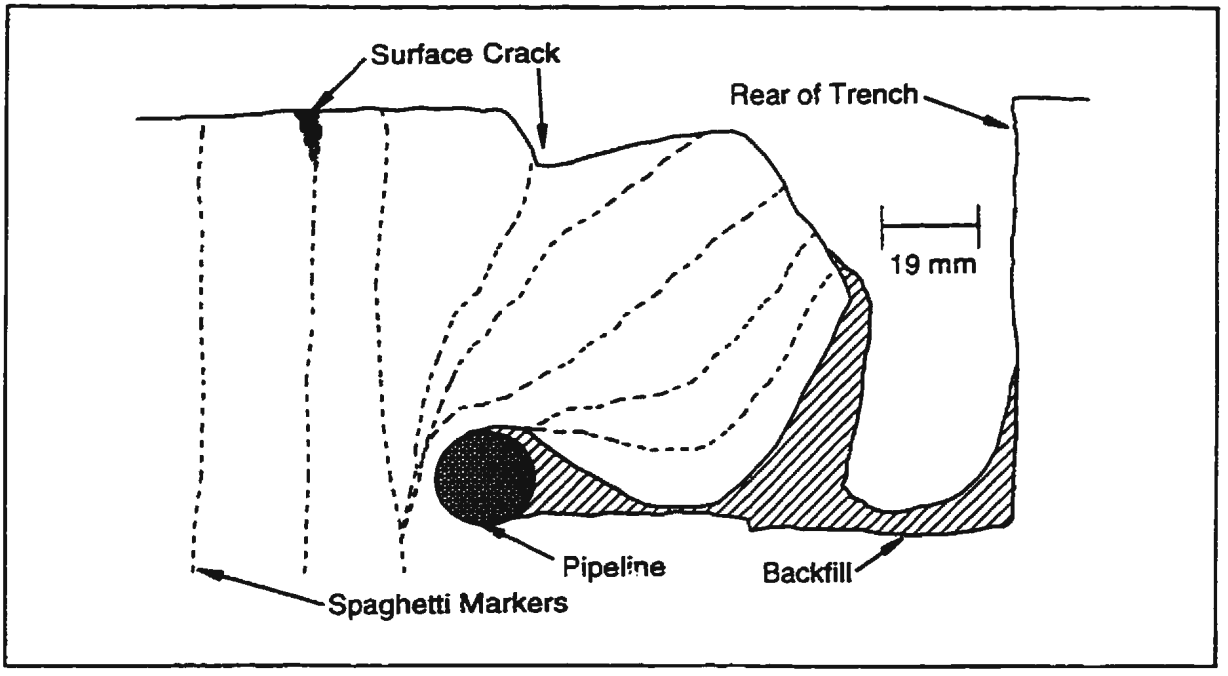

Figure C.13 - *Sketch of excavated cross-section along mid length of model pipeline #1, 65mm cover, Test 02.*

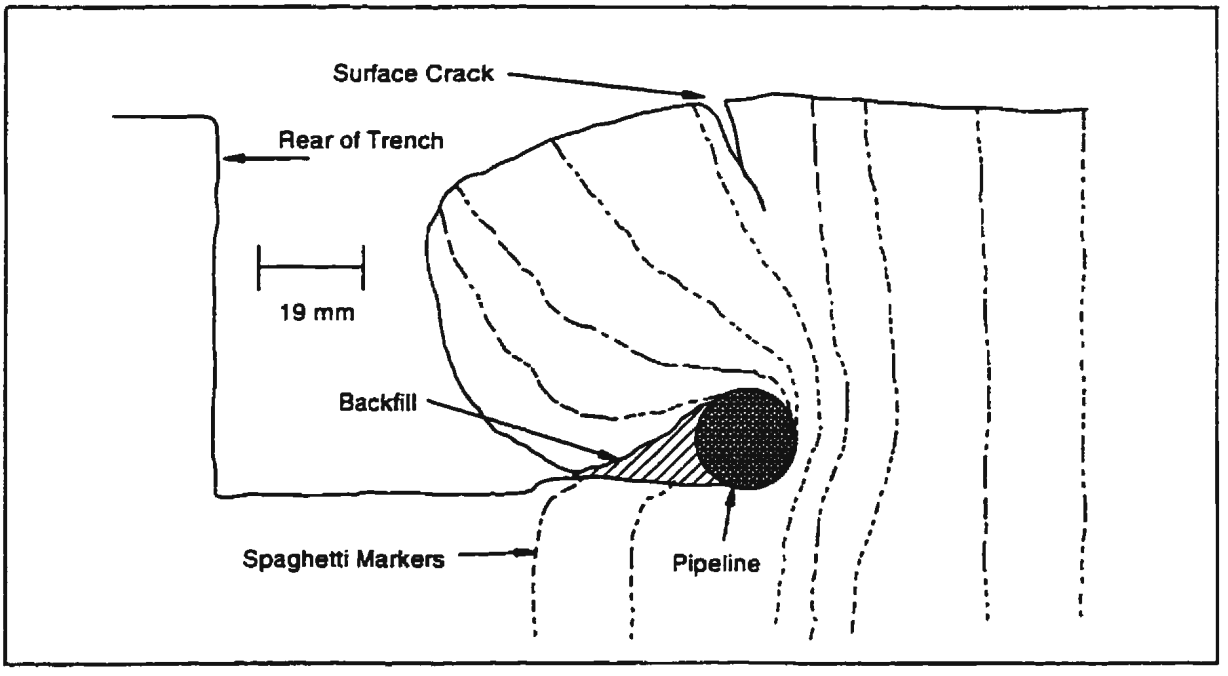

Figure C.14 - *Sketch of excavated cross-section along mid length of model pipeline #2, 50mm cover, Test 02.*

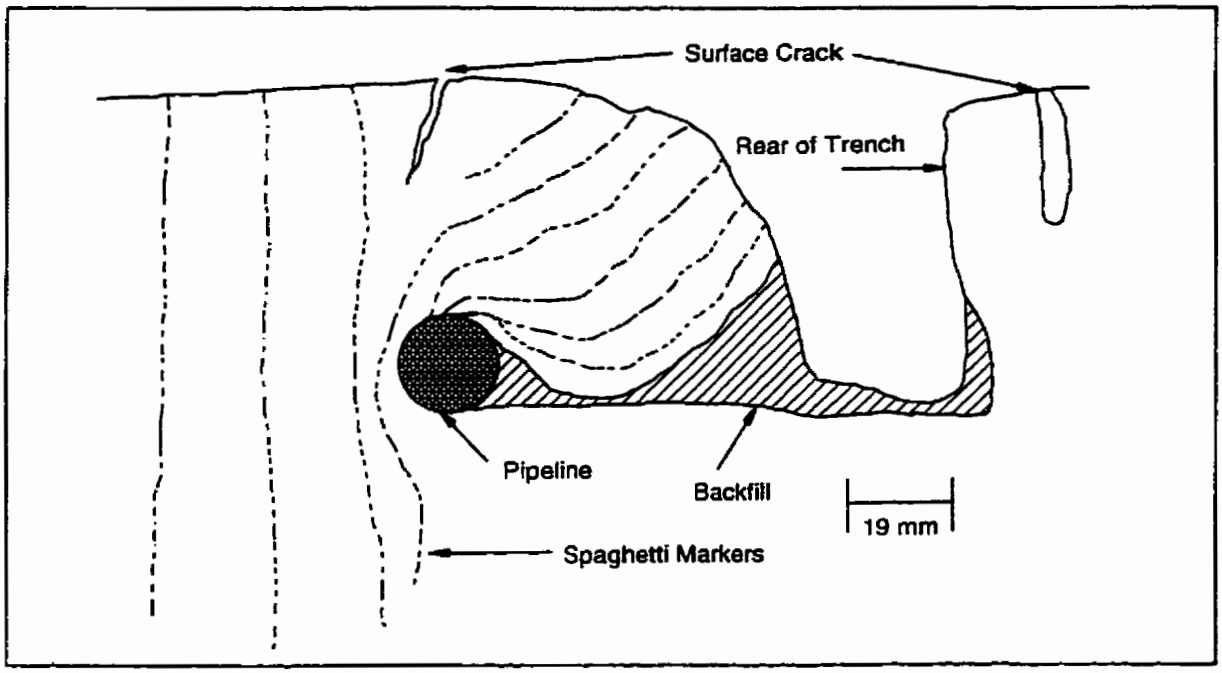

Figure C.15 - *Sketch of excavated cross-section along mid length of model pipeline #3, 38mm cover, Test 02.*

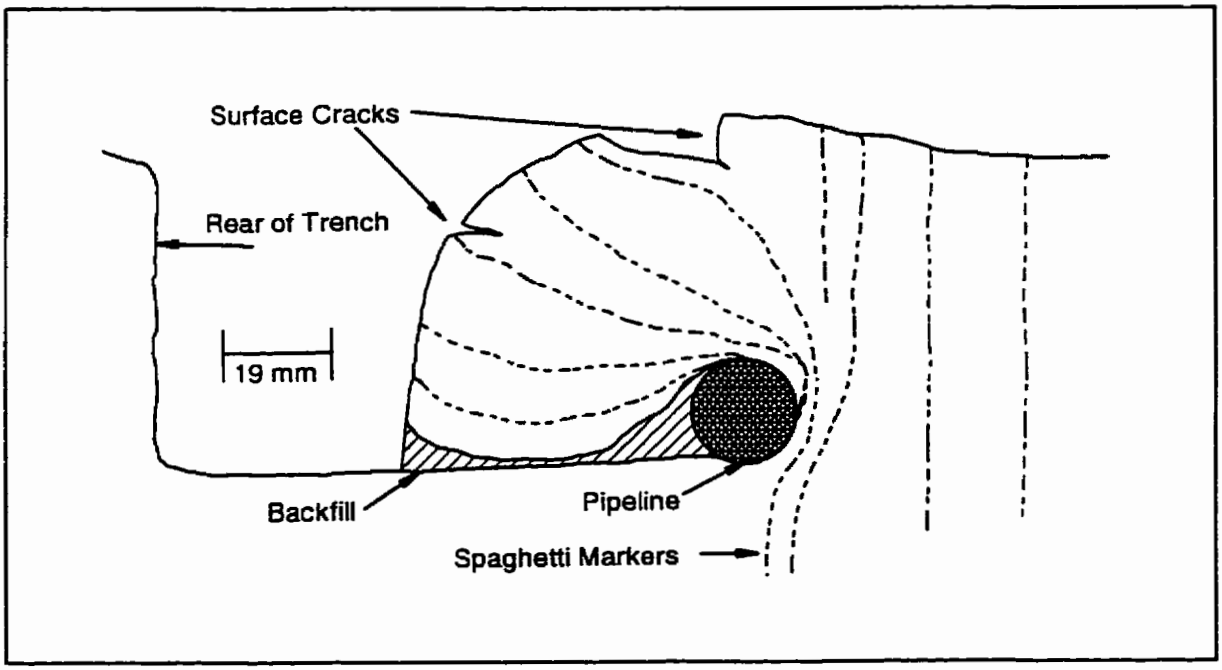

Figure C.16 - *Sketch of excavated cross-section along mid length of model pipeline #4, 27mm cover, Test 02.*

Appendix D

Test 03 - Selected Test Data

Table D.1 - Cone Penetration Test Details for Test 03

CPT No.	X[1] (mm)	Y[1] (mm)	Backfill or Native	Time Tested (hrs)
1	470	590	Backfill	1843
2	350	590	Native	1915
3	510	590	Backfill	1948
4	590	590	Native	2000
5	640	590	Native	2039
6	430	590	Backfill	2057
7	300	590	Native	2114
8	220	590	Native	2130

Notes: 1 - Coordinate convention shown on Figure D.1.

Table D.2 - Interpreted Cone Penetration Resistances for Test 03

Cone Test No.	Interpreted Penetration Resistance (kPa)			
	@ Initial Springline of Pipeline #1	@ Initial Springline of Pipeline #2	@ Initial Springline of Pipeline #3	@ Initial Springline of Pipeline #4
1	27	27	27	27
2	218	218	218	218
3	26	26	26	26
4	256	256	256	256
5	264	264	264	264
6	18	18	18	18
7	255	255	255	255
8	250	250	250	250

Table D.3 - Pipeline Test Details for Test 03

Pipeline No.	Trench Width (mm)	Cover Depth (mm)	X:Y Coordinates of Pipe Centre (mm)	Pipeline Velocity (mm/sec)	Time Tested (hrs)
1	60	16	290 : 500	0.43	1929
2	50	16	650 : 505	0.55	2019
3	40	16	650 : 670	0.69	2049
4	30	16	290 : 665	0.53	2122

Table D.4 - Prototype Test Geometries for Test 03

Pipeline	Distance to Trench Wall in the Direction of Travel (m)	Distance to Trench Wall Towards the Rear of the Pipeline (m)	Distance to a Stiff Retaining Wall in the Direction of Travel (m)	Distance to the Pipeline in the Direction Opposite to Travel (m)	Distance Laterally to a Stiff Retaining Wall (m)	Distance Laterally to the Edge of the Adjacent Pipeline (m)	Distance From Base of Pipeline to Rigid Base, i.e. Bedrock (m)	Water Level Above Rigid Base, i.e. Bedrock (m)	Water Level Below Base of Pipeline (m)
1	1.025	1.025	13.925	7.3	7.75	5.0	5.025	2.715	2.31
2	0.775	0.775	14.175	7.3	7.75	5.0	5.025	2.715	2.31
3	0.525	0.525	14.425	7.3	7.75	5.0	5.025	2.715	2.31
4	0.275	0.275	14.675	7.3	7.75	5.0	5.025	2.715	2.31

Table D.5 - Calculation of Undrained Shear Strength for Test 03

Pipeline	Soil Type	Cone Tests Used to Derive q_c	Interpreted Cone Tip Resistance at Springline, q_c (kPa)	Saturated Bulk Density, γ_{sat} (kN/m^3)	Pore Pressure at Springline, u (kPa)	Depth to Springline, h (m)	Cone Factor, N_c or N_k*	Undrained Shear Strength, c_u (kPa)
1	Native	2,4,5,7,8	285.9	947.2	-22.0	0.0255	8.1/11.3	23.2 - 32.4
1	Backfill	1,3,6	23.7	862.5	---	0.0255	15	1.6
2	Native	2,4,5,7,8	285.9	947.2	-22.0	0.0255	8.1/11.3	23.2 - 32.4
2	Backfill	1,3,6	23.7	862.5	---	0.0255	15	1.6
3	Native	2,4,5,7,8	285.9	947.2	-22.0	0.0255	8.1/11.3	23.2 - 32.4
3	Backfill	1,3,6	23.7	862.5	---	0.0255	15	1.6
4	Native	2,4,5,7,8	285.9	947.2	-22.0	0.0255	8.1/11.3	23.2 - 32.4
4	Backfill	1,3,6	23.7	862.5	---	0.0255	15	1.6

Notes: * - N_c range of values correspond to native material; N_k values correspond to backfill.

Table D.6 - Summary of Prototype Pipeline Data; Test 03

Pipeline →	Pipeline #1	Pipeline #2	Pipeline #3	Pipeline #4
Trench Width	3.0m	2.5m	2.0m	1.5m
Cover Depth	0.80m	0.80m	0.80m	0.80m
Embedment Ratio, H/D	1.842	1.842	1.842	1.842
Average Backfill Undrained Shear Strength @ Springline	1.6kPa	1.6kPa	1.6kPa	1.6kPa
Average Native Undrained Shear Strength @ Springline	27.8kPa	27.8kPa	27.8kPa	27.8kpa
Ultimate Normalized Resistance, N	4.891	5.975	5.275	4.914
Distance into Trench Wall to Ultimate Normalized Resistance	1.398D	1.777D	2.323D	1.664D
Slope to Ultimate Normalized Resistance	1.975	2.304	1.834	2.515
Normalized Resistance at Trench Wall	2.029	1.832*	1.150	1.319
Normalized Resistance at 0.5D Penetration	3.888	4.881*	3.877	3.888
Normalized Resistance at 1D Penetration	4.745	5.496	4.474	4.474
Slope of Interaction Between TW and Breakover	4.791	6.129*	6.892	8.410
Normalized Resistance at Breakover	3.066	5.152*	3.900	3.719
Distance into Trench Wall to Breakover	0.132D	0.548D*	0.417D	0.295D
Slope of Interaction After Breakover	2.213	0.794*	0.892	1.069

Notes: * - Estimated value, force-displacement record is discontinuous.

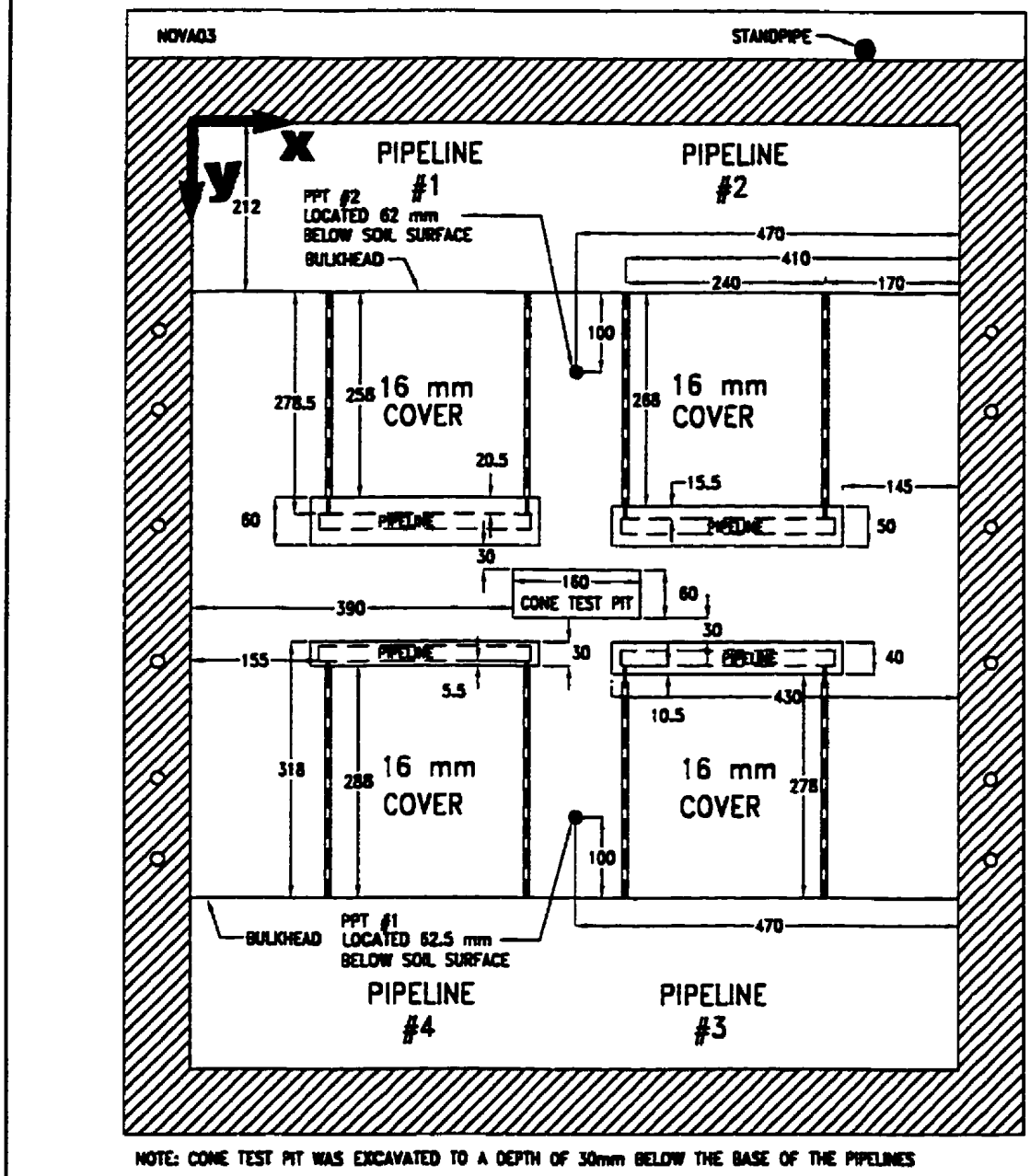

Figure D.1 - *Model Test Geometry, Test 03.*

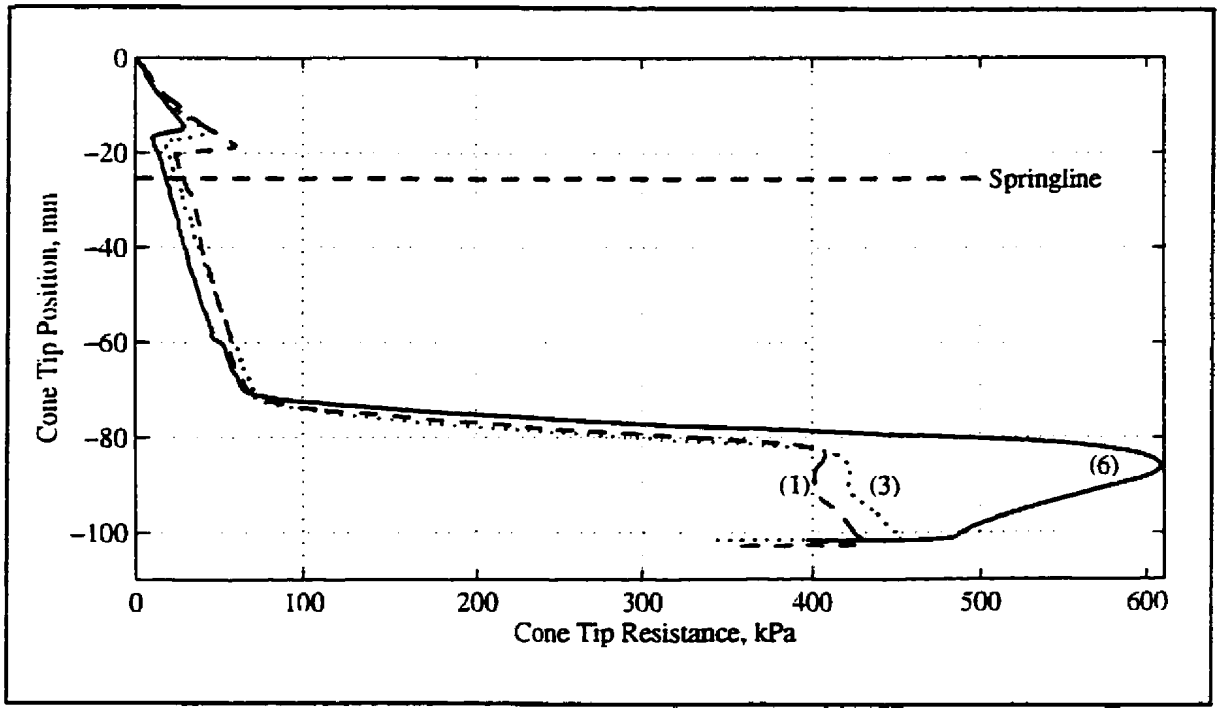

Figure D.2 - *All cone penetration tests, backfill material, Test 03.*

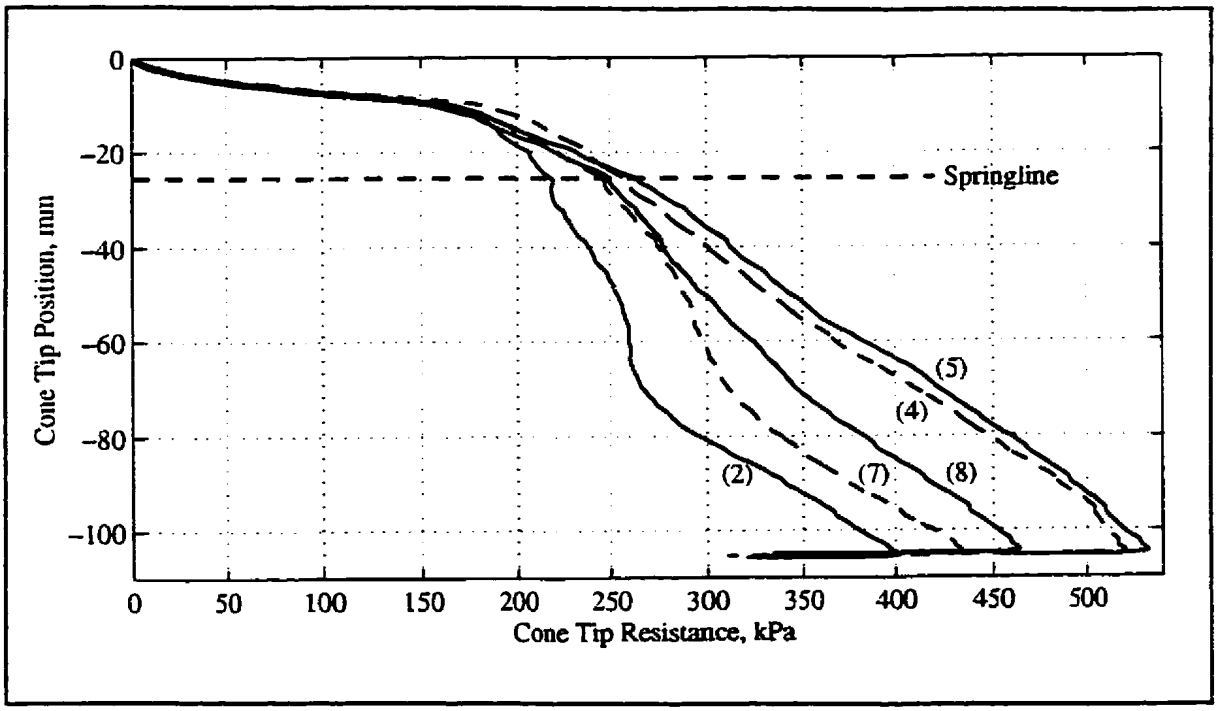

Figure D.3 - *All cone penetration tests, native material, Test 03.*

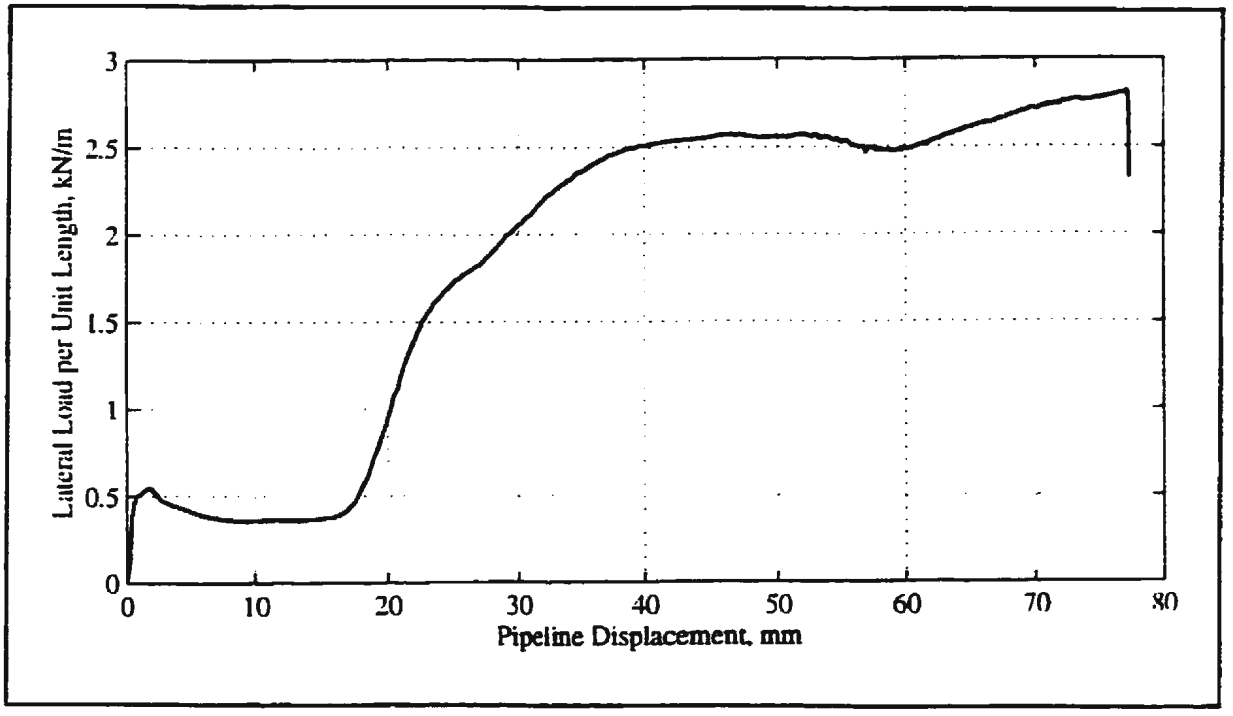

Figure D.4 - *Force-displacement response, model pipeline #1, 60mm wide trench, Test 03.*

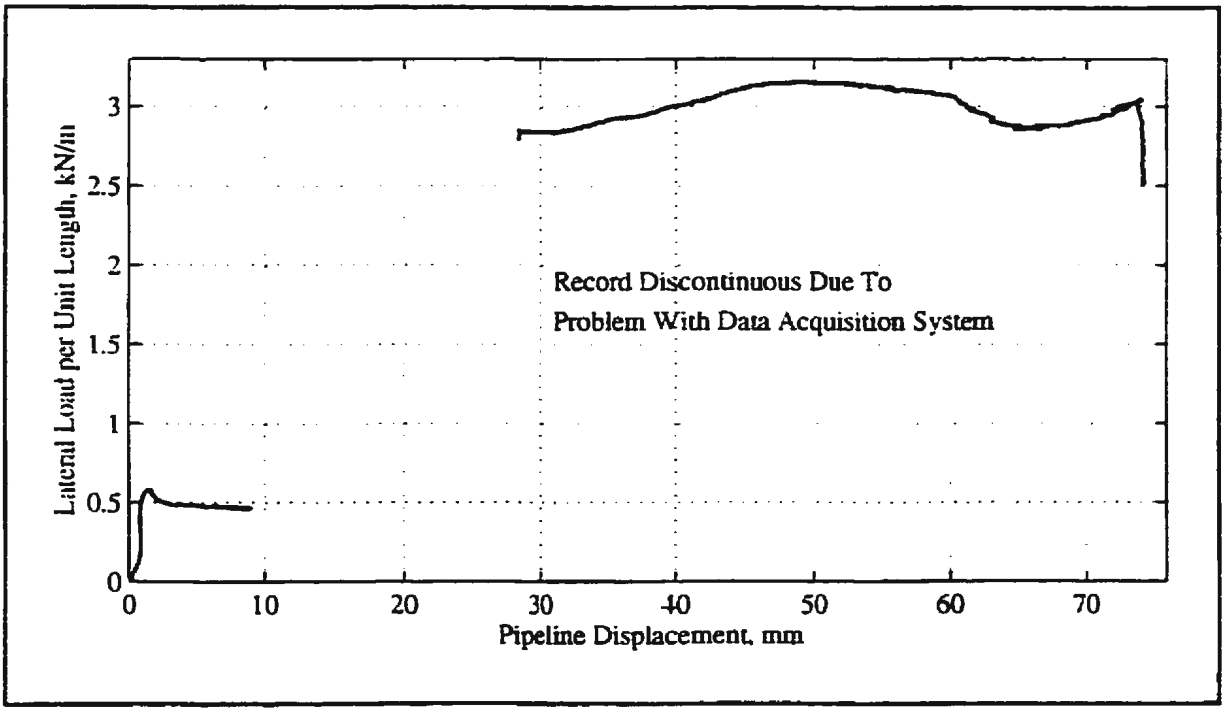

Figure D.5 - *Force-displacement response, model pipeline #2, 50mm wide trench, Test 03.*

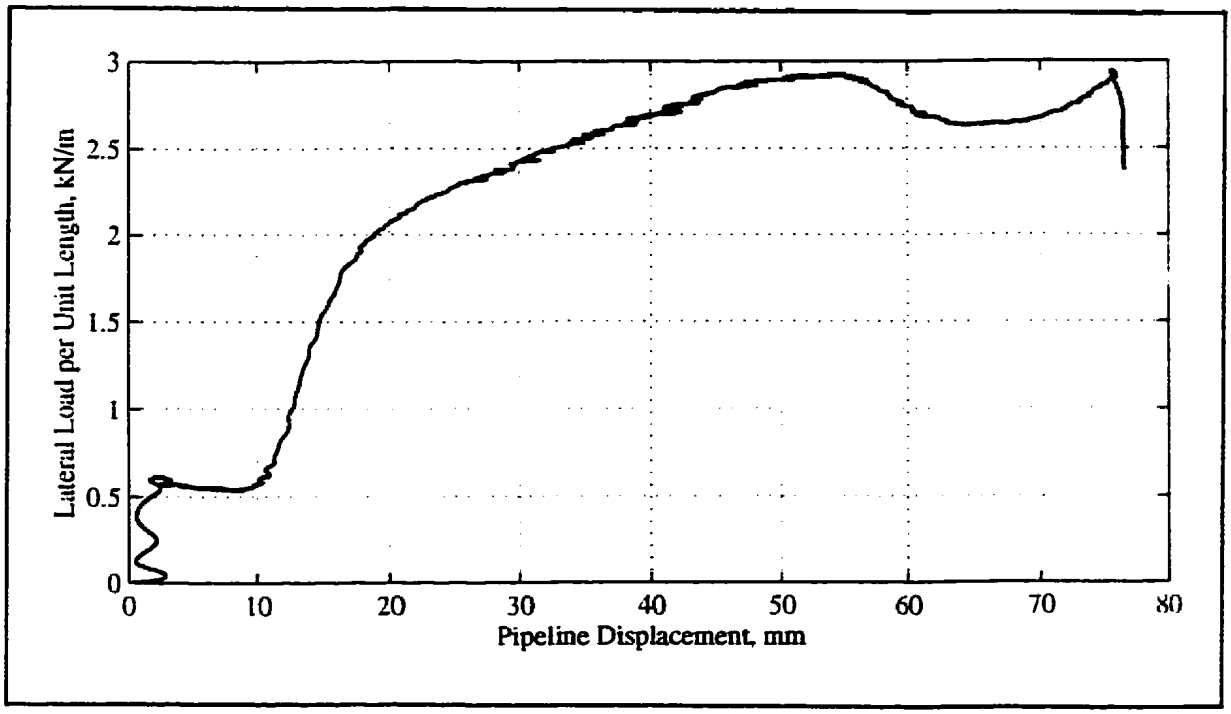

Figure D.6 - *Force-displacement response, model pipeline #3, 40mm wide trench, Test 03.*

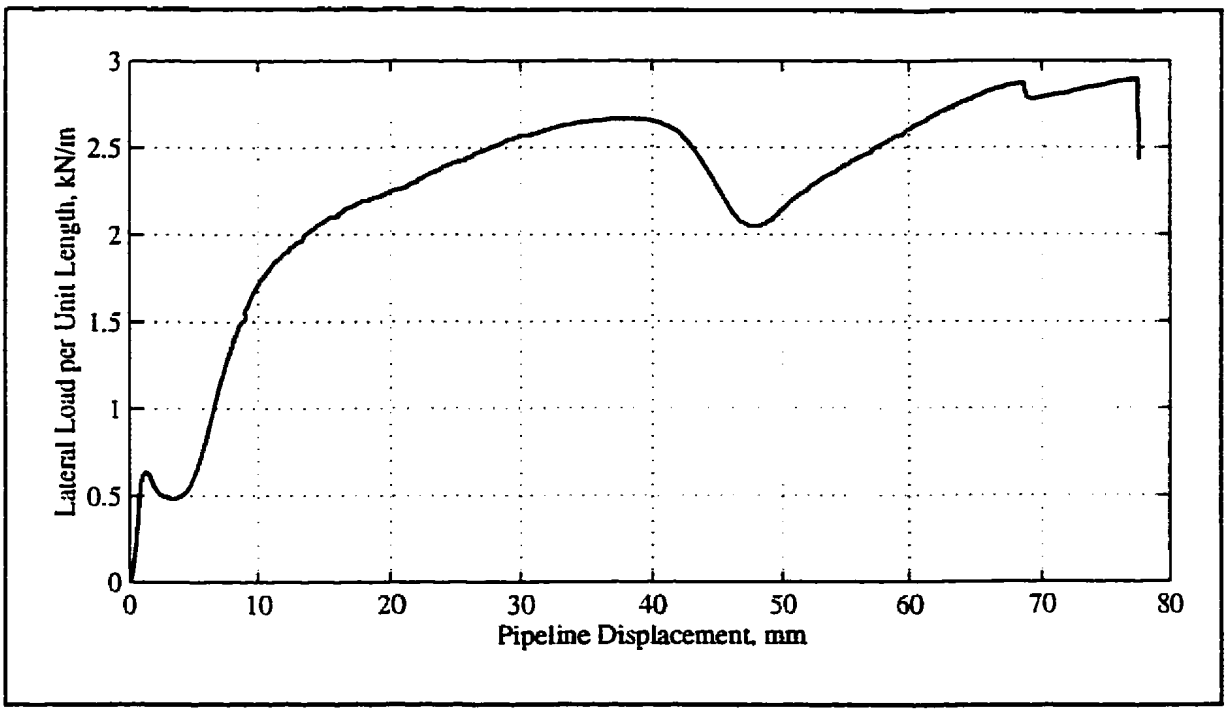

Figure D.7 - *Force-displacement response, model pipeline #4, 30mm wide trench, Test 03.*

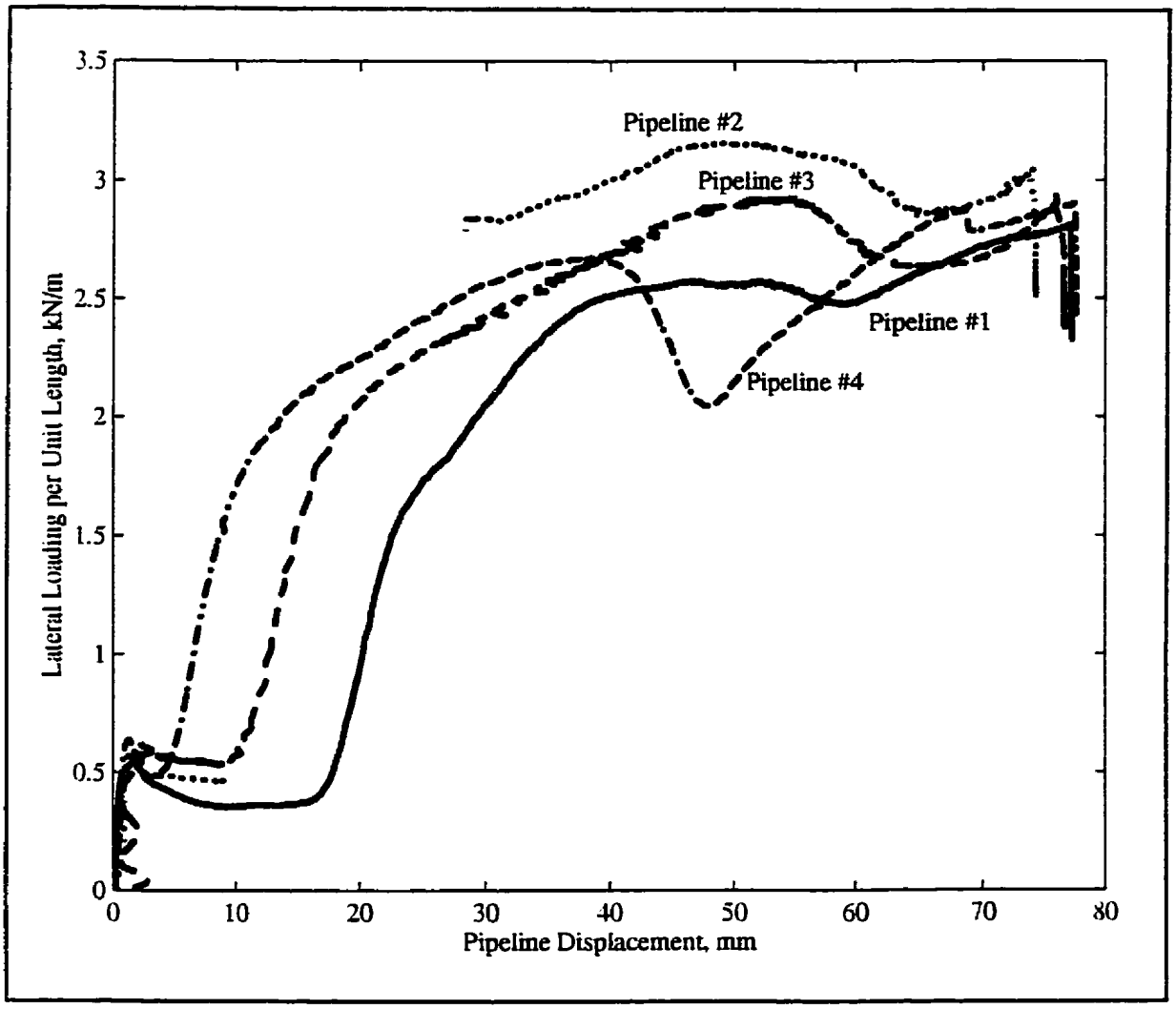

Figure D.8 - Force-displacement response, all model pipelines, Test 03.

Figure D.9 - *Photo of excavated cross-section along mid length of model pipeline #1, 60mm wide trench, Test 03.*

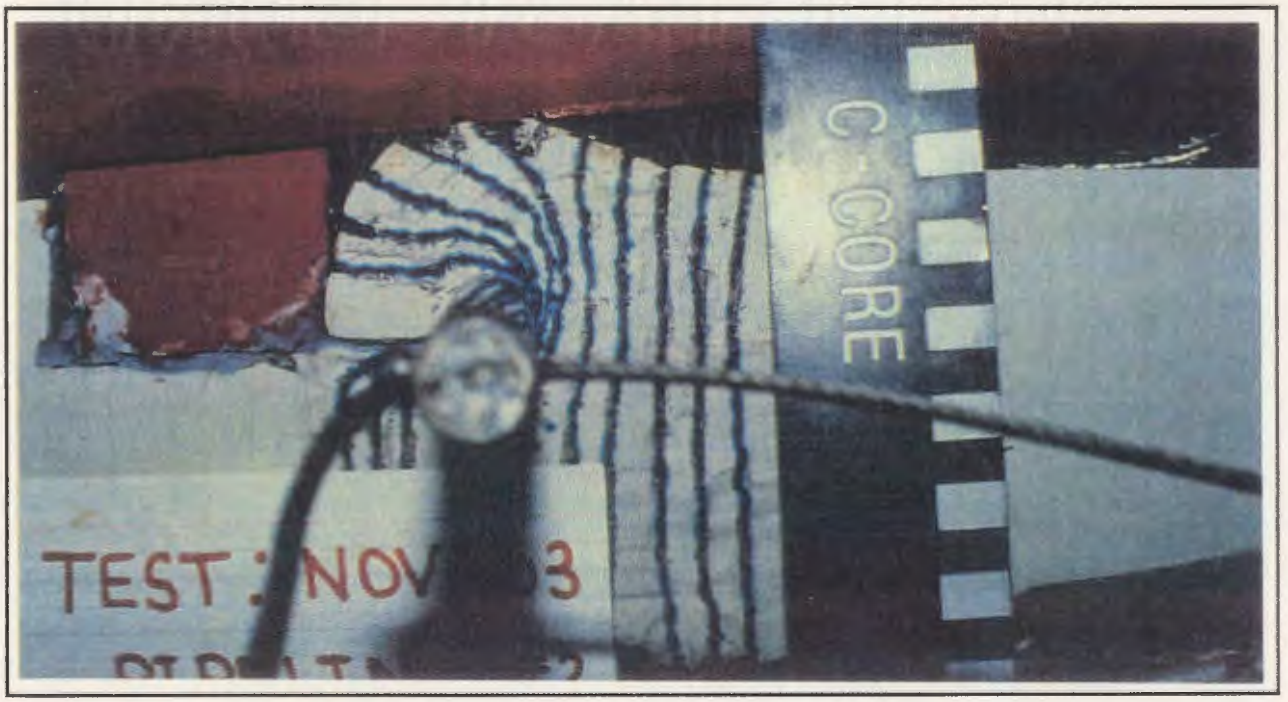

Figure D.10 - *Photo of excavated cross-section along mid length of model pipeline #2, 50mm wide trench, Test 03.*

Figure D.11 - *Photo of excavated cross-section along mid length of model pipeline #3, 40mm wide trench, Test 03.*

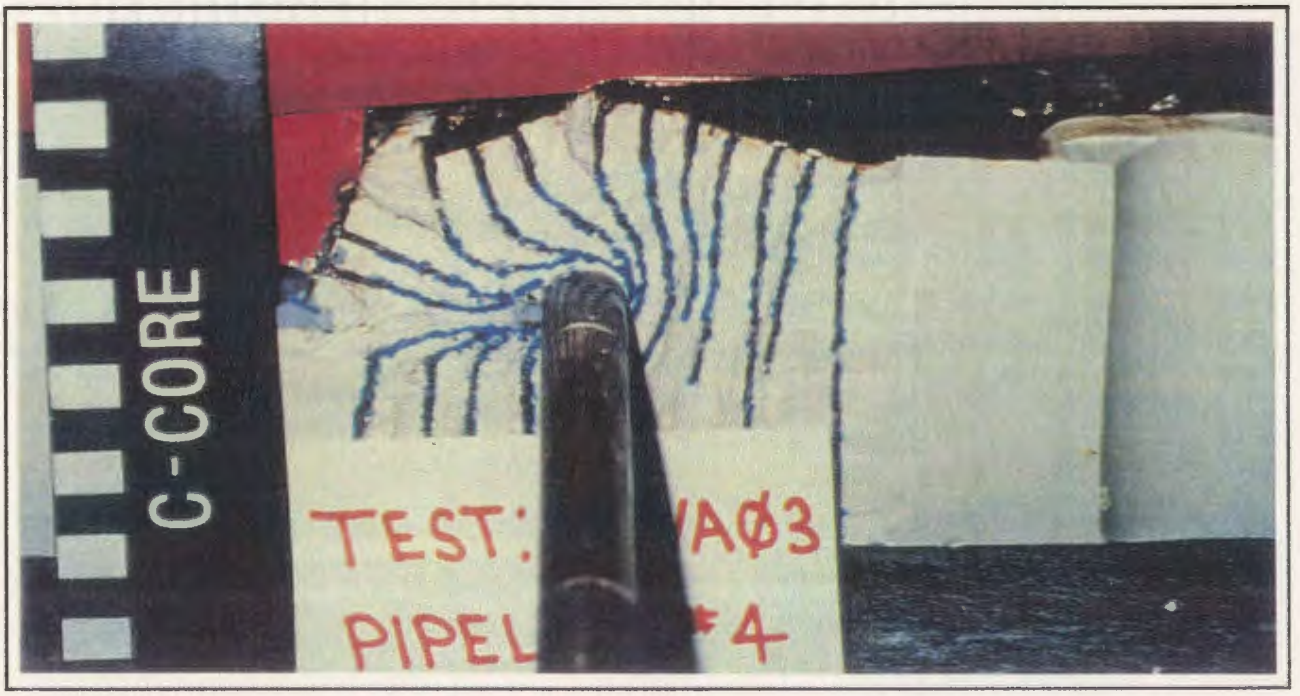

Figure D.12 - *Photo of excavated cross-section along mid length of model pipeline #4, 30mm wide trench, Test 03.*

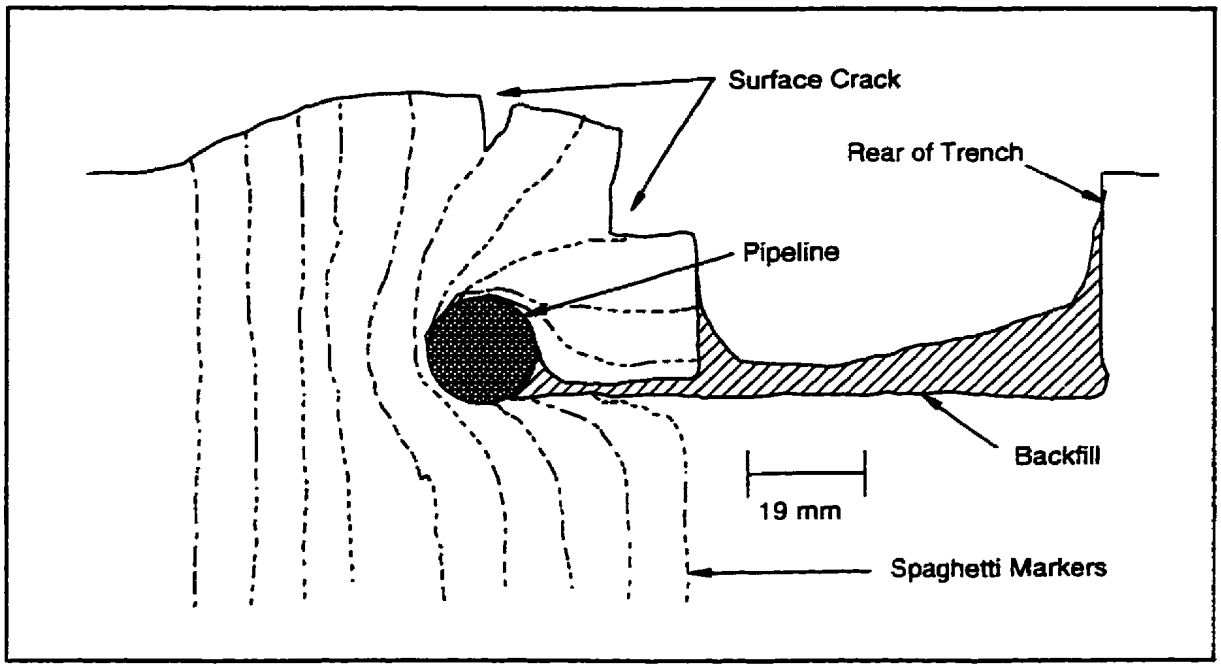

Figure D.13 - *Sketch of excavated cross-section along mid length of model pipeline #1, 60mm wide trench, Test 03.*

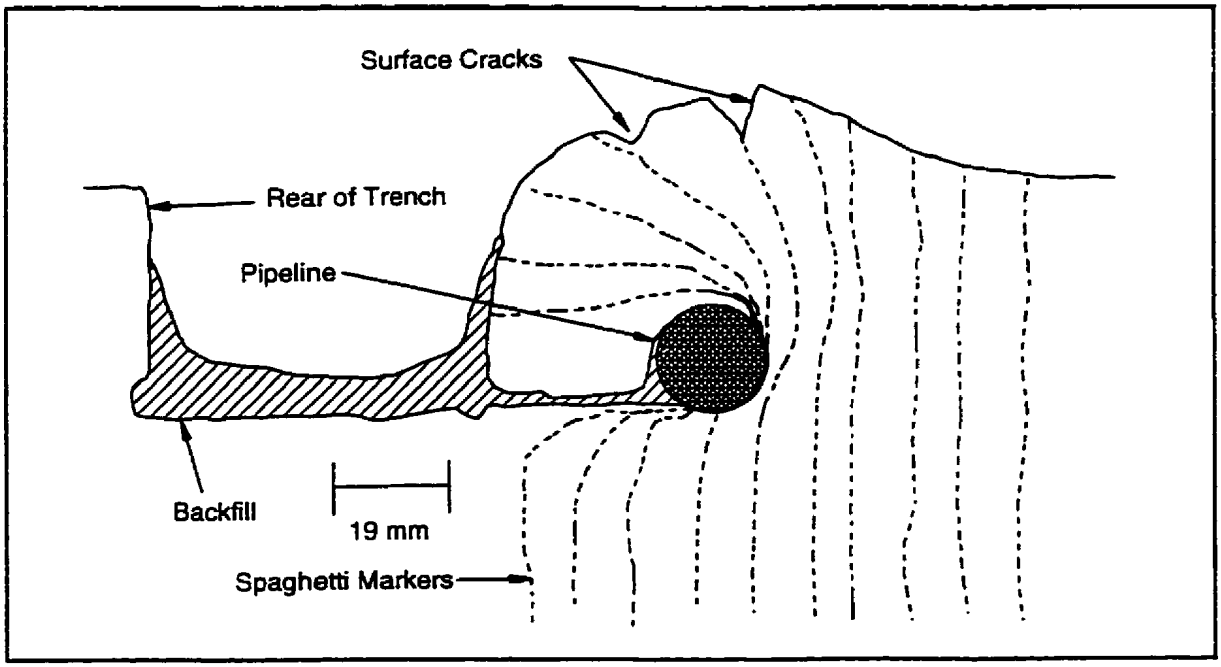

Figure D.14 - *Sketch of excavated cross-section along mid length of model pipeline #2, 50mm wide trench, Test 03.*

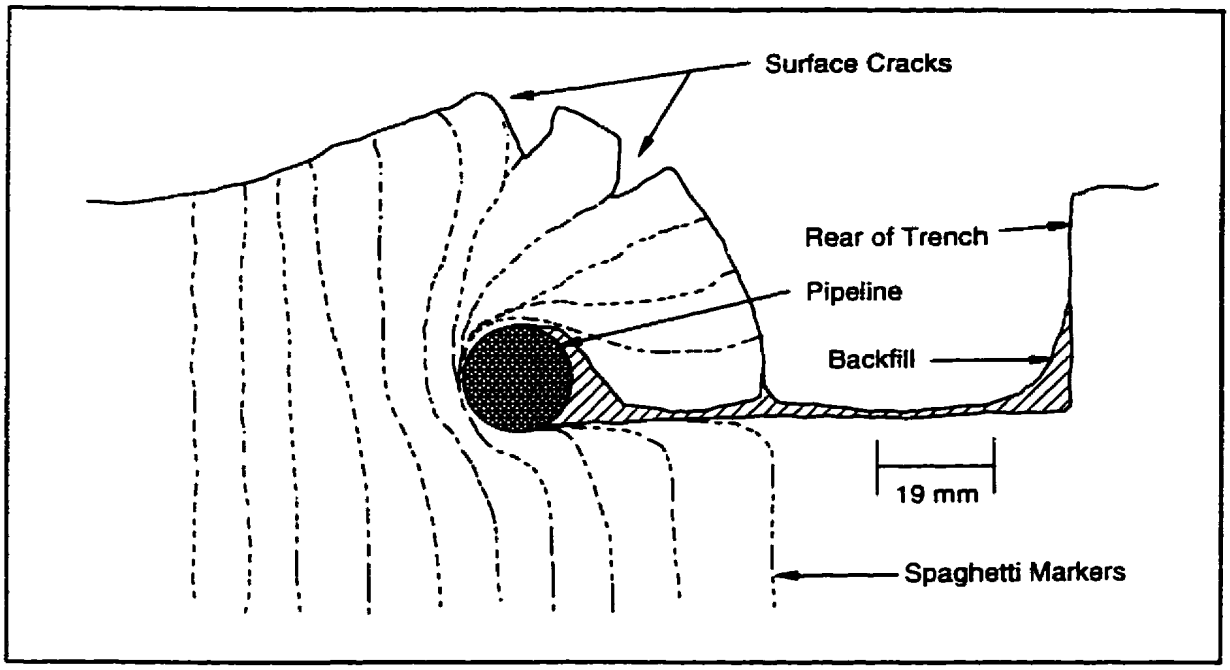

Figure D.15 - *Sketch of excavated cross-section along mid length of model pipeline #3, 40mm wide trench, Test 03.*

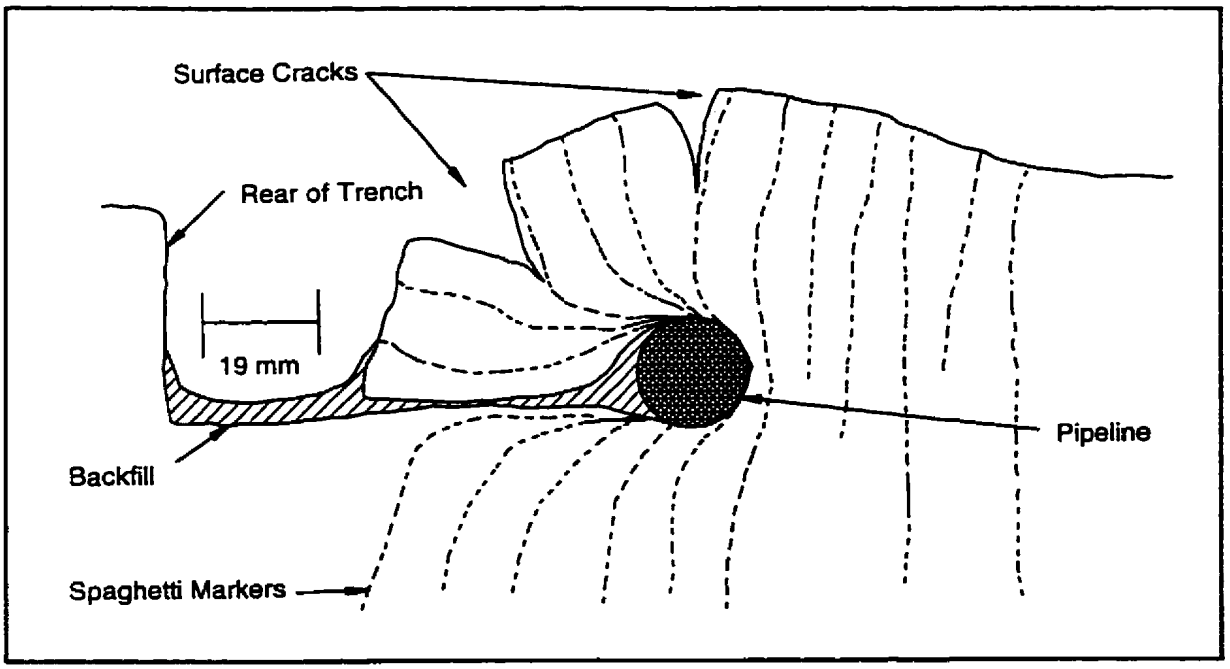

Figure D.16 - *Sketch of excavated cross-section along mid length of model pipeline #4, 30mm wide trench, Test 03.*

Appendix E

Test 04 - Selected Test Data

Table E.1 - Cone Penetration Test Details for Test 04

CPT No.	X[1] (mm)	Y[1] (mm)	Backfill or Native	Time Tested (hrs)
1	470	590	Backfill	1544
2	331	590	Native	1557
3	271	590	Native	0835
4	510	590	Backfill	0845
5	590	590	Native	0855
6	430	590	Backfill	1424
7	230	590	Native	1432
8	189	590	Native	1644
9	305	590	Native	1409
10	450	590	Backfill	1426
11	490	590	Backfill	2013
12	631	590	Native	2025

Notes: 1 - Coordinate convention shown on Figure E.1.

Table E.2 - Interpreted Cone Penetration Resistances for Test 04

Cone Test No.	Interpreted Penetration Resistance (kPa)			
	@ Initial Springline of Pipeline #1	@ Initial Springline of Pipeline #2	@ Initial Springline of Pipeline #3	@ Initial Springline of Pipeline #4
1	20	20	20	20
2	224	224	224	224
3	326	326	326	326
4	22	22	22	22
5	269	269	269	269
6	24	24	24	24
7	301	301	301	301
8	283	283	283	283
9	248	248	248	248
10	29	29	29	29
11	34	34	34	34
12	288	288	288	288

Table E.3 - Pipeline Test Details for Test 04

Pipeline No.	Trench Width (mm)	Cover Depth (mm)	X:Y Coordinates of Pipe Centre (mm)	Pipeline Velocity (mm/sec)	Time Tested (hrs)
1	50	16	290 : 505	0.0008	1613 - Day 1
2	50	16	650 : 505	0.0045	1434 - Day 3
3	50	16	650 : 675	0.0436	1608 - Day 2
4	50	16	290 : 675	0.9288	1450 - Day 2

Table E.4 - Prototype Test Geometries for Test 04

Pipeline	Distance to Trench Wall in the Direction of Travel (m)	Distance to Trench Wall Towards the Rear of the Pipeline (m)	Distance to a Stiff Retaining Wall in the Direction of Travel (m)	Distance to the Pipeline in the Direction Opposite to Travel (m)	Distance Laterally to a Stiff Retaining Wall (m)	Distance Laterally to the Edge of the Adjacent Pipeline (m)	Distance From Base of Pipeline to Rigid Base, i.e. Bedrock (m)	Water Level Above Rigid Base, i.e. Bedrock (m)	Water Level Below Base of Pipeline (m)
1	0.775	0.775	14.175	7.55	7.75	5.0	5.025	3.425	1.6
2	0.775	0.775	14.175	7.55	7.75	5.0	5.025	3.425	1.6
3	0.775	0.775	14.175	7.55	7.75	5.0	5.025	3.425	1.6
4	0.775	0.775	14.175	7.55	7.75	5.0	5.025	3.425	1.6

Table E.5 - Calculation of Undrained Shear Strength for Test 04

Pipeline	Soil Type	Cone Tests Used to Derive q_c	Interpreted Cone Tip Resistance at Springline, q_c (kPa)	Saturated Bulk Density, γ_{sat} (kN/m^3)	Pore Pressure at Springline, u (kPa)	Depth to Springline, h (m)	Cone Factor, N_c or N_k*	Undrained Shear Strength, c_u (kPa)
1	Native	2,3,5,7,8	322.7	956.0	-18.6	0.0255	8.0/11.4	26.2 - 37.3
1	Backfill	1,22,24	22	863.4	---	0.0255	15	1.5
2	Native	9,12	308.2	956.0	-13.6	0.0255	7.9/11.7	24.3 - 35.9
2	Backfill	10,11	31.5	863.4	---	0.0255	15	2.1
3	Native	7,8	335.8	956.0	-18.6	0.0255	8.0/11.4	27.3 - 38.9
3	Backfill	6	24	863.4	---	0.0255	15	1.6
4	Native	7,8	335.8	956.0	-18.6	0.0255	8.0/11.4	27.3 - 38.9
4	Backfill	6	24	863.4	---	0.0255	15	1.6

Notes: * - N_c range of values correspond to native material; N_k values correspond to backfill.

Table E.6 - Summary of Prototype Pipeline Data; Test 04

Pipeline →	Pipeline #1	Pipeline #2	Pipeline #3	Pipeline #4
Trench Width	2.5m	2.5m	2.5m	2.5m
Cover Depth	0.80m	0.80m	0.80m	0.80m
Embedment Ratio, H/D	1.842	1.842	1.842	1.842
Average Backfill Undrained Shear Strength @ Springline	1.5kPa	2.1kPa	1.6kPa	1.6kPa
Average Native Undrained Shear Strength @ Springline	31.8kPa	30.1kPa	33.1kPa	33.1kpa
Ultimate Normalized Resistance, N	11.262* 7.540**	8.152* 4.762**	4.565	4.435
Distance into Trench Wall to Ultimate Normalized Resistance	2.719D* 1.432D**	3.603D* 1.569D**	1.427D	2.101D
Slope to Ultimate Normalized Resistance	3.186	1.845	2.035	1.520
Normalized Resistance at Trench Wall	3.566	1.992	1.262	1.125
Normalized Resistance at 0.5D Penetration	5.607	3.615	3.640	3.652
Normalized Resistance at 1D Penetration	6.762	4.186	4.339	4.085
Slope of Interaction Between TW and Breakover	6.861	5.376	6.773	8.841
Normalized Resistance at Breakover	5.041	3.320	3.302	3.559
Distance into Trench Wall to Breakover	0.248D	0.270D	0.306D	0.292D
Slope of Interaction After Breakover	2.299	1.376	1.562	0.638

Notes: * - Values taken essentially at the end of pipeline pull; not necessarily a peak.
** - Corresponds to the point where the force-displacement curves became linear.

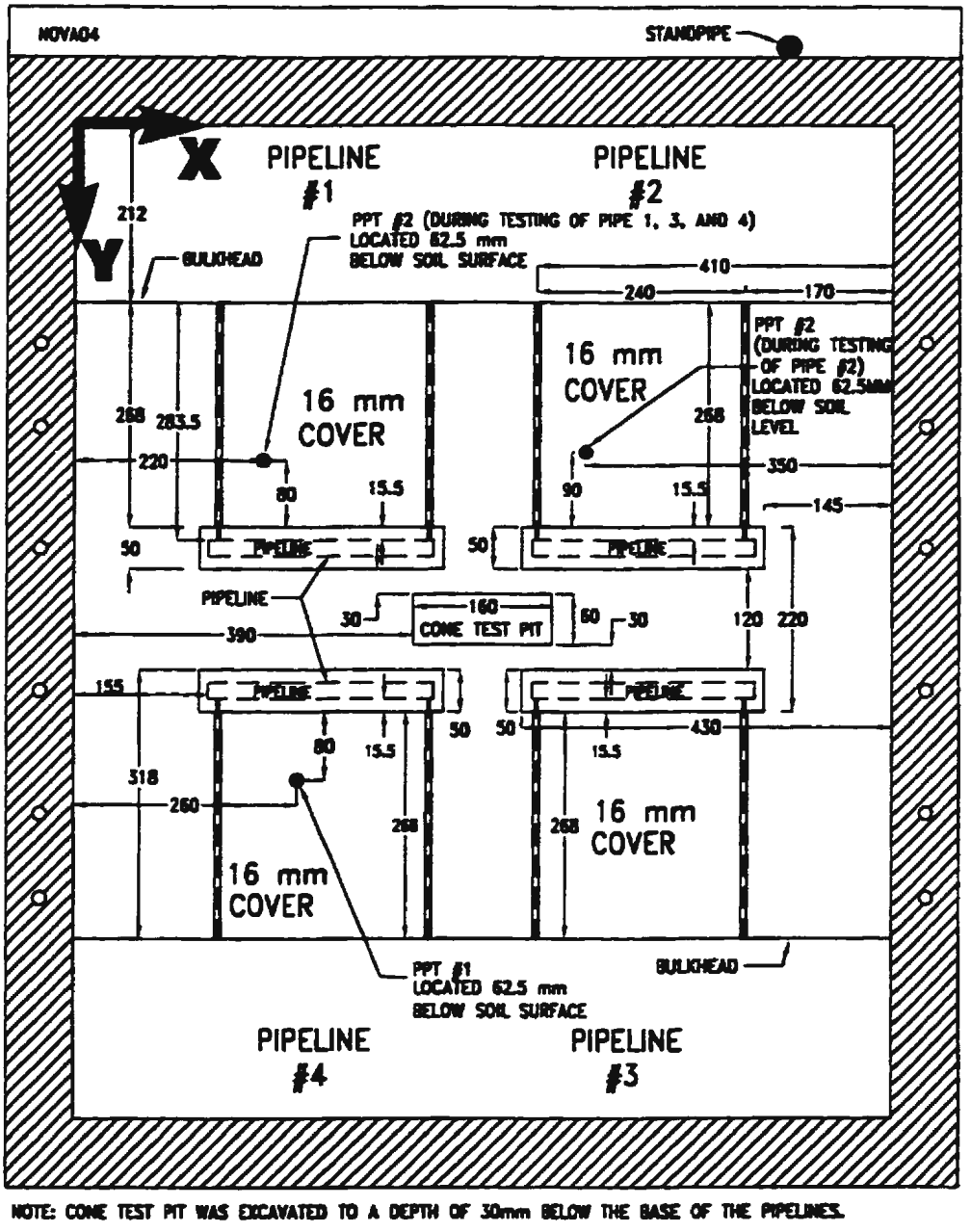

NOTE: CONE TEST PIT WAS EXCAVATED TO A DEPTH OF 30mm BELOW THE BASE OF THE PIPELINES.

Figure E.1 - *Model Test Geometry, Test 04.*

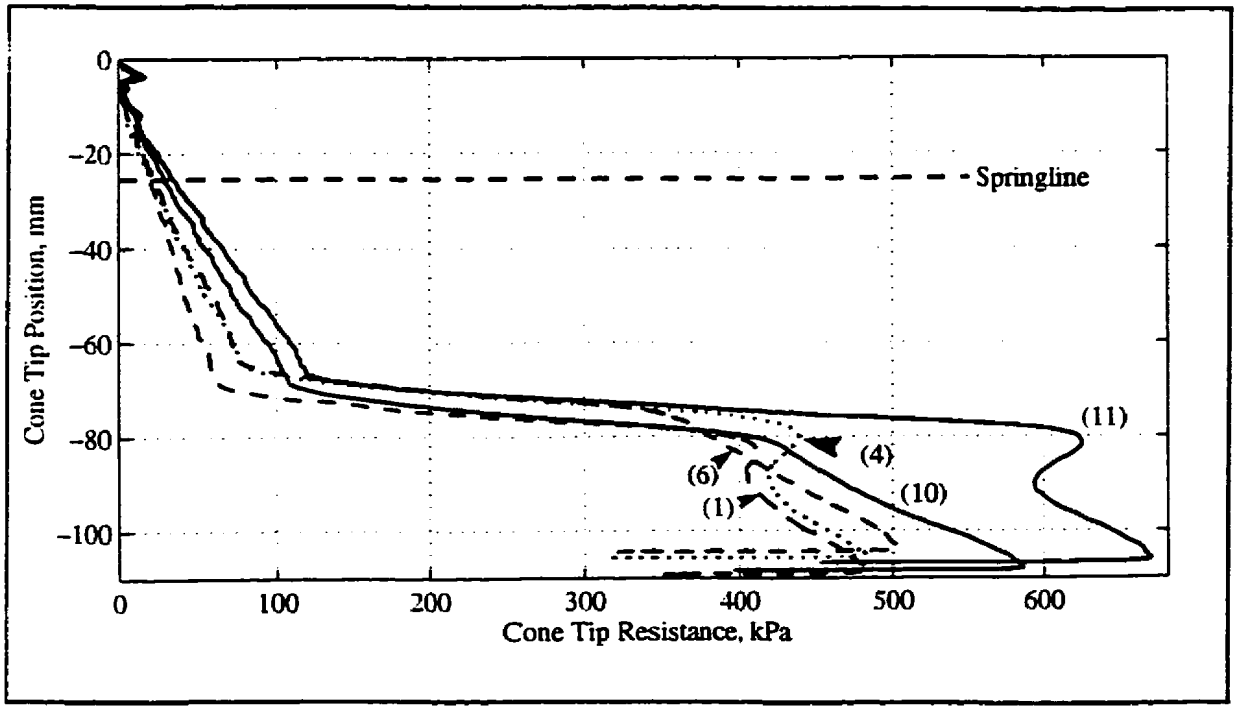

Figure E.2 - *All cone penetration tests, backfill material, Test 04.*

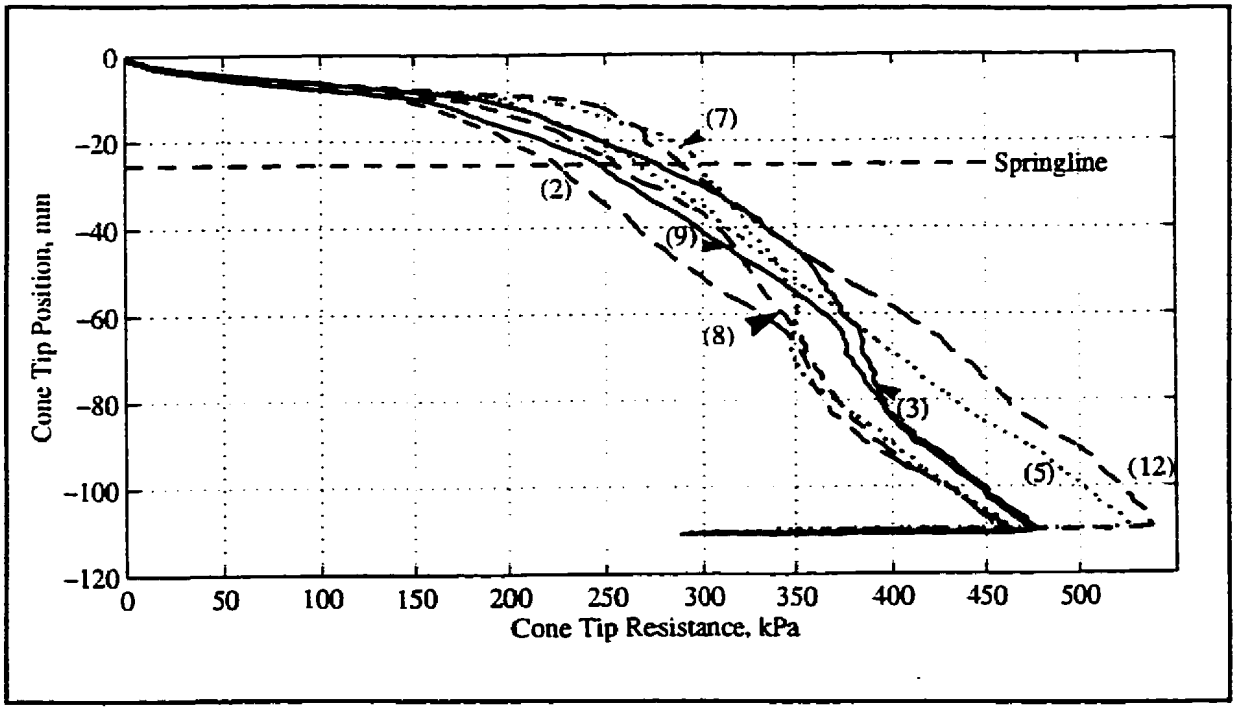

Figure E.3 - *All cone penetration tests, native material, Test 04.*

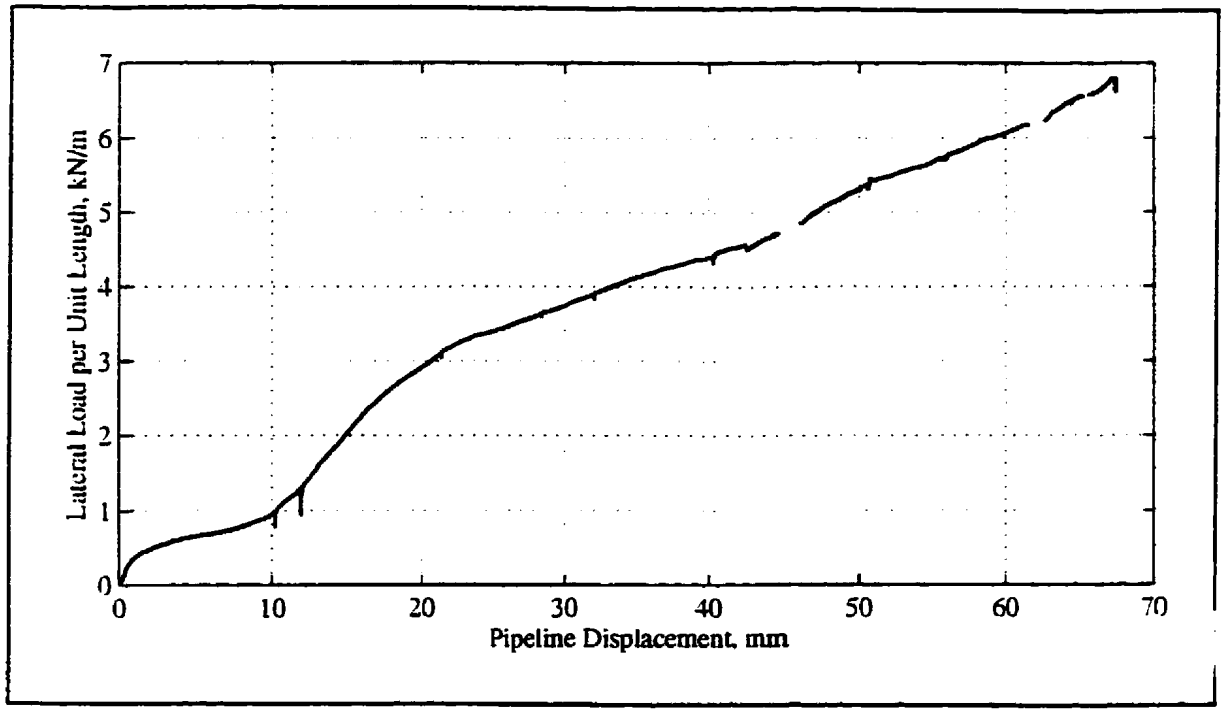

Figure E.4 - *Force-displacement response, model pipeline #1, 0.0008mm/sec, Test 04.*

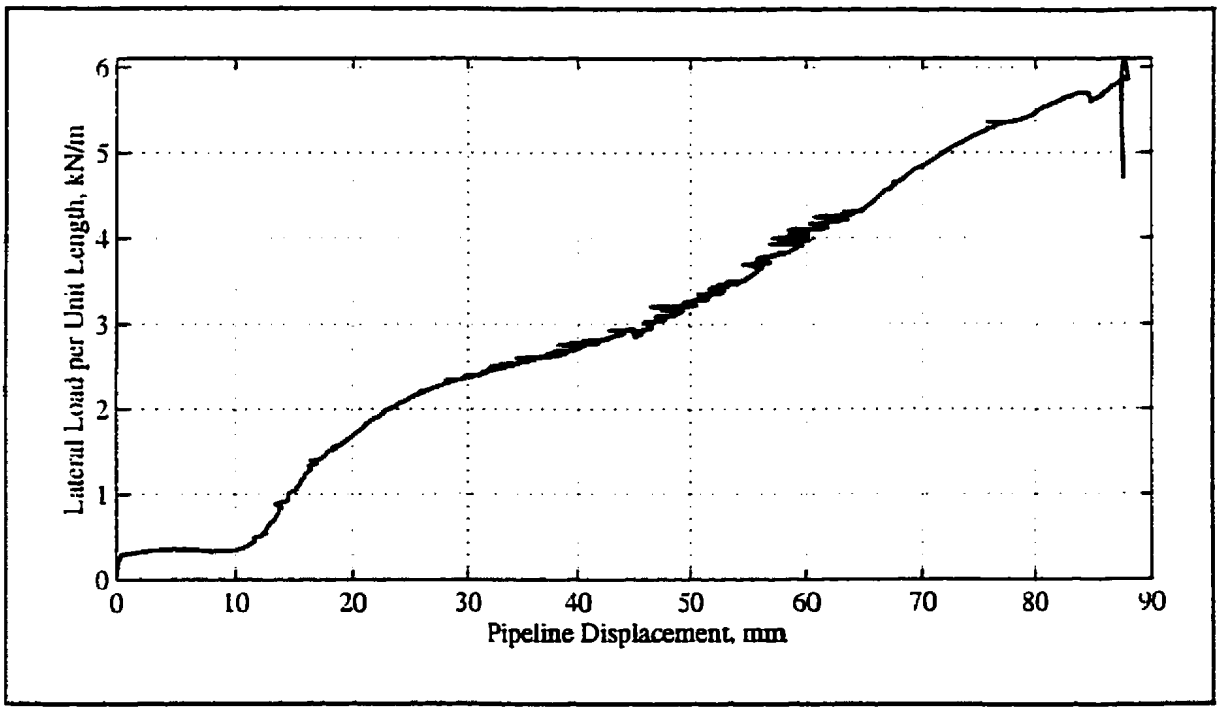

Figure E.5 - *Force-displacement response, model pipeline #2, 0.0045mm/sec, Test 04.*

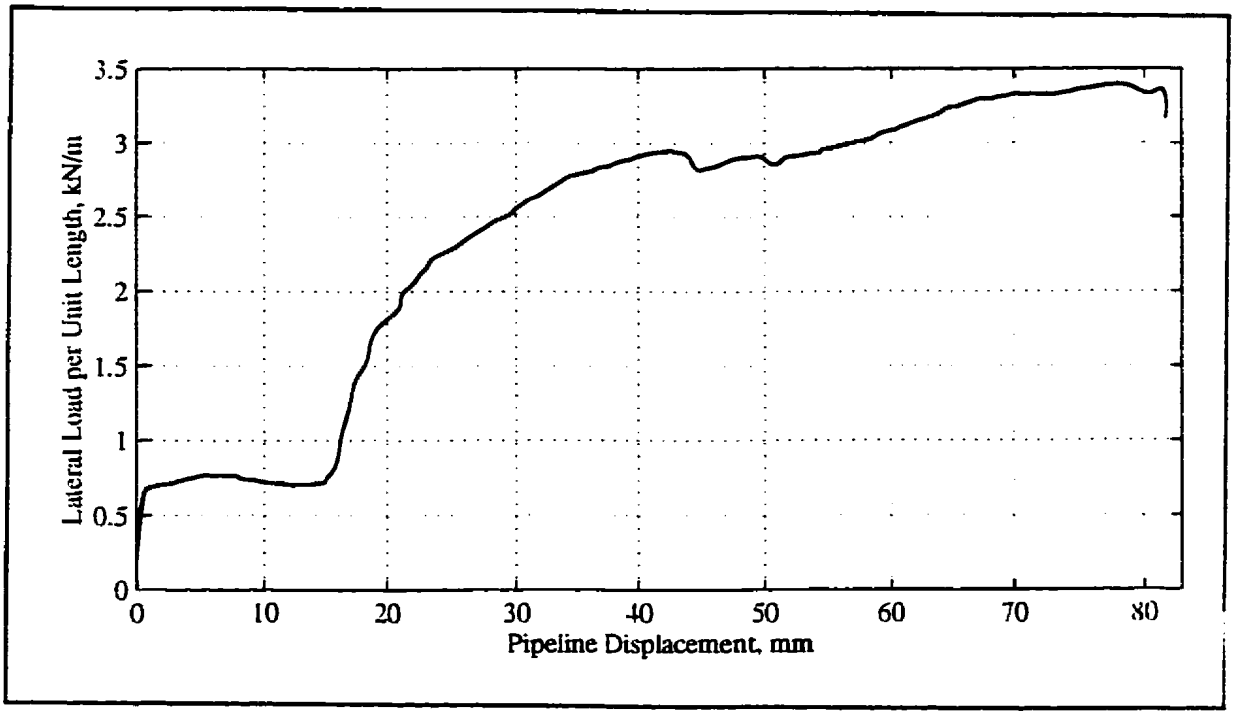

Figure E.6 - *Force-displacement response, model pipeline #3, 0.0436mm/sec, Test 04.*

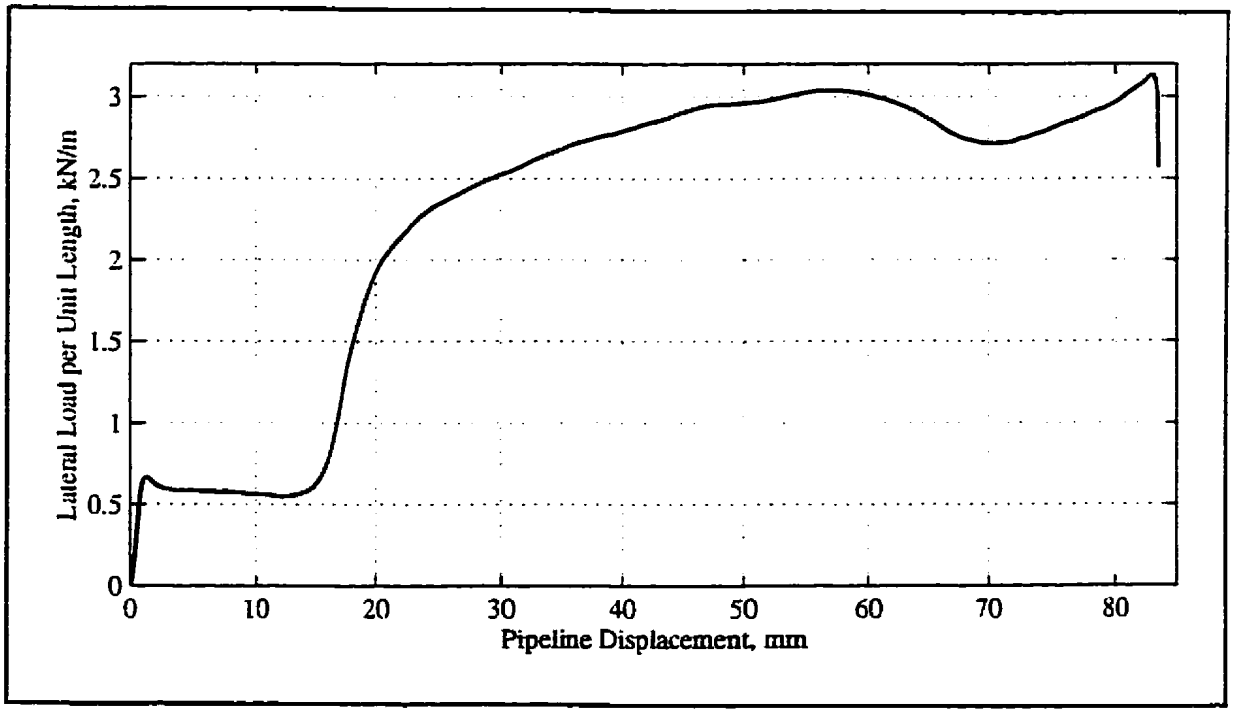

Figure E.7 - *Force-displacement response, model pipeline #4, 0.9288mm/sec, Test 04.*

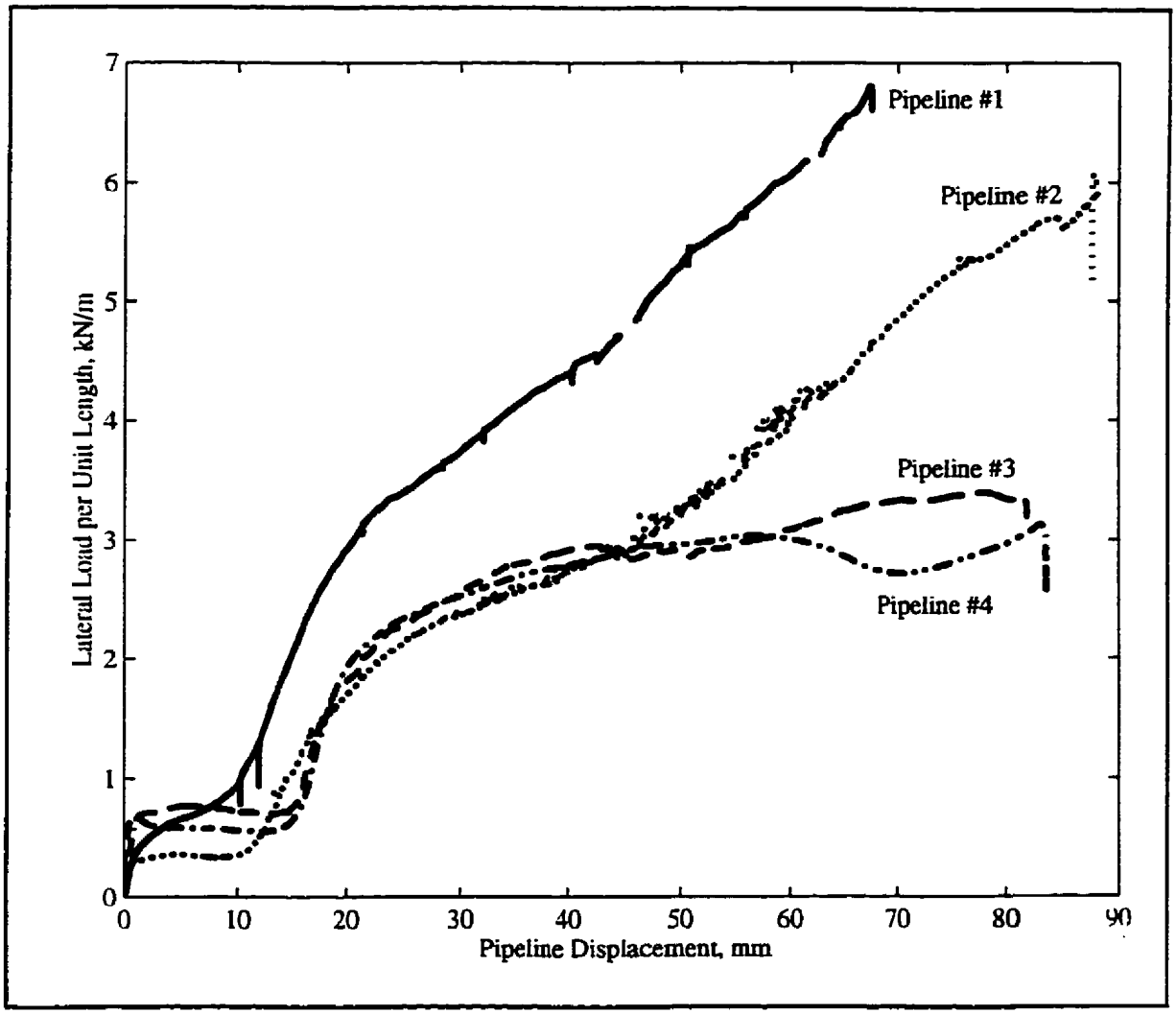

Figure E.8 - Force-displacement response, all model pipelines, Test 04.

Figure E.9 - *Photo of excavated cross-section along mid length of model pipeline #1, 0.0008mm/sec, Test 04.*

Figure E.10 - *Photo of excavated cross-section along mid length of model pipeline #2, 0.0045mm/sec, Test 04.*

Figure E.11 - *Photo of excavated cross-section along mid length of model pipeline #3, 0.0436mm/sec, Test 04.*

Figure E.12 - *Photo of excavated cross-section along mid length of model pipeline #4, 0.9288mm/sec, Test 04.*

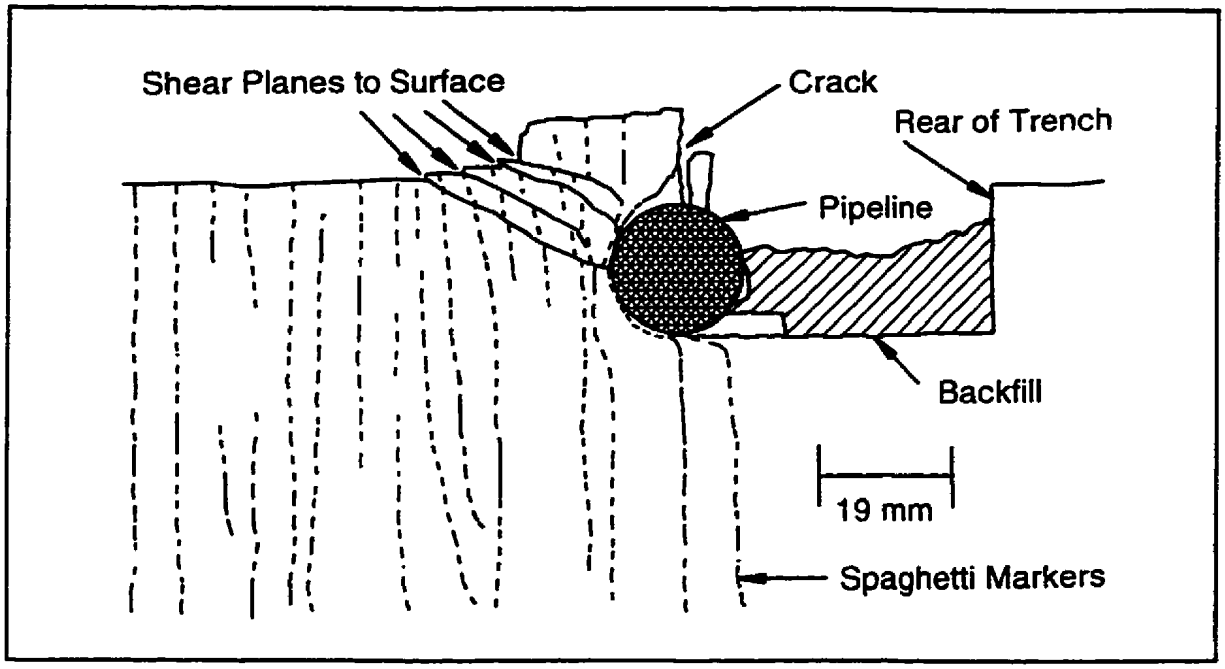

Figure E.13 - *Sketch of excavated cross-section along mid length of model pipeline #1, 0.0008mm/sec, Test 04.*

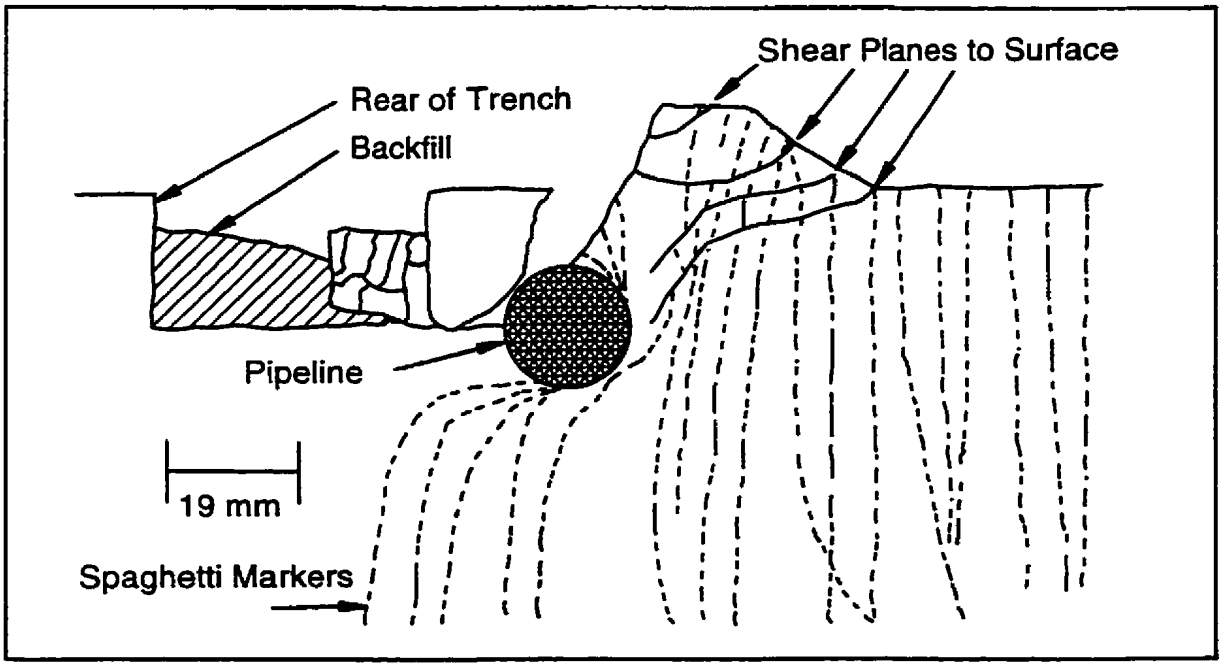

Figure E.14 - *Sketch of excavated cross-section along mid length of model pipeline #2, 0.0045mm/sec, Test 04.*

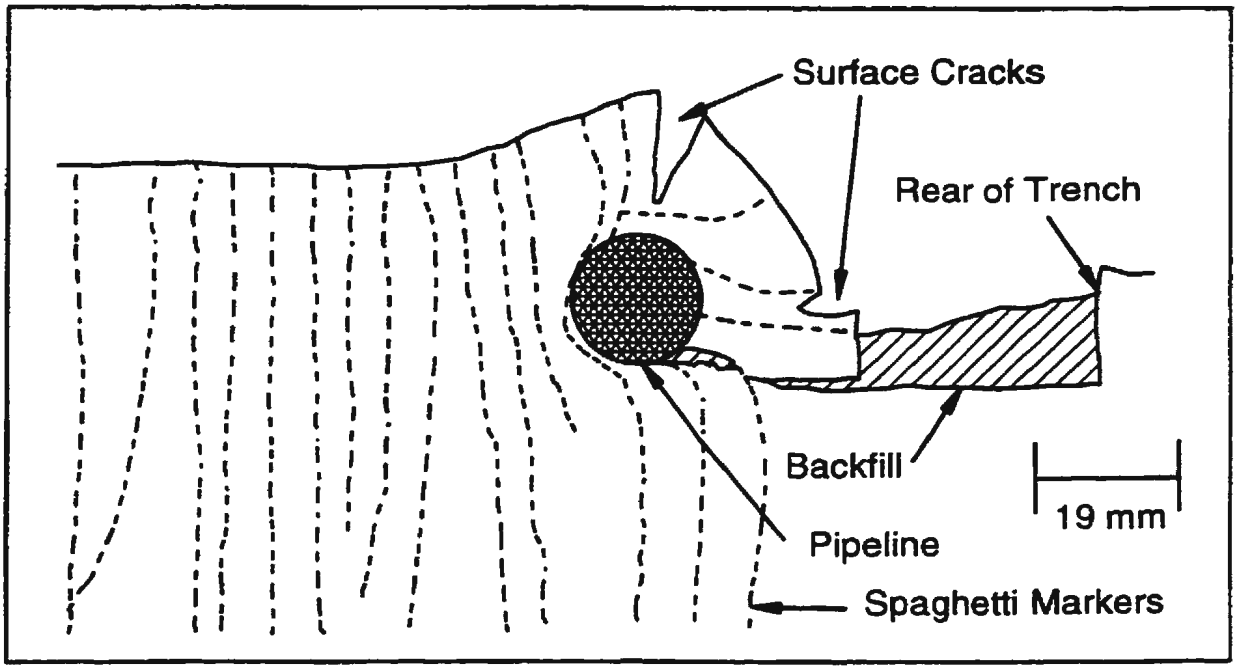

Figure E.15 - *Sketch of excavated cross-section along mid length of model pipeline #3, 0.0436mm/sec, Test 04.*

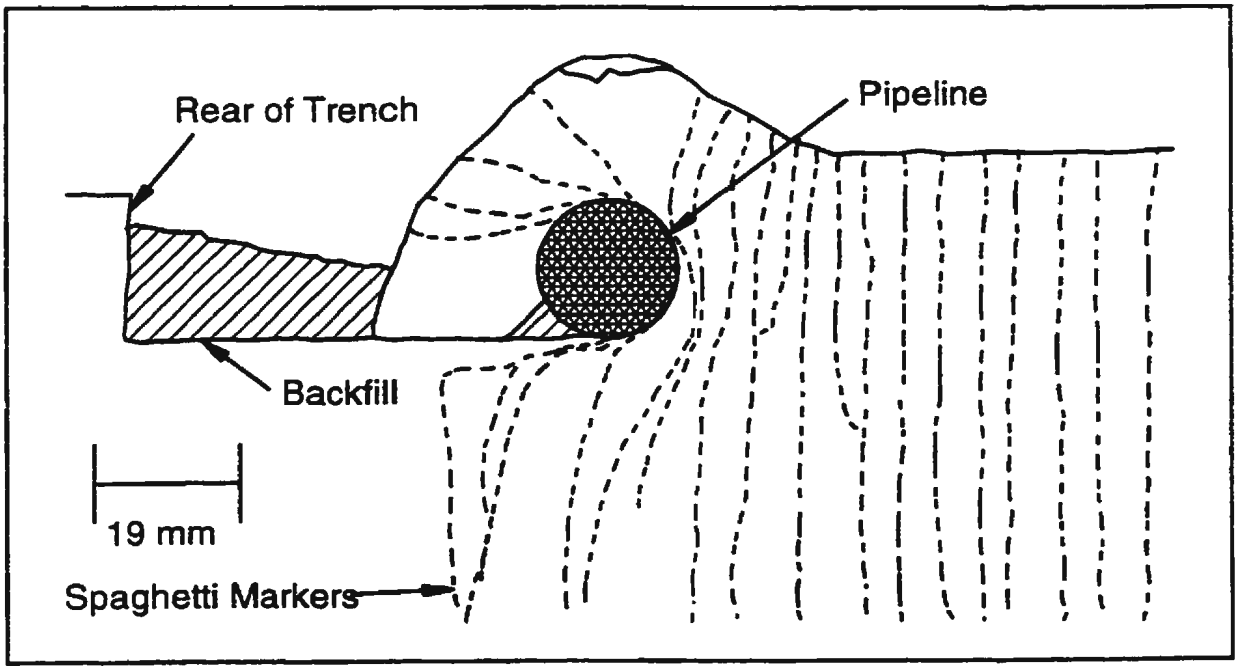

Figure E.16 - *Sketch of excavated cross-section along mid length of model pipeline #4, 0.9288mm/sec, Test 04.*

Appendix F

Test 05 - Selected Test Data

Table F.1 - Cone Penetration Test Details for Test 05

CPT No.	X[1] (mm)	Y[1] (mm)	Backfill or Native	Time Tested (hrs)
1	470	590	Backfill	1352
2	332	590	Native	1430
3	267	590	Native	1459
4	440	590	Backfill	1512
5	590	590	Native	1521
6	635	590	Native	1634
7	510	590	Backfill	1641

Notes: 1 - Coordinate convention shown on Figure F.1.

Table F.2 - Interpreted Cone Penetration Resistances for Test 05

Cone Test No.	Interpreted Penetration Resistance (kPa)			
	@ Initial Springline of Pipeline #1	@ Initial Springline of Pipeline #2	@ Initial Springline of Pipeline #3	@ Initial Springline of Pipeline #4
1	20	15	10	5
2	234	216	199	183
3	259	240	227	211
4	15	10	6	2
5	251	214	187	158
6	272	239	213	186
7	20	13	11	6

Table F.3 - Pipeline Test Details for Test 05

Pipeline No.	Trench Width (mm)	Cover Depth (mm)	X:Y Coordinates of Pipe Centre (mm)	Pipeline Velocity (mm/sec)	Time Tested (hrs)
1	100	32	290 : 480	0.51	1439
2	100	20	650 : 480	0.52	1521
3	100	10	650 : 700	0.48	1619
4	100	0	290 : 700	0.48	1405

Table F.4 - Prototype Test Geometries for Test 05

Pipeline	Distance to Trench Wall in the Direction of Travel (m)	Distance to Trench Wall Towards the Rear of the Pipeline (m)	Distance to a Stiff Retaining Wall in the Direction of Travel (m)	Distance to the Pipeline in the Direction Opposite to Travel (m)	Distance Laterally to a Stiff Retaining Wall (m)	Distance Laterally to the Edge of the Adjacent Pipeline (m)	Distance From Base of Pipeline to Rigid Base, i.e. Bedrock (m)	Water Level Above Rigid Base, i.e. Bedrock (m)	Water Level Below Base of Pipeline (m)
1	0.775	0.775	6.225	4.55	3.875	2.5	2.275	0.425	1.85
2	0.775	0.775	6.225	4.55	3.875	2.5	2.275	0.425	1.85
3	0.775	0.775	6.225	4.55	3.875	2.5	2.275	0.425	1.85
4	0.775	0.775	6.225	4.55	3.875	2.5	2.275	0.425	1.85

Table F.5 - Calculation of Undrained Shear Strength for Test 05

Pipeline	Soil Type	Cone Tests Used to Derive q_c	Interpreted Cone Tip Resistance at Springline, q_c (kPa)	Saturated Bulk Density, γ_{sat} (kN/m^3)	Pore Pressure at Springline, u (kPa)	Depth to Springline, h (m)	Cone Factor, N_c or N_k*	Undrained Shear Strength, c_u (kPa)
1	Native	2,3,5,6	292.1	472.8	-14.5	0.051	7.9/11.6	23.0 - 33.9
1	Backfill	1,4,7	18.3	411.8	---	0.051	15	1.2
2	Native	2,3,5,6	261.3	472.8	-14.5	0.039	7.8/11.9	20.3 - 31.3
2	Backfill	1,4,7	12.7	411.8	---	0.039	15	0.8
3	Native	2,3,5,6	237.5	472.8	-14.5	0.029	7.6/12.2	18.3 - 29.4
3	Backfill	1,4,7	9	411.8	---	0.029	15	0.6
4	Native	2,3,5,6	212.2	472.8	-14.5	0.019	7.4/12.6	16.1 - 27.3
4	Backfill	1,4,7	4.3	411.8	---	0.019	15	0.3

Notes: * - N_c range of values correspond to native material; N_k values correspond to backfill.

Table F.6 - Summary of Prototype Pipeline Data; Test 05

Pipeline →	Pipeline #1	Pipeline #2	Pipeline #3	Pipeline #4
Trench Width	2.5m	2.5m	2.5m	2.5m
Cover Depth	0.80m	0.50m	0.25m	0.00m
Embedment Ratio, H/D	1.842	1.526	1.263	1.000
Average Backfill Undrained Shear Strength @ Springline	1.2kPa	0.8kPa	0.6kPa	0.3kPa
Average Native Undrained Shear Strength @ Springline	28.5kPa	25.8kPa	23.9kPa	21.7kPa
Ultimate Normalized Resistance, N	4.980	5.520	4.365	3.598
Distance into Trench Wall to Ultimate Normalized Resistance	2.184D	1.667D	2.125D	2.260D
Slope to Ultimate Normalized Resistance	1.660	2.223	1.484	1.170
Normalized Resistance at Trench Wall	0.451	1.279	1.947	0.770
Normalized Resistance at 0.5D Penetration	3.156	3.984*	3.320	2.607
Normalized Resistance at 1D Penetration	4.057	5.066	3.822	3.918
Slope of Interaction Between TW and Breakover	8.170	10.221	11.038	5.690
Normalized Resistance at Breakover	3.500	3.320	3.258	2.459
Distance into Trench Wall to Breakover	0.475D	0.218D	0.181D	0.303D
Slope of Interaction After Breakover	1.078	2.380	0.658	0.693

Note: * - Estimated value as normalized force-displacement curve is discontinuous.

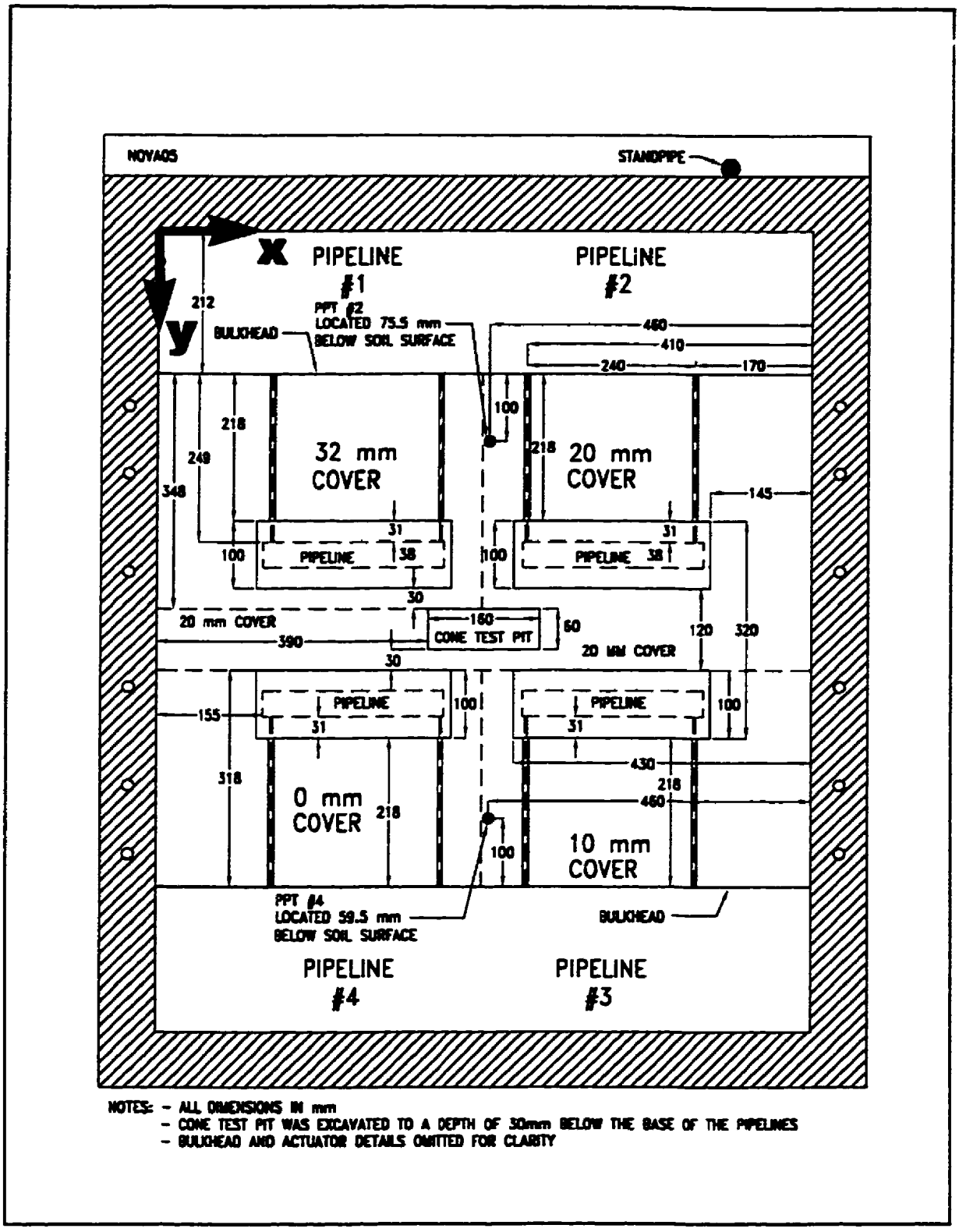

NOTES: - ALL DIMENSIONS IN mm
- CONE TEST PIT WAS EXCAVATED TO A DEPTH OF 30mm BELOW THE BASE OF THE PIPELINES
- BULKHEAD AND ACTUATOR DETAILS OMITTED FOR CLARITY

Figure F.1 - *Model Test Geometry, Test 05.*

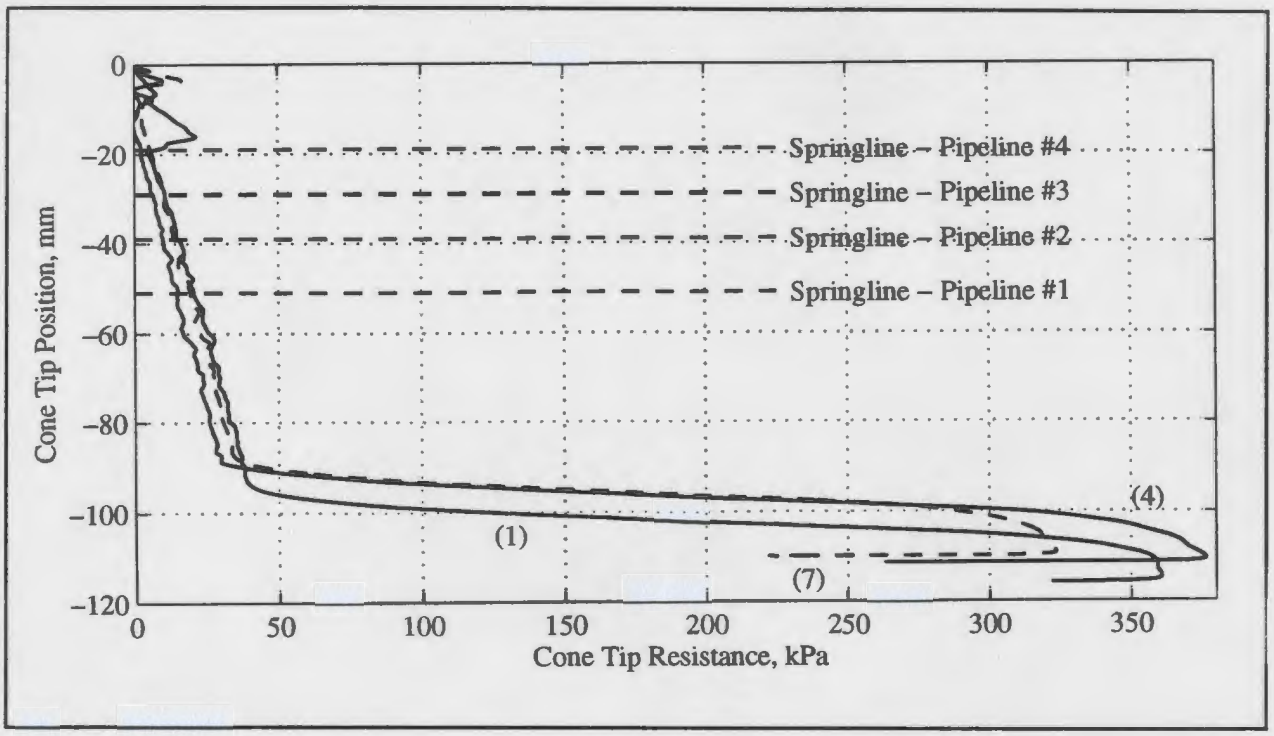

Figure F.2 - *All cone penetration tests, backfill material, Test 05.*

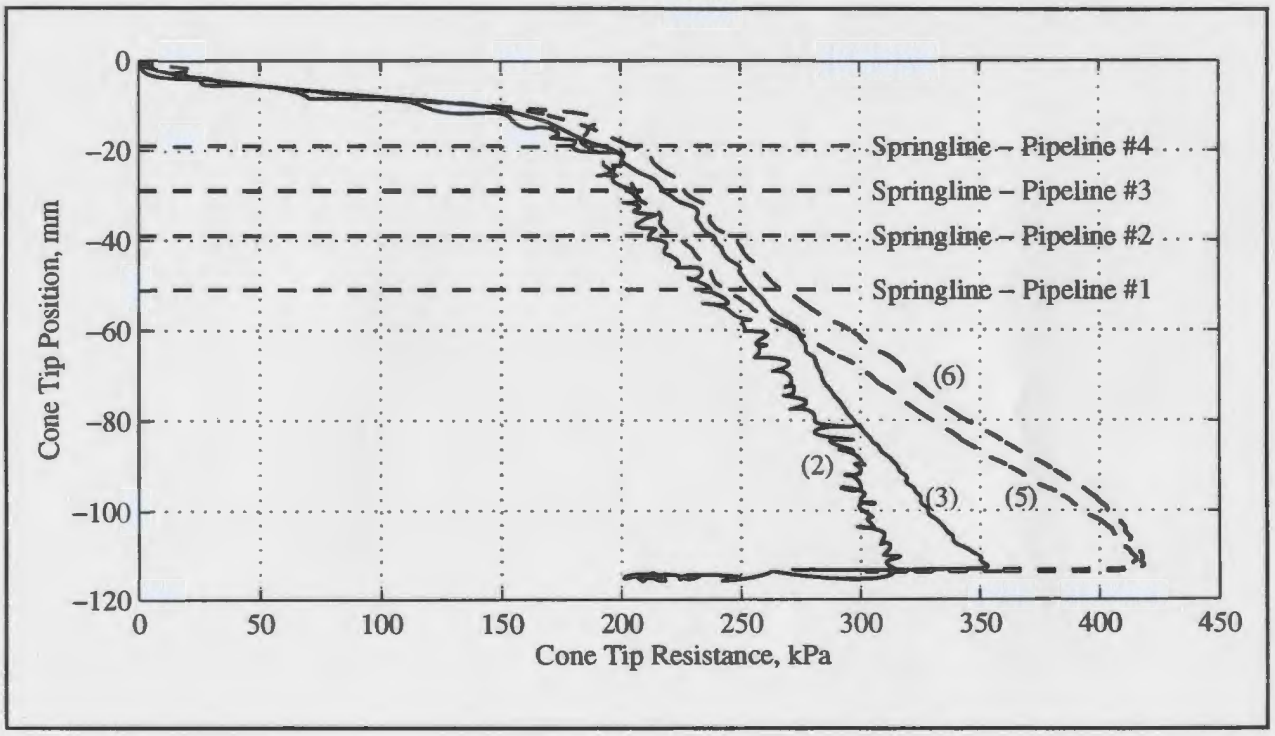

Figure F.3 - *All cone penetration tests, native material, Test 05.*

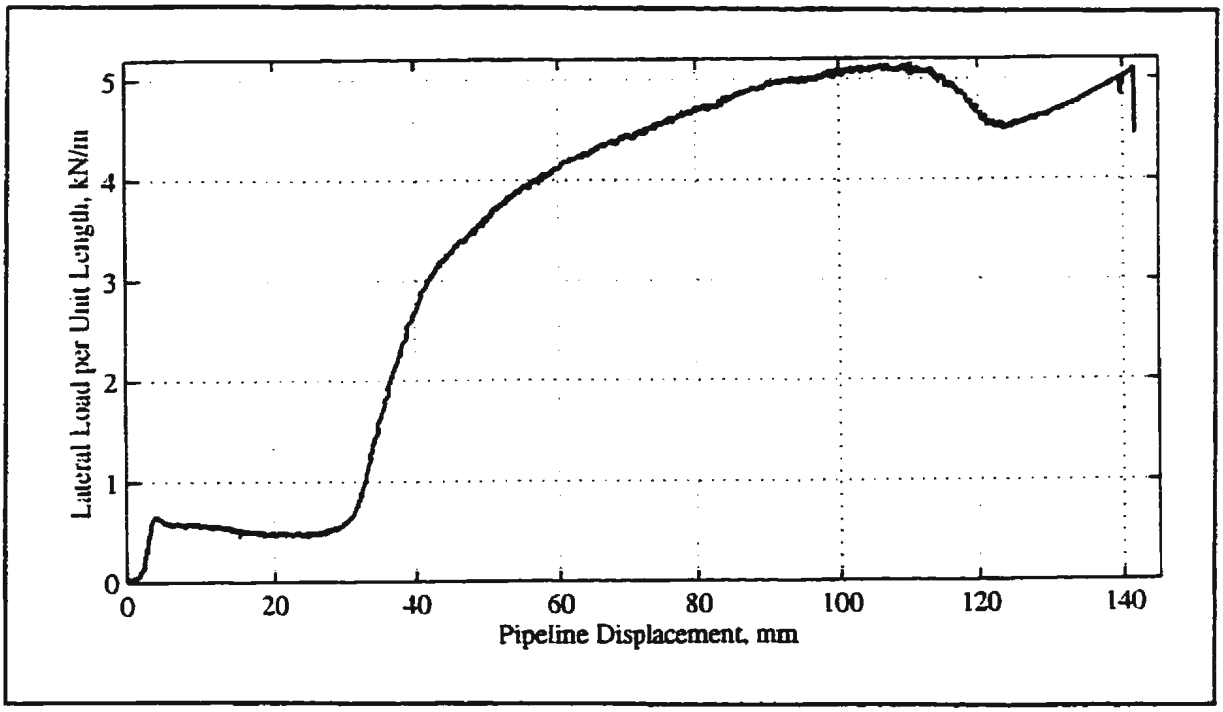

Figure F.4 - *Force-displacement response, model pipeline #1, 32mm cover, Test 05.*

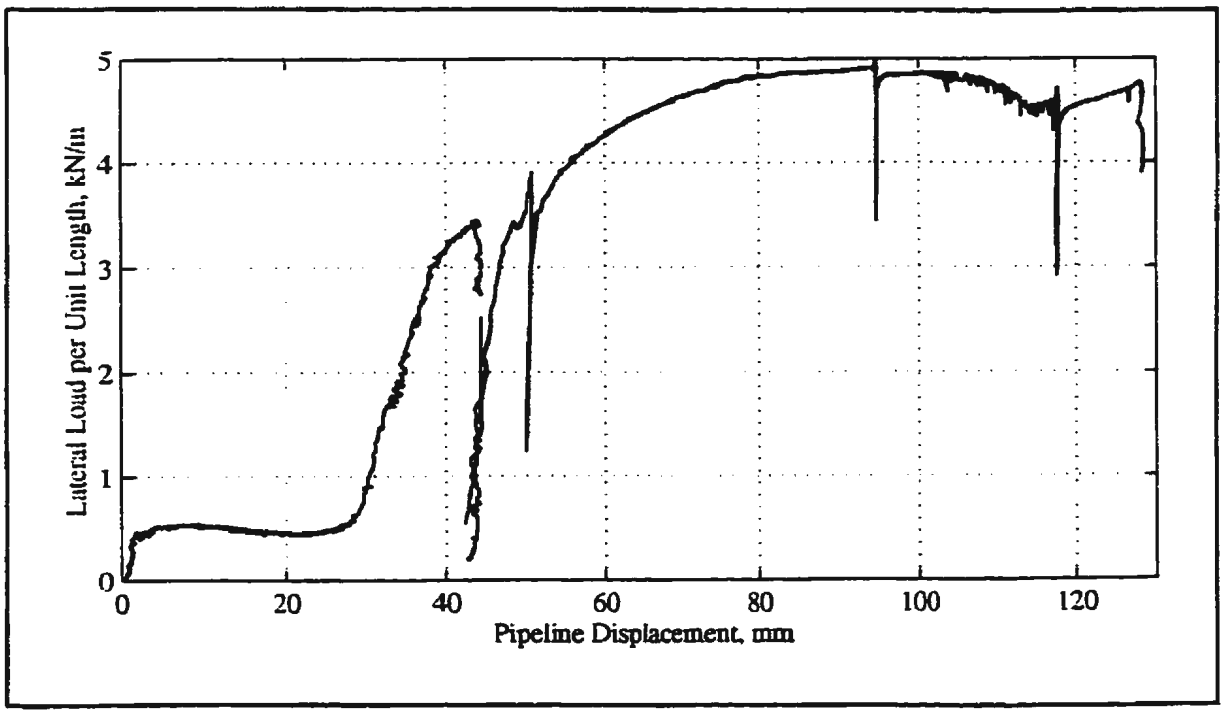

Figure F.5 - *Force-displacement response, model pipeline #2, 20mm cover, Test 05.*

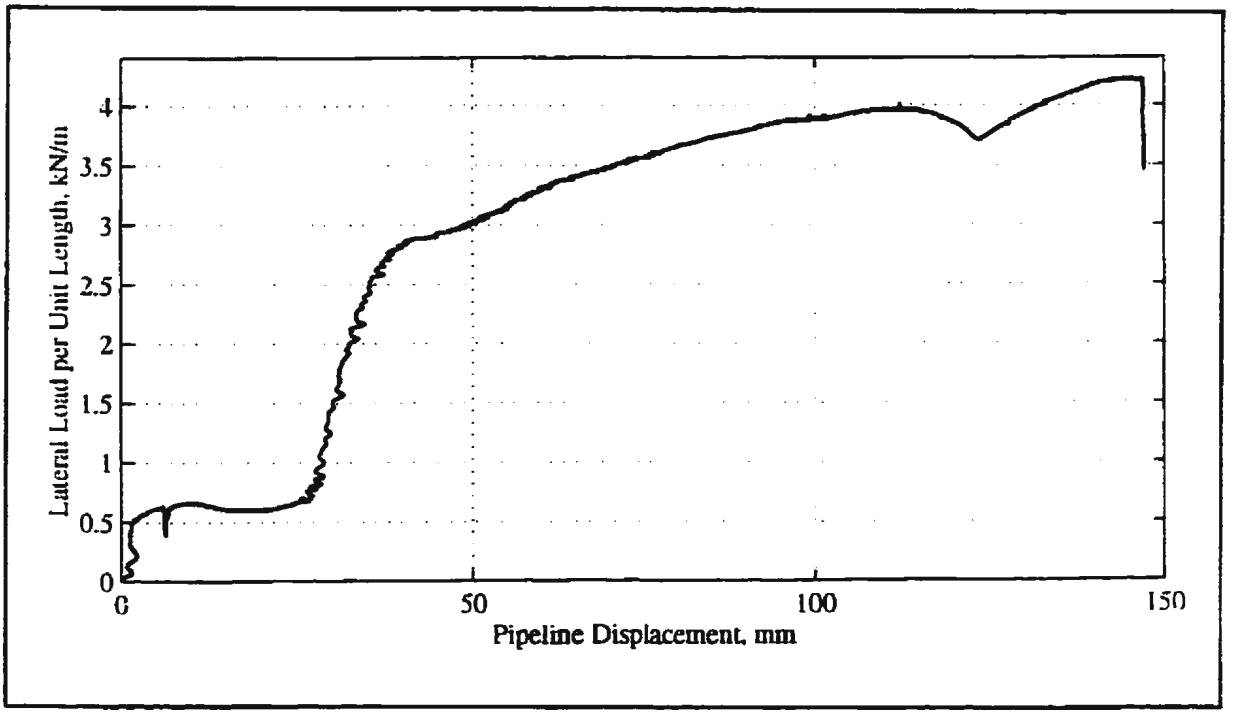

Figure F.6 - *Force-displacement response, model pipeline #3, 10mm cover, Test 05.*

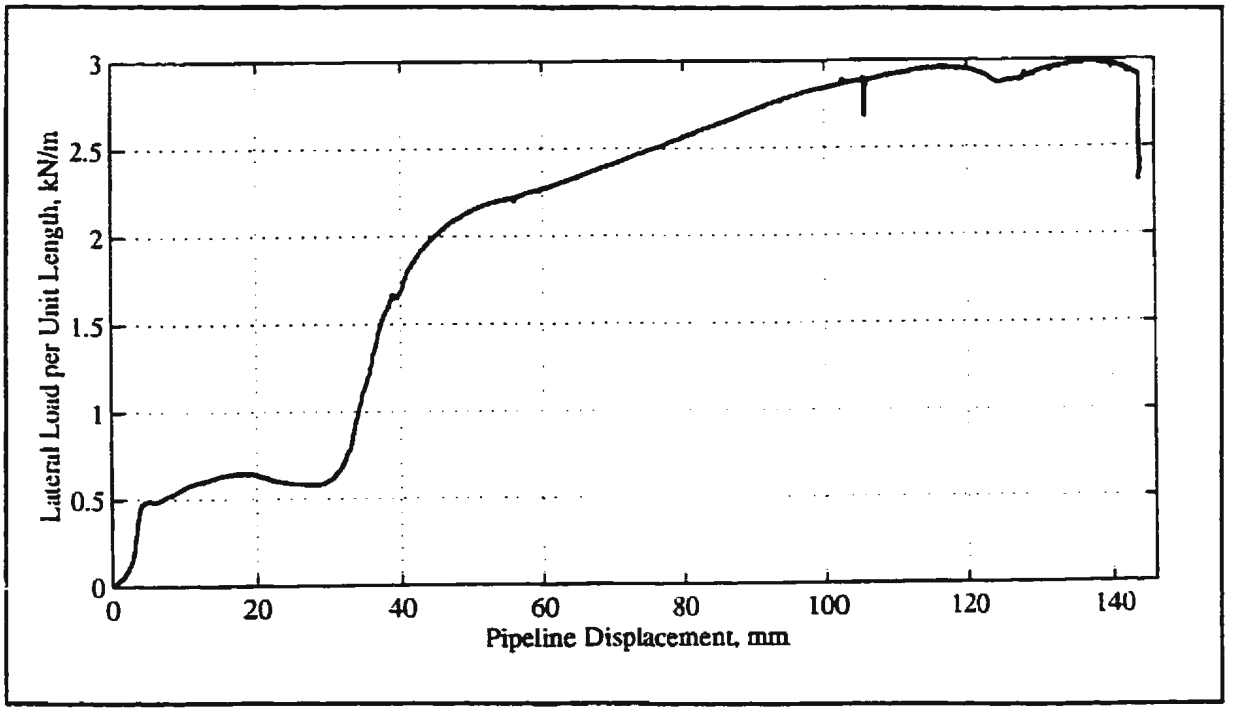

Figure F.7 - *Force-displacement response, model pipeline #4, 0mm cover, Test 05.*

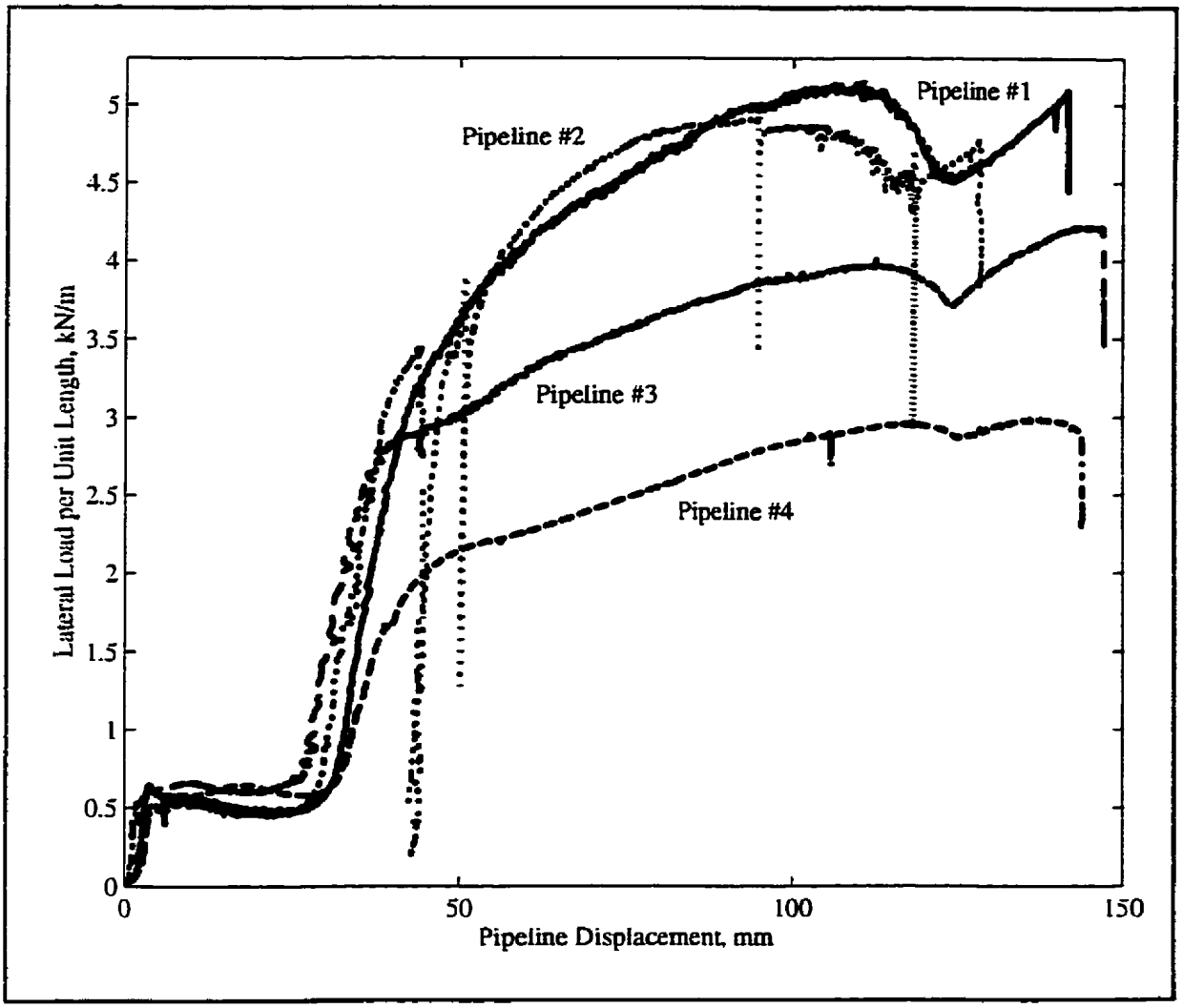

Figure F.8 - Force-displacement response, all model pipelines, Test 05.

Figure F.9 - *Photo of excavated cross-section along mid length of model pipeline #1, 32mm cover, Test 05.*

Figure F.10 - *Photo of excavated cross-section along mid length of model pipeline #2, 20mm cover, Test 05.*

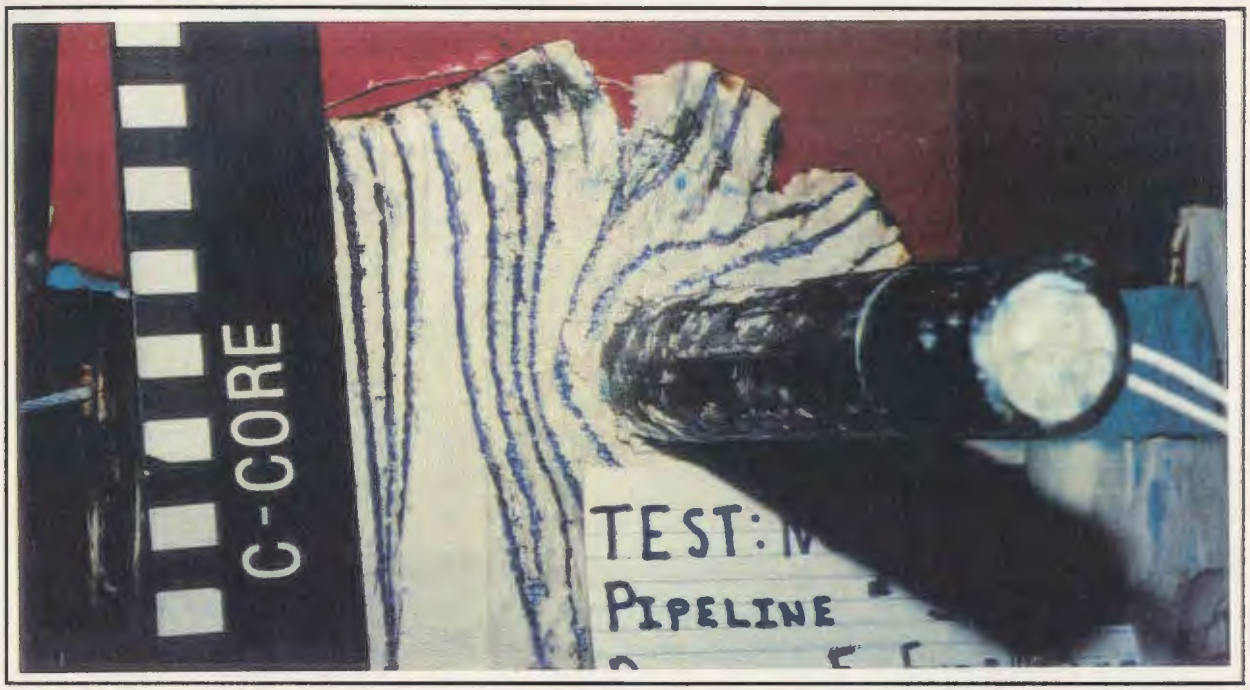

Figure F.11 - *Photo of excavated cross-section along mid length of model pipeline #3, 10mm cover, Test 05.*

Figure F.12 - *Photo of excavated cross-section along mid length of model pipeline #4, 0mm cover, Test 05.*

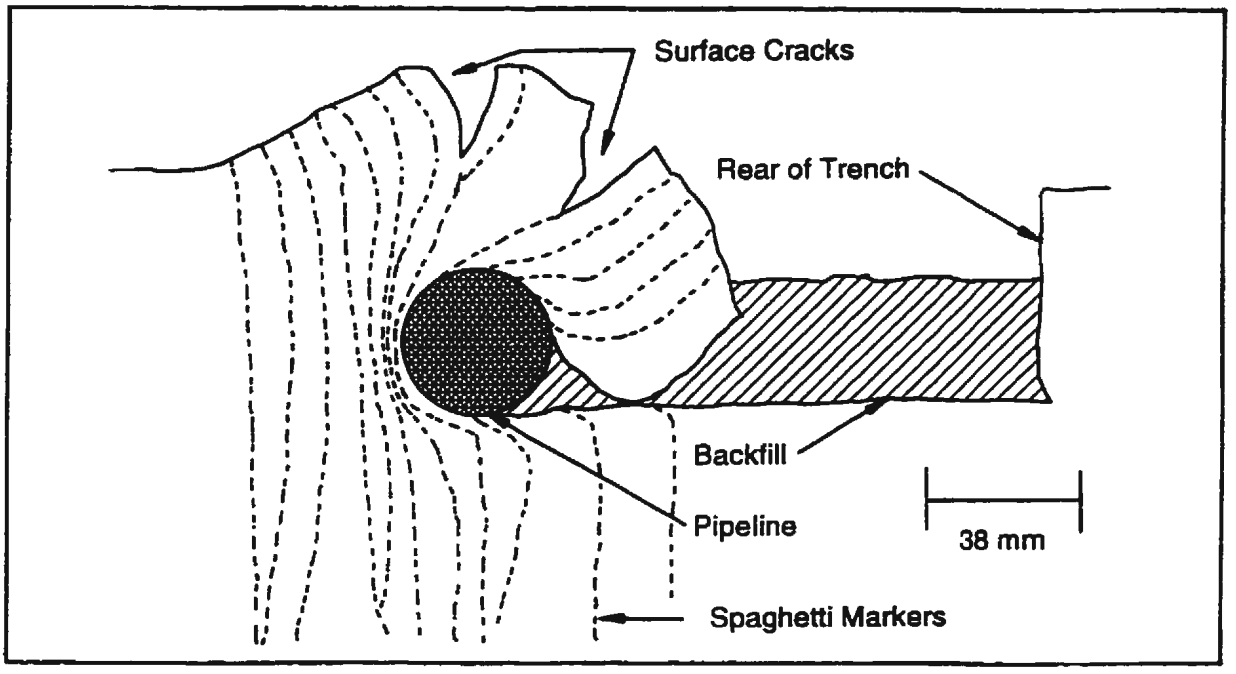

Figure F.13 - *Sketch of excavated cross-section along mid length of model pipeline #1, 32mm cover, Test 05.*

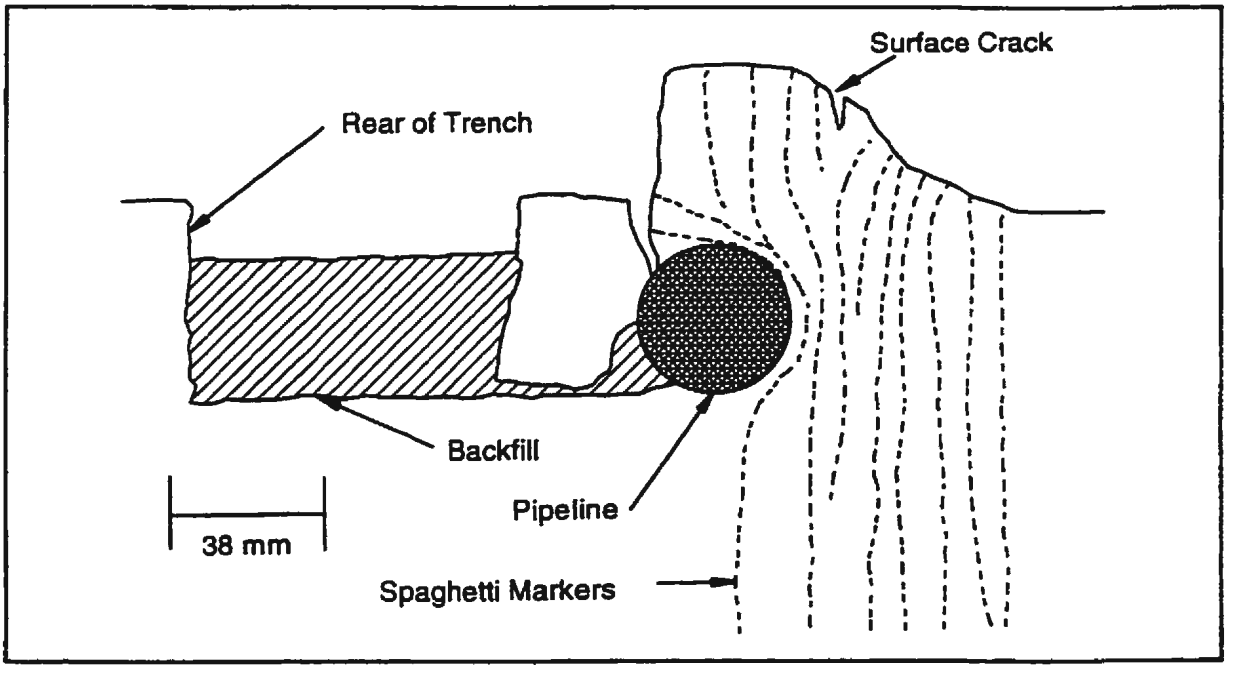

Figure F.14 - *Sketch of excavated cross-section along mid length of model pipeline #2, 20mm cover, Test 05.*

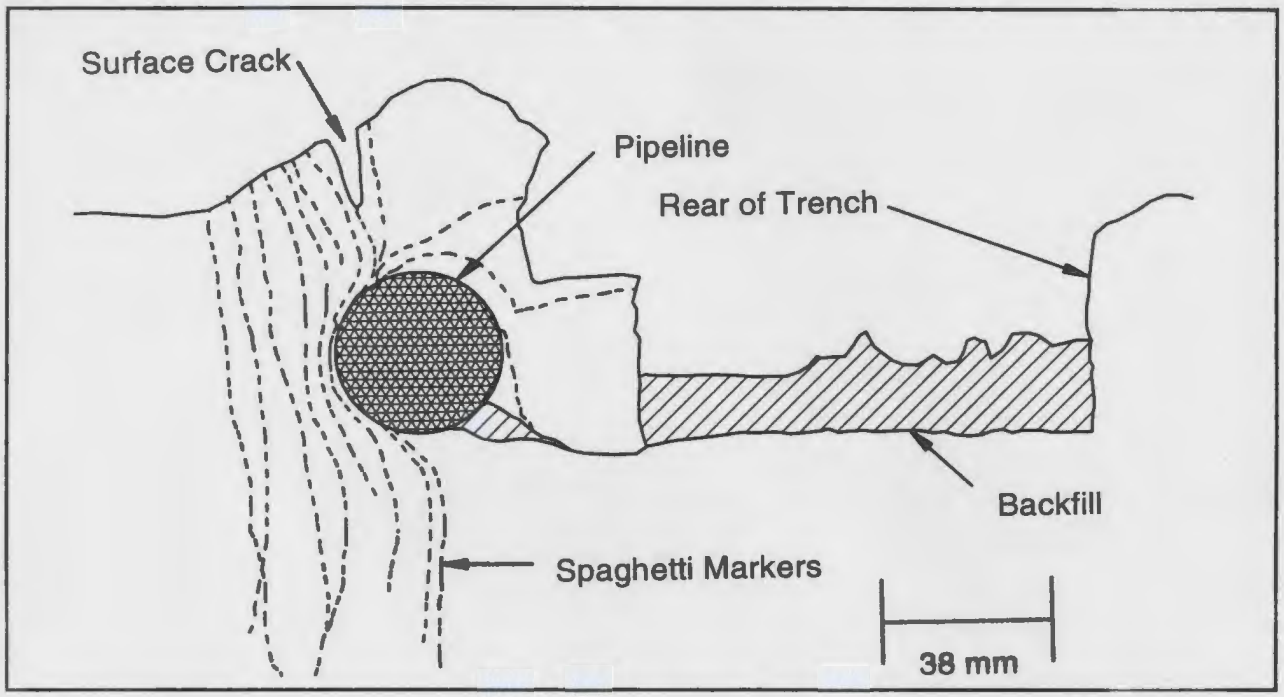

Figure F.15 - *Sketch of excavated cross-section along mid length of model pipeline #3, 10mm cover, Test 05.*

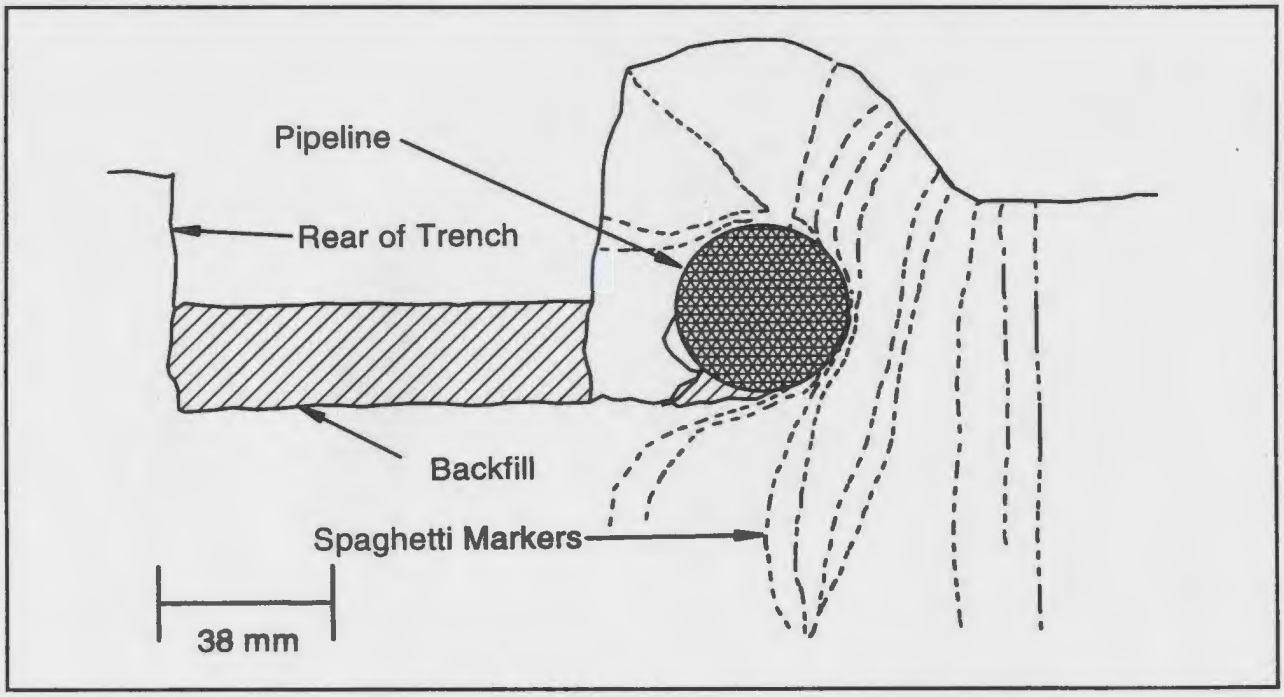

Figure F.16 - *Sketch of excavated cross-section along mid length of model pipeline #4, 0mm cover, Test 05.*

Appendix G

Test 06 - Selected Test Data

Table G.1 - Cone Penetration Test Details for Test 06

CPT No.	X[1] (mm)	Y[1] (mm)	Backfill or Native	Time Tested (hrs)
1	470	590	Backfill	1520
2	350	590	Native	1534
3	310	590	Native	1600
4	269	590	Native	1621
5	431	590	Backfill	1631
6	593	590	Native	1641
7	642	590	Native	1707
8	511	590	Backfill	1715

Notes: 1 - Coordinate convention shown on Figure G.1.

Table G.2 - Interpreted Cone Penetration Resistances for Test 06

Cone Test No.	Interpreted Penetration Resistance (kPa)			
	@ Initial Springline of Pipeline #1	@ Initial Springline of Pipeline #2	@ Initial Springline of Pipeline #3	@ Initial Springline of Pipeline #4
1	24	18	10	6
2	164	147	133	118
3	195	175	158	140
4	200	180	165	149
5	17	14	10	7
6	216	198	180	166
7	226	206	190	172
8	30	23	17	11

Table G.3 - Pipeline Test Details for Test 06

Pipeline No.	Trench Width (mm)	Cover Depth (mm)	X:Y Coordinates of Pipe Centre (mm)	Pipeline Velocity (mm/sec)	Time Tested (hrs)
1	25	8	327.5 : 492.5	1.41	1544
2	25	5	612.5 : 492.5	1.00	1649
3	25	2.5	612.5 : 687.5	1.08	1654
4	25	0	327.5 : 687.5	1.08	1615

Table G.4 - Prototype Test Geometries for Test 06

Pipeline	Distance to Trench Wall in the Direction of Travel (m)	Distance to Trench Wall Towards the Rear of the Pipeline (m)	Distance to a Stiff Retaining Wall in the Direction of Travel (m)	Distance to the Pipeline in the Direction Opposite to Travel (m)	Distance Laterally to a Stiff Retaining Wall (m)	Distance Laterally to the Edge of the Adjacent Pipeline (m)	Distance From Base of Pipeline to Rigid Base, i.e. Bedrock (m)	Water Level Above Rigid Base, i.e. Bedrock (m)	Water Level Below Base of Pipeline (m)
1	0.775	0.775	27.575	18.55	24.0	10.0	10.525	8.9	1.625
2	0.775	0.775	27.575	18.55	24.0	10.0	10.525	8.9	1.625
3	0.775	0.775	27.575	18.55	24.0	10.0	10.525	8.9	1.625
4	0.775	0.775	27.575	18.55	24.0	10.0	10.525	8.9	1.625

Table G.5 - Calculation of Undrained Shear Strength for Test 06

Pipeline	Soil Type	Cone Tests Used to Derive q_c	Interpreted Cone Tip Resistance at Springline, q_c (kPa)	Saturated Bulk Density, γ_{sat} (kN/m^3)	Pore Pressure at Springline, u (kPa)	Depth to Springline, h (m)	Cone Factor, N_c or N_k*	Undrained Shear Strength, c_u (kPa)
1	Native	2,3,4,6,7	230.2	1923.7	-11.8	0.01275	7.8/11.8	17.5 - 26.2
1	Backfill	1,5,8	23.7	1700.3	---	0.01275	15	1.6
2	Native	2,3,4,6,7	208.4	1923.7	-11.8	0.00975	7.7/12.1	15.7 - 24.7
2	Backfill	1,5,8	18.3	1700.3	---	0.00975	15	1.2
3	Native	2,3,4,6,7	190.0	1923.7	-11.8	0.00725	7.5/12.4	14.2 - 23.4
3	Backfill	1,5,8	12.3	1700.3	---	0.00725	15	0.8
4	Native	2,3,4,6,7	171.4	1923.7	-11.8	0.00475	7.3/12.8	12.7 - 22.1
4	Backfill	1,5,8	8.0	1700.3	--	0.00475	15	0.5

Notes: * - N_c range of values correspond to native material; N_k values correspond to backfill.

Table G.6 - Summary of Prototype Pipeline Data; Test 06

Pipeline →	Pipeline #1	Pipeline #2	Pipeline #3	Pipeline #4
Trench Width	2.5m	2.5m	2.5m	2.5m
Cover Depth	0.80m	0.50m	0.25m	0.00m
Embedment Ratio, H/D	1.842	1.526	1.263	1.000
Average Backfill Undrained Shear Strength @ Springline	1.6kPa	1.2kPa	0.8kPa	0.5kPa
Average Native Undrained Shear Strength @ Springline	21.9kPa	20.2kPa	18.8kPa	17.4kPa
Ultimate Normalized Resistance, N	5.128	4.600	2.912	2.361
Distance into Trench Wall to Ultimate Normalized Resistance	7.655D	5.638D	2.242D	2.886D
Slope to Ultimate Normalized Resistance	0.605	0.713	0.952	0.638
Normalized Resistance at Trench Wall	1.082	1.189	0.373	0.541
Normalized Resistance at 0.5D Penetration	3.111	3.002	2.094	1.795
Normalized Resistance at 1D Penetration	4.159	3.402	2.582	1.930
Slope of Interaction Between TW and Breakover	4.673	4.325	3.271	2.947
Normalized Resistance at Breakover	4.238	3.320	2.424	1.869
Distance into Trench Wall to Breakover	0.759D	0.475D	0.652D	0.450D
Slope of Interaction After Breakover	0.131	0.332	0.348	0.158

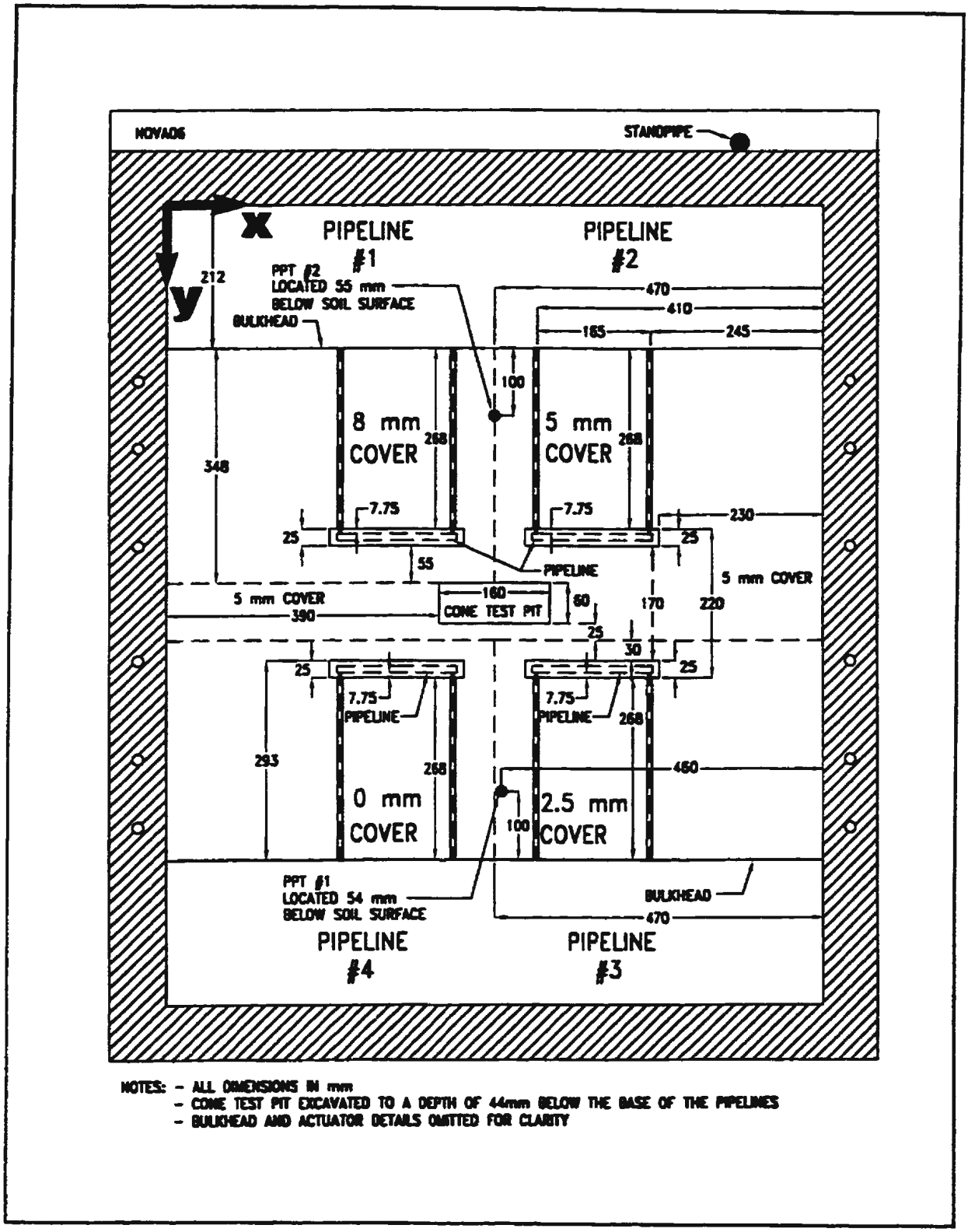

NOTES: - ALL DIMENSIONS IN mm
- CONE TEST PIT EXCAVATED TO A DEPTH OF 44mm BELOW THE BASE OF THE PIPELINES
- BULKHEAD AND ACTUATOR DETAILS OMITTED FOR CLARITY

Figure G.1 - *Model Test Geometry, Test 06.*

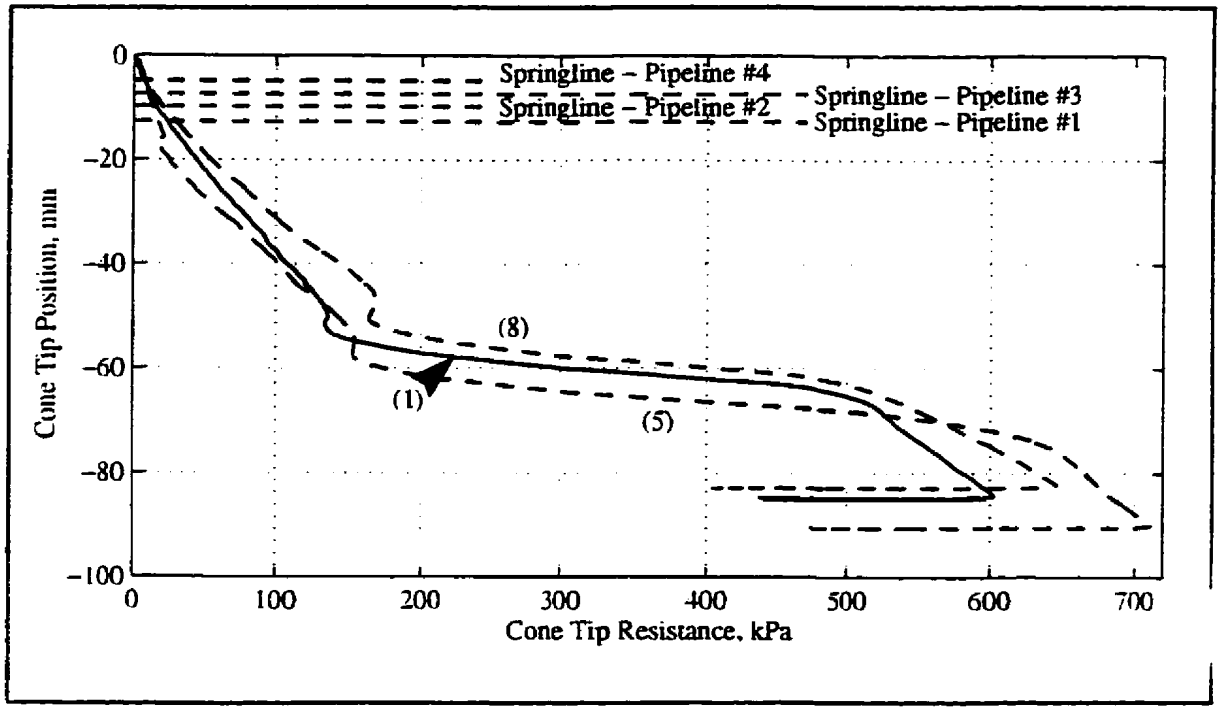

Figure G.2 - *All cone penetration tests, backfill material, Test 06.*

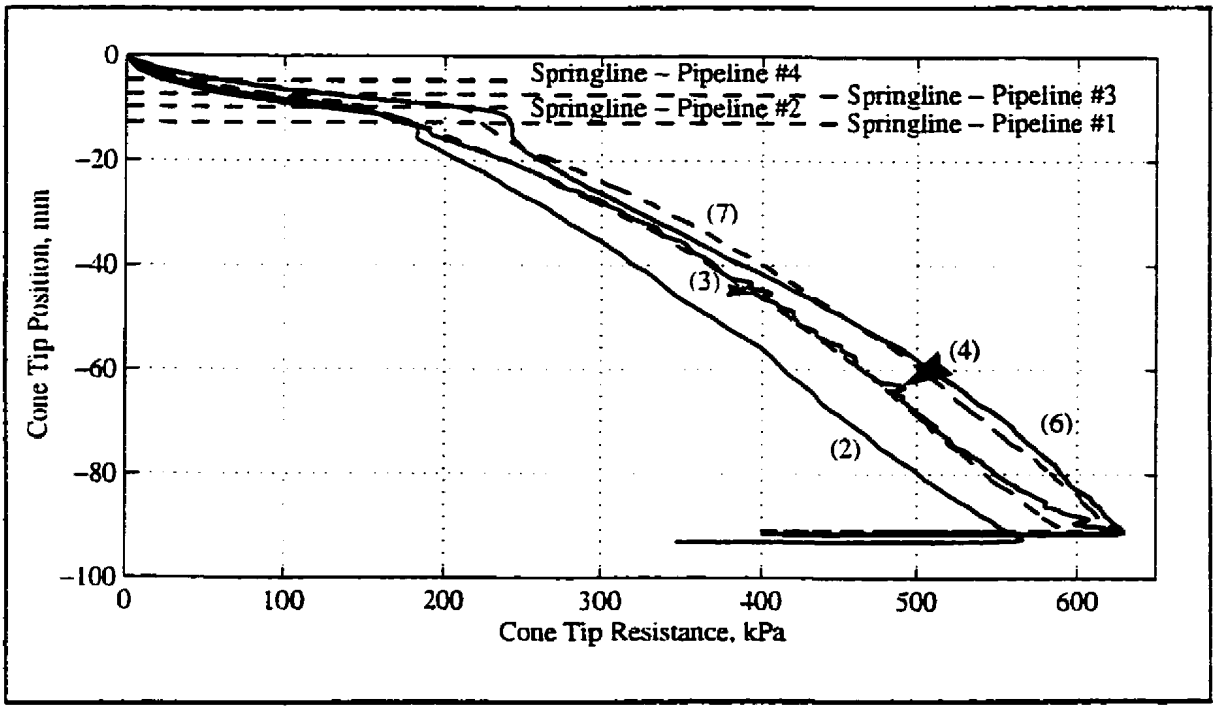

Figure G.3 - *All cone penetration tests, native material, Test 06.*

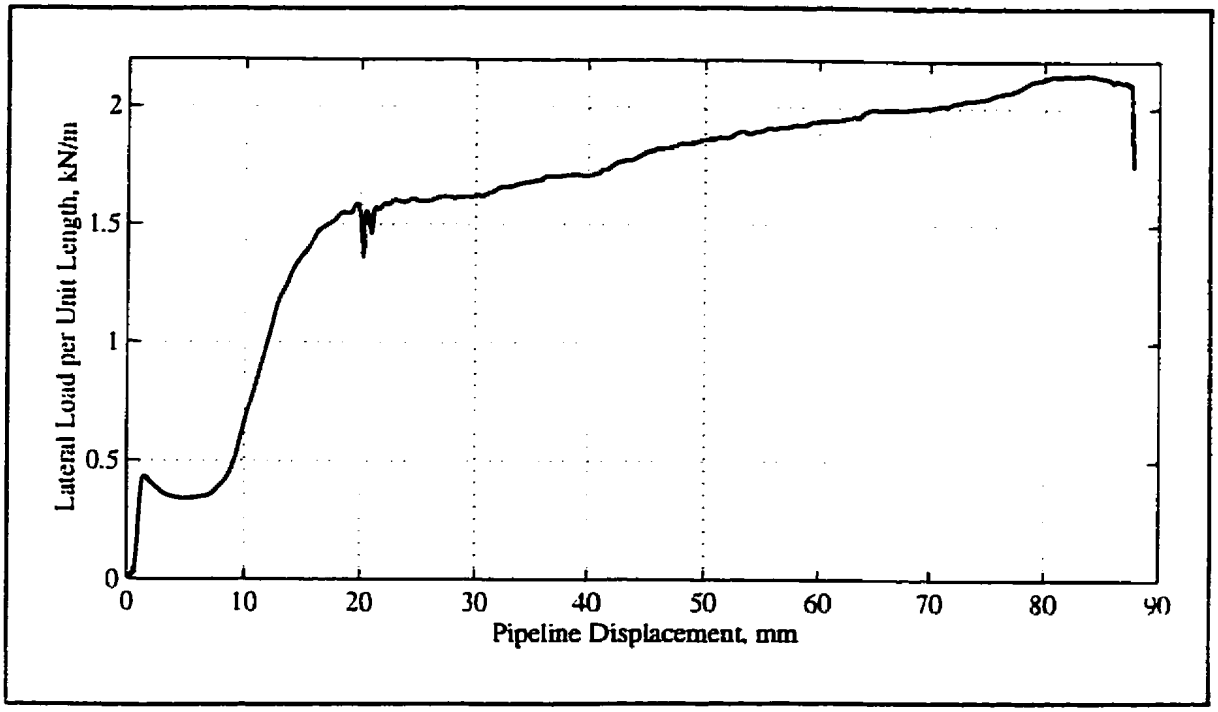

Figure G.4 - *Force-displacement response, model pipeline #1, 8mm cover, Test 06.*

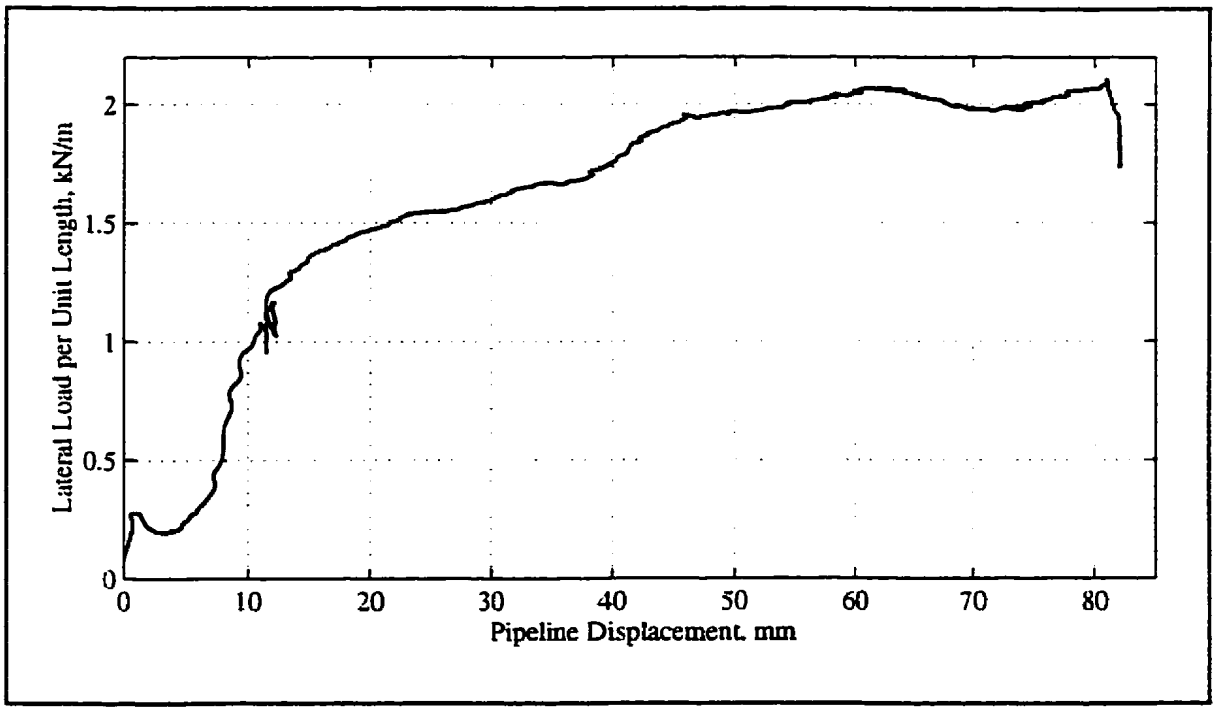

Figure G.5 - *Force-displacement response, model pipeline #2, 5mm cover, Test 06.*

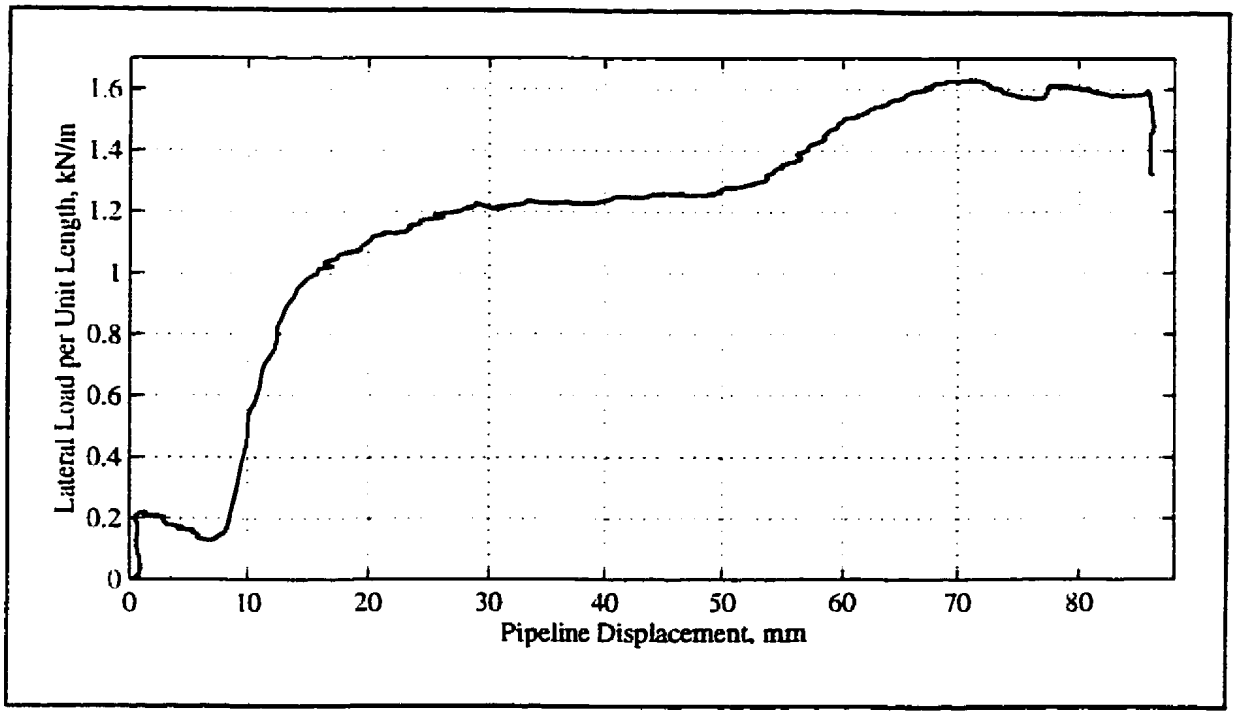

Figure G.6 - *Force-displacement response, model pipeline #3, 2.5mm cover, Test 06.*

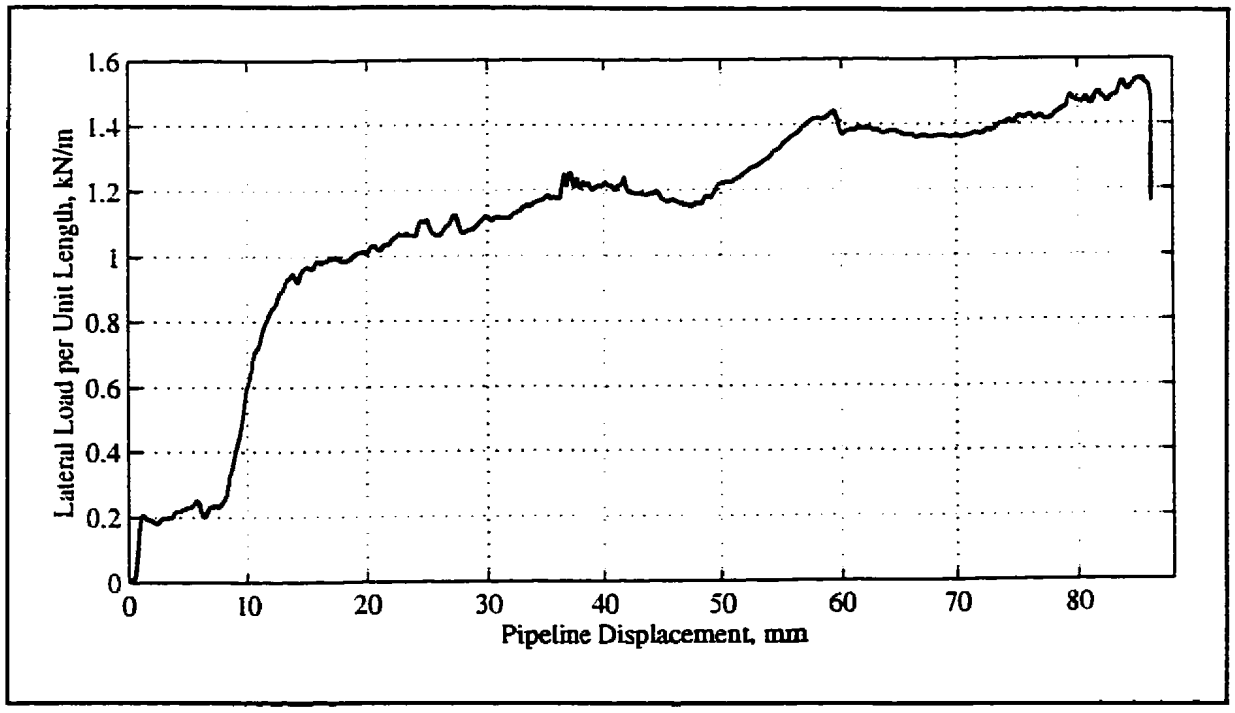

Figure G.7 - *Force-displacement response, model pipeline #4, 0mm cover, Test 06.*

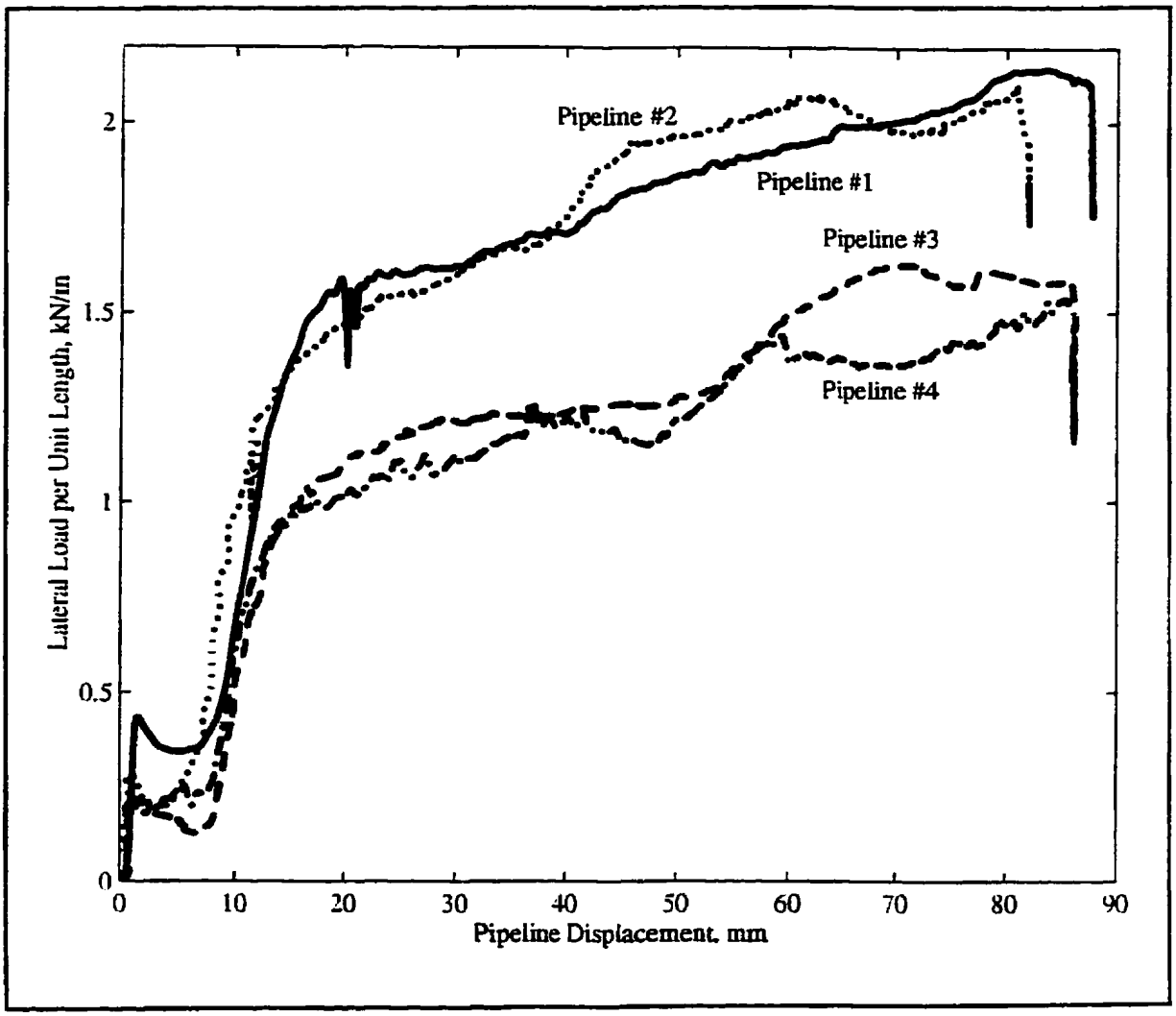

Figure G.8 - Force-displacement response, all model pipelines, Test 06.

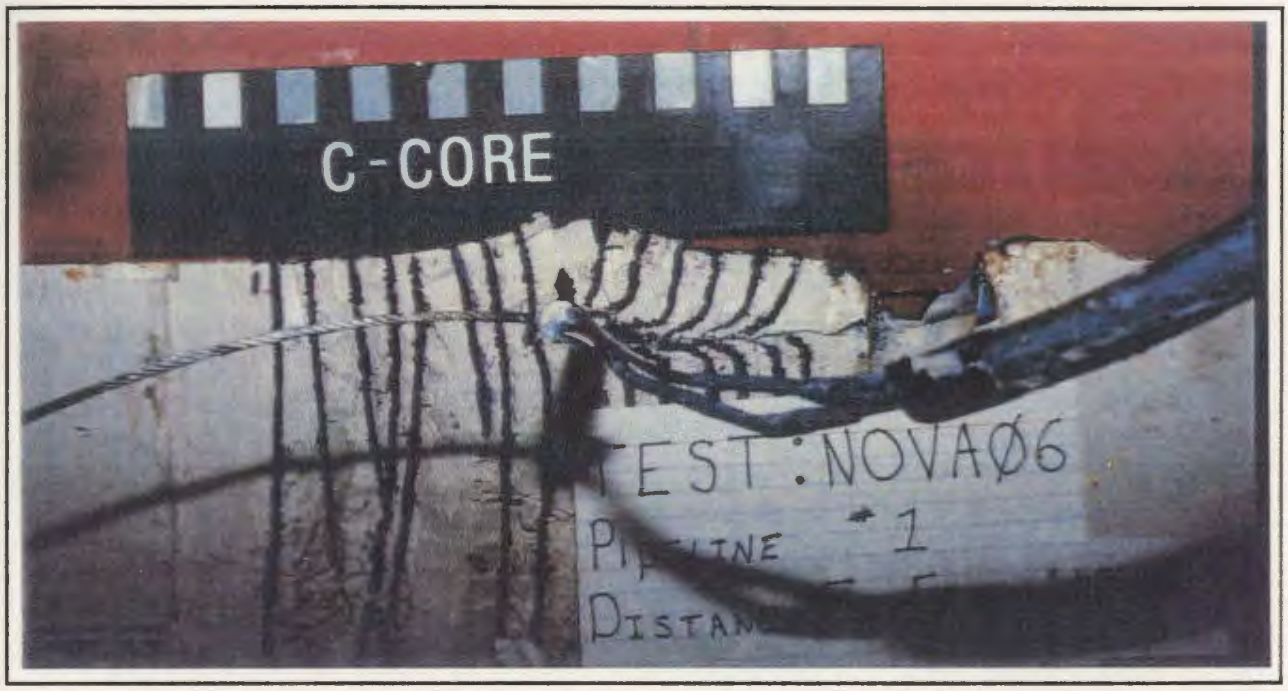

Figure G.9 - *Photo of excavated cross-section along mid length of model pipeline #1, 8mm cover, Test 06.*

Figure G.10 - *Photo of excavated cross-section along mid length of model pipeline #2, 5mm cover, Test 06.*

Figure G.11 - *Photo of excavated cross-section along mid length of model pipeline #3, 2.5mm cover, Test 06.*

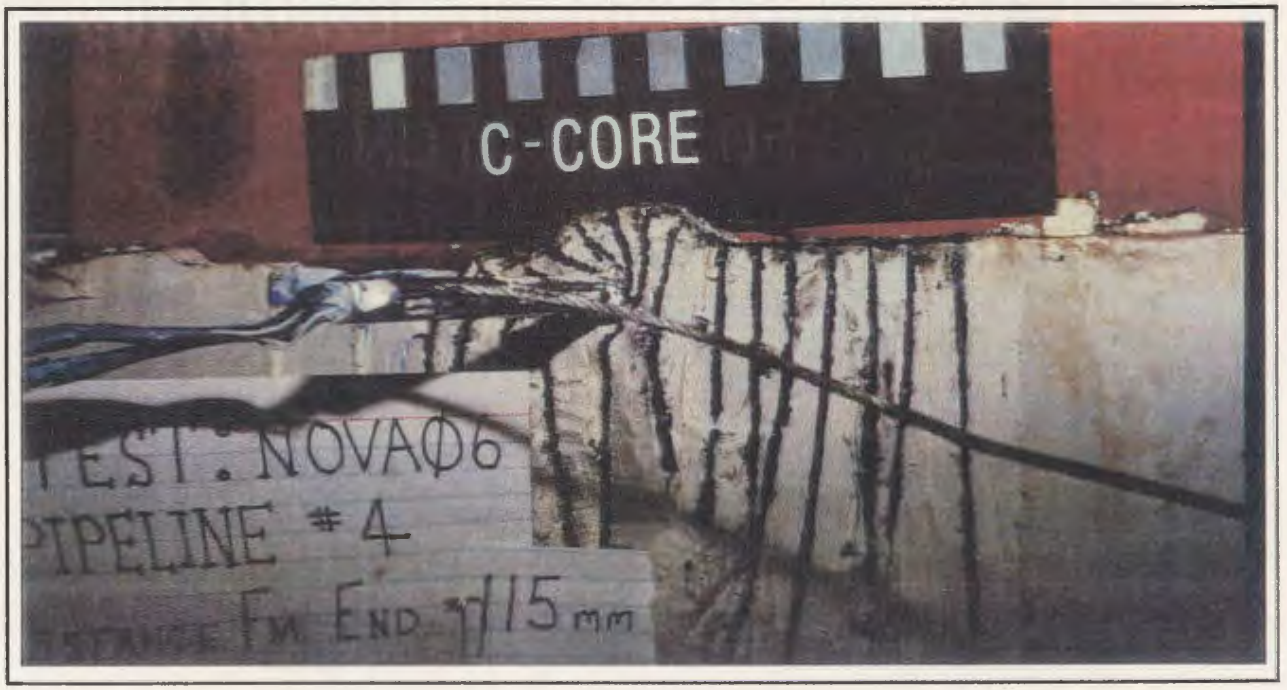

Figure G.12 - *Photo of excavated cross-section along mid length of model pipeline #4, 0mm cover, Test 06.*

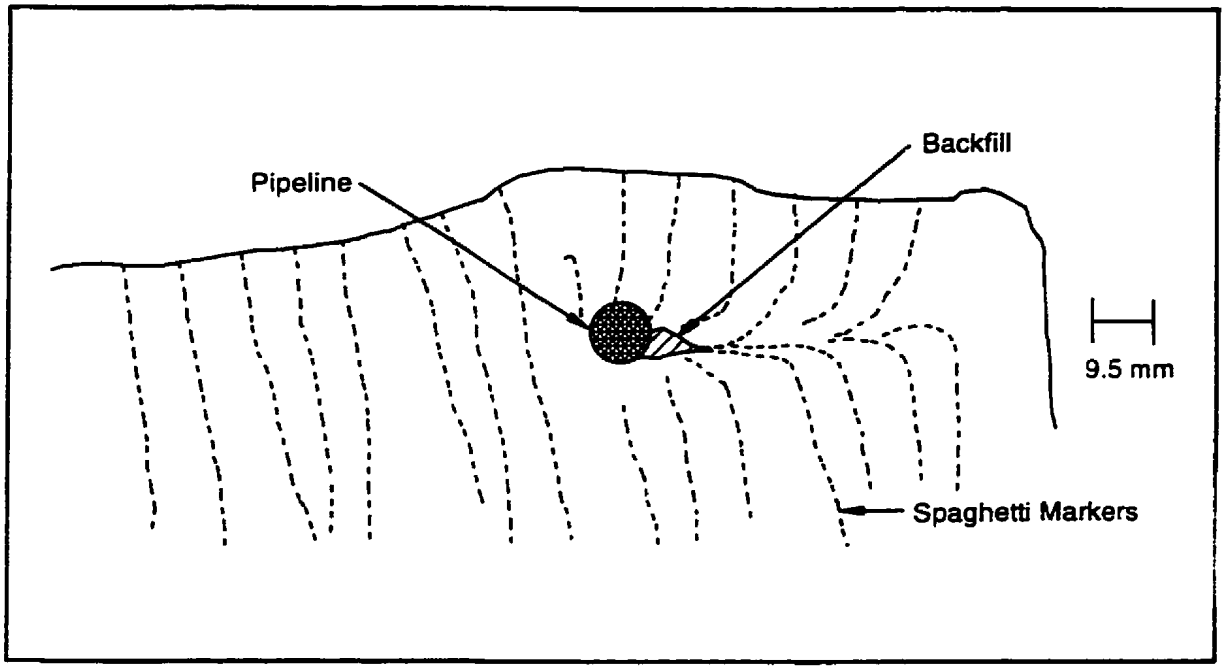

Figure G.13 - *Sketch of excavated cross-section along mid length of model pipeline #1, 8mm cover, Test 06.*

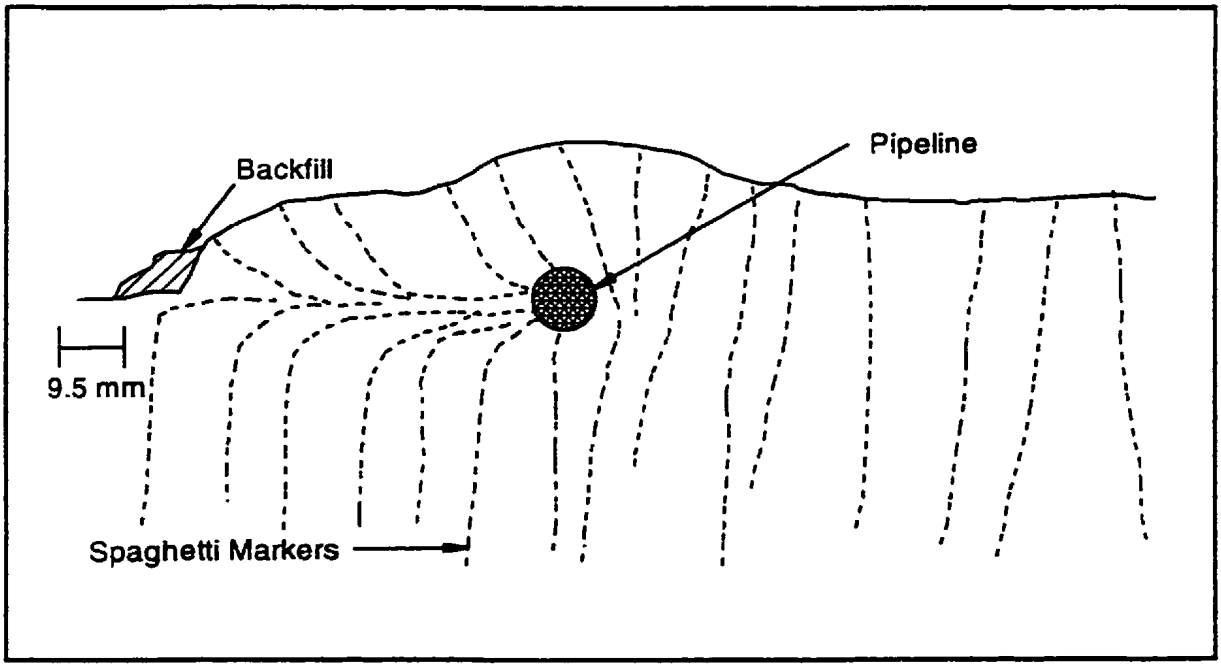

Figure G.14 - *Sketch of excavated cross-section along mid length of model pipeline #2, 5mm cover, Test 06.*

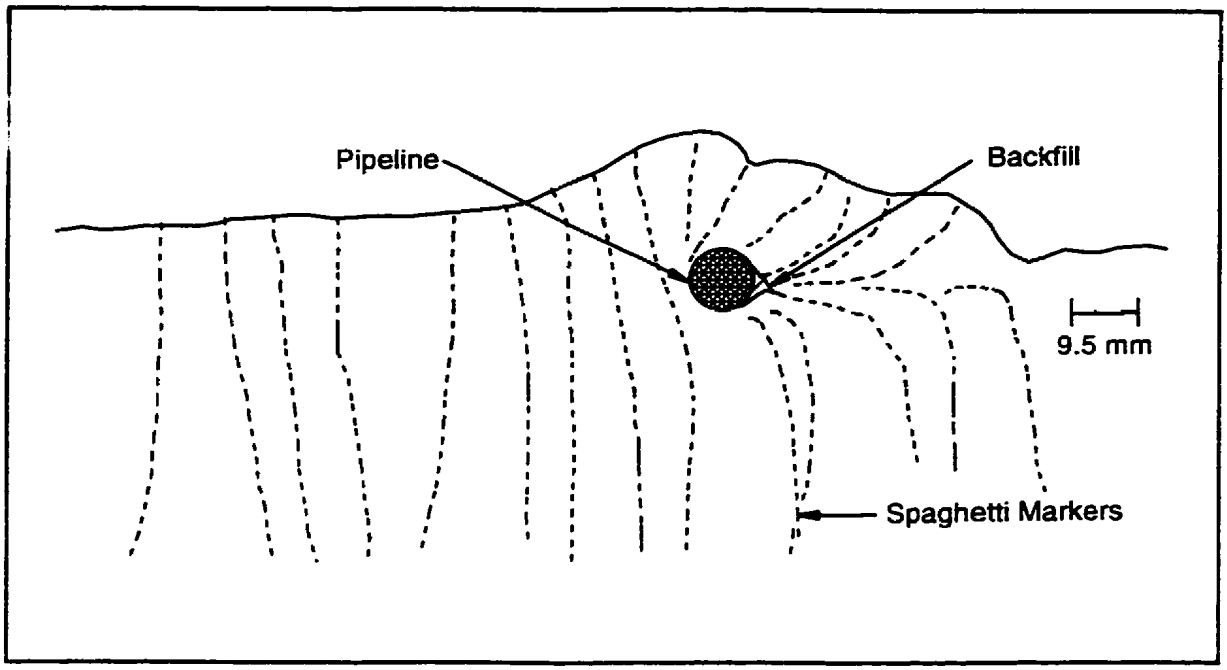

Figure G.15 - *Sketch of excavated cross-section along mid length of model pipeline #3, 2.5mm cover, Test 06.*

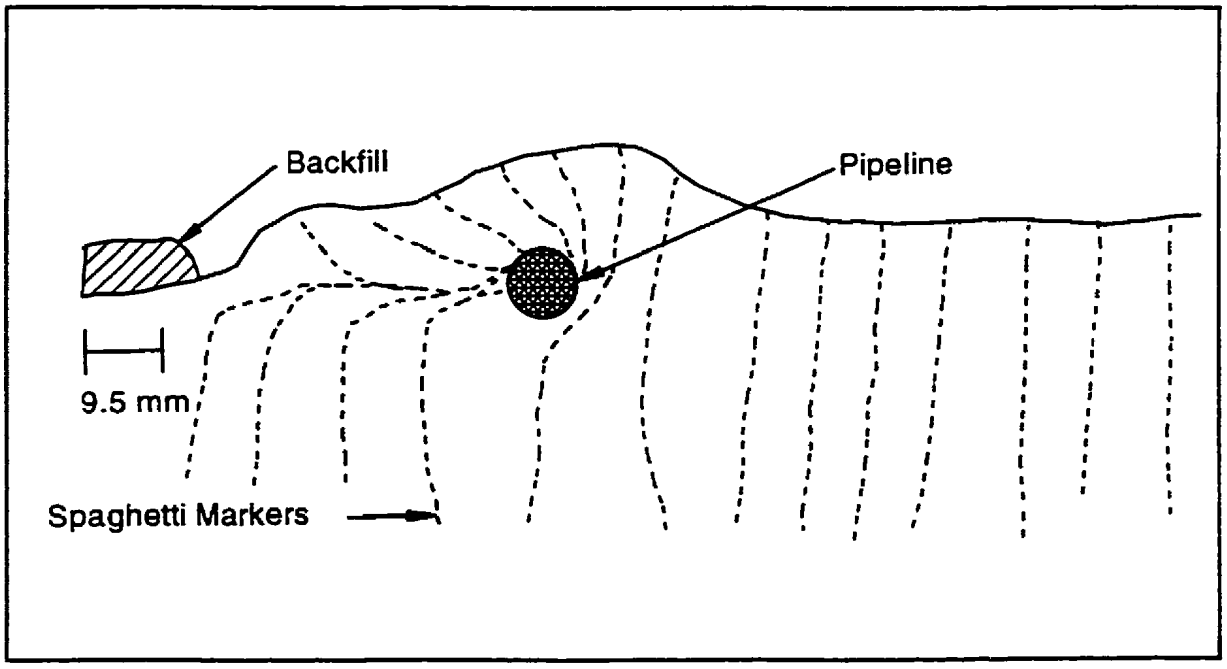

Figure G.16 - *Sketch of excavated cross-section along mid length of model pipeline #4, 0mm cover, Test 06.*

Appendix H

Test 07 - Selected Test Data

Table H.1 - Cone Penetration Test Details for Test 07

CPT No.	X[1] (mm)	Y[1] (mm)	Backfill or Native	Time Tested (hrs)
1	470	590	Backfill	1422
2	333	590	Native	1433
3	260	590	Native	1455
4	650	590	Native	1551
5	510	590	Backfill	1601
6	429	590	Backfill	1927
7	600	590	Native	1935
8	210	590	Native (1g)	1146

Notes: 1 - Coordinate convention shown on Figure H.1.

Table H.2 - Interpreted Cone Penetration Resistances for Test 07

Cone Test No.	Interpreted Penetration Resistance (kPa)			
	@ Initial Springline of Pipeline #1	@ Initial Springline of Pipeline #2	@ Initial Springline of Pipeline #3	@ Initial Springline of Pipeline #4
1	37	37	37	37
2	274	274	274	274
3	268	268	268	268
4	322	322	322	322
5	31	31	31	31
6	40	40	40	40
7	353	353	353	353
8*	263	263	263	263

* - Test conducted at 1g

Table H.3 - Pipeline Test Details for Test 07

Pipeline No.	Trench Width (mm)	Cover Depth (mm)	X:Y Coordinates of Pipe Centre (mm)	Pipeline Velocity (mm/sec)	Time Tested (hrs)
1	50	16	290 : 520.5	0.00071	1509
2	50	16	650 : 520.5	0.0053	1508
3	50	16	650 : 659.5	0.0481	1507
4	50	16	290 : 659.5	0.4292	1441

Table H.4 - Prototype Test Geometries for Test 07

Pipeline	Distance to Trench Wall in the Direction of Travel (m)	Distance to Trench Wall Towards the Rear of the Pipeline (m)	Distance to a Stiff Retaining Wall in the Direction of Travel (m)	Distance to the Pipeline in the Direction Opposite to Travel (m)	Distance Laterally to a Stiff Retaining Wall (m)	Distance Laterally to the Edge of the Adjacent Pipeline (m)	Distance From Base of Pipeline to Rigid Base, i.e. Bedrock (m)	Water Level Above Rigid Base, i.e. Bedrock (m)	Water Level Below Base of Pipeline (m)
1	0.775	0.775	14.175	7.55	7.5	5.0	5.025	3.8	1.225
2	0.775	0.775	14.175	7.55	7.5	5.0	5.025	3.8	1.225
3	0.775	0.775	14.175	7.55	7.5	5.0	5.025	3.8	1.225
4	0.775	0.775	14.175	7.55	7.5	5.0	5.025	3.8	1.225

Table H.5 - Calculation of Undrained Shear Strength for Test 07

Pipeline	Soil Type	Cone Tests Used to Derive q_c	Interpreted Cone Tip Resistance at Springline, q_c (kPa)	Saturated Bulk Density, γ_{sat} (kN/m^3)	Pore Pressure at Springline, u (kPa)	Depth to Springline, h (m)	Cone Factor, N_c or N_k*	Undrained Shear Strength, c_u (kPa)
1	Native	3,4,7	361.4	939.7	-8.5	0.0255	7.7/11.9	28.2 - 43.6
1	Backfill	1,5,6	35.8	901.2	---	0.0255	15	2.4
2	Native	3,4,7	361.4	939.7	-8.5	0.0255	7.7/11.9	28.2 - 43.6
2	Backfill	1,5,6	35.8	901.2	---	0.0255	15	2.4
3	Native	3,4	339.4	939.7	-8.5	0.0255	7.7/11.9	26.4 - 40.8
3	Backfill	1,5	33.9	901.2	---	0.0255	15	2.3
4	Native	2,3	311.8	939.7	-8.5	0.0255	7.7/11.9	24.0 - 37.2
4	Backfill	1	36.8	901.2	---	0.0255	15	2.5

Notes: * - N_c range of values correspond to native material; N_k values correspond to backfill.

Table H.6 - Summary of Prototype Pipeline Data; Test 07

Pipeline →	Pipeline #1	Pipeline #2	Pipeline #3	Pipeline #4
Trench Width	2.5m	2.5m	2.5m	2.5m
Cover Depth	0.80m	0.80m	0.80m	0.80m
Embedment Ratio, H/D	1.842	1.842	1.842	1.842
Average Backfill Undrained Shear Strength @ Springline	2.4kPa	2.4kPa	2.3kPa	2.5kPa
Average Native Undrained Shear Strength @ Springline	35.9kPa	35.9kPa	33.6kPa	30.6kPa
Ultimate Normalized Resistance, N	5.693* 4.842**	5.574 4.947**	4.211	4.221
Distance into Trench Wall to Ultimate Normalized Resistance	1.455D* 0.820D**	1.331D 0.926D**	1.317D	1.606D
Slope to Ultimate Normalized Resistance	2.507	2.596	1.974	1.743
Normalized Resistance at Trench Wall	2.951	2.262***	1.393	1.434
Normalized Resistance at 0.5D Penetration	4.180	3.902	3.402	2.992
Normalized Resistance at 1D Penetration	5.164	5.180	4.098	3.730
Slope of Interaction Between TW and Breakover	5.268	5.483***	5.631	3.511
Normalized Resistance at Breakover	3.492	3.377***	3.012	2.848
Distance into Trench Wall to Breakover	0.094D	0.209D***	0.285D	0.395D
Slope of Interaction After Breakover	1.812	2.180	1.608	1.389

Notes: * - Values taken essentially at the end of pipeline pull; not necessarily a peak.
** - Corresponds to the point where the force-displacement curves became linear.
*** - Estimated value as normalized force-displacement curve is discontinuous.

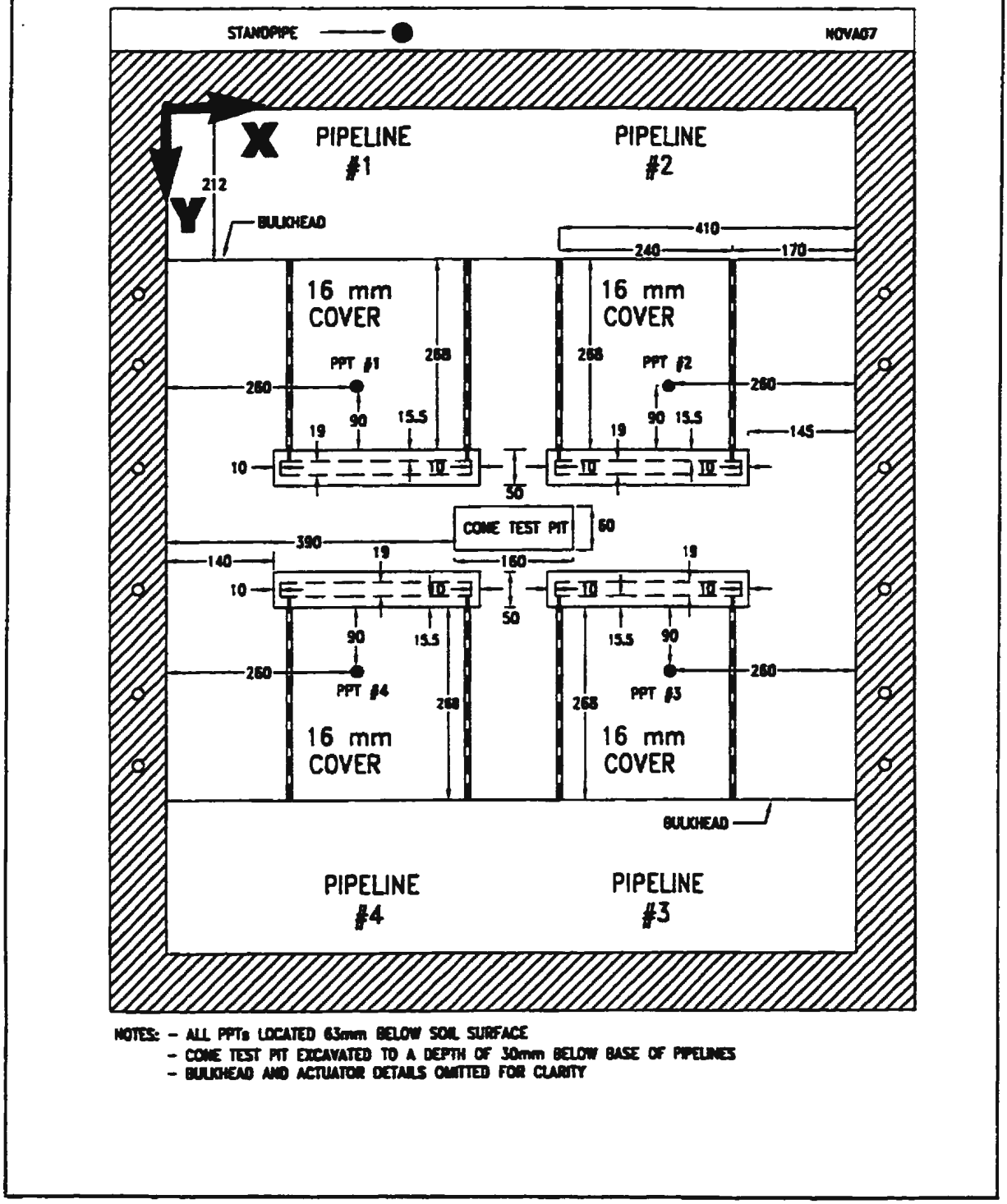

Figure H.1 - *Model Test Geometry, Test 07.*

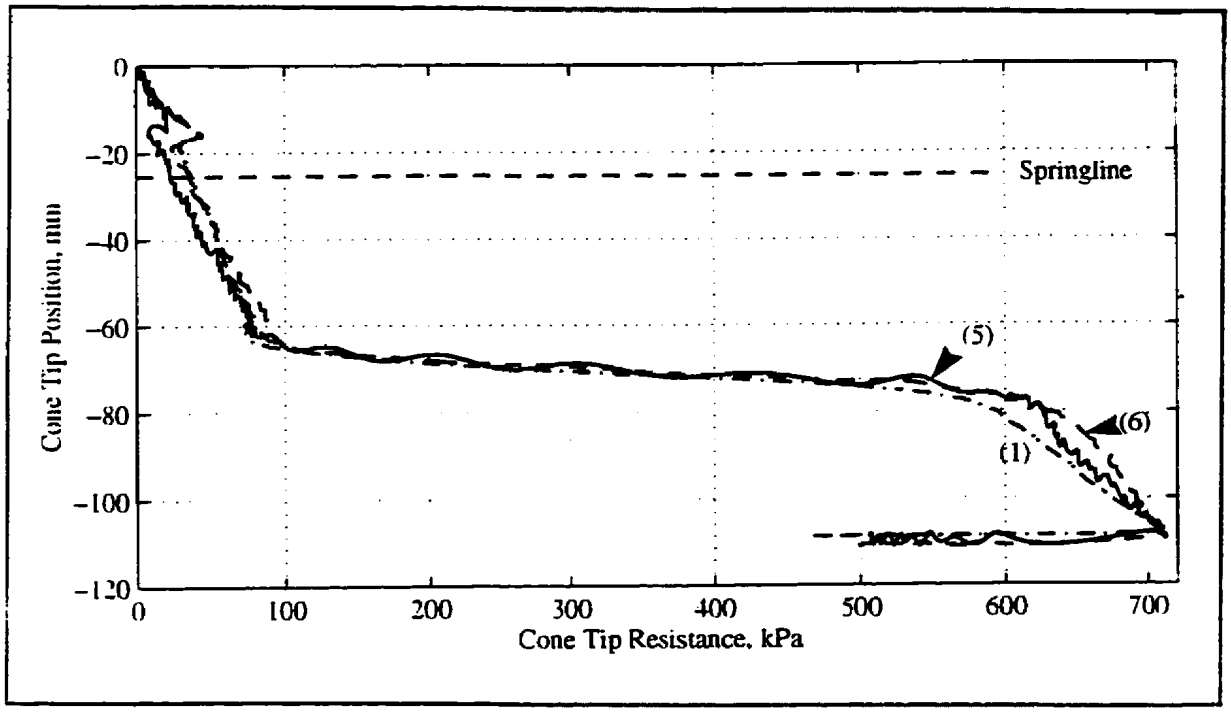

Figure H.2 - *All cone penetration tests, backfill material, Test 07.*

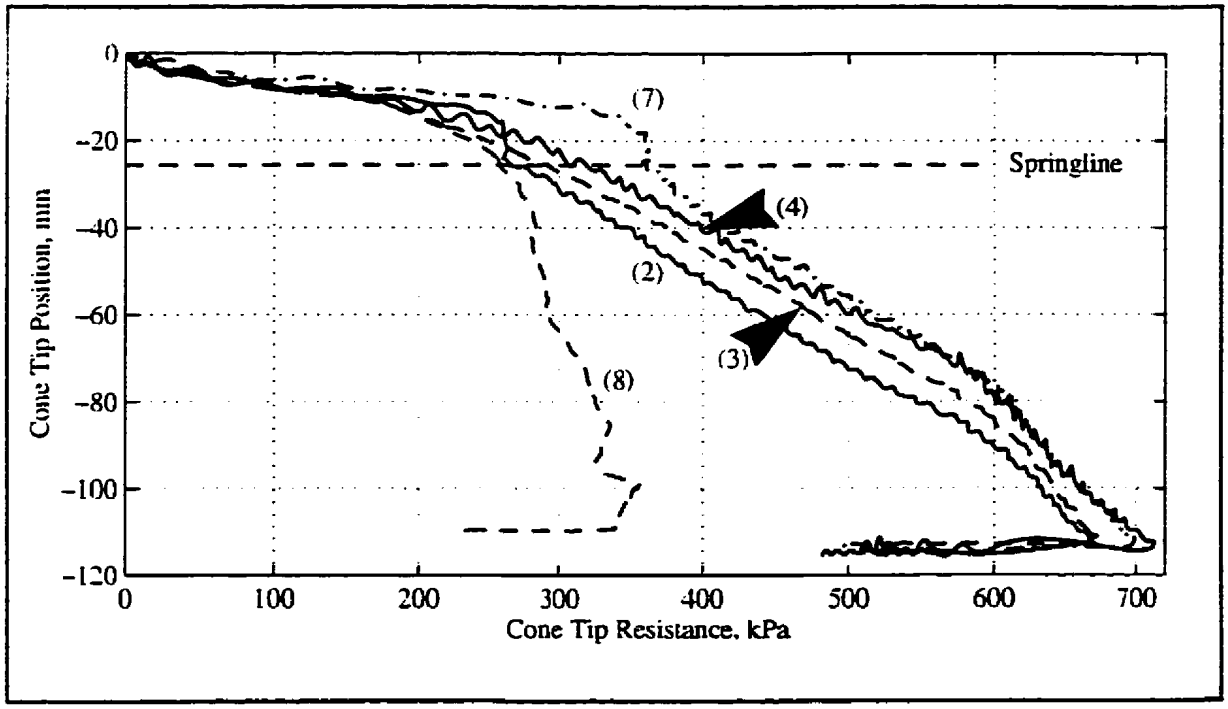

Figure H.3 - *All cone penetration tests, native material, Test 07.*

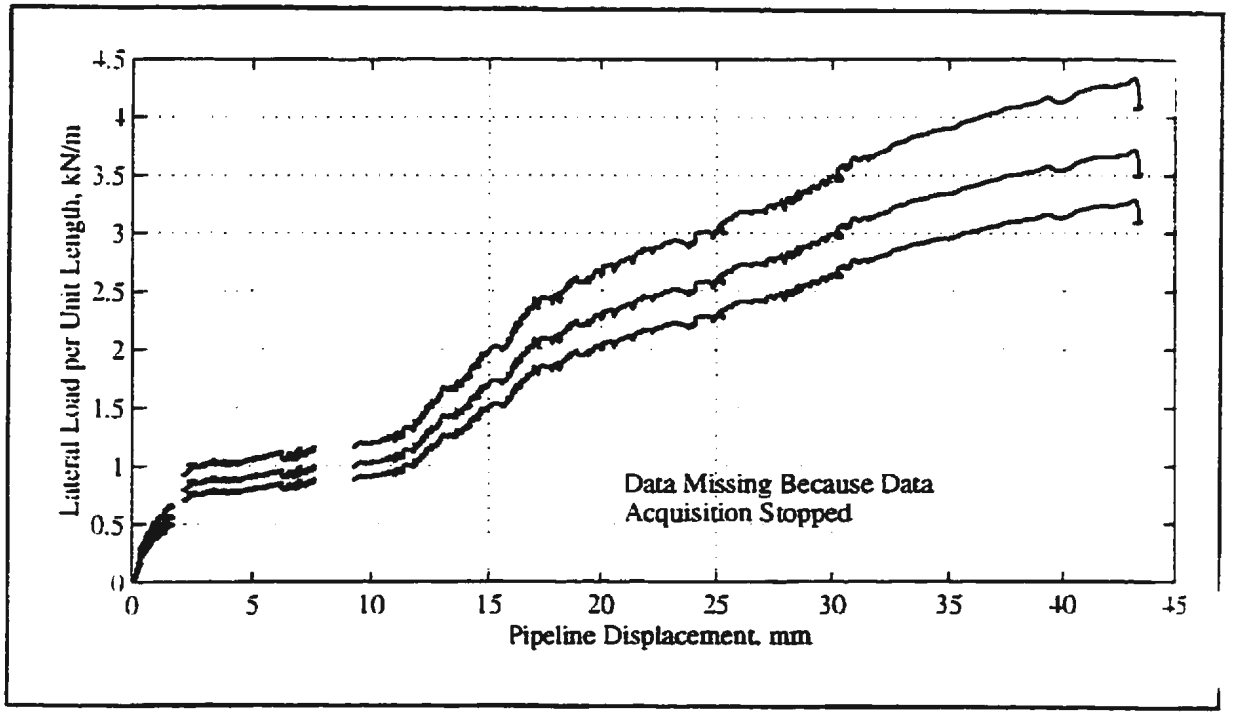

Figure H.4 - *Force-displacement response, model pipeline #1, 0.00071mm/sec, Test 07.*

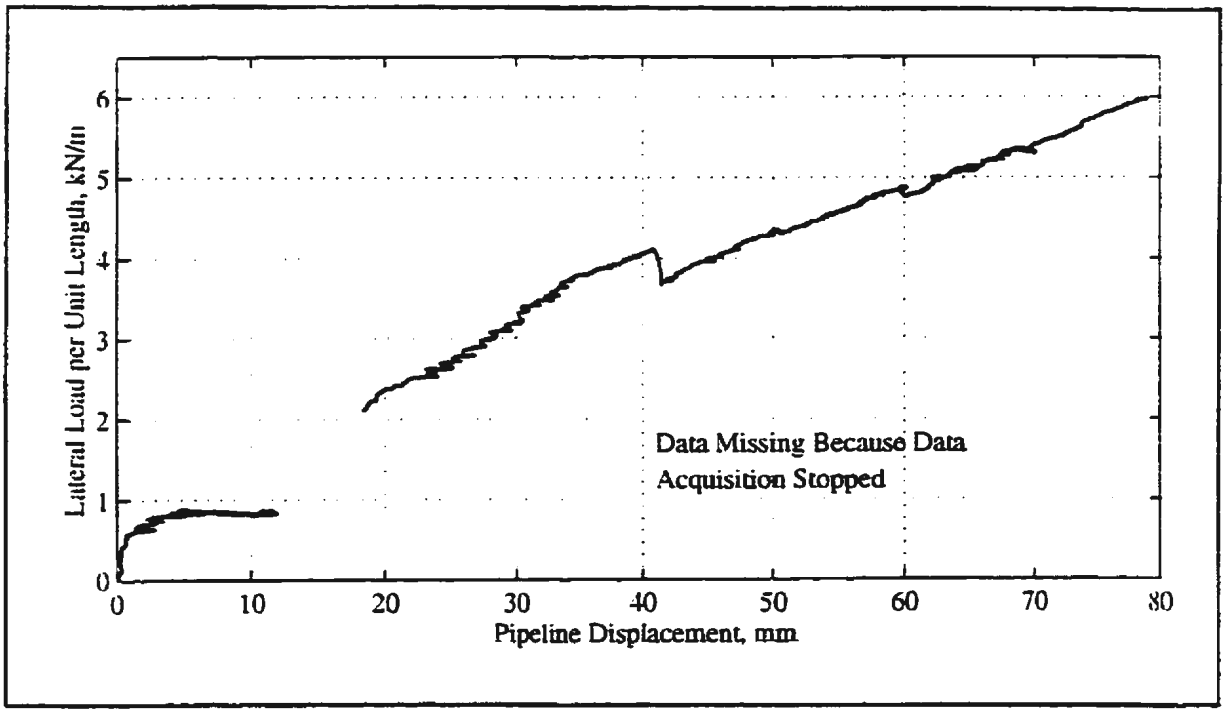

Figure H.5 - *Force-displacement response, model pipeline #2, 0.0053mm/sec, Test 07.*

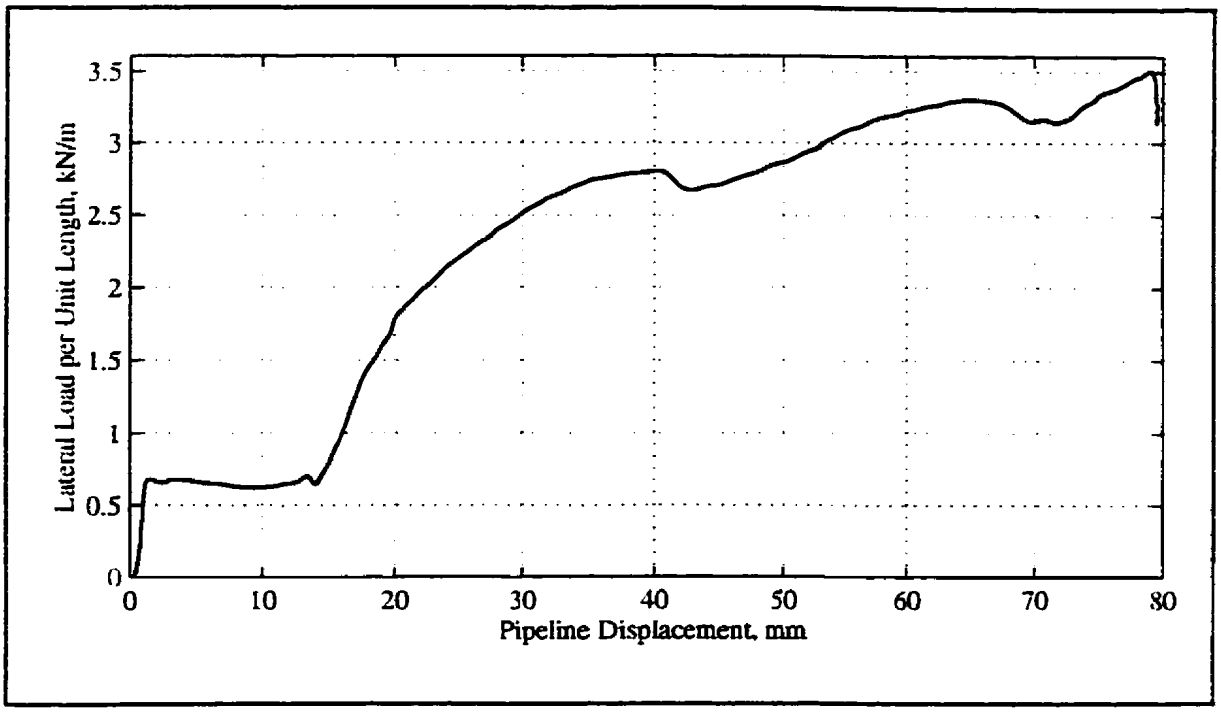

Figure H.6 - *Force-displacement response, model pipeline #3, 0.0481mm/sec, Test 07.*

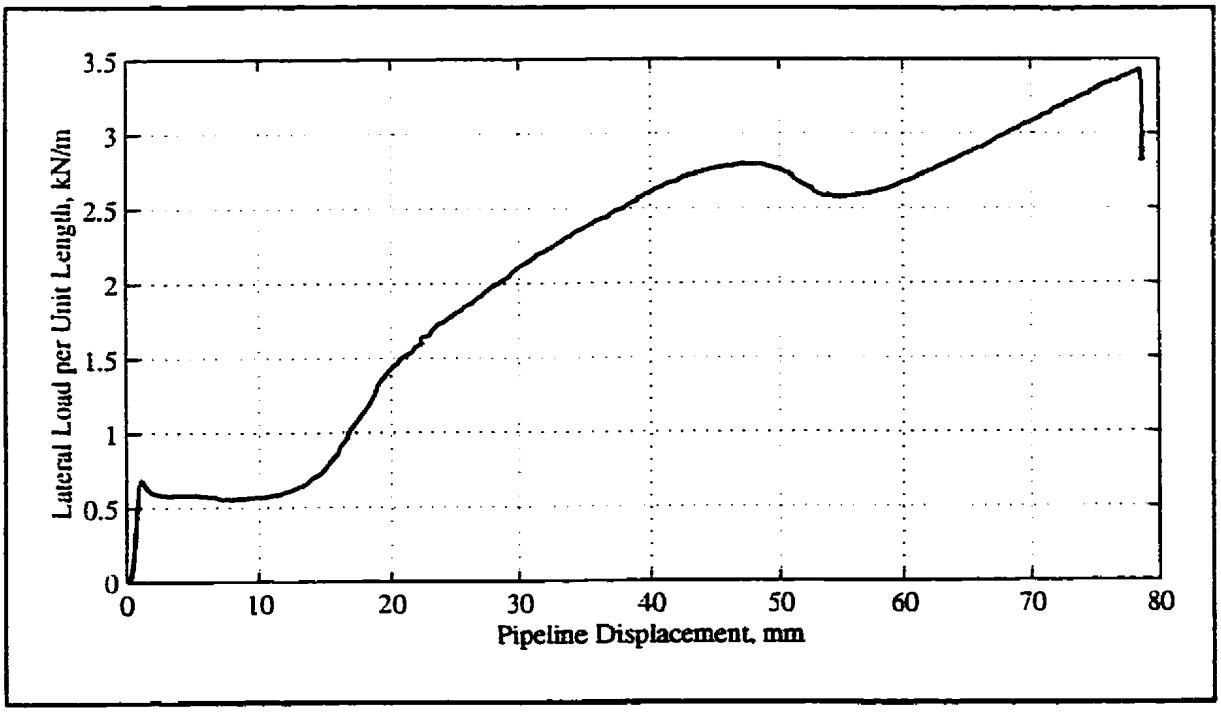

Figure H.7 - *Force-displacement response, model pipeline #4, 0.4292mm/sec, Test 07.*

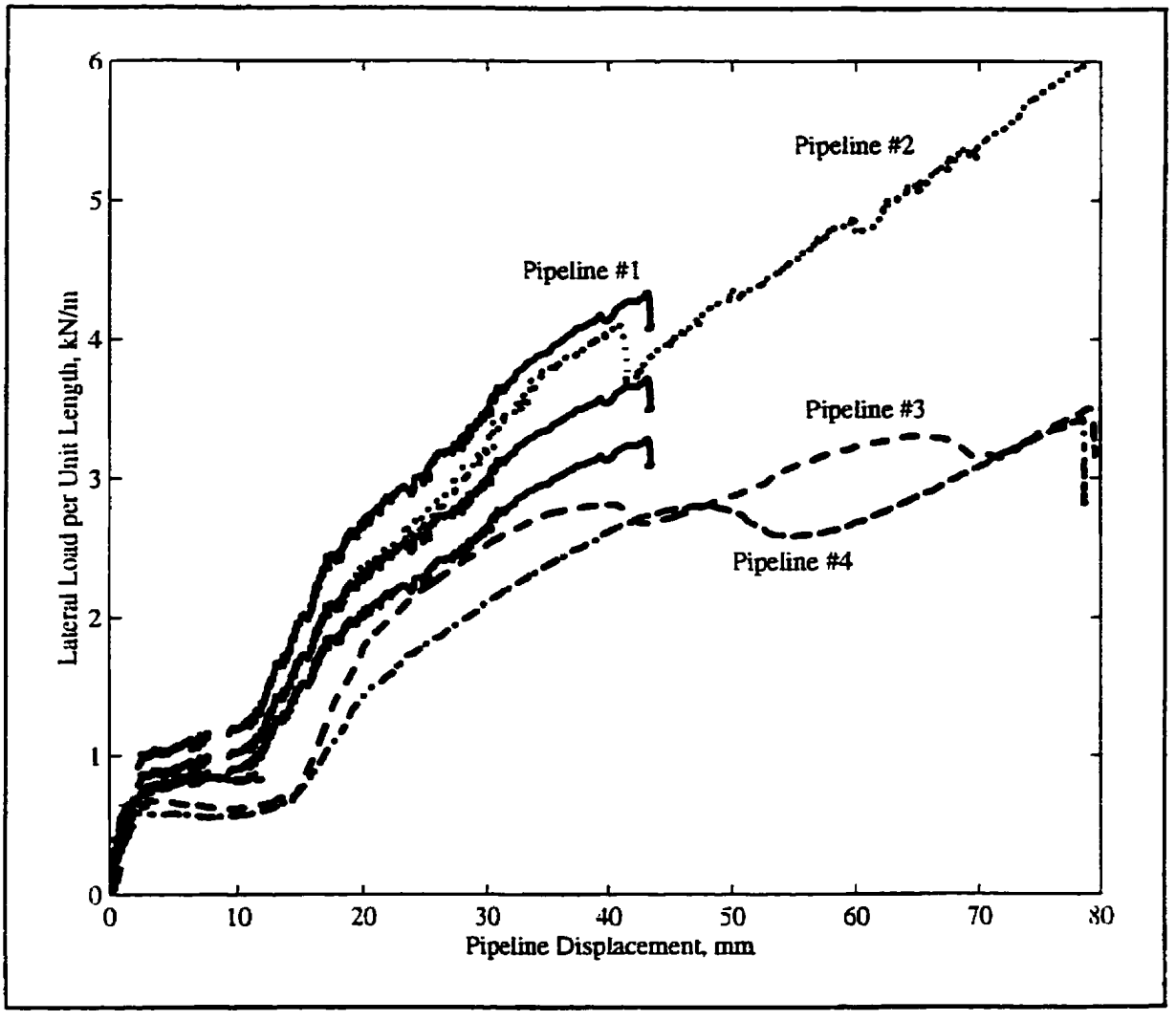

Figure H.8 - Force-displacement response, all model pipelines, Test 07.

Figure H.9 - *Photo of excavated cross-section along mid length of model pipeline #1, 0.00071mm/sec, Test 07.*

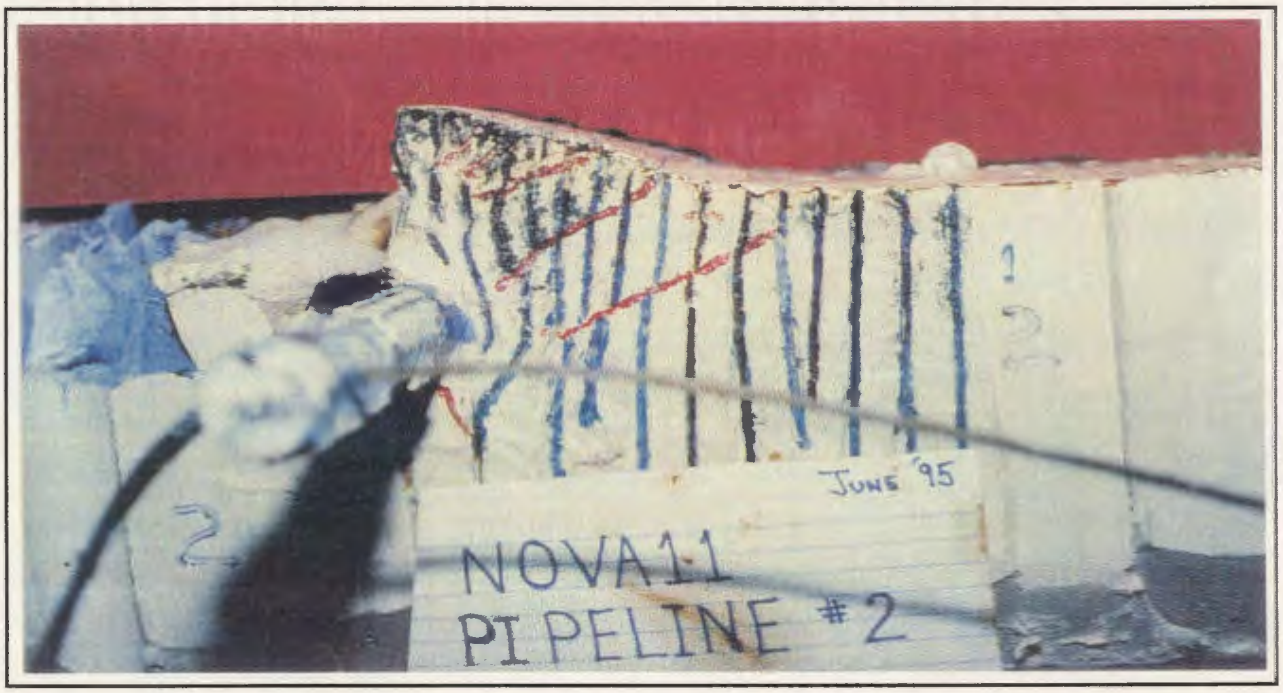

Figure H.10 - *Photo of excavated cross-section along mid length of model pipeline #2, 0.0053mm/sec, Test 07.*

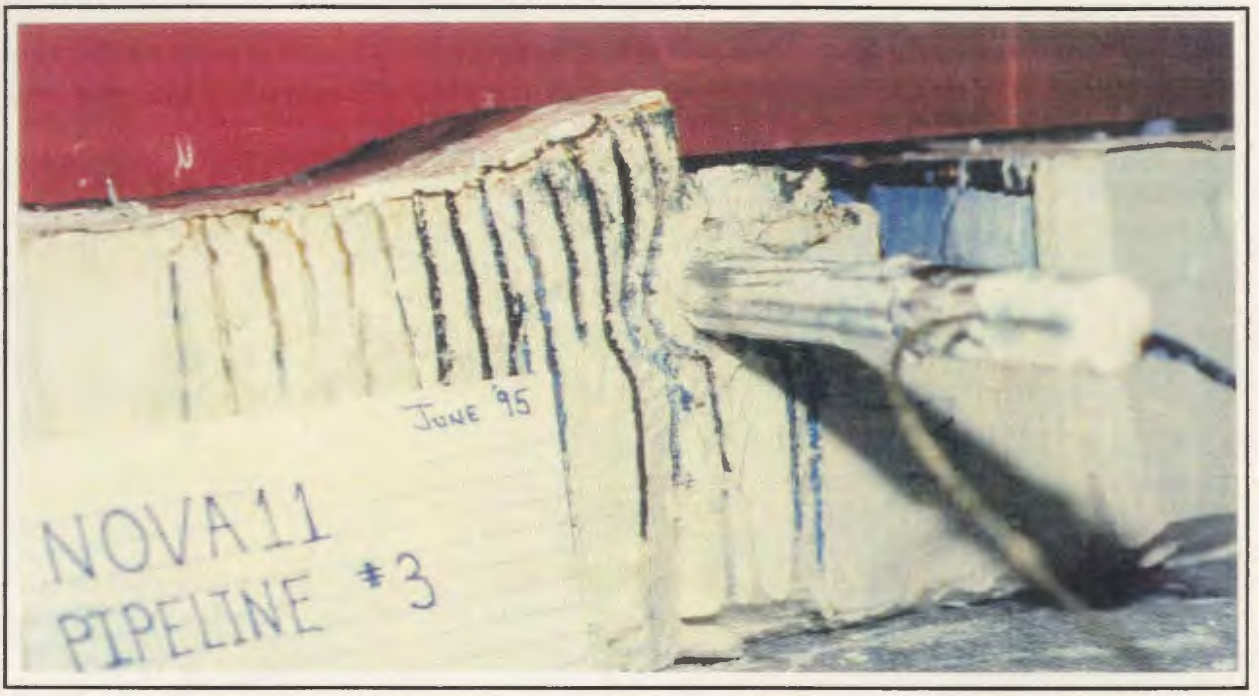

Figure H.11 - *Photo of excavated cross-section along mid length of model pipeline #3, 0.0481mm/sec, Test 07.*

Figure H.12 - *Photo of excavated cross-section along mid length of model pipeline #4, 0.4292mm/sec, Test 07.*

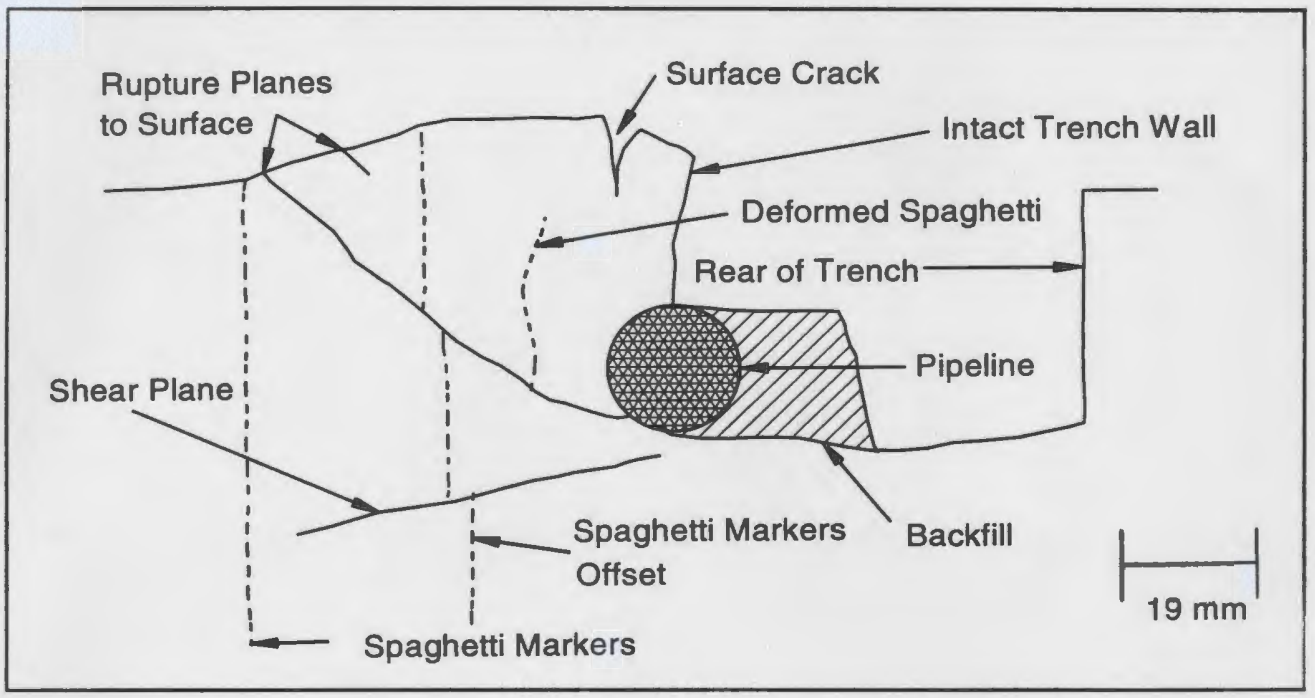

Figure H.13 - *Sketch of excavated cross-section along mid length of model pipeline #1, 0.00071mm/sec, Test 07.*

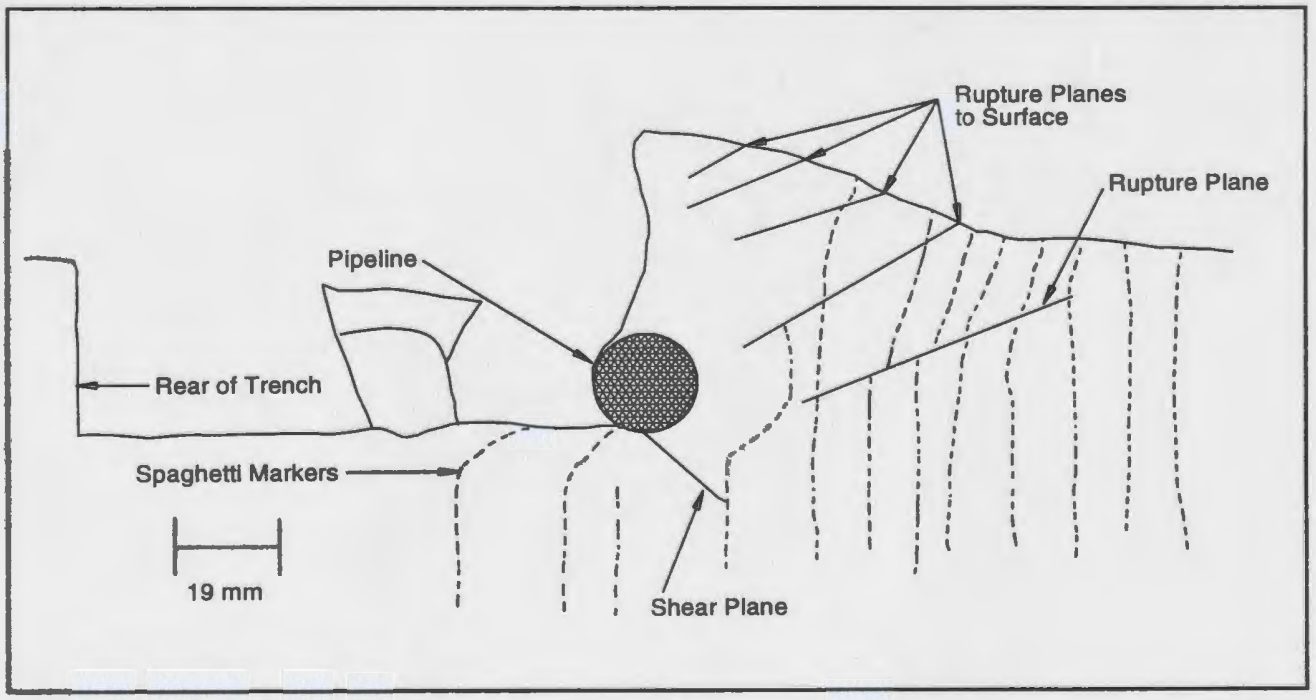

Figure H.14 - *Sketch of excavated cross-section along mid length of model pipeline #2, 0.0053mm/sec, Test 07.*

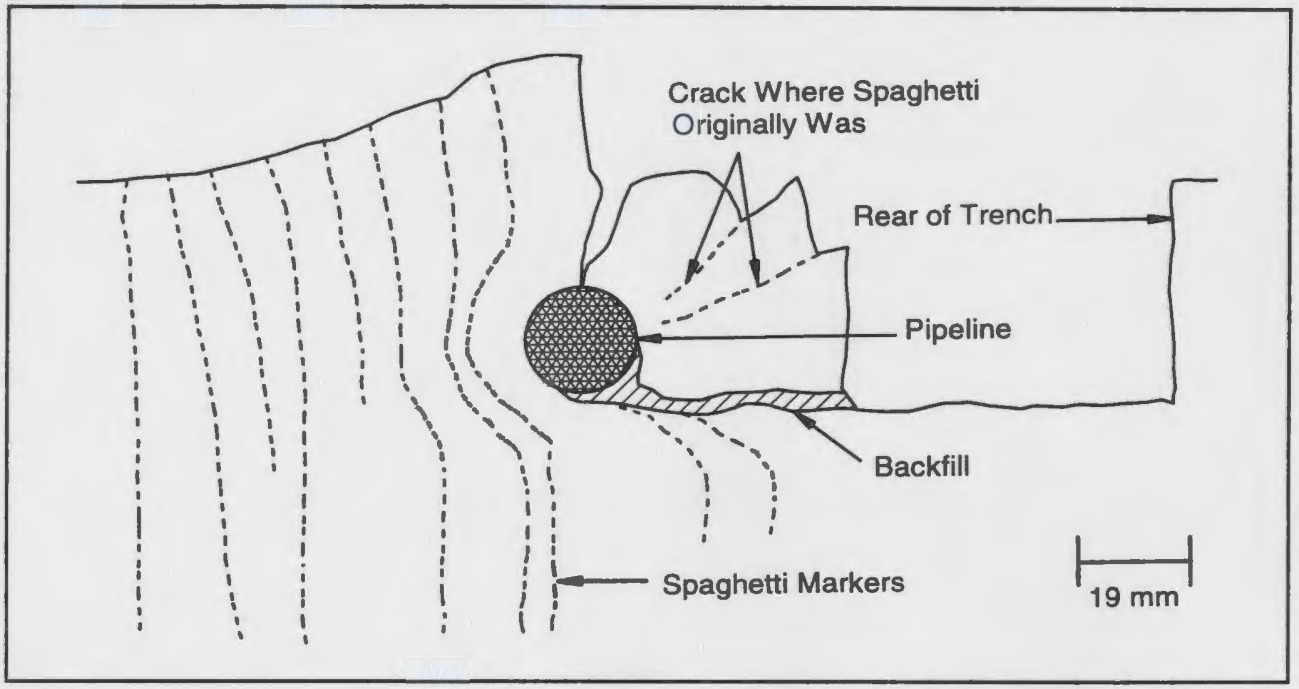

Figure H.15 - *Sketch of excavated cross-section along mid length of model pipeline #3, 0.0481mm/sec, Test 07.*

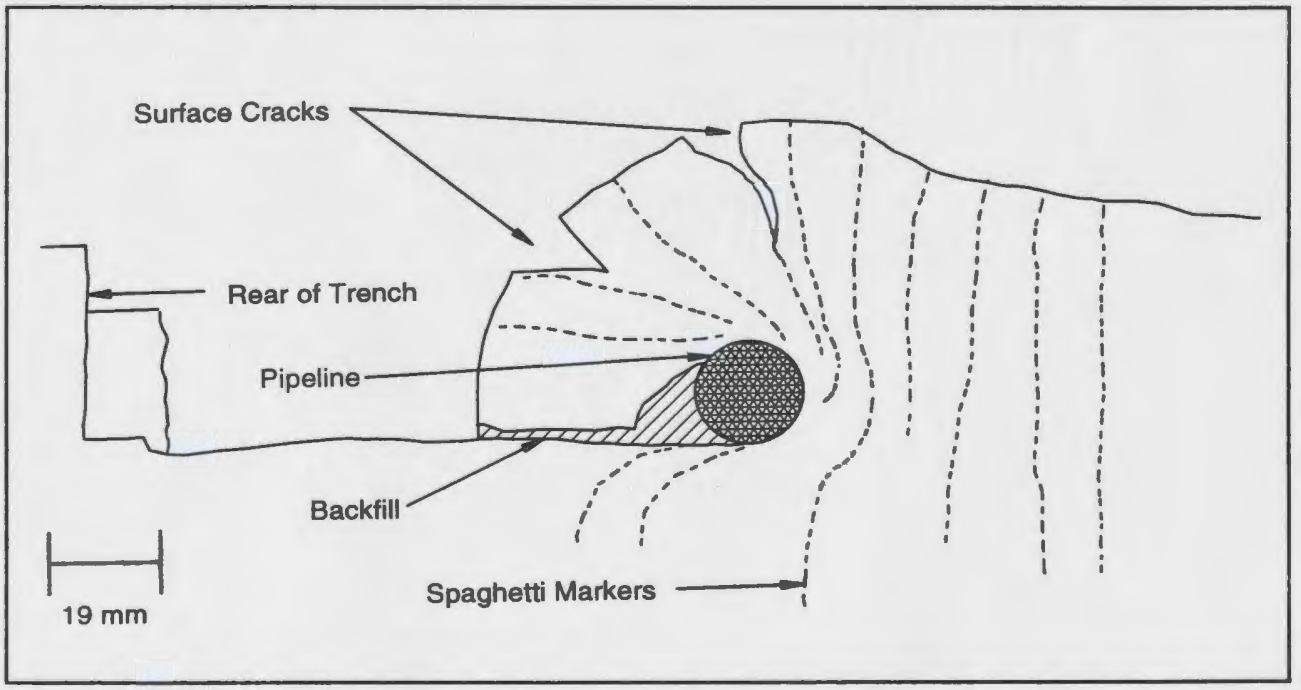

Figure H.16 - *Sketch of excavated cross-section along mid length of model pipeline #4, 0.4292mm/sec, Test 07.*

Appendix I

Test 08 - Selected Test Data

Table I.1 - Cone Penetration Test Details for Test 08

CPT No.	X[1] (mm)	Y[1] (mm)	Backfill or Native	Time Tested (hrs)
1	470	590	Backfill	1303
2	343	590	Native	1312
3	605	590	Native	1339
4	295	590	Native	1446
5	510	590	Backfill	1453
6	652	590	Native	2006
7	430	590	Backfill	2012
8	235	590	Native	1257

Notes: 1 - Coordinate convention shown on Figure I.1.

Table I.2 - Interpreted Cone Penetration Resistances for Test 08

Cone Test No.	Interpreted Penetration Resistance (kPa)			
	@ Initial Springline of Pipeline #1	@ Initial Springline of Pipeline #2	@ Initial Springline of Pipeline #3	@ Initial Springline of Pipeline #4
1	26	26	26	26
2	160	160	160	160
3	190	190	190	190
4	202	202	202	202
5	36	36	36	36
6	221	221	221	221
7	35	35	35	35
8	241	241	241	241

Table I.3 - Pipeline Test Details for Test 08

Pipeline No.	Trench Width (mm)	Cover Depth (mm)	X:Y Coordinates of Pipe Centre (mm)	Pipeline Velocity (mm/sec)	Time Tested (hrs)
1	50	16	290 : 520.5	0.00055	1400
2	50	16	650 : 520.5	0.0053	1400
3	50	16	650 : 659.5	0.0480	1400
4	50	16	290 : 659.5	0.4336	1322

Table I.4 - Prototype Test Geometries for Test 08

Pipeline	Distance to Trench Wall in the Direction of Travel (m)	Distance to Trench Wall Towards the Rear of the Pipeline (m)	Distance to a Stiff Retaining Wall in the Direction of Travel (m)	Distance to the Pipeline in the Direction Opposite to Travel (m)	Distance Laterally to a Stiff Retaining Wall (m)	Distance Laterally to the Edge of the Adjacent Pipeline (m)	Distance From Base of Pipeline to Rigid Base, i.e. Bedrock (m)	Water Level Above Rigid Base, i.e. Bedrock (m)	Water Level Below Base of Pipeline (m)
1	0.775	0.775	14.175	7.55	7.5	5.0	5.025	3.4	1.625
2	0.775	0.775	14.175	7.55	7.5	5.0	5.025	3.4	1.625
3	0.775	0.775	14.175	7.55	7.5	5.0	5.025	3.4	1.625
4	0.775	0.775	14.175	7.55	7.5	5.0	5.025	3.4	1.625

Table I.5 - Calculation of Undrained Shear Strength for Test 08

Pipeline	Soil Type	Cone Tests Used to Derive q_c	Interpreted Cone Tip Resistance at Springline, q_c (kPa)	Saturated Bulk Density, γ_{sat} (kN/m^3)	Pore Pressure at Springline, u (kPa)	Depth to Springline, h (m)	Cone Factor, N_c or N_k*	Undrained Shear Strength, c_u (kPa)
1	Native	3,4,6,8	245.8	917.7	-14.6	0.0255	8.7/10.0	22.3 - 25.5
1	Backfill	1,5,7	32.2	895.2	---	0.0255	15	2.1
2	Native	3,4,6	235.2	917.7	-14.6	0.0255	8.7/10.0	21.2 - 24.3
2	Backfill	1,5,7	32.2	895.2	---	0.0255	15	2.1
3	Native	3,4	225.7	917.7	-14.6	0.0255	8.7/10	20.2 - 23.2
3	Backfill	1,5	30.9	895.2	---	0.0255	15	2.1
4	Native	2,3	201.4	917.7	-14.6	0.0255	8.7/10.0	17.8 - 20.4
4	Backfill	1	25.6	895.2	---	0.0255	15	1.7

Notes: * - N_c range of values correspond to native material; N_k values correspond to backfill.

Table I.6 - Summary of Prototype Pipeline Data; Test 08

Pipeline →	Pipeline #1	Pipeline #2	Pipeline #3	Pipeline #4
Trench Width	2.5m	2.5m	2.5m	2.5m
Cover Depth	0.80m	0.80m	0.80m	0.80m
Embedment Ratio, H/D	1.842	1.842	1.842	1.842
Average Backfill Undrained Shear Strength @ Springline	2.1kPa	2.1kPa	2.1kPa	1.7kPa
Average Native Undrained Shear Strength @ Springline	23.9kPa	22.8kPa	21.7kPa	19.1kPa
Ultimate Normalized Resistance, N	10.279* 7.971**	10.369* 6.521**	5.861	4.805
Distance into Trench Wall to Ultimate Normalized Resistance	1.780D* 0.835D**	2.616D* 0.943D**	1.386D	1.606D
Slope to Ultimate Normalized Resistance	3.960	3.147	2.662	1.984
Normalized Resistance at Trench Wall	3.832	3.697***	2.664	2.316
Normalized Resistance at 0.5D Penetration	6.605	5.500	5.008	3.770
Normalized Resistance at 1D Penetration	8.475	6.762	5.674	4.273
Slope of Interaction Between TW and Breakover	5.738	4.995***	7.937	4.405
Normalized Resistance at Breakover	7.777	5.477***	4.662	3.586
Distance into Trench Wall to Breakover	0.707D	0.361D***	0.257D	0.319D
Slope of Interaction After Breakover	2.317	1.915	1.372	1.032

Notes: * - Values taken essentially at the end of pipeline pull; not necessarily a peak.
** - Corresponds to the point where the force-displacement curves became linear.
*** - Estimated value as normalized force-displacement curve is discontinuous.

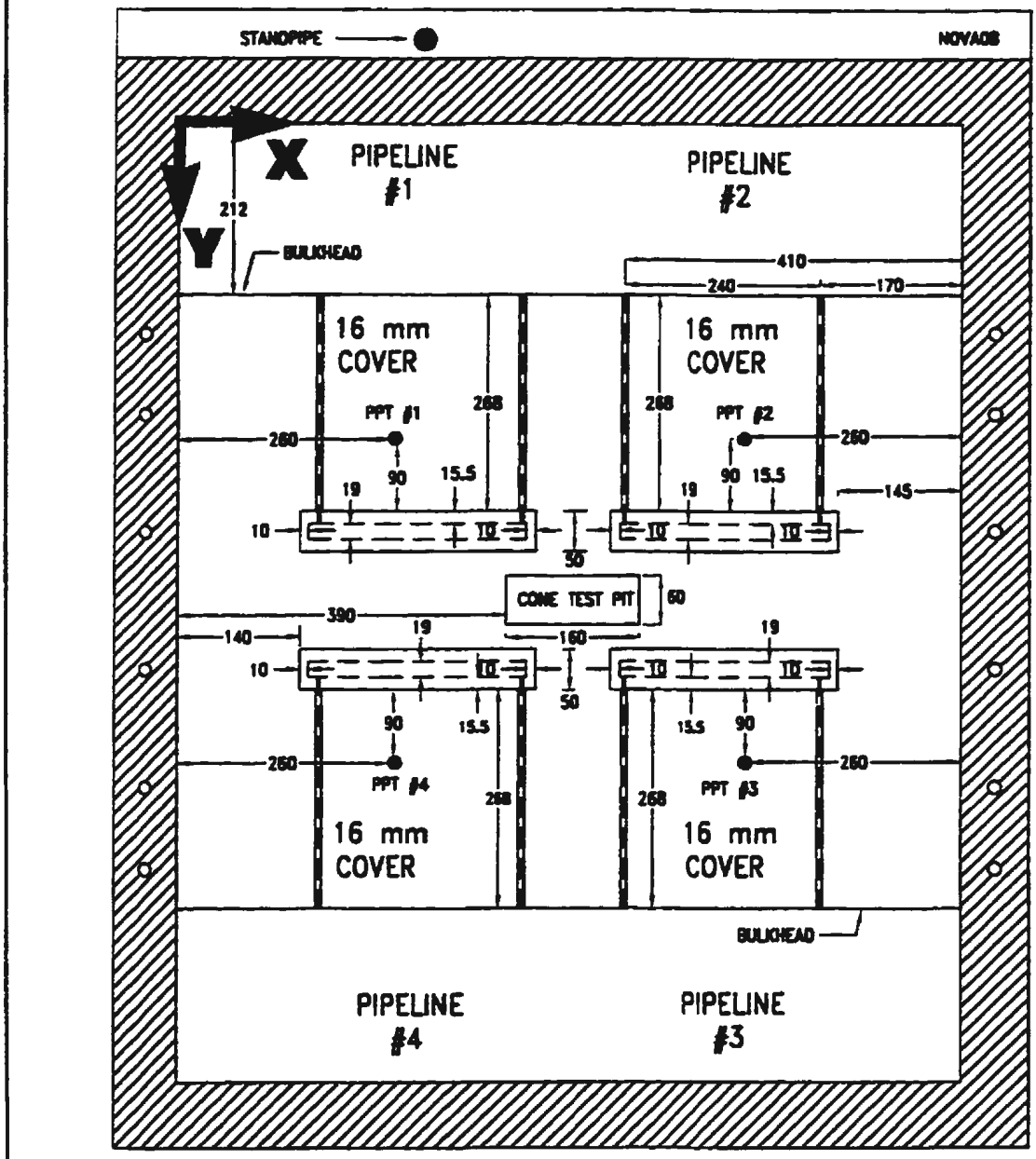

Figure I.1 - *Model Test Geometry, Test 08.*

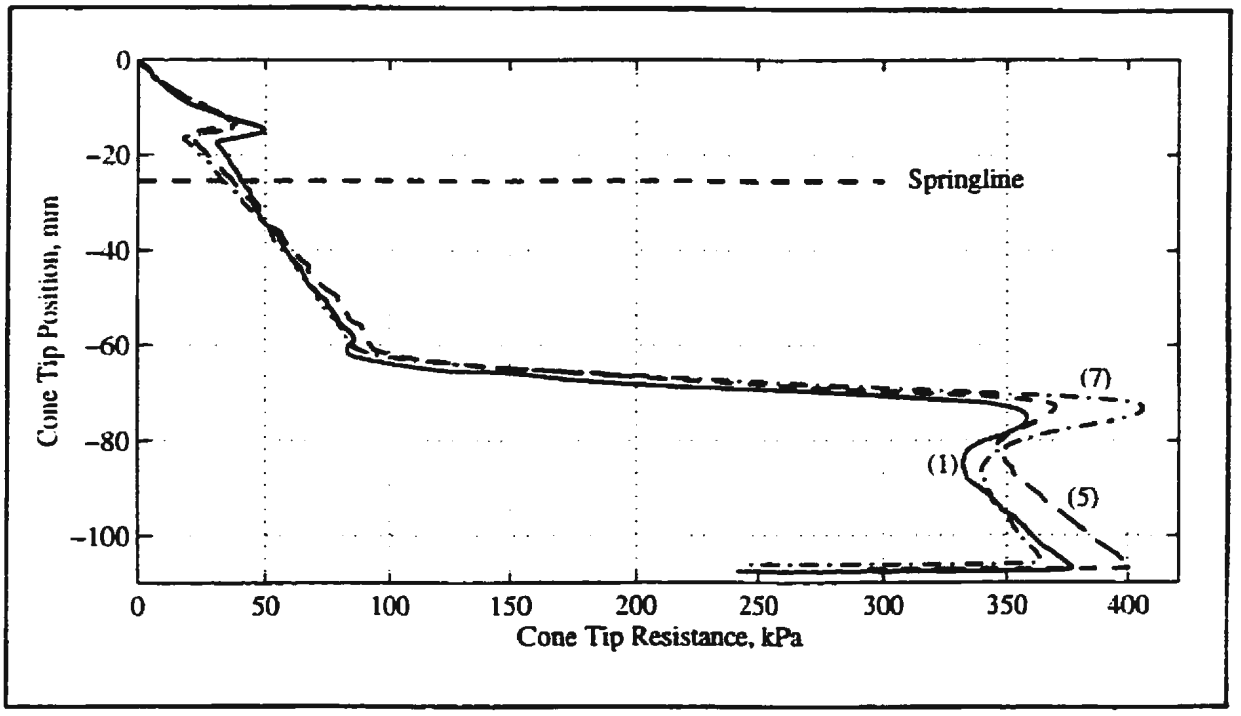

Figure I.2 - *All cone penetration tests, backfill material, Test 08.*

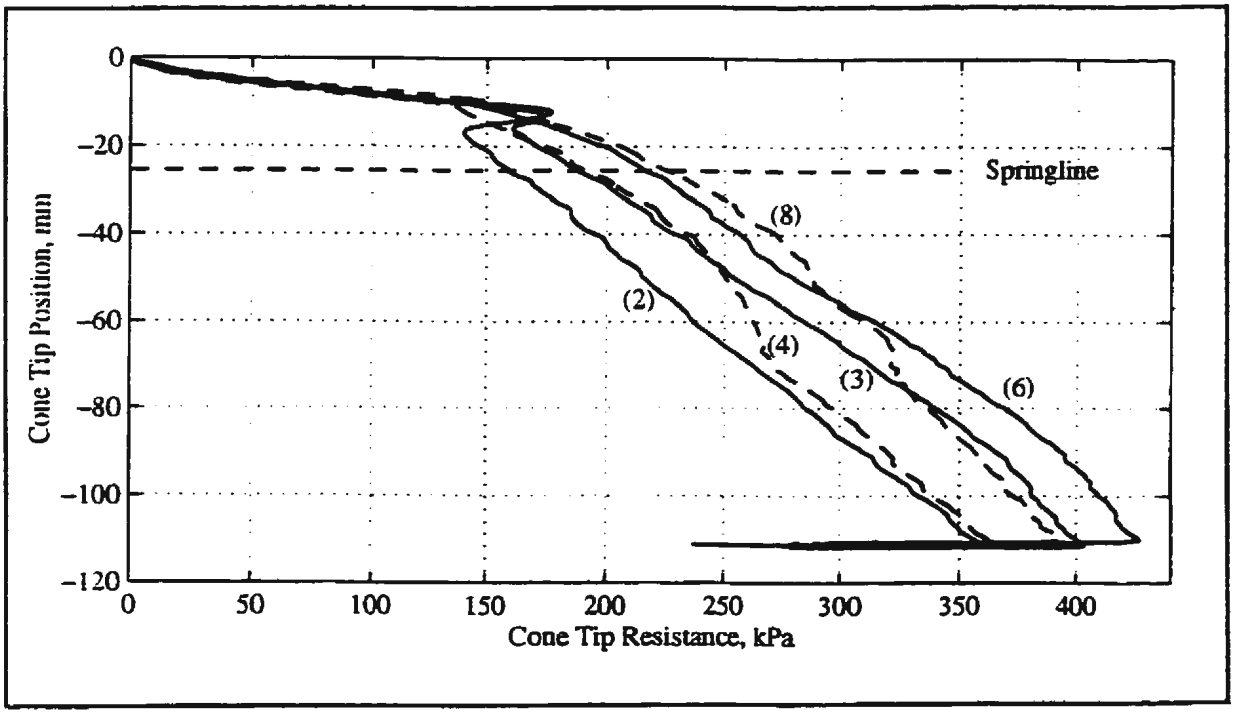

Figure I.3 - *All cone penetration tests, native material, Test 08.*

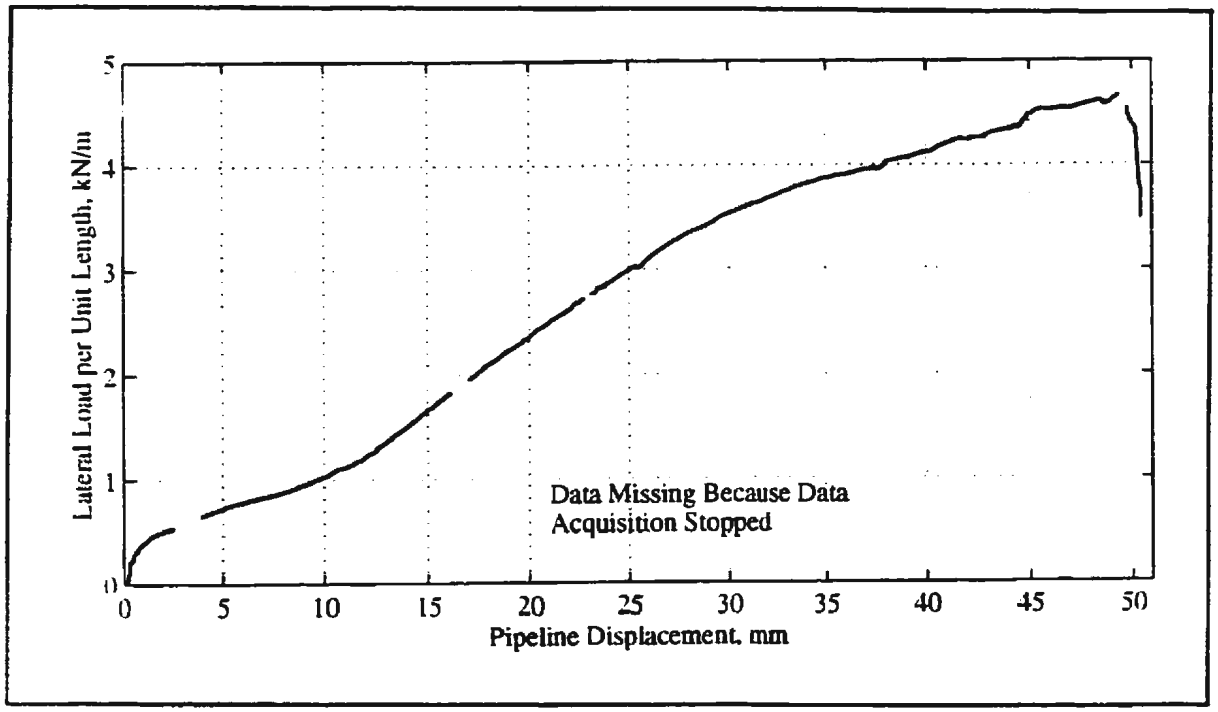

Figure I.4 - *Force-displacement response, model pipeline #1, 0.00055mm/sec, Test 08.*

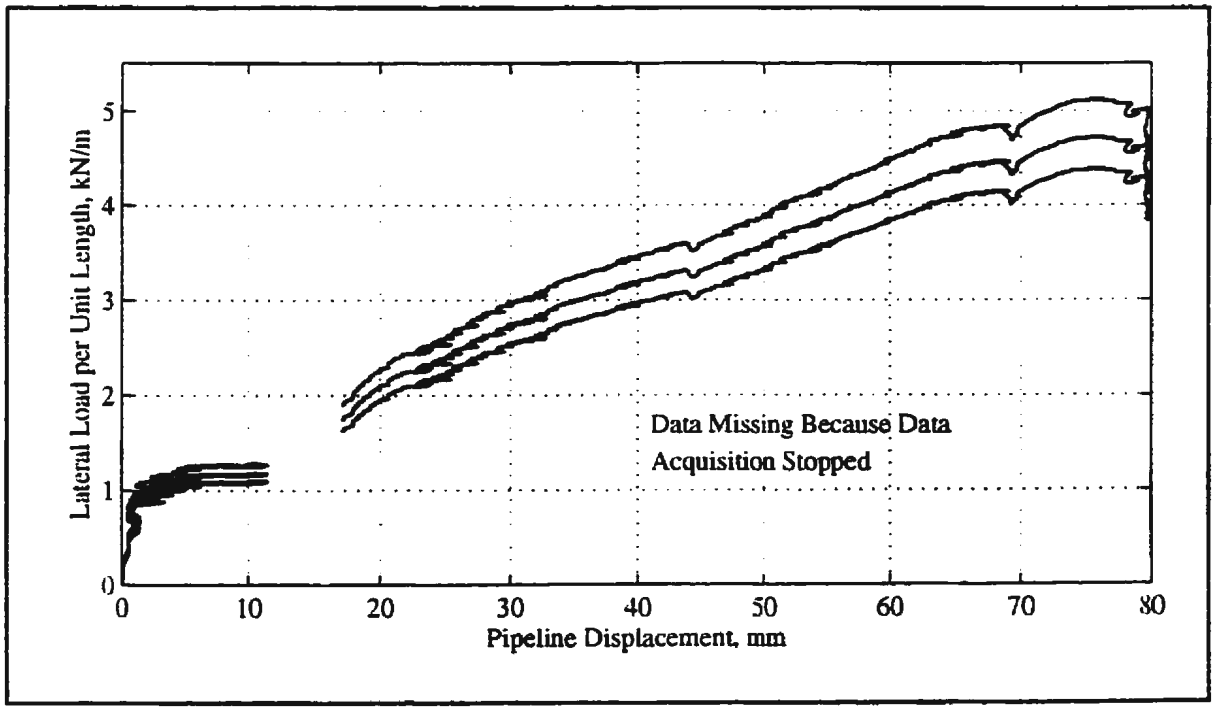

Figure I.5 - *Force-displacement response, model pipeline #2, 0.0053mm/sec, Test 08.*

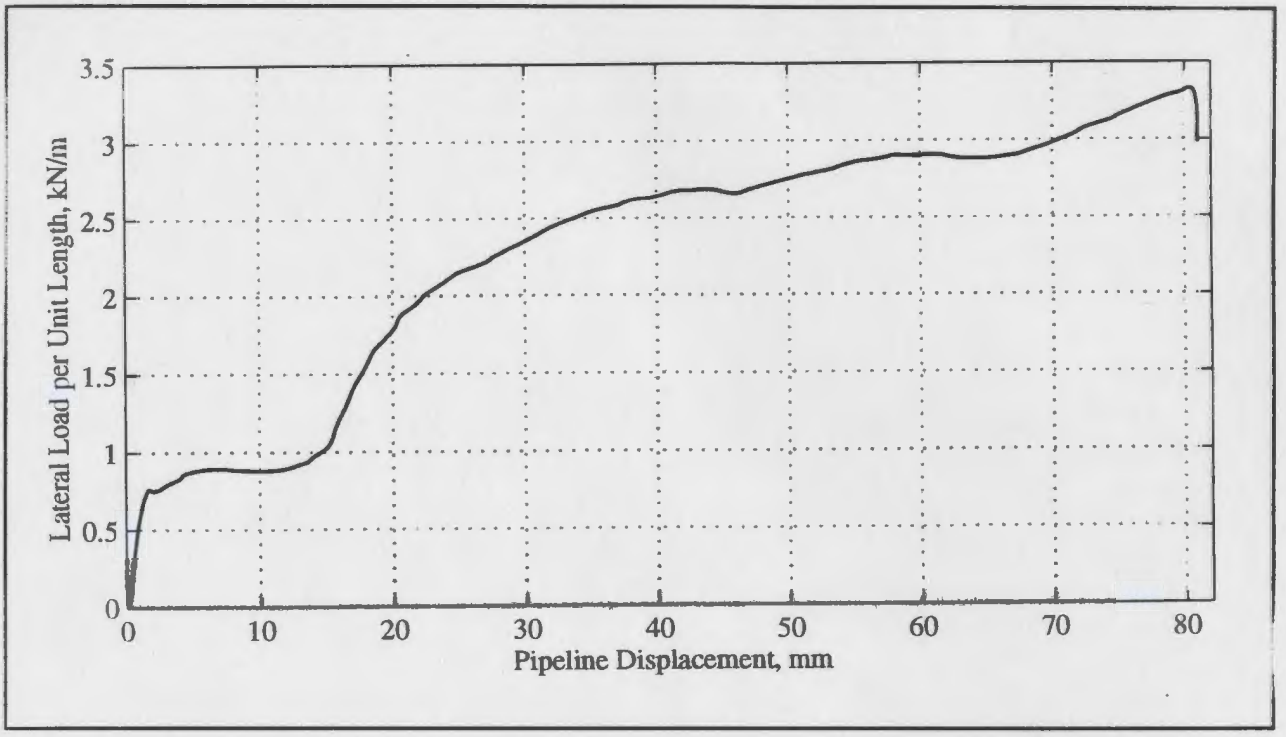

Figure I.6 - *Force-displacement response, model pipeline #3, 0.048mm/sec, Test 08.*

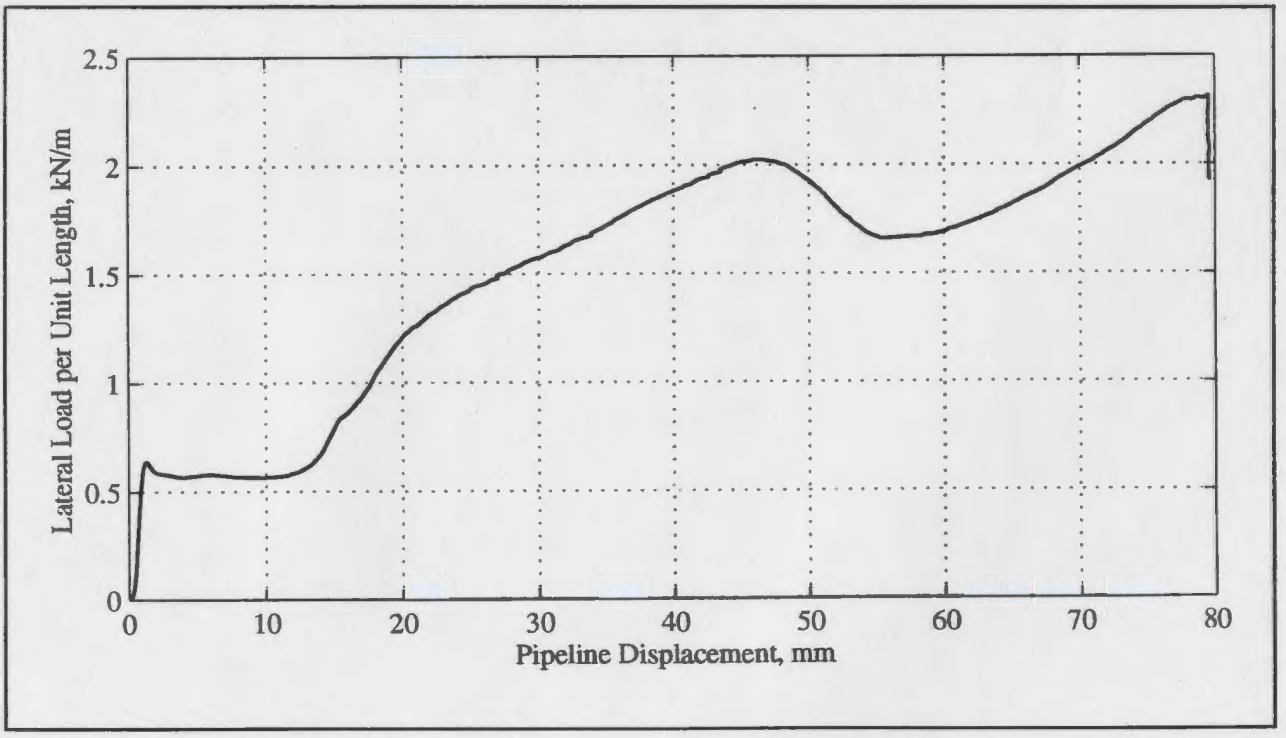

Figure I.7 - *Force-displacement response, model pipeline #4, 0.4336mm/sec, Test 08.*

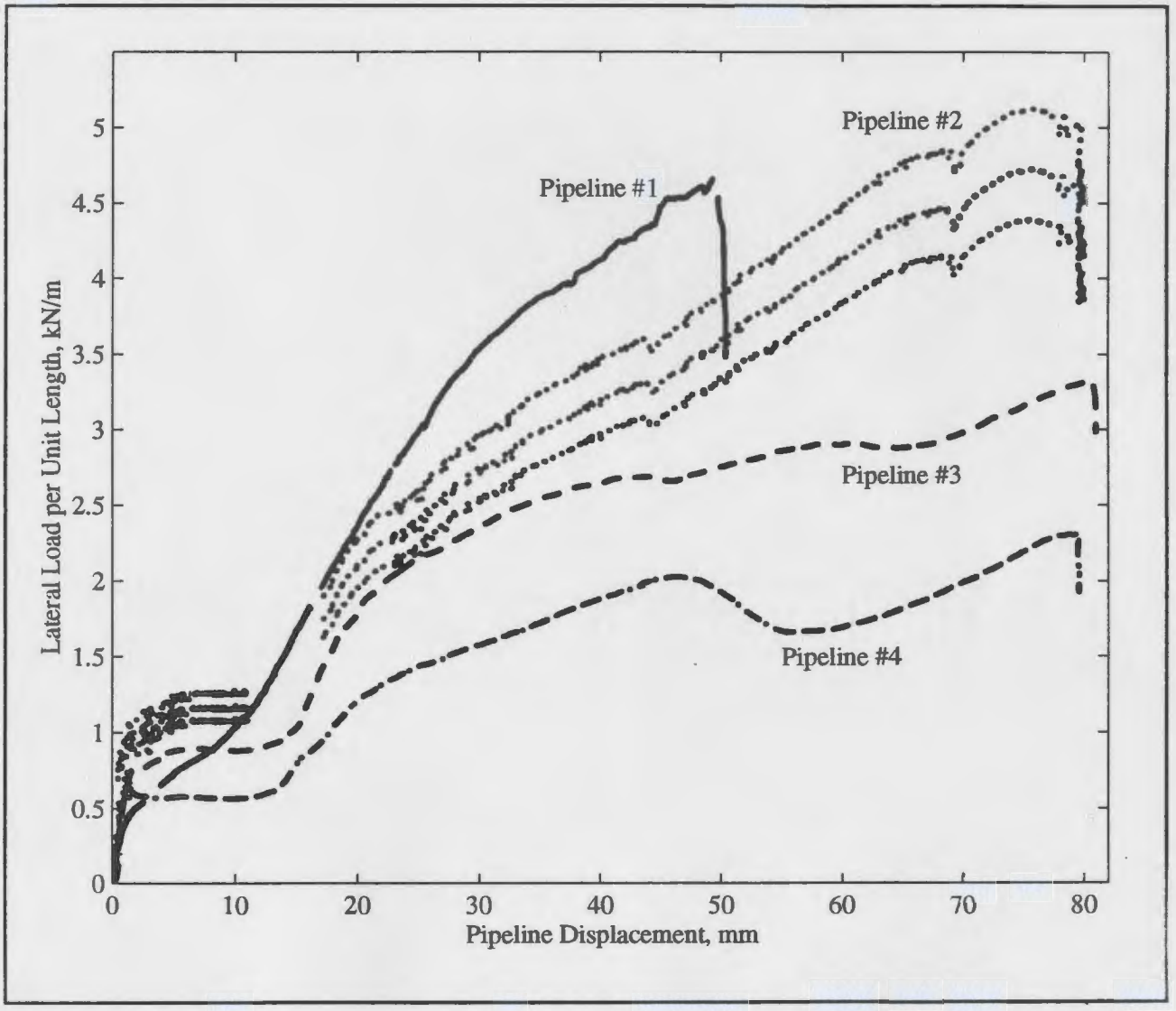

Figure I.8 - Force-displacement response, all model pipelines, Test 08.

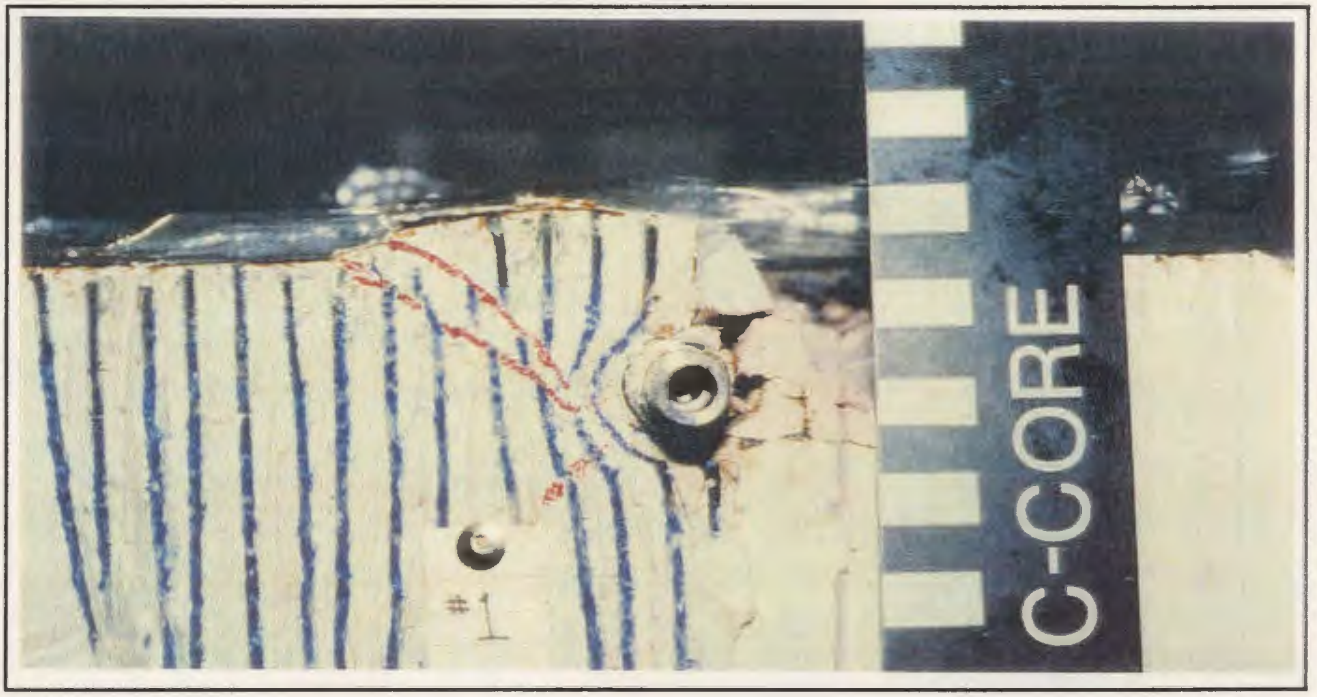

Figure I.9 - *Photo of excavated cross-section along mid length of model pipeline #1, 0.00055mm/sec, Test 08.*

Figure I.10 - *Photo of excavated cross-section along mid length of model pipeline #2, 0.0053mm/sec, Test 08.*

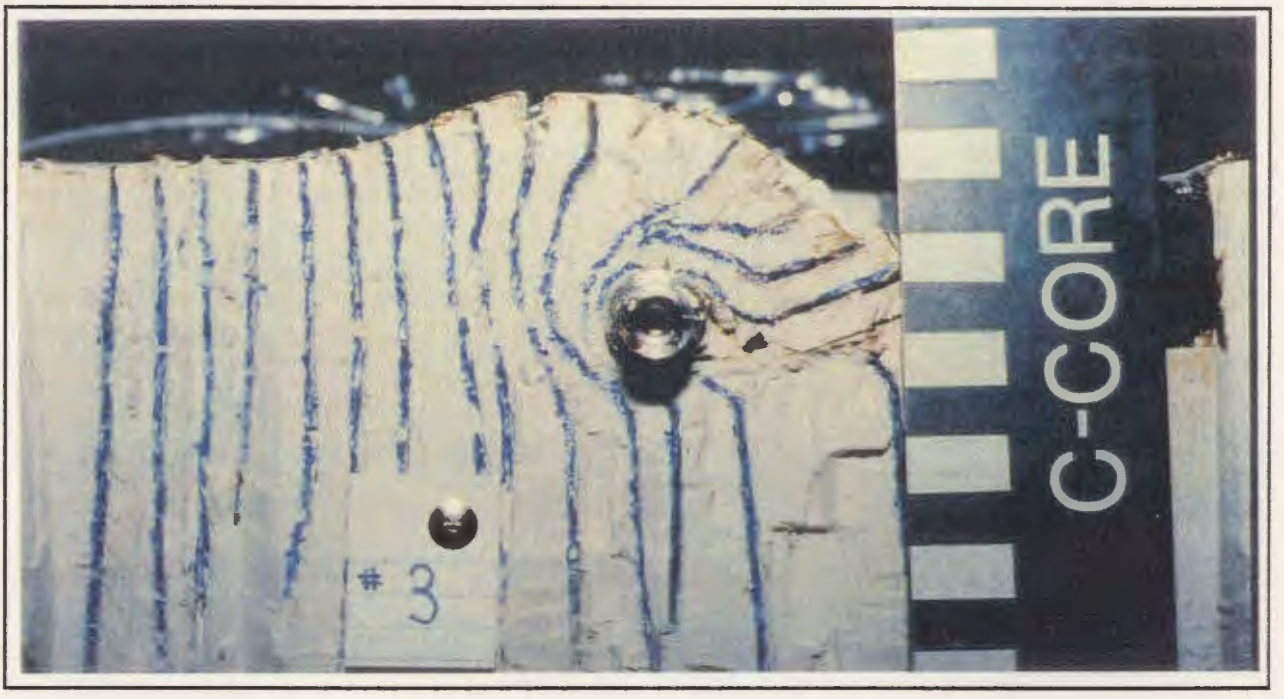

Figure I.11 - *Photo of excavated cross-section along mid length of model pipeline #3, 0.048mm/sec, Test 08.*

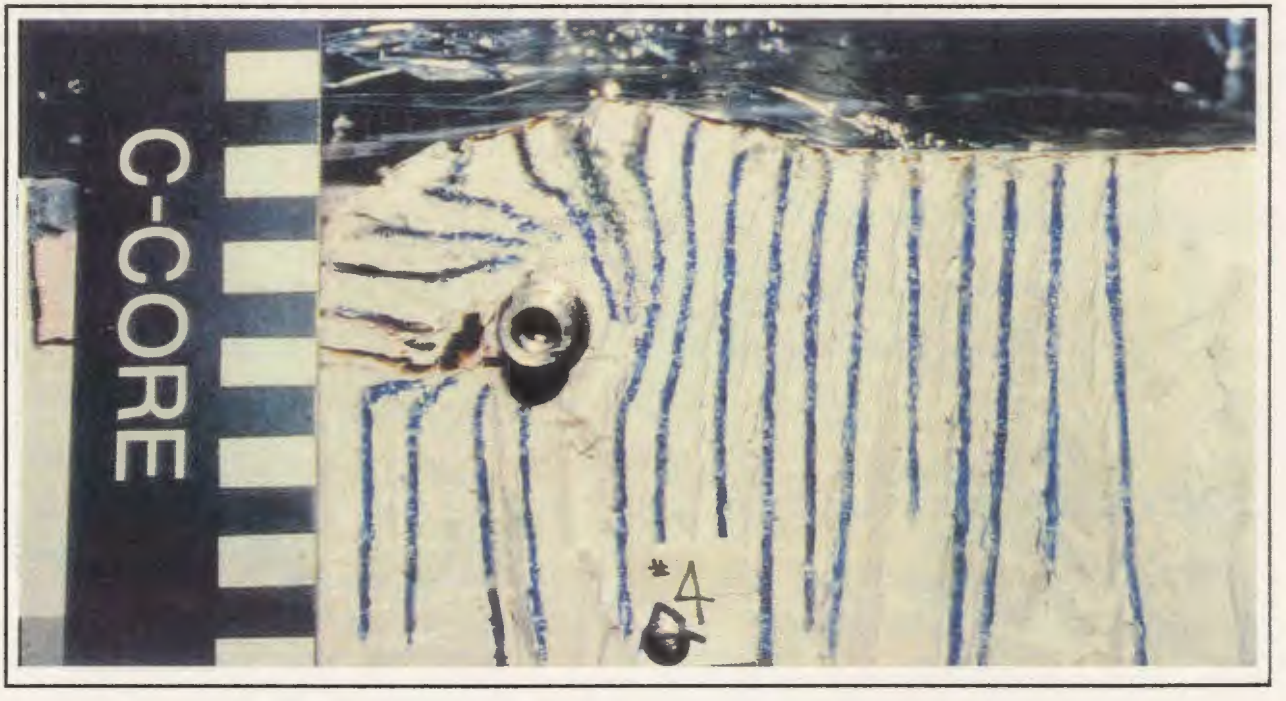

Figure I.12 - *Photo of excavated cross-section along mid length of model pipeline #4, 0.4336mm/sec, Test 08.*

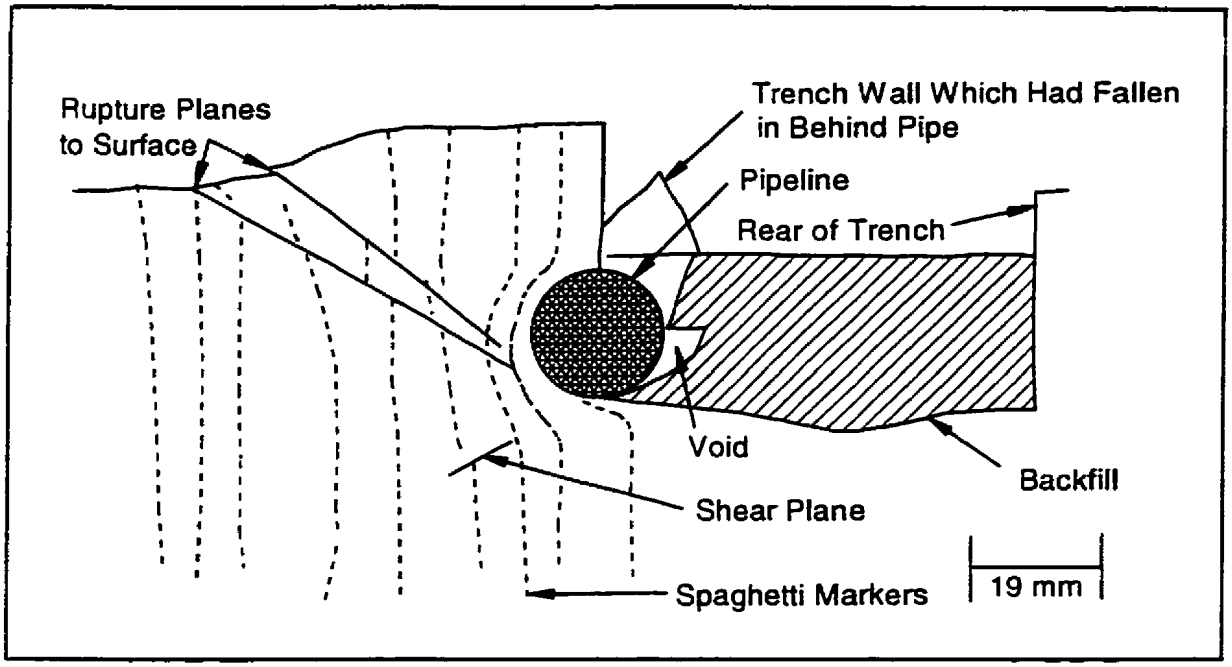

Figure I.13 - *Sketch of excavated cross-section along mid length of model pipeline #1, 0.00055mm/sec, Test 08.*

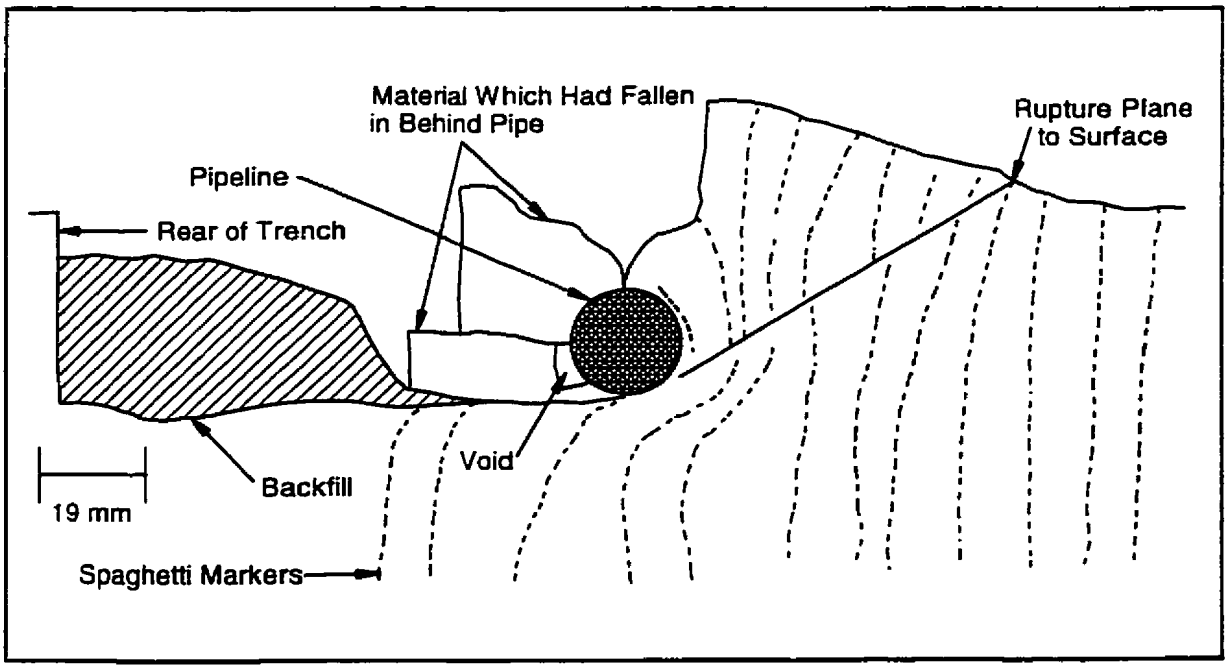

Figure I.14 - *Sketch of excavated cross-section along mid length of model pipeline #2, 0.0053mm/sec, Test 08.*

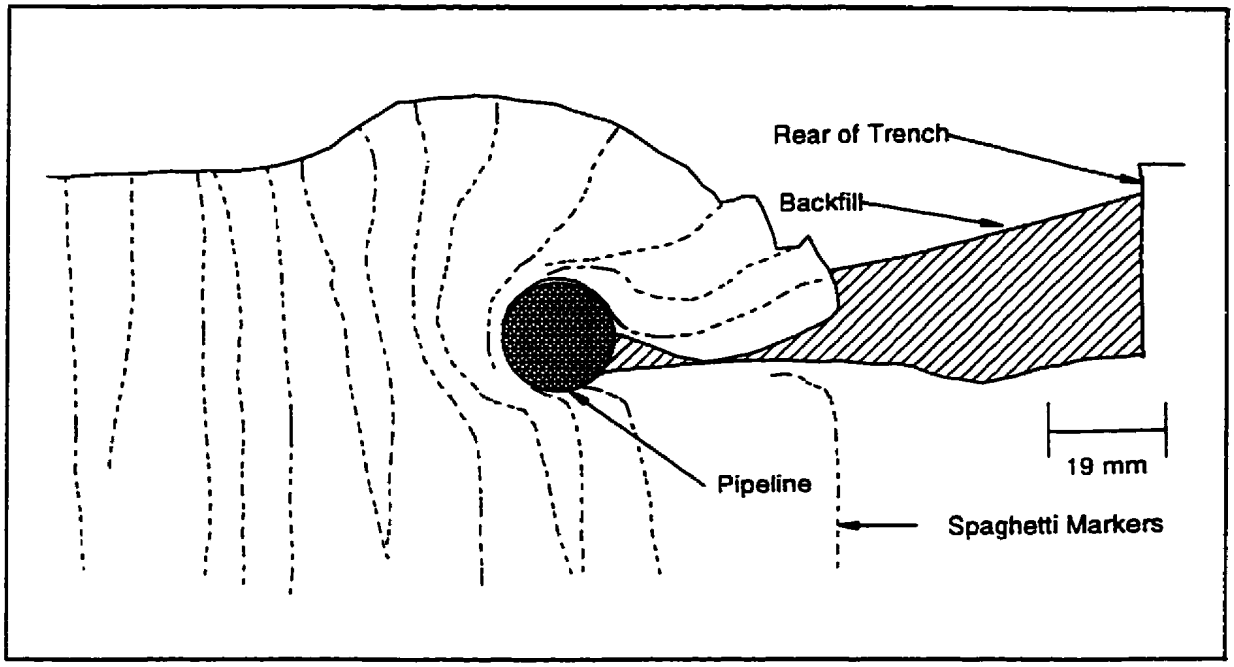

Figure I.15 - *Sketch of excavated cross-section along mid length of model pipeline #3, 0.048mm/sec, Test 08.*

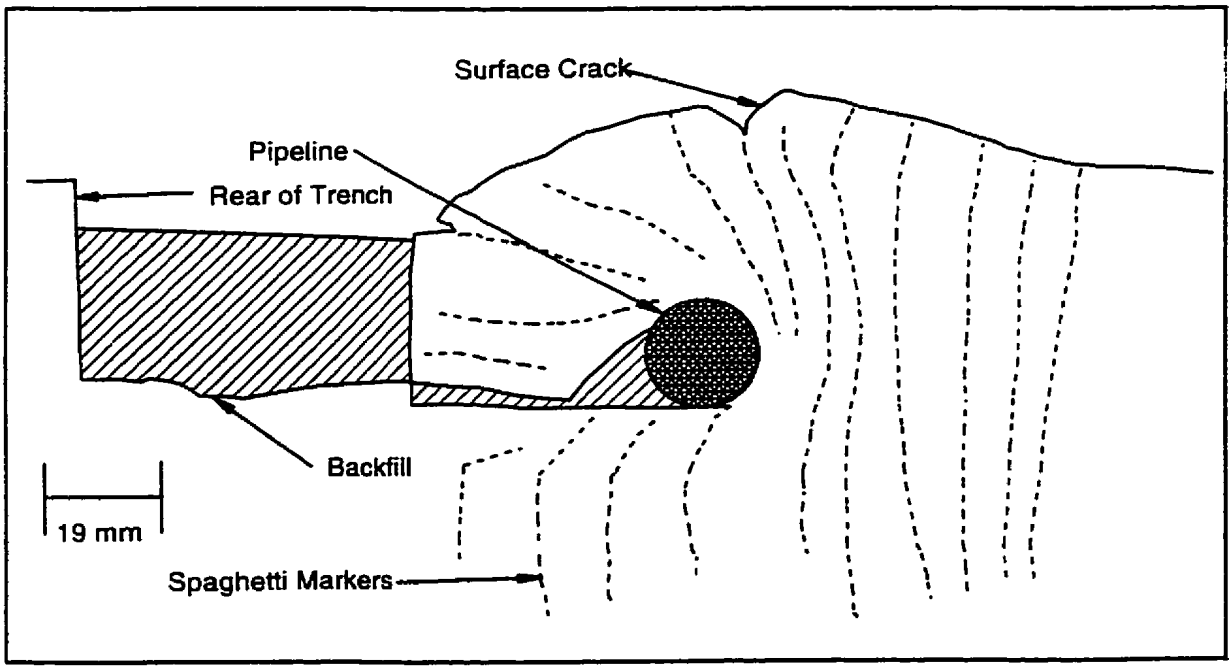

Figure I.16 - *Sketch of excavated cross-section along mid length of model pipeline #4, 0.4336mm/sec, Test 08.*

Appendix J

Test 09 - Selected Test Data

Table J.1 - Cone Penetration Test Details for Test 09

CPT No.	X[1] (mm)	Y[1] (mm)	Backfill or Native	Time Tested (hrs)
1	654	590	Native	2204
2	560	590	Slurry Backfill	2218
3	499	590	Remoulded Backfill	2303
4	440	590	Chunky Backfill	2316
5	308	590	Native	0903
6	265	590	Native	1645
7	225	590	Native	0900*
8	185	590	Native	2112*
9	378	590	Loose Sand Backfill	2126*

Notes: 1 - Coordinate convention shown on Figure J.1.
* - Four days later.

Table J.2 - Interpreted Cone Penetration Resistances for Test 09

Cone Test No.	Interpreted Penetration Resistance (kPa)			
	@ Initial Springline of Pipeline #1	@ Initial Springline of Pipeline #2	@ Initial Springline of Pipeline #3	@ Initial Springline of Pipeline #4
1	410	410	410	410
2	29	---	---	---
3	---	---	370	---
4	---	213	---	---
5	379	379	379	379
6	395	395	395	395
7	340	340	340	340
8	390	390	390	390
9	---	---	---	589

Table J.3 - Pipeline Test Details for Test 09

Pipeline No.	Trench Width (mm)	Cover Depth (mm)	X:Y Coordinates of Pipe Centre (mm)	Pipeline Velocity (mm/sec)	Time Tested (hrs)
1	50	16	290 : 520.5	0.00053	1318 - Aug. 31
2	50	16	650 : 520.5	0.0014	0903 - Sept. 5
3	50	16	650 : 659.5	0.00053	1318 - Aug. 31
4	50	16	290 : 659.5	0.00046	1318 - Aug. 31

Table J.4 - Prototype Test Geometries for Test 09

Pipeline	Distance to Trench Wall in the Direction of Travel (m)	Distance to Trench Wall Towards the Rear of the Pipeline (m)	Distance to a Stiff Retaining Wall in the Direction of Travel (m)	Distance to the Pipeline in the Direction Opposite to Travel (m)	Distance Laterally to a Stiff Retaining Wall (m)	Distance Laterally to the Edge of the Adjacent Pipeline (m)	Distance From Base of Pipeline to Rigid Base, i.e. Bedrock (m)	Water Level Above Rigid Base, i.e. Bedrock (m)	Water Level Below Base of Pipeline (m)
1	0.775	0.775	14.175	7.55	7.5	5.0	5.025	3.3	1.725
2	0.775	0.775	14.175	7.55	7.5	5.0	5.025	3.0	2.025
3	0.775	0.775	14.175	7.55	7.5	5.0	5.025	3.3	1.725
4	0.775	0.775	14.175	7.55	7.5	5.0	5.025	3.3	1.725

Table J.5 - Calculation of Undrained Shear Strength for Test 09

Pipeline	Soil Type	Cone Tests Used to Derive q_c	Interpreted Cone Tip Resistance at Springline, q_c (kPa)	Saturated Bulk Density, γ_{sat} (kN/m^3)	Pore Pressure at Springline, u (kPa)	Depth to Springline h (m)	Cone Factor, N_c or N_k*	Undrained Shear Strength, c_u (kPa)
1	Native	1,5,6	453.6	956.5	-12.3	0.0255	7.9/11.7	36.6 - 54.6
1	Backfill	2	28.9	924.7	---	0.0255	15	1.8
2	Native	7,8	419.2	956.5	-7.4	0.0255	7.7/12.0	32.9 - 51.1
2	Backfill	4	213.2	963.3**	---	0.0255	15	14.2
3	Native	1,5,6	453.6	956.5	-12.3	0.0255	7.9/11.7	36.6 - 54.6
3	Backfill	3	370.3	973.1	---	0.0255	15	24.7
4	Native	1,5,6	453.6	956.5	-12.3	0.0255	7.9/11.7	36.6 - 54.6
4	Backfill	9	588.7	≈ 730	---	0.0255	---	---

Notes: * - N_c range of values correspond to native material; N_k values correspond to backfill.

** - Note: Chunky material only; calculation does not take account voids in backfill.

Table J.6 - Summary of Prototype Pipeline Data; Test 09

Pipeline →	Pipeline #1	Pipeline #2	Pipeline #3	Pipeline #4
Trench Width	2.5m	2.5m	2.5m	2.5m
Cover Depth	0.80m	0.80m	0.80m	0.80m
Embedment Ratio, H/D	1.842	1.842	1.842	1.842
Average Backfill Undrained Shear Strength @ Springline	1.8kPa	14.2kPa	24.7kPa	---
Average Native Undrained Shear Strength @ Springline	45.6kPa	42.0kPa	45.6kPa	45.6kPa
Ultimate Normalized Resistance, N	6.541* 4.420**	8.975* 6.000**	6.380*** 5.435**	4.389* 3.551**
Distance into Trench Wall to Ultimate Normalized Resistance	1.845D* 0.497D**	1.826D* 0.605D**	1.440D*** 0.402D**	1.153D* 0.526D**
Slope to Ultimate Normalized Resistance	2.458	3.397	2.827	2.229
Normalized Resistance at Trench Wall	2.840	3.443	4.569	2.674
Normalized Resistance at 0.5D Penetration	4.475	5.607	5.488	3.569
Normalized Resistance at 1D Penetration	5.336	7.082	6.034	4.223
Slope of Interaction Between TW and Breakover	4.582	4.275	1.978	1.828
Normalized Resistance at Breakover	4.189	5.607	5.434	3.559
Distance into Trench Wall to Breakover	0.303D	0.500D	0.445D	0.500D
Slope of Interaction After Breakover	1.624	2.574	1.237	1.268

Notes: * - Values taken essentially at the end of pipeline pull; not necessarily a peak.
** - Corresponds to the point where the force-displacement curves became linear.
** - Ultimate normalized resistance estimated as pipeline damaged during pull.

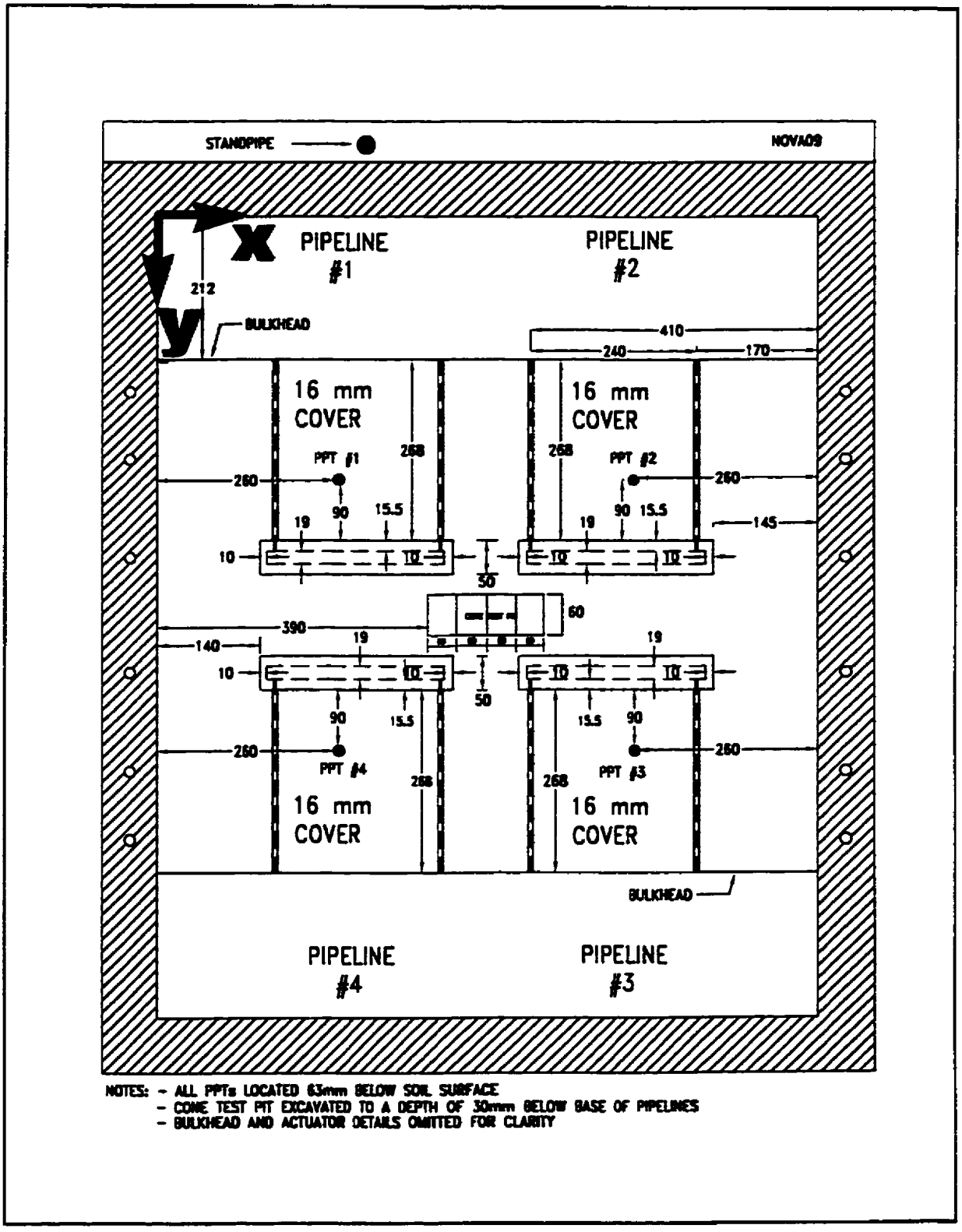

Figure J.1 - *Model Test Geometry, Test 09.*

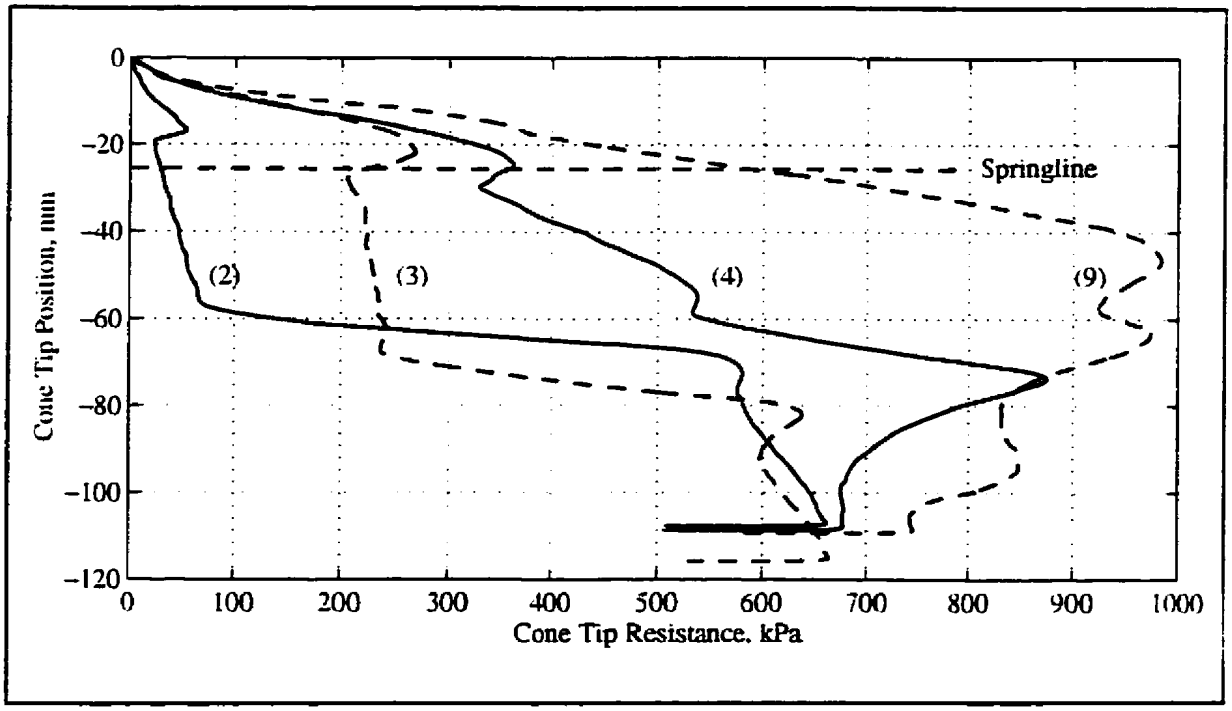

Figure J.2 - *All cone penetration tests, backfill material, Test 09.*

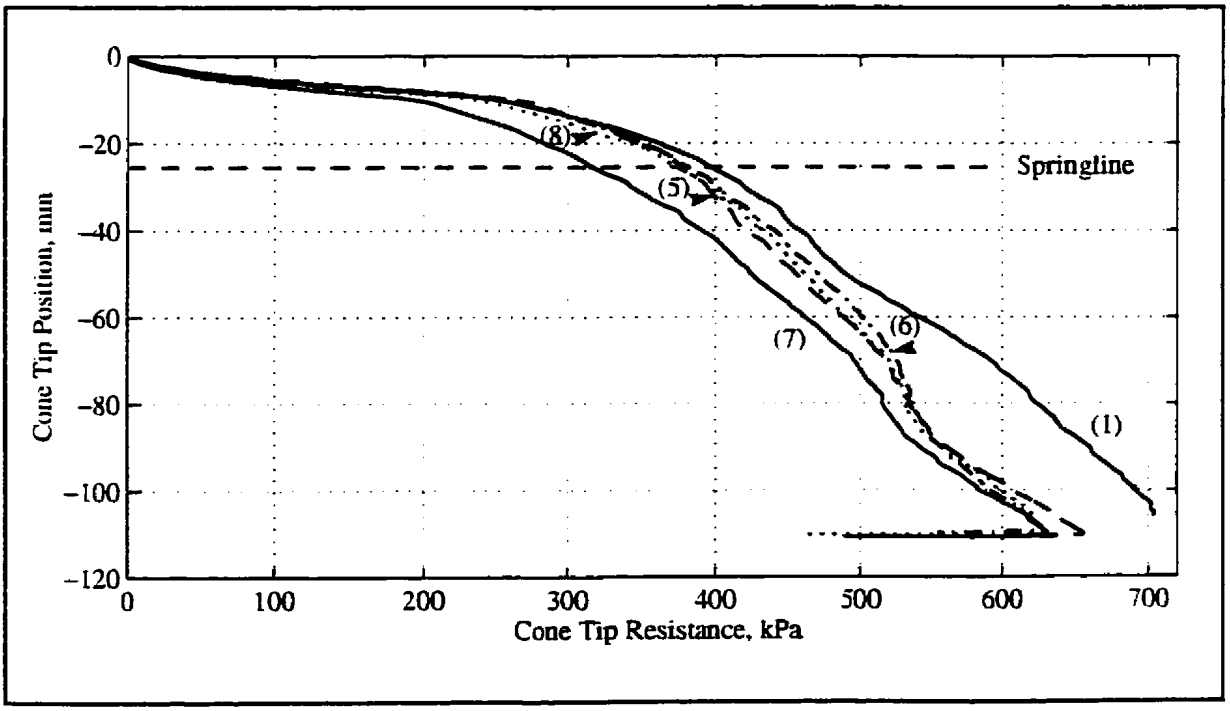

Figure J.3 - *All cone penetration tests, native material, Test 09.*

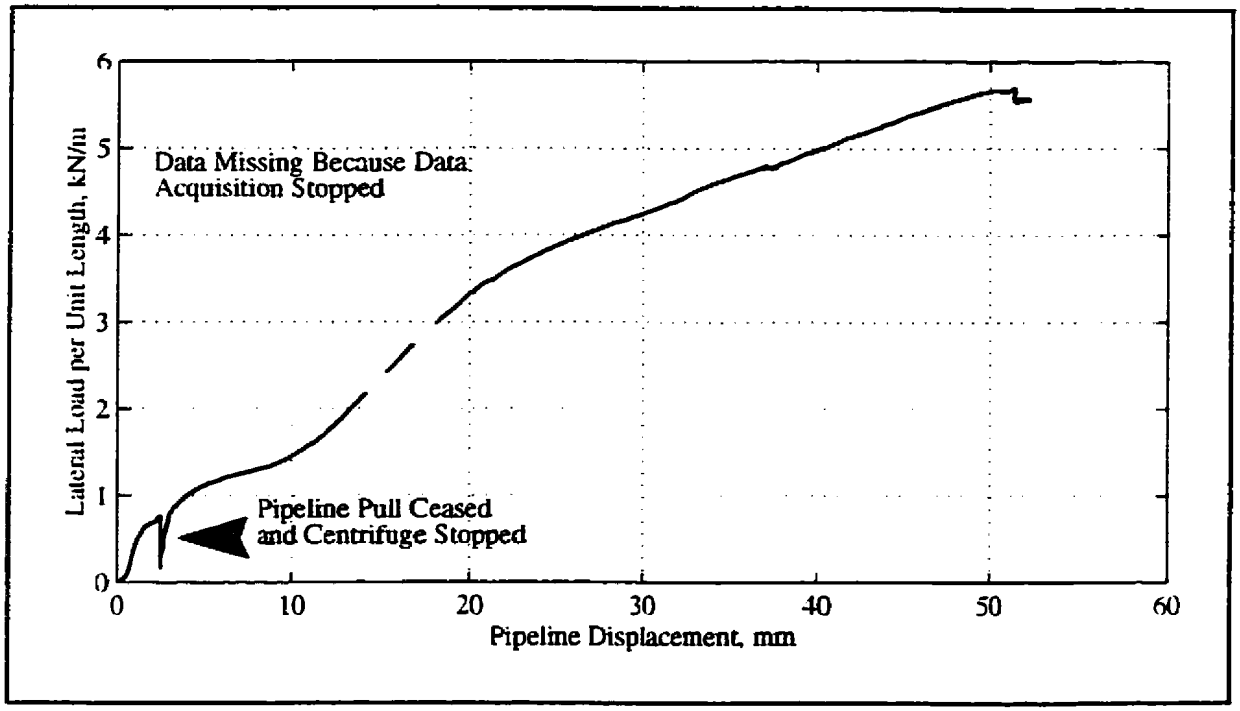

Figure J.4 - *Force-displacement response, model pipeline #1, slurry backfill, Test 09.*

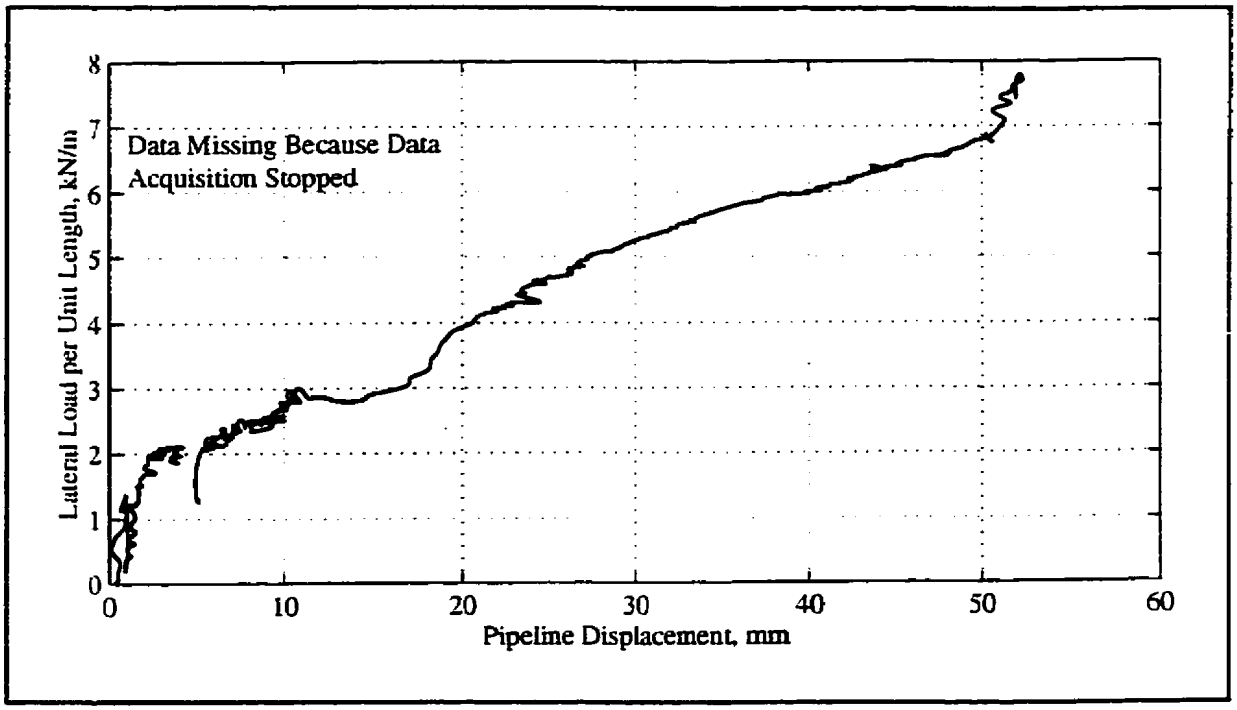

Figure J.5 - *Force-displacement response, model pipeline #2, grated native backfill, Test 09.*

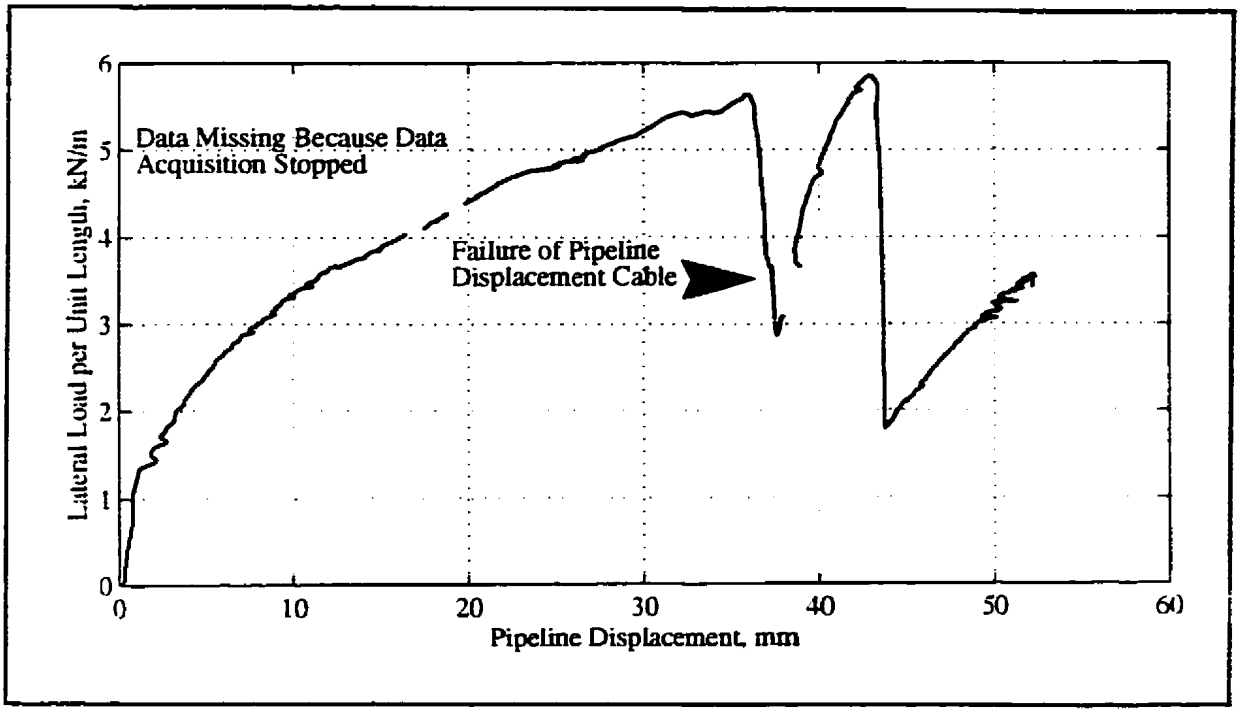

Figure J.6 - *Force-displacement response, model pipeline #3, remoulded backfill, Test 09.*

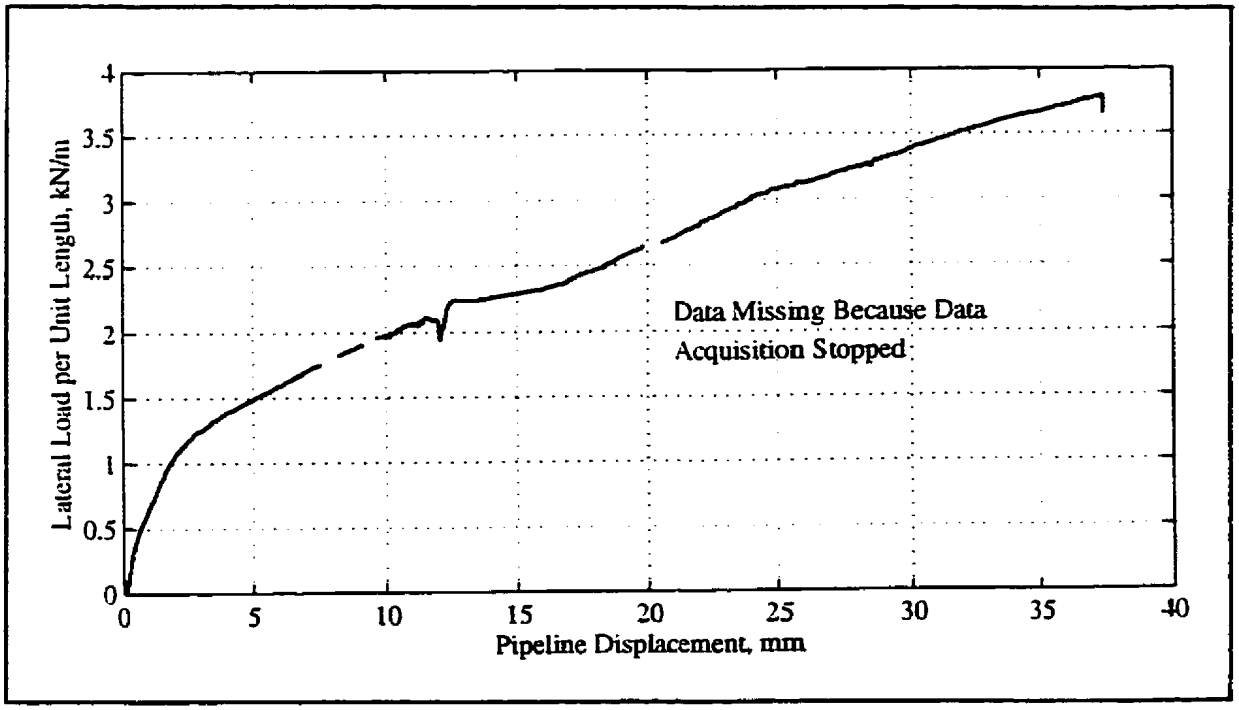

Figure J.7 - *Force-displacement response, model pipeline #4, fine sand backfill, Test 09.*

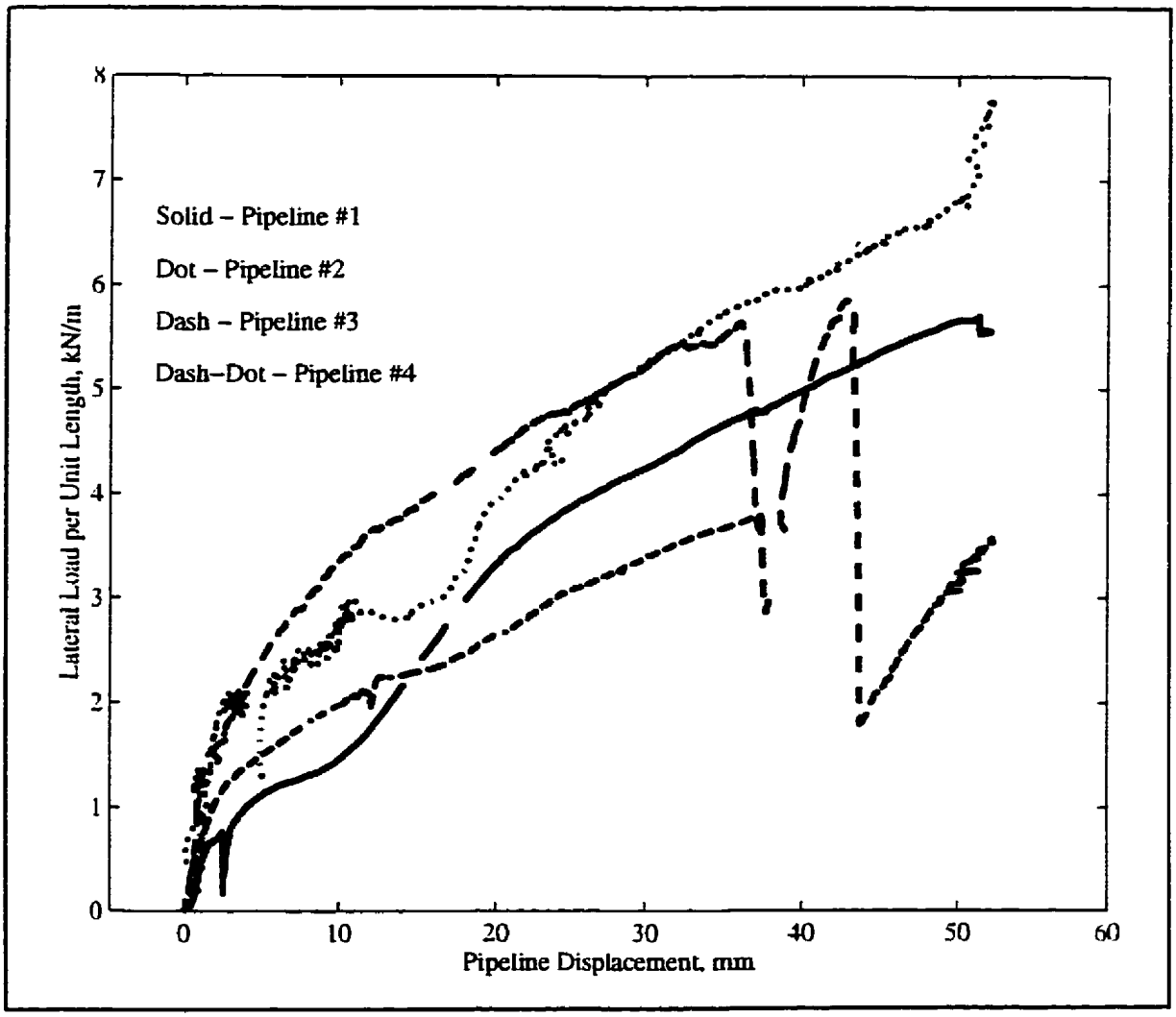

Figure J.8 - Force-displacement response, all model pipelines, Test 09.

Figure J.9 - *Photo of excavated cross-section along mid length of model pipeline #1, slurry backfill, Test 09.*

Figure J.10 - *Photo of excavated cross-section along mid length of model pipeline #2, grated native backfill, Test 09.*

Figure J.11 - *Photo of excavated cross-section along mid length of model pipeline #3, remoulded backfill, Test 09.*

Figure J.12 - *Photo of excavated cross-section along mid length of model pipeline #4, fine sand backfill, Test 09.*

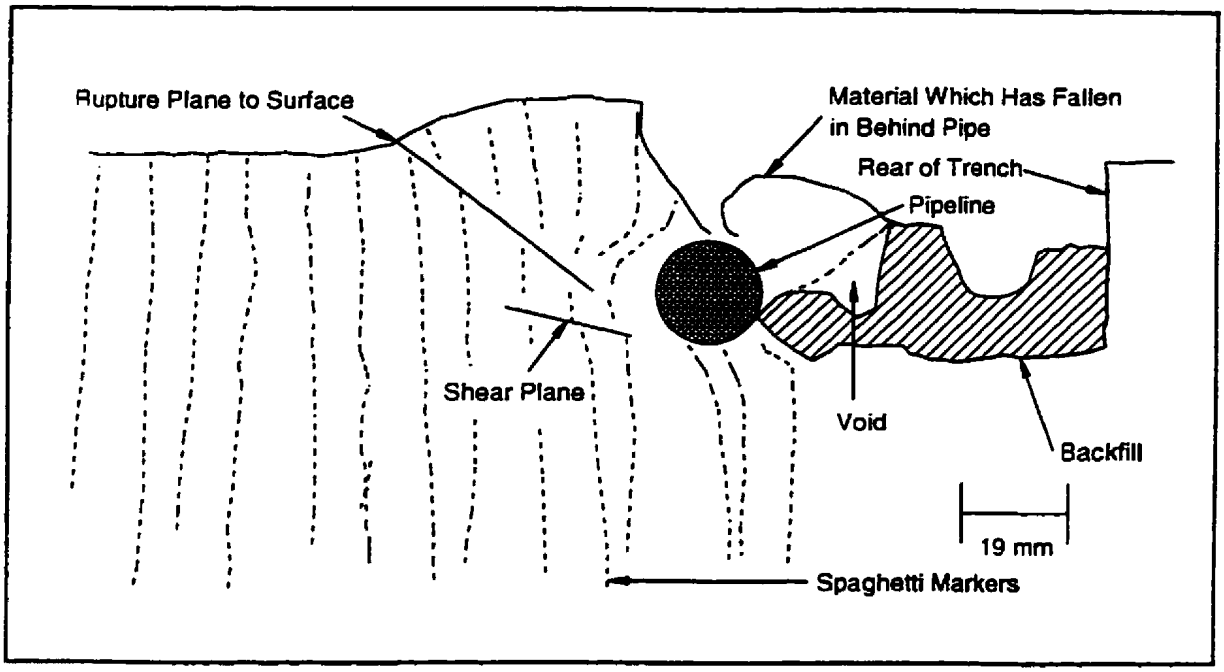

Figure J.13 - *Sketch of excavated cross-section along mid length of model pipeline #1, slurry backfill, Test 09.*

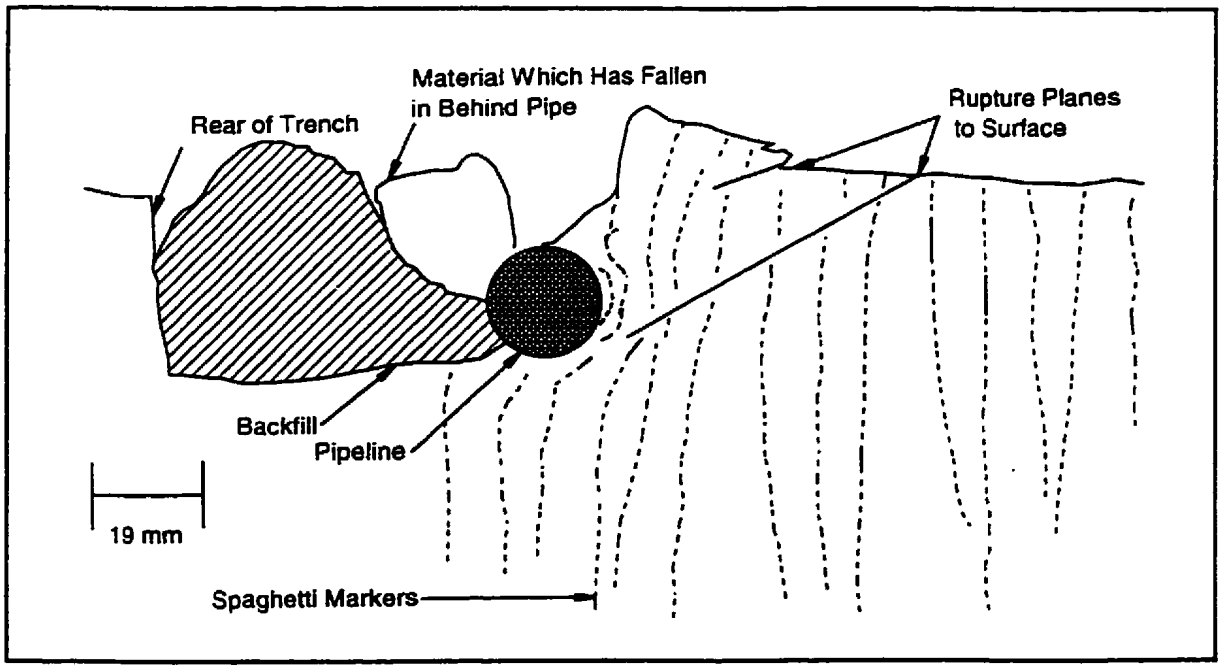

Figure J.14 - *Sketch of excavated cross-section along mid length of model pipeline #2, grated native backfill, Test 09.*

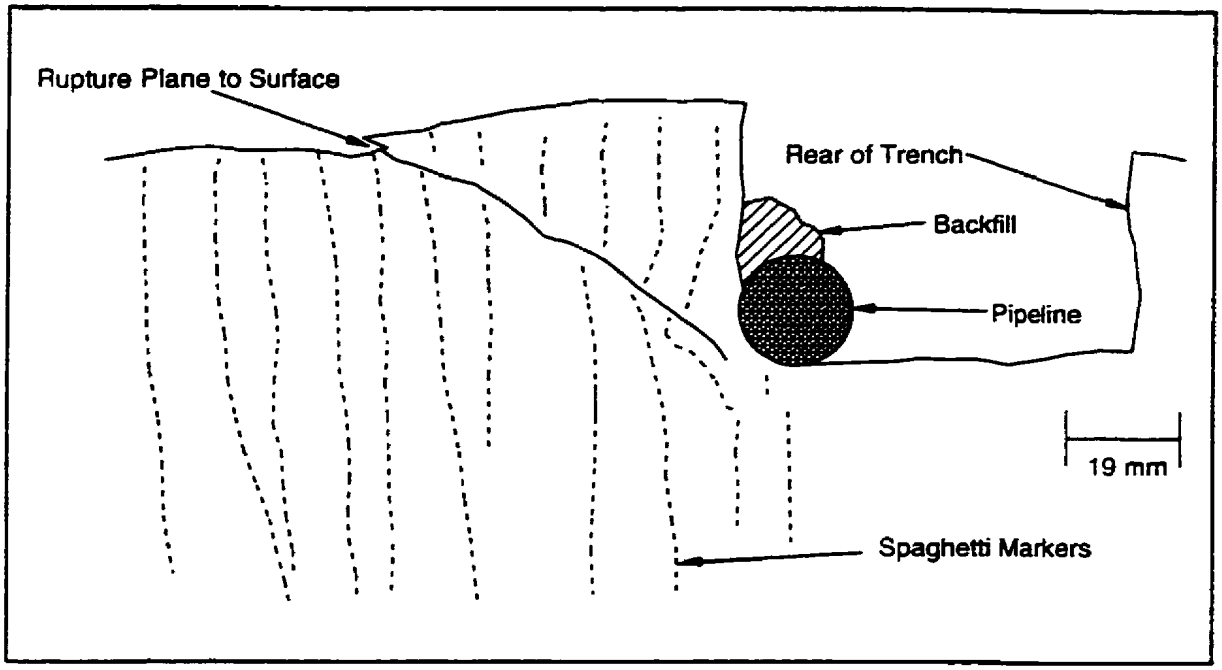

Figure J.15 - *Sketch of excavated cross-section along mid length of model pipeline #3, remoulded backfill, Test 09.*

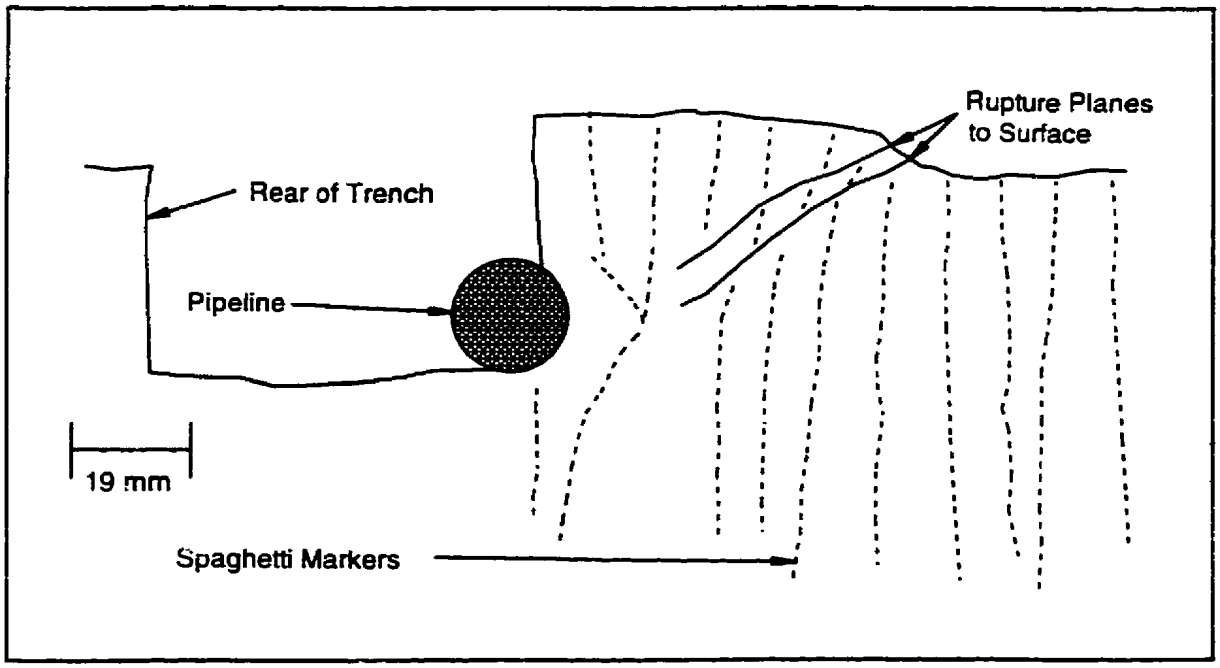

Figure J.16 - *Sketch of excavated cross-section along mid length of model pipeline #4, fine sand backfill, Test 09.*

Appendix K

Internal Deformation Observations

Test	Pipeline	Comments
1	1	Bearing stress calculations conducted for the 50g pipelines indicate that the pipelines would embed themselves less than 0.7mm during centrifuge swingup to 50g. During a relatively shallow interaction, during an undrained displacement of the pipeline, no volume change in the soil would be expected. It might be expected that the soil would take the path of least resistance around the pipeline; the soil in front of the pipeline would flow over top of the pipeline (see Figure 8.1a). If the pipeline moves with constant cover depth, post-test measurements should indicate final cover over the pipeline equal to the initial cover plus the diameter of the pipeline for an undrained interaction. Observations indicate that Pipeline #1 moved essentially horizontally during displacement. The expected cover at end of pipeline travel would be 35mm (consisting of 19mm of soil flowing over pipeline plus 16mm of original soil cover); the final measured cover was 35mm. This measurement is in agreement with above expectation for shallow pipeline burial depths; failure was essentially flow of soil around the top of the pipeline. The embedment ratio at the start of pipeline displacement was assumed to be 1.842 based on a pipeline base elevation of 100.5mm and 16mm of soil cover. Post-test excavation indicated that the pipeline moved essentially horizontal and would therefore have a base elevation of 100.5mm and an equivalent soil cover depth of 16mm which reflects an embedment ratio of 1.842. The "cover depth" and associated "h/D" has been presented in Table 8.1 for the prototype of Pipeline #1. The two values of each parameter represent conditions at the start of the test and during excavation respectively.
1	2	The pipeline appears to have moved down approximately 4mm during travel. Pipeline cover at end of travel was expected to be 33mm (consisting of 4mm downward displacement which would flow over top of the pipeline plus 19mm flow of soil over the pipeline plus 10mm original soil cover); the final measured cover was 31mm. This observation is in acceptable agreement with expectation. Failure was essentially flow of soil around the top of the pipeline. The embedment ratio at the start of pipeline displacement was assumed to be 1.526 based on a pipeline base elevation of 100.5mm and 10mm of soil cover. Post-test excavation indicated that the pipeline moved downwards by approximately 4mm which would suggest a base elevation of 96.5mm or an equivalent increase in cover depth to 14mm which reflects an embedment ratio of 1.737. Therefore, a range in "cover depth" and "h/D" has been presented in Table 8.1 for the prototype of Pipeline #2.
1	3	The pipeline appears to have moved down approximately 3mm during travel. Pipeline cover expected at the end of travel was 27mm (consisting of 3mm of downward displacement which would flow over top of the pipeline plus 19mm of soil flow over top of the pipeline plus 5mm of original soil cover); the final measured cover was 30mm. This measurement is in acceptable agreement with expectation. Failure was essentially flow of soil around the top of the pipeline. The embedment ratio at the start of pipeline displacement was assumed to be 1.263 based on a pipeline base elevation of 100.5mm and 5mm of soil cover. Post-test excavation indicated that the pipeline moved downwards by

Test	Pipeline	Comments
1	3	approximately 3mm which would suggest a base elevation of 97.5mm or an equivalent increase in cover depth to 8mm which reflects an embedment ratio of 1.421. Therefore, a range in "cover depth" and "h/D" has been presented in Table 8.1 for the prototype of Pipeline #3.
1	4	The pipeline appears to have moved down approximately 4mm during travel. The expected cover at end of pipeline travel was 23mm (consisting of 4mm of downward displacement which would flow over top of the pipeline plus 19mm of soil flow over top of the pipeline); the final measured cover was 26mm. This observation is in acceptable agreement with theory. Failure was essentially flow of soil around the top of the pipeline. The embedment ratio at the start of pipeline displacement was assumed to be 1.0 based on a pipeline base elevation of 100.5mm and 0mm of soil cover. Post-test excavation indicated that the pipeline moved downwards by approximately 4mm which would suggest a base elevation of 96.5mm or an equivalent increase in cover depth to 4mm which reflects an embedment ratio of 1.211. Therefore, a range in "cover depth" and "h/D" has been presented in Table 8.1 for the prototype of Pipeline #4.
Comments		Failure mechanisms associated with displacement of the soil in front of the pipelines during this test appears to have been similar; failure was essentially flow of soil around the top of the pipeline.
2	1	There appears to be a noticeable depression at the point where the pipe started, probably caused by the bearing stress of the pipeline. From sketches, the pipeline appears to have interacted with the trench wall, moved up 3mm and then proceeded to move downward until it came to rest at approximately the same level as the base of the trench. During a deeper interaction, it might be expected that the soil would take the path of least resistance around the pipeline; in this case, half the soil would be expected to flow over the pipeline and half under the pipeline (see Figure 8.1b). As this test investigated deeper interactions, the expected cover at the end of travel was 74.5mm (consisting of 65mm of original soil cover plus 9.5mm corresponding to one half the height of soil directly in front of the pipeline) but only 67mm was measured. It was observed that failure was essentially flow of soil around the pipeline. The embedment ratio at the start of pipeline displacement was assumed to be 4.421 based on a pipeline base elevation of 100.5mm and 65mm of soil cover. Post-test excavation indicated that the pipeline ended up essentially horizontal from where it started and would therefore have a base elevation of 100.5mm and an equivalent soil cover depth of 65mm which reflects an embedment ratio of 4.421. The "cover depth" and associated "h/D" has been presented in Table 8.1 for the prototype of Pipeline #1.
2	2	There appears to be a noticeable depression at the point where the pipe started, probably caused by the bearing stress of the pipeline. From sketches, the pipeline appears to have interacted with the trench wall, moved up 2-3mm and then proceeded to move downward until it came to rest approximately 1mm below the base of the trench. The expected cover at the end of travel was 59.5mm (consisting of 50mm of original soil cover plus 9.5mm corresponding to one half

Test	Pipeline	Comments
2	2	the height of soil directly in front of the pipeline) but only 55mm was measured. Failure was essentially flow of soil around the pipeline. The embedment ratio at the start of pipeline displacement was assumed to be 3.632 based on a pipeline base elevation of 100.5mm and 50mm of soil cover. Post-test excavation indicated that the pipeline moved downwards by approximately 1mm which would suggest a base elevation of 99.5mm or an equivalent increase in cover depth to 51mm which reflects an embedment ratio of 3.684. Therefore, a range in "cover depth" and "h/D" has been presented in Table 8.1 for the prototype of Pipeline #2.
2	3	There appears to be a noticeable depression at the point where the pipe started, probably caused by the bearing stress of the pipeline. From sketches, the pipeline appears to have interacted with the trench wall, moved gradually up 2-3mm and then proceeded to move gradually downward until it came to rest approximately at the base of the trench. The expected cover at the end of travel was 47.5mm (consisting of 38mm of original soil cover plus 9.5mm corresponding to one half the height of soil directly in front of the pipeline) and 46mm was measured. Failure was essentially flow of soil around the pipeline. The embedment ratio at the start of pipeline displacement was assumed to be 3.0 based on a pipeline base elevation of 100.5mm and 38mm of soil cover. Post-test excavation indicated that the pipeline ended up essentially horizontal from where it started and would therefore have a base elevation of 100.5mm and an equivalent soil cover depth of 38mm which reflects an embedment ratio of 3.0. The "cover depth" and associated "h/D" has been presented in Table 8.1 for the prototype of Pipeline #3.
2	4	There appears to be a noticeable depression at the point where the pipe started, probably caused by the bearing stress of the pipeline. From sketches, the pipeline appears to have interacted with the trench wall, moved immediately up 2-4mm and then proceeded to move gradually downward until it came to rest approximately at the base of the trench. The expected cover at the end of travel was 36.5mm (consisting of 27mm of original soil cover plus 9.5mm corresponding to one half the height of soil directly in front of the pipeline) but 42mm was measured. Failure was essentially flow of soil around the pipeline. The embedment ratio at the start of pipeline displacement was assumed to be 2.421 based on a pipeline base elevation of 100.5mm and 27mm of soil cover. Post-test excavation indicated that the pipeline ended up essentially horizontal from where it started and would therefore have a base elevation of 100.5mm and an equivalent soil cover depth of 27mm which reflects an embedment ratio of 2.421. The "cover depth" and associated "h/D" has been presented in Table 8.1 for the prototype of Pipeline #4.
Comments		The failure mechanisms from the interactions appear to have been similar. It appears that as the tests become deeper, the assumption of flow of material over and under the pipeline seems reasonable. At some intermediate depth, there would be a transition zone where a proportion of the material would flow over and under the pipeline, the amount of which would be depth dependant.

Test	Pipeline	Comments
3	1	There appears to be a noticeable depression at the point where the pipe started, probably caused by the bearing stress of the pipeline. The pipeline appears to have interacted with the trench wall and moved relatively horizontally with displacement with some 2-3mm variations. The pipe came to rest at the same level as the base of the trench or perhaps 1mm below. The expected cover at end of travel was 35mm (consisting of 16mm of original soil cover plus 19mm of soil directly in front of the pipeline which would have flowed over the pipeline); 34mm was measured. The observations are in good agreement with expectations. Failure was essentially flow of soil around the pipeline. The embedment ratio at the start of pipeline displacement was assumed to be 1.842 based on a pipeline base elevation of 100.5mm and 16mm of soil cover. Post-test excavation indicated that the pipeline ended up essentially horizontal from where it started and would therefore have a base elevation of 100.5mm and an equivalent soil cover depth of 16mm which reflects an embedment ratio of 1.842. The "cover depth" and associated "h/D" has been presented in Table 8.1 for the prototype of Pipeline #1.
3	2	There appears to be a noticeable depression at the point where the pipe started, probably caused by the bearing stress of the pipeline. The pipeline appears to have interacted with the trench wall, moved gradually up 3-4mm and then proceeded downwards so that the pipeline came to rest at the same level as the base of the trench. Expected cover at end of travel was 35mm (consisting of 16mm of original soil cover plus 19mm of soil directly in front of the pipeline which would have flowed over the pipeline); 34mm was measured. The observations are in good agreement with expectations. Failure was essentially flow of soil around the pipeline. The embedment ratio at the start of pipeline displacement was assumed to be 1.842 based on a pipeline base elevation of 100.5mm and 16mm of soil cover. Post-test excavation indicated that the pipeline ended up essentially horizontal from where it started and would therefore have a base elevation of 100.5mm and an equivalent soil cover depth of 16mm which reflects an embedment ratio of 1.842. The "cover depth" and associated "h/D" has been presented in Table 8.1 for the prototype of Pipeline #2.
3	3	There appears to be a noticeable depression at the point where the pipe started, probably caused by the bearing stress of the pipeline. The pipeline appears to have interacted with the trench wall, moved gradually up 2-4mm and then proceeded downwards so that the base of the pipeline came to rest 1-3mm below the base of the trench. Expected cover at the end of travel was 35mm plus 1 to 3mm or 36-38mm (consisting of 16mm of original soil cover plus 19mm of soil directly in front of the pipeline which would have flowed over the pipeline plus the 1 to 3mm associated with the vertical downward movement); 37mm was measured. Measurements were in good agreement with expectations. Failure was essentially flow of soil around the pipeline. The embedment ratio at the start of pipeline displacement was assumed to be 1.842 based on a pipeline base elevation of 100.5mm and 16mm of soil cover. Post-test excavation indicated that the pipeline moved downwards by

Test	Pipeline	Comments
3	3	approximately 2mm which would suggest a base elevation of 98.5mm or an equivalent increase in cover depth to 18mm which reflects an embedment ratio of 1.947. Therefore, a range in "cover depth" and "h/D" has been presented in Table 8.1 for the prototype of Pipeline #3.
3	4	There appears to be a noticeable depression where the pipe started, probably caused by the bearing stress of the pipeline. The pipeline appears to have interacted with the trench wall, moved gradually up 2-3mm and then proceeded downwards so that the base of the pipeline came to rest 1-3mm below the base of the trench. Expected cover at end of travel was 35mm plus 1 to 3mm or 36-38mm (consisting of 16mm of original soil cover plus 19mm of soil directly in front of the pipeline which would have flowed over the pipeline plus the 1 to 3mm associated with the vertical downward movement); 37mm was measured. The observations are in good agreement with expectations. Failure was essentially flow of soil around the pipeline. The embedment ratio at the start of pipeline displacement was assumed to be 1.842 based on a pipeline base elevation of 100.5mm and 16mm of soil cover. Post-test excavation indicated that the pipeline moved downwards by approximately 2mm which would suggest a base elevation of 98.5mm or an equivalent increase in cover depth to 18mm which reflects an embedment ratio of 1.947. Therefore, a range in "cover depth" and "h/D" has been presented in Table 8.1 for the prototype of Pipeline #4.
Comments		The mechanism between these pipeline tests appeared to be similar. No apparent effects of trench width variation could be determined from the internal deformation mechanisms.
4	1	There appeared to be a noticeable depression where pipe started, probably caused by the bearing stress of the pipeline. The pipeline apparently moved out of this depression at the beginning of displacement. Observations indicate that during interaction with the pipe wall, the pipeline rode up approximately 5mm, moved approximately horizontally for a distance and then moved vertically downward approximately 5mm. Because the interaction was considered to be drained, cover at the end of travel of less than 35mm would be expected (consisting of the original 16mm of soil cover plus the 19mm of soil directly in front of the pipeline which would flow over the top of the pipeline); 34mm was measured. Observations are in acceptable agreement with theory. As material passed over the top of the pipe during displacement, the spoil cracked and fell behind the pipeline. Displacements were measured in front of the pipeline extending approximately one pipeline diameter. Failure surfaces were observed in front of the pipeline, the most recent one extending from the toe of the pipeline surface at approximately 40°. The embedment ratio at the start of pipeline displacement was assumed to be 1.842 based on a pipeline base elevation of 100.5mm and 16mm of soil cover. Post-test excavation indicated that the pipeline ended up essentially horizontal from where it started and would therefore have a base elevation of 100.5mm and an equivalent soil cover depth of 16mm which reflects an embedment ratio of

Test	Pipeline	Comments
4	1	1.842. The "cover depth" and associated "h/D" has been presented in Table 8.1 for the prototype of Pipeline #1.
4	2	There appeared to be a noticeable depression where pipe started, probably caused by the bearing stress of the pipeline. The pipeline apparently moved out of this depression at the beginning of displacement. Observations indicate that during interaction with the pipe wall, the pipeline rode up approximately 2-4mm, then moved gradually downward until at rest where the base of the pipeline was approximately 6mm below the trench base. This up-down pattern (as well as the same type of apparent behaviour in other tests) may have been the result of the pipeline trying to follow a path of least resistance. However, the pipeline was restrained by the actuator system and may have tended to move vertically downward as the result of the pipe weight and bearing stress. Again, because the interaction was considered to be drained, cover at the end of travel less than 41mm would be expected (consisting of the original 16mm of soil cover plus the 19mm of soil directly in front of the pipeline which would flow over the top of the pipeline plus the additional 4mm of soil due to the downward vertical movement of the pipeline); an average of 40mm was measured. The observations are in acceptable agreement with expectations. As material passed over the top of the pipe during displacement, the spoil cracked and fell behind the pipeline. Displacements were measured in front of the pipeline extending approximately one pipeline diameter. Failure surfaces were observed in front of the pipeline, the most recent one extended from the toe of the pipeline to the soil surface at approximately 40°. The embedment ratio at the start of pipeline displacement was assumed to be 1.842 based on a pipeline base elevation of 100.5mm and 16mm of soil cover. Post-test excavation indicated that the pipeline moved downwards by approximately 6mm which would suggest a base elevation of 94.5mm or an equivalent increase in cover depth to 22mm which reflects an embedment ratio of 2.158. Therefore, a range in "cover depth" and "h/D" has been presented in Table 8.1 for the prototype of Pipeline #2.
4	3	There appeared to be a noticeable depression where the pipe started, probably caused by the bearing stress of the pipeline. The pipeline apparently moved out of this depression at the beginning of displacement. Observations indicate that during interaction with the pipe wall, the pipeline moved essentially horizontally, followed by downward movement. When it came to rest, the bottom of the pipeline was approximately 2mm below the base of the trench. Because the interaction was considered to be undrained, cover at the end of travel equal to 37mm would be expected (consisting of the original 16mm of soil cover plus the 19mm of soil directly in front of the pipeline which would flow over the top of the pipeline plus the additional 2mm of soil due to the downward vertical movement of the pipeline); an average of 38.5mm was measured. The observations are in acceptable agreement with expectation. As with the other undrained tests, the soil appeared to have flowed over the top of the pipe during displacement. Displacements were measured in front of the pipeline extending approximately one pipeline diameter.

Test	Pipeline	Comments
4	3	The embedment ratio at the start of pipeline displacement was assumed to be 1.842 based on a pipeline base elevation of 100.5mm and 16mm of soil cover. Post-test excavation indicated that the pipeline moved downwards by approximately 2mm which would suggest a base elevation of 98.5mm or an equivalent increase in cover depth to 18mm which reflects an embedment ratio of 1.947. Therefore, a range in "cover depth" and "h/D" has been presented in Table 8.3 for the prototype of Pipeline #3.
4	4	There appears to be a noticeable depression where the pipe started, which was probably caused by the bearing stress of the pipeline. The pipeline apparently moved out of this depression at the beginning of displacement. Observations indicate that after interaction with the trench wall, the pipeline apparently moved downward until, at rest, the base of the pipeline was approximately 5mm below the base of the trench. Because the interaction was considered to be undrained, cover at the end of travel equal to 40mm would be expected (consisting of the original 16mm of soil cover plus the 19mm of soil directly in front of the pipeline which would flow over the top of the pipeline plus the additional 5mm of soil due to the downward vertical movement of the pipeline); an average of 40mm was measured. The observations are in acceptable agreement with theory. As with the other undrained tests, material appeared to have flowed over the top of the pipe during displacement. Displacements were measured in front of the pipeline extending approximately one pipeline diameter. The embedment ratio at the start of pipeline displacement was assumed to be 1.842 based on a pipeline base elevation of 100.5mm and 16mm of soil cover. Post-test excavation indicated that the pipeline moved downwards by approximately 5mm which would suggest a base elevation of 95.5mm or an equivalent increase in cover depth to 21mm which reflects an embedment ratio of 2.105. Therefore, a range in "cover depth" and "h/D" has been presented in Table 8.1 for the prototype of Pipeline #4.
Comments		Failure mechanisms associated with soil displacement in front of Pipeline #1 and Pipeline #2 were similar; conditions during these tests are assumed to have been essentially drained to somewhat drained. Failure mechanisms associated with soil displacement in front of Pipeline #3 and Pipeline #4 were similar; conditions during these tests are assumed to have been somewhat undrained to essentially undrained.
5	1	Bearing stress calculations conducted on the 25g pipelines indicated that the pipelines would embed themselves less than 1.5mm during centrifuge swingup to 25g. The pipeline appears to have interacted with the trench wall and moved relatively horizontally, the base of the pipeline ending up approximately 3mm above the base of the trench. The expected cover at the end of travel was 67mm (consisting of the original 32mm of soil cover plus the 38mm of soil directly in front of the pipeline which would flow over the top of the pipeline minus the 3mm reduction in soil height directly in front of the pipeline due to the upward vertical movement of the pipeline); 66mm was measured. Measurements are in good agreement with expectations. Failure was essentially flow of soil around the pipeline.

Test	Pipeline	Comments
5	1	The embedment ratio at the start of pipeline displacement was assumed to be 1.842 based on a pipeline base elevation of 91mm and 32mm of soil cover. Post-test excavation indicated that the pipeline moved upwards by approximately 3mm which would suggest a base elevation of 94mm or an equivalent decrease in cover depth to 29mm which reflects an embedment ratio of 1.763. Therefore, a range in "cover depth" and "h/D" has been presented in Table 8.1 for the prototype of Pipeline #1.
5	2	The pipeline appears to have interacted with the trench wall and moved up approximately 6mm after which it moved relatively horizontally. The expected cover at the end of travel was 52mm (consisting of the original 20mm of soil cover plus the 38mm of soil directly in front of the pipeline which would flow over the top of the pipeline minus the 6mm reduction in soil height directly in front of the pipeline due to the upward vertical movement of the pipeline); an average of 53.5mm was measured. Observations are in good agreement with expectations. Failure was essentially flow of soil around the pipeline. The embedment ratio at the start of pipeline displacement was assumed to be 1.526 based on a pipeline base elevation of 91mm and 20mm of soil cover. Post-test excavation indicated that the pipeline moved upwards by approximately 5mm which would suggest a base elevation of 96mm or an equivalent decrease in cover depth to 15mm which reflects an embedment ratio of 1.395. Therefore, a range in "cover depth" and "h/D" has been presented in Table 8.1 for the prototype of Pipeline #2.
5	3	The pipeline appears to have interacted with the trench wall and moved relatively horizontally, the base of the pipeline ending up approximately at the same level as the base of the trench. The expected cover at the end of travel was 48mm (consisting of the original 10mm of soil cover plus the 38mm of soil directly in front of the pipeline which would flow over the top of the pipeline); an average of 56mm was measured. Observations are not in good agreement with expectations. Failure was essentially flow of soil around the pipeline. The embedment ratio at the start of pipeline displacement was assumed to be 1.263 based on a pipeline base elevation of 91mm and 10mm of soil cover. Post-test excavation indicated that the pipeline ended up essentially horizontal from where it started and would therefore have a base elevation of 91mm and an equivalent soil cover depth of 10mm which reflects an embedment ratio of 1.263. The "cover depth" and associated "h/D" has been presented in Table 8.1 for the prototype of Pipeline #3.
5	4	The pipeline appears to have interacted with trench wall and moved relatively horizontally, the base of the pipeline was calculated as ending up approximately 1mm below base of the trench. The expected cover at end of travel was 39mm (consisting of the original 38mm of soil directly in front of the pipeline which would flow over the top of the pipeline plus the additional 1mm of soil in front of the pipeline due to the downward vertical movement of the pipeline); an average of 44mm was measured. Observations are not in good agreement with expectations. Failure was essentially flow of soil around the pipeline.

Test	Pipeline	Comments
5	4	The embedment ratio at the start of pipeline displacement was assumed to be 1.0 based on a pipeline base elevation of 91mm and 0mm of soil cover. Post-test excavation indicated that the pipeline moved downwards by approximately 1mm which would suggest a base elevation of 92mm or an equivalent decrease in cover depth to -1mm which reflects an embedment ratio of 0.947. Therefore, a range in "cover depth" and "h/D" has been presented in Table 8.1 for the prototype of Pipeline #4.
Comments		The failure mechanism of soil displacement in front of the pipeline appeared to be similar to that observed during Test 01 in which the interaction was also assumed to be undrained and which had similar geometry.
6	1	Bearing stress calculations conducted on the 100g pipelines indicate that the pipelines could have embed themselves due to self weight at 100g. As the swingup was done in steps, the soil beneath the model pipelines would have had some time to consolidate and increase in strength due to loading from the weight of the pipeline. The pipeline, therefore, would probably not have embed itself until displacement began and it moved onto less- consolidated soil. It is assumed that the pipeline still had the equivalent of 8mm cover prior to the start of displacement (there was no sign of any significant depression in the trench). From sketches made during post test excavation, it appears that during travel the pipeline moved downward approximately 11.5mm so that at the end of travel, a cover depth of 29mm was inferred (consisting of the original 8mm of soil cover plus the 9.5mm of soil directly in front of the pipe plus 11.5mm downward movement). From sketches indicating the pipelines path, it is calculated that the pipeline had the equivalent of 25mm cover as it interacted with the trench wall. The failure of the soil was essentially flow of soil around the pipeline. The embedment ratio at the start of pipeline displacement was assumed to be 1.842 based on a pipeline base elevation of 105mm and 8mm of soil cover. Post-test excavation indicated that the pipeline moved downwards by approximately 11.5mm which would suggest a base elevation of 93.5mm or an equivalent increase in cover depth to 19.5mm which reflects an embedment ratio of 3.053. Therefore, a range in "cover depth" and "h/D" has been presented in Table 8.1 for the prototype of Pipeline #1.
6	2	It is assumed that the pipeline still had the equivalent of 5mm cover prior to the start of displacement (there was no sign of any significant depression in the trench). From sketches made during post test excavation, it appears that during travel the pipeline proceeded downward approximately 12.5mm so that at the end of travel, it is inferred that the pipeline had the equivalent of 27mm cover (consisting of the original 5mm of soil cover plus the 9.5mm of soil directly in front of the pipe plus 12.5mm of downward movement). From sketches indicating the pipelines path, it is calculated that the pipeline had the equivalent of 24mm cover as it interacted with the trench wall. The failure of the soil was essentially flow of soil around the pipeline. The embedment ratio at the start of pipeline displacement was assumed to be 1.526 based on a pipeline base elevation of 105mm and 5mm of soil cover. Post-test excavation indicated that the pipeline moved downwards by approximately

Test	Pipeline	Comments
6	2	12.5mm which would suggest a base elevation of 92.5mm or an equivalent increase in cover depth to 17.5mm which reflects an embedment ratio of 2.842. Therefore, a range in "cover depth" and "h/D" has been presented in Table 8.1 for the prototype of Pipeline #2.
6	3	It is assumed that the pipeline still had the equivalent of 2.5mm cover prior to the start of displacement (there was no sign of any significant depression in the trench). From sketches made during post test excavation, it appears that during travel the pipeline proceeded downward approximately 13mm so that at the end of travel, it is inferred that the pipeline had the equivalent of 25mm cover (consisting of the original 2.5mm of soil cover plus the 9.5mm of soil directly in front of the pipe plus 13mm downward movement). From sketches indicating the pipelines path, it is calculated that the pipeline had the equivalent of 21mm cover as it interacted with the trench wall. The failure of the soil was essentially flow of soil around the pipeline. The embedment ratio at the start of pipeline displacement was assumed to be 1.263 based on a pipeline base elevation of 105mm and 2.5mm of soil cover. Post-test excavation indicated that the pipeline moved downwards by approximately 13mm which would suggest a base elevation of 92mm or an equivalent increase in cover depth to 15.5mm which reflects an embedment ratio of 2.632. Therefore, a range in "cover depth" and "h/D" has been presented in Table 8.1 for the prototype of Pipeline #3.
6	4	It is assumed that the pipeline still had the equivalent of 0mm cover prior to the start of displacement (there was no sign of any significant depression in the trench). From sketches made during post test excavation, it appears that during travel the pipeline proceeded downward approximately 14.5mm so that at the end of travel, it is inferred that the pipeline had the equivalent of 24mm cover (consisting of 9.5mm of soil directly in front of the pipe plus 14.5mm of downward movement). From sketches indicating the pipelines path, it is calculated that the pipeline had the equivalent of 21mm cover as it interacted with the trench wall. The failure of the soil was essentially flow of soil around the pipeline. The embedment ratio at the start of pipeline displacement was assumed to be 1.0 based on a pipeline base elevation of 105mm and 0mm of soil cover. Post-test excavation indicated that the pipeline moved downwards by approximately 14.5mm which would suggest a base elevation of 90.5mm or an equivalent increase in cover depth to 14.5mm which reflects an embedment ratio of 2.526. Therefore, a range in "cover depth" and "h/D" has been presented in Table 8.1 for the prototype of Pipeline #4.
Comments		Failure mechanism of soil displacement in front of the pipeline appeared to be similar to that from Test 01 and Test 05 in which the interaction between the pipeline and the soil was also assumed to be undrained and which had similar geometry. The fact that there was significant vertical displacement of the pipelines with horizontal displacement should be accounted for in the analysis of the experimental data.

Test	Pipeline	Comments
7	1	There was a noticeable depression (1-2mm) where the pipe started, probably caused by the bearing stress of the pipeline. The pipeline moved out of this depression at the beginning of displacement and appears to have moved relatively horizontally during interaction with the trench wall. The base of the pipeline was at an elevation of 100.5mm above the extrusion plate at the start of displacement and finished at an elevation of 98mm. Because the interaction was considered to be drained, cover at the end of travel of less than 37.5mm would be expected(consisting of the original 16mm of soil cover plus the 19mm of soil directly in front of the pipeline which would flow over the top of the pipeline plus the additional 2.5mm of soil directly in front of the pipeline due to the vertical downward pipeline movement); 25mm was measured. Observations are in acceptable agreement with theory. As the pipeline interacted with the trench wall, the trench wall was pushed laterally with the pipeline so that the width of the trench was approximately 59mm at the end of displacement. Displacements were measured in front of the pipeline extending beyond one pipeline diameter. Rupture planes/bands were observed in front of the pipeline extending from the toe of the pipeline to noticeable ruptures at the soil surface at approximately 44°. Tension cracks were observed in front of and above the pipeline. No gaps were noticed between the rear of the pipeline and the backfill. The embedment ratio at the start of pipeline displacement was assumed to be 1.842 based on a pipeline base elevation of 100.5mm and 16mm of soil cover. Post-test excavation indicated a pipeline base elevation of 98mm or an equivalent increase in cover depth to 18.5mm which reflects an embedment ratio of 1.974. Therefore, a range in "cover depth" and "h/D" has been presented in Table 8.1 for the prototype of Pipeline #1.
7	2	There was a noticeable depression (1-2mm) where the pipe started, probably caused by the bearing stress of the pipeline. The pipeline moved out of this depression at the beginning of displacement. Observations indicate that during interaction with the trench wall, the pipeline rode up approximately 2mm, then moved downward until at rest the base of the pipeline was 96mm above the extrusion plate. This up-down pattern may have been the result of the pipeline trying to follow a path of least resistance. However, the pipeline was restrained by the actuator system and may have tended to move vertically downward as the result of the pipe weight and bearing stress. Because the interaction was considered to be partially drained, cover at the end of travel less than 39.5mm would be expected (consisting of the original 16mm of soil cover plus the 19mm of soil directly in front of the pipeline which would flow over the top of the pipeline plus the additional 4.5mm of soil directly in front of the pipeline due to the vertical downward pipeline movement); an average of 40mm was measured. Observations are in acceptable agreement with expectations. As material passed over the top of pipe during displacement, it appears that the soil cracked and fell behind the pipeline. Tension cracks were observed in front of and above the pipeline. Displacements were measured in front of the pipeline extending approximately one pipeline diameter. Failure surfaces were observed in front of the pipeline, the most recent one extending towards the soil surface at approximately 25°. A shear zone was distinguished beneath the pipeline which was approximately 10mm wide.

Test	Pipeline	Comments
7	2	The embedment ratio at the start of pipeline displacement was assumed to be 1.842 based on a pipeline base elevation of 100.5mm and 16mm of soil cover. Post-test excavation indicated a pipeline base elevation of 96mm or an equivalent increase in cover depth to 20.5mm which reflects an embedment ratio of 2.079. Therefore, a range in "cover depth" and "h/D" has been presented in Table 8.1 for the prototype of Pipeline #2.
7	3	There was a noticeable depression (1-2mm) where the pipe started, probably caused by the bearing stress of the pipeline. The pipeline moved out of this depression at the beginning of displacement. Observations indicate that during interaction with the trench wall and subsequently, the pipeline moved essentially horizontally. At rest, the base of the pipeline was 98mm above the extrusion plate. Because the interaction was considered to be partially undrained, cover at the end of travel equal to 37.5mm would be expected (consisting of the original 16mm of soil cover plus the 19mm of soil directly in front of the pipeline which would flow over the top of the pipeline plus the additional 2.5mm of soil directly in front of the pipeline due to the vertical downward pipeline movement); an average of 37.5mm was measured. The observations are in acceptable agreement with expectations. As with other undrained tests, material appears to have flowed over the top of the pipe during displacement. Deformations were measured in front of the pipeline extending greater than one pipeline diameter. Faint rupture bands appeared to run from the base of the pipeline to the soil surface but no noticeable rupture of the soil surface could be distinguished. As the pipeline interacted with the trench wall, native material fell over behind the pipeline. A shear zone was distinguished beneath the pipeline which was approximately 10mm wide. The embedment ratio at the start of pipeline displacement was assumed to be 1.842 based on a pipeline base elevation of 100.5mm and 16mm of soil cover. Post-test excavation indicated a pipeline base elevation of 98mm or an equivalent increase in cover depth to 18.5mm which reflects an embedment ratio of 1.974. Therefore, a range in "cover depth" and "h/D" has been presented in Table 8.1 for the prototype of Pipeline #3.
7	4	There was a minor depression where the pipeline started, which was probably caused by the bearing stress of the pipeline. The pipeline moved out of this depression at the beginning of displacement. Observations indicate that after interaction with the trench wall, the pipeline moved essentially horizontally. After testing, the base of the pipeline was 95mm above the extrusion plate. Because the interaction was considered to be undrained, cover at the end of travel equal to 40.5mm would be expected (consisting of the original 16mm of soil cover plus the 19mm of soil directly in front of the pipeline which would flow over the top of the pipeline plus the additional 5.5mm of soil directly in front of the pipeline due to the vertical downward pipeline movement); approximately 38mm was measured. Observations are in acceptable agreement with expectations. As with other undrained tests, material flowed over the top of the pipe during displacement. Soil displacements were measured in front of the pipeline within one pipeline diameter. Horizontal cracks were noticed above the pipeline extending to the front and rear. Backfill had travelled with the pipeline

Test	Pipeline	Comments
7	4	as it penetrated the trench wall. A shear zone was distinguished beneath the pipeline which was approximately 15mm wide. The embedment ratio at the start of pipeline displacement was assumed to be 1.842 based on a pipeline base elevation of 100.5mm and 16mm of soil cover. Post-test excavation indicated a pipeline base elevation of 95mm or an equivalent increase in cover depth to 21.5mm which reflects an embedment ratio of 2.132. Therefore, a range in "cover depth" and "h/D" has been presented in Table 8.1 for the prototype of Pipeline #4.
Comments		Failure mechanisms associated with soil displacement in front of Pipeline #1 and Pipeline #2 appear to have been similar; conditions during these tests are assumed to have been essentially drained. Failure mechanisms associated with soil displacement in front of Pipeline #3 and Pipeline #4 were similar; conditions during these tests are assumed to have been essentially undrained.
8	1	There was a noticeable depression (3-4mm) where the pipe started, probably caused by the bearing stress of the pipeline. The pipeline moved out of this depression during the first 1D of pipeline movement and then moved relatively horizontally during interaction with the trench wall. The base of the pipeline was at an elevation of 100.5mm at the start of displacement and finished at an elevation of 100mm. Because the interaction was considered to be drained, cover at the end of travel of less than 35.5mm would be expected (consisting of the original 16mm of soil cover plus the 19mm of soil directly in front of the pipeline which would flow over the top of the pipeline plus the additional 0.5mm of soil directly in front of the pipeline due to the vertical downward pipe movement); 25mm was measured. Observations are in acceptable agreement with theory. As the pipeline interacted with the trench wall, the trench wall was pushed laterally with the pipeline after an embedment of approximately 0.5D. The width of the trench was approximately 60mm at the end of displacement. Soil deformations were measured in front of the pipeline extending beyond one pipeline diameter. Linear rupture planes/bands were observed in front of the pipeline extending to noticeable ruptures at the soil surface at approximately 32°. Separation was noted between the backfill and the rear of the pipeline. A shear zone was distinguished beneath the pipeline which was approximately 5-10mm wide. The embedment ratio at the start of pipeline displacement was assumed to be 1.842 based on a pipeline base elevation of 100.5mm and 16mm of soil cover. Post-test excavation indicated a pipeline base elevation of 100mm or an equivalent increase in cover depth to 16.5mm which reflects an embedment ratio of 1.868. Therefore, a range in "cover depth" and "h/D" has been presented in Table 8.1 for the prototype of Pipeline #1.
8	2	There was a noticeable depression (3-5mm) where the pipe started, probably caused by the bearing stress of the pipeline. The pipeline moved out of this depression during the first 1D of pipeline movement. Another slight depression (1-2mm) was noticed at the approximate location where the pipeline began to interact with the trench wall but the pipe appears to have moved out of this depression within a further 1D pipeline displacement. The base of the pipeline

Test	Pipeline	Comments
8	2	was at an elevation of 100.5mm above the extrusion plate at the start of displacement and finished at an elevation of 99mm. Because the interaction was considered to be partially drained, cover at the end of travel less than 36.5mm would be expected (consisting of the original 16mm of soil cover plus the 19mm of soil directly in front of the pipeline which would flow over the top of the pipeline plus the additional 1.5mm of soil directly in front of the pipeline due to the vertical downward pipeline movement); 34mm was measured. Observations are in acceptable agreement with expectations. As material passed over the top of the pipe during displacement, it appears that the soil cracked and fell behind the pipeline. Soil deformations were measured in front of the pipeline extending beyond one pipeline diameter. A linear rupture plane/band was observed in front of the pipeline extending to noticeable ruptures at the soil surface at approximately 33°. A void was observed to the rear of the pipeline. A shear zone was distinguishable beneath the pipeline which was approximately 10mm wide. The embedment ratio at the start of pipeline displacement was assumed to be 1.842 based on a pipeline base elevation of 100.5mm and 16mm of soil cover. Post-test excavation indicated a pipeline base elevation of 99mm or an equivalent increase in cover depth to 17.5mm which reflects an embedment ratio of 1.921. Therefore, a range in "cover depth" and "h/D" has been presented in Table 8.1 for the prototype of Pipeline #2.
8	3	There is a noticeable depression (4-5mm) where the pipe started, probably caused by the bearing stress of the pipeline. The pipeline moved out of this depression over an initial 1D of displacement. Observations indicate that during interaction with the trench wall, the pipeline moved essentially horizontally. After a penetration of approximately 1.5D into the trench wall, the pipeline appears to have moved slightly downward so that at rest, the base of the pipeline was 93mm above the extrusion plate. Because the interaction was considered to be partially undrained, cover at the end of travel approximately equal to 42.5mm would be expected (consisting of the original 16mm of soil cover plus the 19mm of soil directly in front of the pipeline which would flow over the top of the pipeline plus the additional 7.5mm of soil directly in front of the pipeline due to the vertical downward pipeline movement); an average of 36mm was measured. The observations are in acceptable agreement with expectations. As with other undrained tests, material appears to have flowed over the top of the pipeline during displacement. Deformations were measured in front of the pipeline extending greater than one pipeline diameter. A shear zone was distinguished beneath the pipeline which was 10mm wide. The embedment ratio at the start of pipeline displacement was assumed to be 1.842 based on a pipeline base elevation of 100.5mm and 16mm of soil cover. Post-test excavation indicated a pipeline base elevation of 93mm or an equivalent increase in cover depth to 23.5mm which reflects an embedment ratio of 2.237. Therefore, a range in "cover depth" and "h/D" has been presented in Table 8.1 for the prototype of Pipeline #3.
8	4	There is a noticeable depression (3-4mm) from where the pipeline started which was probably caused by the bearing stress of the pipeline. The pipeline moved

Test	Pipeline	Comments
8	4	out of this depression after approximately 1D of displacement. Observations indicate that after interaction with the trench wall, the pipeline suddenly moved vertically downward 3-4mm. From this position, observations indicate that the pipeline moved essentially horizontally. After testing, the base of the pipeline was 92mm above the extrusion plate. Because the interaction was considered to be undrained, cover at the end of travel equal to 43.5mm would be expected(consisting of the original 16mm of soil cover plus the 19mm of soil directly in front of the pipeline which would flow over the top of the pipeline plus the additional 8.5mm of soil directly in front of the pipeline due to the vertical downward pipeline movement); approximately 37mm was measured. Observations are in acceptable agreement with expectations. As with other undrained tests, material appears to have flowed over the top of the pipe during displacement. Soil displacements were measured in front of the pipeline within 1 pipeline diameter. A wedge of backfill (with some Vaseline) was present behind the pipeline. A shear zone was distinguished beneath the pipeline which was approximately 10mm wide. The embedment ratio at the start of pipeline displacement was assumed to be 1.842 based on a pipeline base elevation of 100.5mm and 16mm of soil cover. Post-test excavation indicated a pipeline base elevation of 92mm or an equivalent increase in cover depth to 24.5mm which reflects an embedment ratio of 2.289. Therefore, a range in "cover depth" and "h/D" has been presented in Table 8.1 for the prototype of Pipeline #4.
Comments		Failure mechanisms associated with soil displacement in front of Pipeline #1 and Pipeline #2 appear to have been similar; conditions during these tests are assumed to have been essentially drained. Failure mechanisms associated with soil displacement in front of Pipeline #3 and Pipeline #4 were similar; conditions during these tests are assumed to have been essentially undrained.
9	1	There was a noticeable depression (1-2mm) where the pipeline displacement started, probably caused by the bearing stress of the pipeline. The pipeline moved out of this depression during the first 1D of displacement after which it appears to have moved relatively horizontally. The base of the pipeline was assumed to be at an elevation of 100.5mm above the extrusion plate at the start of displacement and finished at an elevation of approximately 100mm. Because the interaction was considered to be drained, cover at the end of travel less than 35.5mm would be expected (consisting of the original 16mm of soil cover plus the 19mm of soil directly in front of the pipeline which would flow over the top of the pipeline plus the additional 0.5mm of soil due to the downward vertical movement of the pipe); 28-29mm was measured. Observations are in acceptable agreement with theory. Displacements were measured in front of the pipeline extending beyond one pipeline diameter. Straight rupture planes/bands were observed in front of the pipeline extending from the toe of the pipeline to noticeable rupture surfaces at the soil surface at approximately 38° to the horizontal. A wedge of slurry backfill was evident in front of the pipeline which extended horizontally approximately 6mm. A shear zone was distinguished beneath the pipeline which was approximately 5-10mm wide.

Test	Pipeline	Comments
9	1	The embedment ratio at the start of pipeline displacement was assumed to be 1.842 based on a pipeline base elevation of 100.5mm and 16mm of soil cover. Post-test excavation indicated a pipeline base elevation of 100mm or an equivalent increase in cover depth to 16.5mm which reflects an embedment ratio of 1.868. Therefore, a range in "cover depth" and "h/D" has been presented in Table 8.1 for the prototype of Pipeline #1.
9	2	There was a slight depression (2-3mm) where the pipe started, probably caused by the bearing stress of the pipeline. The pipeline appears to have moved out of this depression during the first 0.5D of displacement after which it moved slightly upward with displacement. The base of the pipeline was assumed to be at an elevation of 100.5mm above the extrusion plate at the start of displacement and finished at an elevation of 104mm. Because the interaction was considered to be drained, cover at the end of travel less than 31.5mm would be expected (consisting of the original 16mm of soil cover plus the 19mm of soil directly in front of the pipeline which would flow over the top of the pipeline minus the loss of 3.5mm of soil height directly in front of the pipeline due to the vertical upward pipeline movement); 29mm was measured. Observations are in acceptable agreement with theory. Displacements were measured in front of the pipeline extending beyond one pipeline diameter. Straight rupture planes/bands were observed in front of the pipeline extending from the toe of the pipeline to noticeable rupture surfaces at the soil surface. These ruptures were at an approximate angle of 32° to the horizontal. The pipeline appeared to have essentially separated from the backfill to the rear of the pipeline and no backfill was evident in front of the pipeline. A shear zone was distinguished beneath the pipeline which was approximately 5-10mm wide. The embedment ratio at the start of pipeline displacement was assumed to be 1.842 based on a pipeline base elevation of 100.5mm and 16mm of soil cover. Post-test excavation indicated a pipeline base elevation of 104mm or an equivalent decrease in cover depth to 12.5mm which reflects an embedment ratio of 1.658. Therefore, a range in "cover depth" and "h/D" has been presented in Table 8.1 for the prototype of Pipeline #2.
9	3	There was no noticeable depression at the point of the start of pipeline displacement. The pipeline appears to have moved essentially horizontally during displacement. However, ends of the model pipeline segment were displaced different amounts due to the slippage of the pipeline tension cable as explained earlier. At the cross-sectional excavation halfway along the pipeline length, the trench wall had not collapsed behind the pipeline but rather it appeared that the trench wall had been pushed laterally with the pipeline after an embedment of approximately 0.1-0.2D. The width of the trench, on the path centerline, was approximately 70mm at the end of displacement. The base of the pipeline was assumed to be at an elevation of 100.5mm above the extrusion plate at the start of displacement and finished at an elevation of 98mm. Because the interaction was considered to be drained, cover at the end of travel less than 37.5mm would be expected (consisting of the original 16mm of soil cover plus the 19mm of soil directly in front of the pipeline which would flow over the top of the pipeline plus

Test	Pipeline	Comments
9	3	the additional 2.5mm of soil directly in front of the pipeline due to the vertical downward pipeline movement); approximately 28mm was measured. Observations are in acceptable agreement with theory. Soil displacements were observed in front of the pipeline extending beyond one pipeline diameter. A linear failure surface was observed in front of the pipeline extending to a noticeable rupture at the soil surface. The rupture plane was at an approximate angle of 34° to the horizontal. The backfill appeared to have adhered to the rear of the pipeline. A wedge of backfill extending horizontally 12-13mm in front of the pipeline was evident. A shear zone was distinguished beneath the pipeline which was approximately 5-10mm wide. The embedment ratio at the start of pipeline displacement was assumed to be 1.842 based on a pipeline base elevation of 100.5mm and 16mm of soil cover. Post-test excavation indicated a pipeline base elevation of 98mm or an equivalent increase in cover depth to 18.5mm which reflects an embedment ratio of 1.974. Therefore, a range in "cover depth" and "h/D" has been presented in Table 8.1 for the prototype of Pipeline #3.
9	4	There was no noticeable depression at the point of the start of pipeline displacement. The pipeline appears to have moved essentially horizontally during displacement. At the cross-sectional excavation halfway along the pipeline length, the trench wall had not collapsed behind the pipeline but rather it appeared that the trench wall had been pushed laterally with the pipeline after an embedment of approximately 0.25D. The width of the trench, on the interaction path centerline was approximately 65mm at the end of pipeline displacement. The base of the pipeline was assumed to be at an elevation of 100.5mm above the extrusion plate at the start of displacement and finished at an elevation of 101mm. Because the interaction was considered to be drained, cover at the end of travel less than 34.5mm would be expected (consisting of the original 16mm of soil cover plus the 19mm of soil directly in front of the pipeline which would flow over the top of the pipeline minus the loss of 0.5mm of soil height directly in front of the pipeline due to the vertical upward pipeline movement); approximately 26mm was measured. Observations are in acceptable agreement with theory. Soil displacements were observed in front of the pipeline extending beyond one pipeline diameter. Curvilinear failure surfaces were observed in front of the pipeline extending to noticeable ruptures at the soil surface. These rupture bands were at an approximate angle of 33-34° to the horizontal. A semi-circular zone of loose sand backfill had been carried with the pipeline. This zone extended horizontally approximately 9mm in front of the pipeline. A shear zone extending approximately 5mm below the pipeline could be distinguished. The embedment ratio at the start of pipeline displacement was assumed to be 1.842 based on a pipeline base elevation of 100.5mm and 16mm of soil cover. Post-test excavation indicated a pipeline base elevation of 101mm or an equivalent decrease in cover depth to 15.5mm which reflects an embedment ratio of 1.816. Therefore, a range in "cover depth" and "h/D" has been presented in Table 8.1 for the prototype of Pipeline #4.

Test	Pipeline	Comments
Comments		Failure mechanisms associated with soil displacement in front of the pipelines appear to have been similar; conditions during these tests were essentially drained. The extent and magnitude of backfill observed in front of the pipelines during post-test excavation appears to have been dependent upon the backfill type and condition (i.e. slurry, chunky, remoulded or sand).

Appendix L

Prototype Force-Displacement Curve Corrections

Test	Pipeline	Comments
01	2	Pipeline base elevation at start of travel = 100.5mm; inferred elevation at end of travel = 96.5mm. Expected cover at end of travel = 29mm; equivalent cover at end of travel = 33mm. Correction factor varies from 1 at the trench wall to 33/29 = 1.14 at the end of pipeline travel. This accounts for the apparent increase over the expected h/D. The corrected force-displacement curve is presented in Figure 8.12.
01	3	Pipeline base elevation at start of travel = 100.5mm; inferred elevation at end of travel = 97.5mm. Expected cover at end of travel = 24mm; equivalent cover at end of travel = 27mm. Correction factor varies from 1 at the trench wall to 27/24 = 1.13 at the end of pipeline travel. This accounts for the apparent increase over the expected h/D. The corrected force-displacement curve is presented in Figure 8.12.
01	4	Pipeline base elevation at start of travel = 100.5mm; inferred elevation at end of travel = 96.5mm. Expected cover at end of travel = 19mm; equivalent cover at end of travel = 23mm. Correction factor varies from 1 at the trench wall to 23/19 = 1.21 at the end of pipeline travel. This accounts for the apparent increase over the expected h/D. The corrected force-displacement curve is presented in Figure 8.12.
03	3	Pipeline base elevation at start of travel = 100.5mm; measured elevation at end of travel = 98.5mm. Expected cover at end of travel = 35mm; equivalent cover at end of travel = 37mm. Correction factor varies from 1 at the trench wall to 37/35 = 1.06 at the end of pipeline travel. This accounts for the apparent increase over the expected h/D. The corrected force-displacement curve is presented in Figure 8.13.
03	4	Pipeline base elevation at start of travel = 100.5mm; measured elevation at end of travel = 98.5mm. Expected cover at end of travel = 35mm; equivalent cover at end of travel = 37mm. Correction factor varies from 1 at the trench wall to 37/35 = 1.06 at the end of pipeline travel. This accounts for the apparent increase over the expected h/D. The corrected force-displacement curve is presented in Figure 8.13.
04	2	Pipeline base elevation at start of travel = 100.5mm; measured elevation at end of travel = 94.5mm. Expected cover at end of travel ≤ 35mm; equivalent cover at end of travel ≤ 41mm. Correction factor varies from 1 at the trench wall to 41/35 = 1.17 at the end of pipeline travel. This accounts for the apparent increase over the expected h/D. The corrected force-displacement curve is presented in Figure 8.14.
04	3	Pipeline base elevation at start of travel = 100.5mm; measured elevation at end of travel = 98.5mm. Expected cover at end of travel = 35mm; equivalent cover at end of travel = 37mm. Correction factor varies from 1 at the trench wall to 37/35 = 1.06 at the end of pipeline travel. This accounts for the apparent increase over the expected h/D. The corrected force-displacement curve is presented in Figure 8.14.

Test	Pipeline	Comments
04	4	Pipeline base elevation at start of travel = 100.5mm; measured elevation at end of travel = 95.5mm. Expected cover at end of travel = 35mm; equivalent cover at end of travel = 40mm. Correction factor varies from 1 at the trench wall to 40/35 = 1.14 at the end of pipeline travel. This accounts for the apparent increase over the expected h/D. The corrected force-displacement curve is presented in Figure 8.14.
05	1	Pipeline base elevation at start of travel = 91mm; measured elevation at end of travel = 94mm. Expected cover at end of travel = 70mm; equivalent cover at end of travel = 67mm. Correction factor varies from 1 at the trench wall to 67/70 = 0.96 at the end of pipeline travel. This accounts for the apparent increase over the expected h/D. The corrected force-displacement curve is presented in Figure 8.15.
05	2	Pipeline base elevation at start of travel = 91mm; measured elevation at end of travel = 96mm. Expected cover at end of travel = 58mm; equivalent cover at end of travel = 53mm. Correction factor varies from 1 at the trench wall to 53/58 = 0.91 at the end of pipeline travel. This accounts for the apparent increase over the expected h/D. The corrected force-displacement curve is presented in Figure 8.15.
06	1	Pipeline base elevation at start of travel = 105mm; measured elevation at end of travel = 93.5mm. Expected cover at end of travel = 17.5mm; equivalent cover at end of travel = 29mm. Correction factor varies from 1 prior to displacement to 25/17.5 = 1.43 at the trench wall to 29/17.5 = 1.66 at the end of pipeline travel. This accounts for the apparent increase over the expected h/D. The corrected force-displacement curve is presented in Figure 8.16.
06	2	Pipeline base elevation at start of travel = 105mm; measured elevation at end of travel = 92.5mm. Expected cover at end of travel = 14.5mm; equivalent cover at end of travel = 27mm. Correction factor varies from 1 prior to displacement to 24/14.5 = 1.66 at the trench wall to 27/14.5 = 1.86 at the end of pipeline travel. This accounts for the apparent increase over the expected h/D. The corrected force-displacement curve is presented in Figure 8.16.
06	3	Pipeline base elevation at start of travel = 105mm; measured elevation at end of travel = 92mm. Expected cover at end of travel = 12mm; equivalent cover at end of travel = 25mm. Correction factor varies from 1 prior to displacement to 21/12 = 1.75 at the trench wall to 25/12 = 2.08 at the end of pipeline travel. This accounts for the apparent increase over the expected h/D. The corrected force-displacement curve is presented in Figure 8.16.
06	4	Pipeline base elevation at start of travel = 105mm; measured elevation at end of travel = 90.5mm. Expected cover at end of travel = 9.5mm; equivalent cover at end of travel = 24mm. Correction factor varies from 1 prior to displacement to 21/9.5 = 2.21 at the trench wall to 24/9.5 = 2.53 at the end of pipeline travel. This accounts for the apparent increase over the expected h/D. The corrected force-displacement curve is presented in Figure 8.16.

Test	Pipeline	Comments
07	1	Pipeline base elevation at start of travel = 100.5mm; measured elevation at end of travel = 98mm. Expected cover at end of travel ≤ 35mm; equivalent cover at end of travel ≤ 37.5mm. Correction factor varies from 1 at the trench wall to 37.5/35 = 1.07 at the end of pipeline travel. This accounts for the apparent increase over the expected h/D. The corrected force-displacement curve is presented in Figure 8.17.
07	2	Pipeline base elevation at start of travel = 100.5mm; measured elevation at end of travel = 96mm. Expected cover at end of travel ≤ 35mm; equivalent cover at end of travel ≤ 39.5mm. Correction factor varies from 1 at the trench wall to 39.5/35 = 1.13 at the end of pipeline travel. This accounts for the apparent increase over the expected h/D. The corrected force-displacement curve is presented in Figure 8.17.
07	3	Pipeline base elevation at start of travel = 100.5mm; measured elevation at end of travel = 98mm. Expected cover at end of travel = 35mm; equivalent cover at end of travel = 37.5mm. Correction factor varies from 1 at the trench wall to 37.5/35 = 1.07 at the end of pipeline travel. This accounts for the apparent increase over the expected h/D. The corrected force-displacement curve is presented in Figure 8.17.
07	4	Pipeline base elevation at start of travel = 100.5mm; measured elevation at end of travel = 95mm. Expected cover at end of travel = 35mm; equivalent cover at end of travel = 40.5mm. Correction factor varies from 1 at the trench wall to 40.5/35 = 1.16 at the end of pipeline travel. This accounts for the apparent increase over the expected h/D. The corrected force-displacement curve is presented in Figure 8.17.
08	2	Pipeline base elevation at start of travel = 100.5mm; measured elevation at end of travel = 99mm. Expected cover at end of travel ≤ 35mm; equivalent cover at end of travel ≤ 36.5mm. Correction factor varies from 1 at the trench wall to 36.5/35 = 1.04 at the end of pipeline travel. This accounts for the apparent increase over the expected h/D. The corrected force-displacement curve is presented in Figure 8.18.
08	3	Pipeline base elevation at start of travel = 100.5mm; measured elevation at end of travel = 93mm. Expected cover at end of travel = 35mm; equivalent cover at end of travel = 42.5mm. Correction factor varies from 1 at the trench wall to 42.5/35 = 1.21 at the end of pipeline travel. This accounts for the apparent increase over the expected h/D. The corrected force-displacement curve is presented in Figure 8.18.
08	4	Pipeline base elevation at start of travel = 100.5mm; measured elevation at end of travel = 92mm. Expected cover at end of travel = 35mm; equivalent cover at end of travel = 43.5mm. Correction factor varies from 1 at the trench wall to 43.5/35 = 1.24 at the end of pipeline travel. This accounts for the apparent increase over the expected h/D. The corrected force-displacement curve is presented in Figure 8.18.

Test	Pipeline	Comments
09	2	Pipeline base elevation at start of travel = 100.5mm; measured elevation at end of travel = 104mm. Expected cover at end of travel ≤ 35mm; equivalent cover at end of travel ≤ 31.5mm. Correction factor varies from 1 at the trench wall to 31.5/35 = 0.90 at the end of pipeline travel. This accounts for the apparent decrease in the expected h/D. The corrected force-displacement curve is presented in Figure 8.19.
09	3	Pipeline base elevation at start of travel = 100.5mm; measured elevation at end of travel = 98mm. Expected cover at end of travel ≤ 35mm; equivalent cover at end of travel ≤ 37.5mm. Correction factor varies from 1 at the trench wall to 37.5/35 = 1.07 at the end of pipeline travel. This accounts for the apparent increase over the expected h/D. The corrected force-displacement curve is presented in Figure 8.19.

Appendix M

Summary of Subgrade Modulus Calculation Methods

Reported by	Proposed Formulations	Comments
Skempton (1951)	$k_h = 80 \text{ to } 320 \frac{c_u}{d}$	c_u is the undrained shear strength of the soil and d is the pile diameter.
Terzaghi (1955)[1]	$k_h = \frac{1}{1.5B} \cdot k_{s1}$ k_{s1} is the modulus for a strip, 1ft wide: Consistency / Stiff / Very Stiff / Hard c_u (ton/ft^2) 0.5-1 1-2 2 range of k_{s1} 50-100 100-200 200 proposed k_{s1} 75 100 300	p = k_h*y where p is pressure per unit area. B is the breadth or diameter of the pile in feet. Values of k_{s1} are for overconsolidated clays. c_u is undrained shear strength. k_{s1} is given in ton/ft^3.
Terzaghi (1955)[2]	$k_h = n_h \frac{z}{B}$ n_h is the constant for a pile, 1 ft. wide: Relative Density / Loose / Medium / Dense dry or moist sand 7 21 56 submerged sand 4 14 34	p = k_h*y where p is pressure per unit area. B is the breadth or diameter of the pile in feet. n_h is given in ton/ft^3.

Reported by	Proposed Formulations	Comments
Reese and Matlock (1956)	n_h = 0.6 to 12.7 lb/in^3	for soft NC clay
Peck and Davisson (1962)	n_h = 0.4 to 1.0 lb/in^3	for NC organic clay
Davisson and Prakash (1963)	n_h = 1.0 to 2.0 lb/in^3	for soft NC clay
Broms (1964a)[1]	$K_\alpha = \frac{\alpha K_o}{D}$ where α is and empirical factor and equal to 0.32 for q_u less than 0.5 tons/ft^2 0.36 for q_u between 0.5-2.0 tons/ft^2 0.40 for q_u greater than 0.5 tons/ft^2 and where K_o = 1.67 E_{50} or K_o = 40 to 160 q_u	$p = K_\alpha * y$ based on a wall footing founded on the surface of a semi-infinite, ideal elastic body. D is the diameter of the pile. q_u is the unconfined compressive strength. E_{50} is the secant modulus corresponding to half the ultimate strength.

Reported by	Proposed Formulations	Comments
Broms (1964a)[2]	$K_p = \frac{E_s}{m(1-\mu^2)\sqrt{LD}}$ where m is a numerical factors based on L/D and ranges from 0.95 for L/D=1 to 0.37 for L/D=100	$p = K_p * y$ L is the pile length. D is the pile diameter. μ is the Poisson's ratio of the soil. E_s is the modulus of elasticity of the soil.
Davisson (1970)	$k_h = n_h z$ for granular soils, normally loaded organic silt, and peat. n_h suggested as: Soil Type — Value granular — n_h ranges from 1.5 - 200lb/in^3; n_h generally from 10-100lb/in^3 normally loaded organic silt — n_h ranges 0.4-3.0lb/in^3 peat — $n_h \approx 0.2$lb/in^3 cohesive soils — k is approximately $67c_u$	z is depth below the ground surface

Reported by	Proposed Formulations	Comments
Audibert and Nyman (1977)[1]	$k_h = \frac{2E'}{D}$ Suggested values of E' are as follows: Soil — E', kN/m² sandy clay loam (untamped) — 1600-1800 sandy clay loam (tamped) — 3460-5380 sand — 2410-8270 well graded gravel (untamped) — 4630	The reported E' values are secant values for an unknown amount of deflection.
Audibert and Nyman (1977)[2]	$k_h = \frac{2k_e C'}{1.5D}$ Suggested values of k_e are as follows: Soil — k_e, kN/m³ loose sand — 410-1090 medium sand — 1090-3260 dense sand — > 3260	Proposed formula are for dry or moist granular soil only. C is soil cover.

Reported by	Proposed Formulations	Comments
Audibert and Nyman (1977)[3]	$k_h = \frac{k_e Z}{D}$ Suggested values of k_e are as follows: Soil — k_e, kN/m^3 loose sand — 1170-3530 medium sand — 3530-11670 dense sand — 11670-23350	Proposed formula are for dry or moist granular soil only.
Audibert and Nyman (1977)[4]	$k_h = \frac{2E_s}{1.5D}$	Proposed formula are for cohesive soil only. E_s is the soil Young's Modulus from triaxial compression test.
Crofts *et al.* (1977)	Suggested empirical values of k_h (kN/m^3): Soil — k_h, kN/m^3 very soft to soft clay — 4000 ($c_u < 40$kN/m^2) firm clay — 8000 ($40 < c_u < 75$) stiff clay — 16000 ($75 < c_u < 150$) very stiff or hard — 32000 ($c_u > 150$) very loose to loose sand — 4000 medium dense sand — 8000 dense sand — 16000 very dense sand — 32000	The results are secant values for an unknown magnitude of displacement.

Reported by	Proposed Formulations	Comments
Pyke and Beikae (1984)	Suggested values of k_h (kN/m^3): ν_s — k_h, kN/m^3 0 — $2.3E_s/D$ 0.33 — $2.0E_s/D$ 0.50 — $1.8E_s/D$	Derived for laterally loaded piles surrounded by an infinite elastic medium.
Bowles (1988)[1]	$k_s = A_s + B_s(Z)$ where $A_s = 80(cN_cs_c+0.5\gamma BN_\gamma s_\gamma)$ and $B_s = 80(\gamma N_q s_q)$	Derived from bearing capacity theory for footings but intended for laterally loaded piles.
Bowles (1988)[2]	$k_s = A_s + B_s(Z)$ Suggested values of A_s are as follows: Soil — Range of k_s, MN/m^3 dense sandy gravel — 220-400 medium dense coarse sand — 157-300 medium sand — 110-280 fine or silty, fine sand — 80-200 stiff clay (wet) — 60-220 stiff clay (saturated) — 30-110 medium clay (wet) — 39-140 medium clay (saturated) — 10-80 soft clay — 2-40	Derived from bearing capacity theory for footings but intended for laterally loaded piles. Representative of the A_s term at a depth of 3-6m.

Reported by	Proposed Formulations	Comments
Bowles (1988)[3]	$k_s = \frac{2E_s}{B(1-\mu^2)}$	E_s is the stress-strain secant modulus for soil and can be based on triaxial tests using the secant modulus between 0.25 and 0.5 of the peak deviator stress.
Bowles (1988)[4]	$k_s' = 1 \text{ to } 1.3\ E_s$ where $k_s = \frac{k_s'}{B}$	E_s is the stress-strain secant modulus for soil and can be based on triaxial tests using the secant modulus between 0.25 and 0.5 of the peak deviator stress.
Rajani *et al.* (1993)	Soil — Range of k_s, MPa/m loose sand 5-16 medium sand 9-78 dense sand 63-126 clayey sand 31-78 (medium) silty sand 24-47 (medium) clayey soils $c_u < 50$kPa 0-15 $50 < c_u < 100$kPa 15-30 $100 < c_u < 200$kPa 30-62 $c_u > 200$ >62	Adapted from Bowles (1977) and Poulos and Davis (1980). Suggested for laterally loaded pipelines.